AD_____

Award Number: DAMD17-99-1-9402

TITLE: Training Program in the Molecular Basis of Breast Cancer Research

PRINCIPAL INVESTIGATOR: Z. Dave Sharp, Ph.D.

CONTRACTING ORGANIZATION: The University of Texas Health Sciences Center at San Antonio San Antonio, Texas 78229-3900

REPORT DATE: August 2004

TYPE OF REPORT: Annual Summary

PREPARED FOR: U.S. Army Medical Research and Materiel Command Fort Detrick, Maryland 21702-5012

20041215 007

REPORT DOCUMENTATION PAGE			Form Approved OMB No. 074-0188

Public reporting burden for this collection of information is estimated to average 1 hour per response, including the time for reviewing instructions, searching existing data sources, gathering and maintaining the data needed, and completing and reviewing this collection of information. Send comments regarding this burden estimate or any other aspect of this collection of information, including suggestions for reducing this burden to Washington Headquarters Services, Directorate for Information Operations and Reports, 1215 Jefferson Davis Highway, Suite 1204, Arlington, VA 22202-4302, and to the Office of Management and Budget, Paperwork Reduction Project (0704-0188), Washington, DC 20503

1. AGENCY USE ONLY (Leave blank)	2. REPORT DATE August 2004	3. REPORT TYPE AND DATES COVERED Annual Summary (1 Aug 99-31 Jul 04)	

4. TITLE AND SUBTITLE Training Program in the Molecular Basis of Breast Cancer Research		5. FUNDING NUMBERS DAMD17-99-1-9402

6. AUTHOR(S)
Z. Dave Sharp, Ph.D.

7. PERFORMING ORGANIZATION NAME(S) AND ADDRESS(ES) The University of Texas Health Sciences Center at San Antonio San Antonio, Texas 78229-3900 E-Mail: grants@uthscsa.edu	8. PERFORMING ORGANIZATION REPORT NUMBER

9. SPONSORING / MONITORING AGENCY NAME(S) AND ADDRESS(ES) U.S. Army Medical Research and Materiel Command Fort Detrick, Maryland 21702-5012	10. SPONSORING / MONITORING AGENCY REPORT NUMBER

11. SUPPLEMENTARY NOTES

12a. DISTRIBUTION / AVAILABILITY STATEMENT Approved for Public Release; Distribution Unlimited	12b. DISTRIBUTION CODE

13. ABSTRACT (Maximum 200 Words)

The objective of the program is to train highly qualified doctoral students in the genetic, cellular, and molecular basis of Breast Cancer. The training program, conducted within the Molecular Medicine Ph.D. Program, was administered by a select group of faculty whose research projects were intimately involved in breast cancer. An additional goal of the program was to promote synergistic interactions between the various laboratories engaged in breast cancer research. Breast cancer meetings, Molecular Medicine Distinguished Seminar Series were integral parts of the training program supported by the Breast Cancer Training Program. The major strengths of the program were the high quality of the Program faculty, and the interactive nature of the Breast Cancer research community in San Antonio. The program faculty encompassed scientists and physicians studying different aspects of breast cancer and cancer therapy, as well as fundamental mechanisms of DNA repair, cell growth and cell differentiation. Key research accomplishments during the 1999-2004 reporting period were: **1)** 67 peer-reviewed articles published by students in the program; **2)** DOD BCRP pre-doctoral grants awarded to seven students in the program, **3)** nine faculty awarded DOD BCRP Idea and/or Career Development grants totaling $5 million; **4)** eighteen Ph.D. students supported by the program graduated.

14. SUBJECT TERMS Breast cancer, research training, cancer therapy, DNA repair and tumor suppressor genes, cell growth regulation and cell differentiation			15. NUMBER OF PAGES 164
			16. PRICE CODE

17. SECURITY CLASSIFICATION OF REPORT Unclassified	18. SECURITY CLASSIFICATION OF THIS PAGE Unclassified	19. SECURITY CLASSIFICATION OF ABSTRACT Unclassified	20. LIMITATION OF ABSTRACT Unlimited

NSN 7540-01-280-5500

Standard Form 298 (Rev. 2-89)
Prescribed by ANSI Std. Z39-18
298-102

Table of Contents

INTRODUCTION

This is the final report for the training program supported by DAMD17-99-1-9402. It will also include the period 8/1/03 – 7/31/04, a one-year extension of the funding period.

Brief Description of the Training Program and Its Objectives

The aim of the program was to establish at the University of Texas Health Science Center in San Antonio an in-depth training program in the Molecular Genetics of Breast Cancer. An important goal of the program was to train highly qualified Ph.D. students in the genetic, cellular, and molecular basis of Breast Cancer. Toward these ends, the program has been extremely successful. Based on the publication record of our trainees, our expectation for significant discoveries important for breast cancer was realized. During the period 8/1/03 to 7/31/04, students supported by the training program had 13 publications, and for the entire funding period, 67 papers relevant to breast cancer were published in peer-reviewed journals.

The training program was administered within the Molecular Medicine Ph.D. Program by a select group of faculty whose research projects are relevant to breast cancer. An additional goal of the program was to promote synergistic interactions between the various laboratories engaged in breast cancer research. The Annual Breast Cancer Symposium, which is held annually in San Antonio, was an important aspect of the training. All students supported by the program who resided in San Antonio were required to attend. Finally, an outstanding Molecular Medicine Seminar Series sponsored by the Department of Molecular Medicine was also a requirement for all trainees. The seminars during the entire funding period are listed in the appended materials.

Breast Cancer Research Programs and Faculty.

One of the major strengths of the program was the high quality of the Program faculty, and the interactive nature of the Breast Cancer research community in San Antonio, which encompassed scientists and physicians studying different aspects of breast cancer and cancer therapy, as well as fundamental mechanisms of to maintain genomic stability, cell growth, differentiation and molecular genetics. These faculty are listed below; detailed descriptions of individual research programs were included in the original application or at the time of their appointment.

W.-H. Lee, Ph.D. (Former Director)*	Arun K. Roy, Ph.D.§
C. Kent Osborne, M.D. (Co-Director)	Judy M. Teale, Ph.D.
Powell H. Brown, M.D., Ph.D.	Peter M. Ravdin, M.D. Ph.D.
Peter O'Connell, Ph.D.	Phang-Lang Chen, Ph.D
Gary M. Clark, Ph.D.	Renee Yew, Ph.D.
Suzanne Fuqua, Ph.D.	Tom Boyer, Ph.D.
Alan Tomkinson, Ph.D.	Maria Gazynska, Ph.D.
E. Lee, Ph.D.*	Paul Hasty, DVM
Z. Dave Sharp, Ph.D.¶	Jan Vijg, Ph.D.
Patrick Sung, Ph.D.	Tadayoshi Bessho, Ph.D.*
Greg R. Mundy	Sang Eun Lee, Ph.D.
Bettie Sue Masters, Ph.D.	Hai Rao, Ph.D.
Bandana Chatterjee, Ph.D.	

* Drs. W-H and E Lee moved to UC Irvine, and Dr. Bessho moved to U. Nebraska Medical Center.
¶ Appointed Director as of July 03.
§ Passed Away during the last reporting period.

Relationship between the Breast Cancer Training Program and the Molecular Medicine Graduate Ph.D. Program

The Breast Cancer Training Program was implemented within the context of the Molecular Medicine Graduate Ph.D. Program, an interdisciplinary Ph.D. training program in the Graduate School of Biomedical Sciences at the UTHSCSA. For the academic year 2003-04, there were 33 Ph.D. students enrolled.

The Breast Cancer Training program took advantage of the internationally recognized breast cancer research programs that existed in San Antonio, and offered unique opportunities for students interested in starting careers in breast cancer research. The participating scientists in the breast cancer program represented diverse departments including the Divisions of Medical Oncology and Endocrinology in the Department of Medicine, and the Departments of Cellular and Structural Biology, and Biochemistry. In addition, the University of Texas Institute of Biotechnology and the San Antonio Cancer Institute (SACI), a NIH-designated Cancer Center, represent outstanding resources for training opportunities in clinical and basic science research. The national and international reputation of the participating faculty served to attract a large number of excellent applicants to the breast cancer research track in the Molecular Medicine program.

The breast cancer-training program was administered in the Molecular Medicine Ph.D. program. This was ideal since: **1)** The Molecular Medicine curriculum is specifically designed to integrate fundamental principles of molecular biology with modern medicine. A Molecular Medicine Core course provides students with the mechanisms underlying human disease and provides intensive review of specific diseases (including breast cancer) that may serve as models for how human diseases can be studied at the molecular genetic level. **2)** The Molecular Medicine program requires the participation of both clinical and basic scientists in the training process. The inclusion of MDs on all student advisory committees insured that every graduate of the program has a clear perspective on the clinical relevance of the basic research in their program that, in most instances, served as a guide for the project. **3)** The Molecular Medicine program is an interdepartmental, interdisciplinary program that offers flexibility to students in terms of research laboratories, advisors and committee members. This arrangement offered a real potential for synergism in breast cancer research not possible in traditional department-bound programs. In summary, the Ph.D. program in Molecular Medicine offered a near perfect environment for Ph.D. training in breast cancer and attracted many well-qualified applicants.

Research Support for Program Faculty

An essential component of maintaining a successful and aggressive training program in Breast Cancer Research is the continued research funding of the individual Program Faculty laboratories. The faculty has been extremely successful in obtaining research funding, including over $12.6 million in total direct costs for the 2003-2004 reporting period, and a total of $72.5 million, for the entire period.

Key Research Accomplishments: (For the 2003-04 reporting period).

- Research grants awarded to members of the faculty and to predoctoral students by the Defense Department's Breast Cancer Research Program (BCRP): 12 grants were active during the period totaling $1.2 million for faculty and 6 predoctoral grants awarded to students of program faculty, totaling $523K. Short summaries of the objectives of these grants are presented in the appended materials.

- The publications for the last reporting period (8/1/03 to 7/31/04) summaries of each of trainees in the appendix. The total publications for all trainees are also shown in the appended materials.

- Graduates During the Reporting Period: John Leppard, December 2003; Sean Post, August 2003; Teresa Motycka, July 2004. Summaries of research and future plans are in the appended materials.

Reportable Outcomes for the period 8/1/04 to 7/31/04

- Supported Trainees, Research Description and Publications. The following group of outstanding trainees was supported on the BCRP in the reporting period 8/1/03 – 7/31/04. Summaries of their research are appended, including those supported by DAMD17-99-1-9402 and the previous grant.

Bingnan Gu (08/01/03 - 07/31/04) Aimin Peng (08/01/03 - 07/31/04) Guikai Wu (09/01/03 - 07/31/04) Xianzhi Jiang (08/01/03 - 07/31/04) Yi-Tzu Lin (08/01/03 - 07/31/04)	Seokjoong Kim (11/01/03 - 07/31/04) Xiaolin Qin (11/01/03 - 07/31/04) Chi-Sheng Lu (11/01/03 - 07/31/04)

The accomplishments of these students and their mentors are outstanding examples of how small investments in student training can be amplified in programs grounded in excellence. The 2003-2004 academic year marks the eleventh full year of operation for the Molecular Medicine Ph.D. Program, and is the ninth year for the Training Program in the Molecular Basis of Breast Cancer Research, DAMD17-99-1-9402. The availability of highly qualified applicants to the Molecular Medicine Program over the 2003-04 period was adequate. Overall, 111 applications were received for admission to the Fall 2003 entering class. Five new students began classes in August of 2003. The total number of students at the start of the Fall semester 2003 in the Molecular Medicine Ph.D. Program at all levels was 34, which includes 19 women, and 3 underrepresented minority.

Changes to the Program Faculty:

Drs. Wen-Hwa Lee, and also to Dr. Eva Lee, who both have students in good standing in the Graduate Program in Molecular Medicine, have moved their laboratories to U. of California, Irvine. Although they have both moved their laboratories, they remain members of the faculty since they still have students. Dr. Alan Tomkinson also moved his laboratory to the U. Maryland. His last student in the program, T. Motycka, successfully defended her dissertation in late June, 04, and will graduate in July 04. .

Additions: None during the reporting period.

Changes in the Program Courses: None during the reporting period.

SUMMARY: The BCRP funded by DAMD17-99-1-9402 made adequate progress in attracting and retaining excellent students in breast cancer research during the final period. Students received a high level of training as evidenced by a total of 13 publications on breast cancer by students, and seven faculty had twelve grants totaling $1.2 million. Six students in the Molecular Medicine Program were funded by the BCRP, in the period covered by this report. Three key investigator relocated their laboratories, while two (Drs. WH and E Lee) remained on the training faculty. In summary, the overall progress of the students was excellent.

For entire period of the grant, a total of 67 publications was generated by the trainees supported by DAMD17-99-1-9402. A total of $5 million in DOD BCRP funding was achieved. This is significant for this progress report since Molecular Medicine PhD students (most of whom were supported by this training grant) working in these laboratories are primarily responsible for the science upon which these grants were funded. During the entire funding period, 7 students acquired pre-doctoral fellowships from the DOD BRCP, totaling $523K. This is an impressive record during the period funded by this training grant. Combined with the basic instruction they receive in the Molecular Medicine Ph.D. Program, students graduated as highly skilled researchers who will be competitive for postdoctoral positions in the premiere breast cancer laboratories in the world.

APPENDIX
(Summaries of Research Projects, Research Support, List of Trainee Publications, and Reprints of Trainee Publications.)

Project Summaries and Publications of Ph.D. Trainees (including those supported by the previous grant and DAMD17-99-1-9402)

Note that the Program Director's comments regarding each student's research are in italics below each description.

Students supported by DAMD17-99-1-9402 during the period 8/1/03—7/31/04.

- **Guikai Wu**   **Mentor – Dr. Phang-Lang Chen**

Immortalized cells maintain telomere length through either a telomerase-dependent process or a telomerase-independent pathway termed alternative lengthening of telomeres (ALT). Homologous recombination is implicated in the ALT pathway in both yeast and human ALT cells. In ALT cells, two types of DNA double-strand break repair and homologous recombination factors, the Rad50/Mre11/NBS1 complex and Rad51/Rad52 along with replication factors (RPA) and telomere binding proteins (TRF1 and TRF2), are associated with the ALT-associated PML body (APB). DNA synthesis in late S-G(2) is associated with APBs, which contain telomeric DNA and, are therefore, potential sites for telomere length maintenance. Mr. Gu showed that the breast cancer susceptibility gene product, breast cancer susceptibility gene 1, and the human homologue of yeast Rap1, hRap1, are also associated with APBs specifically during late S-G(2) phase of the cell cycle. He additionally show that the localization of the double-strand break repair factors with APBs is distinct from their association with ionizing radiation-induced nuclear foci. To systematically explore the mechanism involved in the assembly of APBs, we examine the role of Nijmegen breakage syndrome 1 (NBS1) and TRF1 in this process, respectively. He demonstrated that NBS1 plays a key role in the assembly and/or recruitment of Rad50, Mre11, and breast cancer susceptibility gene 1, but not Rad51 or TRF1, to APBs. The NH(2) terminus of NBS1, specifically the BRCA1 COOH-terminal domain, is required for this activity. Although TRF1 interacts with NBS1 directly, it is dispensable for the association of either Rad50/Mre11/NBS1 or Rad51 with APBs. Perturbation of the interactions between NBS1/Mre11 and APBs correlates with reduced BrdUrd incorporation associated with APBs, consistent with decreased DNA synthesis at these sites. Taken together, these results support a model in which NBS1 has a vital role in the assembly of APBs, which function to maintain telomeres in human ALT cells.

All of the proteins in Mr. Wu's project are vital to the DNA repair and response systems of normal and cancer cells. Telomeres are essential for the maintenance of chromosome length and are a target of both cancer and aging research. Accordingly, Mr. Wu's project could have important relevance to the age-related onset of cancer including those of the mammary gland.

Mr. Wu will be defending his dissertation in July, 04.

- **Xianzhi Jiang**   **Mentor – Dr. Phang-Lang Chen**

Since joining Dr. Chen's lab, Mr. Jiang has been participating in the following two research projects: (I) A systematic study of the mechanism involved in the assembly of the ALT-associated promyelocytic leukemia body (APB), and (II) the characterization of a novel non-selenocysteine containing phospholipid hydroperoxide glutathione peroxidase (NPGPx). Regarding the first project, it has been known that NBS1 and TRF1 are associated with ALT- associated PML body (APB). NBS1 physically interacts with TRF1, a telomere-specific binding protein. In order to understand the potential roles of NBS1 and TRF1 in the

assembly of APBs, Mr. Jiang made adenovirus constructs that expressed GFP-TRF1Dmyb fusion protein, which lacks the NBS1 interaction region. Overexpressed TRF1Dmyb protein can form a TRF1Dmyb/TRF1 dimer and thus acts as a dominant negative by depleting endogenous TRF1 from telomere DNA. In collaboration with Guikai Wu, Mr. Jiang demonstrated that NBS1 plays a key role in the assembly and/or recruitment of RAD50, MRE11, and BRCA1, but not RAD51 or TRF1, to APBs. Although TRF1 interacts with NBS1 directly, it is dispensable for the association of either RAD50/MRE11/NBS1 or RAD51 with APBs.

In the second project, Mr. Jiang identified a novel non-selenocysteine containing phospholipid hydroperoxide glutathione peroxidase named as NPGPx. In collaboration with Ahmad Utomo, Mr. Jiang demonstrated that ectopic expression of NPGPx in Brca1-null cells that were sensitive to oxidative stress induce by hydrogen peroxide conferred a similar resistance level to that of the wild-type cells, suggesting the importance of this enzyme in reducing oxidative stress. Unlike mammary gland and other normal tissues, the majority of breast cancer cell lines studied (11 out of 12) expressed very low or undetectable levels of NPGPx irrespective of BRCA1 status. Re-expression of NPGPx in breast cancer lines, MCF-7 and HCC1937, induced resistance to eicosapentaenoic acid (an omega-3 type of polyunsaturated fatty acid) mediated cell death and abrogated proliferative stimulation by linoleic acid (an omega-6 type). Thus NPGPx plays an essential role in breast cancer cells in alleviating oxidative stress generated from polyunsaturated fatty acid metabolism.

Mr. Jiang's projects are clearly important to breast cancer research. The proteins in project one are of obvious importance to DNA repair and genomic stability. Project two is novel and offers fresh insights into the role of oxidative damage and the proteins that participate in assuaging it. Thus the research plan of Mr. Jiang will be important in combating breast cancer on two critically important fronts.

- **Yi-Tzu Lin**   **Mentor – Dr. Wen-Hwa Lee**

Accurate chromosome segregation, a process essential for maintenance of genomic integrity, requires coordination between centrosomes, kinetochores, and chromosomes during M phase progression. Previously, we discovered a novel coil-coiled kinetochore protein, Hec1, which is essential for faithful chromosome segregation. Hec1 interacts directly with Hint1/HZWint1, which in turn binds to Zw10 at the kinetochore to facilitate spindle attachment. Ms. Lin showed that when Hec1 expression is down regulated by a small inhibitory RNA, localization of both Hec1 and Hint1 at kinetochores is abolished. When Hint1 expression is similarly down regulated by siRNA, Hec1 remains at kinetochores. Thus Hec1 is required for the recruitment of Hint1 to kinetochores. Down regulation of Hec1 expression resulted in chromosome missegregation characterized by lagging chromosomes during metaphase, and incomplete segregation during anaphase. These aberrations in turn lead to formation of micronuclei and multiple nuclei. Similar albeit less severe phenotypes were observed in cells treated with Hint1 siRNA. M phase is prolonged in cells treated with Hec1 siRNA, but not completely arrested since cytokinesis occurs. The cells in which Hec1 expression is down regulated fail to activate the spindle checkpoint: they do not accumulate in metaphase after treatment with nocodazole, nor is BubR1 phosphorylated. Taken together, Ms. Lin's results suggest that Hec1 recruits Hint1/Zw10 to the kinetochore for spindle attachment and may serve as a platform for control of the spindle checkpoint. The findings thus provide a molecular mechanism by which Hec1 plays a crucial role in chromosome segregation.

Cells from solid tumors typically display chromosomal aberrations attributed to problems with their segregation during cell division. Ms. Lin's research is especially relevant to breast cancer since these tumors often demonstrate these types of chromosomal defects, which may contributed to their progression.

- **Bingnan Gu**   **Mentor – Dr. Phang-Lang Chen**

CtIP (CtBP-interacting protein) is a co-repressor of transcription that works with CtBP, which was origi-nally identified as a transcriptional repressor that binds to the C-terminal region of oncoprotein E1A1. Published studies suggest a role for CtIP in transcription regulation through interactions with tumor sup-pressors Rb2, and BRCA1 and/or through interactions with transcription repressors CtBP, LMO4 and Ikaros. To systematically study the function of CtIP, Mr. Gu showed that CtIP protein localizes immuno-cytochemically to sites of BrdU-Incorporation representing replication foci (RF) in S-phase of the cell cycle. Deletion mutagenesis indicates that 84 amino acids in the middle of region 463-546 are sufficient to target CtIP to RF. Moreover, neither DNA damage by IR irradiation nor replication stress induced by ~hydroxy urea impair the association of GFP-tagged wide type CtIP with foci, nor does mutations in CtIP (S664/745A) that prevents phosphorylation by the ATM kinase. Finally, small interference RNA-mediated CtIP protein level reductions are correlated with defects in cellular proliferation. These studies have revealed a pivotal role of CtIP in mammalian DNA replication, which is consistent with animal studies showing that homozygous knockout of mouse the CtIP gene is associated with early embryonic lethality.

This study is highly relevant to breast cancer research since CtIP is a BRCA1-associated protein. This association is DNA-damage dependent, and thus potentially links BRCA1 to S phase DNA replication, through its association with CtIP. Mr. Gu's research is in the very early stages, but is clearly on the way to a very significant contribution to breast cancer research.

- **Aimin Peng**   **Mentor – Dr. Phang-Lang Chen**

Mr. Peng works on the role of NFBD1 in mediating cellular responses to DNA damage. The principle goal of cell cycle is to pass on an intact copy of its genome to the daughter cells. However, endogenous or exogenous DNA damage agents, especially those producing double strand breaks (DSB) challenge the integrity of genomic information. DSB can be repaired by either homologous recombination (HR) or non-homologous end joining (NHEJ) pathway. However, to efficiently remove DSB *in vivo*, surveillance mechanisms termed "checkpoints", which arrest cell cycle upon activation, must function coordinately.

The signaling pathway from DSB to checkpoint activation is not entirely understood. Studies demon-strate that activation of checkpoint depends on signaling cascades comprised of molecules that sense DSB (sensors), that transduce DNA damage signals, those that execute cell cycle arrest (effectors). PI-3 like kinase family members, ATM, ATR and DNA-PK are classified as "sensor kinases". DNA damage sig-nals are transduced and amplified by two checkpoint kinases, Chk1 and Chk2, that, together arrest the cell cycle. The key step of activating the checkpoint kinases Chk1 and Chk2 by ATM/ATR involves the utili-zation of adaptor proteins.

Adaptor proteins include *S. cerevisiae* Rad9 (scRad9) and *S. pombe* Crb2 (spCrb2), both of which belong to a conserved family of proteins that contain BRCT domains. The potential adaptors in mammal-ian cells were less studied. Based on structural similarities, BRCA1 and its signaling upstream 53BP1 are both candidates. Another potential scRad9 homologueNFBD1 (<u>n</u>uclear <u>f</u>actor with <u>B</u>RCT <u>d</u>omains pro-tein 1) is similar in structure, contains a FHA (forkhead-associated) region, BRCT (<u>br</u>east cancer suscep-tibility gene 1 <u>c</u>arboxyl <u>t</u>erminus) domains, and internal repeats. Earlier work from our group showed that NFBD1 participates in IR-induced foci (IRIF), suggesting its role in DNA damage response pathway.

Mr. Peng's current studies focus on delineating the function of NFBD1 in regulating DNA damage checkpoint activation. To elucidate its role in the response pathways, vector-based small interfering RNA (siRNA) directed against NFDB1 in human cells demonstrated that its absence is associated with in-creased radio-sensitivity and impaired G2/M checkpoint control. NFBD1, like 53BP1, is recruited into DNA damage sites through g-H2AX, the phosphoylated form of histone 2A variant highlighting DSB area. Furthermore, NFBD1, together with 53BP1, plays a partially redundant role in regulating recruit-ment and/or phosphorylation of the downstream effector protein Chk2. This work has been published.

Mr. Peng also examined the relationship of NFBD1 with other DNA damage response factors. He found that NFBD1 physically associates with NBS1 and TopBP1. Further structural and functional stud-

ies reveal that NFBD1 recruits NBS1 through its FHA domain, while its internal Repeats mediate TopBP1 IRIF association. Mapping analysis also indicates that the internal repeats of NFBD1 associate with BRCT repeat 5 of TopBP1. Interestingly, NFBD1 deleted for its internal repeats is defective in G2/M checkpoint response. Collectively, we propose that NFBD1 interacts with TopBP1 and coordinately participates in G2/M checkpoint control. This is part of a manuscript in preparation.

The sensor kinases ATM/ATR play central roles in sensing and transducing DNA damage signals. In their current model, adaptor proteins facilitate ATM/ATR-dependent phosphorylation by recruiting downstream substrates to the proximity of kinases at DNA damage sites. Mr. Peng's studies revealed a novel link between adaptor proteins NFBD1 and 53BP1, which are also responsible for the recruitment of sensor kinases into DNA damage sites and therefore facilitate their signaling transduction. To this end, Mr. Peng will continue to dissect their molecular and functional relationship. This work has been submitted for publication.

In summary, the DNA damage response pathway is crucial in maintaining of genome stability, conversely, defects of genes involved in this pathway, such as ATM, Chk2, NBS1, BRCA1 etc. frequently associate with severe diseases including cancer. NFBD1, the potential human homologue of yeast Rad9, participates in the DNA damage response pathway. This proposal aims to address the precise role of NFBD1 in mediating DNA damage response signaling pathway, and will provide knowledge guiding the future development of cancer therapy.

This work by Mr. Peng is clearly and compelling important in the breast cancer research field. The signaling control pathways operative in response to DNA-damage are a crucial aspect of the overall cellular response to exogenous stress. This newly identified player, NFBD1 and its relationship to other sensors and transducers, is an important addition to the knowledge base concerning the function of this important stress response pathway. It is clear that Mr. Peng will continue to make significant contributions to breast cancer research as student in Dr. Chen's laboratory.

- **Xiaolin Qin (Sherry)**   **Mentor – Dr. Maria Gaczynska**

Xiaolin Qin has been working on the mechanism of action of the proteasome. The proteasome, an essential non-lysosomal protease in the ubiquitin pathway, is involved in the processing of vital factors controlling cell functioning and also for degrading the bulk of unnecessary or damaged proteins. Importantly, the enzyme is the target for the development of anti-cancer drugs since specific inhibition of proteasome catalytic activity leads to apoptosis. Cancer cells are much more sensitive to the proteasome inhibition when compared to normal cells. Proteasome activity is tightly controlled by the level off translation, by the type of catalytic subunits expressed, and by the interaction of its core with several types of multisubunit regulatory particles. Ms. Qin has been dissecting the stability of complexes composed of the proteasomal catalytic core and regulatory subunits. Specifically, she is investigating the involvement of the proteasomal gating mechanism in stability of the complexes. Focusing on gating mechanism has a two-fold purpose: first, it is an attractive target for a new generation of drugs, which will affect proteasomal active centers indirectly, yet very precisely. Second, the gate could be a target for drugs disrupting interactions of the proteasome with regulatory subunits thus stripping the enzyme from some of its functions. Ms. Qin discovered that: **1)** Mutant proteasomes with disrupted gating mechanism are less structurally stable. **2)** Yeast cells harboring mutant proteasomes with disrupted gating mechanism exhibit a growth defect, especially when cells are in a stationary phase of growth. **3)** Disabling the effector part of the gate by deletion of a 13-amino acid peptide has the most profound effect on the growth of yeast cells.

The work points at certain parts of the proteasome, especially of the proteasome gate, as future targets of the proteasome-modulating drugs.

The work by this trainee is clearly relevant to breast cancer research since proteasomal inhibitors are being actively investigated for use in breast cancer treatments.

- **Chi-Sheng Lu (Jason)**   **Mentor – Dr. Renee Yew**

Mutational inactivation of the breast cancer susceptibility gene, BRCA1, accounts for a large percentage of hereditary breast cancer. Recently, the highly conserved ring finger domain of BRCA1 has been shown to function as a ubiquitin protein ligase, or E3, in the ubiquitination of model substrates. Mr Lu's hypothesis is that BRCA1 effects the ubiquitination of proteins that are either negative regulators of DNA repair or are positive regulators of growth proliferation, leading either to their degradation or to an alteration of their activity. A major advancement in the understanding of BRCA1 and its putative E3 activity, would be the identification of bonafide BRCA1 substrates. Mr. Lu's recent studies using an *in vitro* ubiquitination assay suggest that estrogen receptor α and β may be specific substrates of the BRCA1-BARD1 ubiquitin ligase. To further study the ubiquitination of putative BRCA1-BARD1 substrates, such as ERα and β and to identify novel substrates, Mr. Lu is generating recombinant adenoviruses-expressing BRCA1, both wild type and a C61G RING finger mutant as well as BARD1.

This project has obvious relevance to breast cancer research since BRCA1 alterations are implicated in predisposition to breast and ovarian cancer.

Trainees formerly supported by DAMD17-99-1-9402 and the previous grant.

- ***David Levin***   ***Mentor -- Dr. Alan Tomkinson***

DNA joining events are required to maintain the integrity of the genome. Three human genes encoding DNA ligases have been identified. David is identifying the cellular functions involving the product of the LIG1 gene. Previous studies have implicated DNA ligase I in DNA replication and some pathways of DNA repair. During DNA replication, DNA ligase I presumably functions to join Okazaki fragments. However, under physiological salt conditions, DNA ligase I does not interact with DNA. It is Mr. Levin's working hypothesis that DNA ligase I involvement in different DNA metabolic pathways is mediated by specific protein-protein interactions which serve to recruit DNA ligase I to the DNA substrate. To detect proteins that bind to DNA ligase I, David has fractionated a HeLa nuclear extract by DNA ligase I affinity chromatography. PCNA was specifically retained by the DNA ligase I matrix. To confirm that DNA ligase I and PCNA interact directly, Mr. Levin found that in vitro translated and purified recombinant PCNA bind to the DNA ligase I matrix. In similar experiments, he has shown that DNA ligase I interacts with a GST
(glutathione S transferase)-PCNA fusion protein but not with GST. Using in vitro translated deleted versions of DNA ligase I, Mr. Levin determined that the amino terminal 120 residues of this polypeptide are required for the interaction with PCNA. During DNA replication PCNA acts as a homotrimer that encircles DNA and tethers the DNA polymerase to its template. He showed that DNA ligase I forms a stable complex with PCNA that is topologically linked to a DNA duplex. Thus, it appears that PCNA can also tether DNA ligase I to its DNA substrate. A manuscript describing these studies was published in the Proc. Natl. Acad. Sci. U.S.A.

In addition to interacting with PCNA, the amino terminal domain of DNA ligase I also mediates the localization of this enzyme to replication foci. To determine whether these are separable functions David fine mapped the region that interacts with PCNA and, in collaboration with Dr. Montecucco's group, the region required for recruitment to replication foci. Since the same 19 amino acids are necessary and sufficient for both functions and the same changes in amino acid sequence inactivate both functions, we conclude that DNA ligase I is recruited to replication foci by its interaction with PCNA. A manuscript describing these studies was published in the EMBO Journal.

In recent studies, Mr. Levin has a constructed a mutant version of DNA ligase I that does not interact with PCNA. Importantly the amino acid substitutions do not affect the catalytic activity of DNA ligase I. By transfecting cDNAs encoding the mutant and wild type DNA ligase I into a DNA ligase I-mutant cell line, he has demonstrated the biological significance of the DNA ligase I/PCNA interaction in DNA replication and long patch base excision repair.

This project was relevant to breast cancer since problems with DNA replication and repair undoubtedly underlie the genomic instability associated with tumor formation.

Dr. Levin earned his Ph.D. in Molecular Medicine in the summer of 2000, and is currently a staff scientist at GeneTex, Inc., in San Antonio, Texas.

- ***John Leppard***   ***Mentor -- Alan Tomkinson***

Three genes, *LIG1*, *LIG3* and *LIG4*, encoding DNA ligases have been identified in the mammalian genome. Unlike the *LIG1* and *LIG4* genes, there are no homologues of the *LIG3* gene in lower eukaryotes such as yeast. Biochemical and genetic studies suggest that DNA ligase III participates in base excision repair and the repair of DNA single-strand break. A feature of DNA ligase III that distinguishes it from other eukaryotic DNA ligases is a zinc finger. In published studies we have shown that this zinc finger binds preferentially to nicks in duplex DNA and allows DNA ligase III to efficiently ligate nicks at

physiological salt concentrations. These studies will be extended by determining how the zinc finger of DNA ligase III binds to DNA single-strand breaks but does not hinder access of the catalytic domain of DNA ligase III to ligatable nicks. Furthermore, we will reconstitute the base excision and single-strand break repair pathways mediated by DNA ligase III and elucidate the functional consequences of interactions between DNA ligase III and other DNA repair proteins such as Xrcc1, DNA polymerase beta and poly (ADP-ribose) polymerase that participate in these repair pathways.

Mr. Leppard's research is relevant to breast cancer since genomic instability is likely to be involved at several stages during the progression to malignant breast cancer. Methods to intervene and stabilize the genome could prevent progression and spread of the disease. In addition, information about DNA repair processes in normal and cancer cells may lead to the development of treatment regimes that more effectively kill cancer cells and minimize damage to normal tissues and cells.

***Dr. Leppard is currently obtaining post-doctoral training at the* University of Washington, Seattle, Dept. of Microbiology in the laboratory of Dr. James Champoux. He will be working on the enzymes involved in nucleic acid synthesis and repair.**

Publications:

Leppard JB, Dong Z, Mackey ZB, Tomkinson AE. 2004 Physical and functional interaction between DNA ligase IIIα and poly(ADP-Ribose) polymerase 1 in DNA single-strand break repair. *Mol Cell Biol.* 23:5919-27.

- *Teresa Motycka*   *Mentor -- Alan Tomkinson*

DNA double-strand break repair is important for maintaining genomic stability. If left unrepaired, these lesions may cause cell death. The cell has evolved two major pathways for dealing with these lesions, nonhomologous end-jo ining and homologous recombination. Nonhomologous end-joining fuses the ends of broken DNA irrespective of the sequence at the site of the break, whereas homologous recombination preserves the sequence at the damaged site by using a sister chromatid as a template to copy the genetic information. Genetic studies in the budding yeast Saccharomyces cerevisiae have identified a number of genes important in this pathway, collectively named the RAD52 epistasis group. Of all of these genes, a del etion in rad52 produces the most severe phenotype. Mammalian homologs of RAD52 have been identified and the biochemical activity of the protein products is conserved from yeast to human. In order to gain further understanding of Rad52 function in higher eukaryotes, Ms. Motycka looked for interacting proteins by affinity chromatography and identified those polypeptides that were specifically bound by the resin. She has shown a direct interaction between XPF, a component of a multifunctional DNA structu re-specific endonuclease, with the N-terminus of hRad52. Complex formation between hRad52 and XPF/ERCC1 concomitantly stimulates the DNA structure-specific endonuclease activity of XPF/ERCC1 and attenuates the DNA strand annealing activity of hRad52. These results are consistent with previous genetic studies and provide a novel role for hRad52 in the modulation of XPF/ERCC1 activity. Ms. Motycka are currently examining the biological significance of a second protein-protein interaction identified in our screen. Hypersensitivity to DNA damage results from the deletion of the respective gene, suggesting we may have identified a novel player in Rad52-dependent DNA repair.

An understanding of the mechanisms of DSB in mammalian cells is relevant to breast cancer because the accumulating evidence linking the products of the breast cancer susceptibility genes, BRCA1 and BRCA2, with DSB repair.

Dr. Motycka successfully defended her dissertation in June, 2004. She plans to continue her training in Dr. Tomkinson's laboratory by wrapping up work on the publication of a paper showing the

functional significance of a novel interaction by a yeast INO80 chromatin remodeling complex with Rad52.

Publications:

Motycka TA, Bessho T, Post SM, Sung P, Tomkinson AE. 2004 Physical and functional interaction between the XPF/ERCC1 endonuclease and hRad52. *J Biol Chem.*;279:13634-9. Epub 2004 Jan 20.

- *Suh-Chin(Jackie) Lin*   *Mentor -- Dr. Eva Lee*

The tumor suppressor gene, p53, is frequently mutated in human tumors, including breast carcinoma. P53 null mice develop multiple spontaneous tumors, predominantly lymphoma and sarcoma, within the first 6 months of age. To establish a mouse model of p53-mediated mammary tumor development, Ms. Lin initiated a bigenetic approach employing the cre-loxp system. Through gene targeting in embryonic stem (ES) cells, mice carrying floxed p53 genes in which exons 5 and 6 are flanked by the loxp sequence were generated. A second mouse line carrying a cre transgene under the control of mouse mammary tumor virus LTR (MMTV-cre) has also been generated. Floxed p53 mice were mated with MMTV-cre transgenic mice to produce mice with p53 inactivation in mammary tissue. Indeed, we observed p53 excision in the tissues of double transgenic mice. In addition, adenoviral vectors carrying cre recombinase are being used to inactivate p53. These approaches should provide a mouse mammary tumor model for studies of mammary tumor progression resulting from p53 mutation and for testing therapeutic interventions of mammary tumorigenesis. The resulting mice have demonstrated interesting patterns of tumor development including those of the mammary gland. These animals will be valuable models for testing new approaches to breast cancer treatment and understanding its etiology.

Upon DNA damage, p53 protein becomes phosphorylated and stabilized, leading to subsequent activation of cell cycle checkpoints. It has been shown that ATM is required for IR induced phosphorylation on Ser15 residue of p53. Based on the involvement of p53 in mammary tumorigenesis and on the higher risk of ATM carriers for breast cancer, we have carried out studies to address the cancer susceptibility of ATM heterozygous and ATM null mammary epithelial cells by transplanting mammary gland to wild-type sibling mice. Initial studies have indicated differential checkpoint and apoptotic responses in cells harboring ATM mutation. These studies will establish whether ATM plays important roles in mammary tumorigenesis.

Both of these projects are highly relevant to breast cancer, especially the Dr. Lin's animal models which hold promise in terms of new therapies for breast cancer and its metastases.

Ms. Lin successfully defended her dissertation on December 18, 2000, and continues as a post-doctoral fellow in Dr. Lee's laboratory extending her work on the development of important animal models for human cancer. The below listed publication is evidence of her continuing contribution to breast cancer research.

Publications:

Lin SC, Lee KF, Nikitin AY, Hilsenbeck SG, Cardiff RD, Li A, Kang KW, Frank SA, Lee WH, Lee EY. 2004 Somatic mutation of p53 leads to estrogen receptor alpha-positive and -negative mouse mammary tumors with high frequency of metastasis. *Cancer Res.* 64:3525-32.

- *Sean Post*   *Mentor -- Dr. Eva Lee*

Recent studies indicate that breast cancer susceptibility genes,BRCA1 and BRCA2, are involved in DNA repair. Cells harboring mutations in either gene are hypersensitive to ionizing radiation (IR). Extensive

genetic evidence in yeast indicates that DNA double-stranded breaks are processed by Rad50/Mre11 nuclease complex. It has also been shown that in response to IR, Rad50 assembles into nuclear foci. In mammalian cells, such IR-induced Rad50 foci are not observed in cells established from Nijmegen breakage syndrome (NBS). We and others have shown that the protein product of gene mutated in NBS, Nibrin, forms a stable complex with Rad50/Mre11 and the complex possesses nuclear activity. The E. Lee laboratory demonstrated that IR-induced Rad50 redistribution requires ATM kinase activity. Rad50 is phosphorylated upon IR. Their preliminary studies indicate that such IR-induced Rad50 foci formation and phosphorylation are defective in A-T cells. In addition, IR-induced Rad50 foci formation is aberrant in some sporadiac cancers that express normal ATM, Rad50, Mre11, nibrin, BRCA1 and BRCA2 suggesting involvement of additional protein in this DNA damage response.

Mr. Post characterized IR-induced Rad50 phosphorylation. How phosphorylation affects Rad50 function will be studied. In addition, cross-linking experiments will be carried out to investigate whether there is defective Rad50 protein complex formation in breast cancer cells. These studies will provide insights into the role of ATM kinase cascade in the assembly of double-stranded breakage repair protein. Furthermore, characterization of components in the repair protein complex may lead to the identification of additional players involved in breast carcinoma.

These projects are highly relevant to breast cancer since genomic instability is a hallmark of cancer and is thought to be a major contributor to the tumorigenic process. Mr. Post's research will contribute toward a greater understanding of the mechanisms responsible for maintaining genomic integrity that is undoubtedly involved in breast cancer development and progression.

Mr. Post successfully defended his dissertation research in July of 2003. He is currently obtaining postdoctoral training in Dr. Vicki Lundblad's laboratory at the Baylor College of Medicine. He will be working to understand telomere function in tumorigenesis and aging.

Post SM, Lee EY. Detection of kinase and phosphatase activities. 2004 *Methods Mol Biol.* 241:285-97.

Post SM, Tomkinson AE, Lee EY. 2003 The human checkpoint Rad protein Rad17 is chromatin-associated throughout the cell cycle, localizes to DNA replication sites, and interacts with DNA polymerase epsilon. Nucleic Acids Res. 31:5568-75.

- ***Song Zhao***   *Mentor – Dr. Eva Lee*

Mr. Zhao worked on the functional interactions between ATM and DNA repair proteins with a focus on NBS1. Ataxia-telangiectasia (A-T) and Nijmegen breakage syndrome (NBS) are recessive genetic disorders with susceptibility to cancer and similar cellular phenotypes. The protein product of the gene responsible for A-T, designated ATM, is a member of a family of kinases characterized by a carboxy-terminal phosphatidylinositol 3-kinase-like domain. The NBS1 protein is specifically mutated in patients with Nijmegen breakage syndrome and forms a complex with the DNA repair proteins Rad50 and Mre11. Mr. Zhao showed that phosphorylation of NBS1, induced by ionizing radiation, requires catalytically active ATM. Complexes containing ATM and NBS1 exist in vivo in both untreated cells and cells treated with ionizing radiation. He, along with others in the lab, have identified two residues of NBS1, Ser 278 and Ser 343 that are phosphorylated in vitro by ATM and whose modification in vivo is essential for the cellular response to DNA damage. This response includes S-phase checkpoint activation, formation of the NBS1/Mre11/Rad50 nuclear foci and rescue of hypersensitivity to ionizing radiation. Together, these results demonstrate a biochemical link between cell-cycle checkpoints activated by DNA damage and DNA repair in two genetic diseases with overlapping phenotypes

These projects have clear and compelling relevance to breast cancer since all of the proteins described are vital to the "caretaker" function of the DNA repair and response systems of all cells, to which mam-

mary cells are especially dependent. Dr. Zhao made significant contributions as a graduate student and will undoubtedly continue this level of contribution as a postdoctoral fellow.

Dr. Zhao recently obtained his Ph.D., and is continuing his training as a postdoctoral fellow in Dr. Thomas Kelly's laboratory at the Memorial Sloan Kettering Institute. Dr. Zhao will be working to understand the regulation of DNA replication.

- *Shang Li*   *Mentor -- Dr. Wen-Hwa Lee*

Mutations of the *BRCA1* gene predispose women to the development of breast cancer. The *BRCA1* gene product [BRCA1] is a nuclear phosphoprotein whose cellular function is poorly understood. The C-terminal region of the BRCA1 protein contains an activation domain and two repeats termed BRCT (for BRCA1 C-terminal). In his recent work, Mr. Li identified a BRCT-interacting protein previously identified as CtIP, a protein that interacts with the C-terminal-binding protein (CtBP) of E1A. Together, CtIP and CtBP are postulated to form a transcription corepressor complex. The ability of BRCA1 to transactivate the p21 promoter can be inactivated by mutation of the C-terminal conserved BRCT domains. To explore the mechanisms of this BRCA1 function, the BRCT domains were used as bait in a yeast two-hybrid screen. A known protein, CtIP, a co-repressor with CtBP, was found. CtIP interacts specifically with the BRCT domains of BRCA1, both *in vitro* and *in vivo*, and tumor-derived mutations abolished these interactions. The association of BRCA1 with CtIP was also abrogated in cells treated with DNA-damaging agents including UV, g-irradiation and adriamycin, a response correlated with BRCA1 phosphorylation. The transactivation of the p21 promoter by BRCA1 was diminished by expression of exogenous CtIP and CtBP. These results suggest that the binding of the BRCT domains of BRCA1 to CtIP/CtBP is critical in mediating transcriptional regulation of p21 in response to DNA damage.

This project was directly relevant to breast cancer since it involves the study of a protein whose function appears to central to the mobilizing the response of cells to DNA damage. Perturbations in the systems that maintain genomic integrity underlie initiation and progression of most cancers, including those of the breast.

Dr. Li defended his dissertation in Fall of 2000. He continues his training as a post doctoral fellow in the laboratory of Dr. Elizabeth Blackburn in the department of biochemistry and biophysics at the UCSF. He is working on a novel cancer therapy involving a mutated telomere RNA template.

- *Qing Zhong*   *Mentor -- Dr. Wen-Hwa Lee*

One of Mr. Zhong's project in Dr. Lee's laboratory is a study of the tumor suppressor protein, TSG101. *tsg101* was identified as a tumor susceptibility gene by homozygous function inactivation of allelic loci in mouse 3T3 fibroblasts. To confirm its relevance to breast cancer that was originally reported, antibodies specific for the putative gene product were prepared and used to identify cellular 46 kDa TSG101 protein. A full size 46 kDa TSG101 protein was detected in a panel of 10 breast cancer cell lines and 2 normal breast epithelial cell lines with the same antibodies. A full-length *TSG101* mRNA was also detected using rtPCR. These results indicate that homozygous intragenic deletion of *TSG101* is rare in breast cancer cells. In more recent work, Mr. Zhong demonstrated that TSG101 is a cytoplasmic protein that translocates to the nucleus during S phase of the cell cycle. Interestingly, TSG101 is distributed mainly around the chromosomes during M phase. Microinjection of antibodies selective for TSG101 during G1 or S results in cell cycle arrest and overexpression leads to cell death. These data indicate that neoplastic transformation due to lack of TSG101 could be due to a bypass of cell cycle checkpoints.

Another more recent interest of Mr. Zhong is the role of the breast tumor suppressor BRCA1 in cancer formation. *BRCA1*, encodes a tumor suppressor that is mutated in familial breast and ovarian cancers.

Mr. Zhong's work showed that BRCA1 interacts *in vitro* and *in vivo* with human Rad50, which forms a complex with hMre11 and p95/nibrin. BRCA1 was detected in discrete foci in the nucleus that colocalize with hRad50 after irradiation. Formation of irradiation-induced foci positive for BRCA1, hRad50, hMre11 or p95 were dramatically reduced in HCC1937 breast cancer cells carrying a homozygous mutation in *BRCA1*, but was restored by transfection of wild-type *BRCA1*. Ectopic expression of wild-type, but not mutated *BRCA1* in these cells rendered them less sensitive to the DNA damage agent, methyl methanesulfonate. These data suggest that BRCA1 is important for the cellular responses to DNA damage that are mediated by the hRad50-hMre11-p95 complex.

Dr. Zhong's work on BRCA1 was highly relevant for breast cancer research. By understanding the interaction and functional role of BRCA1 in the DNA repair process could lead to a greater understanding of its role in tumorigenesis and to new forms of cancer therapy aimed at interactions with the repair proteins.

Dr. Zhong successfully defended his dissertation in November, 2000, and obtained his Ph.D. He recently published additional work related to his doctoral research as a postdoctoral fellow in Dr. Wen-Hwa Lee's laboratory. Dr. Zhong is currently continuing his training in Xiaodong Wang's laboratory at the University of Texas Southwestern Medical Center at Dallas, where he is working on the biochemistry and cell biology of apoptosis.

- *Lei Zheng*   *Mentor -- Dr. Wen-Hwa Lee*

Lei accomplished a significant amount of work during this training period. His main goal was to elucidate the molecular basis of genomic instability that occurs in most of human cancers including breast cancer. He started working on a novel mitotic phase specific protein, Hec1, by demonstrating that Hec1 interacts with retinoblastoma protein for maintaining the genomic stability that was published in Mol. Cell. Biol. (1999). He then developed a method to examine the level of chromosome instability by using retrovirus carrying both positive and negative selectable marker that integrated randomly into individual chromosomes, and the frequency of loss of this selectable chromosomal marker (LOM) was measured. The results showed that normal mouse embryonic stem cells had a very low frequency of LOM, which was less than 10^{-8}/cell/generation. In Rb-/- mouse ES cells, the frequency was increased to approximately 10^{-5}/cell/generation, while in Rb+/- ES cells, the frequency was approximately 10^{-7}/cell/generation. LOM was mainly mediated through chromosomal mechanisms and not due to point mutations.

These results revealed that RB haploinsufficiency plays a critical role in the maintenance of chromosome stability. The mystery of why RB heterozygous carriers have early onset tumor formation with high penetrance can be, at least, partially explained by this novel activity. Dr. Lei Zheng made very significant contributions toward this novel aspect with RB function.

Dr. Zheng successfully defended his Ph.D. dissertation in Novermber, 2000. Lei is currently worked on a project involving regulators of gene transcription in Dr. Robert Roeder's at the l Laboratory of Biochemistry and Molecular Biology, The Rockefeller University, New York. After completing his postdoctoral training in Dr. Roeder's laboratory, Dr. Zheng entered an internal medicine residency program of Albert Einstein Medical College in New York, beginning in July, 2003. Already, he has been appointed as the leader of a team of first year residents and medical students. He is planning on applying for Hematology/Oncology subspecialty fellowship that will start in 2006. He is also continues to work in the Roeder lab, mostly advising fellows who are working on the project he started.

Dr. Zheng is clearly going to be a very significant physician scientist, a further testament to the value of supporting graduate student-based research programs.

- *Horng-Ru Lin*   *Mentor: Dr. Renee Yew*

BRCA1 or BRCA2 germline mutations predispose women to early onset, familial breast cancer. Current studies on BRCA1 and BRCA2 suggest their roles in the maintenance of genome integrity. However, in contrast to the clear studies of BRCA1, there has been very little characterization of the BRCA2 protein and evidence that speaks to a dynamic function of BRCA2 in this regard. That is, the intrinsic biological nature of the BRCA2 protein remains enigmatic. Therefore, this project is to try to reveal the physiological function of the BRCA2 protein by characterizing its posttranslational processing, such as phosphorylation.

The novelty of the work lies in the following. First, it demonstrates BRCA2 is a phosphoprotein in vivo. Second, BRCA2 is hyperphosphorylated specifically in mitosis. Third, dephosphorylation of BRCA2 corresponds to the timing of cells' exit from mitosis. These findings imply that BRCA2 may play an important role in mitosis. To further characterize the phosphorylated amino acids of BRCA2 will provide fresh insights into functional study of BRCA2, which has obvious relevance to breast cancer.

Because of personal issues, Mr. Lin did not accompany Dr. Wen-Hwa Lee when he recently moved his laboratory to UC Irvine. Mr. Lin is currently working in Dr. Renee Yew's laboratory on a project to better understand regulation of the cell cycle, a critically important area in cancer biology.

Research description under Dr. Yew:

- *Stephen Van Komen*   *Mentor – Dr. Patrick Sung*

In yeast homologous recombination, Rad54, a member of Swi2/Snf2 family of proteins, functionally cooperates with the Rad51 recombinase in making D-loop, the first DNA joint formed between recombining chromosomes. Mr. Van Komen's biochemical studies have indicated that yeast Rad54 modulates DNA topology at the expense of ATP hydrolysis, producing extensive unconstrained supercoils in DNA. This supercoiling ability is likely to be indispensable for D-loop formation. Given the high degree of structural and functional conservation among yeast and human recombination factors, Mr. Van Komen hypothesize that human Rad51 and Rad54 also function together to make D-loop. This hypothesis is being tested with human Rad51 and Rad54 proteins purified from insect cells infected with recombinant baculoviruses. In addition, whether human Rad54 has ATP hydrolysis-driven DNA supercoiling ability is also being examined.

Mr. Van Komen's research is directly relevant to breast cancer since double strand breaks in DNA and their repair is an issue pertinent to breast cancer. Since the tumor suppressor, BRCA2, interacts with Rad51, it is critically important to understand the biochemistry of this important enzyme in DNA repair.

Dr. Van Komen continues as a postdoctoral fellow in Dr. Sung's laboratory, which has recently moved to Yale University. The below papers show Dr. Van Komen's continuing contributions to our understanding of DNA repair in response to damage, which is one of the most vibrant areas of cancer biology.

Publications:

Lewis LK, Storici F, **Van Komen S**, Calero S, Sung P, Resnick MA. 2004 Role of the nuclease activity of Saccharomyces cerevisiae Mre11 in repair of DNA double-strand breaks in mitotic cells. *Genetics.* 166:1701-13.

Smirnova M, **Van Komen S**, Sung P, Klein HL. 2004 Effects of tumor-associated mutations on Rad54 functions. *J Biol Chem.* 279:24081-8. Epub 2004 Mar 31.

Krejci L, Macris M, Li Y, **Van Komen S**, Villemain J, Ellenberger T, Klein H, Sung P. 2004 Role of

ATP hydrolysis in the antirecombinase function of Saccharomyces cerevisiae Srs2 protein. *J Biol Chem.* 279:23193-9. Epub 2004 Mar 27.

Trujillo KM, Roh DH, Chen L, **Van Komen S,** Tomkinson A, Sung P. 2003 Yeast xrs2 binds DNA and helps target rad50 and mre11 to DNA ends. *J Biol Chem.* 278:48957-64. Epub 2003 Sep 30.

Krejci L, Chen L, **Van Komen S,** Sung P, Tomkinson A. 2003 Mending the break: two DNA double-strand break repair machines in eukaryotes. *Prog Nucleic Acid Res Mol Biol.*;74:159-201. Review.

- **Deanna Jansen**

Ms. Jansen's husband was transferred to a new military base and, for family reasons, she decided to withdraw from the program. At some point, she plans to complete her Ph.D. training.

- **Stefan Sigurdsson**   **Mentor – Dr. Patrick Sung**

The RAD51 encoded product exhibits structural and functional similarities to the Escherichia coli recombination protein RecA. RecA promotes the pairing and strand exchange between homologous DNA molecules to form heteroduplex DNA. We have shown that hRad51 also makes DNA joints avidly and promotes highly efficient DNA strand exchange. Two Rad51-like proteins, Rad51B and Rad51C, are found associated in a heterodimeric complex. We have co-expressed the Rad51B and Rad51C proteins in insect cells and purified the Rad51B-Rad51C complex to near homogeneity. Biochemical experiments have revealed that Rad51B-Rad51C binds DNA and enhances the recombinase activity of the Rad51 protein. This recombination mediator function of Rad51B-Rad51C is likely indispensable for efficient recombination in vivo. Recently, hRad51 was shown to interact with the breast tumor suppressor BRCA2. The biochemical studies by Mr. Sigurdsson should be useful for understanding the molecular basis of breast tumor suppression by the recombination machinery.

Genomic caretaking by the recombination systems is vital to the "health" of the information residing in DNA. Corruption of the information by insults arising from internal and external sources is known to be involved in genesis of cancer. Thus, the system elucidated by Mr. Sigurdsson is very important for all cancers including those of the mammary glands.

Dr. Sigurdsson recently successfully defended his dissertation. He is continuing to pursue research in DNA repair as a postdoctoral fellow in Dr. Sung's laboratory. Upon his wife's graduation from Medical School, he will be pursuing other postdoctoral training opportunities in breast cancer research. His authorship in a high profile paper in *Nature* below is an indication of his continuing contribution to our understanding of the maintenance of genomic stability, a hallmark of tumor suppression by cellular caretakers.

Publications:

Sehorn MG, **Sigurdsson S,** Bussen W, Unger VM, Sung P. 2004 Human meiotic recombinase Dmc1 promotes ATP-dependent homologous DNA strand exchange. *Nature* 429:433-7.

- **Ahmad Utomo**   **Mentor – Dr. Wen-Hwa Lee**

A drastic reduction in the expression of a novel phospholipid hydroperoxide glutathione peroxidase (PHGPx), which incorporates cysteine instead of selenocysteine in the conserved catalytic motif was observed in a microarray analysis using cDNAs amplified from mRNA of Brca1-null mouse embryonic fibroblasts (MEFs). This non-selenocysteine PHGPx named as NPGPx is a cytoplasmic protein with a mo-

lecular weight of approximately 22 kDa. Ectopic expression of NPGPx in Brca1-null cells, which are sensitive to oxidative stress induced by hydrogen peroxide, conferred a similar resistance level equal to that of the wild-type cells, suggesting the importance of this enzyme in reducing oxidative stress. Expression of NPGPx was found in many tissues, including developing mammary gland. However, the majority of breast cancer cell lines studied (11 out of 12) expressed very low or undetectable levels of NPGPx irrespective of BRCA1 status. Re-expression of NPGPx in breast cancer lines, MCF-7 and HCC1937, induced resistance to eicosapentaenoic acid (an omega-3 type of polyunsaturated fatty acid) mediated cell death, and abrogated proliferative stimulation by linoleic acid (an omega-6 type). Thus, NPGPx plays an essential role in breast cancer cells in alleviating oxidative stress generated from polyunsaturated fatty acid metabolism.

The data and novel insights derived from Mr. Utomo's research might help explain breast cancer development due to defects in responding to oxidative damage. If true, affected family members of families carrying alterations in BRCA1 might benefit from avoidance of situations where oxidative damage is increased.

Dr. Utomo successfully defended his dissertation and was recently awarded his Ph.D. He is continuing his training as a postdoctoral fellow at the Harvard Medical School in the laboratory of Dr. Tanya Mayadas.

- **Chang-Ching Liu**   **Mentor – Dr. Wen-Hwa Lee**

The Rad50/MRE11/NBS1 complex is involved in a variety of cellular processes, including both non-homologous end-joining and homologous recombination pathways involved in DNA double-strand breaks repair, cell cycle checkpoint activation, telomere maintenance, and meiosis. In order to understand the mechanism underlying the function of this repair complex, a novel Rad50-interacting protein (RINT-1) was identified by a yeast two-hybrid screen in our laboratory. RINT-1, an evolutionarily conserved protein from Drosophila to human beings, has been shown to interact with Rad50 preferentially at late S and G2/M phases through its central and c-terminal conserved region. To further explore the function of interaction between RINT-1 and Rad50, several stable MCF7 clonal cell lines that express GFP fusions containing only the Rad50 binding region of RINT-1 were established. Overexpression of the fusion protein leads to a defective radiation-induced G2/M checkpoint. This observation is related to the repair function of Rad50 and another Rad50-interacting protein, BRCA1, which is also thought to play a role in radiation-induced G2/M checkpoint control. Like Rad50 and BRCA1, inactivation of RINT-1 causes early embryonic lethality. Blastocysts were isolated at day 3.5 of pregnancy from Rint-1+/- intercross and were cultured in vitro for 7 days. Unlike wild type and Rint-1+/- embryos, whose inner cell mass continued to expand and differentiate, Rint-1-/- cells stop their expansion subsequent to day 4 and died.

To study the cellular function of RINT-1 besides its roles in response to DNA damage, Ms. Liu established an U2OS cell line expressing full-length RINT-1 protein coupled with GFP and discovered that RINT-1 localizes to the centrosome in a microtubule-independent manner. GFP-RINT-1 proteins localize at the centrosomes throughout the cell cycle and move to the midbody along with the mother centrosome before cytokinesis. Endogenous RINT-1 proteins reside in the centrosomal fractions isolated from LEM cells, and are found in purified centrosomes. Interestingly, GFP fusions with either the N-terminal coiled-coil domain or the conserved Rad50 binding region of RINT-1 are recruited to the centrosome. Using the N-terminal coiled-coil domain of RINT-1 as bait in a yeast two-hybrid screen, Ms. Liu found two centrosomal proteins potentially interacting with RINT-1; PA28b and p150glued. Similar to the p150glued component of the dynactin complex, adenovirally overexpressed N-terminal RINT-1 polypeptides decorated the entire length of interphase microtubules. Overexpressed N-terminal RINT-1 polypeptides also resulted in the formation of cytoplasmic dots outside the centrosome, a phenomenon also observed when peptides of a coiled-coil centrosomal protein, Cep135, were overexpressed. The centrosome is a major microtubule-organizing center in animal cells. It duplicates only once during the cell cycle and ensures the formation of bipolar spindles, which distribute replicated chromosomes equally to daughter cells. De-

fective centrosomes, exemplified by an excess number of centrioles and pericentriolar material, are characteristic of solid tumors in general and breast tumors in particular, and may contribute to their genomic instability by the formation of multipolar mitotic spindles. Recent molecular evidence suggests that centrosomes are also involve in stress response mechanisms, cell cycle checkpoint control, and cell cycle progression. It has been shown that inactivation of the other Rad50-interacting proteins, MRE11 and Brca1, lead to centrosome amplification and embryonic lethality. Future studies of the roles played by RINT-1 in regulation of centrosomal activities may provide insight about how DNA repair pathways coordinate with the cell cycle progression and the regulation of centrosome function.

This on the basic biology of centrosomes and their roles in cells division is applicable to all cells including those that form tumors. It is especially relevant to breast tumors since they often display chromosomal aberrations attributed to defects involving centrosomal proteins.

Note: Miss. Liu withdrew from the graduate program to return to home to assist with a critically ill member of her immediate family.

- **Wei Tan**   **Mentor – Dr. Thomas Boyer**

The breast and ovarian-specific tumor suppressor BRCA1 has been implicated in both activation and repression of gene transcription by virtue of its direct interaction with sequence-specific DNA-binding transcription factors. However, the mechanistic basis by which BRCA1 mediates the transcriptional activity of these regulatory proteins remains largely unknown. Mr. Tan has been studying the functional interaction between BRCA1 and ZBRK1, a BRCA1-dependent KRAB-zinc finger transcriptional repressor as a model system to understand the mechanistic basis by which BRCA1 mediates sequence-specific transcription control. During the reporting period, Mr. Tan succeeded in identifying and initiating the molecular characterization of a portable BRCA1-dependent transcriptional repression domain within the ZBRK1 C-terminus. Mr. Tan found that this C-terminal repression domain functions in a BRCA1-, HDAC-, and promoter-specific manner, and is thus functionally distinguishable from the N-terminal KRAB repression domain in ZBRK1, which exhibits no BRCA1 dependency and broad promoter specificity. Significantly, Mr. Tan also found that the BRCA1-dependent transcriptional repression domain modulates sequence-specific DNA-binding by the minimal ZBRK1 DNA-binding domain. These findings thus reveal a dual function for the BRCA1-binding domain on ZBRK1 in sequence-specific DNA-binding and transcriptional repression by DNA-bound ZBRK1. Mr. Tan is currently engaged in experiments to complete the functional characterization of this BRCA1-dependent repression domain, and he is in the process of writing up his results in manuscript form.

This project is applicable to breast cancer since all of these proteins are involved in the transcriptional response to DNA damage medicated by BRCA1. Understanding this response system, which includes the ZBRK1 protein, is critical to preventing and treating breast cancer.

Publications:

Tan W, Zheng L, Lee WH, Boyer TG. 2004 Functional dissection of transcription factor ZBRK1 reveals zinc fingers with dual roles in DNA-binding and BRCA1-dependent transcriptional repression. *J Biol Chem.* 279:6576-87. Epub 2003 Dec 02.

- **Sangeetha Vijayakumar**   **Mentor – Dr. Wen-Hwa Lee**

The Suv3 helicase of yeast *Saccharomyces cerevisiae* has been classified as a mitochondrial RNA helicase. Yeast genetic studies revealed that suv3-null yeast fails to grow in glycerol media and forms petite colonies, implicating a role in energy metabolism. Because the helicase domains in both yeast and human Suv3 vary considerably from typical RNA helicase motifs, homogenously purified Suv3 was required by

Ms. Vijayakumar in order to verify its putative enzymatic activities. Ms. Vijayakumar expressed a form of human Suv3 carrying an N-terminal deletion of 46 amino acids (ΔNhSuv3) in yeast suv3 null mutants and demonstrated that ΔNhSuv3 fully complements the null phenotype. Through a five-step chromatographic procedure, ΔNhSuv3 (83 kDa) and its partially degraded 70 kDa protein (hSuv3-70), which constitutes amino acids 68 to 685, were purified to homogeneity. Both proteins have ATPase activities, but mutants with an invariant lysine in the ATP binding site, K213, changed to alanine (A) or arginine (R) lose activity. At pH 7.5, ΔNhSuv3 unwinds only RNA/DNA hetero duplex, while hSuv3-70, which retains all the core catalytic domains, can unwind multiple substrates including homoduplexes of RNA and DNA and heteroduplexes of RNA-DNA. However, under low pH ($\leq$ 5.0) reaction conditions, ΔNhSuv3 also exhibits ATP-dependent multi-substrate specificity similar to that of hSuv3-70. Consistently, ΔNhSuv3 binds to homo duplexes of both RNA and DNA at pH 5.0, but not at pH 7.5, Moreover, data from circular dichroism analysis suggests that at pH 5.0, ΔNhSuv3 adopts a similar conformation to that of hSuv3-70, which in turn may govern its differential substrate specificity.

Human Suv3 is likely to be involved in critical functions in both normal and breast cancer cells. Knowledge regarding its function will, therefore, be a significant contribution toward understanding the development and/or maintenance of the tumorigenic state.

Publications:

Shu Z, **Vijayakumar S**, Chen CF, Chen PL, Lee WH. 2004 Purified human SUV3p exhibits multiple-substrate unwinding activity upon conformational change. *Biochemistry.* 43:4781-90.

Note: Ms. Vijayakumar recently transferred to Dr. Alan Tomkinson's laboratory at U. Maryland. There she is going to work on DNA ligases and other proteins involved in DNA repair.

DoD RESEARCH SUPPORT

An essential component of maintaining a successful and aggressive training program in Breast Cancer Research is the continued research funding of the individual Program Faculty laboratories.

Program Faculty Breast Cancer Research Awards

Tadayoshi Bessho, Ph.D. *(Dr. Bessho has transferred his laboratory to the University of Nebraska)*

Idea Award (DAMD17-03-1-0225)
Project Title: Biochemical Characterization of BRCA2
Project Period: 04/01/03 - 03/31/06
Project Total: $414,115 Total for entire project

Thomas G. Boyer, Ph.D.

Idea Award (DAMD17-03-1-0272)
Project Title: BRCA1 Regulation of Estrogen Signaling in the Breast
Project Period: 06/01/02 - 05/31/06
Project Total: $433,182 Total for entire project

These studies should reveal novel insight concerning how mutational inactivation of a ubiquitously expressed tumor suppressor could have restricted consequences in the breast and ovary.

Career Development Award (DAMD17-02-1-0584)
Project Title: Regulation of BRCA1 function by DNA damage-induced site-specific phosphorylation.
Project Period: 05/15/02 - 06/15/05
Project Total: $176,516 Total for entire project

Considerable evidence implicates DNA-damage-induced site-specific phosphorylation of BRCA1 as a critical regulator of its caretaker properties. Dr. Boyer hypothesizes that DNA damage-induced site-specific phosphorylation of BRCA1 regulates its transcription and/or DNA double-strand break repair activities.

Idea Award (DAMD17-01-1-0408)
Project Title: Regulation of BRCA1 function by DNA damage-induced site-specific phosphorylation.
Project Period: 04/01/01 - 03/31/04

Project Total: $414,599 Total for entire project

Considerable evidence implicates DNA-damage-induced site-specific phosphorylation of BRCA1 as a critical regulator of its caretaker properties. Dr. Boyer hypothesizes that DNA damage-induced site-specific phosphorylation of BRCA1 regulates its transcription and/or DNA double-strand break repair activities.

Phang-Lang Chen, Ph.D.

Idea Award (DAMD17-99-1-9398)
Project Title: BRCA2 and the DNA double strand break repair machinery
Project Period: 10/01/99 – 10/31/03
Project Total: $304,500

To understand the cellular function of BRCA2, and to elucidate its role in the development and progression of breast cancer.

Idea Award (DAMD17-01-1-0409)
Project Title: Small chemical molecules disrupt BRCA2 and Rad51 interaction for adjuvant BC
Project Period: 04/01/01 – 05/31/05
Project Total: $433,500

To isolate small molecules which disrupt the interactions between BRCA2 and Rad51 using reverse yeast two-hybrid screening. To evaluate the ability of the identified molecules to sensitize cultured breast cancer cells to the genotoxic and cytotoxic effects of ionizing radiation; and to assess the efficacy of the small molecules as adjuvant.

Barbara A. Christy, Ph.D.

Training/Recruitment Award (DAMD17-03-1-0308)
Project Title: Summer Undergraduate Fellowships in Breast Cancer Research
Project Period: 04/15/03 - 04/14/06
Project Total: $105,840 Total for entire project

Funding received from this award will support a summer training program for undergraduate students interested in scientific research. The students will participate in breast cancer-related research in laboratories of the Department of Molecular Medicine of the University of Texas Health Science Center at San Antonio.

Maria Gaczynska, Ph.D.

Concept Award (DAMD17-03-1-0636)

Project Title: Proteasome-Related Molecular Signature of Breast Cancer
Project Period: 09/01/03 - 08/31/04
Project Total: $109,500 Total for entire project

The major goal of this proposal is to define a common proteasome-related denominator for breast cancer cells.

Idea Award (DAMD17-01-1-0410)
Project Title: Molecular characteristics of multicorn, a new large proteolytic assembly and potential   anticancer drug target in human breast cancer cells
Project Period: 04/01/01 – 05/31/05
Project Total: $324,056

The goal of this project is to clone and express the gene of human multicorn monomer, study the mechanism controlling the multicorn activity through its oligomerization and phosphorylation, and test molecular characterization of the multicorn at different stages of the cell cycle.

E. Paul Hasty, D.V.M

Idea Award (DAMD17-02-1-0587)
Project Title: Development of anti-cancer therapeutics that modulate the RAD51-BRCA2 complex.
Project Period: 02/15/02 – 02/15/05
Project Total: $436,500

RAD51 is important for repairing double-strand breaks in DNA by recombination; interestingly, this function is likely to be essential since mammalian cells deleted for RAD51 exhibit chromosomal instability, are unable to sustain proliferation and senesce or die. Our specific aims are: characterize antp-26mer for biological activity on tissue culture cells, perform a deletion and substitution analysis on the antp-26mer, and test peptides for potential as anti-cancer therapeutics in mice.

Z. Dave Sharp, Ph.D.

Concept Award (W81XWH-04-1-0700)
Project Title: Nuclear Dynamics of BRCA1-dependent Transcription Regulation
Project Period: 07/15/04 - 08/14/05
Project Total: $109,500 Total for entire project

The purpose is to develop a biosensor system to visualize transcription control by ZBRK1 and BRCA1 in a single living and/or fixed cells.

Patrick Sung, Ph.D.

Career Development Award (DAMD17-98-1-8247)
Project Title: Interactions among BRCA1, BRCA2 & components of the recombination machinery
Project Period: 06/01/98 – 05/31/03
Project Total: $200,000

The main goal of this project is to purify BRCA1 and BRCA2 and study their biochemical properties.

Idea Award (DAMD17-98-1-8247)
Project Title: Interactions among BRCA1, BRCA2 & components of the recombination machinery
Project Period: 06/01/98 – 05/31/03
Project Total: $303,311

The main goal of this project is to purify BRCA1 and BRCA2 and study their biochemical properties.

P. Renee Yew, Ph.D.

Career Development Award (DAMD17-02-1-0589)
Project Title: The role of BRCA1-dependent ubiquitination in Breast Cancer
Project Period: 06/01/02 - 05/31/05
Project Total: $181,960

Mutational inactivation of the BRCA1 gene accounts for a large percentage of hereditary breast cancer. Although the BRCA1 gene product has been implicated to function in a number of different cellular processes including DNA repair and transcription, it is still unclear how BRCA1 biochemically mediates its cellular function as a tumor suppressor protein. It has been suggested that the BRCA1 gene product functions as an ubiquitin protein ligase or E3 enzyme in a manner similar to a growing number of proteins that comprise a family of ring finger proteins. If this putative E3 activity of BRCA1 can be shown to be a physiological function of full length BRCA1 in the cell, this could greatly aid in determining the molecular mechanisms by which BRCA1 mediates its cellular function.

Idea Award (DAMD17-01-1-0415)
Project Title: The role of BRCA1-dependent ubiquitination in Breast Cancer
Project Period: 04/01/01 - 03/31/05
Project Total: $411,006

Mutational inactivation of the BRCA1 gene accounts for a large percentage of hereditary breast cancer. Although the BRCA1 gene product has been implicated to function in a number of different cellular processes including DNA repair and transcription, it is still unclear how BRCA1 biochemically mediates its cellular function as a tumor suppressor protein. It has been suggested that the BRCA1 gene product functions as an ubiquitin protein ligase or E3 enzyme in a manner similar to a growing number of proteins that comprise a family of ring finger proteins. If this putative E3 activity of BRCA1 can be shown to be a physiological function of full length BRCA1 in the cell, this could greatly aid in determining the molecular mechanisms by which BRCA1 mediates its cellular function.

Predoctoral Breast Cancer Research Awards to Supported Trainees

Predoctoral training grants awarded to current trainees by the Defense Department's Breast Cancer Research Program (BCRP):

Karen Block (P. Renee Yew – Mentor)/DAMD17-02-1-0583
(PI changed from Karen Block to Srikanth Appikonda effective 02/18/04)
Project Title: The role of Ubiquitin-Mediated Proteolysis of cyclin D in Breast Cancer
Project Period: 04/01/02-04/30/05
Project Total: $65,636

Recent studies have indicated that cyclin D protein levels are modulated post-transcriptionally by the ubiquitin-mediated protein degradation pathway. The specific E2 and E3 enzymes postulated to target cyclin D for ubiquitination are the ubiquitin conjugating enzyme, CDC34, and the ubiquitin protein ligase called SCF (Skp1, cullin, F-box, ring protiein). We will define and characterize how the regulation of CDC34-SCF activity modulates cyclin D proteolysis during the normal cell cycle and in breast cancer cells.

Valerie Boka (E. Paul Hasty – Mentor)/W81XWH-04-1-0325
Project Title: A Mouse Model to Investigate the Role of DBC2 in Breast Cancer
Project Period: 02/15/04-03/14/07
Project Total: $90,000

Major goals are 1) to characterize the phenotype of *DBC2*-mutant mouse ES cell and MEF clones; and 2) to generate and analyze *DBC2* knockout mice.

Wendy Bussen (Patrick Sung – Mentor)/W81XWH-04-1-0410
Project Title: The Role of the BLM Helicase in Homologous Recombination
Project Period: 04/01/04-03/01/06
Project Total: $85,467

The major goals of this proposal are to destabilize hRad51 presynaptic filament by BLM helicase, to define the role of BLM in the SDSA pathway, and to address the significance of ATP hydrolysis in BLM function.

Sean Post (Eva Lee – Mentor)/DAMD17-02-1-0588
(PI changed from Sean Post to Wei Tan effective 09/17/03)
Project Title: Phosphorylation of hRad17 by ATR is required for cell cycle checkpoint activation
Project Period: 04/01/02 - 03/31/05
Total Award: $61,342

The goal of this study is to determine the relationship between ATR, hRad17, Chk2, and BRCA1 and demonstrate how these potential protein networks regulate checkpoint activation. Based on the reuqirement of SpRad3 and SpRad17 for checkpoint activation through SpCds1 in fission yeast and the ability of Chk2 to phosphorylate BRCA2 Ser988 in humans, it is my hypothesis that ATR mediated phosphorylation of hRad17 is required to activate cell cycle checkpoints, through Chk2 and BRCA1.

Stefan Sigurdsson (Patrick Sung – Mentor)/DAMD17-01-1-0412
Project Title: Functions of Human Rad51 and Other Recombination Factors In DNA Double-Strand
                    Break Repair.
Project Period: 04/01/01 - 05/31/04
Total Award: $66,000

Homologous recombination and recombinational repair of DNA double-strand breaks are mediated by proteins of the *RAD52* epistasis group. Rad51 is a key factor in these processes and the protein can assemble on ssDNA substrates to form a nucleoprotein filament. With the help from other factors, the Rad51-ssDNA nucleoprotein filament searches for a DNA homlog and catalyzes formation of a heteroduplex DNA joint with the homolog. The biochemical reaction that forms heteroduplex DNA joints is called ☐homologous DNA pairing and strand exchange. A number of Rad51-like proteins are known in human cells, but their function in recombination and DNA repair is currently unknown. I have shown that two of these Rad51-like proteins, Rad51B and Rad51C, are associated in a stable heterodimer. I will further define the homologous DNA pairing and strand exchange activity of human Rad51. In addition, a variety of experiments will be conducted to test the hypothesis that the Rad51B-Rad51C complex promotes the assembly of the Rad51-ssDNA nucleoprotein filament and enhances the efficiency of Rad51-mediate d homologous DNA pairing and strand exchange. The information garnered from this study should contribute significantly to our understanding of how DNA double-strand breaks are repaired in human cells.

Stephen Van Komen (Patrick Sung – Mentor)/DAMD17-01-1-0414
Project Title: Functional interactions of HRAD54 with the RAD51 recombinase
Project Period: 04/01/01 - 03/31/03

Total Award: $65,173

Homologous recombination is essential for the accurate repair of DNA double-strand breaks. Products of the BRCA1 and BRCA2 breast and ovarian susceptibility genes have recently been shown to associate with key members of the recombinational machinery including the Rad51 recombinase. Rad51 is homologous to the bacterial homologous DNA pairing and strand exchange enzyme, RecA. Unlike RecA, yeast Rad51 has little ability to promote pairing between homologous linear ssDNA and covalently closed duplex to form an important recombination intermediate known as a D-loop. Importantly, yeast Rad54, another recombination factor, promotes robust D-loop formation by Rad51. Recently, I have shown that yeast Rad54 uses the free energy from ATP hydrolysis to remodel DNA structure in a fashion that generates both positively and negatively supercoiled domains in the DNA template, and that DNA supercoiling by Rad54 is important for the D-loop reaction. Given the conservation between yeast and human recombination factors, I hypothesize that human Rad54 supercoils DNA and promotes D-loop formation with human Rad51 in a similar manner. Using highly purified human Rad51 and Rad54 proteins, I will study the functional interactions between these two factors in D-loop formation and in supercoiling DNA. The results from these studies will be important for understanding the human recombinational machinery and may provide a system for dissecting the role of BRCA1, BRCA2, and other tumor suppressors in recombination and DNA double-strand break repair.

Xining Zhu (P. Renee Yew -- Mentor)/DAMD17-03-1-0364
Project Title: Identification and Characterization of the BRCA1 Ubiquitin Ligase and its Substrates
Project Period: 05/01/03 – 04/30/06
Project Total: $90,000

The specific aims proposed here will address the physiological significance of a BRCA1 E3 activity, potential BRCA1 target substrates, and the significance of a BRCA1 E3 activity to breast cancer biology. The specific aims of this study are: (1) to develop an *in vitro* ubiquitination assay using full length BRCA1 and BRCA1-associated RING domain 1 protein (BARD1) proteins; and (2) to identify potential BRCA1 substrates and to study the biological significance of the BRCA1-dependent ubiquitination of substrates. This study addresses a highly novel putative activity of BRCA1 that could have a large impact on our understanding of familial breast cancer development.

Postdoctoral Breast Cancer Research Awards to Supported Trainees

Postdoctoral training grants awarded to current postdoctoral fellows by the Defense Department's Breast Cancer Research Program (BCRP):

Qing Gao, Ph.D., (W.H. Lee – Mentor)/DAMD17-00-1-0457
(PI changed from Qing Zhong to Qing Gao 11/02; Subcontract set-up with UC Irvine for Longen Zhou effective 01/16/04))

Project Title: Involvement of BRCA2 BRC repeats in RAD51 mediated DNA repair
Project Period: 12/01/00 – 11/30/04
Project Total: $141,330

To test the importance of BRC repeats in BRCA2 for binding to RAD51 in response to DNA damage. To determine the critical residues in the BC repeats of BRCA2 and the significance of these residues for BRCA2/RAD51 interactions. To determine if BRCA2, through BRC repeats, directly affects DNA repair mechanisms mediated by RAD51; and to test small BRC repeat peptides in vivo for their ability to overcome tumor resistance to DNA damaging agents.

TRAINEE PUBLICATIONS

LINDA DEGRAFFENRIED
deGraffenried LA, Hilsenbeck SG, and Fuqua SAW. Sp1 is Essential for Estrogen Receptor Alpha Gene Transcription. (2002) J Steroid Biochem Mol Biol. Sep: 82(1) 7-18.

JENNIFER GOOCH
Lee AV, Jackson JG, **Gooch JL,** Hilsenbeck SG, Coronado-Heinsohn E, Osborne CK, Yee D. Enhancement of the insulin-like growth factor signaling in human breast cancer: Estrogen regulation of insulin receptor substrate-1 (IRS-1) in vitro and in vivo. (1999) *Molecular Endocrinology*, 13(5): 787-796.

Gooch JL, Van Den Berg CL, Yee D. Insulin-like growth factor (IGF) -I rescues breast cancer cells from chemotherapy-induced cell death: proliferative and anti-apoptotic effects. (1999) *Breast Cancer Research and Treatment* 56:1-10.

Gooch JL, Yee D. Strain-specific differences in the formation of apoptotic DNA ladders in MCF-7 breast cancer cells. (1999) *Cancer Letters*, 144:31-7.

Gooch JL, Herrera R, Yee D. The role of p21 in IFN-gamma-mediated growth inhibition in human breast cancer cells.(2000) *Cell Growth and Differentiation*, 11:335-42.

Lee AV, **Gooch JL,** Osterreich S, Guler B, Yee D. IGF-I-induced degradation of IRS-1 is mediated by the 26S proteosome and requires PI-3 kinase. (2000) *Molecular Cell Biology*, 20:1489-96

Gooch JL, Tang Y, Ricono JM, & Abboud HE. Insulin-like Growth Factor-I Induces Renal Cell Hypertrophy via a Calcineurin-dependent Mechanism. (2001) *J Biol Chem* **276,** 42492-500.

XIANZHI JIANG
Wu G, **Jiang X**, Lee W-H, Chen P-L. Assembly of functional ALT-associated promyelocytic leukemia bodies requires Nijmegen Breakage Syndrome 1. (2003) Cancer Res. 63:2589-95.

JOHN LEPPARD
Mackey ZB, Niedergang C, Menissier-de Murcia J, **Leppard JB,** Au K, Chen J, de Murcia G, and Tomkinson AE. DNA ligase III is recruited to DNA strand breaks by a zinc finger motif homologous to that of Poly (ADP-ribose) polymerase. (1999) J. Biol. Chem. 274, 21679-21687.

Tomkinson AE, Chen L, Dong Z, **Leppard JB**, Levin DS, Mackey ZB, & Motycka TA. Completion of base excision repair by mammalian DNA ligases. (2001) *Prog Nucleic Acid Res Mol Biol* **68,** 151-64.

DAVID LEVIN

Matsumoto Y, Gary R, **Levin DS,** Tomkinson AE, and Park M. Reconstitution of long patch base excision repair with purified human proteins. (1999) J. Biol. Chem. 274(47):33703-8

Levin DS, McKenna AE, Motycka TA, Matsumoto Y, & Tomkinson AE. Interaction between PCNA and DNA ligase I is critical for joining of Okazaki fragments and long-patch base-excision repair. (2000) *Curr Biol* **10,** 919-22.

Tomkinson AE, Chen L, Dong Z, Leppard JB, **Levin DS**, Mackey ZB, & Motycka TA. Completion of base excision repair by mammalian DNA ligases. Interaction between PCNA and DNA ligase I is critical for joining of Okazaki fragments and long-patch base-excision repair. (2001) *Prog Nucleic Acid Res Mol Biol* **68,** 151-64.

SHANG LI

Li S, Chen P-L, Subramanian T, Chinnadurai G, Tomlinson G, Osborne CK, Sharp ZD, and Lee W-H. Dissociation of BRCA1 Binding to CtIP upon DNA Damage Mediates p21 Expression. (1999) J. Biol. Chem. 274:11334-11338.

Zhong Q, Chen C-F, **Li S,** Chen Y, Wang CC, Xiao J, Chen P-L, Sharp ZD, and Lee W-H. Association of BRCA1 with the hRad50-hMre11-p95 complex and the DNA damage response. (1999) Science 285, 747-750.

Zheng L, Pan H, **Li S**, Flesken-Nikitin A, Chen P-L, Boyer TG, Lee W-H. Sequence-Specific Transcriptional Corepressor Function for BRCA1 through a Novel Zinc Finger Protein, ZBRK1. (2000) *Mol Cell* 6:757-768.

Li S, Ting NS, Zheng L, Chen P-L, Ziv Y, Shiloh Y, Lee E Y-H P, Lee W-H Functional link of BRCA1 and ataxia telangiectasia gene product in DNA damage response. (2000) *Nature*;406:210-215.

Zheng L, **Li S,** Boyer TG, and and Lee, W-H. Lessons learned from BRCA1 and BRCA2 (2000) Oncogene, 19: 6159-6175.

HORNG-RU LIN

Lin H-R, Ting NS, Qin J, Lee W-H. M-phase specific phosphorylation of BRCA2 by Polo-like Kinase 1 correlates with dissociation of p300/CBP-associated factor, P/CAF. (2003) J Biol Chem. Jun 17. [Epub ahead of print].

SUH-CHIN LIN

Dasika GK, **Lin S-C,** Zhao S, Sung P, Tomkinson AE and Lee E Y-H P. DNA Damage-induced cell cycle checkpoints and DNA strand break repair in development and tumorigenesis. (1999) Oncogene 18, 7883-7899.

Zhao S, Weng Y-C, Yuan S-S F, Lin Y-T, Hsu HC., **Lin S-C,** Gerbino E, Song MH, Zdzienicka MZ, Gatti RA, Shay JW, Ziv Y, Shiloh Y, & Lee E Y-H P. Functional link between ataxia-telangiectasia and Nijmegen breakage syndrome gene products. (2000) *Nature* **405,** 473-7.

Skapek SX, **Lin S-C,** Jablonski MM, McKeller RN, Tan M, Hu N, Lee E Y-H P Persistent expression of cyclin D1 disrupts normal photoreceptor differentiation and retina development. (2001) *Oncogene* **20**:6742-51.

Lin S-C, Skapek SX, Papermaster DS, Hankin M, & Lee, E Y-H P. The proliferative and apoptotic activities of E2F1 in the mouse retina. (2001) *Oncogene* **20,** 7073-84.

ZACHARY MACKEY
Mackey ZB, Niedergang C, Menissier-de Murcia J, Leppard JB, Au K, Chen J, de Murcia G, and Tomkinson AE. DNA ligase III is recruited to DNA strand breaks by a zinc finger motif homologous to that of Poly (ADP-ribose) polymerase. (1999) J. Biol. Chem. 274, 21679-21687

TERESA MOTYCKA
Levin DS, McKenna AE, **Motycka TA,** Matsumoto Y, Tomkinson AE. Interaction between PCNA and DNA ligase I is critical for joining of Okazaki fragments and long-patch base-excision repair. Curr Biol. (2000) 10(15):919-22.

Tomkinson AE, Chen L, Dong Z, Leppard JB, Levin DS, Mackey ZB, & **Motycka TA.** Completion of Base Excision Repair by Mammalian DNA Ligases. Progress in Nucleic Acid Research and Molecular Biology (2001) 68: 151-164.

AIMIN PENG
Peng A, Chen P-L. NFBD1, like 53BP1, is an early and redundant transducer mediating Chk2 phosphorylation in response to DNA damage. J Biol Chem. (2003) 278(11):8873-76.

SEAN POST
Post S, Weng Y-C, Cimprich K, Chen LB, Xu Y, & Lee E Y-H P. Phosphorylation of serines 635 and 645 of human Rad17 is cell cycle regulated and is required for G(1)/S checkpoint activation in response to DNA damage. (2001) *Proc Natl Acad Sci U S A* **98,** 13102-7.

JILL GILROY RICONO

Ghosh Choudhury G, **Ricono JM.** Increased effect of interferon gamma on PDGF-induced c-fos gene transcription in glomerular mesangial cells: differential effect of the transcriptional coactivator CBP on STAT1alpha activation. (2000) *Biochem Biophys Res Commun* 273:1069-77

Gooch JL., Tang Y, **Ricono JM,** & Abboud HE. Insulin-like Growth Factor-I Induces Renal Cell Hypertrophy via a Calcineurin-dependent Mechanism. (2001) *J Biol Chem* **276,** 42492-500.

Ricono JM, Arar M, Ghosh Choudhury G, & Abboud HE. Effect of Platelet-Derived Growth Factor (PDGF) Isoforms in Rat Metanephric Mesenchymal Cells. (2001) *Am J Physiol Renal Physiol* **8, 8.**

STEFAN SIGURDSSON

Van Komen S, Petukhova G, **Sigurdsson S,** Stratton S, Sung P. Superhelicity-driven homologous DNA pairing by yeast recombination factors Rad51 and Rad54. (2000) *Mol Cell* 6:563-72

Sigurdsson S, Trujillo K, Song B, Stratton S, Sung P. Basis for avid homologous DNA strand exchange by human Rad51 and RPA (2000) J. Biol. Chem. 276: 8798-806

Sigurdsson S, Van Komen S, Bussen W, Schild D, Albala JS, Sung P. Mediator function of the human Rad51B-Rad51C complex in Rad51/RPA-catalyzed DNA strand exchange. (2001) Genes Dev. 15:3308-18.

Van Komen S, Petukhova G, **Sigurdsson S,** Sung P. Functional cross-talk among Rad51, Rad54, and replication protein A in heteroduplex DNA joint formation. (2002) J Biol Chem. 277:43578-87.

Sigurdsson S, Van Komen S, Petukhova G, Sung P. Homologous DNA pairing by human recombination factors Rad51 and Rad54. (2002) J Biol Chem. 277:42790-4.

STEPHEN VAN KOMEN

Petukhova G, **Van Komen S,** Vergano S, Klein H, and Sung P. Yeast Rad54 promotes Rad51-dependent homologous DNA pairing via ATP hydrolysis-driven change in DNA double helix conformation. (1999) J. Biol. Chem. 274:29453-62.

Sung P, Trujillo K, and **Van Komen S.** Recombination factors of Saccharomyces cerevisiae. (2000) Mutation Research 451:257-275.

Van Komen S, Petukhova G, Sigurdsson S, Stratton S, Sung P. Superhelicity-driven homologous DNA pairing by yeast recombination factors Rad51 and Rad54. (2000) *Mol Cell* 6:563-572.

Sigurdsson S, **Van Komen S**, Bussen W, Schild D, Albala JS, Sung P. Mediator function of the human Rad51B-Rad51C complex in Rad51/RPA-catalyzed DNA strand exchange. (2001) Genes Dev. 15:3308-18.

Van Komen S, Petukhova G, Sigurdsson S, Sung P. Functional cross-talk among Rad51, Rad54, and replication protein A in heteroduplex DNA joint formation. (2002) J Biol Chem. 277:43578-87.

Sigurdsson S, **Van Komen S**, Petukhova G, Sung P. Homologous DNA pairing by human recombination factors Rad51 and Rad54. (2002) J Biol Chem. 277:42790-4.

Wolner B, **Van Komen S**, Sung P, Peterson CL. Recruitment of the recombinational repair machinery to a DNA double-strand break in yeast. (2003) Mol Cell. Jul;12(1):221-32.

Krejci L, **Van Komen S**, Li Y, Villemain J, Reddy MS, Klein H, Ellenberger T, Sung P. DNA helicase Srs2 disrupts the Rad51 presynaptic filament. (2003) Nature, May 15;423:305-9.

Jaskelioff M, **Van Komen S**, Krebs JE, Sung P, Peterson CL. Rad54p is a chromatin remodeling enzyme required for heteroduplex DNA joint formation with chromatin. (2003) J Biol Chem. 278(11):9212-8.

GUIKAI WU
Wu G, Lee W-H, and Chen P-L. NBS1 and TRF1 Colocalize at Promyelocytic Leukemia Bodies during Late S/G2 Phases in Immortalized Telomerase-negative Cells. (2000) J Biol Chem 275:39, 30618-30622.

Wu G, Jiang X, Lee W-H, Chen P-L. Assembly of functional ALT-associated promyelocytic leukemia bodies requires Nijmegen Breakage Syndrome 1. (2003) Cancer Res. 63:2589-95.

SHYNG-SHIOU "FRANK" YUAN
Yuan S-S F, Cox LA, Dasika GK, and Lee E.Y.-H.P. Cloning and functional studies of a novel gene aberrantly expressed in *Rb-/-* mouse embryos. (1999) Dev. Biol. 207:62-75.

Chen G, **Yuan S-S F.**, Liu W, Xu Y, Trujillo K, Song B.-W., Cong F, Goff SP, Arlinghaus R, Baltimore D, Park MS, Sung P, and Lee E.Y.-H. P. Radiation-induced Assembly of Rad51 and Rad52 recombination complex requires ATM and c-Abl. (1999) J. Biol. Chem. 274:12748- 12752.

Yuan S-S F., Lee, S.-Y., Chen, G., Song, M., Tomlinson, G. E., and Lee, E.Y.-H.P. BRCA2 is Required for Ionizing Radiation-induced Assembly of Rad51 Complex *in Vivo*. (1999) Cancer Res. 59: 3547-3551.

Zhao S, Weng YC, **Yuan S-S F**, Lin YT, Hsu HC, Lin SC, Gerbino E, Song MH, Zdzienicka MZ, Gatti RA, Shay JW, Ziv Y, Shiloh Y, Lee E.Y.-H.P. Functional link between ataxia-telangiectasia and Nijmegen breakage syndrome gene products. (2000) *Nature* 405:473-7

Yuan S-S F, Su JH, Hou MF, Yang FW, Zhao S, Lee E Y-H P. Arsenic-induced Mre11 phosphorylation is cell cycle-dependent and defective in NBS cells. (2002) DNA Repair (Amst). 1:137-42.

SONG ZHAO

Dasika GK, Lin S-C, **Zhao S**, Sung P, Tomkinson AE and Lee E Y-H P. DNA Damage-induced cell cycle checkpoints and DNA strand break repair in development and tumorigenesis. (1999) Oncogene 18, 7883-7899.

Zhao S, Weng Y-C, Yuan S-S F, Lin YT, Hsu HC, Lin SC, Gerbino E, Song MH, Zdzienicka MZ, Gatti RA, Shay JW, Ziv Y, Shiloh Y, Lee E Y-H P. Functional link between ataxia-telangiectasia and Nijmegen breakage syndrome gene products. (2000) *Nature* 405:473-7.

Yuan S-S F, Su JH, Hou MF, Yang FW, **Zhao S**, Lee E Y-H P. Arsenic-induced Mre11 phosphorylation is cell cycle-dependent and defective in NBS cells. (2002) DNA Repair (Amst). 1:137-42.

Zhao S, Renthal W, Lee E Y-H P. Functional analysis of FHA and BRCT domains of NBS1 in chromatin association and DNA damage responses. (2002) Nucleic Acids Res. 30:4815-22.

Yazdi PT, Wang Y, **Zhao S**, Patel N, Lee EY, Qin J. SMC1 is a downstream effector in the ATM/NBS1 branch of the human S-phase checkpoint. (2002) Genes Dev. 16:571-82.

LEI ZHENG

Zheng L, Chen Y, and Lee W-H. Hec1p, an evolutionarily conserved coiled-coil protein, modulates chromosome segregation through interaction with SMC proteins. (1999) Mol Cell Biol *19*, 5417-5428.

Zheng L, Chen Y, Riley DJ, Chen P-L., and Lee W-H. Retinoblastoma protein enhances the fidelity of chromosome segregation mediated by a novel coiled-coil protein, HsHec1p (2000) Molecular Cell Biology. 20:3529-3537.

Zheng L, Pan H, Li S, Flesken-Nikitin A, Chen P-L, Boyer TG, Lee W-H. Sequence-Specific Transcriptional Corepressor Function for BRCA1 through a Novel Zinc Finger Protein, ZBRK1. (2000) *Mol Cell* 6:757-768

Li S, Ting NS, **Zheng L**, Chen P-L, Ziv Y, Shiloh Y, Lee E Y-H P, Lee W-H. Functional link of BRCA1 and ataxia telangiectasia gene product in DNA damage response. (2000) *Nature*;406:210-215.

Zheng L, Li S, Boyer TG, and and Lee, W-H. Lessons learned from BRCA1 and BRCA2 (2000) Oncogene, 19: 6159-6175.

Zheng L, Pan H, Li S, Flesken-Nikitin A, Chen P-L, Boyer T, and Lee W-H. A novel zinc-finger protein, ZBRK1, represses transcription of the GADD45 gene mediated by BRCA1. (2000) Molecular Cell, 6: 757-768.

Chen Y, Riley DJ, **Zheng L**, Chen P-L, Lee W-H. Phosphorylation of the mitotic regulator protein Hec1 by Nek2 kinase is essential for faithful chromosome segregation. (2002) J Biol Chem. 277:49408-49416.

Zheng L, Lee W-H. Retinoblastoma tumor suppressor and genome stability. (20002) Adv Cancer Res.;85:13-50.

Peng H, **Zheng L**, Lee W-H, Rux JJ, Rauscher FJ. A common DNA-binding site for SZF1 and the BRCA1-associated zinc finger protein, ZBRK1. (2002) Cancer Res. 62:3773-3781.

Zheng L, Flesken-Nikitin A, Chen P-L and Lee W-H. Deficiency of Retinoblastoma gene in mouse embryonic stem cells leads to genetic instability. (2002) Cancer Research 62:2498-2502.

Zheng L, Roeder RG, Luo Y. S phase activation of the histone H2B promoter by OCA-S, a coactivator complex that contains GAPDH as a key component (2003) Cell 114:255-66.

QING ZHONG
Zhong Q., Chen C-F, Li S, Chen Y, Wang CC, Xiao J, Chen P-L, Sharp ZD, and Lee W-H. Association of BRCA1 with the hRad50-hMre11-p95 complex and the DNA damage response. (1999) Science 285, 747-750.

Chen C-F, Chen P-L, **Zhong Q**, Sharp ZD, Lee W-H. Expression of BRC repeats in breast cancer cells disrupts the BRCA2-Rad51 complex and leads to radiation hypersensitivity and loss of G(2)/M checkpoint control. (1999) *J Biol Chem* 274:32931-32935.

Zhong Q, Boyer TG, Chen P-L, Lee W-H. Deficient nonhomologous end-joining activity in cell-free extracts from Brca1-null fibroblasts. (2002) *Cancer Res.* 62(14):3966-3970.

Zhong Q, Chen C-F, Chen P-L, Lee W-H. BRCA1 facilitates microhomology-mediated end joining of DNA double strand breaks. (2002) J Biol Chem. 277:28641-28647.

Nijhawan D, Fang M, Traer E, **Zhong Q**, Gao W, Du F, Wang X. Elimination of Mcl-1 is required for the initiation of apoptosis following ultraviolet irradiation. (2003) Genes Dev. 17(12):1475-1486.

Physical and Functional Interaction between DNA Ligase IIIα and Poly(ADP-Ribose) Polymerase 1 in DNA Single-Strand Break Repair

John B. Leppard, Zhiwan Dong, Zachary B. Mackey,† and Alan E. Tomkinson*

*Department of Molecular Medicine, Institute of Biotechnology, The University of Texas
Health Science Center at San Antonio, San Antonio, Texas 78245*

The repair of DNA single-strand breaks in mammalian cells is mediated by poly(ADP-ribose) polymerase 1 (PARP-1), DNA ligase IIIα, and XRCC1. Since these proteins are not found in lower eukaryotes, this DNA repair pathway plays a unique role in maintaining genome stability in more complex organisms. XRCC1 not only forms a stable complex with DNA ligase IIIα but also interacts with several other DNA repair factors. Here we have used affinity chromatography to identify proteins that associate with DNA ligase III. PARP-1 binds directly to an N-terminal region of DNA ligase III immediately adjacent to its zinc finger. In further studies, we have shown that DNA ligase III also binds directly to poly(ADP-ribose) and preferentially associates with poly(ADP-ribosyl)ated PARP-1 in vitro and in vivo. Our biochemical studies have revealed that the zinc finger of DNA ligase III increases DNA joining in the presence of either poly(ADP-ribosyl)ated PARP-1 or poly(ADP-ribose). This provides a mechanism for the recruitment of the DNA ligase IIIα-XRCC1 complex to in vivo DNA single-strand breaks and suggests that the zinc finger of DNA ligase III enables this complex and associated repair factors to locate the strand break in the presence of the negatively charged poly(ADP-ribose) polymer.

Three human genes, *LIG1*, *LIG3*, and *LIG4*, that encode DNA ligases have been identified (30). Unlike the *LIG1* and *LIG4* genes, which appear to be conserved among all eukaryotes, the *LIG3* gene has been found only in the genomes of mammals and of the amphibian *Xenopus laevis* (6, 22, 32). Intriguingly, the *LIG3* gene is more closely related to poxvirus DNA ligase genes than to those for the other eukaryotic DNA ligases (6, 10). Furthermore, the *LIG3* gene is more complex than the other *LIG* genes in that it encodes multiple products that appear to have distinct biological functions.

Alternative splicing of the *LIG3* gene transcript generates two species of mRNA, designated α and β, that encode polypeptides with different C termini (17, 22). DNA ligase IIIα mRNA is ubiquitously expressed, whereas DNA ligase IIIβ mRNA has been detected only in germ cells (17, 22). The unique C terminus of DNA ligase IIIα, which exhibits homology with the BRCT motif initially identified in the product of the breast cancer susceptibility gene *BRCA1* (5, 11), mediates formation of a stable complex with the DNA repair protein XRCC1 (3, 4, 17, 21, 29). In contrast, no protein partner or biochemical activity has been ascribed to the unique C terminus of DNA ligase IIIβ. Further heterogeneity of products from the *LIG3* gene is generated by translation initiation at different ATG codons within DNA ligase III mRNA, generating mitochondrial and nuclear forms of DNA ligase III (14, 15, 22).

A unique feature of the DNA ligases encoded by the *LIG3* gene is the zinc finger motif situated at the N termini of these polypeptides (32). Interestingly, this motif is closely related to the two tandem-arrayed zinc fingers that constitute the DNA binding domain of poly(ADP-ribose) polymerase 1 (PARP-1), a nuclear protein that binds avidly to DNA strand breaks and catalyzes ADP-ribosylation of itself and other proteins by using NAD as a cofactor (7, 32). Previous studies have shown that the zinc finger of DNA ligase III enables this enzyme to bind to DNA strand breaks, in particular single-strand breaks, and to efficiently ligate DNA nicks at physiological salt concentrations (16). However, the zinc finger is not required either for catalytic activity in vitro or for in vivo function in a heterologous organism (16).

Although *Lig3* mutant mammalian cell lines are not currently available, the *xrcc1* mutant Chinese hamster cell lines EM9 and EMC11 are functionally DNA ligase III deficient because, in the absence of XRCC1 protein, the levels of nuclear DNA ligase IIIα protein are significantly reduced (3, 4, 28, 36). Genetic and biochemical studies with these mutant cells have implicated XRCC1 in the short-patch subpathway of DNA base excision repair and DNA single-strand break repair (8, 28, 29). XRCC1 itself has no known catalytic activity, but this protein binds to nicked DNA (18) and to several other DNA repair proteins, including PARP-1 (19), PARP-2 (26), DNA polymerase β (Pol β) (2, 12), polynucleotide kinase (33), and apurinic-apyrimidinic (AP) endonuclease (31), in addition to DNA ligase IIIα (3, 17, 21). Based on these observations, it has been suggested that XRCC1 acts as a scaffolding factor in the assembly of multiprotein DNA repair complexes. Recent studies demonstrating that XRCC1 may also function independently of DNA ligase IIIα (20, 27) and that the mitochondrial

* Corresponding author. Mailing address: Department of Molecular Medicine, Institute of Biotechnology, The University of Texas Health Science Center at San Antonio, 15355 Lambda Dr., San Antonio, TX 78245. Phone: (210) 567-7327. Fax: (210) 567-7324. E-mail: TOMKINSON@UTHSCSA.EDU.

† Present address: Department of Pathology, University of California, San Francisco, San Francisco, CA 94143.

form of DNA ligase IIIα functions independently of XRCC1 (14, 15) indicate that the roles of DNA ligase IIIα in somatic cells cannot be deduced solely on the basis of its interaction with XRCC1.

Using DNA ligase IIIβ as the ligand, we fractionated a HeLa extract by affinity chromatography and identified a specific association between DNA ligase III and the DNA strand break binding factor, PARP-1. In subsequent studies, we show that DNA ligase III not only directly interacts with PARP-1 but preferentially binds to poly(ADP-ribosyl)ated PARP-1, providing a mechanism for the recruitment of the DNA ligase IIIα-XRCC1 complex to DNA single-strand breaks in somatic cells. Finally, we demonstrate that the zinc finger of DNA ligase III is required for efficient ligation in the presence of poly(ADP-ribosyl)ated PARP-1, suggesting that this DNA binding activity allows the ligase to locate DNA nicks in the presence of the negatively charged poly(ADP-ribose) polymer (PAR).

MATERIALS AND METHODS

Plasmids. The plasmid pTG-LigIII that encodes full-length DNA ligase IIIβ as a glutathione S-transferase (GST) fusion protein has been described previously (17). Removal of an XhoI fragment corresponding to nucleotides 459 to 2589 of DNA ligase III cDNA followed by religation generated the plasmid pTG-LigIII$_{1-152}$ that encodes the N-terminal 152 amino acids of DNA ligase III as a GST fusion protein. The DNA sequence encoding the last 692 amino acids of DNA ligase IIIβ was amplified by PCR and then subcloned into the pGSTag vector (24) to generate the plasmid pTG-LigIIIβ$_{170-862}$ that encodes a C-terminal fragment of DNA ligase IIIβ containing the catalytic domain as a GST fusion protein. Plasmids encoding His-tagged versions of DNA ligase III have been described previously (16).

Expression and purification of recombinant DNA ligase III. Plasmids encoding the GST fusion derivatives of DNA ligase III were transformed into Escherichia coli BL21. One-liter cultures were grown at 37°C in Terrific Broth medium containing 100 μg of ampicillin/ml. At an optical density at 600 nm of 0.6, isopropyl thiogalactoside was added to a final concentration of 1 mM and incubation was continued for 4 h. Cells were collected by centrifugation and then resuspended in a 100-ml solution of 50 mM Tris-HCl (pH 7.5), 100 mM NaCl, 5 mM EDTA, 0.1% Nonidet P-40, 1 mM phenylmethanesulfonyl fluoride (PMSF), and 1 mM benzamidine-HCl. After clarification by sonication, GST fusion proteins were purified from the lysate by stepwise elution from a phosphocellulose column and then further purified to near homogeneity by glutathione-Sepharose affinity chromatography. His-tagged versions of human DNA ligase IIIβ were expressed and purified as described previously (16). Unless specifically noted, the experiments were carried out with DNA ligase IIIβ translated from the preferred internal ATG site (6, 14). This form of the protein and its truncated derivatives, which lack the mitochondrial leader sequence (14), are referred to as DNA ligase III. Recombinant human PARP-1 purified from baculovirus-infected insect SF9 cells (9) was a gift from Gilbert de Murcia.

Fractionation of a HeLa nuclear extract by DNA ligase IIIβ affinity chromatography. Purified GST (2 mg) and GST-DNA ligase IIIβ (2 mg) were each covalently attached to 1 ml of Affigel-10 beads (Bio-Rad) according to the manufacturer's instructions. Nuclear extracts were prepared from a frozen pellet of HeLa S3 cells (5 × 10^9 cells) as described previously (34) and dialyzed against a solution containing 50 mM Tris-HCl (pH 7.5), 50 mM KCl, 0.5 mM EDTA, 10 μg of leupeptin/ml, 1 mM PMSF, and 1 mM benzamidine-HCl. Nuclear extract (20 mg) was loaded onto Affigel beads liganded by either GST or GST-DNA ligase IIIβ that had been preequilibrated with buffer A (100 mM morpholinepropanesulfonic acid [MOPS, pH 7.5], 50 mM NaCl, 10 μg of leupeptin/ml, 1 mM PMSF, 1 mM benzamidine-HCl). After a wash with buffer A, bound proteins were eluted stepwise with buffer A containing 0.15 M NaCl and then 0.3 M NaCl. Proteins in equivalent column fractions were separated by sodium dodecyl sulfate-polyacrylamide gel electrophoresis (SDS-PAGE) (13) and then detected by using the Silver Stain Plus kit (Bio-Rad).

Mass spectrometry. Proteins that were preferentially retained by the GST-DNA ligase IIIβ beads were separated by preparative SDS-PAGE and stained with Coomassie blue. Bands were cut out of the gel and diced into small pieces. The gel pieces were vortexed with 100 μl of 25 mM ammonium bicarbonate-50% acetonitrile three times and then dried in a SpeedVac SC100 for 20 min. The

dried gel pieces were resuspended in 20 μl of 25 mM ammonium bicarbonate containing 5 μg of sequencing-grade trypsin (Promega)/ml, vortexed for 10 min, and then incubated at 4°C for 30 min. The supernatant was discarded and 20 μl of 25 mM ammonium bicarbonate was added to the gel pieces, which were then incubated at 37°C for 16 h. After the addition of 100 μl of H$_2$O, samples were vortexed for 10 min. The supernatant was collected and added to 5 μl of 50% acetonitrile-5% formic acid in a 0.65-ml siliconized tube. The gel pieces were washed two more times with 5 μl of 50% acetonitrile-5% formic acid, and the supernatants were all combined. The pooled supernatants were reduced to 10 μl in a SpeedVac and then diluted by the addition of 100 μl of H$_2$O. After concentration to 5 μl, an equal volume of 50% acetonitrile-5% formic acid was added, and an aliquot (1 μl) was analyzed by matrix-assisted laser desorption ionization–time of flight (MALDI-TOF) mass spectrometry (Voyager-DE Pro; Applied Biosystems). Peptides in the sample were compared against those in the University of California, San Francisco, MS-FIT database (ProteinProspector package) for identification.

Immunoblotting. Proteins were separated by SDS-PAGE and then transferred onto nitrocellulose membranes. The membranes were incubated with antibodies against DNA ligase III (GeneTex), Ku70 and Ku80 (NeoMarkers), PARP-1 (Trevigen), PAR (Trevigen), or XRCC1 (NeoMarkers) in 50 mM Tris-HCl (pH 7.5), 150 mM NaCl, and 0.05% Tween 20 containing 2% dried milk overnight at 4°C. After incubation with the appropriate secondary antibody linked to horseradish peroxidase, antigen-antibody complexes were detected by enhanced chemiluminescence (Pierce).

Yeast two-hybrid genetic screen. PARP-1 and DNA ligase IIIα cDNAs were cloned into the two-hybrid vectors pGADT7 and pGBKT7 (Clontech), respectively. Plasmids were transformed individually into the isogenic haploid Saccharomyces cerevisiae strains PJ69-4a and PJ69-4α. Diploids were selected on synthetic medium lacking tryptophan and leucine and replica plated onto plates of synthetic complete medium supplemented with 30 mM 3-amino-1,2,4-triazole but lacking tryptophan, leucine, and histidine. Colonies were incubated at 30°C for 3 days and then assayed for β-galactosidase activity (1). To confirm the protein-protein interaction, the colonies were transferred onto synthetic medium lacking tryptophan, leucine, and adenine.

Pull-down assays. Nickel-agarose beads (10 μl) liganded by either His-tagged DNA ligase IIIβ (2 μg) or DNA ligase IIIβ lacking the zinc finger (2 μg) were washed with buffer B (50 mM Tris-HCl [pH 8.0], 200 mM NaCl, 20 imidazole) and then resuspended in 0.5 ml of buffer B containing 5 mg of bovine serum albumin/ml and purified PARP-1 (1 μg). After incubation at 4°C with constant rotation for 1 h, the beads were washed extensively with buffer B. Proteins were eluted from the beads with SDS sample buffer. After separation by SDS-PAGE, PARP-1 was detected by immunoblotting.

Surface plasmon resonance. A 40-bp hairpin duplex containing a single-strand break was biotinylated at the 3′ terminus and coupled to a streptavidin-coated Biacore CM-5 sensor chip. Full-length DNA ligase IIIβ, DNA ligase IIIβ lacking the zinc finger, or PARP-1 dialyzed against 10 mM HEPES (pH 7.4)–150 mM NaCl–3 mM EDTA was injected (60 μl at 5 μl/min) at various concentrations and monitored for association and dissociation. Dissociation constants were calculated using BIAevaluation software (version 3.1) in which experimental data are fitted with kinetic models.

DNase I footprinting. An 80-mer oligonucleotide (50 pmol) was end labeled with [γ-^{32}P]ATP (6,000 Ci/mmol; NEN) and polynucleotide kinase (New England Biolabs) and then annealed with two complementary oligonucleotides (50 pmol of each) to generate a labeled 80-bp duplex with a single nick. Radiolabeled nicked duplexes (800 fmol) and DNA ligase IIIβ were incubated on ice for 10 min in a solution containing 50 mM Tris-HCl (pH 8.0), 0.1 M KCl, 12.5 mM MgCl$_2$, 1.0 mM EDTA, 20% glycerol, and 1.0 mM dithiothreitol. The DNase I cleavage reaction was started with the addition of 50 μl of 5 mM CaCl$_2$–10 mM MgCl$_2$ and 75 μl of DNase I (50 U/ml; Promega) at room temperature. Reactions were terminated after 1 min by the addition of 90 μl of stop solution (0.05% bromophenol blue, 0.05% xylene cyanol, 0.2 M NaCl, 0.03 M EDTA, 1% SDS, and 100 μg of yeast RNA/ml). After phenol-chloroform extraction and ethanol precipitation, DNA was electrophoresed through a 15% polyacrylamide gel containing 8 M urea. Labeled DNA products in the dried gel were detected by autoradiography.

Kinase protection assay. A 50-bp duplex oligonucleotide containing a single-nucleotide gap with only the 5′ terminus at the gap unphosphorylated (0.5 pmol) was preincubated in kinase buffer with 3 pmol of either full-length DNA ligase IIIβ or PARP-1 in the presence or absence of 1 mM NAD. After 10 min at room temperature, 10 U of T4 polynucleotide kinase was added and incubation was continued for 5 min. Reactions were stopped by phenol-chloroform extraction. DNA was precipitated with ethanol and then electrophoresed through a 6%

denaturing polyacrylamide gel for 1.5 h. Labeled DNA products in the dried gel were detected and quantitated by phosphorimager analysis.

DNA ligation assays. The substrate used in DNA joining assays was a 50-bp duplex oligonucleotide containing a single nick. The 5′ terminus of the 30-mer at the nick was end labeled with polynucleotide kinase and [γ-^{32}P]ATP. DNA substrate (1 pmol) was preincubated in ligation buffer with either 4 or 2 pmol of full-length PARP-1 for 10 min at room temperature in the presence or absence of 1 mM NAD as indicated. Subsequently, DNA ligase IIIβ, truncated DNA ligase IIIβ lacking the zinc finger, or DNA ligase I (50 or 100 fmol as indicated) was added and incubation was continued for 10 min at room temperature. Reactions were stopped with 5 μl of gel loading dye (0.05% bromophenol blue, 0.05% xylene cyanol, and 20 mM EDTA in 100% formamide), and then DNA was electrophoresed through a 6% denaturing polyacrylamide gel for 1.5 h. Labeled DNA products in the dried gel were detected and quantitated by phosphorimager analysis.

Immunoprecipitation. For immunoprecipitation of purified proteins, protein A/G Sepharose beads (10 μl) were incubated with monoclonal anti-PARP-1 or anti-PAR antibody and then washed twice with 100 mM MOPS (pH 7.5)–50 mM NaCl. The beads were resuspended in 0.5 ml of the same buffer containing 5 mg of bovine serum albumin/ml and either purified PARP-1 (1 μg) or PAR (0.2 μg; Trevigen) and then incubated at 4°C with constant rotation for 1 h. Purified DNA ligase IIIβ (1 μg) or truncated DNA ligase IIIβ lacking the zinc finger (1 μg) was added to the reaction mixture, which was incubated at 4°C with constant rotation for 1 h. The beads were washed extensively, and the proteins were eluted with SDS sample buffer. After separation by SDS-PAGE, proteins were detected by immunoblotting with the appropriate antibody.

HeLa cells were cultured in Dulbecco modified Eagle medium supplemented with 10% fetal bovine serum prior to incubation with 5 mM hydrogen peroxide (H_2O_2) in serum-free media for 1 h at 37°C. Following H_2O_2 treatment or mock treatment, cells were harvested and lysed in a solution containing 50 mM Tris-HCl (pH 7.5), 150 mM NaCl, 1 mM EDTA, 0.5% Nonidet-P40, 10 μg of leupeptin/ml, 1 mM PMSF, and 1 mM benzamidine-HCl. The lysate was then cleared by centrifugation for 10 min at 16,000 × g at 4°C. PARP-1 polyclonal antibody (3 μl; Serotec) was combined with 2 mg of cleared lysate and protein A/G Sepharose beads (15-μl bed volume) preequilibrated with lysis buffer and then incubated with constant rotation at 4°C for 16 h. After extensive washing, proteins were eluted from the beads with SDS sample buffer and then separated by SDS-PAGE. Proteins were detected by immunoblotting.

RESULTS

DNA ligase III interacts directly with PARP-1. To identify proteins in somatic cells that associate with DNA ligase IIIα independently of XRCC1, we fractionated a HeLa nuclear extract by affinity chromatography by using GST-DNA ligase IIIβ, which lacks the C-terminal XRCC1-interacting domain of DNA ligase IIIα (6, 21) as the ligand. Analysis of proteins in the column eluates by silver staining after SDS-PAGE revealed the presence of three polypeptides with molecular masses of 110, 80, and 70 kDa that were much more abundant in the 0.3 M NaCl eluate from the DNA ligase column than in that from the GST column (Fig. 1A). To identify these polypeptides, the bands were excised from the gel and, after in situ digestion by trypsin, the masses of peptides were determined by MALDI-TOF and compared against those in a public database. This initial identification was confirmed by immunoblotting with antibodies against PARP-1 (Fig. 1B) and Ku80 and Ku70 (Fig. 1C).

Since both PARP-1 and the Ku70/Ku80 heterodimer are abundant nuclear proteins that bind avidly to DNA strand breaks, the preferential binding of these factors to the DNA ligase III column could have been mediated by DNA. Because of genetic and biochemical studies linking PARP-1 and DNA ligase IIIα with the repair of DNA single-strand breaks (2, 19, 29, 36), we chose to further characterize the association between these proteins by using different approaches. PARP-1 and DNA ligase III were found to specifically interact both in

FIG. 1. Identification of DNA ligase III-associated proteins by affinity chromatography. A HeLa nuclear extract was fractionated by using a DNA ligase III affinity chromatography column as described in Materials and Methods. (A) Proteins in comparable fractions eluted with 0.3 M NaCl from the beads liganded by GST and by GST-DNA ligase III (Lig III) were detected by silver staining after separation by SDS-PAGE. The polypeptides indicated were identified by MALDI-TOF mass spectrometry. The identities of PARP-1, Ku70, and Ku80 were verified by immunoblotting with PARP-1 (B) and Ku70 and Ku80 (C) monoclonal antibodies.

the yeast two-hybrid in vivo assay (Fig. 2A) and in pull-down assays with purified proteins (Fig. 2B). By deletion analysis, the PARP-1 binding site was localized to residues 55 to 152 of the nuclear form of DNA ligase III (6, 14). Together, these results provide compelling evidence that PARP-1 and DNA ligase III interact directly in a reaction that is dependent on the N-terminal region of DNA ligase III adjacent to the zinc finger motif.

Binding of PARP-1 and DNA ligase III to DNA single-strand breaks. The direct interaction between PARP-1 and DNA ligase III, both of which possess similar zinc finger motifs at their N termini (32), suggests that these DNA binding domains may functionally interact in the repair of DNA single-strand breaks. To begin to examine this idea, we initially characterized the binding of DNA ligase III to DNA single-strand breaks. Using surface plasmon resonance, we monitored the binding and release (Fig. 3A) of DNA ligase III from an immobilized DNA substrate containing a single-strand break. From this data, the dissociation constant of DNA ligase III was calculated to be 5 nM. In similar experiments, the dissociation constant of truncated DNA ligase III lacking the zinc finger and that of PARP-1 were calculated to be 300 nM and 0.5 pM, respectively (data not shown). Thus, we conclude that the zinc finger is the major single-strand break binding activity in DNA ligase III and that the DNA binding domain of PARP-1 containing the two tandem-arrayed zinc fingers binds to DNA strand breaks with much higher affinity than does the single zinc finger of DNA ligase III.

Next, the binding of DNA ligase III to a nonligatable DNA single-strand break was visualized by DNase I footprinting. Full-length DNA ligase III protected a region of 14 to 18 nucleotides in the intact strand that encompassed the strand break plus about 4 nucleotides on the 5′ side and about 14 nucleotides on the 3′ side of the break (Fig. 3B). The size and asymmetry of this footprint are similar to those observed with both PARP-1 and an N-terminal fragment of DNA ligase III that had been denatured by SDS-PAGE and then immobilized on a nitrocellulose membrane (16). These results suggest that

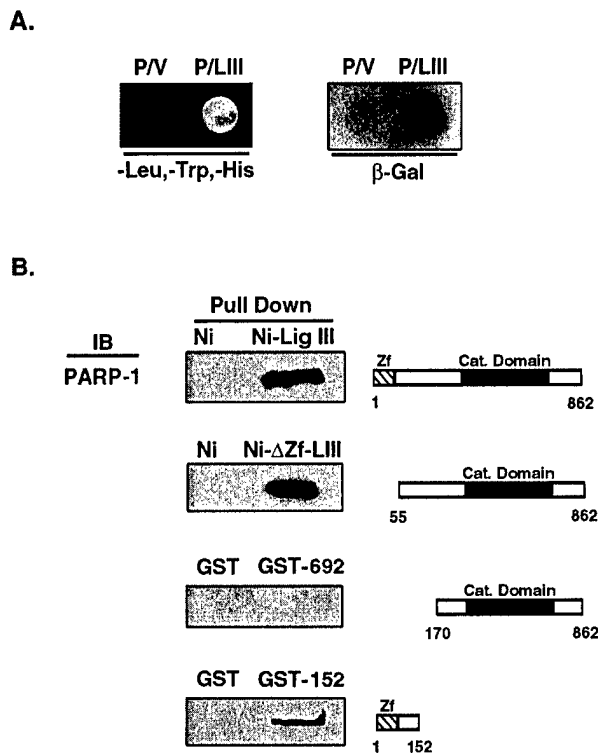**A.**

-Leu,-Trp,-His β-Gal

B.

FIG. 2. (A) The yeast two-hybrid genetic screen was employed to determine whether DNA ligase III interacts directly with PARP-1. Yeast strains were constructed as described in Materials and Methods. Colonies were tested for growth on triple dropout medium (-Leu, -Trp,-His) and subjected to a β-galactosidase (β-Gal) filter assay to detect protein-protein interactions as indicated. P/LIII, yeast strain expressing PARP-1 fused to the GAL4 activation domain (P) and DNA ligase III fused to the GAL4 DNA binding domain (LIII); P/V, yeast strain expressing the GAL4 binding domain (V) and PARP-1 fused to the GAL4 activation domain (P). (B) Mapping of the region of DNA ligase III that interacts with PARP-1. Pull-down assays with glutathione Sepharose and nickel beads were performed as described in Materials and Methods with purified PARP-1 (10 nM) and tagged versions of DNA ligase III. Ni, nickel beads only; Ni-Lig III, nickel beads liganded by His-tagged full-length DNA ligase III; Ni-ΔZf-LIII, nickel beads liganded by His-tagged DNA ligase III lacking the N-terminal 55 amino acids; GST, glutathione Sepharose beads liganded by GST; GST-692, glutathione Sepharose beads liganded by a GST fusion protein containing the C-terminal 692 residues of DNA ligase III; GST-152, glutathione Sepharose beads liganded by a GST fusion protein containing the N-terminal 152 residues of DNA ligase III; Zf, zinc finger; cat. domain, catalytic domain. The binding of PARP-1 to the beads was detected by immunoblotting (IB) with PARP-1 monoclonal antibody.

binding of DNA ligase III to a DNA single-strand break will cover regions of the broken strand immediately adjacent to the break and block access to the termini at the break. To test this directly, we examined whether the complex formed by DNA ligase III at a DNA single-strand break prevented T4 polynucleotide kinase from reacting with the 5' terminus of the DNA strand break. In accord with the footprinting results, preincubation of DNA ligase III with a DNA substrate containing a single-nucleotide gap effectively inhibited T4 polynucleotide kinase activity (Fig. 3C). As expected, purified PARP-1 also inhibited T4 polynucleotide kinase activity in the absence of NAD. However, in the presence of NAD, PARP-1 did not inhibit T4 polynucleotide kinase activity (Fig. 3C), indicating

that, upon automodification, PARP-1 dissociates from the DNA strand break.

Effect of PARP-1 on DNA joining by DNA ligase III. By quantitative immunoblotting of extracts from proliferating T24 and HeLa cells, we estimate that there are 2×10^5 PARP-1 molecules, 8×10^4 XRCC1 molecules, and 3×10^4 DNA ligase IIIα molecules per cell (Z. Dong and A. E. Tomkinson, unpublished results). Based on this numerical advantage and its higher affinity for DNA single-strand breaks, it seems likely that PARP-1 will bind to in vivo DNA single-strand breaks before DNA ligase IIIα does. In accord with the results of the kinase protection assays (Fig. 3C), DNA joining by DNA ligases I and III was almost completely inhibited by PARP-1 in the absence of NAD (Fig. 4A and B). However, in the presence of NAD when PARP-1 became poly(ADP-ribosyl)ated (Fig. 4C), DNA ligase I recovered maximum joining activity (Fig. 4A and B), providing further evidence that poly(ADP-ribosyl)ated PARP-1 dissociates from the DNA strand break. In contrast, both intact DNA ligase III and the truncated version of DNA ligase III lacking the zinc finger failed to recover maximum joining activity in the presence of poly(ADP-ribosyl)ated PARP-1 (Fig. 4A and B). Taken together, these results show that DNA joining by DNA ligase III but not DNA ligase I is partially inhibited by high levels of poly(ADP-ribosyl)ated PARP-1 and suggest that the interaction between DNA ligase III and PARP-1 modulates DNA joining.

DNA ligase III binds directly to PAR. With the use of a peptide binding assay, a putative PAR binding site (residues 12 to 34) has been identified within the zinc finger domain of DNA ligase III (23). To demonstrate that DNA ligase III does indeed interact with PAR, we performed coimmunoprecipitation experiments with PAR antibody. As expected, DNA ligase III was efficiently coimmunoprecipitated by the PAR antibody only in the presence of PAR (Fig. 5A). However, the truncated version of DNA ligase III lacking the zinc finger was also coimmunoprecipitated in a PAR-dependent manner, indicating that there are other PAR binding regions within DNA ligase III and that the previously identified PAR binding site within the zinc finger domain (23) may not be the predominant PAR binding site in DNA ligase III. In a similar experiment, DNA ligase I was not coimmunoprecipitated by the PAR antibody either in the presence or in the absence of PAR (data not shown).

Since the negatively charged PAR resembles the phosphodiester backbone of DNA, we examined the effect of PAR on DNA joining. Although both intact DNA ligase III and the truncated version of DNA ligase III lacking the zinc finger interact with PAR (Fig. 5A), PAR was significantly less effective at inhibiting DNA joining by intact DNA ligase III (<10% inhibition) (Fig. 5B) than that by the truncated version lacking the zinc finger (40% inhibition) (Fig. 5B). A similar effect was observed over a range of PAR concentrations from 0.5 to 50 nM (data not shown). These results suggest that the DNA ligase III zinc finger may facilitate recognition of the DNA nick in the context of the negatively charged PAR.

This model predicts that poly(ADP-ribosyl)ated PARP-1 should be more effective at inhibiting the truncated version lacking the zinc finger than it should be at inhibiting full-length DNA ligase III. Although we showed in Fig. 4 that the presence of the DNA ligase III zinc finger resulted in a greater

A.

Single-Strand
Break

↓

ᵀᵀCTGTCGCCCTT ATTCCGATAGTGACTACAATGGTCATU-Biotin
ᵀTGACAGCGGGAATAAGGCTATCACTGATGTTACCAGTA

Chip Surface →

Sensorgram

B.

single-strand
break

5'——42——↓——38——3'
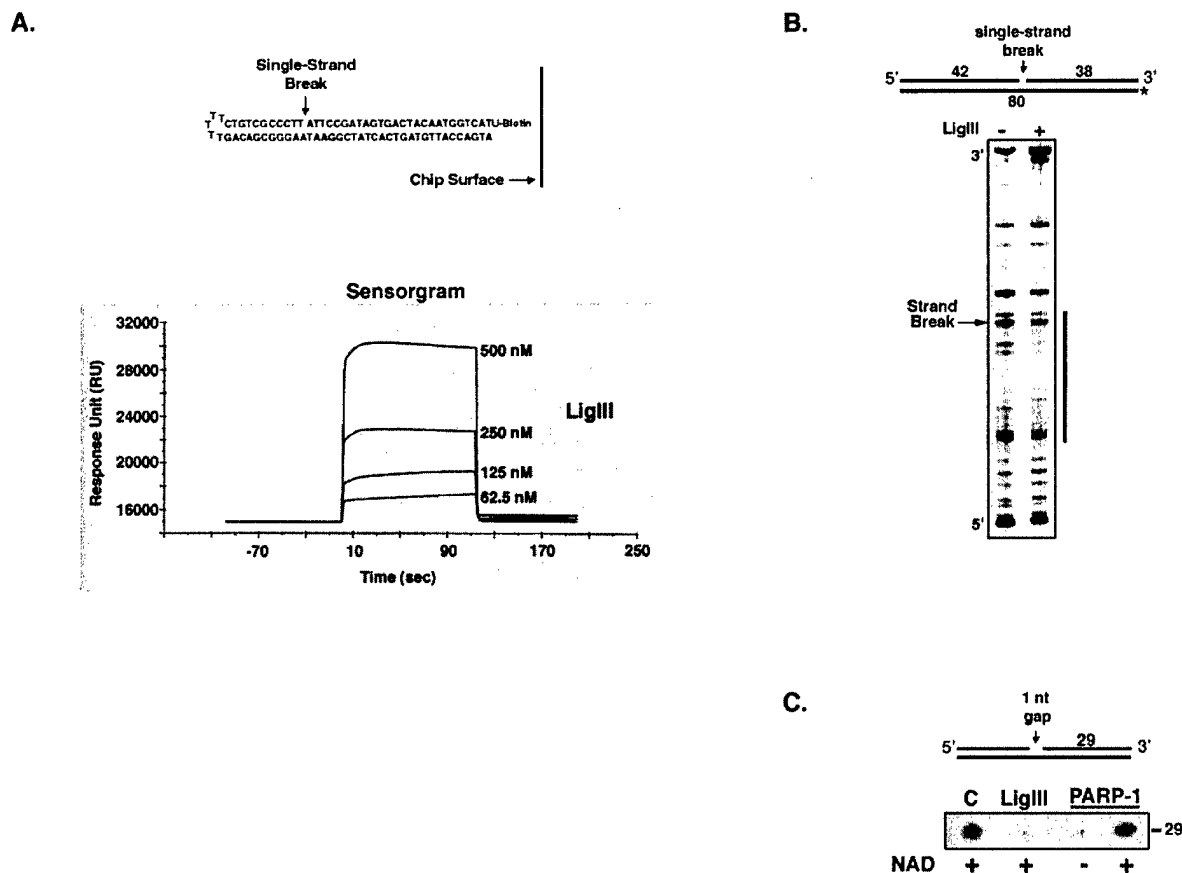————80————*

LigIII — +

C.

1 nt
gap

5'————↓——29——3'

FIG. 3. Binding of DNA ligase III and PARP-1 to DNA single-strand interruptions. Effects of NAD on DNA binding by PARP-1 are shown. (A) Analysis of the binding of DNA ligase III to a DNA single-strand break by surface plasmon resonance. (Top panel) Schematic representation of the nicked hairpin oligonucleotide immobilized on the chip surface. (Bottom panel) Representative sensorgram showing the binding and release of untagged full-length DNA ligase III (LigIII), injected at the concentrations indicated, from the nicked hairpin oligonucleotide immobilized on the chip surface. (B) Visualization of DNA ligase III bound to a DNA single-strand break by DNase I footprinting. Intact DNA ligase III (LigIII; 20 nM) was preincubated with the labeled, nicked DNA substrate (16 nM) indicated and then incubated with DNase I as described in Materials and Methods. After separation by denaturing gel electrophoresis, labeled oligonucleotides were detected by autoradiography. −, no enzyme. The vertical line indicates the region protected from DNase I activity. (C) Effect of DNA strand break binding by DNA ligase III and PARP-1 on T4 polynucleotide kinase activity. Intact DNA ligase III (150 nM) or PARP-1 (150 nM) was preincubated with the indicated DNA substrate containing a single-nucleotide (1 nt) gap in the presence (+) or absence (−) of NAD as indicated prior to incubation with polynucleotide kinase and [γ-^{32}P]ATP as described in Materials and Methods. After separation by denaturing gel electrophoresis, labeled 29-mer oligonucleotide was detected and quantitated by phosphorimager analysis. Lane C, no PARP-1 or DNA ligase III.

recovery from inhibition by poly(ADP-ribosyl)ated PARP-1, the ratio of PARP-1 to DNA ligase III in these experiments was more than 10-fold higher than the in vivo ratio. Therefore, we examined the effect of PARP-1 on the DNA joining activity of DNA ligase III at a molar ratio that more closely reflects physiological conditions. In these reactions, unmodified PARP-1 inhibited DNA joining by less than 10% (Fig. 6). Formation of poly(ADP-ribosyl)ated PARP-1 by preincubation with the nicked DNA substrate and NAD resulted in a small increase in DNA joining by intact DNA ligase III (Fig. 6). In contrast, there was a decrease of about 30% in DNA joining by the truncated version of DNA ligase III lacking the zinc finger motif in similar reactions (Fig. 6). Taken together, these results strongly support the idea that the DNA ligase III zinc finger enhances the ability of DNA ligase III to detect DNA nicks in the presence of either PAR or poly(ADP-ribosyl)ated PARP-1.

DNA ligase III preferentially interacts with poly(ADP-ribosyl)ated PARP-1 in vitro and in vivo. The direct binding of DNA ligase III to both PAR and PARP-1 suggests that this enzyme may preferentially bind to poly(ADP-ribosyl)ated PARP-1. In support of this idea, about fivefold more intact and truncated DNA ligase III was specifically coimmunoprecipitated by the PARP-1 antibody in the presence of automodified PARP-1 than in identical experiments with unmodified PARP-1 (Fig. 7A). The preferential interaction of DNA ligase III with poly(ADP-ribosyl)ated PARP-1 provides an attractive mechanism for the recruitment of DNA ligase IIIα to in vivo DNA single-strand breaks in the nuclei of somatic cells. To provide support for this hypothesis, extracts were prepared from undamaged cells and from cells treated with H_2O_2 to induce PAR synthesis and PARP-1 automodification. Although DNA damage did not cause a significant change in the cellular levels of DNA ligase IIIα or XRCC1, coimmunopre-

A.

B.

C.

IB:
Anti-PAR

FIG. 4. Effect of DNA binding by PARP-1 on DNA joining. (A) Purified PARP-1 (200 nM) was preincubated with a labeled DNA duplex containing a single ligatable nick (50 nM) in the presence (+) or absence (−) of NAD. Subsequently, intact DNA ligase III (Lig III; 2.5 nM), a truncated version lacking the zinc finger (ΔZf-Lig III; 2.5 nM), or DNA ligase I (Lig I; 2.5 nM) was added to the reaction mixture as indicated. After incubation for 10 min at 25°C, labeled oligonucleotides were separated by denaturing gel electrophoresis. The labeled substrate (30-mer) and ligated product (50-mer) were detected and quantitated by phosphorimager analysis. (B) The results of three independent DNA joining assays are shown graphically. White bars, intact DNA ligase III; grey bars, truncated version of DNA ligase III lacking the zinc finger; black bars, DNA ligase I. (C) Purified PARP-1 (100 nM) was preincubated with a labeled DNA duplex containing a single ligatable nick (100 nM) in the presence (+) or absence (−) of NAD. After separation by SDS-PAGE, poly(ADP-ribosyl)ated PARP-1 was detected by immunoblotting (IB) with a monoclonal antibody against PAR. The positions of unmodified and poly(ADP-ribosyl)ated PARP-1 are indicated.

cipitation of the DNA ligase IIIα-XRCC1 complex by the PARP-1 antibody was DNA damage dependent (Fig. 7B). Pretreatment of the cells with the PARP-1 inhibitor 1,5-isoquinolinediol prevented the DNA damage-dependent association between PARP-1 and the DNA ligase IIIα-XRCC1 complex (Fig. 7B). Similar results were observed with another PARP-1 inhibitor, 3-aminobenzamide (data not shown). Since there are two- to threefold more XRCC1 molecules than DNA ligase IIIα molecules per cell, it is likely that there is a pool of free

XRCC1 molecules. Notably, the ratio of DNA ligase IIIα to XRCC1 was significantly higher in the immunoprecipitates than in the cell extract (Fig. 7B), indicating that it is XRCC1 complexed with DNA ligase IIIα rather than free XRCC1 that preferentially associates with poly(ADP-ribosyl)ated PARP-1. Thus, our results indicate that the DNA ligase IIIα-XRCC1 complex is recruited to in vivo DNA strand breaks by its interaction with poly(ADP-ribosyl)ated PARP-1.

DISCUSSION

The apparent absence of homologs of the *LIG3* gene from the genomes of *Drosophila, Caenorhabditis elegans,* and *S. cerevisiae* indicates that this gene is restricted to mammals and amphibians and is presumably involved in DNA repair transactions that are unique to these higher eukaryotes (6, 16, 22, 27, 32). Because the nuclear form of DNA ligase IIIα is unstable without its partner protein XRCC1 (3, 4), it was assumed that DNA ligase IIIα functions together with XRCC1 in short-patch DNA base excision repair and the repair of DNA single-strand breaks (8, 28, 29, 36). However, recent studies have shown that the DNA ligase IIIα-XRCC1 complex is critical for repair for cells in the G₁ phase of the cell cycle and in noncycling cells but that DNA ligase IIIα but not XRCC1 is dispensable for repair in cells in S phase (20, 27). To gain

A.

IP: Anti-PAR polymer

B.

FIG. 5. Interaction of DNA ligase III with PAR. Effects of PAR on DNA joining by DNA ligase III are shown. (A) Intact DNA ligase III (Lig III; 10 nM) or a truncated version lacking the zinc finger (ΔZf-LIII; 10 nM) was incubated with PAR antibody in the presence (+) or absence (−) of PAR. After separation of immunoprecipitated (IP) proteins by SDS-PAGE, DNA ligase III was detected by immunoblotting (IB). (B) DNA joining reactions with intact DNA ligase III (5 nM) or a truncated version lacking the zinc finger (5 nM) were carried out as described in Materials and Methods in the presence or absence of 0.5 nM PAR as indicated. The results of four independent DNA joining assays are shown graphically. White bars, intact DNA ligase III; grey bars, truncated version of DNA ligase III lacking the zinc finger.

A.

B.

FIG. 6. Effect of poly(ADP-ribosyl)ated PARP-1 on DNA joining by DNA ligase III. (A) Purified PARP-1 (100 nM) was preincubated with a labeled DNA duplex containing a single ligatable nick (50 nM) in the presence (+) or absence (−) of NAD. Subsequently, intact DNA ligase III (Lig III; 5 nM) or a truncated version lacking the zinc finger (ΔZf-Lig III; 5 nM) was added to the reaction mixture as indicated. After incubation for 10 min at 25°C, labeled oligonucleotides were separated by denaturing gel electrophoresis. The labeled substrate (30-mer) and ligated product (50-mer) were detected and quantitated by phosphorimager analysis. (B) The results of three independent DNA joining assays are shown graphically. White bars, full-length DNA ligase IIIβ; grey bars, truncated version of DNA ligase IIIβ lacking the zinc finger.

insights into the DNA repair events mediated by DNA ligase IIIα in the nuclei of somatic cells, we fractionated a HeLa nuclear extract by affinity chromatography and identified PARP-1 as a protein that specifically associates with DNA ligase III. In subsequent studies, we demonstrated that there is a direct physical interaction between PARP-1 and DNA ligase III that occurs via the region of amino acids immediately adjacent to the N-terminal zinc finger of DNA ligase III. Intriguingly, the DNA ligase III zinc finger is closely related to the tandem-arrayed N-terminal zinc fingers that constitute the DNA binding domain of PARP-1 (32). Our detection of a direct physical interaction between PARP-1 and the DNA binding region of DNA ligase III prompted us to determine whether these proteins functionally interact in DNA single-strand break repair.

Based on its relative abundance and high binding affinity, it seems likely that PARP-1 is the first factor to bind to DNA single-strand breaks in vivo (Fig. 8), resulting in activation of its polymerase activity and automodification since PARP-1 itself is the major acceptor for PAR (25). Although poly(ADP-ribosyl)ated PARP-1 dissociates from the DNA strand break (35), it is likely that PARP-1 molecules shuttle on and off the strand break, generating a network of PARs in the vicinity of the DNA strand break because of the relatively large number

of PARP molecules per cell combined with the action of the poly(ADP-ribose) glycohydrolase (35). Presumably, this network of negatively charged polymers protects the DNA break by nonspecifically binding DNA metabolizing enzymes, such as nucleases, that recognize the negatively charged phosphodiester backbone of DNA (25, 35). The DNA damage-dependent association of DNA ligase IIIα with poly(ADP-ribosyl)ated PARP-1 in vivo suggests that the DNA ligase IIIα-XRCC1 complex is specifically recruited to the poly(ADP-ribosyl)ated PARP-1 molecules near the DNA strand break.

Although the binding to poly(ADP-ribosyl)ated PARP-1 provides a molecular mechanism for the relocation of the DNA ligase IIIα-XRCC1 complex to the vicinity of DNA damage sites in vivo, the complex then has to recognize and interact with DNA single-strand breaks when it is bound to negatively charged, automodified PARP-1. It has been previously shown that the DNA ligase III zinc finger is not required either for DNA joining activity in vitro or for the in vivo complementation of an *E. coli lig* mutant (16). These observations suggest that the DNA ligase III zinc finger may play a critical role only

A.

B.

FIG. 7. DNA ligase III preferentially binds to poly(ADP-ribosyl)ated PARP-1 in vitro. Effects of DNA damage on the association between PARP-1 and DNA ligase III-XRCC1 in vivo are shown. (A) Purified PARP-1 (500 nM) was preincubated with a labeled DNA duplex containing a single ligatable nick (300 nM) in the presence (+) or absence (−) of NAD. After treatment with DNase I, intact DNA ligase III (10 nM) or a truncated version lacking the zinc finger (10 nM) was added to the reaction mixture as indicated. Proteins immunoprecipitated (IP) by PARP-1 antibody were separated by SDS-PAGE and then detected by immunoblotting (IB) with the indicated antibody. Upper panel, intact DNA ligase III (Lig III); middle panel, truncated version of DNA ligase III lacking the zinc finger (ΔZf-Lig III); lower panel, unmodified PARP-1 y(ADP-ribosyl)ated PARP-1 [P-(ADPR)n]. (B) Effect of H_2O_2 treatment on the association of PARP-1, DNA ligase IIIα, and XRCC1. Whole cell extracts (WCE) were prepared from undamaged (−) or damaged (+) HeLa cells as described in Materials and Methods. Equivalent aliquots of the cells to be damaged were pretreated with 1,5-isoquinolinediol (DiQ; 100 μM) as indicated for 1 h prior to and during H_2O_2 treatment. Proteins immunoprecipitated by PARP-1 antibody were separated by SDS-PAGE and then detected by immunoblotting with the indicated antibody. DNA ligase IIIα and XRCC1 in the extracts from undamaged cells were detected by direct immunoblotting.
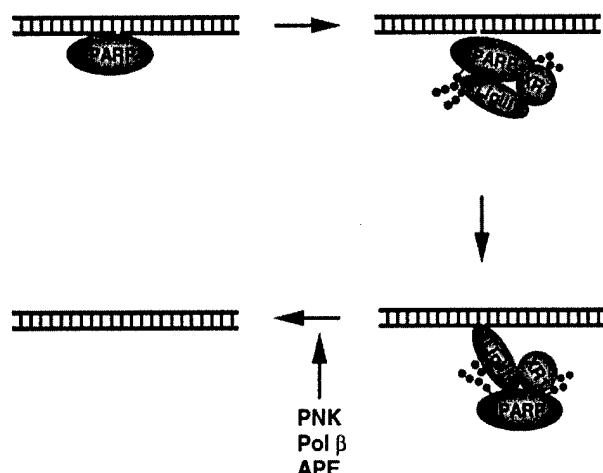
FIG. 8. Model of the repair of DNA single-strand breaks by PARP-1 and DNA ligase III-XRCC1. The binding of PARP-1 to a DNA single-strand break activates PARP-1's polymerase activity that in turn results in automodification and dissociation of poly(ADP-ribosyl)ated PARP-1 from the strand break. DNA ligase IIIα (LigIII)-XRCC1 (XR1) associates with poly(ADP-ribosyl)ated PARP-1 in the vicinity of the DNA strand break. The zinc finger of DNA ligase IIIα enables this ternary complex to specifically recognize and bind to the DNA strand break despite the presence of negatively charged PARs. Additional repair factors such as polynucleotide kinase (PNK), Pol β, and AP endonuclease (APE) that process damaged termini are recruited via interactions with XRCC1. After the generation of ligatable termini, repair is completed by DNA ligase IIIα.

in the presence of PARP-1 and PAR. In support of this idea, we found that intact DNA ligase III was more effective at DNA joining than a truncated version of DNA ligase III lacking the zinc finger in the presence of either PAR or poly(ADP-ribosyl)ated PARP-1. Taken together, these results suggest that the role of the DNA ligase III zinc finger is to enable this enzyme to functionally interact with DNA single-strand breaks when it is complexed with poly(ADP-ribosyl)ated PARP-1 (Fig. 8). Although the effect of the DNA ligase III zinc finger was relatively small in the in vitro assays with naked DNA substrates, it may be more critical in vivo when the DNA strand breaks occur in chromatin with the adjacent histones probably poly(ADP-ribosyl)ated by PARP-1 (7, 25). Since the majority of DNA single-strand breaks will not have ligatable termini, it is likely that end processing enzymes, such as polynucleotide kinase, AP endonuclease, and Pol β, are recruited to the DNA ligase IIIα-XRCC1-DNA strand break complex via their interaction with XRCC1 (2, 12, 31, 33). Further biochemical and molecular genetic studies are needed to elucidate the complex relationship between PARP-1, DNA ligase IIIα-XRCC1, and XRCC1 in the network of DNA repair pathways that maintain genome stability in higher eukaryotes.

ACKNOWLEDGMENTS

REFERENCES

1. Ausubel, F. M., R. Brent, R. Kingston, D. Morre, J. Seidman, A. Smith, and K. Struhl. 1994. Current protocols in molecular biology. John Wiley and Sons, Inc., New York, N.Y.
2. Caldecott, K. W., S. Aoufouchi, P. Johnson, and S. Shall. 1996. XRCC1 polypeptide interacts with DNA polymerase β and possibly poly (ADP-ribose) polymerase, and DNA ligase III is a novel molecular nick-sensor in vitro. Nucleic Acids Res. 24:4387–4394.
3. Caldecott, K. W., C. K. McKeown, J. D. Tucker, S. Ljunquist, and L. H. Thompson. 1994. An interaction between the mammalian DNA repair protein XRCC1 and DNA ligase III. Mol. Cell. Biol. 14:68–76.
4. Caldecott, K. W., C. K. McKeown, J. D. Tucker, L. Stanker, and L. H. Thompson. 1996. Characterization of the Xrcc1-DNA ligase III complex in vitro and its absence from mutant hamster cells. Nucleic Acids Res. 23:4836–4843.
5. Callebaut, I., and J. P. Mornon. 1997. From BRCA1 to RAP1: a widespread BRCT module closely associated with DNA repair. FEBS Lett. 400:25–30.
6. Chen, J., A. E. Tomkinson, W. Ramos, Z. B. Mackey, S. Danehower, C. A. Walter, R. A. Schultz, J. M. Besterman, and I. Husain. 1995. Mammalian DNA ligase III: molecular cloning, chromosomal localization, and expression in spermatocytes undergoing meiotic recombination. Mol. Cell. Biol. 15:5412–5422.
7. de Murcia, G., and J. Menissier-de Murcia. 1994. Poly(ADP) ribose polymerase: a molecular nick sensor. Trends Biochem. Sci. 19:172–176.
8. Frosina, G., P. Fortini, O. Rossi, F. Carrozzino, G. Raspaglio, L. S. Cox, D. P. Dane, A. Abbondandolo, and E. Dogliotti. 1996. Two pathways of base excision repair in mammalian cells. J. Biol. Chem. 271:9573–9578.
9. Giner, H., F. Simonin, G. de Murcia, and J. Menissier-de Murcia. 1992. Overproduction and large scale purification of human poly (ADP-ribose) polymerase using a baculovirus expression system. Gene 11:279–283.
10. Husain, I., A. E. Tomkinson, W. A. Burkhart, M. B. Moyer, W. Ramos, Z. B. Mackey, J. M. Besterman, and J. Chen. 1995. Purification and characterization of DNA ligase III from bovine testes. J. Biol. Chem. 270:9683–9690.
11. Koonin, E. V., S. F. Alschul, and P. Bork. 1996. Functional motifs. Nat. Genet. 13:266–267.
12. Kubota, Y., R. A. Nash, A. Klungland, P. Schar, D. E. Barnes, and T. Lindahl. 1996. Reconstitution of DNA base excision-repair with purified human proteins: interaction between DNA polymerase β and the XRCC1 protein. EMBO J. 15:6662–6670.
13. Laemmli, U. K. 1970. Cleavage of structural proteins during the assembly of the head of bacteriophage T4. Nature 227:680–685.
14. Lakshmipathy, U., and C. Campbell. 1999. The human DNA ligase III gene encodes nuclear and mitochondrial proteins. Mol. Cell. Biol. 19:3869–3876.
15. Lakshmipathy, U., and C. Campbell. 2000. Mitochondrial DNA ligase III function is independent of Xrcc1. Nucleic Acids Res. 28:3880–3886.
16. Mackey, Z. B., C. Niedergang, J. M. Murcia, J. Leppard, K. Au, J. Chen, G. de Murcia, and A. E. Tomkinson. 1999. DNA ligase III is recruited to DNA strand breaks by a zinc finger motif homologous to that of poly(ADP-ribose) polymerase. Identification of two functionally distinct DNA binding regions within DNA ligase III. J. Biol. Chem. 274:21679–21687.
17. Mackey, Z. B., W. Ramos, D. S. Levin, C. A. Walter, J. R. McCarrey, and A. E. Tomkinson. 1996. An alternative splicing event, which occurs in mouse pachytene spermatocytes, generates a form of DNA ligase III with distinct biochemical properties that may function in meiotic recombination. Mol. Cell. Biol. 17:989–998.
18. Marintchev, A., M. Mullen, M. W. Maciejewski, B. Pan, M. R. Gryk, and G. P. Mullen. 1999. Solution structure of the single-strand break repair protein XRCC1 N-terminal domain. Nat. Struct. Biol. 6:884–893.
19. Masson, M., C. Niedergang, V. Schreiebr, S. Muller, J. Menissier de Murcia, and G. de Murcia. 1998. XRCC1 is specifically associated with poly(ADP-ribose) polymerase and negatively regulates its activity following DNA damage. Mol. Cell. Biol. 18:3563–3571.
20. Moore, D. J., R. M. Taylor, P. Clements, and K. W. Caldecott. 2000. Mutation of a BRCT domain selectively disrupts DNA single-strand break repair in noncycling Chinese hamster ovary cells. Proc. Natl. Acad. Sci. USA 97:13649–13654.
21. Nash, R. A., K. Caldecott, D. E. Barnes, and T. Lindahl. 1997. XRCC1 protein interacts with one of two distinct forms of DNA ligase III. Biochemistry 36:5207–5211.
22. Perez-Jannotti, R. M., S. M. Klein, and D. F. Bogenhagen. 2001. Two forms of mitochondrial DNA ligase III are produced in Xenopus laevis oocytes. J. Biol. Chem. 276:48978–48987.
23. Pleschke, J. M., H. E. Kleczkowska, M. Strohm, and F. R. Althaus. 2000. Poly(ADP-ribose) binds to specific domains in checkpoint proteins. J. Biol. Chem. 275:40974–40980.
24. Ron, D., and H. Dressler. 1992. pGSTag—a versatile bacterial expression plasmid for enzymatic labeling of recombinant proteins. BioTechniques 13:866–868.
25. Satoh, M., and T. Lindahl. 1992. Role of poly(ADP-ribose) formation in DNA repair. Nature 356:356–358.
26. Schreiber, V., J. C. Ame, P. Dolle, I. Schultz, B. Rinaldi, V. Fraulob, J.

Menissier-de Murcia, and G. de Murcia. 2002. Poly(ADP-ribose) polymerase-2 (PARP-2) is required for efficient base excision repair in association with PARP-1 and XRCC1. J. Biol. Chem. 277:23028–23036.

27. Taylor, R. M., D. J. Moore, J. Whitehouse, P. Johnson, and K. W. Caldecott. 2000. A cell cycle-specific requirement for the XRCC1 BRCT II domain during mammalian DNA strand break repair. Mol. Cell. Biol. 20:735–740.

28. Thompson, L. H., K. W. Brookman, L. E. Dillehay, A. V. Carrano, J. A. Mazrimas, C. L. Mooney, and J. L. Minkler. 1982. A CHO-cell strain having hypersensitivity to mutagens, a defect in strand break repair, and an extraordinary baseline frequency of sister chromatid exchange. Mutat. Res. 95:247–254.

29. Thompson, L. H., K. W. Brookman, N. J. Jones, S. A. Allen, and A. V. Carrano. 1990. Molecular cloning of the human XRCC1 gene, which corrects defective DNA strand break repair and sister chromatid exchange. Mol. Cell. Biol. 10:6160–6171.

30. Tomkinson, A. E., and Z. B. Mackey. 1998. Structure and function of mammalian DNA ligases. Mutat. Res. 407:1–9.

31. Vidal, A. E., S. Boiteux, I. D. Hickson, and J. P. Radicella. 2001. XRCC1 coordinates the initial and late stages of DNA abasic site repair though protein-protein interactions. EMBO J. 20:6530–6539.

32. Wei, Y.-F., P. Robins, K. Carter, K. Caldecott, D. J. C. Pappin, G.-L. Yu, R.-P. Wang, B. K. Shell, R. A. Nash, P. Schar, D. E. Barnes, W. A. Haseltine, and T. Lindahl. 1995. Molecular cloning and expression of human cDNAs encoding a novel DNA ligase IV and DNA ligase III, an enzyme active in DNA repair and genetic recombination. Mol. Cell. Biol. 15:3206–3216.

33. Whitehouse, C. J., R. M. Taylor, A. Thistlethwaite, H. Zhang, F. Karimi-Busheri, D. D. Lasko, M. Weinfeld, and K. W. Caldecott. 2001. XRCC1 stimulates human polynucleotide kinase at damaged DNA termini and accelerates DNA single-strand break repair. Cell 104:107–117.

34. Wu, Y., R. Hickey, K. Lawlor, P. Wills, F. Yu, H. Ozer, R. Starr, J. Y. Quan, M. Lee, and M. Malkas. 1994. A 17S multiprotein form of murine DNA polymerase mediates polyoma virus DNA synthesis. J. Cell. Biochem. 54:32–46.

35. Zahradka, P., and K. Ebisuzaki. 1982. A shuttle mechanism for DNA-protein interactions. The regulation of poly(ADP-ribose) polymerase. Eur. J. Biochem. 127:579–585.

36. Zdzienicka, M. Z., G. P. Vanderschans, A. T. Natarajan, L. H. Thompson, I. Neuteboom, and J. W. I. M. Simmons. 1992. A Chinese hamster ovary cell mutant (EMC-11) with sensitivity to simple alkylating agents and a very high level of sister chromatid exchanges. Mutagenesis 7:265–269.

Somatic Mutation of *p53* Leads to Estrogen Receptor α-Positive and -Negative Mouse Mammary Tumors with High Frequency of Metastasis

Suh-Chin J. Lin,[1,2] Kuo-Fen Lee,[4] Alexander Yu. Nikitin,[5] Susan G. Hilsenbeck,[6] Robert D. Cardiff,[7] Aihua Li,[1,2] Keon-Wook Kang,[1,2] Steven A. Frank,[3] Wen-Hwa Lee,[2] and Eva Y-H. P. Lee[1,2]

[1]*Departments of Developmental and Cell Biology,* [2]*Biological Chemistry, and* [3]*Ecology and Evolutionary Biology, University of California, Irvine, California;* [4]*The Salk Institute for Biological Studies, La Jolla, California;* [5]*Department of Biomedical Sciences, Cornell University, Ithaca, New York;* [6]*Department of Medicine and Department of Molecular and Cellular Biology, Breast Center, Baylor College of Medicine, Houston, Texas; and* [7]*Center for Comparative Medicine, University of California, Davis, California*

ABSTRACT

Approximately 70% of human breast cancers are estrogen receptor α (ERα)-positive, but the origins of ERα-positive and -negative tumors remain unclear. Hormonal regulation of mammary gland development in mice is similar to that in humans; however, most mouse models produce only ERα-negative tumors. In addition, these mouse tumors metastasize at a low rate relative to human breast tumors. We report here that somatic mutations of *p53* in mouse mammary epithelial cells using the Cre/loxP system leads to ERα-positive and -negative tumors. *p53* inactivation under a constitutive active *WAPCre^e* in prepubertal/pubertal mice, but not under *MMTVCre* in adult mice, leads to the development of ERα-positive tumors, suggesting that target cells or developmental stages can determine ERα status in mammary tumors. Importantly, these tumors have a high rate of metastasis. An inverse relationship between the number of targeted cells and median tumor latency was also observed. Median tumor latency reaches a plateau when targeted cell numbers exceed 20%, implying the existence of saturation kinetics for breast carcinogenesis. Genetic alterations commonly observed in human breast cancer including *c-myc* amplification and Her2/Neu/erbB2 activation were seen in these mouse tumors. Thus, this tumor system reproduces many important features of human breast cancer and provides tools for the study of the origins of ERα-positive and -negative breast tumors in mice.

INTRODUCTION

Breast carcinogenesis requires multiple genetic changes including inactivation of tumor suppressor genes and activation of oncogenes (1). Mutations in *p53* are observed in close to half of human cancers including breast carcinomas (2). *p53* is also mutated in families with Li-Fraumeni syndrome in which early-onset female breast cancer is the most prevalent type of tumor (3). p53 is a transcription factor that regulates genes critical for cell cycle arrest and for apoptosis after genotoxic stress, thus preventing genome instability (4–6). In addition, amplification and/or overexpression of *c-myc*, *Her2/Neu/erbB2*, and *cyclin D1* oncogenes are seen in a significant portion of breast cancers (2, 7).

p53 knockout mice are cancer prone and develop early-onset lymphoma and sarcoma (8, 9) but rarely mammary tumors (10) because of early mortality. To circumvent this problem, *p53^null* mammary epithelium is transplanted into the fat pad of wild-type recipients and leads to the formation of breast tumors (11). Although this offers a potential model to study breast tumors, the influence of the transplantation process on carcinogenesis is not clear. Also, the transplanted cells are *p53^null*, whereas in human tumors somatic mutations are acquired in a subset of cells during tumor progression. Previously, Jonkers *et al.* (12) reported that no mammary tumor formation was observed in p53 conditional-mutant mice carrying K14Cre transgene. Therefore, conditional inactiva-

tion of *p53* in mouse mammary epithelial cells is necessary to generate a mouse model mimicking human carcinogenesis.

In addition to genetic mutations, steroid hormones play a critical role in breast carcinogenesis (13). About 70% of human breast cancers are estrogen receptor α (ERα)-positive and estrogen-dependent (14), and ERα and progesterone receptor (PR) expression is an important indicator of potential responses to hormonal therapy (15). However, the factors that control ERα expression in tumor cells are unknown. Thus far, most established mouse models seldom produce ERα-positive mammary tumors (16). In a C3(1)/SV40 T-antigen-transgenic model, ERα expression decreases during early mammary tumor progression (from low- to high-grade mammary intraepithelial neoplasia and becomes undetectable in invasive tumors (17). In *Brca1*- and *Brca2*-linked mammary tumors, the majority of tumors show no detectable ERα expression (18–20).

In humans, breast cancers frequently metastasize to other organs such as liver, lung, and specifically bone (21). Metastasis rather than primary tumors are responsible for most cancer mortality (21, 22). Less than 5% of patients with metastatic breast cancer have a long-term remission after treatment (22). In established mouse mammary tumor models, the tumor cells infrequently colonize other organs. Only 10% *Brca1* tumors (18), 10% *pten^{+/−}* tumors (23), and 0% *Brca2* tumors (12, 20) metastasize. Many mouse mammary tumor virus (MMTV)/oncogene-bearing transgenic mice have a rare occurrence of metastasis (24), but metastatic tumors are observed in polyomavirus middle T antigen and neu proto-oncogene transgenic mice (25, 26).

We have generated a mouse breast tumor model by using Cre/loxp method to specifically inactivate *p53* in mammary epithelial cells. This conditional inactivation of *p53* leads to ERα-positive and -negative mammary tumors with a high rate of metastasis. We found that *p53* inactivation during specific developmental stages critically determines ERα expression in mammary tumors. This breast tumor system provides a close model of the human disease and will be useful for both mechanistic and therapeutic studies of ERα-positive breast cancer.

MATERIALS AND METHODS

Targeting Vector Construction. A 10.75-kb clone covering exons 1–10 of *p53* was isolated from a 129sv mouse genomic library. The 3.4-kb *Xho*I-*Hind*III fragment containing exons 2–9 was subcloned into pBR322. A replacement-type targeting vector was made by inserting the first *loxP* site into a *Bam*HI site located in intron 6. A *neo*-cassette flanked by two *loxP* sites was inserted into the *Pvu*II site in intron 4. The resulting construct was cleaved with *Xho*I and *Hind*III, blunt-ended and subcloned into p2TK (27). The finished targeting construct is designated p53neoloxp³2TK.

MMTVCre Transgene Construction. The backbone of the *MMTVCre* transgene is pBSpKCR3 (28) containing part of the rabbit β-*globin* gene (the end of exon 2, intron 2, and exon 3), and the polyadenylation site. A 1.6-kb *Bgl*II-*Hind*III fragment composed of the *Cre* transgene with a nuclear localization signal was inserted within exon 3 of the *globin* gene of pBSpKCR3. A 1.5-kb *Hind*III-*Nhe*I fragment containing the *MMTV-LTR* was cut from pMAM (Clontech, Palo Alto, California) and subcloned 5' to exon 2 of the *globin* gene. The finished transgene construct is designated pMMTV_βCre.

MMTVCre-Transgenic Mice Production. The 4.3-kb *Xho*I fragment containing the *MMTVCre* transgene was excised and purified. The transgenic

founders were generated by microinjecting the *MMTVCre* transgene fragment into the male pronucleus of fertilized eggs derived from CB6F1 × C57BL/6 intercrosses. Transgenic founders were identified by Southern analysis or PCR of tail DNA. The primers for the *Cre* transgene (363-bp amplified) were CreF (5'-GGTGTCCAATTTACTGACCGTACA-3') and CreR (5'-CGGATCCGC-CGCATAACCAGTG-3'). All mice were maintained in accordance with the guidelines of Laboratory Animal Research of The University of Texas Health Science Center at San Antonio and Institutional Animal Care and Use Committee of University of California, Irvine.

Generation of Conditional *p53* Mutant Mice. J1 embryonic stem cells were electroporated with *Sal*I-linearized *p53neoloxp³2TK* and selected with G418 and 1-(2-deoxy-2-fluoro-β-D-arabinofuranosyl)-5-iodouracil. Embryonic stem cells harboring homologous recombination were identified by Southern blotting using a 3' probe external to the targeting region. The *neo*-cassette was removed from targeted embryonic stem cells by transient expression of *pSPCre*. Of 231 clones analyzed by Southern blotting, two contained a recombination that removed only *neo*. These two clones were expanded and injected into C57BL/6 blastocysts. Chimeric males were mated with C57BL/6 females, and germline transmission of the mutant allele was verified by Southern and PCR analyses. Subsequently, *p53^{fp/fp}MMTVCre* mice were generated by crossing *p53^{fp/fp}* mice with *MMTVCre* mice. For PCR analysis, the following primers were used: primer x (5'-TGGGA-CAGCCAAGTCTGTTA-3'); y (5'-GCTGCAGGTCACCTGTAG-3'); z (5'-CATGCAGGAGCTATTACACA-3'); and p (5'-TACTCTCCTCCCCTCAATA-AGCTAT-3'). Primers "y" and "z" flank the *loxP* site in intron 6 and amplify a 119-bp fragment from wild-type *p53* and 158 bp from the *FP* allele. Primer pair x/z amplifies a ~500-bp fragment from the deleted allele after Cre-mediated recombination. Primer pair p/q amplifies a 327-bp product in the wild-type allele as well as a 253-bp fragment for the pseudogene.

In vivo functional analysis of Cre recombinase in double-transgenic mice carrying Cre and *R26R* reporter transgenes. To evaluate Cre activity *in vivo*, Cre mice were crossed with the *Rosa 26 reporter* (*R26R*) strain (29). Mammary glands from double-transgenic *Cre; R26R* mice were collected at different developmental stages and stained with X-gal for lacZ expression (30).

Histology and Immunohistochemistry. Collected tissues were fixed in 4% paraformaldehyde and processed through paraffin embedding following standard procedures. Sections were stained with H&E for histopathological evaluation. Immunostaining was performed following the protocol described in the Vectastain Elite ABC kit (Vector Laboratories, Burlingame, CA). For antigen retrieval, slides were heated for 20 min in 10 mM citrate buffer (pH 6.0) in a microwave oven. The antibodies used were CK8 and CK14 (1:2,000 and 1:300; The Binding Site, Birmingham, United Kingdom), ERα (1:2,000, MC-20; Santa Cruz Biotechnology, Santa Cruz, CA), PR and Neu/erbB2 (1:500 and 1:2,000; DAKO, Carpinteria, CA), and p53 (1:2,000, CM5; Novocastra Laboratories, Newcastle, United Kingdom).

Western Analysis and Fluorescence Microscopy. Tumor cells were grown in DMEM/F12 medium containing 15% fetal bovine serum, 10 ng/ml epidermal growth factor, and 1 μg/ml insulin. Cell lysates were prepared using EBC (50mM Tris-HCl, 120 mM NaCl, 1 mM EDTA, pH 8.0, 50 mM NaF, 0.5% NP-40) buffer, and lysates (50 μg) were separated by 10% gel electrophoresis and electrophoretically transferred to nitrocellulose paper. The nitrocellulose paper was incubated with anti-ERα (1:1,000, MC-20; Santa Cruz Biotechnology), anti-ERβ (1:1,000, PA1–311; Affinity Bioreagents, Golden, CO) or anti-actin (1:20,000; Sigma, St. Louis, MO) antibodies, followed by incubation with horseradish peroxidase or alkaline phosphatase-conjugated secondary antibodies, and developed using an enhanced chemiluminescence (ECL) or 5-bromo-4-chloro-3-indolyl phosphate/nitroblue tetrazolium solution. Tumor cells were infected with Ad-25ERE-GFP adenoviruses at a multiplicity of infection of ~100. Cells were precultured in serum-free DMEM/F12 for 1 day and treated with 10 nM 17-β estradiol. Green fluorescent protein fluorescence was detected 24 h after 17-β estradiol treatment.

RESULTS

Generation of the Floxed *p53* Allele. We engineered the floxed *p53* allele (designated *p53^{fp}*) by inserting the *loxP* sites into introns 4 and 6 of *p53* through a two-step process (Fig. 1, *A* and *B*). The phosphoglycerate kinase neomycin resistance cassette was subsequently removed by transient expression of Cre recombinase. Deletion

of exons 5 and 6 led to an in-frame deletion of 99 codons (codons 123–221) that encode part of the DNA-binding domain. The presence of *loxP* sites in introns 4 and 6 did not interfere with the transcription of *p53*, and the full-length p53 protein was detected in *p53^{fp/fp}* mouse embryonic fibroblasts in the absence of Cre recombinase (Fig. 1*C*). A smaller protein product of expected mass of 39 kDa, designated p53^{Δ5,6}, was detected in *p53^{fp/fp}* mouse embryonic fibroblasts infected with Cre adenoviruses (Fig. 1*C*). IR-induced responses demonstrate that p53^{Δ5,6} is transcriptionally inactive and fails to increase p21 target gene transcription. In contrast to wild-type p53, mutant p53^{Δ5,6} protein was not stabilized after IR (Fig. 1*D*). No p53 protein was detected from mouse embryonic fibroblasts derived from *p53-null* (*p53^{-/-}*) mice (Fig. 1, *C* and *D*).

Characterization of Cre-Transgenic Mice. To introduce somatic *p53* mutation in the mammary gland, different lines of mice expressing Cre under the control of MMTV-long terminal repeat, *MMTVCre^a*, and *MMTVCre^b* (collectively termed *MMTVCre*) were generated. In addition, to express Cre specifically in mammary luminal epithelial cells, *WAPrtTACre*-transgenic mice in which Cre is regulated by the whey acidic protein (WAP) promoter were also used (31). In the *MMTVCre^a* line, Cre activity was restricted to the mammary gland, whereas in *MMTVCre^b* and *WAPrtTACre* lines, Cre-mediated deletion was observed in many tissues (Fig. 2*A*). In contrast to the founder mice, when the *WAPrtTACre* transgene was bred to floxed *p53* or reporter mice (see below), its activity became independent of doxycycline and pregnancy, likely attributable to modification of the transgene, and/or the unstable nature of the multicopy transgene. The altered transgene will be referred to as *WAPCre^c* hereafter.

Because transgene activity varies depending on promoter and insertion sites, Cre-transgenic mice were crossed with *R26R* mice expressing LacZ after the removal of the floxed stop sequence by Cre (29) to identify the cell types targeted by Cre-mediated recombination in the mammary gland (Fig. 2*B*; Table 1; data not shown). In nulliparous *MMTVCre^a; R26R* mice, LacZ was detected in ~0.7% cells of mammary gland. The expression remained low during 1st pregnancy and reached ~2.9% at 2nd pregnancy in both luminal epithelial and myoepithlial cells but not in stromal fibroblasts and adipocytes. In *MMTVCre^b; R26R* mice, LacZ expression was also found in 5.6% of those cells in 2-week-old and ~20% in 7-week-old nulliparous mice. The expression increased to >60% in pregnant mice. The increased percentage of targeted cells in multiparous mice is expected, because MMTV promoter activities are up-regulated during pregnancy. In *WAPCre^c; R26R* mice, LacZ activities were robust with 66% positive cells in 1-week-old and >90% in 17-day-old and 6-week-old nulliparous and pregnant mice. Thus, there are significantly higher numbers of targeted cells in *WAPCre^c* than in *MMTVCre* mice during prepubertal/pubertal stages.

Effects of *p53* Inactivation on Spontaneous Mammary Carcinogenesis. As expected, these mice develop tumors with different spectrums. The most common tumor type is mammary tumor, and the majority of mammary tumor-bearing mice (60–80%) had multiple primary mammary tumors (Fig. 3; Table 2). Mammary tumor latency varied depending partly on numbers of targeted cells and parity of mice. Nulliparous *p53^{fp/fp}MMTVCre^a* females developed mammary tumors between 14 and 24 months of age with a median tumor latency (MTL) of 17.5 months with almost complete penetrance (23 of 24 mice), whereas all multiparous *p53^{fp/fp}MMTVCre^a* mice developed mammary tumors with a significantly shortened latency, between 11.5 and 24 months of age with a MTL of 15.5 months (*P* = 0.004, generalized Wilcoxon statistic). Both larger numbers of targeted cells as well as pregnancy-mediated cell proliferation could contribute to the shortened MTL. Nulliparous *p53^{fp/fp}MMTVCre^b* females developed mammary tumors between 6 and 14 months of age with a MTL of 10.5 months in nearly 50% of mice (9 of 19 mice), whereas
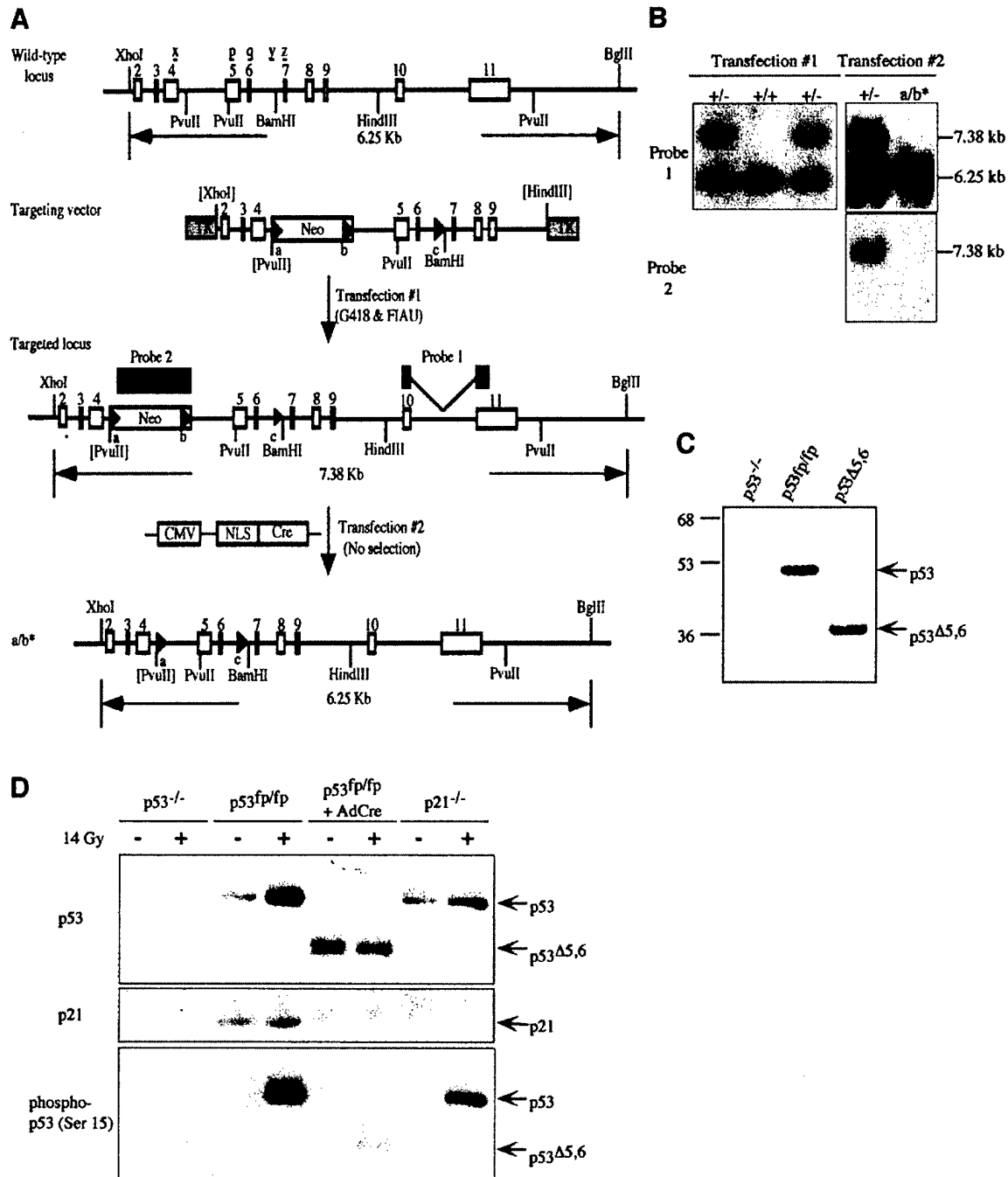
Fig. 1. Generation of conditionally inactivated p53 alleles. A, maps of a portion of the wild-type p53 locus, the targeting construct p53neoloxp[3]2TK, the targeted p53 locus, and the floxed p53 allele (a/b*). B, Southern analysis of embryonic stem clones. DNA was digested with XhoI plus BglII and hybridized with probe 1 containing exon 10 and part of exon 11 (top) or probe 2 containing neo sequence (bottom). Clone a/b* carried a/b recombination, as shown by a 6.25-kb band when hybridized with probe 1 (top) and without signal when hybridized with probe 2 (bottom). The sizes of wild-type (6.25 kb) and targeted (7.38 kb) bands are also shown. C, Western analysis of p53 protein in mouse embryonic fibroblasts (MEFs). Expression of p53 protein in MEFs prepared from p53-null (p53^{−/−}) mice and p53-floxed (p53[fp/fp]) mice, and in Cre adenoviruses infected p53[fp/fp] MEFs are shown. D, Western analysis of p53 protein levels (top), p21 induction (middle), and Ser-15 phosphorylation of p53 (bottom) in MEFs treated with 14Gy IR. FIAU, 1-(2-deoxy-2-fluoro-β-D-arabinofuranosyl)-5-iodouracil; TK, thymidine kinase; CMV, cytomegalovirus; NLS, nuclear localization signal.

multiparous p53[fp/fp]MMTVCre[b] mice developed mammary tumors between 7 and 12 months of age with a MTL of 11 months in 60% of mice (12 of 20 mice). The MTL of p53[fp/fp]MMTVCre[b] mice is significantly shorter than that of p53[fp/fp]MMTVCre[a] mice (P < 0.001), indicating distinct mammary carcinogenesis kinetics in mice with 1 or 3% versus ≥20% of p53-mutated cells. However, there is no statistical difference in the median MTL between 20% targeted cells in nulliparous and 60% in multiparous p53[fp/fp]MMTVCre[b] mice (P = 0.29). The lower penetrance of mammary tumors in

p53[fp/fp]MMTVCre[b] was attributable to the presence of other tumor types leading to early death. In p53[fp/fp]WAPCre[c] mice, mammary tumors developed between 8 and 12.5 months of age with a MTL of 9.5 months with high penetrance (13 of 14 mice). Consistent with the findings in p53[fp/fp]MMTVCre[b], increasing targeted cells to >90% did not shorten the MTL further (P = 0.29). Of note, only one 23.5-month-old multiparous heterozygous p53[+/fp]MMTVCre[a] mouse developed palpable mammary tumor in a cohort of mice between 20 and 26 months of ages (n = 12; data not shown). The apparent long tumor

Fig. 2. Characterization of Cre activity. *A,* PCR analysis of Cre-mediated excision of floxed *p53* alleles in *p53^{fp/fp}; Cre* mice. Primer pair x/z amplified a ~500-bp product in the deleted allele and a 377-bp fragment for the pseudogene, and primer pair p/q amplified a 327-bp product in the wild-type allele as well as a 253-bp fragment for the pseudogene. Tissue DNA samples were derived from *p53^{fp/fp}MMTVCre^a* (*a*), *p53^{fp/fp}MMTVCre^b* (*b*), and *p53^{fp/fp}WAPCre^c* (*c*) mice. Nontransgenic, non-Cre-transgenic mammary gland; Mg (1st), (3rd), (4th), and (parous), mammary gland of 1st, 3rd, 4th pregnancy and of a parous female. *B,* β-galactosidase staining of cells in the mammary gland of *Cre; R26R* mice. *a-c,* mammary gland from *MMTVCre^a; R26R* mice, nulliparous (*a*), 1st pregnancy (*b*), 2nd pregnancy (*c*). *Arrow* in *c* indicates β-galactosidase detection in a myoepithelial cell; *d-f,* mammary gland from *MMTVCre^b; R26R* mice, 2-week-old (*d*), nulliparous (*e*), 1st pregnancy (*f*); *g-i,* mammary gland from *WAPrtACre; R26R* mice, 1-week-old (*g*), nulliparous (*e*), 1st pregnancy (*f*). Counterstained with nuclear fast red. Original magnifications, ×200.

Table 1 *Cre-mediated recombination in Cre; R26R mice*

Cre transgene	Nulliparous/ pregnant	Site	X-gal positive cells (%) (mean ± SE)[a]
MMTVCre[a]	Nulliparous (d42)	End bud/duct	0.73 ± 0.37 (n = 12)
	1st pregnancy	Alveoli	0.22 ± 0.12 (n = 12)
	2nd pregnancy	Alveoli	2.85 ± 0.44 (n = 12)
MMTVCre[b]	Nulliparous (d50)	End bud/duct	18.97 ± 3.19 (n = 12)
	1st pregnancy	Alveoli	56.71 ± 0.06 (n = 12)
WAPCre[c]	Nulliparous (d44)	End bud/duct	90.73 ± 0.02 (n = 12)
	1st pregnancy	Alveoli	96.80 ± 0.02 (n = 24)

[a] SE, standard error.

latency suggests that the internally truncated mutant p53 protein expressed under the endogenous promoter might not work in a dominant-negative manner.

Mammary tumors in all groups of mice are heterogeneous including adenocarcinoma, myoepithelial adenocarcinoma, adenosquamous carcinoma, and spindle cell tumor (Fig. 4, A-D). The majority of tumors were poorly differentiated invasive adenocarcinomas that share the most histopathological similarity with human tumors. In addition to mammary tumors, a few $p53^{fp/fp}MMTVCre^a$ mice also developed lymphoma caused by a very low level of Cre activity in the lymphocytes or a low spontaneous incidence in aged C57BL/6 × 129sv mice. On the other hand, other tumor types were found in $p53^{fp/fp}$-$MMTVCre^b$ and $p53^{fp/fp}WAPCre^c$ mice caused by a broader Cre expression pattern (Table 2; Fig. 2A).

Importantly, up to half of $p53^{fp/fp}MMTVCre^a$ mice had mammary tumor metastasis either in lung and/or liver after gross examination (Table 2; Fig. 4, E and F). Metastatic mammary tumor foci were also detected in $p53^{fp/fp}MMTVCre^b$ and $p53^{fp/fp}WAPCre^c$ mice (Table 2).

Molecular Characterization of Mammary Tumors. Estrogen is critical in the etiology of breast cancer and ERα mediates estrogen

responsiveness in breast cancer. Significantly, 40% of the $p53^{fp/fp}WAPCre^c$ mice ($n = 15$) had both ERα- and PR-positive tumors (Fig. 4H), compared with 42 tumors from $p53^{fp/fp}MMTVCre$ mice that were all ERα- and PR-negative (Fig. 4G). The percentage of ERα-positive cells in ERα-positive tumors is over 90% whereas in ERα-negative tumors, no ERα-positive tumor cells were seen. The expression of ERα in tumors from $p53^{fp/fp}WAPCre^c$ but not $p53^{fp/fp}$-$MMTVCre$ mice was further confirmed by Western blotting analysis (Fig. 4L). In contrast to ERα, ERβ was expressed in all tumors (Fig. 4L and data not shown). The closely correlated expression of ERα and PR, a downstream target of ER, suggests that ERα is functional in ERα-positive tumors. To further test this notion, adenoviruses carrying green fluorescent protein regulated by estrogen-response elements (EREs; 32) were used to infect tumor cells prepared from $p53^{fp/fp}$-$MMTVCre$ and $p53^{fp/fp}WAPCre^c$ mice. After treatment with estradiol, green fluorescent protein-positive cells were detected in tumor cells from $p53^{fp/fp}WAPCre^c$ but not $p53^{fp/fp}MMTVCre$ mice (Fig. 4M). Thus, ERα in the ERα-positive $p53^{fp/fp}WAPCre^c$ tumors is transcriptionally active.

Deregulation of ERα expression during the premalignant stages of human breast carcinogenesis has been reported (33). Correspondingly, an increase of ERα-positive cells as well as clusters of ERα-positive cells (Fig. 4, J-K), in contrast to singularly distributed ERα-positive cells in the normal gland, was observed in mammary intraepithelial neoplasia (34) but not in hyperplasia without atypia (Fig. 4I). Thus, similar to human breast cancer, there are multistep histopathological changes and alterations in the ERα expression pattern during the progression of mammary carcinogenesis in these models.

Frequent genetic changes and prognostic markers of human breast cancer have been identified. To test whether this mouse model parallels human breast cancer in these alterations, selected genes were

Fig. 3. Tumor-free survival curves in $p53^{fp/fp}$; Cre mice. Survival curves were computed using the Kaplan-Meier product-limit method and compared using the generalized Wilcoxon statistic. Animals sacrificed before development of a mammary tumor are censored at the time of sacrifice and are shown with *vertical tick marks* plus *asters*. The numbers of mice are as follows: nulliparous $p53^{fp/fp}MMTVCre^a$ ($n = 23$); multiparous $p53^{fp/fp}MMTVCre^a$ ($n = 43$); nulliparous $p53^{fp/fp}MMTVCre^b$ ($n = 19$); multiparous $p53^{fp/fp}MMTVCre^b$ ($n = 20$); and parous $p53^{fp/fp}WAPCre^c$ ($n = 14$).

Table 2 *Tumor formation in $p53^{fp/fp}$; Cre mice*

Cre transgene	MMTVCre[a] (Nulliparous)	MMTVCre[a] (Multiparous)	MMTVCre[b] (Nulliparous)	MMTVCre[b] (Multiparous)	WAPCre[c] (Parous)
Total number of mice	14	37	19	20	12
Mammary tumor	14 (100%)	37 (100%)	9 (47%)	12 (60%)	11 (92%)
Lymphoma	2 (14%)	6 (16%)	15 (79%)	15 (75%)	5 (42%)
Other tumor types[a]	−[c]	−	−	−	2 (17%)
Metastasis[b]	7 (50%)	13 (35%)	1 of 3 (33%), IC[d]	1 of 4 (25%), IC	4 (36%)
Multiple mammary tumors	11 (79%)	22 (59%)	3 of 4 (75%), IC	7 of 10 (70%), IC	8 (67%)
Median tumor latency (months)	17.5	15.5	10.5	11	9.5

[a] Other tumor types, such as soft tissue tumors.
[b] The number of mammary tumor bearing-mice had metastasis of mammary tumor origin.
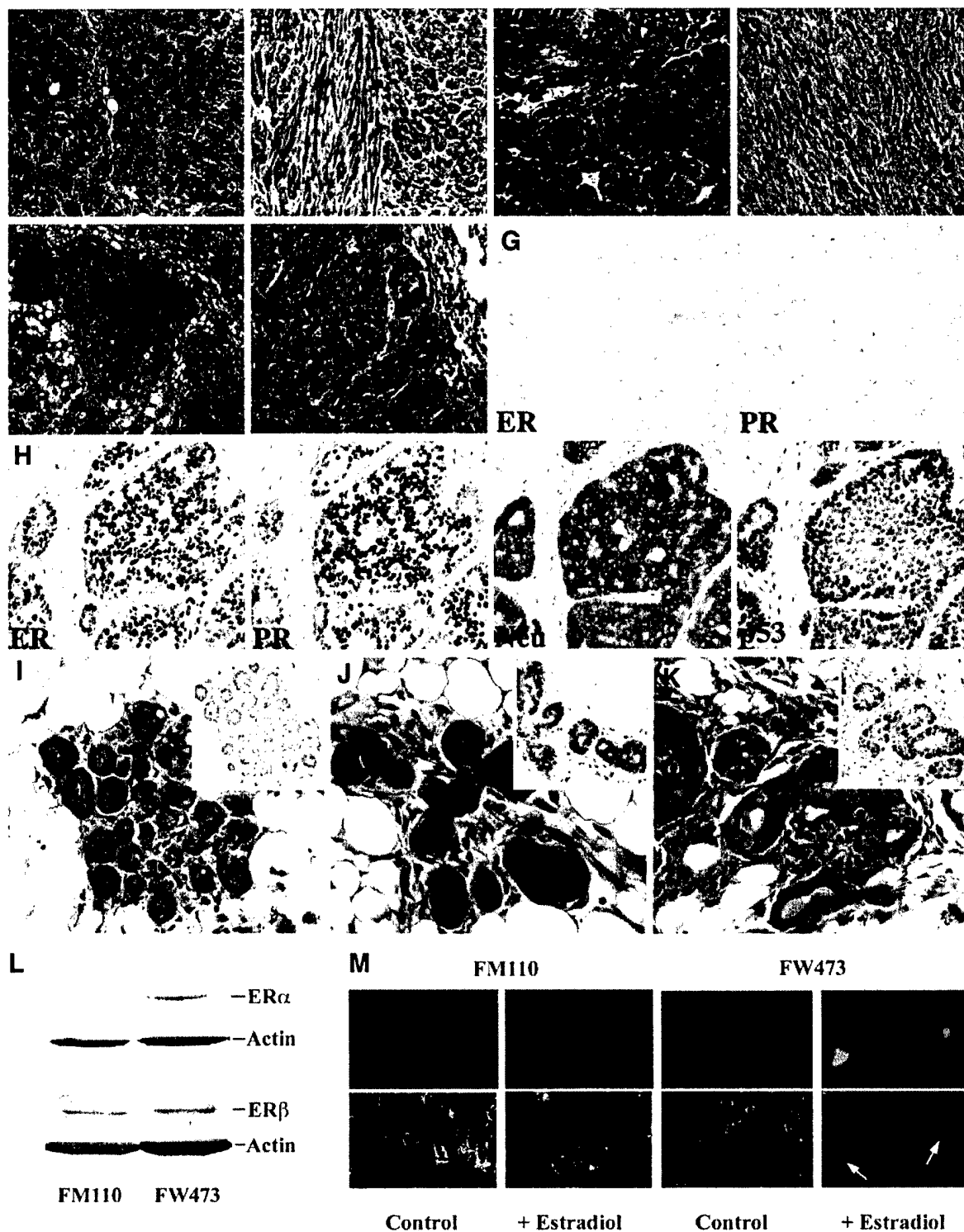[c] −, not detected.
[d] IC, incomplete.

Fig. 4. Histological characterization of mammary tumors. Primary mammary tumors from p53^{fp/fp}; Cre mice showed various histological features, including adenocarcinoma (A), myoepithelial adenocarcinoma (B), squamous cell carcinoma (C), and spindle cell tumor (D). Metastatic mammary tumors in the liver (E) and lung (F). Immunophenotypes of mammary tumors showing estrogen receptor α (ERα)- and PR-negative staining (G), and ERα-, PR-, Neu-, and p53-positive staining (H). I-K, premalignant lesions of mammary gland. I, hyperplasia without atypia with negligible ERα expression (inset). J-K, mammary intraepithelial neoplasia (MIN) with increased ERα expression (inset). L, Western analysis of ERα and ERβ expression in tumors from p53^{fp/fp}MMTVCre^a (FM110) and p53^{fp/fp}WAPCre^c (FW473) mice. M, estrogen and estrogen receptor responsiveness of tumor cells. Fluorescence microscopy analysis of ERα-negative tumor cells (FM110) and of ERα-positive tumor cells (FW473) infected with Ad-25ERE-GFP in the presence or absence of estradiol. Original magnifications, ×200 (A-F) and ×400 (G-K).

examined (Fig. 5). Amplification or overexpression of c-myc proto-oncogene is frequently observed in human breast cancer (35). In this model, c-myc amplification is found in ~35% of mammary tumors from p53^{fp/fp}MMTVCre mice (Fig. 5A). About two-thirds of tumors from p53^{fp/fp}MMTVCre and p53^{fp/fp}WAPCre^c mice showed Neu/

erbB2 overexpression by immunostaining and Western blot analysis using anti-Neu/erbB2 and phosphotyrosine antibodies (Figs. 4H and 5B). Overexpressed Neu/erbB2 appears to be active because tyrosine residues of the receptors are phosphorylated (Fig. 5B). In addition, the activity of matrix metalloproteinase (MMP), matrix metalloproteinase

A

B

C

D

Fig. 5. Molecular characterization of mammary tumors. *A*, Southern blotting analysis of *c-myc* amplification in mammary tumors. The gene from which each probe is derived is given at *left*. The number between *top* and *bottom blots* indicates the relative intensity of *c-myc* signal (fold) of tumors (*T*) compared with the normal control sample (*N*) after normalized with the intensity of *p53* signal. *B*, Western analysis of erbB2 levels using anti-erbB2 (Neu) and phosphotyrosine (p-Tyr) antibodies, truncated p53 protein (p53$^{\Delta5,6}$), and a loading control (p84). *T*, mammary tumors; *N*, normal mammary gland control; *P*, mammary tumor from an *MMTV-Neu*-transgenic mouse. *C*, changes in the relative activity of matrix metalloproteinase 9 (MMP9) and MMP2 in mammary tumors assayed by gelatin zymography. The value was normalized as a ratio to the activity of normal mammary gland. *D*, changes in the expression of several prognostic markers in mammary tumors. The relative levels of mRNAs of AYK1, CDC25B, cyclin E2, and MCM6 were analyzed by reverse transcription-PCR. Each value was normalized using the amount of ribosomal protein S16 reverse transcription-PCR product and was expressed as a ratio to the amount of mRNA in normal mammary gland.

9 but not matrix metalloproteinase 2, was increased dramatically (Fig. 5*C*). Several prognostic markers [*e.g.*, AYK1 (STK15), CDC25B, cyclin E2, and MCM6] identified recently through gene expression profiling in human breast cancer (36, 37) also showed enhanced expression in these tumors (Fig. 5*D*).

DISCUSSION

Mice in a C57BL/6 × 129sv background are normally resistant to mammary tumor development (38, 39), but loss of *p53* leads to a nearly complete incidence of mammary tumor with a high rate of metastasis to lung or liver. As the number of *p53*-inactivated cells increases, the MTL shortens. MTL reaches a plateau when ≥20% of the cells are targeted, indicating that there is a limit to the rate of breast carcinogenesis. Because ERα-positive mammary tumors develop in prepubertal/pubertal but not in adult mice, the timing of *p53* inactivation might be critical for determining ERα expression. Genetic changes (*e.g.*, in *c-myc* and Her2/Neu/erbB2) and prognostic markers [*e.g.*, AYK1 (STK15), CDC25B, cyclin E2, and MCM6] associated with human breast cancer are also seen in these mouse tumors.

Despite the use of different promoters with Cre, both luminal epithelial

and myoepithelial cells were targeted by Cre recombinase, as indicated by the *Rosa26* reporter strain (29). Heterogeneous tumor types (adenocarcinomas, myoepithelial adenocarcinomas, adenosquamous carcinomas, and spindle cell tumors) were seen in all mouse strains (Fig. 4). The majority of tumors were poorly differentiated invasive adenocarcinomas, which were also the most similar to human tumors histopathologically. Nonmammary tumors were also found, probably attributable to Cre expression in other tissues (Table 2; Fig. 2*A*). About 50% of mammary tumors metastasize to lung or liver (Table 2). Both histopathology and microarray analyses (data not shown) support that lung lesions are indeed tumor metastases. The metastasis frequency correlated with neither specific Cre-transgenic line nor tumor latency, consistent with previous observations (40). This tumor system recapitulates the high frequency of metastasis seen in advanced human breast cancer. By contrast, the experience of some investigators indicated that most mouse tumor models represent an early nonmetastatic stage of tumor development (41). Lung metastasis was also found in *p53$^{-/-}$*-BALB/c mammary gland transplant models (42); however, the precise metastasis rate is not clear.

These mouse mammary tumors exhibit a pattern of mutation and gene dysregulation similar to human breast cancer. Amplification or overexpression of the *c-myc* and *erbB2* proto-oncogenes is frequently observed in human breast cancer (7, 35). About 35% of these mammary tumors were found to have *c-myc* amplification and two-thirds showed erbB2 overexpression. Matrix metalloproteinase 9 and cell cycle regulators such as AYK1 (STK15), CDC25B, cyclin E2, and MCM6 were up-regulated in these tumor cells. This is consistent with the recent results showing that overexpression of these genes in human breast cancer reflects poor prognosis (36, 37). The high frequencies of c-myc amplification and overexpression of erbB2 and cell cycle regulators in *p53*-mutated tumors suggest that these genetic alterations have pivotal roles during tumor progression.

An inverse relationship between the number of targeted cells and MTL was observed. It is reasonable to assume that larger numbers of targeted cells are more likely to acquire critical genetic changes leading to tumor development with shorter latency. Indeed, similar genetic (*e.g.*, *c-myc*) and gene expression changes (*e.g.*, Neu/erbB2, AYK1, CDC25B, cyclin E2, and MCM6) were seen at high frequencies in tumors of both short and long latency. Intriguingly, when the number of targeted cells exceeded 20%, MTL did not shorten further. To explain this phenomena, we assume that cancer initiation depends in part on the accumulation of a certain number of key mutations (43). If the key rate-limiting process was simply the accumulation of one additional mutation, then after the average cell has gone through *T* rounds of cell division, the probability of obtaining the key mutation is *NuT*, where *N* is the number of target cells with the predisposing mutation and *u* is the mutation rate per cell division. If there are two rate-limiting mutational steps, then the probability of obtaining both mutations is, from the gamma distribution, approximately $N(uT)^2/2$. If we suppose *u* is approximately 10^{-6}, and there are about $T = 10$ rounds of cell division, then saturation would happen when *N* is of the order 10^{10}, which is probably much higher than the actual number of cells at saturation. Thus, to explain the saturation kinetics, there are two alternatives. First, the mutation rate per cell division may be higher than 10^{-6}. This may occur because mutations of *p53* increase the mutation rate per cell division. Second, some precancerous clonal expansion may be occurring, which would increase the number of rounds of cell division and therefore decrease the number *N* of initial predisposing target cells needed to achieve saturation. On the basis of results of the *MMTVCre^b* line, it can be concluded that a saturation kinetic is reached by targeting ~20% of mouse mammary epithelial cells. In the *WAPCre^c* line, it is likely that a different population of mammary epithelial cells is targeted; however, the tumor kinetics is similar to that of *MMTVCre^b*. In addition to the number of targeted

cells, it is plausible that the tumor latency might also be reflective of the type of cells targeted. Because multiple cell types are targeted in the models described here, the contribution of cell numbers and types of cells cannot be clearly differentiated.

On the basis of microarray profiling analysis, human breast cancers can be classified into five subtypes (44). It is not clear whether these heterogeneous tumor types are originated from different cells of the mammary gland or specific cancer-initiating cells are targeted and heterogeneity develops subsequently during tumor progression. Recent studies have revealed that a population of breast cancer cells possess stem cell-like properties (45). However, it remains to be studied whether cancer-initiating cells of ERα-positive and -negative tumors are different. In WAPCre^c mice both ERα-positive and -negative mammary tumors were found, although mutations of p53 in MMTVCre mice resulted in only ERα-negative tumors. Parity may not be relevant because ERα-positive tumors were found in both nulliparous and parous p53$^{fp/fp}$WAPCre^c mice. It is plausible that ERα-positive stem cells, in addition to ERα-negative stem cells, are targeted in WAPCre^c mice. In contrast, in MMTVCre mice, only ERα-negative stem cells are targeted. Because nearly 90% of cells are LacZ-positive during second pregnancy in MMTVCre mice (data not shown), this might suggest that only a small population of cells give rise to ERα-positive tumors in these adult parous mice. The Cre transgenes are active at different developmental stages in WAPCre^c and MMTVCre mice. Whether developmental stages affect the abundance of ERα-positive progenitor cells is not clear. Because it is feasible to isolate ERα-positive epithelial cells from normal mammary glands and tumors (32),[8] molecular mechanisms underlying ERα-positive and -negative mammary carcinogenesis can be systematically addressed using this model.

ACKNOWLEDGMENTS

REFERENCES

1. Bieche I, Lidereau R. Genetic alterations in breast cancer. Genes Chromosomes Cancer 1995;14:227–51.
2. Hollstein M, Hergenhahn M, Yang Q, Bartsch H, Wang ZQ, Hainaut P. New approaches to understanding p53 gene tumor mutation spectra. Mutat Res 1999;431:199–209.
3. Malkin D. Germline p53 mutations and heritable cancer. Annu Rev Genet 1994;28:443–65.
4. Hahn WC, Weinberg RA. Modelling the molecular circuitry of cancer. Nat Rev Cancer 2002;2:331–41.
5. Sharpless NE, DePinho RA. p53: good cop/bad cop. Cell 2002;110:9–12.
6. Vogelstein B, Lane D, Levine AJ. Surfing the p53 network. Nature (Lond) 2000;408:307–10.
7. Brison O. Gene amplification and tumor progression. Biochim Biophys Acta 1993;1155:25–41.
8. Donehower LA, Harvey M, Slagle BL, McArthur MJ, Montgomery CA, Butel J, Bradley A. Mice deficient for p53 are developmentally normal but susceptible to spontaneous tumours. Nature (Lond) 1992;356:215–21.
9. Jacks T, Remington L, Williams BO, et al. Tumor spectrum analysis in p53-mutant mice. Curr Biol 1994;4:1–7.
10. Harvey M, McArthur MJ, Montgomery CA Jr, Butel JS, Bradley A, Donehower LA. Spontaneous and carcinogen-induced tumorigenesis in p53-deficient mice [see comments]. Nat Genet 1993;5:225–9.
11. Jerry DJ, Kittrell FS, Kuperwasser C, et al. A mammary-specific model demonstrates the role of the p53 tumor suppressor gene in tumor development. Oncogene 2000; 19:1052–8.
12. Jonkers J, Meuwissen R, van der Gulden H, Peterse H, van der Valk M, Berns A. Synergistic tumor suppressor activity of BRCA2 and p53 in a conditional mouse model for breast cancer. Nat Genet 2001;29:418–25.
13. Anderson E. The role of oestrogen and progesterone receptors in human mammary development and tumorigenesis. Breast Cancer Res 2002;4:197–201.
14. Masood S. Estrogen and progesterone receptors in cytology: a comprehensive review. Diagn Cytopathol 1992;8:475–91.
15. Trichopoulos D, MacMahon B, Cole P. Menopause and breast cancer risk. J Natl Cancer Inst (Bethesda) 1972;48:605–13.
16. Nandi S, Guzman RC, Yang J. Hormones and mammary carcinogenesis in mice, rats, and humans: a unifying hypothesis. Proc Natl Acad Sci USA 1995;92:3650–7.
17. Yoshidome K, Shibata MA, Couldrey C, Korach KS, Green JE. Estrogen promotes mammary tumor development in C3(1)/SV40 large T-antigen transgenic mice: paradoxical loss of estrogen receptor alpha expression during tumor progression. Cancer Res 2000;60:6901–10.
18. Brodie SG, Xu X, Qiao W, Li WM, Cao L, Deng CX. Multiple genetic changes are associated with mammary tumorigenesis in Brca1 conditional knockout mice. Oncogene 2001;20:7514–23.
19. Ludwig T, Fisher P, Ganesan S, Efstratiadis A. Tumorigenesis in mice carrying a truncating Brca1 mutation. Genes Dev 2001;15:1188–93.
20. Ludwig T, Fisher P, Murty V, Efstratiadis A. Development of mammary adenocarcinomas by tissue-specific knockout of Brca2 in mice. Oncogene 2001;20:3937–48.
21. Parker B, Sukumar S. Distant metastasis in breast cancer: molecular mechanisms and therapeutic targets. Cancer Biol Ther 2003;2:14–21.
22. Greenberg PA, Hortobagyi GN, Smith TL, Ziegler LD, Frye DK, Buzdar AU. Long-term follow-up of patients with complete remission following combination chemotherapy for metastatic breast cancer. J Clin Oncol 1996;14:2197–205.
23. Stambolic V, Tsao MS, Macpherson D, Suzuki A, Chapman WB, Mak TW. High incidence of breast and endometrial neoplasia resembling human Cowden syndrome in pten± mice. Cancer Res 2000;60:3605–11.
24. Pattengale PK, Stewart TA, Leder A, et al. Animal models of human disease. Pathology and molecular biology of spontaneous neoplasms occurring in transgenic mice carrying and expressing activated cellular oncogenes. Am J Pathol 1989;135:39–61.
25. Guy CT, Cardiff RD, Muller WJ. Induction of mammary tumors by expression of polyomavirus middle T oncogene: a transgenic mouse model for metastatic disease. Mol Cell Biol 1992;12:954–61.
26. Guy CT, Webster MA, Schaller M, Parsons TJ, Cardiff RD, Muller WJ. Expression of the neu protooncogene in the mammary epithelium of transgenic mice induces metastatic disease. Proc Natl Acad Sci USA 1992;89:10578–82.
27. Lee EY, Chang CY, Hu N, et al. Mice deficient for Rb are nonviable and show defects in neurogenesis and haematopoiesis [see comments]. Nature (Lond) 1992;359:288–94.
28. Howes KA, Ransom N, Papermaster DS, Lasudry JG, Albert DM, Windle JJ. Apoptosis or retinoblastoma: alternative fates of photoreceptors expressing the HPV-16 E7 gene in the presence or absence of p53 [published erratum appears in Genes Dev 1994;8:1738]. Genes Dev 1994;8:1300–10.
29. Soriano P. Generalized lacZ expression with the ROSA26 Cre reporter strain [letter]. Nat Genet 1999;21:70–1.
30. Wagner KU, McAllister K, Ward T, Davis B, Wiseman R, Hennighausen L. Spatial and temporal expression of the Cre gene under the control of the MMTV-LTR in different lines of transgenic mice. Transgenic Res 2001;10:545–53.
31. Utomo AR, Nikitin AY, Lee WH. Temporal, spatial, and cell type-specific control of Cre-mediated DNA recombination in transgenic mice. Nat Biotechnol 1999;17:1091–6.
32. Seth P, Porter D, Lahti-Domenici J, Geng Y, Richardson A, Polyak K. Cellular and molecular targets of estrogen in normal human breast tissue. Cancer Res 2002;62:4540–4.
33. Shoker BS, Jarvis C, Sibson DR, Walker C, Sloane JP. Oestrogen receptor expression in the normal and pre-cancerous breast. J Pathol 1999;188:237–44.
34. Cardiff RD, Anver MR, Gusterson BA, et al. The mammary pathology of genetically engineered mice: the consensus report and recommendations from the Annapolis meeting [see comments]. Oncogene 2000;19:968–88.
35. Liao DJ, Dickson RB. c-Myc in breast cancer. Endocr Relat Cancer 2000;7:143–64.
36. Perou CM, Sorlie T, Eisen MB, et al. Molecular portraits of human breast tumours. Nature (Lond) 2000;406:747–52.
37. van 't Veer LJ, Dai H, van de Vijver MJ, et al. Gene expression profiling predicts clinical outcome of breast cancer. Nature (Lond) 2002;415:530–6.
38. Ullrich RL, Bowles ND, Satterfield LC, Davis CM. Strain-dependent susceptibility to radiation-induced mammary cancer is a result of differences in epithelial cell sensitivity to transformation. Radiat Res 1996;146:353–5.
39. Medina D. Mammary tumorigenesis in chemical carcinogen-treated mice. I. Incidence in BALB-c and C57BL mice. J Natl Cancer Inst (Bethesda) 1974;53:213–21.
40. Lifsted T, Le Voyer T, Williams M, et al. Identification of inbred mouse strains harboring genetic modifiers of mammary tumor age of onset and metastatic progression. Int J Cancer 1998;77:640–4.
41. Van Dyke T, Jacks T. Cancer modeling in the modern era: progress and challenges. Cell 2002;108:135–44.
42. Kuperwasser C, Hurlbut GD, Kittrell FS, et al. Development of spontaneous mammary tumors in BALB/c p53 heterozygous mice: a model for Li-Fraumeni syndrome. Am J Pathol 2000;157:2151–9.
43. Knudson AG. Antioncogenes and human cancer. Proc Natl Acad Sci USA 1993;90:10914–21.
44. Sorlie T, Perou CM, Tibshirani R, et al. Gene expression patterns of breast carcinomas distinguish tumor subclasses with clinical implications. Proc Natl Acad Sci USA 2001;98:10869–74.
45. Al-Hajj M, Wicha MS, Benito-Hernandez A, Morrison SJ, Clarke MF. Prospective identification of tumorigenic breast cancer cells. Proc Natl Acad Sci USA 2003;100:3983–8.

[8] M. J. McArthur, C. A. Montgomery, J. Butel, A. Bradley, unpublished data.

The human checkpoint Rad protein Rad17 is chromatin-associated throughout the cell cycle, localizes to DNA replication sites, and interacts with DNA polymerase ε

Sean M. Post, Alan E. Tomkinson and Eva Y.-H. P. Lee*

Department of Molecular Medicine/Institute of Biotechnology, University of Texas Health Science Center at San Antonio, 15355 Lambda Drive, San Antonio, TX 78245, USA

ABSTRACT

The checkpoint Rad proteins Rad17, Rad9, Rad1, Hus1, ATR, and ATRIP become associated with chromatin in response to DNA damage caused by genotoxic agents and replication inhibitors, as well as during unperturbed DNA replication in S phase. Here we show that murine Rad17 is phosphorylated at two sites that were previously shown to be modified in response to DNA damage, independent of DNA damage and ATM, in proliferating tissue. In contrast to studies with *Xenopus laevis* extracts but similar to observations in *Schizosaccharomyces pombe*, the level of chromatin-bound hRad17 remains relatively constant during the cell cycle and does not change significantly in response to DNA damage or replication block. However, phosphorylated hRad17 preferentially associates with the sites of ongoing DNA replication and interacts with the DNA replication protein, DNA polymerase ε. These results provide a link between the DNA damage checkpoint machinery and the replication apparatus and suggest that hRad17 may play a role in monitoring the progress of DNA replication via its interaction with DNA polymerase ε.

INTRODUCTION

Damage to the genome, arising from replication errors and environmental factors, pose a grave threat to genomic stability and can ultimately lead to cancer formation. Cell cycle checkpoints prevent this damaged DNA from being replicated and passed on to future daughter cells (1,2). A group of six proteins called the checkpoint Rad proteins, first identified in *Schizosaccharomyces pombe* and *Saccharomyces cerevisiae*, mediate checkpoint activation, including the intra-S checkpoint and the S/M checkpoint, in response to DNA damage

during DNA replication or incomplete replication, respectively (3,4). Human homologs of these checkpoint Rad proteins (hRad17, hRad9, hRad1, hHus1, ATRIP, and ATR) are required to activate cell cycle checkpoints through a signaling cascade to the downstream checkpoint effector Chk1 (5–11). Upon activation, Chk1 phosphorylates and thereby negatively regulates the phosphatase Cdc25 and activates the kinase Wee1 (12–16). Activation of Chk1 also results in the inactivation of Cdc2, which is required for the cell to progress through the G$_2$/M checkpoint (17,18). In mice, this checkpoint-signaling cascade appears to be required for embryogenesis. Cells derived from early embryos of Atr$^{-/-}$-, Hus1$^{-/-}$- and Chk1$^{-/-}$-deficient mice are sensitive to DNA damage, have an aberrant G$_2$/M checkpoint and exhibit spontaneous genomic instability (8,19–23).

Xenopus laevis egg extracts have been used to elucidate the role of checkpoint Rad proteins in the regulation of DNA replication and checkpoint activation during DNA synthesis. Initiation of DNA replication by the primase activity of DNA polymerase α is required for the chromatin association of *X.laevis* (Xl)ATR (24). Immunodepletion of XlATR, even in untreated extracts, abrogates the phosphorylation of Chk1 and the subsequent S/M replication checkpoint, resulting in a shortened cell cycle (25,26). Additionally, XlHus1 and XlRad17 are required for the S/M replication checkpoint and checkpoints activated in response to DNA damage or replication inhibitors (27–29). Unlike the replication-dependent loading of XlRad17, a significant portion of fission yeast *S.pombe* (Sp)Rad17 is bound to the chromatin throughout the cell cycle (30); however, there is a dynamic change in the amount of chromatin-bound SpRad17 in response to different genotoxic agents. Exposure to replication inhibitors results in the release of SpRad17 from the chromatin (31), whereas treatment with DNA-damaging agents causes an increase in chromatin-associated SpRad17 (30). Although these data suggest that the checkpoint Rad proteins function during S phase to monitor the progression of DNA replication and/or replication forks, it is not known how the checkpoint Rad proteins perform this monitoring function.

*To whom correspondence should be addressed at present address. Tel: +1 949 824 9766; Fax: +1 949 824 9767; Email: elee@uci.edu
Present address:
Eva Y.-H. P. Lee, Department of Biological Chemistry and Department of Developmental and Cell Biology, University of California–Irvine, Sprague Hall, Room 122, 839 Medical Science Court, Irvine, CA 92697, USA

Rad17 is closely related to the five replication factor C (RFC) subunits (32–35). The pentameric RFC complex loads proliferating cell nuclear antigen (PCNA) onto the DNA during replication. hRad17 replaces the large subunit of RFC, p140, in an alternative form of the clamp-loading complex that interacts with the PCNA-like heterotrimeric Rad9–Rad1–Hus1 (9-1-1) complex (36). Recent biochemical studies with the homologous complexes isolated from budding yeast have demonstrated that the alternative RFC-like complex linked with checkpoint activation has clamp-loading activity (37). In agreement with the functional interaction between the hRad17 clamp-loading complex and the 9-1-1 complex *in vitro*, DNA damage-dependent chromatin association of hRad9 requires hRad17 *in vivo* (7). Furthermore, phosphorylation of hRad17 by ATR on Ser635 and Ser645 in response to DNA damage and replication block stimulates the interaction between hRad17 and the 9-1-1 complex (38). Interestingly, hRad17 is also phosphorylated on these same two serine residues during unperturbed S phase, suggesting a role for hRad17 during DNA replication (6). In support of this idea, human cells engineered for conditional deletion of hRad17 alleles undergo endoreduplication after loss of hRad17 function (39). Recent reports have demonstrated that the checkpoint Rad protein hRad9 interacts with TopBP1, a DNA polymerase ε subunit, even in the absence of DNA damage (40). Additionally, hRad9 was shown to interact with PCNA (41,42). These observations suggest that the checkpoint Rad proteins may monitor DNA replication by interacting with the DNA replication machinery.

As noted above, there are differences in the regulation of Rad17 subnuclear localization among different eukaryotes. Therefore, we have examined the behavior of mammalian Rad17 during S phase. Here we show that mammalian Rad17 is phosphorylated during unperturbed S phase in replicating tissue in a DNA damage-independent and ATM-independent manner. We demonstrate that the level of chromatin-associated hRad17 remains constant throughout the cell cycle, in response to genotoxic agents, and regardless of phosphorylation status. Finally, we show that phosphorylated hRad17 localizes to sites of DNA replication and interacts with the DNA replication machinery.

MATERIALS AND METHODS

Collection of murine tissues samples

One-month-old wild-type ($Atm^{+/+}$) and ATM-deficient ($Atm^{-/-}$) mice were treated with 10 Gy ionizing radiation (IR) and then killed 1 h post-treatment. IR was performed using a ^{137}Cs γ-irradiator (Shepherd) at 2.08 Gy/min. Tissues were collected and frozen in liquid nitrogen. Extracts were prepared by grinding frozen tissues prior to resuspension in lysis 250 buffer (50 mM Tris pH 7.4, 250 mM NaCl, 2 mM EDTA and 1.0% NP-40) supplemented with a cocktail of protease and phosphatase inhibitors containing 10 μg/ml aprotinin, 1 mM phenylmethylsulfonyl fluoride, 100 mM sodium fluoride, 1 mM sodium orthovanidate, 1 mM benzamide and 1 mM β-glycerophosphate. Proteins were separated by SDS–PAGE and transferred to PVDF membranes (Millipore). Membranes were incubated with the indicated antibodies

and antigen–antibody complexes were detected with an enhanced chemiluminescence kit (Amersham).

Antibodies

Mouse α-hRad17 (31E9) monoclonal antibodies have been described previously (35). Characterization of the rabbit α-hRad17 phospho-specific polyclonal antibodies has been reported previously (6). Mouse α-HA.11 (Babco), α-DNA polymerase ε (93H3A) (NeoMarkers), α-PCNA (PC10) (Santa Cruz), α-Flag (M2) (Sigma) and α-Mek2 (Cell Signaling) were purchased from commercial sources. Rabbit α-Orc2 was a kind gift from Dr Bruce Stillman.

Generation of cell lines

MCF-7 cells were cultured in Dulbecco's modified Eagle's medium (DMEM) (Gibco) supplemented with 15% fetal calf serum (FCS) (Gibco) and 1 mg/ml insulin (Sigma). To generate tetracycline-inducible stable cell lines, MCF-7 cells were transfected with the doxycycline repressible plasmid pUHG 15-1 and selected in 1 mg/ml neomycin for 2 weeks. Regulation of protein expression in selected cells was determined by transient transfection with the reporter plasmid pTRE-2dGFP (Clontech) in the presence or absence of doxycycline. Cells expressing N-terminal HA-tagged hRad17 were generated by co-transfecting each construct, at a 10:1 ratio with pPuro (Stratagene), followed by selection in 500 ng/ml puromycin (Sigma). Stable MCF-7 clones expressing the wild-type or the phosphorylation site mutant of hRad17 were maintained in DMEM supplemented with 15% FCS, 1 mg/ml insulin, 400 μg/ml G-418 (Gibco), 100 ng/ml puromycin and 1 mg/ml doxycycline (Sigma). Expression of wild-type and phosphorylation site mutants of HA-hRad17 was induced by removing doxycycline from the medium for 72 h. Expression of recombinant protein was determined by immunoblotting. Synchronized and unsynchronized T24 cell lines and HeLa cell lines were cultured as previously described (6,43).

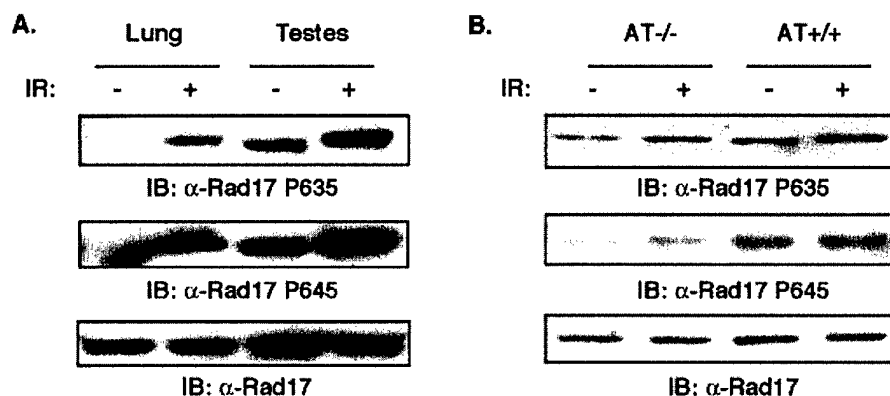### Fluorescence-activated cell sorting

The human bladder carcinoma T24 cells were density arrested and released as described previously (6,43,44). After trypsinization, cells were harvested, washed with phosphate-buffered saline (PBS), resuspended in 70% ice-cold ethanol and then incubated at 4°C for 30 min. Cells were spun down, washed with PBS and resuspended in PBS containing 0.1% Triton X-100 and 200 μg/ml RNase A (Sigma) prior to incubation for 30 min at room temperature. Finally, cells were stained with 20 μg/ml propidium iodide and then analyzed using a FACScan (Becton-Dickinson).

DNA damage and replication inhibition

Hydroxyurea was added to cell culture medium at a final concentration of 1 mM for 24 h, aphidicolin at a final concentration of 5 μg/ml for 20 h and actinomycin D at a final concentration of 1 μg/ml for 6 h. Cell extracts were prepared from mock- or IR-treated cells 1 h post-treatment.

Cell lysate preparation

Whole cell extracts were prepared by lysing cells in RIPA buffer (50 mM Tris, 150 mM NaCl, 1.0% NP-40, 0.5% DOC and 0.1% SDS) supplemented with protease and phosphatase

Figure 1. Phosphorylation of MmRad17 in replicating and quiescent mouse tissues. (A) Phosphorylation of MmRad17 in testis and lung tissues. Mice were mock-treated or treated with 10 Gy IR and killed 1 h post-treatment. Lysates were prepared from testes and lung tissues for western blotting analysis. (B) Phosphorylation of MmRad17 in *Atm*^{-/-} mice. Mice were treated as described above.

inhibitors as above. Chromatin fractionation was performed using modifications to a previously described method (7,44,45). Briefly, equal numbers of synchronized or treated cells were washed twice in ice-cold PBS followed by incubation in buffer A (10 mM HEPES pH 7.9, 10 mM KCl, 1.5 mM MgCl, 0.34 M sucrose, 10% glycerol, 0.5% Triton X-100 and protease and phosphatase inhibitors) for 5 min. After low speed centrifugation, the supernatant cytoplasmic fraction (Cyto) was removed. The pellet containing nuclei was washed in buffer A and then lysed in buffer B (3 mM EDTA, 0.2 mM EGTA and protease and phosphatase inhibitors). Soluble nuclear proteins (Nuc Sol) were separated from the chromatin fraction (Chr) by low speed centrifugation. The chromatin-enriched pellet was washed in buffer B and resuspended in 2× SDS sample buffer and sonicated three times for 15 s.

Immunofluoresence

T24 cells were seeded onto 12 mm glass coverslips that had been pre-coated for 30 min with 0.1% gelatin and prepared for immunostaining as described previously (46). Briefly, cells were washed twice in cold PBS and then permeabilized by incubation in PBS containing 0.5% Triton X-100, 2 mM EDTA and 1% bovine serum albumin (BSA) for 15 min at 4°C. After washing with PBS, cells were fixed in 100% methanol at –20°C for 15 min. Cells were washed with PBS and then blocked by incubation with PBS containing 10% FCS for 2 h at room temperature. Antibodies were added and incubated in PBS containing 5% FCS for 2 h. Cells were washed five times in Tris-buffered saline with Tween-20 (TBST) for 10 min and then incubated with goat α-mouse conjugated with fluorescein isothiocyanate (Jackson Immunochemical), goat α-rabbit conjugated with rhodamine B isothiocyanate (Jackson Immunochemical) and 4′,6-diami-dino-2-phenylindole (DAPI) for 1.5 h. After washing in TBST, coverslips were mounted on slides using Immunon mountant.

For bromodeoxyuridine (BrdU) and hRad17 co-localiza-tion, T24 cells were incubated in medium supplemented with 10 μM BrdU for 15 min prior to fixation. Cells were washed twice in cold PBS followed by permeabilization and fixation as above. After treatment with 4 N HCl containing 0.2% Triton X-100 for 10 min, cells were washed with PBS, then
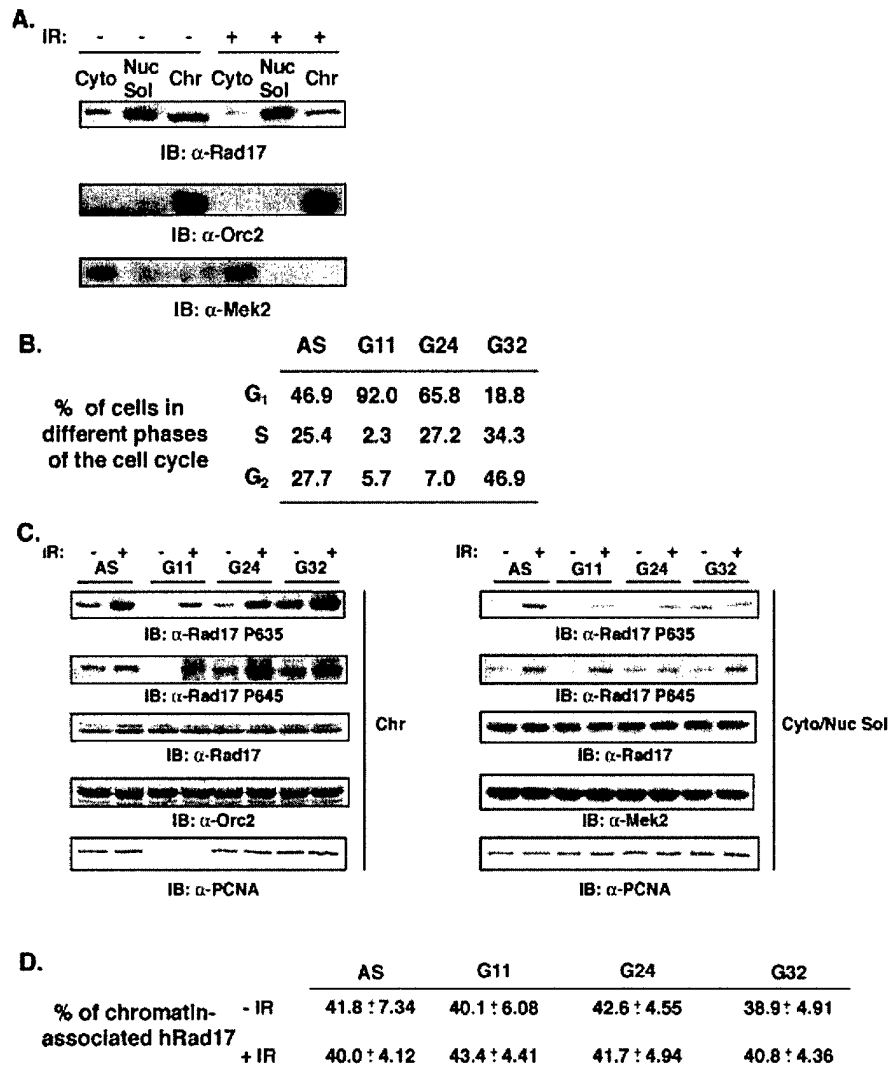
incubated with 50 mM glycine for 5 min, washed once with PBS and then blocked in PBS containing 10% FCS for 2 h at room temperature. Finally, cells were incubated with mouse α-BrdU (Becton Dickinson) and rabbit α-hRad17-phosphoSer645 in PBS containing 5% FCS for 2 h and then visualized as described above.

Immunoprecipitation

Cell lysates were prepared in lysis 250 buffer containing ethidium bromide at a final concentration of 20 μg/ml and supplemented with phosphatase and proteases inhibitors as above. The clarified lysates were incubated with the indicated antibodies followed by incubation with protein G–Sepharose beads for 2 h. Immunoprecipitates were washed four times in lysis 250 buffer and boiled in 2× SDS sample buffer. Proteins were separated by SDS–PAGE and transferred to PVDF membranes (Millipore).

In vitro hRad17 and DNA polymerase ε interaction

The pGEX4T-3 plasmid expressing full-length hRad17 as a GST fusion protein has been described (6). Digestion of this plasmid with EcoRV and SmaI followed by religation generated plasmid GST–hRad17[1-320] that encoded the N-terminal 320 residues of hRad17. Fragments of hRad17 cDNA encoding residues 319–670 and 491–670 were amplified by PCR and then subcloned into pGEX4T-3 to generate plasmids GST–hRad17[319-670] and GST–hRad17[419-670], which encode these C-terminal fragments of hRad17 as GST fusions proteins. GST fusion proteins were expressed and purified according to the manufacturer's protocol (Amersham). Full-length DNA polymerase ε cDNA, a gift from Dr Stuart Linn, was used as a template to synthesize ^{35}S-labeled DNA polymerase ε coupled by *in vitro* transcription–translation using the TNT T7 Quick Kit (Promega). For the GST pull-down assays, equal amounts of GST, GST–hRad17 or GST–hRad17 fragments bound to glutathione–Sepharose beads were incubated with labeled DNA polymerase ε in 50 mM Tris (pH 7.4), 120 mM NaCl, 2 mM EDTA, 0.1% NP-40 and 10% BSA for 2 h at 4°C. After extensive washing, bound proteins were released from the beads by boiling in 2× SDS sample buffer. Labeled DNA polymerase ε was visualized by fluorography after SDS–PAGE.

Figure 2. Chromatin association of hRad17 during the cell cycle and after IR. (A) Analysis of cytoplasmic, nuclear soluble and chromatin-bound proteins. Human T24 fibroblasts were mock-treated or treated with 10 Gy IR and harvested 1 h post-treatment. Cells were fractionated as described in Materials and Methods. After separation by SDS–PAGE, proteins in the cytoplasmic (Cyto), soluble nuclear (Nuc Sol) and chromatin-enriched (Chr) fractions were detected by immunoblotting with the indicated antibodies. Mek2 and Orc2 served as controls for the soluble and chromatin fractions, respectively. (B) Cell cycle distribution of T24 cells determined by FACS analysis. T24 cells were released from density arrest and harvested at the indicated time points, G11, G24 and G32, representing 11, 24 and 32 h after density release, respectively. (C) Chromatin association of hRad17 during the cell cycle. T24 cells were released from density arrest and harvested as above. Cells subjected to DNA damage were harvested 1 h post-treatment. The left panel represents the chromatin-enriched fraction (Chr) while the right panel corresponds to the soluble fractions (Cyto and Nuc Sol). Sample analysis was as described in (A). (D) Percentage of chromatin-associated hRad17 during the cell cycle. Levels of soluble and chromatin-associated hRad17 were determined by densitometry analysis. The average and standard deviation were determined from three separate experiments.

RESULTS

Mammalian Rad17 is phosphorylated in undamaged replicating tissue in an ATM-independent manner

We previously demonstrated that the two DNA damage-dependent phosphorylation sites of hRad17, Ser635 and Ser645, are also phosphorylated at the start of DNA replication in cultured synchronized cells (6). To demonstrate that these phosphorylation events were not caused by the synchronization protocol, we examined the phosphorylation status of murine Rad17 in replicating and non-replicating tissues. Phosphorylation on both Ser647 and Ser657 residues of *Mus musculus* (Mm)Rad17, corresponding to hRad17

Ser635 and Ser645, was observed in extracts from both undamaged and IR-treated testes (Fig. 1A). In contrast to replicating tissue, the same two residues were phosphorylated only after DNA damage in quiescent lung tissue. Since the kinase activity of ATR increases in response to S phase (25), and ATM and ATR are both involved in the activation of S phase-dependent checkpoints (47,48), we asked whether ATM influences the phosphorylation of mammalian Rad17 in replicating tissues after IR. The absence of ATM had little effect on the phosphorylation of MmRad17 in the presence or absence of DNA damage in testes (Fig. 1B). These results, coupled with our previous data demonstrating that ATM is not required for the ionizing irradiation-dependent phosphorylation of Rad17 in quiescent and cycling cells (6), indicates that

A.

IB: α-HA

IB: α-Orc2

IB: α-Mek2

B.

IB: α-HA

IB: α-Orc2

IB: α-Mek2

Figure 3. Replication inhibitors and phosphorylation status does not effect the chromatin association of hRad17. (A) Chromatin association of recombinant wild-type HA-tagged hRad17 in response to DNA damage and replication block. (B) Chromatin association of recombinant phosphomutant HA-tagged hRad17 in response to DNA damage and replication block. Cells expressing HA-tagged hRad17 were mock-treated, treated with 1 μg/ml actinomycin D for 6 h, 5 μg/ml aphidicolin for 20 h or 10 Gy IR or 1 mM hydroxyurea for 24 h. Cells lysates were fractionated as in Figure 2 and subjected to immunoblotting using the indicated antibodies. Doxycycline-treated and untreated whole cell extracts served as a control for loading and expression of HA-hRad17.

mammalian Rad17 is normally phosphorylated during replication in an ATM-independent manner and suggests that hRad17 monitors the progression of DNA replication in unperturbed cells.

Chromatin-associated levels of hRad17 remain constant throughout the cell cycle and in response to DNA damage

Using a fractionation procedure first described in the Stillman laboratory (45), we have examined whether the distribution of hRad17 between the nucleoplasmic and chromatin fractions changes either as a function of cell cycle progression or in response to DNA damage. In asynchronous cells, the majority of hRad17 is in the nucleoplasmic fraction, but an appreciable amount was present in the chromatin fraction (Fig. 2A). In agreement with data from the Elledge laboratory, the level of chromatin-associated hRad17 was not significantly altered by DNA damage (7).
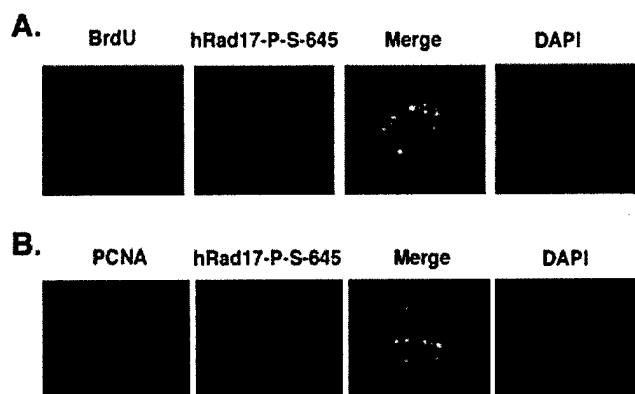
To directly address whether hRad17 is shuttled on and off chromatin during the cell cycle, we density arrested, released and harvested human T24 cells at different phases of the cell cycle. The cell cycle distributions of these synchronized cells were determined by FACS analysis (Fig. 2B). As expected, the replication protein PCNA associates with chromatin at the start of S phase. In contrast to the S phase-dependent chromatin association of PCNA, we observed that ~35–45% of hRad17 is associated with chromatin throughout the cell

cycle, as determined by densitometry (Fig. 2C and D). Thus, the behavior of hRad17 is different from that of XlRad17 (28), which associates with chromatin at the start of DNA replication, but similar to that of *S.pombe*, in which a fraction of Rad17 remains bound throughout the cell cycle (30). Furthermore, DNA damage did not affect the amount of hRad17 localized to the chromatin in specific cell cycle phases (Fig. 2C and data not shown). In contrast to the steady-state levels of chromatin-bound hRad17, there were significant changes in the phosphorylation of chromatin-bound hRad17 during cell cycle progression and in response to DNA damage. hRad17 Ser635 and Ser645 became phosphorylated at the start of S phase in undamaged cells and in IR-treated G_1 cells (Fig. 2C). These results demonstrate that a pool of hRad17 remains bound to the chromatin at all phases of the cell cycle and that the association of hRad17 with the chromatin is not regulated by DNA damage.

Replication inhibitors and phosphorylation status does not effect the chromatin association of hRad17

Next we wanted to determine if hRad17 disassociates from chromatin after treatment with replication inhibitors and, if so, whether phosphorylation of hRad17 is required for this release. To address these questions, we created a stable cell line expressing HA-tagged versions of the wild-type and a phosphorylation site mutant hRad17 from a tetracycline-regulated promoter. Unlike fission yeast (31), the replication

A.

B.

Figure 4. Co-localization of phosphorylated hRad17 with sites of active DNA replication in T24 cells. (A) Co-localization of hRad17-phosphoSer645 with sites of DNA synthesis. hRad17-phosphoSer645 (red fluorescence) and BrdU (green fluorescence) were detected by indirect immunofluorescence. DAPI staining serves a marker for nuclear staining (blue fluorescence, right panel). (B) Co-localization of hRad17-phosphoSer645 with PCNA. PCNA (green fluorescence), hRad17-phosphoSer645 and DNA were detected as above.

A.

B.

Figure 5. Interaction between hRad17 and DNA polymerase ε. (A) Co-immunoprecipitation of phosphorylated hRad17 and DNA polymerase ε. Extracts from mock-treated or irradiated HeLa cells were prepared as described in Materials and Methods. After immunoprecipitation with α-hRad17-phosphoSer645, α-DNA polymerase ε or α-hRad17 antibodies, proteins in the immunoprecipitates were separated by SDS–PAGE and immunoblotted with α-hRad17-phosphoSer645 or α-DNA polymerase ε antibodies. Whole cell extracts served as a positive control and immunoprecipitation with α-Flag antibodies served as a negative control. (B) Interaction between ^{35}S-labeled *in vitro* transcribed/translated DNA polymerase ε and GST–hRad17. *In vitro* transcribed/translated DNA polymerase ε was incubated with equal amounts of GST–full-length hRad17–, GST–N-hRad17$^{1–320}$–, GST–C-hRad17$^{319–670}$– or GST–hRad17$^{419–670}$–Sepharose beads and then separated by SDS–PAGE followed by fluorography. One-tenth load of ^{35}S-labeled *in vitro* transcribed/translated DNA polymerase ε served as a control.

inhibitors hydroxyurea, aphidicolin and actinomycin D did not disrupt the chromatin association of hRad17 (Fig. 3A and B). Furthermore, the identical behavior of the phosphorylation site mutant form of hRad17 indicates that phosphorylation of hRad17 is not required for either the initial association with chromatin or in maintaining the interaction between hRad17 and chromatin after DNA damage or replication block (Fig. 3A and B).

Chromatin-associated and phosphorylated hRad17 co-localizes to sites of DNA replication

Since hRad17 is phosphorylated at the beginning of S phase, we examined whether phosphorylated hRad17 associates with the replication machinery or sites of DNA replication by immunocytochemistry. Prior to fixation, we used a protein extraction method first described in Aboussekhra *et al.* to remove cytoplasmic and soluble nuclear proteins (46). Immunostaining of the fixed T24 cells revealed that phosphorylated hRad17 is extraction resistant and co-localizes with sites of active DNA replication as determined by co-localization with α-BrdU and α-PCNA (Fig. 4A and B). Thus, phosphorylated hRad17 is localized at the sites of ongoing DNA replication.

Human Rad17 interacts with the replication protein DNA polymerase ε

Since phosphorylated hRad17 co-localizes with sites of DNA replication, we examined whether the phosphorylated hRad17 associates with replication proteins. Using lysates from untreated and IR-treated cells, the catalytic subunit of DNA polymerase ε was co-immunoprecipitated by the hRad17 phospho-specific antibody (Fig. 5A). These antibodies have been extensively characterized and shown to exclusively recognize phosphorylated Rad17 (6). In reciprocal experiments, phosphorylated hRad17 was immunoprecipitated by the α-DNA polymerase ε antibody (Fig. 5A). This appears to reflect a specific association between hRad17 and DNA polymerase ε because α-Flag antibodies were unable to immunoprecipitate either DNA polymerase ε or hRad17 and

another replication protein, PCNA, was not co-immunoprecipitated by the hRad17 phospho-specific antibody (data not shown).

Next, we performed *in vitro* binding assays to determine if there is an interaction between these proteins. Full-length *in vitro* transcribed/translated DNA polymerase ε interacted with GST–hRad17 but not GST alone (Fig. 5B). To determine which region of hRad17 interacts with DNA polymerase ε, we generated a GST–N-terminal fragment of hRad17 containing amino acids 1–320 and two GST–C-terminal fragments of hRad17 containing amino acids 319–670 and 419–670, respectively. Similar to the full-length GST–hRad17, both the N-terminal fragment of hRad17$^{1–320}$ and the large C-terminal fragment of hRad17$^{319–670}$ specifically interact with *in vitro* transcribed/translated DNA polymerase ε (Fig. 5B). In contrast, the small C-terminal fragment, encoding amino acids 419–670 of hRad17, did not interact with DNA polymerase ε *in vitro* (Fig. 5B). Together these results demonstrate that hRad17 associates with DNA polymerase ε in cell extracts and suggests that this association is mediated by a direct interaction between DNA polymerase ε and the N- and C-terminal regions of hRad17.

DISCUSSION

Although phosphorylation of hRad17 is required for DNA damage-induced checkpoint activation (6,38), the same residues are also phosphorylated in unperturbed S phase proliferating cells *in vitro* and *in vivo* (Fig. 1) (6). This

phosphorylation pattern is similar to the S phase-dependent checkpoint-signaling pathway observed in both human and *X.laevis*, in which Chk1 is also phosphorylated by ATR in the absence of exogenous DNA damage during DNA replication (25,49). The simplest explanation for these signaling events is that low levels of DNA damage occur during DNA replication and activate the cell cycle checkpoint-signaling cascade. However, DNA damage-dependent checkpoint activation appears unlikely, as hRad9 does not exhibit the characteristic DNA damage-induced mobility shift caused by phosphorylation in the absence of exogenous DNA-damaging agents during S phase (42,50). Thus, it appears that hRad17 phosphorylation occurs as a normal consequence of DNA replication and may reflect the participation of hRad17 in a function associated with DNA replication, in addition to the DNA damage-induced checkpoint pathway.

Here we have shown that ~40% of hRad17 is constitutively chromatin-associated independent of cell cycle phase or the start of DNA replication. This behavior is similar to that observed in *S.pombe* but differs from the observations in *X.laevis* (28,30). Several lines of evidence indicate that phosphorylation of hRad17 does not affect its chromatin association. First, the amount of chromatin-associated hRad17 remains relatively unchanged throughout the cell cycle or in response to genotoxic stress. Second, both the wild-type and phosphorylation site mutant forms of hRad17 associate with chromatin before and after treatment with genotoxic agents (Fig. 3). This further demonstrates that ATR-dependent phosphorylation is not required for Rad17 association with chromatin and is consistent with the observation that the lack of DNA damage- and replication block-induced phosphorylation of hRad17 in Hus1$^{-/-}$ cells does not affect the chromatin association of hRad17 (7).

Interestingly, we observed that phosphorylated hRad17 co-localizes to sites of ongoing DNA replication as determined by co-immunostaining with α-BrdU and α-PCNA antibodies (Fig. 4A and B). These data, coupled with the recent finding of endoreduplication in the absence of hRad17, strongly support the notion that hRad17 has a key role in the regulation of DNA replication and suggest that chromatin-associated, phosphorylated hRad17 may serve as a sensor of DNA replication progression (39). In support of this replication surveillance model, we found that the phosphorylated form of hRad17 associates with DNA polymerase ε, a DNA replication enzyme that has also been implicated in cell cycle checkpoints (51,52). Although it is not known whether hRad17 phosphorylation regulates its interaction with DNA polymerase ε, this interaction provides a physical link between checkpoint and DNA replication proteins. In addition to our results linking DNA polymerase ε with the hRad17 clamp-loading complex, there is a conserved and direct interaction between TopBP1 in humans (Dpb11 in budding yeast), a subunit of DNA polymerase ε and hRad9 (Ddc1 in budding yeast) that occurs in the absence of DNA damage (40,53). Thus, DNA polymerase ε interacts with both the checkpoint clamp-loader and the checkpoint clamp complex, providing a possible molecular mechanism for the proposed checkpoint activities of DNA polymerase ε and the participation of hRad17 in the regulation of DNA replication.

Even though phosphorylated hRad17 interacts with the replication machinery and localizes to sites of DNA replication during unperturbed S phase, the possibility remains that hRad17 may only localize to sites of stalled forks or where DNA damage is sensed during S phase, because not all α-phospho-hRad17 and α-BrdU or α-PCNA foci overlap (Fig. 4A and B). A possible role for phosphorylated hRad17 is that it may monitor replication fork stability and sense replication blocks during unperturbed replication. Alternatively, it may inhibit DNA reduplication, likely through its interactions with components of the replication machinery. Although the effect of hRad17 phosphorylation on DNA replication remains to be elucidated, our research provides evidence that phosphorylated hRad17 links the checkpoint Rad proteins and the replication machinery.

ACKNOWLEDGEMENTS

REFERENCES

1. Zhou,B. and Elledge,S. (2000) The DNA damage response: putting checkpoints in perspective. *Nature*, **408**, 433–439.
2. Melo,J. and Toczyski,D. (2002) A unified view of the DNA-damage checkpoint. *Curr. Opin. Cell Biol.*, **14**, 237–245.
3. Caspari,T. and Carr,A.M. (1999) DNA structure checkpoint pathways in *Schizosaccharomyces pombe*. *Biochimie*, **81**, 173–181.
4. Nyberg,K.A., Michelson,R.J., Putnam,C.W. and Weinert,T.A. (2002) Toward maintaining the genome: DNA damage and replication checkpoints. *Annu. Rev. Genet.*, **36**, 617–656.
5. Roos-Mattjus,P., Hopkins,K.M., Oestreich,A.J., Vroman,B.T., Johnson,K.L., Naylor,S., Lieberman,H.B. and Karnitz,L.M. (2003) Phosphorylation of human Rad9 is required for genotoxin-activated checkpoint signaling. *J. Biol. Chem.*, **278**, 24428–24437.
6. Post,S., Weng,Y.C., Cimprich,K., Chen,L.B., Xu,Y. and Lee,E.Y. (2001) Phosphorylation of serines 635 and 645 of human Rad17 is cell cycle regulated and is required for G(1)/S checkpoint activation in response to DNA damage. *Proc. Natl Acad. Sci. USA*, **98**, 13102–13107.
7. Zou,L., Cortez,D. and Elledge,S.J. (2002) Regulation of ATR substrate selection by Rad17-dependent loading of Rad9 complexes onto chromatin. *Genes Dev.*, **16**, 198–208.
8. Weiss,R.S., Matsuoka,S., Elledge,S.J. and Leder,P. (2002) Hus1 acts upstream of chk1 in a mammalian DNA damage response pathway. *Curr. Biol.*, **12**, 73–77.
9. Cortez,D., Guntuku,S., Qin,J. and Elledge,S.J. (2001) ATR and ATRIP: partners in checkpoint signaling. *Science*, **294**, 1713–1716.
10. Cliby,W.A., Roberts,C.J., Cimprich,K.A., Stringer,C.M., Lamb,J.R., Schreiber,S.L. and Friend,S.H. (1998) Overexpression of a kinase-inactive ATR protein causes sensitivity to DNA-damaging agents and defects in cell cycle checkpoints. *EMBO J.*, **17**, 159–169.
11. Cimprich,K.A., Shin,T.B., Keith,C.T. and Schreiber,S.L. (1996) cDNA cloning and gene mapping of a candidate human cell cycle checkpoint protein. *Proc. Natl Acad. Sci. USA*, **93**, 2850–2855.
12. Zeng,Y., Forbes,K.C., Wu,Z., Moreno,S., Piwnica-Worms,H. and Enoch,T. (1998) Replication checkpoint requires phosphorylation of the phosphatase Cdc25 by Cds1 or Chk1. *Nature*, **395**, 507–510.
13. Mailand,N., Falck,J., Lukas,C., Syljuasen,R.G., Welcker,M., Bartek,J. and Lukas,J. (2000) Rapid destruction of human Cdc25A in response to DNA damage. *Science*, **288**, 1425–1429.
14. Kumagai,A., Guo,Z., Emami,K.H., Wang,S.X. and Dunphy,W.G. (1998) The *Xenopus* Chk1 protein kinase mediates a caffeine-sensitive pathway of checkpoint control in cell-free extracts. *J. Cell Biol.*, **142**, 1559–1569.

15. Furnari,B., Blasina,A., Boddy,M.N., McGowan,C.H. and Russell,P. (1999) Cdc25 inhibited *in vivo* and *in vitro* by checkpoint kinases Cds1 and Chk1. *Mol. Biol. Cell*, **10**, 833–845.

16. Yu,L., Orlandi,L., Wang,P., Orr,M.S., Senderowicz,A.M., Sausville,E.A., Silvestrini,R., Watanabe,N., Piwnica-Worms,H. and O'Connor,P.M. (1998) UCN-01 abrogates G2 arrest through a Cdc2-dependent pathway that is associated with inactivation of the Wee1Hu kinase and activation of the Cdc25C phosphatase. *J. Biol. Chem.*, **273**, 33455–33464.

17. Rhind,N., Furnari,B. and Russell,P. (1997) Cdc2 tyrosine phosphorylation is required for the DNA damage checkpoint in fission yeast. *Genes Dev.*, **11**, 504–511.

18. Poon,R.Y., Chau,M.S., Yamashita,K. and Hunter,T. (1997) The role of Cdc2 feedback loop control in the DNA damage checkpoint in mammalian cells. *Cancer Res.*, **57**, 5168–5178.

19. de Klein,A., Muijtjens,M., van Os,R., Verhoeven,Y., Smit,B., Carr,A.M., Lehmann,A.R. and Hoeijmakers,J.H. (2000) Targeted disruption of the cell-cycle checkpoint gene ATR leads to early embryonic lethality in mice. *Curr. Biol.*, **10**, 479–482.

20. Brown,E.J. and Baltimore,D. (2003) Essential and dispensable roles of ATR in cell cycle arrest and genome maintenance. *Genes Dev.*, **17**, 615–628.

21. Brown,E.J. and Baltimore,D. (2000) ATR disruption leads to chromosomal fragmentation and early embryonic lethality. *Genes Dev.*, **14**, 397–402.

22. Takai,H., Tominaga,K., Motoyama,N., Minamishima,Y.A., Nagahama,H., Tsukiyama,T., Ikeda,K., Nakayama,K., Nakanishi,M. and Nakayama,K. (2000) Aberrant cell cycle checkpoint function and early embryonic death in Chk1(–/–) mice. *Genes Dev.*, **14**, 1439–1447.

23. Liu,Q., Guntuku,S., Cui,X.S., Matsuoka,S., Cortez,D., Tamai,K., Luo,G., Carattini-Rivera,S., DeMayo,F., Bradley,A., Donehower,L.A. and Elledge,S.J. (2000) Chk1 is an essential kinase that is regulated by Atr and required for the G(2)/M DNA damage checkpoint. *Genes Dev.*, **14**, 1448–1459.

24. Michael,W.M., Ott,R., Fanning,E. and Newport,J. (2000) Activation of the DNA replication checkpoint through RNA synthesis by primase. *Science*, **289**, 2133–2137.

25. Hekmat-Nejad,M., You,Z., Yee,M., Newport,J.W. and Cimprich,K.A. (2000) *Xenopus* ATR is a replication-dependent chromatin-binding protein required for the DNA replication checkpoint. *Curr. Biol.*, **10**, 1565–1573.

26. Guo,Z., Kumagai,A., Wang,S.X. and Dunphy,W.G. (2000) Requirement for Atr in phosphorylation of Chk1 and cell cycle regulation in response to DNA replication blocks and UV-damaged DNA in *Xenopus* egg extracts. *Genes Dev.*, **14**, 2745–2756.

27. Stokes,M.P., Van Hatten,R., Lindsay,H.D. and Michael,W.M. (2002) DNA replication is required for the checkpoint response to damaged DNA in *Xenopus* egg extracts. *J. Cell Biol.*, **158**, 863–872.

28. Lee,J., Kumagai,A. and Dunphy,W.G. (2003) Claspin, a Chk1-regulatory protein, monitors DNA replication on chromatin independently of RPA, ATR and Rad17. *Mol. Cell*, **11**, 329–340.

29. You,Z., Kong,L. and Newport,J. (2002) The role of single-stranded DNA and polymerase alpha in establishing the ATR, Hus1 DNA replication checkpoint. *J. Biol. Chem.*, **277**, 27088–27093.

30. Griffiths,D., Uchiyama,M., Nurse,P. and Wang,T.S. (2000) A novel mutant allele of the chromatin-bound fission yeast checkpoint protein Rad17 separates the DNA structure checkpoints. *J. Cell Sci.*, **113**, 1075–1088.

31. Kai,M., Tanaka,H. and Wang,T.S. (2001) Fission yeast Rad17 associates with chromatin in response to aberrant genomic structures. *Mol. Cell. Biol.*, **21**, 3289–3301.

32. Griffiths,D.J., Barbet,N.C., McCready,S., Lehmann,A.R. and Carr,A.M. (1995) Fission yeast rad17: a homologue of budding yeast RAD24 that shares regions of sequence similarity with DNA polymerase accessory proteins. *EMBO J.*, **14**, 5812–5823.

33. Dean,F.B., Lian,L. and O'Donnell,M. (1998) cDNA cloning and gene mapping of human homologs for *Schizosaccharomyces pombe* rad17, rad1 and hus1 and cloning of homologs from mouse, *Caenorhabditis elegans* and *Drosophila melanogaster*. *Genomics*, **54**, 424–436.

34. Bluyssen,H.A.R., Naus,N.C., van Os,R.I., Jaspers,I., Hoeijmakers,J.H.J. and de Klein,A. (1999) Human and mouse homologs of the *Schizosaccharomyces pombe* rad17(+) cell cycle checkpoint control gene. *Genomics*, **55**, 219–228.

35. Bao,S., Chang,M.S., Auclair,D., Sun,Y., Wang,Y., Wong,W.K., Zhang,J., Liu,Y., Qian,X., Sutherland,R., Magi-Galluzi,C., Weisberg,E., Cheng,E.Y., Hao,L., Sasaki,H., Campbell,M.S., Kraeft,S.K., Loda,M., Lo,K.M. and Chen,L.B. (1999) HRad17, a human homologue of the *Schizosaccharomyces pombe* checkpoint gene rad17, is overexpressed in colon carcinoma. *Cancer Res.*, **59**, 2023–2028.

36. Bermudez,V.P., Lindsey-Boltz,L.A., Cesare,A.J., Maniwa,Y., Griffith,J.D., Hurwitz,J. and Sancar,A. (2003) Loading of the human 9-1-1 checkpoint complex onto DNA by the checkpoint clamp loader hRad17-replication factor C complex *in vitro*. *Proc. Natl Acad. Sci. USA*, **100**, 1633–1638.

37. Majka,J. and Burgers,P.M. (2003) Yeast Rad17/Mec3/Ddc1: a sliding clamp for the DNA damage checkpoint. *Proc. Natl Acad. Sci. USA*, **100**, 2249–2254.

38. Bao,S., Tibbetts,R.S., Brumbaugh,K.M., Fang,Y., Richardson,D.A., Ali,A., Chen,S.M., Abraham,R.T. and Wang,X.F. (2001) ATR/ATM-mediated phosphorylation of human Rad17 is required for genotoxic stress responses. *Nature*, **411**, 969–974.

39. Wang,X., Zou,L., Zheng,H., Wei,Q., Elledge,S.J. and Li,L. (2003) Genomic instability and endoreduplication triggered by RAD17 deletion. *Genes Dev.*, **17**, 965–970.

40. Makiniemi,M., Hillukkala,T., Tuusa,J., Reini,K., Vaara,M., Huang,D., Pospiech,H., Majuri,I., Westerling,T., Makela,T.P. and Syvaoja,J.E. (2001) BRCT domain-containing protein TopBP1 functions in DNA replication and damage response. *J. Biol. Chem.*, **276**, 30399–30406.

41. Komatsu,K., Wharton,W., Hang,H., Wu,C., Singh,S., Lieberman,H.B., Pledger,W.J. and Wang,H.G. (2000) PCNA interacts with hHus1/hRad9 in response to DNA damage and replication inhibition. *Oncogene*, **19**, 5291–5297.

42. Dahm,K. and Hubscher,U. (2002) Colocalization of human Rad17 and PCNA in late S phase of the cell cycle upon replication block. *Oncogene*, **21**, 7710–7719.

43. Chen,P.L., Scully,P., Shew,J.Y., Wang,J.Y. and Lee,W.H. (1989) Phosphorylation of the retinoblastoma gene product is modulated during the cell cycle and cellular differentiation. *Cell*, **58**, 1193–1198.

44. Zhao,S., Renthal,W. and Lee,E.Y. (2002) Functional analysis of FHA and BRCT domains of NBS1 in chromatin association and DNA damage responses. *Nucleic Acids Res.*, **30**, 4815–4822.

45. Mendez,J. and Stillman,B. (2000) Chromatin association of human origin recognition complex, cdc6 and minichromosome maintenance proteins during the cell cycle: assembly of prereplication complexes in late mitosis. *Mol. Cell. Biol.*, **20**, 8602–8612.

46. Aboussekhra,A. and Wood,R.D. (1995) Detection of nucleotide excision repair incisions in human fibroblasts by immunostaining for PCNA. *Exp. Cell Res.*, **221**, 326–332.

47. Guo,N., Faller,D.V. and Vaziri,C. (2002) Carcinogen-induced S-phase arrest is Chk1 mediated and caffeine sensitive. *Cell Growth Differ.*, **13**, 77–86.

48. Sarkaria,J.N., Busby,E.C., Tibbetts,R.S., Roos,P., Taya,Y., Karnitz,L.M. and Abraham,R.T. (1999) Inhibition of ATM and ATR kinase activities by the radiosensitizing agent, caffeine. *Cancer Res.*, **59**, 4375–4382.

49. Jiang,K., Pereira,E., Maxfield,M., Russell,B., Goudelock,D.M. and Sanchez,Y. (2003) Regulation of Chk1 includes chromatin association and 14-3-3 binding following phosphorylation on Ser345. *J. Biol. Chem.*, **278**, 25207–25217.

50. Chen,M.J., Lin,Y.T., Lieberman,H.B., Chen,G. and Lee,E.Y. (2001) ATM-dependent phosphorylation of human Rad9 is required for ionizing radiation-induced checkpoint activation. *J. Biol. Chem.*, **276**, 16580–16586.

51. Navas,T.A., Zhou,Z. and Elledge,S.J. (1995) DNA polymerase epsilon links the DNA replication machinery to the S phase checkpoint. *Cell*, **80**, 29–39.

52. Dua,R., Levy,D.L. and Campbell,J.L. (1998) Role of the putative zinc finger domain of *Saccharomyces cerevisiae* DNA polymerase epsilon in DNA replication and the S/M checkpoint pathway. *J. Biol. Chem.*, **273**, 30046–30055.

53. Wang,H. and Elledge,S.J. (2002) Genetic and physical interactions between DPB11 and DDC1 in the yeast DNA damage response pathway. *Genetics*, **160**, 1295–1304.

Role of the Nuclease Activity of *Saccharomyces cerevisiae* Mre11 in Repair of DNA Double-Strand Breaks in Mitotic Cells

L. Kevin Lewis,*[,1] Francesca Storici,[†] Stephen Van Komen,[‡] Shanna Calero,* Patrick Sung[‡] and Michael A. Resnick[†]

*Department of Chemistry and Biochemistry, Texas State University, San Marcos, Texas 78666, [†]Laboratory of Molecular Genetics, National Institute of Environmental Health Sciences, National Institutes of Health, Research Triangle Park, North Carolina 27709 and [‡]Molecular Biophysics and Biochemistry, Yale University School of Medicine, New Haven, Connecticut 06520

ABSTRACT

The Rad50:Mre11:Xrs2 (RMX) complex functions in repair of DNA double-strand breaks (DSBs) by recombination and nonhomologous end-joining (NHEJ) and is also required for telomere stability. The Mre11 subunit exhibits nuclease activities *in vitro*, but the role of these activities in repair in mitotic cells has not been established. In this study we have performed a comparative study of three mutants (*mre11-D16A*, *-D56N*, and *-H125N*) previously shown to have reduced nuclease activities *in vitro*. In ends-in and ends-out chromosome recombination assays using defined plasmid and oligonucleotide DNA substrates, *mre11-D16A* cells were as deficient as *mre11* null strains, but defects were small in *mre11-D56N* and *-H125N* mutants. *mre11-D16A* cells, but not the other mutants, also displayed strong sensitivity to ionizing radiation, with residual resistance largely dependent on the presence of the partially redundant nuclease Exo1. *mre11-D16A* mutants were also most sensitive to the S-phase-dependent clastogens hydroxyurea and methyl methanesulfonate but, as previously observed for *D56N* and *H125N* mutants, were not defective in NHEJ. Importantly, the affinity of purified Mre11-D16A protein for Rad50 and Xrs2 was indistinguishable from wild type and the mutant protein formed complexes with equivalent stoichiometry. Although the role of the nuclease activity has been questioned in previous studies, the comparative data presented here suggest that the nuclease function of Mre11 is required for RMX-mediated recombinational repair and telomere stabilization in mitotic cells.

E UKARYOTIC organisms repair broken chromosomes by at least two distinct DNA repair pathways, homologous recombination and nonhomologous end-joining (NHEJ). The conserved *Saccharomyces cerevisiae* Rad50, Mre11, and Xrs2 proteins (referred to as RMX) play a unique role in that they function in both recombination and NHEJ repair. Yeast cells containing inactivated RMX genes are defective in NHEJ assays (*e.g.*, homology-independent plasmid recircularization, sensitivity to *in vivo* expression of *Eco*RI endonuclease, deletion formation within dicentric plasmids, etc.) and also exhibit reduced efficiency of DSB-induced homologous recombination (LEWIS and RESNICK 2000; SUNG *et al.* 2000; SYMINGTON 2002). RMX mutants also have greatly increased frequencies of spontaneous chromosome rearrangements, shortened telomeres, defects in S-phase checkpoint responses to DNA damage, hypersensitivity to clastogenic chemicals and ionizing radiation and reduced recombination in meiosis (CHEN and KOLODNER 1999; KOUPRINA *et al.* 1999; LEWIS and RESNICK 2000; GRENON *et al.* 2001; USUI *et al.* 2001; CHANG *et al.* 2002;

D'AMOURS and JACKSON 2002; MYUNG and KOLODNER 2002).

Several of the metabolic defects described for yeast RMX mutants are also observed in mammalian cells upon inactivation of the corresponding gene orthologs. For example, mutations within the human genes hMRE-11 and hNBS1 (hNBS1 is the apparent human equivalent of yeast *XRS2*) cause the human disorders Nijmegen breakage syndrome and ataxia telangiectasia-like disorder, respectively (STEWART *et al.* 1999). Cells derived from individuals with these disorders display multiple DNA damage response defects, including hypersensitivity to ionizing radiation and defective checkpoint responses. In addition, individuals with these disorders have an increased incidence of cancer (PETRINI 1999; D'AMOURS and JACKSON 2002). Further evidence suggesting a role for inactivation of the complex in cancer development has been obtained from directed sequencing of hMRE11 genes from random (FUKUDA *et al.* 2001) and mismatch repair-deficient tumor cells (GIANNINI *et al.* 2002).

The Mre11 subunit of RMX has manganese-dependent 3′-to-5′ dsDNA exonuclease and ssDNA endonuclease activities that are active on a number of linear and circular DNA structures, including the tops of hairpin structures formed by inverted repeat sequences *in*

[1]*Corresponding author:* Department of Chemistry and Biochemistry, Texas State University, 601 University Dr., San Marcos, TX 78666.
E-mail: ll18@txstate.edu

vitro and *in vivo* (HOPFNER *et al.* 2000; TRUJILLO and SUNG 2001; LOBACHEV *et al.* 2002). The purified enzyme also has DNA strand annealing and dissociation activities (D'AMOURS and JACKSON 2002). Sequence comparisons have indicated that Mre11 contains five conserved sequence motifs found in many phosphodiesterase enzymes (although some reports recognize only four motifs) and these regions appear to harbor the nuclease activities of the enzyme (BAUM 1995; SHARPLES and LEACH 1995; BRESSAN *et al.* 1998; TSUBOUCHI and OGAWA 1998; USUI *et al.* 1998; MOREAU *et al.* 1999; HOPFNER *et al.* 2001, 2002).

The Rad50 subunit of RMX is a large ATP-binding protein whose sequence contains typical Walker A and B ATPase motifs on either side of two extended coiled-coil domains (ALANI *et al.* 1990; HOPFNER *et al.* 2000). The function of Xrs2 remains unclear, although recent work demonstrating protein:protein interactions between this subunit and Lif1, a component of the DNA ligase IV complex, suggest an important role in RMX-mediated repair by NHEJ (CHEN *et al.* 2001). Studies of the equivalent protein in higher eukaryotes (NBS1) indicate that some activities of the complex, *e.g.* duplex DNA unwinding, are also dependent upon the presence of this subunit (PAULL and GELLERT 1999).

Structural studies of archaebacterial, yeast, and human Rad50 and Mre11 suggest that these proteins combine to form multimers whose unit structure consists of two molecules of each polypeptide (ANDERSON *et al.* 2001; CHEN *et al.* 2001; DE JAGER *et al.* 2001; HOPFNER *et al.* 2002). According to recent models, each Rad50 subunit forms a folded, antiparallel structure that places the N- and C-terminal Walker A and B motifs in proximity with each other. Association of two Mre11 molecules with the joined ends of two folded Rad50 subunits then forms the DNA-binding portion of the complex. Larger multimeric structures that can potentially form bridges between broken DNA ends or between adjacent sister chromatids have also been suggested, possibly resulting from Zn^{2+}-mediated joining of Rad50 molecules at a "hinge" or "hook" region (DE JAGER *et al.* 2001; HOPFNER *et al.* 2002).

The specific mechanism(s) by which the RMX nuclease complex mediates repair by recombination and NHEJ, activates checkpoints, inhibits chromosome rearrangements, and stabilizes telomeres is unknown. We and others established that some DSB repair phenotypes of RMX mutants can be suppressed by overexpression of the gene encoding Exo1, a 5'-to-3' exonuclease (and also by telomerase RNA; LEWIS *et al.* 2002), suggesting that a critical function that has been lost in these mutants is DSB end-processing (CHAMANKHAH *et al.* 2000; SYMINGTON *et al.* 2000; TSUBOUCHI and OGAWA 2000; MOREAU *et al.* 2001; LEWIS *et al.* 2002). More specifically, these experiments revealed that the nuclease activity of Exo1 could partially substitute for RMX in recombinational repair, but not repair by the NHEJ

pathway. The results with Exo1 are inconsistent with recent analyses of mutants with substitutions in the conserved phosphoesterase motifs of Mre11 (*e.g.*, -D56N, -H125N, and -H125L/D126V), which suggested that nuclease activity is not required for several major functions of RMX in mitotic cells, including recombination, NHEJ, and telomere stabilization (BRESSAN *et al.* 1999; MOREAU *et al.* 1999; SYMINGTON *et al.* 2000; TSUKAMOTO *et al.* 2001; LOBACHEV *et al.* 2002).

While the Mre11 nuclease is clearly required for processing of special DNA structures, such as meiotic DSBs containing attached proteins or certain DNA secondary structures in mitotic cells (RATTRAY *et al.* 2001; LOBACHEV *et al.* 2002; SYMINGTON 2002), previous studies of known nuclease-defective alleles observed only minor effects on repair of DSBs induced by ionizing radiation, chemicals, or site-specific endonucleases during mitotic growth. We report here that cells expressing a mutant Mre11 protein (Mre11-D16A; motif I), which is deficient in endonuclease and exonuclease activities, but which retains the ability to bind DNA and to form multimers with Mre11, has multiple DNA metabolic defects that are consistent with a role for its nuclease function(s) in recombinational repair of DSBs and telomere stabilization, but not NHEJ in mitotic cells. Several phenotypes of *mre11-D16A* cells differ only in severity from cells expressing two other Mre11 variants shown to have reduced nuclease activities *in vitro*. Together with past observations of recombination-specific suppression by *EXO1*, these results suggest that catalytic activities established for Mre11 *in vitro* are in fact important for major functions of the enzyme *in vivo* such as repair of DSBs by homologous recombination and stabilization of telomeres.

MATERIALS AND METHODS

Strains and plasmids: Yeast strains used for this work are shown in Table 1. *rad50::hisG-URA3-hisG* disruptions were generated using pNKY83 (a generous gift from N. Kleckner) digested with *Eco*RI + *Bgl*II and *exo1::URA3* disruptions were created using plasmid p244 cut with *Hind*III + *Kpn*I (TRAN *et al.* 1999). Geneticin/G418 (BRL) and Hygromycin B (Boehringer Mannheim, Indianapolis) were added to plates for selection of resistant strains at concentrations of 200 and 300 μg/ml, respectively. 5-Fluoroorotic acid (5-FOA) used for selection of Ura⁻ cells was purchased from United States Biological. Methyl methanesulfonate (MMS) was obtained from Fluka (Buchs, Switzerland) and hydroxyurea (HU) was purchased from Sigma (St. Louis).

Plasmids used for expression studies were as follows: pRS314 (*CEN/ARS, TRP1*; SIKORSKI and HIETER 1989), pMre11-D16A (*CEN/ARS, TRP1 mre11-D16A*; this work), pSM258 (*CEN/ARS, TRP1, MRE11*; a kind gift from L. Symington), pSM304 (as pSM258, but *mre11-H125N*), pSM312 (as PSM258, but *mre11-D56N*), and pRS316Gal (LEWIS *et al.* 1998).

Site-specific mutagenesis of chromosomal and plasmid loci: A recently developed technique (*delitto perfetto*; STORICI *et al.* 2001) was employed to create substitutions in *MRE11* at its natural locus on chromosome XIII (Figure 1A). A DNA frag-

ment containing selectable and counterselectable markers for G418^r and *URA3* flanked by *MRE11* sequences was generated using primers MRE11.G and MRE11.U to amplify DNA in the cassette plasmid pCORE (Storici *et al.* 2001). Sequences of these and all other primers are available upon request. This fragment was used to insert the cassette into the *MRE11* gene on chromosome XIII between nucleotides (nt) G46 and A47 of the coding region. Cells were subsequently transformed with the 80-mer MRE11.a and MRE11.b and 5-FOA^r G418-sensitive cells were selected. Genomic *MRE11* DNAs from three independent transformants were sequenced and found to contain a single mutation at codon 16 from GAT to GCT, changing the coding from aspartate to alanine. Using the same approach plasmid pSM258 (*CEN/ARS, TRP1, MRE11*) was modified in an *MRE11*-deleted strain background (YLKL-555) to create pMre11-D16A. All PCR reactions utilized Platinum Pfx enzyme (GIBCO/Invitrogen).

Ends-in and ends-out chromosome recombination and NHEJ assays: Plasmid NHEJ assays were performed by LiAc transformation as previously described (Lewis *et al.* 2002) using uncut or *Bam*HI-cut pRS314 with strains VL6α (*MRE11*), YLKL503 (*mre11Δ*), and YLKL641 (*mre11-D16A*). In these experiments the uncut pRS314 DNA serves as a control for variability in transformation efficiencies among different strains.

Ends-in recombination proficiencies of cells expressing mutant *mre11* alleles were assessed using strain YLKL503 (*mre11Δ*) containing pRS314, pSM258, pSM304, pSM312, or pMre11-D16A. Cells were transformed with pLKL37Y that had been cut inside *URA3* with *Nco*I. pLKL37Y was created in the following way: A 1.2-kb *Hin*dIII *URA3* gene fragment obtained from YEp24 was made blunt with T4 DNA polymerase and cloned into *Sal*I/*Not*I-cut pRS303 that had also been made flush by extension of sticky ends with T4 DNA polymerase. The resulting plasmid, pLKL37Y, is an integrating vector containing *URA3* and *HIS3*. After digestion with *Nco*I and transformation, Ura$^+$ colonies formed by recombinational integration of the plasmid into the *ura3-52* locus on chromosome V were scored. In this assay most transformants are Ura$^+$ His$^+$ integrants (see Figure 3B), with a small fraction (≤1%) of Ura$^+$ His$^-$ cells presumed to arise by conversion of *ura3-52* on the chromosome. All transformation efficiencies (transformants per microgram of DNA) were normalized to those for uncut *CEN/ARS* plasmid DNA (pRS316Gal) transformed into the same competent cell preparations on the same day. Results presented are the mean ±SD of 3–5 experiments for each strain.

Ends-out gene conversion assays were performed using derivatives of the strain BY4742-TRP5-HP53 (Table 1). This strain contains a selectable-counterselectable HygB^r + GALp::p53-V122A CORE cassette inserted into nucleotides 1002 and 1003 of the *TRP5* gene in strain BY4742. This strain is used for quantitative analysis of oligonucleotide-mediated recombination events that result in perfect excision of the CORE cassette. The cassette used for these studies differs from the cassette previously described in Storici *et al.* (2001) in that hygromycin B resistance is selectable and resistance to the growth inhibitory effects of p53-V122A expression can be counterselected (Storici and Resnick 2003). p53-V122 is a variant of human p53 that is highly toxic to yeast cells when expressed from the *GAL1* promoter (Storici and Resnick 2003). *MRE11*, *mre11Δ*, and *mre11-D16A* cells (BY4742-TRP5-HP53, YLKL770, and YLKL771, respectively) were transformed with complementary 95-nt oligonucleotides TRP5.e and TRP5.f and frequencies of HygB^s p53$^-$ cells quantitated as described previously for recombination-dependent *delitto perfetto* mutagenesis (Storici *et al.* 2001). The *rad52Δ* control cells used for Figure 4 were identical to the above strains except that an alternative cassette, *URA3* + G418^r, was employed. BY4742-TRP5-CORE and YLKL769 were used for the latter assays.

Binding of Rad50 and Xrs2 to wild-type and mutant Mre11 and Mre11-D16A proteins: 6His-Mre11 and 6His-Mre11-D16A were purified from *Escherichia coli* strains tailored to express these proteins (Furuse *et al.* 1998). Nontagged Rad50, Mre11, and Xrs2 were overexpressed in yeast and purified to near homogeneity as described previously (Trujillo and Sung 2001; Trujillo *et al.* 2003). The concentrations of Rad50, Mre11, 6His-Mre11, 6His-Mre11-D16A, and Xrs2 were determined by densitometric scanning of 7.5% SDS-PAGE gels containing multiple loadings of the purified proteins against known amounts of bovine serum albumin run on the same gel (Trujillo *et al.* 2003).

Binding studies were conducted by incubating purified Rad50 (5 μg, 1.1 μM) or Xrs2 (2.3 μg, 0.8 μM) with and without purified Mre11 (3.5 μg, 1.5 μM) or Mre11-6His (3.5 μg, 1.5 μM) at 0° in 30 μl of B buffer (20 mM KH$_2$PO$_4$, pH 7.4, 0.5 mM EDTA, 1 mM dithiothreitol) containing 150 mM KCl, 5 μg BSA, 10 mM imidazole, and 0.01% Igepal (Sigma). After 60 min of incubation, 10 μl of nickel-NTA-agarose beads (QIAGEN, Valencia, CA) were added and the reaction mixtures were left at 0° for another 60 min, with gentle tapping every 2 min. The beads were washed twice with 30 μl of B buffer containing 20 mM imidazole before eluting the bound proteins from the nickel matrix with 30 μl of 200 mM imidazole in B buffer.

Cell survival assays: Survival after treatment with gamma radiation was monitored after exposure to a ^{137}Cesium source emitting at a dose rate of 2.7 krad/min. Two or three independent log phase cultures containing YLKL503 (*mre11Δ*) cells with pRS314 or different *MRE11* plasmids (see above) were irradiated and placed on ice and mean fractions of surviving cells were calculated after dilutions were spread onto synthetic glucose plates without tryptophan. Hydroxyurea survival assays were performed by dilution pronging and fivefold dilutions of cells as described (Lewis *et al.* 2002). Strains used for the assays were YLKL503 containing pRS314 and *MRE11* plasmids as above. Control strains were YLKL532 (Δ*rad51*) and YLKL-593 (Δ*yku70*) containing pRS314. Cells were propagated on synthetic glucose plates minus tryptophan with increasing concentrations of hydroxyurea.

RESULTS

The *mre11-D16A* mutation greatly increases sensitivity to ionizing radiation: The endo- and exonuclease activities of Mre11 reside in conserved phosphodiesterase motifs located in the amino terminus of the protein (Figure 1B; Hopfner *et al.* 2001; D'Amours and Jackson 2002). The aspartic acid residue in phosphoesterase domain I (D16) is associated with a manganese ion in the crystal structure of *Pyrococcus furiosus* Mre11 (the corresponding aspartic acid in P. f. Mre11 is the eighth residue of the protein; Hopfner *et al.* 2001). Conversion of this negatively charged residue to a neutral alanine produces a protein that has no detectable nuclease activities *in vitro*, but which retains the ability to bind to DNA and to other Mre11 molecules (Furuse *et al.* 1998). Our study was designed to assess the precise consequences of this and other substitutions known to produce proteins with no detectable nuclease activity on DSB repair capabilities in mitotic cells.

To determine the impact of the D16A substitution on DNA repair in mitotic cells, the *MRE11* locus on

TABLE 1

Yeast strains used in this study

Strain	Genotype	Reference
VL6α	*MATα ura3-52 his3-Δ200 trp1-Δ63 lys2-801 ade2-101 met14*	LARIONOV *et al.* (1994)
YLKL499	VL6α, *Δrad50::hisG*	LEWIS *et al.* (2002)
YLKL503	VL6α, *Δmre11::G418*	LEWIS *et al.* (2002)
YLKL532	VL6α, *Δrad51::hisG*	LEWIS *et al.* (2002)
YLKL546	VL6α, *Δexo1::G418*	LEWIS *et al.* (2002)
YLKL640	VL6α, *rad50-K40A*	This work
YLKL641	VL6α, *mre11-D16A*	This work
YLKL724	YLKL641, *exo1::URA3*	This work
YLKL725	YLKL503, *exo1::URA3*	This work
VL6-48α	VL6α, *Δleu2::G418*	V. Larionov
YLKL555	VL6-48α, *Δmre11::HygB*	LEWIS *et al.* (2002)
YLKL684	VL6-48α, *Δrad50::hisG*	This work
YLKL593	VL6-48α, *Δyku70::HIS3*	This work
BY4742	*MATα ura3Δ0 leu2Δ0 his3Δ1 lys2Δ0*	BRACHMANN *et al.* (1998)
YLKL649	BY4742, *Δrad50::G418*	This work
BY4742-TRP5-CORE	BY4742, *trp5::[G418ʳ KlURA3]*	STORICI *et al.* (2001)
YLKL769	BY4742-TRP5-CORE, *Δrad52:LEU2*	This work
BY4742-TRP5-HP53	BY4742, *trp5::[HygBʳ p53]*	STORICI and RESNICK (2003)
YLKL770	BY4742-TRP5-HP53, *Δmre11*	This work
YLKL771	BY4742-TRP5-HP53, *mre11-D16A*	This work

chromosome XIII of strain VL6α was altered by the *delitto perfetto* method of oligonucleotide-mediated, site-specific mutagenesis (STORICI *et al.* 2001; STORICI and RESNICK 2003) as shown in Figure 1A. Initially, a two-gene "CORE" cassette was integrated into *MRE11* by PCR fragment-mediated gene targeting. One of the CORE genes provides for selection by resistance to G418 and the other for counterselection against *URA3* after subsequent transformation with oligonucleotides. After transformation of cassette-containing cells with long, complementary oligonucleotides containing one or more sequence changes, transformants containing perfectly excised cassettes were identified by 5-FOA counterselection of Ura⁻ cells and confirmation of loss of the selectable marker (G418ʳ) along with sequencing of the resulting DNA locus (see MATERIALS AND METHODS). A plasmid-borne version of *MRE11* on pSM258 was similarly converted to *mre11-D16A* after propagation in an *MRE11*-deleted strain background, producing the plasmid pMre11-D16A.

mre11 null cells are hypersensitive to killing by many physical and chemical agents that induce DSBs, including ionizing radiation. For example, haploid *mre11* mutants are fully as sensitive to ionizing radiation as strongly recombination-defective *rad51*, *rad52*, and *rad54* strains (SAEKI *et al.* 1980; LEWIS and RESNICK 2000; BENNETT *et al.* 2001). Survival of logarithmically growing cells containing *mre11-D16A* was found to be reduced at all doses tested, although cells were not as sensitive as *mre11Δ* strains (Figure 2A). In contrast, the widely studied phosphoesterase motif II and III mutants *mre11-D56N* and *-H125N* displayed near-wild-type resistance

up to 20 krad, corresponding to ~10–15 DSBs per haploid genome (RESNICK and MARTIN 1976). This result is consistent with a recent report demonstrating that the latter two mutants have a weak radiation sensitivity that becomes apparent at relatively high doses (30–70 krad; MOREAU *et al.* 2001).

Past experiments have established that the 5'-to-3' exonuclease encoded by *EXO1* can partially substitute for the RMX complex in recombinational repair of DSBs (CHAMANKHAH *et al.* 2000; TSUBOUCHI and OGAWA 2000; MOREAU *et al.* 2001; LEWIS *et al.* 2002). Haploid *exo1* mutants are not sensitive to radiation, but *exo1 rmx* double mutants exhibit slightly more gamma sensitivity than *rmx* single mutants and reduced repair proficiency in plasmid DSB repair assays (SYMINGTON *et al.* 2000; LEWIS *et al.* 2002). To assess the possibility that the residual radiation resistance of nuclease-defective *mre11-D16A* cells is due to basal level expression of Exo1, double-mutant strains were constructed and tested for radiation sensitivity. *exo1 mre11-D16A* double mutants exhibited ~10-fold more killing at 20 krad than *mre11-D16A* cells did (Figure 2B). This suggests that a large fraction of radiation-induced DSBs in *mre11-D16A* cells are processed by the 5'-to-3' exonuclease activity of Exo1. However, killing did not reach the level of *exo1 mre11Δ* double mutants, which were slightly more sensitive than *mre11* single mutants.

Radiation-induced DSBs are repaired primarily by homologous recombinational mechanisms and current models propose that RMX initiates recombination by processing DSB ends to generate 3' single-strand overhangs (SUNG *et al.* 2000; SYMINGTON 2002). The gamma

A

MRE11

——————◻▨▨▨▨▨▨▨▨▨▨▨▨▨▨▨▨◻——Chr. XIII

URA3 G418^r

▨◼◻▨

Insertion of CORE cassette into locus

URA3 G418^r

——▨▨▨▨◻◼◻◼◻▨▨▨▨▨▨——

m
▨▨▨▨▨▨

Replacement of cassette by recombination with 95 nt oligonucleotide
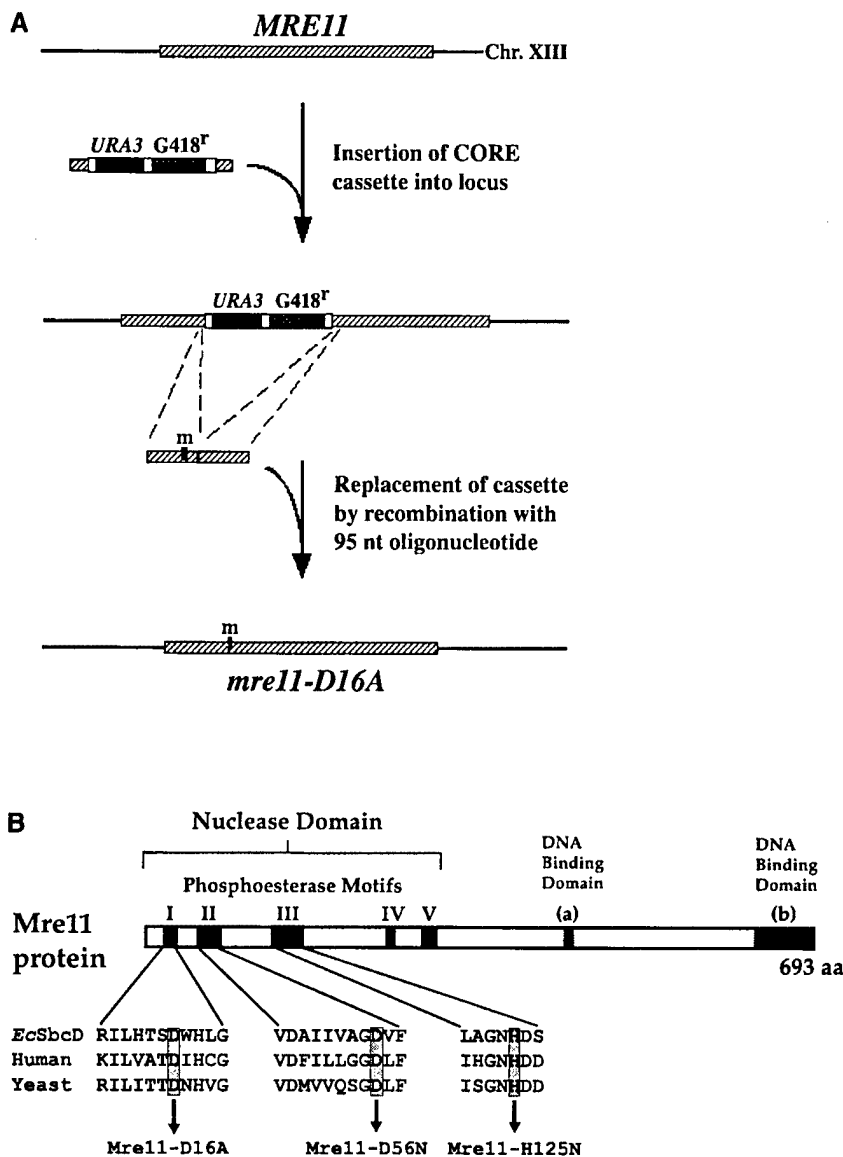
m
———————▨▨▨▨▨▨▨▨▨▨▨▨▨——————

mre11-D16A

FIGURE 1.—Site-specific mutagenesis of the *MRE11* gene using oligonucleotides. (A) Schematic of the *delitto perfetto* method of oligonucleotide-mediated mutagenesis. (B) Phosphoesterase motifs within Mre11 and three substitutions resulting in proteins with reduced activity in *in vitro* assays.

B

Nuclease Domain

DNA Binding Domain (a)   DNA Binding Domain (b)

Phosphoesterase Motifs

Mre11 protein

I II   III   IV V   (a)   (b)

693 aa

*Ec*SbcD	RILHTSDWHLG	VDAIIVAGDVF	LAGNHDS
Human	KILVATDIHCG	VDFILLGGDLF	IHGNHDD
Yeast	RILITTDNHVG	VDMVVQSGDLF	ISGNHDD

Mre11-D16A   Mre11-D56N Mre11-H125N

sensitivity of the *mre11-D16A* mutants is in agreement with this model and may also be an indication that Mre11-D16A protein has reduced nuclease activity relative to the Mre11-D56N and Mre11-H125N enzymes (see DIS-CUSSION).

mre11-D16A cells are unable to repair a site-specific DSB by homologous recombination, but are proficient in NHEJ repair: To address the consequences of the *MRE11* mutations on repair by the two pathways we utilized separate assays that each relied on repair of a defined DSB structure created in a plasmid (shown schematically in Figure 3, A and B). For each assay a single, cohesive-ended DSB with 5′ overhangs that were four bases long served as substrate for repair (see MATE-RIALS AND METHODS). Cells lacking Rad50, Mre11, or Xrs2 have reduced ability to recircularize linear plas-mids *in vivo* after cell transformation if the DSB is in a region that lacks homology with chromosomal DNA. This reduction in recombination-independent repair

by NHEJ, typically ~10- to 100-fold, is not observed in mutants deficient only in the recombination pathway (*e.g.*, *rad51* or *rad52*). NHEJ repair events were scored as transformant cells that had recircularized the broken plasmid under conditions where repair by homologous recombination was not possible. Repair of the DSB by NHEJ was reduced 20-fold in *mre11Δ* strains (Figure 4A). Similar to a previous report for *mre11-D56N* and *mre11-H125N* mutants (MOREAU *et al.* 1999), *mre11-D16A* strains exhibited approximately wild-type levels of NHEJ repair. This observation reinforces the idea that the nuclease functions of the complex are not required for RMX-mediated NHEJ repair. The proficiency at NHEJ also implies that each of the mutants is able to form productive RMX complexes *in vivo*.

RMX mutants exhibit reduced frequencies of ends-in (CROMIE and LEACH 2000; SYMINGTON 2002) DSB-induced plasmid:chromosome recombination. For as-sessment of DSB repair by recombination, cells were
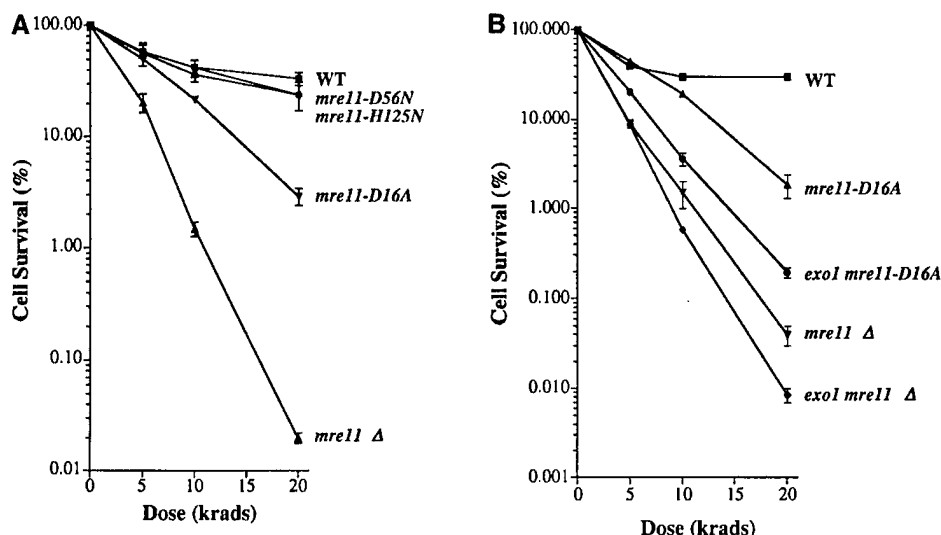
FIGURE 2.—Radiation-induced killing in three nuclease-defective mutant strains. (A) Dose response curves obtained using logarithmically growing haploid cells expressing Mre11-D16A, Mre11-D56N, or Mre11-H125N proteins. (B) Impact of inactivation of the 5'-to-3' exonuclease activity of Exo1 on radiation sensitivities of *mre11* null and *mre11-D16A* cells.

transformed with a linearized integrating plasmid that could undergo recombination with a homologous chromosomal locus (shown schematically in Figure 3B). Cells were transformed with a *HIS3 URA3* DNA fragment (cut within *URA3* using *Nco*I) that could recombine with the chromosomal *ura3-52* locus. Nearly all Ura⁺ recombinants arose from integration of the entire cut plasmid into the chromosome by ends-in recombination to produce Ura⁺ His⁺ cells, but a small fraction (typically ~0.5–1% in wild-type cells) of DSBs were repaired by gene conversion of the chromosomal locus to produce Ura⁺ His⁻ colonies (see below). For all experiments, transformation efficiencies (recombinants formed per microgram of DNA) were normalized to those for uncut *CEN/ARS* plasmids transformed into the same competent cell preparations on the same day.

The efficiency of ends-in recombinational repair was reduced ~20-fold in *mre11Δ* strains (Figure 4B). Interestingly, *mre11-D16A* cells were as defective in recombinational repair of the plasmid DSBs as *mre11Δ* strains. In contrast, recombination was much higher in strains expressing the *mre11-D56N* and *-H125N* mutants (25 and 33% of wild-type levels, respectively). Over 99% of transformant colonies from wild-type cells contained integrated plasmids and were phenotypically Ura⁺ His⁺, with the remainder being Ura⁺ His⁻ gene convertants. The corresponding numbers for *mre11Δ* and *mre11-D16A* cells were 99 and 96%, suggesting that crossover and noncrossover frequencies were not greatly affected.

We also determined if the severe recombination defect observed in the *mre11-D16A* cells was restricted to the types of ends-in plasmid:chromosome targeting events analyzed in Figure 4B. The chromosome mutagenesis procedure employed to create *mre11-D16A* involved replacement of a selectable-counterselectable cassette with homologous DNA contained within an oligonucleotide. This process requires a functional *RAD52* gene (STORICI *et al.* 2001) and involves the alternative,

"ends-out" form of DSB-induced recombination (CROMIE and LEACH 2000; SYMINGTON 2002). The scheme used for the assays is depicted in Figure 3C. Briefly, wild-type and mutant cells containing a *HygBʳ GALp::p53-V122* cassette integrated into *TRP5* were transformed with 95-mer DNA composed of upstream and downstream *TRP5* sequences as described (STORICI *et al.* 2001). Correct recombinational repair events resulted in cells that were *HygBˢ p53⁻* and *TRP5⁺*. As shown in Figure 4C, no recombinants were observed when *rad52* cells were assayed. Recombination frequencies in *mre11Δ* and *mre11-D16A* strains (recorded as integration events per 0.5 nmol of oligonucleotide DNA) were decreased to 2.1 and 1.3% of wild-type levels, respectively. Thus, *mre11-D16A* mutants are approximately as deficient as *mre11* null cells in both classes of recombination events.

The nuclease mutants are differentially sensitive to the S-phase clastogens HU and MMS: Exposure of cells to high levels of the ribonucleotide reductase inhibitor HU leads to replication inhibition and formation of DSBs in chromosomal DNA (MERRILL and HOLM 1999; D'AMOURS and JACKSON 2001). In contrast, low levels of HU produce few DSBs, but do result in activation of the S-phase checkpoint and killing of cells that are deficient in this checkpoint response. Early checkpoint activation events such as phosphorylation of Rad53 are inhibited and survival of RMX mutants is reduced after exposure to low levels of HU (D'AMOURS and JACKSON 2001). Like HU, the DNA-methylating agent MMS induces DSBs during replication and is lethal to mutants defective in DSB repair and the S-phase checkpoint (LEWIS and RESNICK 2000; USUI *et al.* 2001; CHANG *et al.* 2002).

We examined sensitivities of several repair-deficient mutant strains to a range of HU and MMS concentrations (Figure 5). Growth inhibition was apparent in *mre11Δ* strains at concentrations of HU as low as 5.0
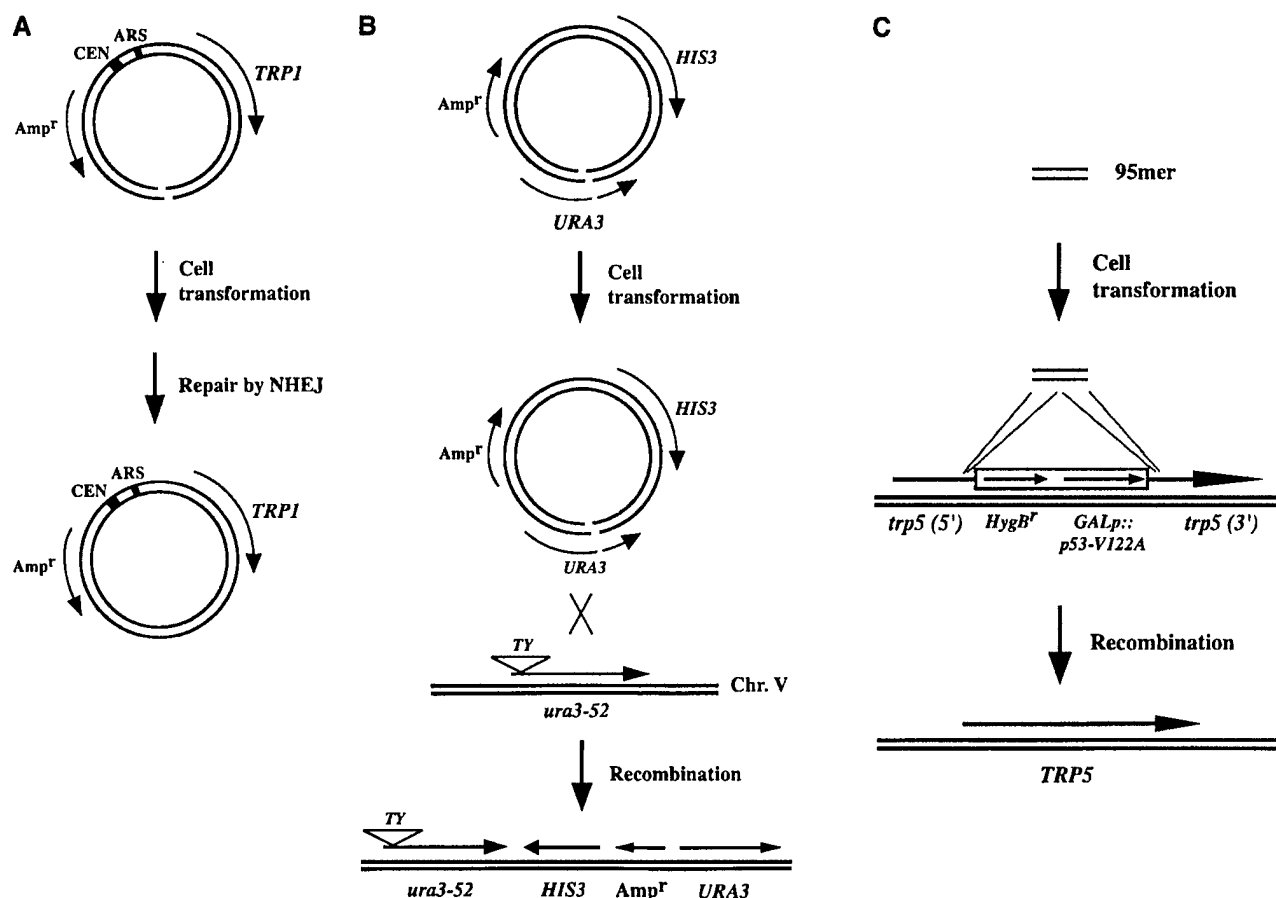
A

ARS
CEN

TRP1

Amp^r

↓ Cell transformation

↓ Repair by NHEJ

ARS
CEN

TRP1

Amp^r

B

HIS3

Amp^r

URA3

↓ Cell transformation

HIS3

Amp^r

URA3

X

TY

Chr. V

ura3-52

↓ Recombination

TY

ura3-52   HIS3   Amp^r URA3

C

═══ 95mer

↓ Cell transformation

trp5 (5')   HygB^r GALp::   trp5 (3')
p53-V122A

↓ Recombination

TRP5

FIGURE 3.—Plasmid assay systems used to monitor repair of a single, cohesive-ended DSB by (A) NHEJ, (B) ends-in plasmid:chromosome homologous recombination, or (C) ends-out recombination using 95-mer oligonucleotide substrates.

mM. These cells were moderately more sensitive than Rec⁻ rad51 cells and much more sensitive than NHEJ-deficient yku70 cells. Cells expressing the phosphoesterase mutants Mre11-D16A, -D56N, and -H125N required much higher doses of HU to detect loss of viability than did mre11 null cells. The mre11-D16A strains exhibited killing at a lower dose (40 mM) than that of either of the other nuclease mutants. A similar general pattern of survival was observed when cells were exposed to MMS (Figure 5B). Relative sensitivities could again be ordered as mre11Δ > rad51Δ > mre11-D16A > mre11-D56N or mre11-H125N (most sensitive to least sensitive). The greater killing of mre11-D16A cells compared to the other two mutants is qualitatively consistent with the radiation survival curves (Figure 2A).

Purified Mre11-D16A protein binds efficiently to Rad50 and Xrs2: Mre11 interacts with Rad50 and Xrs2 to form a trimeric complex (SUNG et al. 2000; SYMINGTON 2002). To ask whether Mre11-D16A protein retains the ability to bind Rad50 and Xrs2, purified six-histidine-tagged Mre11-D16A was mixed with purified Rad50 or Xrs2, and the complexes formed between the protein pairs were isolated using nickel-NTA-agarose beads, which have high affinity for the histidine tag on Mre11-D16A. We included as positive control six-histidine-tagged wild-type Mre11 protein. As shown in Figure 6, A and B, while Rad50 and Xrs2 have no affinity for the nickel-NTA-agarose beads, a substantial portion of these two proteins became associated with the beads when tagged Mre11-D16A was present, indicating complex formation. Importantly, the histidine-tagged Mre11-D16A protein has the same affinity for Rad50 and Xrs2 as histidine-tagged wild-type Mre11 (Figure 6, A and B, lanes 4 and 8). Consistent with the affinity pulldown results, Mre11-D16A forms a trimeric complex with Rad50 and Xrs2 that has a component stoichiometry indistinguishable from that assembled with wild-type Mre11 (CHEN et al. 2001; data not shown). These results, in conjunction with the previous work of FURUSE et al. (1998), demonstrate that Mre11-D16A protein is proficient at both DNA binding and RMX complex formation.

DISCUSSION

The RMX complex is required for successful completion of several specific DNA metabolic processes in mitotic cells. These functions include repair by recombination and end-joining, telomere length maintenance, DNA replication-associated cell cycle checkpoints, inhi-
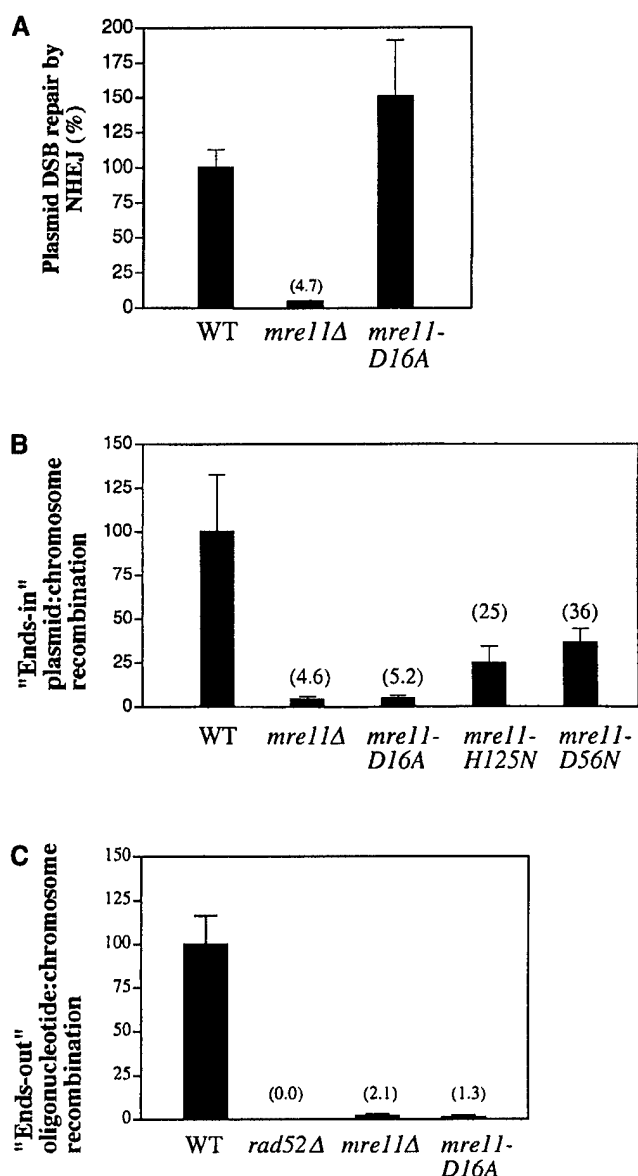
FIGURE 4.—DSB repair proficiencies of haploid cells expressing altered Mre11 proteins with reduced nuclease activity. Efficiencies of repair in wild-type cells by (A) end-joining, (B) ends-in recombination, and (C) ends-out recombination. Transformation efficiencies (repair events per microgram of DNA) in A and B were normalized to those for uncut *CEN/ARS* plasmids transformed into the same competent cell preparations on the same day. Numbers in parentheses indicate means derived from 3–5 assays for each strain. No recombinants were detected for *rad52Δ* strains in C. Error bars indicate standard deviations.

FIGURE 5.—Assessment of S-phase clastogen sensitivities of *mre11-D16A*, *mre11-D56N*, and *mre11-H125N* mutants. Haploid yeast cells were pronged to synthetic glucose plates lacking tryptophan and containing increasing concentrations of (A) hydroxyurea or (B) MMS.

bition of gross chromosomal rearrangements and processing of transiently formed DNA secondary structures such as hairpins (summarized in D'AMOURS and JACKSON 2002; SYMINGTON 2002). Several recent studies have examined possible correlations between the nuclease activities of the purified complex detected *in vitro* and the multiple roles *in vivo*. Most experiments focused on expression and characterization of mutant Mre11

proteins containing alterations within one or more conserved phosphoesterase motifs in the nuclease domain. Four mutant proteins described in the literature, Mre11-D16A (motif I, FURUSE *et al.* 1998), Mre11-D56N and Mre11-H125N (motifs II and III, MOREAU *et al.* 1999; SYMINGTON *et al.* 2000; D'AMOURS and JACKSON 2001; RATTRAY *et al.* 2001; TSUKAMOTO *et al.* 2001; LOBACHEV *et al.* 2002), and Mre11-H213Y (motif IV, TSUBOUCHI and OGAWA 1998; USUI *et al.* 1998; CHAMANKHAH and XIAO 1999; LEE *et al.* 2002), have been evaluated for both *in vitro* nuclease activities and multiple *in vivo* consequences. The D16, D56, and H213 residues are each associated with an Mn^{2+} ion in the crystal structure of Mre11, while the histidine at position 125 is thought to be involved in the phosphodiester hydrolysis reaction (HOPFNER *et al.* 2001).

Characteristics of cells expressing each of the mutant proteins are summarized in Table 2. An additional less well-characterized mutant, *mre11-H125L/D126V*, was included in the table because of its similarity to the *mre11-H125N* allele, although nuclease activities of this protein have not been measured *in vitro*. One of the mutants listed in the table, *mre11-H213Y*, behaves essentially like a null mutation in most *in vivo* assays and is also defective in protein:protein interactions. Thus, this protein is deficient in nuclease activities and also in other functions of the enzyme.

Three of the mutant proteins depicted in Table 2 (D56N, H125N, and D16A) are particularly useful for
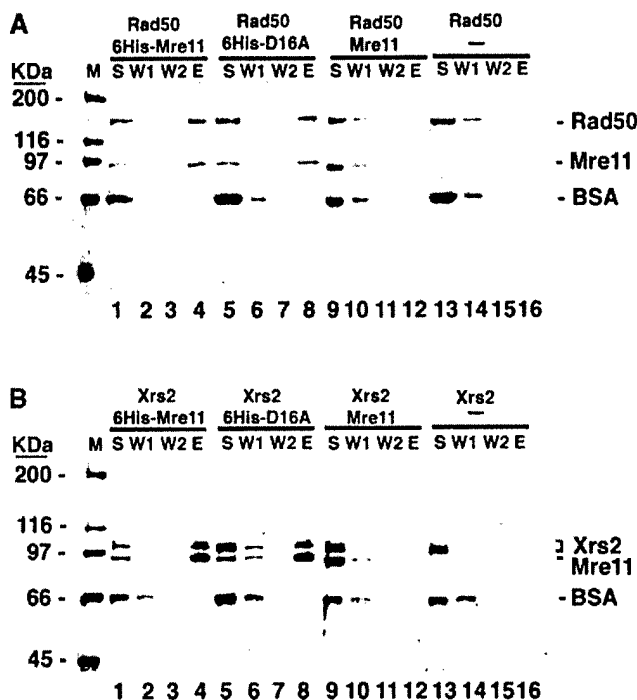
FIGURE 6.—Analysis of binding of wild-type Mre11 and mutant Mre11-D16A protein to Rad50 and Xrs2. (A) Rad50 alone, Rad50 with nontagged Mre11, Rad50 with 6His-Mre11, or Rad50 with 6His-Mre11-D16A (6His-D16A) were incubated with nickel-NTA-agarose beads and washed twice with buffer before the bound proteins were eluted with 200 mM imidazole. The supernatant (S), first wash (W1), second wash (W2), and eluate (E) fractions were run in a 7.5% denaturing polyacrylamide gel followed by staining with Coomassie blue. (B) Xrs2 alone, Xrs2 with Mre11, Xrs2 with 6His-Mre11, and Xrs2 with 6His-Mre11-D16A (6His-D16A) were incubated with nickel-NTA-agarose and bound proteins were eluted as in A. Note that binding of Rad50 and Xrs2 to the nickel-NTA matrix is dependent on the histidine tag on the Mre11 protein (compare lanes 4 and 12 in both A and B).

analysis of cellular requirements for the Mre11 nuclease activities. Each of these proteins has been reported to have no detectable nuclease activities *in vitro*, but the mutant proteins retain many Mre11 functions. For example, each of the proteins is proficient for DNA repair by NHEJ and the purified proteins are capable of RMX complex formation *in vitro* (SYMINGTON 2002; Figure 6; Table 2).

Several common DNA repair and chromosome stability defects are found in cells expressing the altered proteins. For example, all of the mutants are unable to complete meiotic DSB processing. In addition, each mutant is more sensitive than wild-type cells to ionizing radiation, MMS, and HU. *mre11-D16A* cells consistently demonstrated a stronger sensitivity to the clastogens than did the *D56N* and *H125N* mutants. In the two assays of recombinational repair of a defined DSB presented here, the *D16A* mutant behaved as a null while the *D56N* and *H125N* mutants displayed modest reductions. This result is qualitatively consistent with the relative radiation, MMS, and HU

sensitivities. Another property of *mre11-D16A* strains is that telomeres are shortened in these mutants, unlike *mre11-D56N* or *mre11-H125N* cells (FURUSE *et al.* 1998; MOREAU *et al.* 1999). This property has previously been observed in RMX-deleted cells and in strains containing deletions of other NHEJ genes, including *YKU70, YKU80, SIR2, SIR3,* and *SIR4* (LEWIS and RESNICK 2000). If this defect in telomere maintenance is due to a greater reduction in nuclease activity in the Mre11-D16A protein (discussed below), it would be supportive of models that postulate a role for RMX in processing of chromosome ends to generate single-stranded DNA overhangs (DIEDE and GOTTSCHLING 2001).

Of central importance is the question of why the *D16A* mutant has more severe defects in mitotic cells than the other phosphoesterase mutants do. The RMX complex has ssDNA endonuclease and 3'-to-5' dsDNA exonuclease activities, as well as a weak DNA helicase activity. In addition, the Mre11 subunit forms specific associations with DNA, Rad50, Xrs2, and possibly other proteins (Sae2?) and may also be subject to post-translational modification in mitotic cells (D'AMOURS and JACKSON 2002; SYMINGTON 2002). Although each of these activities and associations may vary in the three nuclease mutants, we favor the simplest explanation; *i.e.*, the D16A protein is more defective than the other mutants in nuclease processing of DSBs *in vivo*.

Support for this proposal comes from several considerations. First, many phenotypic differences between the mutants are simply a matter of degree. For example, radiation, MMS, and HU sensitivities and plasmid:chromosome recombination are reduced in all of the mutants and *mre11-D16A* cells are simply more defective than the others.

Second, studies utilizing either overexpression or inactivation of *EXO1* in RMX mutants also provide support. Overexpression of the 5'-to-3' exo activity of Exo1 partially rescues repair of DSBs induced by radiation, MMS, *Eco*RI, and HO in RMX mutants, as well as the mitotic recombination defects of the mutants (LEE *et al.* 2002; LEWIS *et al.* 2002; SYMINGTON 2002 and references within). This effect is likely due to enhanced processing of the broken DNA ends by Exo1 to create 3' tailed substrates for the Rad51/Rad52 strand exchange complex. We note, however, that *EXO1* overexpression does not rescue meiotic DSB repair (involving removal of DNA ends containing attached protein by Mre11 endonuclease activity), inverted repeat-stimulated recombination (thought to involve endonuclease cleavage of hairpin loops), or shortening of telomeres (which might also involve endo cleavage of T-loop structures; DIEDE and GOTTSCHLING 2001; SYMINGTON 2002; K. LOBACHEV and M. RESNICK, unpublished results). These latter results clearly point to the importance of the endonuclease activity of Mre11 *in vivo*. The endo activity may also be important in resection of damage-induced DSB ends in mitotic cells, possibly in conjunction with the

TABLE 2

Impact of Mre11 proteins with reduced *in vitro* nuclease activities on DNA repair and stability

Allele	*In vitro* nuclease activities		Associations			Plasmid NHEJ	Spontaneous diploid recombination	Survival		DSB repair by recombination		Telomere stability	Meiotic recombination
	Endo	Exo	DNA	Mre11	R/X[a]			Radiation	MMS	Ends-in	Ends-out		
MRE11	+	+	+	+	+	+	+	+	+	+	+	+	+
mre11Δ	NA	NA	NA	NA	NA	−−−	+++	−−−	−−−	−−−	−−−	−−−	−−−
mre11-D16A	−−−	−−−	+	+	+	+	+	−−−	−−−	−−−	−−−	−	−−−
mre11-D56N	−−−	−−−	ND	ND	+	+	+	+/−[b]	+/−[b]	−	ND	+	−−−
mre11-H125N	−−−	−−−	ND	ND	+	+	+	+/−[b]	+/−[b]	−	ND	+	−−−
mre11-H125L/ D126V (mre11-3)	ND	ND	ND	ND	+	ND	+	+/−[b]	+	ND	ND	+	−
mre11-H213Y (mre11-58)	−−−	−−−	ND	−−−	−−−	ND	+++	ND	−−/−−−[c]	ND	ND	−	−−−

References are as follows: Mre11-D56N and Mre11-H125N (MOREAU *et al.* 1999; SYMINGTON 2002; this work), Mre11-H125L/D126V (BRESSAN *et al.* 1998; LEE *et al.* 2002), Mre11-D16A (FURUSE *et al.* 1998; this work), and Mre11-H213Y (Mre11-58; TSUBOUCHI and OGAWA 1998; USUI *et al.* 1998; CHAMANKHAH and XIAO 1999; LEE *et al.* 2002). NA, not applicable; ND, no data; +, wild-type efficiency; +++, higher than wild type; −, slight deficiency; −−, moderate deficiency; −−−, strong deficiency.

[a] Binding of mutant Mre11 protein to Rad50/Xrs2.

[b] Mutants exhibit more killing than wild-type cells only at high doses of radiation (>30 krad) or high concentrations of MMS (this work; MOREAU *et al.* 1999); survival of mre11-H125L/D126V mutants was also near wild type over the dose range 0–30 krad (BRESSAN *et al.* 1998).

[c] Different levels of MMS sensitivity were reported (TSUBOUCHI and OGAWA 1998; USUI *et al.* 1998; LEE *et al.* 2002).

weak helicase activity of the complex (TRUJILLO and SUNG 2001; SYMINGTON 2002). The major point here is that increased levels of a nuclease (Exo1) rescues clastogen sensitivities and recombination defects of RMX mutants during mitotic growth, suggesting that nuclease processing is the function that is missing.

Analyses of the ionizing radiation sensitivities of *mre11-D16A* and *mre11-H125* mutants with and without a functional *EXO1* gene present also lend support to this premise. *mre11-D16A* strains were more sensitive than the other nuclease mutants and *mre11-D16A exo1* double mutants exhibited a linear, dose-dependent reduction in survival that was greater than that of *mre11-D16A* single mutants (~10-fold difference at 20 krad). This indicates that much of the resistance in the *D16A* single mutants was due to basal levels of Exo1. The strong sensitivity of these cells and its dependence on Exo1 seem most consistent with the idea that very little or no nuclease activity is retained in the Mre11-D16A complex *in vivo*, although other factors may also be involved.

In contrast to results with D16A, radiation survival was high in *mre11-H125N* mutants and was not reduced further in *mre11-H125N exo1* double mutants at doses up to 30 krad (MOREAU *et al.* 2001; Figure 2), which corresponds to ~40 DSBs per G_2 cell (RESNICK and MARTIN 1976). If the Mre11-H125N protein is nuclease deficient, then this result would indicate that cells lacking both RMX and Exo1 nuclease activities are largely proficient at processing of radiation-induced DSBs for recombinational repair. Put another way, this would mean that the major enzymatic activities defined for Mre11 (and Exo1) *in vitro* are not essential for a major function of the complex *in vivo* (repair of chemically and physically induced DSBs). It seems more likely that survival is high in *mre11-H125N* cells lacking the "backup" Exo1 nuclease activity because the mutant RMX complex has residual nuclease activity *in vivo*.

Another question that must be addressed is the following: If the nuclease activity of *mre11-D16A* mutants is absent (or greatly reduced), why is radiation resistance not reduced to the level of *mre11* null strains? We suggest that an important difference here is the presence or absence of the RMX complex bound to DSB ends. Structural studies have indicated that two Mre11 molecules bind to the proximal ends of two folded, fibrous Rad50 subunits to form the DNA-binding portion of the complex (ANDERSON *et al.* 2001; CHEN *et al.* 2001; DE JAGER *et al.* 2001; HOPFNER *et al.* 2002). The structures imply that RMX might potentially form a bridge between two DNA ends in a broken molecule or between adjacent sister chromatids in a replicated chromosome. The latter structure would be consistent with the observation that Rad50 is structurally similar to SMC proteins required for sister chromatid cohesion (HOPFNER *et al.* 2000). It is possible that this "tethering" function of RMX is retained in the mutant Rad50/Mre11-D16A/

Xrs2 complex, although nuclease activities are reduced. We infer that this tethering, combined with redundant nuclease activities, provides an explanation for the observation that the radiation sensitivity of *mre11-D16A* cells did not reach that of *mre11Δ* cells. After exposure to ionizing radiation, the tethering function would keep sister chromatids (or possibly broken DNA ends) in proximity and enhance the likelihood that a break is processed by Exo1 or another partially redundant nuclease and repaired by the dominant pathway of radiation repair in yeast, homologous recombination.

mre11-D16A mutants were not as radiation sensitive as *mre11Δ* cells, but they were as defective as null cells in the ends-in and ends-out recombination assays. It is possible that the impact of RMX DNA bridging is less in the plasmid:chromosome and oligonucleotide:chromosome DSB repair assays than in the radiation survival assays, since the latter are almost completely dependent on sister chromatid exchanges. DNA tethering by mutant RM*X complexes may also explain why spontaneous recombination rates of diploid cells are not elevated in the three mutants with reduced nuclease activities (Table 2). Unlike other RAD52 group mutants, diploid strains lacking RMX display increased spontaneous recombination between homologous chromosomes, possibly because of a reduced preference for interactions between sister chromatids (SYMINGTON 2002). The absence of high spontaneous recombination rates in the three nuclease mutants may be an indication that RMX complexes containing Mre11-D16A, Mre11-D56N, and Mre11-H125N are still capable of forming bridges between sister chromatids, and therefore the strong preference for sister-sister recombination has been retained.

mre11-D56N and *mre11-H125N* mutants have only slight reductions in mitotic DSB repair, but they show strong defects in assays of inverted repeat-stimulated recombination in mitotic cells and DSB processing in meiotic cells (this work; RATTRAY *et al.* 2001; LOBACHEV *et al.* 2002; SYMINGTON 2002). The latter two processes are likely to involve endonucleolytic cleavage of transiently formed hairpin structures and protein-bound DNA ends, respectively, and they cannot be rescued by overexpression of *EXO1*. It is possible that the mutant D56N and H125N complexes have a reduced level of endonuclease activity *in vivo* and that the type of endprocessing required for these structures cannot be supplied by backup enzymes such as Exo1. If this is true, then the reduced levels of RMX endonuclease activity in the mutants might be limiting for these repair events, but not for others that can also be performed by redundant nucleases. Other possibilities, such as impacts on helicase activity or postendonucleolytic processing by the exonuclease cannot be ruled out, however.

Finally, we note that D16 of *S. cerevisiae* Mre11 is completely conserved among many related yeasts (H125 also), but D56 is changed to a valine in the yeast *S. kluyveri* (Saccharomyces Genome Database; http://www.

yeastgenome.org/). The reduced evolutionary conservation of this aspartic acid, one of several residues found in association with Mn²⁺ ions in the *P. furiosus* Mre11 crystal structure, suggests that its contributions to the phosphodiesterase reaction may be less critical than those of other residues such as D16.

In summary, cells expressing Mre11-D16A exhibit several dramatic mitotic DNA repair defects that are more severe than those seen in two widely studied phosphoesterase mutants with reduced *in vitro* nuclease activities. The mutant protein exhibits normal RMX complex formation and DNA binding *in vitro* and *mre11-D16A* cells are proficient at NHEJ repair *in vivo*. We suggest that the strong radiation sensitivity and recombination defects are due primarily to lack of nuclease processing by the mutant Rad50/Mre11-D16A/Xrs2 complex. This conclusion is contrary to those of previous mutant studies proposing a limited role for the Mre11 nuclease activity in mitotic cells (*e.g.*, BRESSAN *et al.* 1999; MOREAU *et al.* 1999; SYMINGTON *et al.* 2000; TSUKAMOTO *et al.* 2001; LOBACHEV *et al.* 2002) and suggests the possibility that some mutants such as *mre11-D56N* and *-H125N* may have residual nuclease activity *in vivo*. We note that more subtle distinctions are also possible. For example, the endo- and exonuclease activities, whose precise roles in DNA processing *in vivo* remain unclear, may be differentially affected in the mutants. It is likely that the residual radiation resistance in haploid *mre11-D16A* mutants and the absence of high spontaneous recombination in *mre11-D16A* diploids arise, at least in part, because the mutant complex retains the ability to tether sister chromatids and/or DSB ends. It is intriguing that telomeres are shortened in *mre11-D16A* cells. This result might also be due to a greater loss of nuclease activities in this mutant and supports the idea that chromosome ends (possibly forming T-loop structures) may require processing by RMX to create substrates for DNA replication by telomerase (DIEDE and GOTTSCHLING 2001).

LITERATURE CITED

ALANI, E., R. PADMORE and N. KLECKNER, 1990 Analysis of wild-type and *rad50* mutants of yeast suggests an intimate relationship between meiotic chromosome synapsis and recombination. Cell **61:** 419–436.

ANDERSON, D. E., K. M. TRUJILLO, P. SUNG and H. P. ERICKSON, 2001 Structure of the Rad50-Mre11 DNA repair complex from *Saccharomyces cerevisiae* by electron microscopy. J. Biol. Chem. **276:** 37027–37033.

BAUM, B., 1995 Mre11 and *S. pombe* Rad32 are phosphoesterases. Yeast Update Newsl. **3** (7): 1.

BENNETT, C. B., L. K. LEWIS, G. KARTHIKEYAN, K. S. LOBACHEV, Y. H. JIN *et al.*, 2001 Genes required for ionizing radiation resistance in yeast. Nat. Genet. **29:** 426–434.

BRACHMANN, C. B., A. DAVIES, G. J. COST, E. CAPUTO, J. LI *et al.*, 1998

Designer deletion strains derived from *Saccharomyces cerevisiae* S288C: a useful set of strains and plasmids for PCR-mediated gene disruption and other applications. Yeast **14:** 115–132.

BRESSAN, D. A., H. A. OLIVARES, B. E. NELMS and J. H. PETRINI, 1998 Alteration of N-terminal phosphoesterase signature motifs inactivates *Saccharomyces cerevisiae* Mre11. Genetics **150:** 591–600.

BRESSAN, D. A., B. K. BAXTER and J. H. PETRINI, 1999 The Mre11-Rad50-Xrs2 protein complex facilitates homologous recombination-based double-strand break repair in *Saccharomyces cerevisiae.* Mol. Cell. Biol. **19:** 7681–7687.

CHAMANKHAH, M., and W. XIAO, 1999 Formation of the yeast Mre11-Rad50-Xrs2 complex is correlated with DNA repair and telomere maintenance. Nucleic Acids Res. **27:** 2072–2079.

CHAMANKHAH, M., T. FONTANIE and W. XIAO, 2000 The *Saccharomyces cerevisiae mre11(ts)* allele confers a separation of DNA repair and telomere maintenance functions. Genetics **155:** 569–576.

CHANG, M., M. BELLAOUI, C. BOONE and G. W. BROWN, 2002 A genome-wide screen for methyl methanesulfonate-sensitive mutants reveals genes required for S phase progression in the presence of DNA damage. Proc. Natl. Acad. Sci. USA **99:** 16934–16939.

CHEN, C., and R. D. KOLODNER, 1999 Gross chromosomal rearrangements in *Saccharomyces cerevisiae* replication and recombination defective mutants. Nat. Genet. **23:** 81–85.

CHEN, L., K. TRUJILLO, W. RAMOS, P. SUNG and A. E. TOMKINSON, 2001 Promotion of Dnl4-catalyzed DNA end-joining by the Rad50/Mre11/Xrs2 and Hdf1/Hdf2 complexes. Mol. Cell **8:** 1105–1115.

CROMIE, G. A., and D. R. LEACH, 2000 Control of crossing over. Mol. Cell **6:** 815–826.

D'AMOURS, D., and S. P. JACKSON, 2001 The yeast Xrs2 complex functions in S phase checkpoint regulation. Genes Dev. **15:** 2238–2249.

D'AMOURS, D., and S. P. JACKSON, 2002 The Mre11 complex: at the crossroads of DNA repair and checkpoint signalling. Nat. Rev. Mol. Cell. Biol. **3:** 317–327.

DE JAGER, M., J. VAN NOORT, D. C. VAN GENT, C. DEKKER, R. KANAAR *et al.*, 2001 Human Rad50/Mre11 is a flexible complex that can tether DNA ends. Mol. Cell **8:** 1129–1135.

DIEDE, S. J., and D. E. GOTTSCHLING, 2001 Exonuclease activity is required for sequence addition and Cdc13p loading at a de novo telomere. Curr. Biol. **11:** 1336–1340.

FUKUDA, T., T. SUMIYOSHI, M. TAKAHASHI, T. KATAOKA, T. ASAHARA *et al.*, 2001 Alterations of the double-strand break repair gene MRE11 in cancer. Cancer Res. **61:** 23–26.

FURUSE, M., Y. NAGASE, H. TSUBOUCHI, K. MURAKAMI-MUROFUSHI, T. SHIBATA *et al.*, 1998 Distinct roles of two separable in vitro activities of yeast Mre11 in mitotic and meiotic recombination. EMBO J. **17:** 6412–6425.

GIANNINI, G., E. RISTORI, F. CERIGNOLI, C. RINALDI, M. ZANI *et al.*, 2002 Human MRE11 is inactivated in mismatch repair-deficient cancers. EMBO Rep. **3:** 248–254.

GRENON, M., C. GILBERT and N. F. LOWNDES, 2001 Checkpoint activation in response to double-strand breaks requires the Mre11/Rad50/Xrs2 complex. Nat. Cell Biol. **3:** 844–847.

HOPFNER, K. P., A. KARCHER, D. S. SHIN, L. CRAIG, L. M. ARTHUR *et al.*, 2000 Structural biology of Rad50 ATPase: ATP-driven conformational control in DNA double-strand break repair and the ABC-ATPase superfamily. Cell **101:** 789–800.

HOPFNER, K. P., A. KARCHER, L. CRAIG, T. T. WOO, J. P. CARNEY *et al.*, 2001 Structural biochemistry and interaction architecture of the DNA double-strand break repair Mre11 nuclease and Rad50-ATPase. Cell **105:** 473–485.

HOPFNER, K. P., L. CRAIG, G. MONCALIAN, R. A. ZINKEL, T. USUIT *et al.*, 2002 The Rad50 zinc-hook is a structure joining Mre11 complexes in DNA recombination and repair. Nature **418:** 562–566.

KOUPRINA, N., N. NIKOLAISHVILI, J. GRAVES, M. KORIABINE, M. A. RESNICK *et al.*, 1999 Integrity of human YACs during propagation in recombination-deficient yeast strains. Genomics **56:** 262–273.

LARIONOV, V., N. KOUPRINA, N. NIKOLAISHVILI and M. A. RESNICK, 1994 Recombination during transformation as a source of chimeric mammalian artificial chromosomes in yeast (YACs). Nucleic Acids Res. **22:** 4154–4162.

LEE, S. E., D. A. BRESSAN, J. H. J. PETRINI and J. E. HABER, 2002 Complementation between N-terminal *Saccharomyces cerevisiae mre11*

alleles in DNA repair and telomere length maintenance. DNA Repair **1:** 27–40.

LEWIS, L. K., and M. A. RESNICK, 2000 Tying up loose ends: nonhomologous end-joining in *Saccharomyces cerevisiae.* Mutat. Res. **451:** 71–89.

LEWIS, L. K., J. M. KIRCHNER and M. A. RESNICK, 1998 Requirement for end-joining and checkpoint functions, but not *RAD52*-mediated recombination after *Eco*RI endonuclease cleavage of *Saccharomyces cerevisiae* DNA. Mol. Cell. Biol. **18:** 1891–1902.

LEWIS, L. K., G. KARTHIKEYAN, J. W. WESTMORELAND and M. A. RESNICK, 2002 Differential suppression of DNA repair deficiencies of yeast *rad50, mre11* and *xrs2* mutants by *EXO1* and *TLC1* (the RNA component of telomerase). Genetics **160:** 49–62.

LOBACHEV, K. S., D. A. GORDENIN and M. A. RESNICK, 2002 The Mre11 complex is required for repair of hairpin-capped double-strand breaks and prevention of chromosome rearrangements. Cell **108:** 183–193.

MERRILL, B. J., and C. HOLM, 1999 A requirement for recombinational repair in *Saccharomyces cerevisiae* is caused by DNA replication defects of *mec1* mutants. Genetics **153:** 595–605.

MOREAU, S., J. R. FERGUSON and L. S. SYMINGTON, 1999 The nuclease activity of Mre11 is required for meiosis but not for mating type switching, end-joining, or telomere maintenance. Mol. Cell. Biol. **19:** 556–566.

MOREAU, S., E. A. MORGAN and L. S. SYMINGTON, 2001 Overlapping functions of the *Saccharomyces cerevisiae* Mre11, Exo1 and Rad27 nucleases in DNA metabolism. Genetics **159:** 1423–1433.

MYUNG, K., and R. D. KOLODNER, 2002 Suppression of genome instability by redundant S-phase checkpoint pathways in *Saccharomyces cerevisiae.* Proc. Natl. Acad. Sci. USA **99:** 4500–4507.

PAULL, T. T., and M. GELLERT, 1999 Nbs1 potentiates ATP-driven DNA unwinding and endonuclease cleavage by the Mre11/Rad50 complex. Genes Dev. **13:** 1276–1288.

PETRINI, J. H., 1999 The mammalian Mre11-Rad50-Nbs1 protein complex: integration of functions in the cellular DNA-damage response. Am. J. Hum. Genet. **64:** 1264–1269.

RATTRAY, A. J., C. B. McGILL, B. K. SHAFER and J. N. STRATHERN, 2001 Fidelity of mitotic double-strand-break repair in *Saccharomyces cerevisiae*: a role for *SAE2/COM1.* Genetics **158:** 109–122.

RESNICK, M. A., and P. MARTIN, 1976 The repair of double-strand breaks in the nuclear DNA of *Saccharomyces cerevisiae* and its genetic control. Mol. Gen. Genet. **143:** 119–129.

SAEKI, T., I. MACHIDA and S. NAKAI, 1980 Genetic control of diploid recovery after gamma-irradiation in the yeast *Saccharomyces cerevisiae.* Mutat. Res. **73:** 251–265.

SHARPLES, G. J., and D. R. LEACH, 1995 Structural and functional similarities between the SbcCD proteins of *Escherichia coli* and the RAD50 and MRE11 (RAD32) recombination and repair proteins of yeast. Mol. Microbiol. **17:** 1215–1217.

SIKORSKI, R. S., and P. HIETER, 1989 A system of shuttle vectors and

yeast host strains designed for efficient manipulation of DNA in *Saccharomyces cerevisiae.* Genetics **122:** 19–27.

STEWART, G. S., R. S. MASER, T. STANKOVIC, D. A. BRESSAN, M. I. KAPLAN *et al.,* 1999 The DNA double-strand break repair gene hMRE11 is mutated in individuals with an Ataxia-Telangiectasia-like disorder. Cell **99:** 577–587.

STORICI, F., and M. A. RESNICK, 2003 *Delitto perfetto* targeted mutagenesis in yeast with oligonucleotides, pp. 191–209 in *Genetic Engineering,* Vol. 25, edited by J. K. SETLOW. Kluwer Academic/Plenum Publishers, Dordrecht, The Netherlands.

STORICI, F., L. K. LEWIS and M. A. RESNICK, 2001 *In vivo* site-directed mutagenesis using oligonucleotides. Nat. Biotechnol. **19:** 773–776.

SUNG, P., K. M. TRUJILLO and S. VAN KOMEN, 2000 Recombination factors of *Saccharomyces cerevisiae.* Mutat. Res. **451:** 257–275.

SYMINGTON, L. S., 2002 Role of RAD52 epistasis group genes in homologous recombination and double-strand break repair. Microbiol. Mol. Biol. Rev. **66:** 630–670.

SYMINGTON, L. S., L. E. KANG and S. MOREAU, 2000 Alteration of gene conversion tract length and associated crossing over during plasmid gap repair in nuclease-deficient strains of *Saccharomyces cerevisiae.* Nucleic Acids Res. **28:** 4649–4656.

TRAN, H. T., D. A. GORDENIN and M. A. RESNICK, 1999 The 3′→5′ exonucleases of DNA polymerases delta and epsilon and the 5′→3′ exonuclease Exo1 have major roles in postreplication mutation avoidance in *Saccharomyces cerevisiae.* Mol. Cell. Biol. **19:** 2000–2007.

TRUJILLO, K. M., and P. SUNG, 2001 DNA structure-specific nuclease activities in the *Saccharomyces cerevisiae* Rad50:Mre11 complex. J. Biol. Chem. **276:** 35458–35464.

TRUJILLO, K. M., D. H. ROH, L. CHEN, S. VAN KOMEN, A. TOMKINSON *et al.,* 2003 Yeast Xrs2 binds DNA and helps target Rad50 and Mre11 to DNA ends. J. Biol. Chem. **278:** 48957–48964.

TSUBOUCHI, H., and H. OGAWA, 1998 A novel mre11 mutation impairs processing of double-strand breaks of DNA during both mitosis and meiosis. Mol. Cell. Biol. **18:** 260–268.

TSUBOUCHI, H., and H. OGAWA, 2000 Exo1 roles for repair of DNA double-strand breaks and meiotic crossing over in *Saccharomyces cerevisiae.* Mol. Biol. Cell **11:** 2221–2233.

TSUKAMOTO, Y., A. K. TAGGART and V. A. ZAKIAN, 2001 The role of the Mre11-Rad50-Xrs2 complex in telomerase-mediated lengthening of *Saccharomyces cerevisiae* telomeres. Curr. Biol. **11:** 1328–1335.

USUI, T., T. OHTA, H. OSHIUMI, J. TOMIZAWA, H. OGAWA *et al.,* 1998 Complex formation and functional versatility of Mre11 of budding yeast in recombination. Cell **95:** 705–716.

USUI, T., H. OGAWA and J. H. PETRINI, 2001 A DNA damage response pathway controlled by Tel1 and the Mre11 complex. Mol. Cell **7:** 1255–1266.

Effects of Tumor-associated Mutations on Rad54 Functions*

Marina Smirnova‡§, Stephen Van Komen§¶, Patrick Sung¶‖, and Hannah L. Klein‡**

From the ‡Department of Biochemistry and Kaplan Comprehensive Cancer Institute, New York University School of Medicine, New York, New York 10016 and the ¶Department of Molecular Biophysics and Biochemistry, Yale University School of Medicine, New Haven, Connecticut 06520

Yeast *RAD54* gene, a member of the *RAD52* epistasis group, plays an important role in homologous recombination and DNA double strand break repair. Rad54 belongs to the Snf2/Swi2 protein family, and it possesses a robust DNA-dependent ATPase activity, uses free energy from ATP hydrolysis to supercoil DNA, and cooperates with the Rad51 recombinase in DNA joint formation. There are two *RAD54*-homologous genes in human cells, *hRAD54* and *RAD54B*. Mutations in these human genes have been found in tumors. These tumor-associated mutations map to conserved regions of the hRad54 and hRad54B proteins. Here we introduced the equivalent mutations into the *Saccharomyces cerevisiae RAD54* gene in an effort to examine the functional consequences of these gene changes. One mutant, *rad54 G484R*, showed sensitivity to DNA-damaging agents and reduced homologous recombination rates, indicating a loss of function. Even though the purified rad54 G484R mutant protein retained the ability to bind DNA and interact with Rad51, it was nearly devoid of ATPase activity and was similarly defective in DNA supercoiling and D-loop formation. Two other mutants, *rad54 N616S* and *rad54 D442Y*, were not sensitive to genotoxic agents and behaved like the wild type allele in homologous recombination assays. Consistent with the mild phenotype associated with the *rad54 N616S* allele, its encoded protein was similar to wild type Rad54 protein in biochemical attributes. Because dysfunctional homologous recombination gives rise to genome instability, our results are consistent with the premise that tumor-associated mutations in hRad54 and Rad54B could contribute to the tumor phenotype or enhance the genome instability seen in tumor cells.

In *Saccharomyces cerevisiae*, homologous recombination (HR)[1] represents an important means for the repair of DNA

double strand breaks and other types of DNA damage and also for restarting stalled replication forks (1–5). HR depends on the use of a homologous DNA molecule as a template to eliminate double strand breaks and other lesions mostly with high fidelity. Impaired HR results in genetic instability and sensitivity to genotoxic agents (6) and can lead to cancer in humans (7).

Double strand break repair by HR is dependent on genes of the *RAD52* epistasis group, *RAD50*, *RAD51*, *RAD54*, *RAD55*, *RAD57*, *RAD59*, *RDH54/TID1*, *MRE11*, and *XRS2*, in which structure and function have been highly conserved (6). Before repair can occur, the ends of double strand breaks are processed by nucleolytic resection of the 5′ ends of the breaks to yield ssDNA, which is then bound by Rad51 to form a helical nucleoprotein filament often referred to as the presynaptic filament. Nucleation of Rad51 onto the ssDNA is facilitated by recombination mediators, including Rad52, the Rad55-Rad57 complex, and Rad54 (6, 8). Once assembled, the presynaptic filament mediates a search for homology in the homologous dsDNA partner and forms a DNA joint molecule (called D-loop) with the latter. The length of the nascent DNA joint molecule is extended by DNA branch migration (9), and the D-loop is resolved by one of several pathways that yields recombinants with or without associated crossovers (6).

The *RAD54* gene encodes a dsDNA-dependent ATPase of the Swi2/Snf2 family (10). Rad54 protein physically interacts with Rad51 protein (11–13) and binds ssDNA preferentially. Rad54 utilizes the free energy from ATP hydrolysis to translocate on dsDNA and induces dynamic topological changes in the DNA (8, 14, 15). The ATPase and DNA supercoiling activities of Rad54 are stimulated by Rad51 (15, 16). Rad54 protein appears to play a role in different steps of the HR process. Rad54 promotes assembly of the presynaptic filament apparently by loading Rad51 onto ssDNA and enhancing filament stability (17, 18). Although Rad51 has only a weak ability to form the D-loop, the inclusion of Rad54 renders D-loop formation highly robust (11, 15, 19, 20). The negative supercoils produced by Rad54 result in transient opening of the DNA strands (15), which may aid in strand invasion by the presynaptic filament in the D-loop reaction. Rad54 also stimulates DNA branch migration by severalfold (21) and cooperates with the presynaptic filament in chromatin remodeling (22–24). In addition, Rad54 can dissociate Rad51 from duplex DNA, an activity believed to be germane for Rad51 recycling and the promotion of DNA repair synthesis during recombination (25).

The protein encoded by *RDH54/TID1* is structurally related to Rad54 protein. Rdh54/Tid1 protein is important for meiotic recombination but has a relatively minor role in mitotic recombination (26, 27). Rdh54/Tid1 also possesses a dsDNA-activated ATPase activity via its dsDNA, binds Rad51, translocates on and supercoils dsDNA, and greatly stimulates D-loop

[1] The abbreviations used are: HR, homologous recombination; ssDNA, single strand DNA; dsDNA, double strand DNA; MMS, methyl methanesulfonate; HU, hydroxyurea; BSA, bovine serum albumin; SC, synthetic complete; YEPD, yeast extract peptone dextrose.

formation (8, 28). It remains to be seen whether or not Rdh54/ Tids affects presynaptic filament assembly, stimulates DNA branch migration, functions in chromatin remodeling, and removes Rad51 from duplex DNA.

Two Rad54 homologous proteins have been found in different eukaryotic species (29). The human hRad54 protein has 68% similarity with ScRad54 protein. A second human homologue, *RAD54B*, was described subsequently (30). The NH$_2$-terminal region of *RAD54B* shares homology with yeast *RDH54*. *In vitro* experiments show a dsDNA-dependent ATPase in hRad54 and that hRad54 translocates on dsDNA (14, 31) and promotes transient separation of the strands in duplex DNA (31). Interaction with hRad51 stimulates the ATPase activity, DNA supercoiling, and the DNA strand opening activities of hRad54. hRad51 and hRad54 cooperate in the formation of D-loops (31). Except for the demonstration of a dsDNA-dependent ATPase activity (32), the Rad54B protein remains poorly characterized.

In vertebrate cells, interference with HR has a strong impact on viability and genomic stability. For instance, cells with hypomorphic mutations in the *RAD51* gene are genetically unstable and sensitive to DNA-damaging agents, and disruption of the *RAD51* gene is lethal (33, 34). The importance of HR in cancer avoidance is best appreciated in studies of the breast tumor suppressor genes *BRCA1* and *BRCA2*. Cells with mutations in *BRCA1* and *BRCA2* are impaired for HR and show a high rate of chromosome aberration, sensitivity to DNA-damaging agents, and elevated mutation rates (35–42). BRCA2 binds Rad51 through a series of BRC repeats and is thought to promote the assembly of the presynaptic filament (40–42).

As expected, Rad54 and Rad54B both function in HR in mammalian cells. Inactivation of the mouse *RAD54* gene causes a marked sensitivity to DNA-damaging agents in embryonic stem cells, but somatic cells deleted for Rad54 show only a slight increase in radiosensitivity (43–46). Inactivation of the *RAD54B* gene in a colon cancer cell line resulted in a severe reduction of targeted integration frequency, whereas sensitivity to DNA-damaging agents and sister chromatid exchange was not significantly affected (47). hRad54 protein co-localizes with hRad51 and BRCA1 in the nucleus (48, 49), and significant colocalization of Rad54B with hRad51 and BRCA1 has also been observed (50). Interestingly, several point mutations in conserved regions of the *hRAD54* and *RAD54B* genes have been found in primary tumors (30, 51), but the functional consequences of these mutations on gene function and their causal relationship to the tumor phenotype is not known. To ascertain the possible effects of the tumor-associated *hRAD54* and *RAD54B* mutations on protein functions, we introduced these mutations into the homologous sites in the *S. cerevisiae RAD54* gene. We found that two mutations, *rad54 N616S* and *rad54 D442Y*, engendered little or no phenotype but that another mutation, *rad54 G484R*, behaved similarly to the *rad54Δ* null allele. The severe phenotype seen with the *rad54 G484R* allele was because of an inability of the mutant protein to hydrolyze ATP. The implications of our results are discussed.

EXPERIMENTAL PROCEDURES

Media, Growth Condition, and Genetic Analysis—Standard media were prepared as described (52). All strains were grown at 30 °C. Genetic analysis was performed according to standard procedure (52).

Construction of rad54 Mutants—Mutations were introduced into the *S. cerevisiae RAD54* gene using the QuikChange site-directed mutagenesis kit (Stratagene). Mutagenic PCR primers were used in PCR reactions with the *RAD54* gene cloned into the pUC18 vector as a template. Mutation confirmation was performed by restriction enzyme digestion, which specifically recognizes each change, and by DNA sequencing to ensure that no other mutations were introduced inadvertently. For genetic analyses, pRS306 (*URA3*, integrating) derivatives containing the *rad54 D442Y*, *rad54 G484R*, or *rad54 N616S* allele were linearized

by HindIII, purified, and then used for transforming wild type yeast strain HKY579-1A. Chromosomal integrants were selected on SC-ura media. After 2 days of growth on YEPD, the integrants were transferred to 5-fluoroorotic acid-containing media. 5-Fluoroorotic acid-resistant colonies were analyzed for the presence of the *RAD54* mutations by PCR analysis of the genomic *RAD54* gene, using the restriction enzymes diagnostic for each mutation and DNA sequencing of the PCR products.

For protein purification, the *rad54 G484R* and *rad54 N616S* alleles were cloned into pPM231.6His (2μ, *LEU2-d, GAL-PGK-6His*) to add a six-histidine sequence at the NH$_2$-terminal end of the *rad54*-encoded products and place the histidine-tagged mutant genes under the control of the galactose-inducible *GAL-PGK* promoter for expression in yeast cells (11). Plasmids pR54.G484R.1 (2μ, *LEU2-d, GAL-PGK-6His-rad54 G484R*) and pR54.N616S.1 (2μ, *LEU2-d, GAL-PGK-6His-rad54 N616S*) were transformed into the protease-deficient strain BJ5464.

Yeast Strains—Yeast strains for genetic studies were all derived from the W303 *RAD5* strain and have the basic genotype *ade2-1 leu2-3,112 his3-11,15 trp1-1 ura3-1 can1-100*. Strains with point mutations in the *RAD54* gene were crossed with strains HKY660-2B *MATa leu2-rI::URA3::leu2-bsteII*, HKY661-4D *MATa rdh54::HIS3 leu2-rI::URA3::leu2-bsteII*, HKY590-6D *MATa srs2::HIS3*, HKY885 *MATa pol30-50*, and MSY127-5A *MATa top3::HIS3*. For the chromosome-loss assay, we constructed diploids from a set of strains with *ade2-1 can1-100 hom3-10* (or *ADE2 CAN1 HOM3*) in addition to the *RAD54* mutations. Sources of the markers were strains HKY1025-47D *MATa CAN1 ADE2 HOM3* and HKY1026-8C *MATa can-100 ade2-1 hom3-10*. The protease-deficient strain BJ5464 used in protein purification has the genotype *MATa, ura3-52, trp-1, leu2Δ1, his3Δ200, pep4::HIS3, prbΔ1.6R*.

DNA Substrates—ϕX 174 viral (+) strand DNA was purchased from New England Biolabs, and the ϕX-replicative form I DNA (~90% supercoiled) was from Invitrogen. Relaxation of the ϕX-replicative form I DNA by calf thymus topoisomerase I was carried out as described previously (19). pBluescript form I dsDNA was prepared using standard methods (53). For the DNA binding experiments, the 83-mer oligonucleotide (Oligo 3) (19) with the sequence 5′-TTG ATA AGA GGT CAT TTT TGC GGA TGG CTT AGA GCT TAA TTG CTG AAT CTG GTG CTG TAG CTC AAC ATG TTT TAA ATA TGC AA-3′ was 5′ end-labeled with [γ-^{32}P]ATP (Amersham Biosciences) and T4 polynucleotide kinase (Promega). The unincorporated nucleotide was removed with a Spin 30 column (Bio-Rad), and the radiolabeled oligo was annealed to its exact complement. The resulting duplex was purified from a 10% polyacrylamide gel by overnight diffusion at 4 °C into TAE buffer (40 mM Tris acetate, pH 7.5, 0.5 mM EDTA) (19). The 90-mer oligonucleotide D1 used in the D-loop reaction is complementary to pBluescript SK DNA from positions 1932 to 2022 and has the sequence 5′-AAA TCA ATC TAA AGT ATA TAT GAG TAA ACT TGG TCT GAC AGT TAC CAA TGC TTA ATC AGT GAG GCA CCT ATC TCA GCG ATC TGT CTA TTT-3′. The oligonucleotide was 5′ end-labeled with T4 polynucleotide kinase (Promega) and [γ-^{32}P]ATP (Amersham Biosciences) and then purified using the MERmaid spin kit (Bio101). All the DNA substrates were stored in TE buffer (10 mM Tris-HCl, pH 7.0, 0.5 mM EDTA).
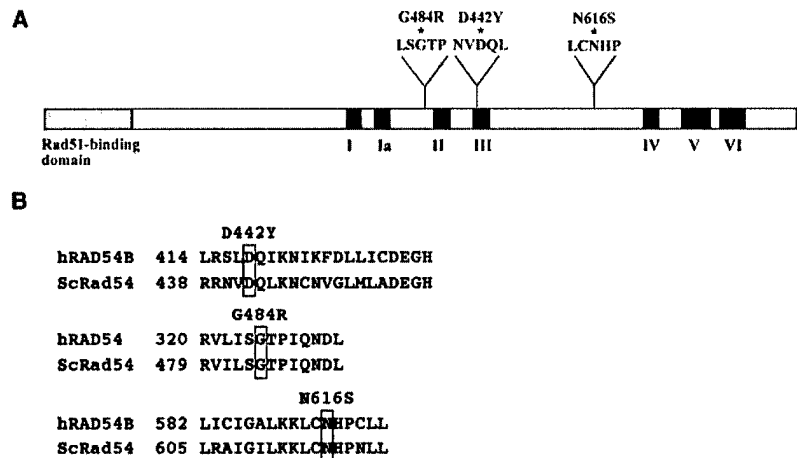
Determination of Intrachromosomal Recombination Rates—Recombination rates were determined as described previously (54). Spore segregants from crosses of the *rad54* mutants with the recombination reporter strains were used. Nine colonies from each spore segregant were used for each fluctuation test, and three to six fluctuation tests were performed for each *rad54* mutant.

MMS and HU Sensitivity—To determine methyl methanesulfonate (MMS) and hydroxyurea (HU) sensitivity of the *rad54* mutants, cells were grown in liquid YEPD to saturation. The cells were then diluted, and 4-μl aliquots were spotted onto fresh YEPD plates containing 0.016% MMS or 200 mM HU.

For UV sensitivity, cells from overnight cultures were diluted, and 4-μl aliquots were spotted onto fresh YEPD plates and exposed to UV irradiation. After exposure, the plates were kept in the dark to avoid photoreactivation.

Determination of Chromosome Loss Rates in Diploids—Rates of chromosome loss were determined as described previously (55). Fresh zygotes were isolated for each genotype. After growth for 3–4 days at 30 °C on YEPD medium, zygotic colonies were resuspended in water. Appropriate dilutions were applied onto SC plates for measurement of the total number of colony-forming units and onto SC plates plus canavanine to select for canavanine-resistant mitotic segregants. These were then replica-plated to SC plates lacking threonine. Colonies that grew only on SC plus canavanine plates, Can^r Hom$^-$, were counted to determine the chromosome loss rates. Fluctuation tests were conducted

A

B

D442Y

hRAD54B 414 LRSLDQIKNIKFDLLICDEGH
ScRad54 438 RRNVDQLKNCNVGLMLADEGH

G484R

hRAD54 320 RVLISGTPIQNDL
ScRad54 479 RVILSGTPIQNDL

N616S

hRAD54B 582 LICIGALKKLCNHPCLL
ScRad54 605 LRAIGILKKLCNHPNLL

FIG. 1. **Schematic representation of the domain structure of the *S. cerevisiae* gene *RAD54* and position of the point mutations.** *A*, the conserved helicase domains I–VI are shown as well as the Rad51 binding domain. Positions of the mutations D442Y, G484R, and N616S relative to the helicase domains are shown. *B*, alignment of the hRad54B and hRad54 amino acid domains with the ScRad54 domains, showing that all amino acid changes are within conserved residues and conserved domains of the proteins.

according to the median method (56). These tests were repeated three to five times for each genotype.

Protein Expression and Purification—The rad54 N616S and rad54 G484R mutant proteins were purified to near homogeneity from cells of the BJ5464 strain harboring pR54.G484R.1 or pR54.N616S.1 using the procedure described for wild type Rad54 protein (11). The two mutant rad54 proteins behaved like the wild type protein in all of the fractionation steps. Rad51 was overexpressed and purified to near homogeneity from yeast as described by Sung (57). *Escherichia coli* topoisomerase I was purified to near homogeneity from *E. coli* JM103 (Stratagene) cells transformed with pJW312 as described by Lynn *et al.* (58). The concentration of purified Rad54, rad54 G484R, rad54 N616S, and *E. coli* topoisomerase I was determined by densitometric scanning of 8% SDS-polyacrylamide gels with multiple loadings of these proteins against known quantities of bovine serum albumin (BSA) and ovalbumin. The concentration of purified Rad51 was determined using the extinction coefficient 1.29×10^4 (59).

ATPase Assay—The indicated amounts of Rad54, rad54 G484R, and rad54 N616S proteins were incubated with ϕX174-replicative form I DNA (30 μM base pairs) in 10 μl of buffer A (30 mM Tris-HCl, pH 7.4, 5 mM $MgCl_2$, 1 mM dithiothreitol, 50 mM KCl, and 100 μg/ml BSA) and 1.5 mM [γ-^{32}P]ATP (Amersham Biosciences) for the indicated times at 23 °C. The amount of ATP hydrolysis was determined by thin layer chromatography as described by Petukhova *et al.* (11). To examine the effect of Rad51 on ATP hydrolysis by Rad54 and the rad54 mutants, Rad51 (360 nM) was premixed with Rad54, rad54 G484R, and rad54 N616S (50 nM each) at 0 °C for 15 min prior to the addition of DNA and incubation at 23 °C.

DNA Mobility Shift—The indicated amounts (40–200 nM) of Rad54, rad54 G484R, and rad54 N616S and the ^{32}P-labeled 83-mer duplex substrate (1.5 μM nucleotides) were incubated for 8 min at 23 °C in 10 μl of buffer A with 2.5 mM ATP and an ATP-regenerating system consisting of 10 mM creatine phosphate and 30 μg/ml creatine kinase. After adding 2 μl of loading buffer (30 mM Tris-HCl, pH 7.4, 2 mM EDTA, 0.1% orange G, 50% glycerol), the reaction mixtures were analyzed in 9% native polyacrylamide gels run in TAE buffer at 4 °C. The gels were dried and subject to analysis in a Personal FX phosphorimaging device employing the Quantity One software (Bio-Rad).

Rad51 and Rad54 Complex Formation—Rad51 and BSA were covalently conjugated to Affi-Gel 15 beads (Bio-Rad) to yield matrices containing 3 mg/ml Rad51 and 12 mg/ml BSA as described by Petukhova *et al.* (11). To examine binding of Rad54, rad54 G484R, and rad54 N616S to the affinity beads, these proteins (4 μg each) were gently mixed with 6 μl of Affi-Rad51 or Affi-BSA beads every 3 min for 45 min at 4 °C in 30 μl of binding buffer (25 mM Tris-HCl, pH 7.5, 10% glycerol, 0.01% Nonidet P-40, and 0.5 mM dithiothreitol) containing 150 mM KCl. The beads were collected by centrifugation, and the supernatant was removed. After being washed twice with 100 μl of binding buffer with 300 mM KCl, the Affi-Rad51 and Affi-BSA beads were treated with 30 μl of 3% SDS at 37 °C for 10 min to elute the bound Rad54 or mutant rad54 protein. The supernatant containing unbound Rad54 or mutant rad54 protein (10 μl), the two washes (15 μl), and the SDS eluate (10 μl) were subject to SDS-PAGE in an 8% gel to determine their content of Rad54 or mutant rad54 protein.

D-loop Reaction—The radiolabeled oligonucleotide D1 (3.6 μM nucleotides) was incubated with Rad51 (1.5 μM) in 10.5 μl of buffer A and an ATP-regenerating system consisting of 20 mM creatine phosphate and

30 μg/ml creatine kinase for 5 min at 37 °C followed by the incorporation of the indicated amounts (80–400 nM) of Rad54, rad54 G484R, or rad54 N616S in 1 μl storage buffer (20 mM KH_2PO_4, pH 7.4, 10% glycerol, 0.5 mM EDTA, 0.5 mM dithiothreitol, 300 mM KCl) and a 2-min incubation at 23 °C. The reaction was initiated by adding the pBluescript-replicative form I DNA (35 μM base pairs) in 1 μl TE (10 mM Tris-HCl, pH 7.5, 0.2 mM EDTA). The reaction mixtures were incubated at 23 °C for 4 min and processed for electrophoresis in 0.9% agarose gels in TAE buffer at 23 °C as described previously (20). The gels were dried, and the radiolabeled DNA species were visualized and quantified in the phosphorimaging device. The percent D-loop refers to the quantity of the replicative form I substrate that had been converted into D-loop.

Topoisomerase I-linked DNA Supercoiling Assay—The indicated amounts of Rad54, rad54 G484R, and rad54 N616S were incubated with topologically relaxed ϕX 174 DNA (18.5 μM base pairs) for 3 min at 23 °C in 9.5 μl of buffer R (35 mM Tris-HCl, pH 7.6, 2.5 mM ATP, 3 mM $MgCl_2$, 100 μg/ml bovine serum albumin, 1 mM dithiothreitol, and an ATP regenerating system consisting of 20 mM creatine phosphate and 30 μg/ml creatine kinase) with 50 mM KCl followed by the addition of 150 ng of *E. coli* topoisomerase I in 0.5 μl of storage buffer. The reactions were incubated at 23 °C for 10 min and processed for agarose gel electrophoresis as described previously (19). To examine the effect of Rad51, it was mixed with Rad54, rad54 G484R, and rad54 N616S at 4 °C for 20 min prior to the addition of the DNA substrate and incubation with topoisomerase.

RESULTS AND DISCUSSION

Phenotypes of the rad54D442Y, rad54 N616S, and rad54 G484R Mutants—The human cancer cell lines Kco15, Ly6, and Br7 harbor mutations in *RAD54B* and *hRAD54* genes at positions that are highly conserved among Rad54-homologous proteins. In Kco15, in a region close to helicase domain II, a conserved Asp residue at codon 418 of Rad54B (equivalent to Asp-442 in yeast Rad54) is mutated to Tyr (30) (Fig. 1). In Ly6, the Asn at codon 593 (equivalent to Asn-616 in yeast Rad54), a residue within a conserved region between helicase motifs III and IV, is mutated to Ser in Rad54B (30) (Fig. 1). In Br7, in the helicase motif III of hRad54, the conserved Gly residue at codon 325 (equivalent to Gly-484 in yeast Rad54) is mutated to Arg (51) (Fig. 1). We introduced point mutations into the *S. cerevisiae RAD54* gene corresponding to the aforementioned mutations found in the human cancer cell lines (Fig. 1).

Strains carrying the *rad54* mutations (*D442Y, N616S,* and *G484R*) were examined for sensitivity to MMS, HU, and UV irradiation. The *rad54 G484R* mutant showed a degree of sensitivity to all three DNA-damaging agents very similar to that seen with the deletion mutant *rad54Δ* (Fig. 2). In crosses of *rad54 G484R* by *RAD54*, the *rad54 G484R* spore segregants showed slower mitotic growth compared with the *RAD54* strain. In contrast, *rad54 D442Y* and *rad54 N616S* were not hypersensitive to MMS, HU, or UV irradiation (Fig. 2), and they did not exhibit any growth defect.
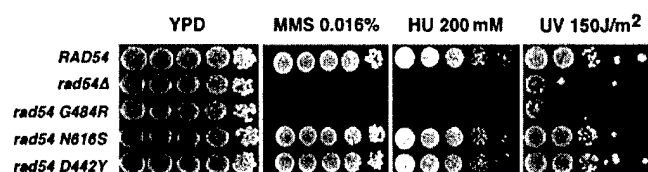
FIG. 2. **DNA damage sensitivities of the** *rad54* **mutants.** Cells of each genotype were grown overnight in YEPD, the culture was serially diluted 10-fold, and 4 μl from each dilution was spotted onto YEPD plates containing 0.016% MMS, 200 mM HU, or without any addition (*YPD*). The cells were also spotted onto YEPD plates and exposed to UV irradiation at a dose of 150 J/m^2 exposure. The plates were photographed after 3 days of growth at 30 °C.

Homozygous *rad54* mutant diploids demonstrated differences in spore viability, a reflection of meiotic recombination success. The *rad54 G484R* diploid has impaired spore viability of 63% compared with spore viability of 93% for *RAD54* and 68% for the *rad54Δ* null allele diploid. The *rad54 D442Y* and *rad54 N616S* homozygous mutant diploids had spore viability of 97 and 98%, respectively.

Effect of the rad54 Mutations on Intrachromosomal Recombination—Intrachromosomal gene conversion is strongly reduced in the *rad54Δ* mutant (19). To determine the effect of the *rad54* mutations on intrachromosomal gene conversion, we tested recombination in haploid *rad54 N616S, rad54 D442Y*, and *rad54 G484R* strains using the *leu2-rI::URA3::leu2-bsteII* direct repeat. We measured gene conversion and deletion events by determining the rates of the Leu$^+$ Ura$^+$ colonies and 5-fluoroorotic acid-resistant (Ura$^-$) events, respectively. As shown in Fig. 3, the *rad54 G484R* mutant has a reduced rate of gene conversion and an increased gene deletion rate compared with wild type, and the magnitude of the effects is very similar to that observed with the null mutant *rad54Δ*. Intrachromosomal gene conversion and deletion rates in the *rad54 D442Y* and *rad54 N616S* mutants do not differ from the wild type strain.

Chromosome Loss in rad54 Mutants—Chromosome stability is strongly impaired in the *rad54Δ* deletion mutant (55). We examined the effect of the three *rad54* point mutations on chromosome stability in homozygous mutant diploids. Chromosome stability was measured by a genetic assay for loss of one copy of chromosome V. One chromosome V homologue was marked with *hom3-10* and *can1-100*, whereas the other homologue harbored the wild type alleles of these genes. Can^r Hom$^-$ segregants were classified as chromosome loss events (55).

The chromosome loss rate in the *rad54 G484R* diploid was elevated to the same level as that observed in the *rad54Δ* diploid, an increase of about 40-fold over the *RAD54* rate (Fig. 4). The *rad54 N616S* and *rad54 D442Y* mutant diploids had a wild type rate of chromosome loss, again suggesting that these mutations do not significantly affect the function of Rad54 (Fig. 4).

Genetic Interactions—To further assess the phenotype of the *rad54 G484R* mutant, we studied the genetic interactions of this allele with mutations known to be lethal in a *rad54Δ* background. The *srs2Δ* mutation is lethal in a *rad54Δ* strain (60). Genetic analysis of the crosses between *rad54 G484R* and *srs2Δ* shows synthetic lethality as well.

Synthetic lethality of the *rad54 G484R* and *rad54Δ* mutations with the *pol30-52* mutation in the *POL30* gene, which encodes the DNA polymerase processivity clamp PCNA, was also found. Mutations in the *RAD54* gene can suppress the slow growth and hyper-recombination phenotypes of the *top3* mutant (61). Our genetic analysis showed that the *rad54 G484R* mutation could suppress the slow growth of *top3Δ*. Recombination rate determinations revealed that the *rad54 G484R* mu-
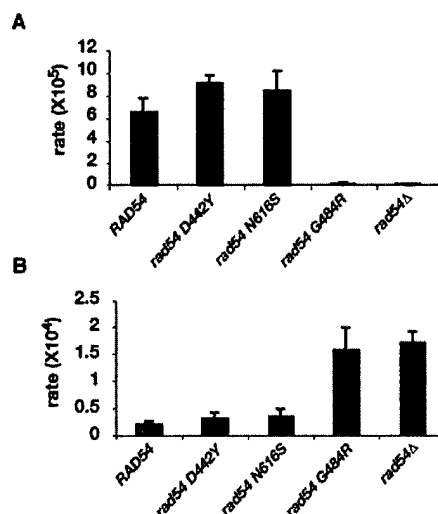

FIG. 3. **Effects of the** *rad54 D442Y, rad54 G484R,* **and** *rad54 N616S* **mutations on homologous recombination.** Rates of intrachromosomal gene conversion and deletion in the haploid mutants were determined using the direct repeat *leu2-rI::URA3::leu2-bsteII.* For rate determinations, three spore segregants from crosses of the *rad54* mutants with HKY660-2B were used. *A,* rates of gene conversion were determined as rates of Leu$^+$ Ura$^+$ mitotic segregants. *B,* deletion rates were determined as rates of 5-fluoroorotic acid-resistant mitotic segregants. The mean of the rates, from three to six independent rate determinations, is presented with the standard deviation.
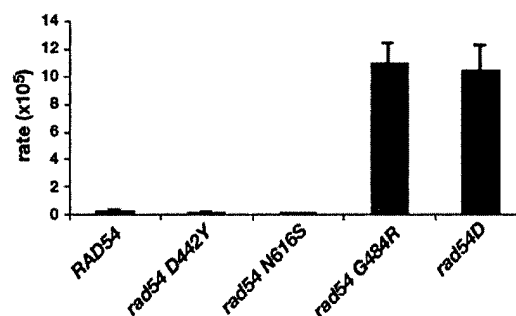

FIG. 4. **Rates of chromosome loss in** *rad54* **diploids.** Determination of chromosome loss rates in mutant and wild type diploids was performed as described under "Experimental Procedures." All diploids were isogenic to the W303 parental strain. Chromosome loss rates were determined three times for each genotype. The mean and standard deviation of these rates is shown.

tation resulted in a 20-fold decrease in gene conversion of the *top3Δ* mutant compared with the *RAD54 top3Δ* strain. In contrast, the *rad54 N616S* and *rad54 D442Y* mutants are viable in combination with *srs2Δ* or *pol30-52* and do not show any effect on the hyper-recombination phenotype of the *top3Δ* mutant.

As detailed above, the *rad54 N616S* and *rad54 D442Y* mutants did not exhibit increased sensitivity to genotoxic agents and had wild type levels of mitotic gene conversion and chromosome loss. However, the *rad54 N616S* mutation was not completely benign. We observed that diploid strains hemizygous for the *rad54 N616S* allele (*rad54 N616S/rad54Δ*) had increased MMS sensitivity compared with the homozygous *rad54 N616S* diploid (*rad54 N616S/rad54 N616S*). Hemizygous *RAD54* strains (*RAD54/rad54Δ*) did not show any increased MMS sensitivity.

Further evidence of a subtle functional impairment in the *rad54 N616S* mutant was revealed by double mutant studies of HU and MMS sensitivity. The double mutants *rad54 N616S rdh54Δ* and *rad54 N616S srs2Δ* had a slight enhancement of MMS and HU sensitivity compared with the single mutants (Fig. 5). We did not, however, find any change in rates of gene conversion and deletion formation in these double mutants
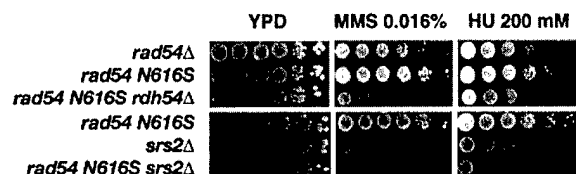
FIG. 5. Enhancement of MMS and HU sensitivity in *rad54 N616S rdh54Δ* and *rad54 N616S srs2Δ* double mutants. MMS and HU sensitivities were determined as described in Fig. 2. Double mutants were generated in crosses of *rad54 N616S* mutant with HKY661-4D and HKY590-6D strains. The plates were photographed after 3 days of growth at 30 °C on YEPD plates containing 0.016% MMS or 200 mM HU or without any addition (*YPD*).
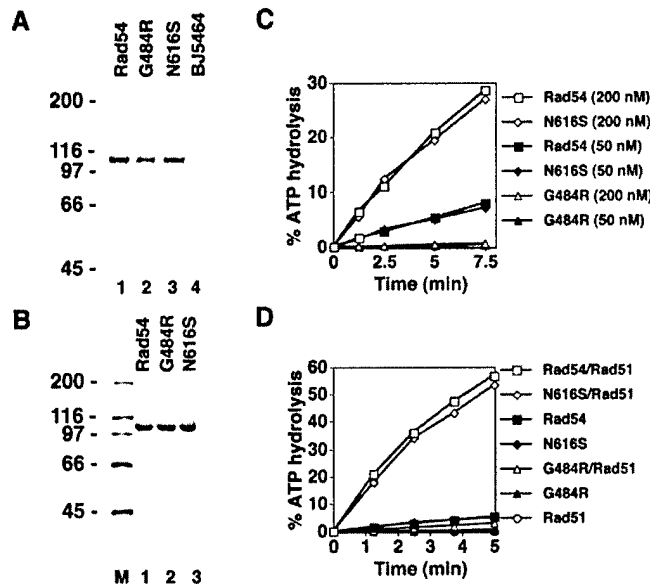

FIG. 6. ATP hydrolysis by Rad54, rad54 G484R, and rad54 N616S. *A*, immunoblot analysis of extract from yeast strain BJ5464 harboring the empty protein expression vector pPM231.6His (*lane 4*) and plasmids pR54.1, pR54.G484R.1, and pR54.N616S.1 that express Rad54 (*lane 1*), rad54 G484R (*lane 2*), and rad54 N616S (*lane 3*), respectively, using anti-Rad54 antibodies as described by Petukhova *et al.* (11). *B*, purified Rad54, rad54 G484R (G484R), and rad54 N616S (N616S) proteins, 1.8 μg of each, were run beside size markers (*M*) in an 8% denaturing polyacrylamide gel and then stained with Coomassie Blue. *C*, time course of ATP hydrolysis by Rad54, rad54 G484R, and rad54 N616S. Rad54, rad54 G484R, and rad54 N616S (all 50 and 200 nM) were incubated with 1.5 mM [γ-^{32}P]ATP and ϕX-replicative form I DNA (18.5 μM base pairs) for the indicated times. *D*, to examine the effect of Rad51 on ATPase hydrolysis by the mutant rad54 proteins, 50 nM Rad54, rad54 G484R, and rad54 N616S were incubated with radiolabeled ATP, ϕX DNA, and 200 nM Rad51 or without Rad51 for the indicated times. Rad51 was also incubated with the radiolabeled ATP and ϕX-replicative DNA for the indicated times.

FIG. 7. DNA binding by Rad54, rad54 G484R, and rad54 N616S. *A*, ^{32}P-labeled 83-mer duplex (1.5 μM nucleotides) was incubated with Rad54 protein (*panel I, lanes 2–6*), rad54 G484R (*panel II, lanes 2–6*), and rad54 N616S (*panel III, lanes 2–6*) all at 40, 80, 120, 160, and 200 nM. The reaction mixtures were analyzed in nondenaturing polyacrylamide gels, which were dried and subjected to phosphorimaging analysis. No protein was added in *lanes 1*. *B*, graphical representation of the results in *A*.

(data not shown). Surprisingly, the mitotic recombination rate of the *rad54 N616S srs2Δ* double mutant showed an increase of 15-fold over the *srs2Δ* rate. The double mutant colonies grew slowly with uneven edges featuring lethal sectors.

rad54 G484R, but Not rad54 N616S, Is Impaired for ATP Hydrolysis—To examine the effects of the tumor-associated hRad54 and Rad54B mutations on the biochemical activities of Rad54, the rad54 G484R and rad54 N616S proteins were overexpressed in yeast cells (Fig. 6*A*) and purified to near homogeneity (Fig. 6*B*) by following the procedures devised for the purification of the wild type protein (19). We used thin layer chromatography to examine the ability of the rad54 G484R and rad54 N616S mutant proteins to hydrolyze ATP in the presence of dsDNA. The results, as summarized in Fig. 6*C*, indicated that whereas rad54 N616S is just as proficient as the wild type protein in ATP hydrolysis, the rad54 G484R mutant protein
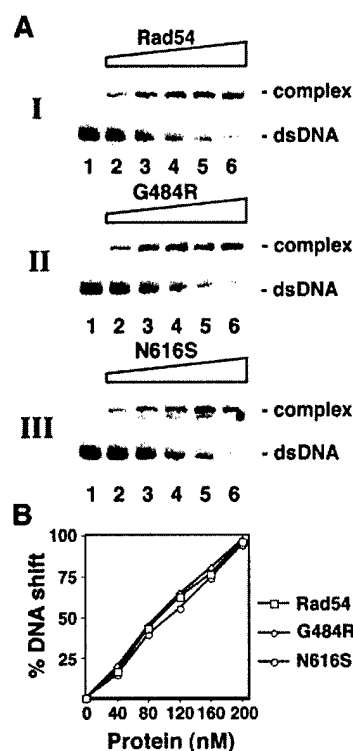
possesses little or no ATPase activity (Fig. 6*C*).

Published studies have shown that through a specific protein-protein interaction, Rad51 greatly stimulates the ATPase of Rad54 (15, 16). We examined whether Rad51 can enhance the ATPase activity of these mutant proteins. As shown in Fig. 6*D*, Rad51 greatly enhanced the ATPase activity of wild type Rad54 and rad54 N616S. In contrast, the addition of Rad51 did not enable rad54 G484R to hydrolyze ATP.

rad54 G484R and rad54 N616S Bind DNA and Rad51—The data above show a pronounced defect of the rad54 G484R mutant in ATP hydrolysis. Because the Rad54 ATPase activity requires dsDNA as a cofactor, it was of considerable interest to examine whether the noted defect associated with the rad54 G484R mutant was due to an inability to bind DNA. DNA mobility shift experiments were performed to address this point. Rad54, rad54 G484R, and rad54 N616S were incubated with a ^{32}P-labeled 83-mer duplex, and the levels of nucleoprotein complex formed were compared. Importantly, the results from this experiment showed that rad54 G484R is just as proficient in DNA binding as the rad54 N616S and wild type proteins (Fig. 7).

Rad54 physically interacts with Rad51 *in vitro* and *in vivo* (11–13). To determine whether the mutant rad54 G484R and rad54 N616S proteins retain the ability to bind Rad51, purified rad54 G484R and rad54 N616S were mixed with Affi-gel 15 beads containing either Rad51 (Affi-Rad51) or bovine serum albumin (Affi-BSA). After washing with buffer, Rad54 and rad54 mutant proteins that remained bound to the Affi-beads were eluted by SDS and then analyzed by SDS-PAGE. As indicated from Fig. 8, as much of the rad54 G484R (*panel II*) and rad54 N616S (*panel III*) as the wild type (*panel I*) protein were found associated with the Affi-Rad51 beads. As ex-

FIG. 8. rad54 G484R and rad54 N616S mutant proteins physically interact with Rad51. Purified Rad54, rad54 G484R, and rad54 N616S were mixed with Affi-Gel 15 beads containing either Rad51 (*Affi-Rad51*) or bovine serum albumin (*Affi-BSA*). The beads were collected by centrifugation, washed twice with buffer containing 300 mM KCl, and then eluted with SDS. The supernatant (*S*), first wash (*W1*), second wash (*W2*), and SDS-eluate (*E*) were run in an 8% denaturing polyacrylamide gel followed by staining with Coomassie Blue.

FIG. 9. Rad54-mediated DNA supercoiling is inactivated by the G484R mutation. *A*, schematic of the *E. coli* topoisomerase I-linked DNA supercoiling assay, as described by Ristic *et al.* (14) and Van Komen *et al.* (15). ATP hydrolysis fuels the translocation of a Rad54 oligomer on DNA, producing a positively supercoiled domain ahead of protein movement and a negatively supercoiled domain behind. The addition of *E. coli* topoisomerase I removes the negative supercoils, resulting in the formation of a positively supercoiled species called Form OW upon deproteinization. *B*, Rad54 protein (*lanes 2–4*), rad54 G484R (*lanes 5–7*), and rad54 N616S (*lanes 8–10*) (all at 45, 90, and 135 nM) were incubated with topologically relaxed DNA (9 μM base pairs) and *E. coli* topoisomerase I. To test the effect of Rad51, this protein at 100 and 300 nM was added to DNA supercoiling reactions that contained the lowest amount (45 nM) of Rad54 or rad54 mutant. In *lane 1*, relaxed DNA was incubated in buffer with topoisomerase but without any recombination protein. In *lane 17*, Rad51 (300 nM) was incubated with relaxed DNA and topoisomerase. All the reactions were carried out at 23 °C for 10 min. The reaction mixtures were deproteinized and then analyzed in a 0.9% agarose gel followed by staining with ethidium bromide.

FIG. 10. The rad54 G484R mutant has greatly attenuated activity in the D-loop reaction. *A*, schematic of the D-loop reaction. Pairing of the radiolabeled 90-mer oligonucleotide with pBluescript form I DNA yields a D-loop. *B*, D-loop reactions with Rad51 only (*panels I, II*, and *III, lane 2*), Rad54 only (400 nM in *panel I, lane 3*), rad54 G484R only (400 nM in *panel II, lane 3*), rad54 N616S only (400 nM in *panel III, lane 3*), Rad51 and Rad54 (80, 160, 240, 320, and 400 nM in *panel I, lanes 4–8*), Rad51 and rad54 G484R (80, 160, 240, 320, and 400 nM in *panel II, lanes 4–8*), and Rad51 and rad54 G616S (80, 160, 240, 320, and 400 nM in *panel III, lanes 4–8*). Rad51 was at 1.5 μM, and the completed reaction mixtures were incubated for 4 min. In *lane 1* of each panel, the DNA substrates were incubated in buffer without any recombinant proteins. The reaction mixtures were deproteinized and resolved in 0.9% agarose gels, which were dried and subjected to phosphorimaging analysis. *C*, graphical representation of the results in *B*.

pected, neither wild type Rad54 nor the two rad54 mutants bound to the Affi-BSA beads (Fig. 8). Thus, the two rad54 mutants are as proficient as wild type Rad54 in complex formation with Rad51.

rad54 G484R, but Not rad54 N616S, Is Defective in DNA Supercoiling—Biochemical analyses and scanning force microscopy have indicated that the free energy derived from ATP hydrolysis fuels the translocation of Rad54 on duplex DNA. As Rad54 tracks on dsDNA, positive and negative supercoils that are equal in magnitude are generated, with the positive supercoils accumulating ahead of protein movement and the negative supercoils trailing it (8, 14, 15). The supercoiling activity of Rad54 is greatly stimulated via a specific interaction of Rad54 with the Rad51-ssDNA nucleoprotein filament. During recombination, the tracking of Rad54 on duplex DNA and the negative supercoils that accompany this motion are believed
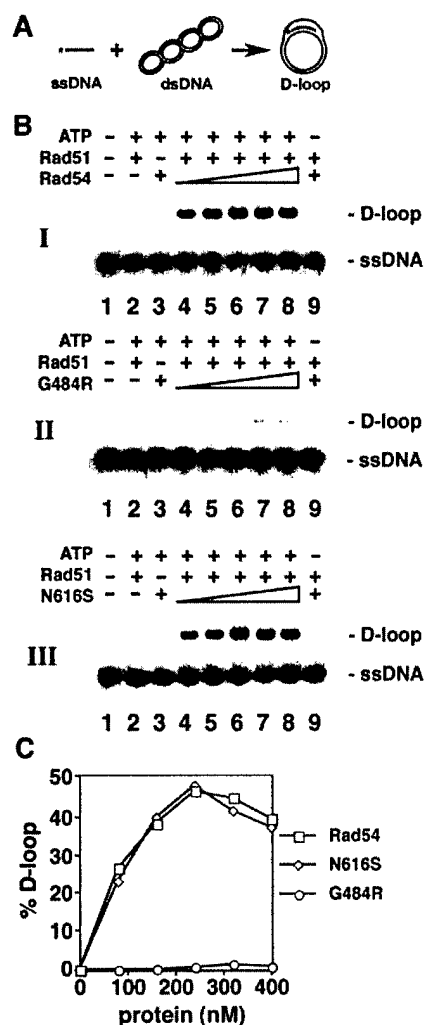
to enhance the rate at which the incoming duplex DNA can be sampled by the presynaptic filament for homology and to promote DNA joint formation upon location of DNA homology (9).

We have previously devised a topoisomerase I-linked assay to gauge the DNA supercoiling activity of Rad54 (15). Briefly, the negative supercoils generated by Rad54 are removed by *E. coli* topoisomerase I to result in the formation of a positively supercoiled species called Form OW (overwound), which is separated from the topologically relaxed input DNA by agarose gel electrophoresis ((15); Fig. 9A). We used this topoisomerase-linked assay to determine the ability of rad54 G484R and rad54 N616S to supercoil DNA. Fig. 9B shows that although rad54 N616S (*lanes 8–10*) was as capable of producing Form OW as the wild type protein (*lanes 2–4*), the rad54 G484R (*lanes 5–7*) mutant is devoid of this activity.

As with its ATPase activity, the DNA supercoiling activity of Rad54 is greatly stimulated via a specific interaction with Rad51 (15, 16). Consistent with data from the experiment that examined the Rad54 ATPase function (Fig. 6D), Rad51 enhanced the DNA supercoiling activity of rad54 N616S to the same extent as it did the wild type protein (Fig. 9B, *lanes 11* and *12*), but it did not impart DNA supercoiling activity to the rad54 G484R mutant (Fig. 9B, *lanes 13* and *14*).

Promotion of Rad51-mediated D-loop Formation—During the initial stage of homologous recombination, the Rad51-ssDNA nucleoprotein filament invades the homologous duplex donor to form a D-loop. The D-loop reaction can be studied by monitoring the incorporation of an oligonucleotide into a homologous supercoiled DNA molecule (Fig. 10A). Although Rad51, by itself, has only a modest ability to form the D-loop (11), the addition of Rad54 protein renders D-loop formation robust (11). Promotion of the D-loop reaction requires the ATPase activity of Rad54 (19). We examined the ability of rad54 G484R and rad54 N616S to enhance Rad51-mediated D-loop formation. To do this, Rad51 was incubated with the radiolabeled oligonucleotide before the homologous duplex (pBluescript-replicative form I DNA) and increasing amounts of Rad54, rad54 G484R, and rad54 N616S were incorporated. The wild type Rad54 and the rad54 N616S mutant were equally effective in the D-loop reaction, whereas only a negligible amount of D-loop was detected when rad54 G484R was used (Fig. 10, *B* and *C*).

Implications of Our Genetic and Biochemical Results—We have constructed several mutations in yeast *RAD54* to test the genetic and biochemical consequences of *hRAD54* and *hRAD54B* mutations found in human tumors. Of the three mutations tested, *rad54 G484R* showed great impairment of Rad54 activity both in genetic and biochemical assays. Whether this is related to the fact that the human mutation in this case, Br7, was in the *hRAD54* gene (and not the *hRAD54B* gene) is not known, as we have not tested yeast *RDH54* with a similar mutation. Nonetheless, our studies have revealed that the Br7 cell line most likely has no hRad54 activity and that the helicase III domain is essential for hRad54 activity.

In all of the genetic and biochemical aspects examined, the *rad54 G484R* mutant was as defective as the null allele deletion mutant. The *in vivo* phenotypes of reduced recombination and increased DNA damage sensitivities and genomic instability can be correlated with the loss of ATP hydrolysis activity and, consequently, DNA supercoiling, DNA strand opening, and Rad51-mediated D-loop formation. However, the rad54 G484R protein still retains the ability to bind DNA and Rad51 protein, demonstrating that nucleoprotein complex formation between Rad54 and DNA and association with Rad51 are not sufficient for DNA damage repair, DNA damage avoidance, and maintenance of genomic stability.

In contrast, the *rad54 D442Y* and *rad54 N616S* mutants that correspond to two tumor-associated mutations (D418Y and N593S, respectively) found in the *hRAD54B* gene (30) have no demonstrable deficiency in Rad54 protein activity and, accordingly, do not engender any discernible phenotype as single mutants. In double mutant studies, the *rad54 N616S* mutant showed an enhancement of DNA damage sensitivity. Overall, our genetic observations are consistent with the premise that the *rad54 N616S* mutant could have phenotypic consequences in certain mutant backgrounds.

In conclusion, our results suggest that the tumor-associated *hRAD54* mutation (G325R) noted in the Br7 cell line (51) probably enhances genomic instability in tumor cells. It is possible that this mutation accelerates the tumor phenotype by enhancing genomic instability in an already mutant cell line or may have a more causative role in tumorigenesis. Further experiments are required to test these possibilities.

REFERENCES

1. Cox, M. M., Goodman, M. F., Kreuzer, K. N., Sherratt, D. J., Sandler, S. J., and Marians, K. J. (2000) *Nature* **404**, 37–41
2. Cox, M. M. (2001) *Annu. Rev. Genet.* **35**, 53–82
3. Helleday, T. (2003) *Mutat. Res.* **532**, 103–115
4. Michel, B. (2000) *Trends Biochem. Sci.* **25**, 173–178
5. Michel, B., Flores, M. J., Viguera, E., Grompone, G., Seigneur, M., and Bidnenko, V. (2001) *Proc. Natl. Acad. Sci. U. S. A.* **98**, 8181–8188
6. Symington, L. S. (2002) *Microbiol. Mol. Biol. Rev.* **66**, 630–670
7. Pierce, A. J., Stark, J. M., Araujo, F. D., Moynahan, M. E., Berwick, M., and Jasin, M. (2001) *Trends Cell Biol.* **11**, (suppl.) S52–S59
8. Krejci, L., Chen, L., Van Komen, S., Sung, P., and Tomkinson, A. (2003) *Prog. Nucleic Acid Res. Mol. Biol.* **74**, 159–201
9. Sung, P., Krejci, L., Van Komen, S., and Sehorn, M. G. (2003) *J. Biol. Chem.* **278**, 42729–42732
10. Eisen, J. A., Sweder, K. S., and Hanawalt, P. C. (1995) *Nucleic Acids Res.* **23**, 2715–2723
11. Petukhova, G., Stratton, S., and Sung, P. (1998) *Nature* **393**, 91–94
12. Jiang, H., Xie, Y., Houston, P., Stemke-Hale, K., Mortensen, U. H., Rothstein, R., and Kodadek, T. (1996) *J. Biol. Chem.* **271**, 33181–33186
13. Clever, B., Interthal, H., Schmuckli-Maurer, J., King, J., Sigrist, M., and Heyer, W. D. (1997) *EMBO J.* **16**, 2535–2544
14. Ristic, D., Wyman, C., Paulusma, C., and Kanaar, R. (2001) *Proc. Natl. Acad. Sci. U. S. A.* **98**, 8454–8460
15. Van Komen, S., Petukhova, G., Sigurdsson, S., Stratton, S., and Sung, P. (2000) *Mol. Cell* **6**, 563–572
16. Mazin, A. V., Bornarth, C. J., Solinger, J. A., Heyer, W. D., and Kowalczykowski, S. C. (2000) *Mol. Cell* **6**, 583–592
17. Wolner, B., Van Komen, S., Sung, P., and Peterson, C. L. (2003) *Mol. Cell* **12**, 221–232
18. Mazin, A. V., Alexeev, A. A., and Kowalczykowski, S. C. (2003) *J. Biol. Chem.* **278**, 14029–14036
19. Petukhova, G., Van Komen, S., Vergano, S., Klein, H., and Sung, P. (1999) *J. Biol. Chem.* **274**, 29453–29462
20. Van Komen, S., Petukhova, G., Sigurdsson, S., and Sung, P. (2002) *J. Biol. Chem.* **277**, 43578–43587
21. Solinger, J. A., and Heyer, W. D. (2001) *Proc. Natl. Acad. Sci. U. S. A.* **98**, 8447–8453
22. Jaskelioff, M., Van Komen, S., Krebs, J. E., Sung, P., and Peterson, C. L. (2003) *J. Biol. Chem.* **278**, 9212–9218
23. Alexeev, A., Mazin, A., and Kowalczykowski, S. C. (2003) *Nat. Struct. Biol.* **10**, 182–186
24. Alexiadis, V., and Kadonaga, J. T. (2002) *Genes Dev.* **16**, 2767–2771
25. Solinger, J. A., Kiianitsa, K., and Heyer, W. D. (2002) *Mol. Cell* **10**, 1175–1188
26. Klein, H. L. (1997) *Genetics* **147**, 1533–1543
27. Shinohara, M., Shita-Yamaguchi, E., Buerstedde, J. M., Shinagawa, H., Ogawa, H., and Shinohara, A. (1997) *Genetics* **147**, 1545–1556
28. Petukhova, G., Sung, P., and Klein, H. (2000) *Genes Dev.* **14**, 2206–2215
29. Kanaar, R., Troelstra, C., Swagemakers, S. M., Essers, J., Smit, B., Franssen, J. H., Pastink, A., Bezzubova, O. Y., Buerstedde, J. M., Clever, B., Heyer, W. D., and Hoeijmakers, J. H. (1996) *Curr. Biol.* **6**, 828–838
30. Hiramoto, T., Nakanishi, T., Sumiyoshi, T., Fukuda, T., Matsuura, S., Tauchi, H., Komatsu, K., Shibasaki, Y., Inui, H., Watatani, M., Yasutomi, M., Sumii, K., Kajiyama, G., Kamada, N., Miyagawa, K., and Kamiya, K. (1999) *Oncogene* **18**, 3422–3426
31. Sigurdsson, S., Van Komen, S., Petukhova, G., and Sung, P. (2002) *J. Biol. Chem.* **277**, 42790–42794
32. Tanaka, K., Kagawa, W., Kinebuchi, T., Kurumizaka, H., and Miyagawa, K. (2002) *Nucleic Acids Res.* **30**, 1346–1353
33. Lim, D. S., and Hasty, P. (1996) *Mol. Cell. Biol.* **16**, 7133–7143
34. Sonoda, E., Sasaki, M. S., Buerstedde, J. M., Bezzubova, O., Shinohara, A., Ogawa, H., Takata, M., Yamaguchi-Iwai, Y., and Takeda, S. (1998) *EMBO J.* **17**, 598–608
35. Stark, J. M., and Jasin, M. (2003) *Mol. Cell. Biol.* **23**, 733–743
36. Xu, X., Weaver, Z., Linke, S. P., Li, C., Gotay, J., Wang, X. W., Harris, C. C., Ried, T., and Deng, C. X. (1999) *Mol. Cell* **3**, 389–395
37. Yu, V. P., Koehler, M., Steinlein, C., Schmid, M., Hanakahi, L. A., van Gool, A. J., West, S. C., and Venkitaraman, A. R. (2000) *Genes Dev.* **14**, 1400–1406
38. Moynahan, M. E., Chiu, J. W., Koller, B. H., and Jasin, M. (1999) *Mol. Cell* **4**, 511–518
39. Moynahan, M. E., Pierce, A. J., and Jasin, M. (2001) *Mol. Cell* **7**, 263–272
40. Tutt, A., Bertwistle, D., Valentine, J., Gabriel, A., Swift, S., Ross, G., Griffin, C., Thacker, J., and Ashworth, A. (2001) *EMBO J.* **20**, 4704–4716
41. Tutt, A. N., van Oostrom, C. T., Ross, G. M., van Steeg, H., and Ashworth, A. (2002) *EMBO Rep.* **3**, 255–260
42. Xia, F., Taghian, D. G., DeFrank, J. S., Zeng, Z. C., Willers, H., Iliakis, G., and Powell, S. N. (2001) *Proc. Natl. Acad. Sci. U. S. A.* **98**, 8644–8649
43. Bezzubova, O., Silbergleit, A., Yamaguchi-Iwai, Y., Takeda, S., and Buerstedde, J. M. (1997) *Cell* **89**, 185–193
44. Essers, J., Hendriks, R. W., Swagemakers, S. M., Troelstra, C., de Wit, J., Bootsma, D., Hoeijmakers, J. H., and Kanaar, R. (1997) *Cell* **89**, 195–204
45. Essers, J., van Steeg, H., de Wit, J., Swagemakers, S. M., Vermeij, M., Hoeijmakers, J. H., and Kanaar, R. (2000) *EMBO J.* **19**, 1703–1710
46. Takata, M., Sasaki, M. S., Sonoda, E., Morrison, C., Hashimoto, M., Utsumi, H., Yamaguchi-Iwai, Y., Shinohara, A., and Takeda, S. (1998) *EMBO J.* **17**, 5497–5508
47. Miyagawa, K., Tsuruga, T., Kinomura, A., Usui, K., Katsura, M., Tashiro, S.,

Mishima, H., and Tanaka, K. (2002) *EMBO J.* **21,** 175–180

48. Scully, R., Chen, J., Plug, A., Xiao, Y., Weaver, D., Feunteun, J., Ashley, T., and Livingston, D. M. (1997) *Cell* **88,** 265–275
49. Tan, T. L., Essers, J., Citterio, E., Swagemakers, S. M., de Wit, J., Benson, F. E., Hoeijmakers, J. H., and Kanaar, R. (1999) *Curr. Biol.* **9,** 325–328
50. Tanaka, K., Hiramoto, T., Fukuda, T., and Miyagawa, K. (2000) *J. Biol. Chem.* **275,** 26316–26321
51. Matsuda, M., Miyagawa, K., Takahashi, M., Fukuda, T., Kataoka, T., Asahara, T., Inui, H., Watatani, M., Yasutomi, M., Kamada, N., Dohi, K., and Kamiya, K. (1999) *Oncogene* **18,** 3427–3430
52. Sherman, F., Fink, G. R., and Hicks, J. B. (1986) *Methods in Yeast Genetics*, Cold Spring Harbor Laboratory Press, Cold Spring Harbor, NY
53. Sambrook, J., Fritsch, E. F., and Maniatis, T. (1989) *Molecular Cloning: A Laboratory Manual*, 2nd Ed., Cold Spring Harbor Laboratory Press, Cold Spring Harbor, NY
54. Aguilera, A., and Klein, H. L. (1988) *Genetics* **119,** 779–790
55. Klein, H. L. (2001) *Genetics* **159,** 1501–1509
56. Lea, D. E., and Coulson, C. A. (1948) *J. Genet.* **49,** 264–284
57. Sung, P. (1994) *Science* **265,** 1241–1243
58. Lynn, R. M., Bjornsti, M. A., Caron, P. R., and Wang, J. C. (1989) *Proc. Natl. Acad. Sci. U. S. A.* **86,** 3559–3563
59. Sugiyama, T., Zaitseva, E. M., and Kowalczykowski, S. C. (1997) *J. Biol. Chem.* **272,** 7940–7945
60. Palladino, F., and Klein, H. L. (1992) *Genetics* **132,** 23–37
61. Shor, E., Gangloff, S., Wagner, M., Weinstein, J., Price, G., and Rothstein, R. (2002) *Genetics* **162,** 647–662

Role of ATP Hydrolysis in the Antirecombinase Function of *Saccharomyces cerevisiae* Srs2 Protein*

Lumir Krejci‡, Margaret Macris‡, Ying Li§, Stephen Van Komen‡, Jana Villemain¶,
Thomas Ellenberger§, Hannah Klein‖, and Patrick Sung‡**

From the ‡Department of Molecular Biophysics and Biochemistry, Yale University School of Medicine, New Haven, Connecticut 06520, the §Department of Biological Chemistry and Molecular Pharmacology, Harvard Medical School, Boston, Massachusetts 02115, the ¶Institute of Biotechnology and Department of Molecular Medicine, University of Texas Health Science Center at San Antonio, San Antonio, Texas 78245, and the ‖Department of Biochemistry, New York University School of Medicine, New York, New York 10016

Mutants of the *Saccharomyces cerevisiae SRS2* gene are hyperrecombinogenic and sensitive to genotoxic agents, and they exhibit a synthetic lethality with mutations that compromise DNA repair or other chromosomal processes. In addition, *srs2* mutants fail to adapt or recover from DNA damage checkpoint-imposed G_2/M arrest. These phenotypic consequences of ablating *SRS2* function are effectively overcome by deleting genes of the *RAD52* epistasis group that promote homologous recombination, implicating an untimely recombination as the underlying cause of the *srs2* mutant phenotypes. The *SRS2*-encoded protein has a single-stranded (ss) DNA-dependent ATPase activity, a DNA helicase activity, and an ability to disassemble the Rad51-ssDNA nucleoprotein filament, which is the key catalytic intermediate in Rad51-mediated recombination reactions. To address the role of ATP hydrolysis in Srs2 protein function, we have constructed two mutant variants that are altered in the Walker type A sequence involved in the binding and hydrolysis of ATP. The srs2 K41A and srs2 K41R mutant proteins are both devoid of ATPase and helicase activities and the ability to displace Rad51 from ssDNA. Accordingly, yeast strains harboring these *srs2* mutations are hyperrecombinogenic and sensitive to methylmethane sulfonate, and they become inviable upon introducing either the *sgs1Δ* or *rad54Δ* mutation. These results highlight the importance of the ATP hydrolysis-fueled DNA motor activity in *SRS2* functions.

DNA helicases perform important functions in various chromosomal transactions, including replication, repair, recombination, and transcription (1, 2). These proteins utilize the chemical energy from the hydrolysis of a nucleoside triphosphate to dissociate DNA structures and nucleoprotein complexes. Interestingly, mutations in several DNA helicases are involved in the pathogenesis of human diseases. For instance, mutations in the XPB and XPD helicases, which constitute subunits of the transcription factor TFIIH that has a dual role in nucleotide excision repair, lead to the cancer prone syndrome xeroderma pigmentosum (3). Furthermore, mutations in the BLM, WRN, and RecQ4 proteins, members of the RecQ helicase family, cause the cancer-prone Bloom, Werner, and Rothmund-Thomson syndromes, respectively (4, 5).
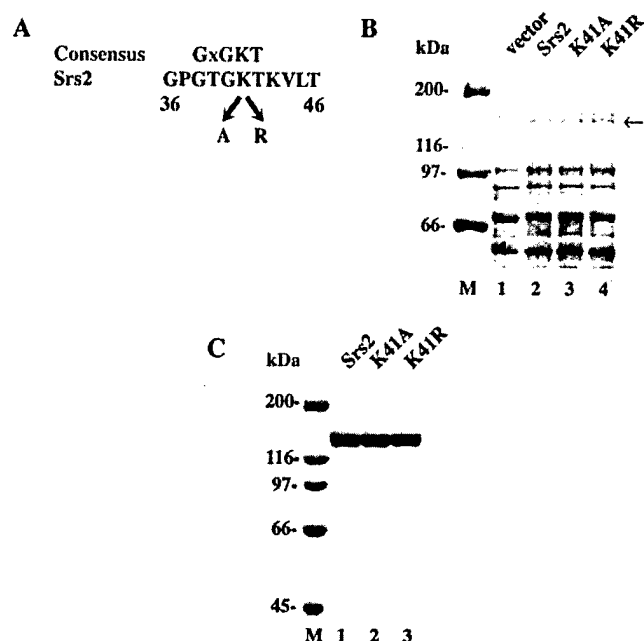
We are interested in the biology of various DNA helicases that influence homologous recombination and DNA repair processes. One such helicase is encoded by the *Saccharomyces cerevisiae SRS2* gene, altered forms of which were first described as either suppressors of the DNA damage sensitivity of *rad6* and *rad18* mutants (6) or as hyperrecombination mutants (7). Detailed genetic analyses have shown that a major function of *SRS2* is to attenuate homologous recombination activity to allow for the channeling of certain DNA lesions into the *RAD6/RAD18*-mediated postreplication repair pathway (8, 9). Accordingly, *srs2* mutants are sensitive to DNA damaging agents and show a hyperrecombination phenotype. Genetic deletion of the *RAD51* or *RAD52*, key members of the *RAD52* epistasis group functioning in homologous recombination, alleviates the DNA damage sensitivity and hyperrecombination phenotypes of *srs2* mutants (8), implicating untimely recombination events as the progenitor of these *srs2* phenotypes. *Srs2* mutations are lethal when combined with mutations in a variety of genes needed for DNA repair and other chromosomal processes, *e.g.* with mutations in the DNA repair and recombination gene *RAD54* and also with mutations in *SGS1*, which codes for the sole RecQ helicase in *S. cerevisiae* (10, 11). The synthetic lethality encountered in the *srs2 sgs1* and *srs2 rad54* double mutants is suppressed by inactivating key recombination genes (11). The available genetic evidence therefore implicates Srs2 protein in the attenuation of recombination events that produce toxic DNA structures or nucleoprotein intermediates (12, 13).

In congruence with the genetic data, biochemical assays have shown that the Srs2 protein strongly suppresses the recombinase activity of Rad51. Interestingly, although Srs2 has the ability to unwind DNA (14, 15) and had been predicted to dissociate DNA intermediates in recombination reactions, its antirecombinase function can be attributed to an ability to disassemble the Rad51-single-stranded DNA (ssDNA)[1] nucleoprotein filament (14, 15), the key catalytic intermediate in recombination reactions (16). Likewise, the failure of *srs2* mu-
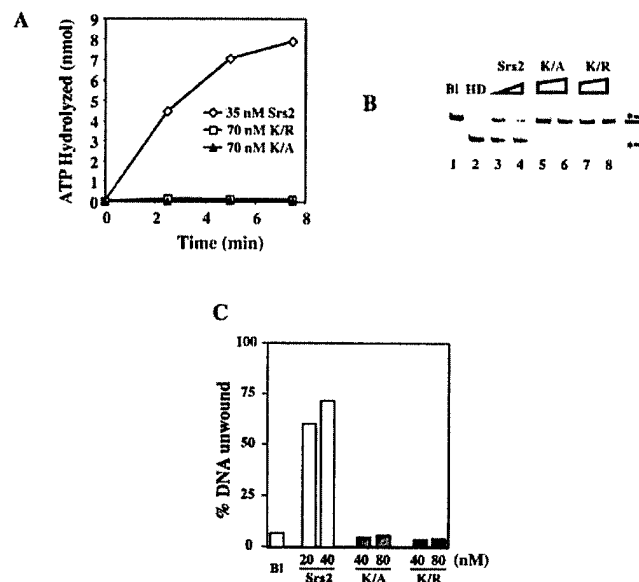
[1] The abbreviations used are: ssDNA, single-stranded DNA; MMS, methylmethane sulfonate; BSA, bovine serum albumin; dsDNA, double-stranded DNA; RPA, replicative protein A.
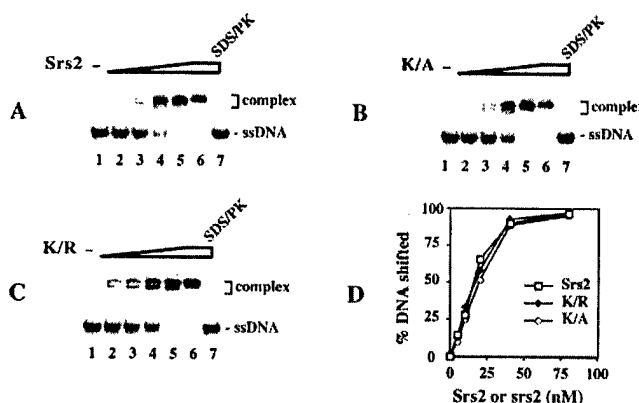
FIG. 1. **Expression and purification of srs2 K41A and srs2 K41R mutant proteins.** *A*, sequence of the Walker type A motif in Srs2 and the two mutant alleles, K41A (*A*) and K41R (*R*), constructed for this study. *B*, extracts from *E. coli* cells harboring the empty protein expression vector pET11c (*vector, lane 1*) and plasmids that express wild-type Srs2 (*lane 2*), srs2 K41A (*K41A, lane 3*) and srs2 K41R (*K41R, lane 4*) proteins were subjected to SDS-PAGE in a 7.5% gel and stained with Coomassie Blue. The *arrow* marks the position of the wild-type Srs2 and mutant srs2 proteins. *C*, purified Srs2 (*lane 1*), srs2 K41A (*K41A, lane 2*), and srs2 K41R (*K41R, lane 3*) proteins, 2 μg of each, were run in a 7.5% SDS-PAGE and then stained with Coomassie Blue.

tants to recover from or adapt to DNA damage checkpoint-imposed G_2/M cell cycle arrest has been linked to a failure to remove Rad51 from DNA (17). These results imply that, in addition to its ability to unwind double-stranded DNA, Srs2 has a motor activity that clears proteins from single-stranded DNA. Srs2 physically interacts with Rad51 in the yeast two-hybrid system and *in vitro* (14), and it has been suggested that complex formation between Srs2 and Rad51 helps target the former to DNA sites where Rad51 nucleoprotein filaments have assembled (14). In addition to the recombination-related phenotypes, the *srs2Δ* mutant is partially deficient in the activation of the intra-S DNA damage checkpoint in response to treatment with methylmethane sulfonate (MMS) (18). Additionally, two independent studies (19, 20) have implicated *SRS2* in DNA double-strand break repair by the synthesis-dependent single-strand annealing mechanism as well. Srs2 also appears to influence the efficiency of single-strand annealing (17).

As summarized above, Srs2 appears to have a multifunctional role in nuclear processes including an ability to unwind DNA and disassemble the Rad51-ssDNA nucleoprotein filament. Here, we address the role of ATP in Srs2 protein functions by mutating the highly conserved lysine residue in the Walker type A motif expected to be involved in ATP binding and hydrolysis. We show that the resulting srs2 K41A and srs2 K41R mutant proteins are devoid of ATPase and helicase activities and are unable to dislodge Rad51 from DNA. Genetic analyses reveal that the *srs2 K41A* and *srs2 K41R* mutations cause hyperrecombination, sensitivity to MMS, and synthetic lethality with the *sgs1Δ* or *rad54Δ* mutation. Our results thus reveal a requirement for the Srs2 DNA motor activity in recombination attenuation. However, the *srs2 K41A* and *srs2 K41R* mutants are less sensitive to MMS than *srs2* null cells

FIG. 2. **Biochemical properties of srs2 Walker mutants.** *A*, the ssDNA-dependent ATP hydrolysis activities of Srs2 (35 nM), srs2 K41A (*K/A*, 70 nM), and srs2 K41R (*K/R*, 70 nM) proteins were measured as described under "Materials and Methods." *B*, the DNA unwinding activities of Srs2 (20 and 40 nM in *lanes 3* and *4*), srs2 K41A (*K/A*, 40 and 80 nM in *lanes 5* and *6*), and srs2 K41R (*K/R*, 40 and 80 nM in *lanes 7* and *8*) proteins were assayed using a 3'-tailed DNA helicase substrate. The reaction mixtures were deproteinized and resolved in a native 12% polyacrylamide gel. *HD*, heat-denatured substrate; *Bl*, reaction mixture that did not contain any protein. *C*, quantification of the data in *B*.

FIG. 3. **srs2 K41A and srs2 K41R proteins have normal DNA binding activity.** Increasing concentrations (5, 10, 20, 40, and 80 nM in *lanes 2–6*, respectively) of Srs2 (*A*), srs2 K41A (*K/A* in *B*), and srs2 K41R (*K/R* in *C*) were incubated with a ^{32}P-labeled ssDNA oligonucleotide, and the reaction mixtures were analyzed in 12% native polyacrylamide gels. In *lane 7*, the highest concentration (80 nM) of Srs2 or srs2 mutant was incubated with the oligonucleotide substrate, but the reaction mixture was treated with SDS and proteinase K (*SDS/PK*) prior to gel analysis. In *lane 1*, the oligonucleotide substrate was incubated without protein. The percent DNA substrate shifted by Srs2, srs2 K41A, and srs2 K41R was determined by phosphorimaging analysis of the dried gels, and the data points are plotted in *D*.

and exhibit a more pronounced hyperrecombinational phenotype than the latter. It therefore seems possible that Srs2 has additional functions that are not strictly linked to ATP hydrolysis and Rad51 removal from DNA.

MATERIALS AND METHODS

Yeast Media and Strains—Yeast extract-peptone-dextrose (YPD) medium, synthetic complete (SC) medium, and synthetic complete media without leucine (SC-Leu), without uracil (SC-Ura), and without leucine and uracil (SC-Leu-Ura) were prepared as described (21). Media containing 5-fluoro-orotic acid were prepared as described (21). Except where noted, all strains are *RAD5* derivatives of W303 (22). The re-
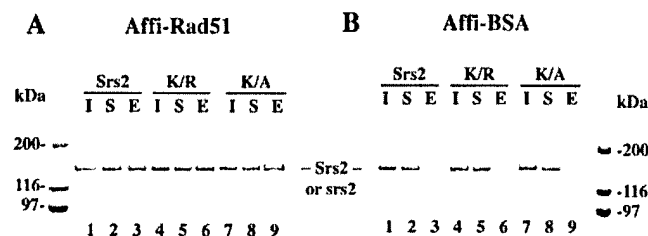
FIG. 4. **Interaction of mutant srs2 proteins with Rad51.** Srs2, srs2 K41A (*K/A*), and srs2 K41R (*K/R*) proteins were mixed with Affi-Rad51 beads (*A*) and Affi-BSA beads (*B*). The starting material (*I*), supernatant that contained unbound Srs2, srs2 K41A, or srs2 K41R (*S*), and the SDS eluate (*E*) were resolved by SDS-PAGE in a 10% gel and then stained with Coomassie Blue.
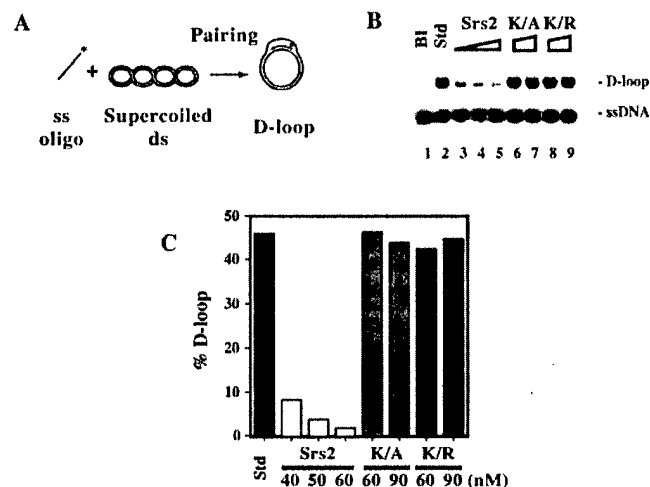

FIG. 5. **Mutant srs2 proteins fail to attenuate Rad51/Rad54/RPA-mediated D-loop reaction.** *A*, D-loop reaction scheme. The radiolabeled 90-mer oligonucleotide D1 is paired with homologous pBluescript form I DNA to yield a D-loop. *B*, in *lanes 2–9*, radiolabeled D1 was incubated with Rad51, Rad54, RPA, and with or without Srs2 (40, 50, and 60 nM in *lanes 3–5*), srs2 K41A (*K/A*, 60 and 90 nM in *lanes 6* and *7*), or srs2 K41R (*K/R*, 60 and 90 nM in *lanes 8* and *9*) and then pBluescript form I DNA was incorporated. The reaction (*lane 2*) without Srs2 or mutant srs2 is designated as *Std. Lane 1* contained the DNA substrates but no protein (*Bl*). The reaction mixtures were incubated for 4 min, deproteinized, and then subject to electrophoresis in a 1% agarose gel. The gel was dried and analyzed in the PhosphorImager. *C*, the data points from phosphorimaging analysis of the gel in *B* are plotted.

maining strains were derived from HKY344-27C and carry *leu2-112::URA3::leu2-k* and *his3-513::TRP1::his3-537* recombination reporters (7).

Plasmid Construction—To generate the *SRS2*::pUC18 plasmid, the ORF of *SRS2* was amplified using the following primers: C*GGGATC-CA*CATATGTCGTCGAACAATGATCTTTGGTTGC (sense, BamHI site italic, NdeI underline) and CG*GGATCC*GGAATTCCCTACTAATCGA-TGACTATGATTTCACCG (antisense, BamHI site italic, EcoRI site underline). The PCR product was digested with BamHI and ligated into the BamHI-digested pUC18. The mutations in the Walker A site in Srs2, K41A, and K41R, were introduced by using mutagenic DNA primers and QuikChange site-directed mutagenesis kit (Stratagene). The mutations were confirmed by DNA sequencing. For protein purification, the *srs2 K41R* and *srs2 K41A* mutant genes were introduced into the pET11c vector. pBS::SRS2 and YIpLac211-srs2 were constructed as follows. The 3.1-kb NdeI-BglII fragments containing the K41R or K41A segments of the mutated *SRS2* gene were used to replace the wild-type *SRS2* segment in plasmid pRL101 (9). Next, a 6.4-kb EcoRI-SalI fragment containing all of the *SRS2* coding region plus 927 bp upstream of the ATG start codon and 1602 bp downstream of the stop codon was inserted into the EcoRI and SalI sites of the polylinker of YIpLac211, which carries the *URA3* selectable marker, to form pHK284 (*srs2 K41A*) and pHK286 (*srs2 K41R*). These plasmids were linearized with BglII and then used to transform W303 and HKY344–27C strains. After selecting for Ura⁺ transformants, cells were grown non-selectively and
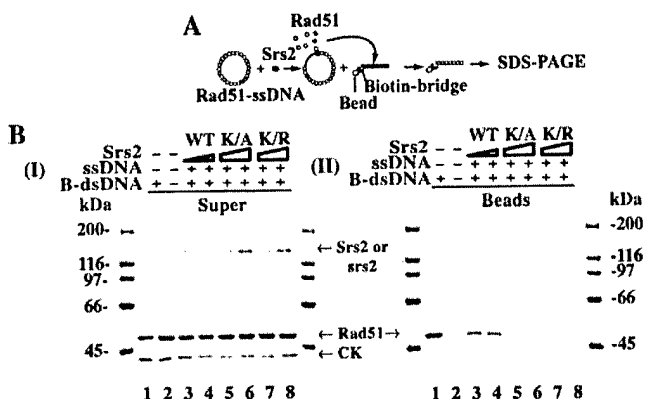

FIG. 6. **Disassembly of Rad51-ssDNA nucleoprotein filaments is coupled to ATP hydrolysis by Srs2.** *A*, Rad51 molecules displaced by Srs2 can be trapped on immobilized DNA duplex attached to streptavidin magnetic beads. Rad51 associated with the magnetic bead-bound duplex is eluted by SDS followed by SDS-PAGE analysis. *B*, pre-assembled Rad51-ssDNA nucleoprotein filaments (*lanes 2–8*) were incubated with Srs2 (*WT*, 60 and 90 nM in *lanes 3* and *4*), srs2 K41A (*K/A*, 90 and 180 nM in *lanes 5* and *6*), or srs2 K41R (*K/R*, 90 and 180 nM in *lanes 7* and *8*), and the reaction mixtures mixed with streptavidin magnetic beads containing biotinylated dsDNA (*lanes 3–8*). In *lane 1*, free Rad51 was mixed with streptavidin magnetic beads that contained biotinylated dsDNA, and in *lane 2*, free Rad51 was mixed with streptavidin magnetic beads that did not contain any dsDNA. The supernatant (*Super, panel I*) and bead-bound (*Beads, panel II*) fractions were subjected to SDS-PAGE in a 7.5% gel and stained with Coomassie Blue. *CK* denotes creatine kinase in the buffer.
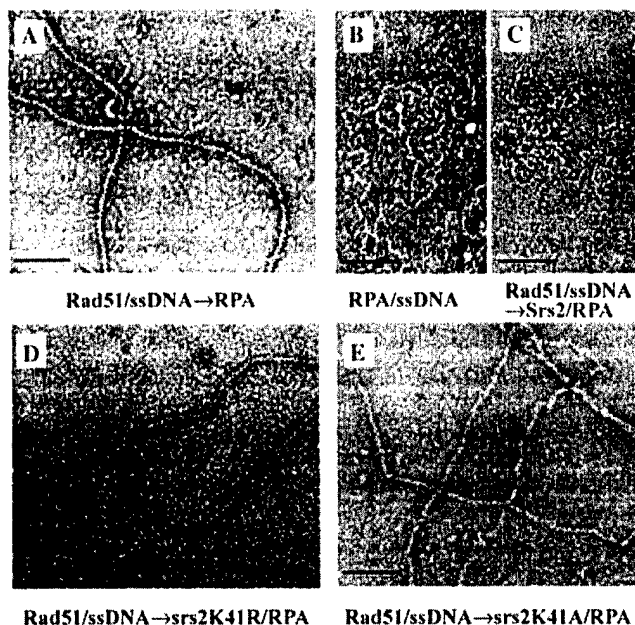

Rad51/ssDNA→RPA   RPA/ssDNA   Rad51/ssDNA →Srs2/RPA

Rad51/ssDNA→srs2K41R/RPA   Rad51/ssDNA→srs2K41A/RPA

FIG. 7. **Electron micrographs showing effects of Srs2 and mutant srs2 proteins on Rad51-ssDNA filaments.** *A*, Rad51 was incubated with ssDNA before RPA was added, and an example of the resulting Rad51-ssDNA nucleoprotein filaments is shown. *B*, RPA was incubated with ssDNA, and an example of the RPA-ssDNA nucleoprotein complex that formed is shown. *C*, incubation of preformed Rad51-ssDNA nucleoprotein filaments with Srs2 caused the displacement of Rad51 from DNA and the formation of RPA-ssDNA nucleoprotein complexes, an example of which is shown. *D* and *E*, srs2 K41R and srs2 K41A were incapable of disrupting the Rad51-ssDNA nucleoprotein filaments. The *dark bar* represents 100 nm.

then streaked on 5-fluoro-orotic acid plates. Fluoro-orotic acid-resistant colonies were tested for MMS sensitivity. MMS-sensitive colonies were examined for the presence of the *srs2* mutations by PCR amplification of the genomic region surrounding the *SRS2 K41* site. Primers used were CTTTTTCTTTTGCGCTGTAT and TCCCGAACTAAAGAAG-GTGC. The mutant *srs2 K41A* and *K41R* sites carry an adjacent StyI

TABLE I

Gene conversion in srs2 K41A and srs2 K41R strains

Strains used for the gene conversion tests are derived from HKY344-27C and are of the genotype *leu2-112::URA3::leu2-k his3-513::TRP1::his3-537 ura3-52 trp1 ade1-101*. Strains used are HKY344-27C, HKY344-109D, and HKY1355-7B for *SRS2*, HKY1355-8B, HKY1355-12C, and HKY1355-16C for *srs2 K41A*, HKY1439-5C, HKY1439-9C, and HKY1439-10A for *srs2 K41R*, and F103-2A56, F126-1C, and F121-8C for *srs2Δ*.

Genotype	Leu + Ura + rate	Increase	His + Trp + rate	Increase
		-fold		-fold
SRS2	$5.65 \times 10^{-6} \pm 1.24 \times 10^{-6}$		$3.92 \times 10^{-6} \pm 1.65 \times 10^{-6}$	
srs2 K41A	$5.22 \times 10^{-5} \pm 3.63 \times 10^{-5}$	9.24	$6.15 \times 10^{-5} \pm 1.14 \times 10^{-5}$	15.69
srs2 K41R	$6.96 \times 10^{-5} \pm 3.75 \times 10^{-5}$	12.32	$6.77 \times 10^{-5} \pm 3.11 \times 10^{-5}$	17.27
srs2Δ	$1.93 \times 10^{-5} \pm 3.06 \times 10^{-6}$	3.42	Not done	

site that is not present in the wild-type sequence. PCR products were tested for the StyI site by restriction digestion and agarose gel electrophoresis.

Srs2 Expression and Purification—srs2 K41A and srs2 K41R proteins were overexpressed in *Escherichia coli* cells and purified to near homogeneity as described previously for wild-type Srs2 (14, 23). Rad51 was overexpressed in yeast and purified to near homogeneity as described (16). The concentration of the wild-type Srs2 and mutant srs2 proteins was determined by densitometric scanning of SDS-polyacrylamide gels containing multiple loadings of purified proteins against known quantities of bovine serum albumin. The concentrations of Rad51 and RPA were determined using extinction coefficients of 1.29×10^4 and 8.8×10^4 at 280 nm, respectively (24).

DNA Substrates—The H2 and D1 oligonucleotides used in the construction of the helicase substrate have been described (23). Oligo-1 used in the DNA binding experiments has also been described (25). The oligonucleotides were purified from 12% polyacrylamide gels and 5'-end-labeled with [γ-^{32}P] ATP using T4 polynucleotide kinase. The unincorporated nucleotide was removed from the oligonucleotides using Spin30 columns (Bio-Rad). The DNA helicase substrate was obtained by heating equimolar amounts of H2 and radiolabeled D1 oligonucleotides to 95 °C for 10 min in buffer B (50 mM Tris-HCl, pH 7.5, 10 mM MgCl$_2$, 100 mM NaCl), followed by slow cooling to room temperature. The annealed substrate was purified from a 12% non-denaturing polyacrylamide gel, as described (23). The ϕX174 (+) strand was purchased from New England Biolabs.

ATPase Assay—Srs2 (35 nM) was incubated with viral ssDNA (25 μM nucleotides) in 10 μl of buffer A (30 mM Tris-HCl, pH 7.2, 2.5 mM MgCl$_2$, 1 mM dithiothreitol, 150 mM KCl, and 100 μg/ml BSA) and 1 mM [γ-^{32}P] ATP for the indicated times at 37 °C. The released phosphate was separated from unhydrolyzed ATP by thin layer chromatography, as described (26). The levels of hydrolysis were determined by phosphorimaging analysis of the thin layer chromatography plates in a Personal Molecular Imager FX (Bio-Rad).

DNA Helicase Assay—Srs2 (20 and 40 nM), srs2 K41R (40 and 80 nM), or srs2 K41A (40 and 80 nM) was incubated at 30 °C for 5 min with the helicase substrate (300 nM nucleotides) in 10 μl of buffer H (30 mM Tris-HCl, pH 7.5, 2.5 mM MgCl$_2$, 1 mM dithiothreitol, 100 mM KCl, 2 mM ATP, and 100 μg/ml BSA). The reaction mixtures were resolved by electrophoresis in a 12% non-denaturing polyacrylamide gel run in TAE buffer (40 mM Tris-HCl, pH 7.4, 0.5 mM EDTA) at 4 °C. The gel was dried onto Whatman DE81 paper and analyzed in the PhosphorImager.

DNA Mobility Shift—Varying amounts of Srs2, srs2 K41A or srs2 K41R (0–80 nM) was incubated with ^{32}P-labeled oligo-1 (1.36 μM nucleotides) at 37 °C in 10 μl of buffer D (40 mM Tris-HCl, pH 7.8, 50 mM KCl, 1 mM dithiothreitol, and 100 μg/ml BSA) for 10 min. After the addition of gel loading buffer (50% glycerol, 20 mM Tris-HCl, pH 7.4, 2 mM EDTA, 0.05% orange G), the reaction mixtures were resolved in 12% native polyacrylamide gels in TAE buffer (40 mM Tris acetate, 1 mM EDTA) at 4 °C, and the DNA species were quantified using Quantity One software (Bio-Rad). To release the DNA substrate from bound Srs2 and srs2 mutants, the reaction mixtures were treated with 0.5% SDS and 0.5 mg/ml proteinase K at 37 °C for 10 min before being subject to electrophoresis.

Binding of Srs2 to Rad51 Affi-beads—Affi-gel 15 beads containing Rad51 (Affi-Rad51; 5 mg/ml) and bovine serum albumin (Affi-BSA, 12 mg/ml) were prepared as described previously (26). Purified Srs2, srs2 K41A, or srs2 K41R, 5 μg of each, was mixed with 5 μl of Affi-Rad51 or Affi-BSA in 60 μl of phosphate-buffered saline (10 mM Na$_2$HPO$_4$, 1.8 mM KH$_2$PO$_4$, pH 7.4, and 150 mM NaCl) for 30 min on ice. The beads were washed twice with 150 μl of the same buffer before being treated with 25 μl of 2% SDS to elute bound protein. The starting material, a supernatant that contained unbound Srs2, srs2 K41A, or srs2 K41R,

TABLE II

Mutation rates in srs2 K41A and srs2 K41R strains

Strains used for the *CAN1* mutation rate determinations are derived from *CAN1* versions of W303 and are of the genotype *leu2-3, 112 his3-11, 15 ADE2 ura3-1 trp1-1 RAD5 CAN1*. Strains used are HKY1025-47D for *SRS2*, HKY1434-4A for *srs2 K41A*, HKY1433-8A for *srs2 K41R*, and HKY1303-1B for *srs2Δ*.

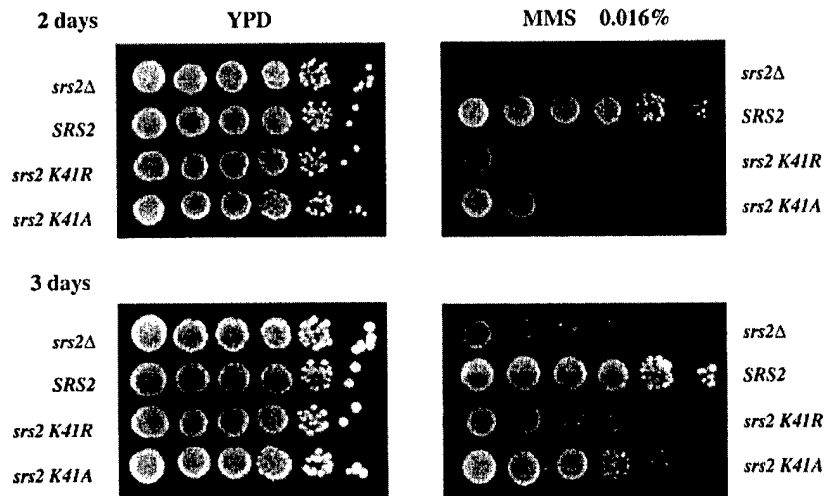| Genotype	Can^r rate	Increase
		-fold
SRS2	9.30×10^{-8}	
srs2 K41A	9.33×10^{-8}	1.0
srs2 K41R	4.66×10^{-8}	0.5
srs2Δ	1.41×10^{-7}	1.5

and the SDS eluate, 10 μl of each, were analyzed by 10% SDS-PAGE and staining with Coomassie Blue.

D-loop Reaction—The reactions were carried out in Buffer R (35 mM Tris-HCl, pH 7.4, 2.0 mM ATP, 2.5 mM MgCl$_2$, 50 mM KCl, 1 mM dithiothreitol, containing an ATP-regenerating system consisting of 20 mM creatine phosphate, 20 μg/ml creatine kinase) and had a final volume of 12.5 μl. The radiolabeled oligonucleotide D1 (3 μM nucleotides) was incubated with Rad51 (1 μM) for 5 min at 37 °C to assemble Rad51-ssDNA nucleoprotein filaments, followed by the incorporation of Rad54 (150 nM) and RPA (200 nM) and a 2 min incubation at 23 °C. The D-loop reaction was initiated by the addition of pBluescript replicative form I DNA (50 μM base pairs). The reaction mixtures were incubated at 30 °C for 4 min, deproteinized by treatment with SDS (0.5%) and proteinase K (0.5 mg/ml) at 37 °C for 10 min, and then run in a 1% agarose gel in TAE buffer. The gel was dried and subject to phosphorimaging analysis. The percentage D-loop refers to the quantity of the replicative form I substrate that had been converted into D-loop. When present, Srs2 (40, 50, and 60 nM), srs2 K41A (60 and 90 nM), and srs2 K41R (60 and 90 nM) were added to the pre-assembled Rad51-ssDNA nucleoprotein filaments, followed by a 4-min incubation at 37 °C before Rad54 and RPA were incorporated.

Transfer of Rad51 to Bead-bound Biotinylated dsDNA—M13mp18 circular (+) strand (7.2 μM nucleotides) was incubated for 5 min with Rad51 (2.4 μM) at 37 °C, followed by the addition of Srs2 (60 and 90 nM), srs2 K41A (90 and 180 nM), or srs2 K41R (90 and 180 nM) in a final volume of 20 μl of buffer R containing 0.01% igepal. After 3 min at 37 °C, 4 μl of magnetic beads containing dsDNA (14) were added to the reaction mixture, followed by constant mixing for 5 min at 23 °C. The beads were captured with the Magnetic Particle Separator (Roche Molecular Biochemicals), washed twice with the same buffer, and the bound Rad51 was eluted with 20 μl of 1% SDS. The supernatant, which contained unbound Rad51, and the SDS eluate (10 μl of each) were analyzed by SDS-PAGE.

Electron Microscopy—The reactions were carried out in buffer R and had a final volume of 12.5 μl. To assemble the Rad51 presynaptic filament, M13mp18(+) strand (7.2 μM nucleotides) and Rad51 (2.4 μM) were incubated at 37 °C for 5 min, followed by the addition of RPA (350 nM) and a 3 min incubation. To test the effects of Srs2 and mutant srs2 proteins, 60 nM of these proteins were incubated with the pre-assembled Rad51-ssDNA nucleoprotein filaments at 37 °C for 3 min. For electron microscopy, 2.5 μl of each reaction mixture was applied to copper grids coated with thin carbon film, after glow-discharging the grids for 2 min. The grids were washed twice with buffer R and stained for 30 s with 0.75% uranyl formate. After air-drying, the grids were examined with a Philips Tecnai 12 electron microscope under low-dose conditions. Images were recorded with a charge-coupled device camera (Gatan).

FIG. 8. **MMS sensitivity of the *srs2 K41A* and *srs2 K41R* mutants.** srs2 mutant strains grow normally on YPD plates but are sensitive when grown on plates containing MMS. Overnight cultures were serially diluted, and 3-μl aliquots were dropped on the plates. The pictures were taken after two and three days of incubation at 30 °C.

Genetic Studies—MMS sensitivity was determined using freshly made YPD plates containing 0.016% MMS. Overnight cultures of strains to be tested were serially diluted, and 3-μl aliquots of each dilution were applied onto YPD and YPD+MMS plates. Growth was assessed after 2 and 3 days at 30 °C. Forward mutation rates of *CAN1* were determined in haploid *CAN1* strains by fluctuation tests. These tests were conducted according to the median method (27) and were repeated three to five times for each genotype. Gene conversion between intrachromosomal *leu2-112* and *leu2-k* as well as between *his3-513* and *his3-537* heteroalleles was measured in haploid strain HKY344-27C and its isogenic derivatives.

RESULTS

srs2 Variants Mutated for the Walker Type A ATP Binding Motif—Srs2 contains canonical Walker-type ATP binding motifs. For addressing the role of ATP binding and hydrolysis in Srs2 functions, we have substituted the highly conserved lysine residue (lysine 41) in the Walker type A motif with either alanine or arginine using site-directed mutagenesis (Fig. 1A). The *srs2 K41A* and *srs2 K41R* mutant genes were sequenced to ensure that no unintended change had been introduced during the mutagenesis procedure. To express the srs2 K41A and srs2 K41R proteins, the mutant genes were placed under the isopropyl-1-thio-β-D-galactopyranoside-inducible T7 promoter in the *E. coli* expression vector pET11c, which we previously used for the expression and purification of wild-type Srs2 (14). Expression of the srs2 K41A and srs2 K41R mutant proteins in *E. coli* was verified by SDS-PAGE analysis of cell extracts (Fig. 1B) and by immunoblot analysis of these extracts with affinity-purified anti-Srs2 polyclonal antibodies (14). The srs2 K41A and srs2 K41R mutant proteins were purified to near homogeneity (Fig. 1C) using the chromatographic procedure that we have developed for wild-type Srs2 (14).

Biochemical Properties of srs2 K41A and srs2 K41R Mutant Proteins—Based on studies with the equivalent Walker mutations in other DNA-dependent ATPases (28, 29), the srs2 K41A and srs2 K41R mutant proteins were expected to be defective in ATP hydrolysis. This expectation was confirmed by examining the ATPase activity of purified proteins with [α-^{32}P] ATP and thin layer chromatography (14, 23). We showed previously that ATP hydrolysis by Srs2 occurs only in the presence of DNA with ssDNA being much more effective than dsDNA in this regard (9, 23). As summarized in Fig. 2A, although robust ATPase activity was observed with wild-type Srs2 in the presence of ssDNA (14, 23), the two srs2 mutant proteins showed less than 1% of the wild-type level of ATP hydrolysis. Likewise, no significant ATP hydrolysis by either of the srs2 mutants was seen when the ssDNA was omitted or substituted with dsDNA (data not shown). We next examined the two srs2 mutant

proteins for DNA helicase activity using a ^{32}P-labeled substrate that contained a 40-bp duplex region adjacent to a 40-nucleotide 3'-ssDNA overhang (Fig. 2B and Ref. 23). As shown in Fig. 2B, although wild-type Srs2 at 40 nM unwound greater than 70% of the substrate after 5 min of incubation, neither of the srs2 mutants, even at the increased concentration of 80 nM, showed a significant helicase activity under the same conditions (Fig. 2B) or even after a prolonged incubation (data not shown).

Even though the results presented in Fig. 2 were consistent with the premise that the K41A and K41R mutations abolish the ATPase activity of Srs2, there existed the possible caveat that this defect had originated from a loss of DNA binding by the mutant proteins. For this reason, we compared the DNA binding ability of the two Walker mutants to that of the wild-type protein by a DNA mobility shift assay. To do this, increasing amounts of wild-type Srs2 and the two mutant proteins were incubated with a ^{32}P-labeled 83-mer oligonucleotide, followed by resolution of the reaction mixtures in non-denaturing polyacrylamide gels and phosphorimaging analysis of the dried gels to detect and quantify the DNA mobility shift. As shown in Fig. 3, both srs2 mutant proteins were just as proficient as wild-type Srs2 in DNA binding. Consistent with this result, using the same DNA substrate, we found that DNA binding by wild-type Srs2 and the two srs2 mutant proteins is not influenced by ATP (data not shown).

Attenuation of Rad51-mediated Homologous DNA Pairing and Strand Exchange by Srs2 Requires ATP Hydrolysis—Recently, we (14) and Fabre and co-workers (15) demonstrated that Srs2 is highly adept at attenuating Rad51-mediated homologous DNA pairing and strand exchange, the biochemical reaction that serves to link recombining chromosomes (30). In addition, a physical interaction between Rad51 and Srs2 was demonstrated by us (14). Before examining the srs2 K41A and srs2 K41R mutant proteins for their ability to suppress the Rad51 recombinase activity, we first verified that the srs2 mutant proteins retain the ability to interact with Rad51. For this, purified Srs2, srs2 K41A, and srs2 K41R proteins were each mixed with Affi-Gel beads that contained covalently conjugated Rad51 protein (Affi-Rad51) or Affi-Gel beads that contained conjugated bovine serum albumin (Affi-BSA). After being washed with buffer, the Affi-Rad51 and Affi-BSA beads were treated with SDS to elute bound Srs2 and srs2 mutant proteins. As shown in Fig. 4A, the two srs2 mutant proteins interacted with Rad51 just as avidly as wild-type Srs2 did. As expected, neither the wild-type Srs2 protein nor either of the srs2 mutants was retained on the Affi-BSA control beads (Fig. 4B).

We employed the D-loop assay (Fig. 5*A*) for testing the proficiency of the srs2 K41A and srs2 K41R mutant proteins in recombination attenuation. As reported in our published work, the addition of a catalytic quantity of Srs2 (40–60 nM) to the D-loop reaction containing Rad51 (1 μM), Rad54 (150 nM), and RPA (200 nM) caused pronounced inhibition (Fig. 5, *B* and *C*). For instance, at 50 nM Srs2, the level of D-loop was suppressed by greater than 10-fold (Fig. 5, *B* and *C*). Importantly, as much as 90 nM of srs2 K41A and srs2 K41R did not exert any inhibitory effect on the D-loop reaction (Fig. 5, *B* and *C*), thus revealing a requirement for the Srs2 ATPase activity in the attenuation of the Rad51 recombinase activity. We independently verified this conclusion by using a homologous DNA pairing and strand exchange system that employs φX174 (+) strand DNA and linear duplex as substrates (Refs. 14 and 16, data not shown).

Disassembly of Rad51-ssDNA Nucleoprotein Filament by Srs2 Requires ATP Hydrolysis—The results above have verified that the ATPase activity of Srs2 protein is indispensable for attenuating Rad51-mediated recombination reactions *in vitro*. We have devised previously a bead-based biochemical assay to monitor the Srs2-mediated dissociation of Rad51 from ssDNA. Briefly, Rad51 molecules displaced by Srs2 from the presynaptic filament are trapped on a biotinylated duplex DNA fragment tethered to streptavidin-conjugated magnetic beads, followed by elution of Rad51 from the beads and SDS-PAGE analysis (Fig. 6*A*, and Ref. 14). As reported previously, incubation of Rad51 nucleoprotein filaments with Srs2 protein (60–90 nM) resulted in the release of Rad51 from the filaments as indicated by Rad51 being trapped on the streptavidin-magnetic beads that contained duplex DNA (Fig. 6*B*). Importantly, neither of the srs2 mutants, even in an amount twice that of Srs2 (180 nM), was capable of releasing Rad51 protein from the nucleoprotein filaments (Fig. 6*B*).

We also used electron microscopy to examine the ability of the two srs2 mutant proteins to catalyze the disassembly of the presynaptic filament, following the guidelines described in Krejci *et al.* (14). Briefly, the Rad51 presynaptic filament, which is extended and has a striated appearance (Fig. 7*A*), was incubated with Srs2 or the srs2 mutant proteins in the presence of RPA, and the dissociation of the Rad51 filament was gauged by the disappearance of the filament and the concomitant appearance of RPA-ssDNA nucleoprotein complexes, which appear as compact structures with bulges of bound protein molecules (14) (Fig. 7*B*). As expected, incubation of the Rad51 presynaptic filament with Srs2 led to its replacement by the RPA-ssDNA complex (Fig. 7*C*). However, the Rad51 filament was completely stable in the presence of either srs2 K41R (Fig. 7*D*) or srs2 K41A (Fig. 7*E*). Taken together, the results from the biochemical and electron microscopy analyses (Figs. 6 and 7) clearly indicated that disassembly of the Rad51 presynaptic filament by Srs2 requires the ATPase activity of the latter.

Genetic Characterization of the srs2 K41A and srs2 K41R Mutant Alleles—Previous studies (8, 9) of *SRS2* have highlighted the role of *SRS2* in attenuating Rad51-mediated recombination. We determined the effect of loss of Srs2 ATP hydrolysis on mitotic gene conversion, using two reporters that measure intra-chromosomal gene conversion between heteroalleles. As shown in Table I, both *srs2 K41A* and *srs2 K41R* elevated the gene conversion rates with both reporters. Interestingly, the hyperrecombination phenotype of two srs2 mutants was even more pronounced than that of the srs2 deletion mutant. Thus, the results show clearly that the antirecombination function of Srs2 requires the ATPase activity of this protein. Although the rate of gene conversion is increased in
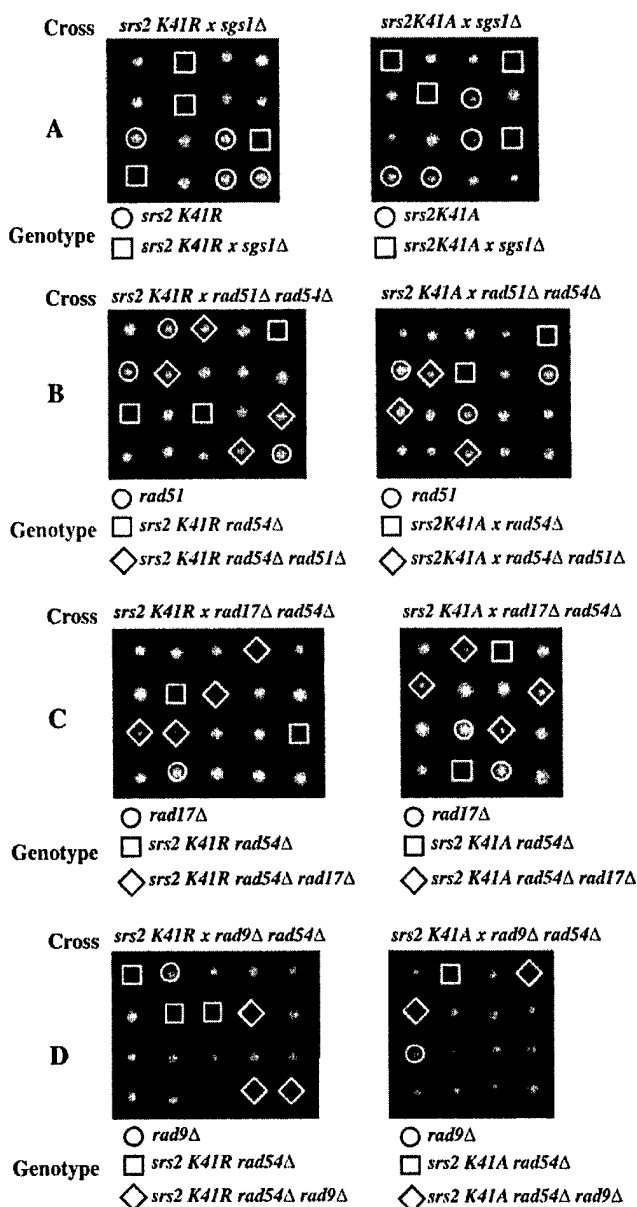

FIG. 9. **Synthetic lethal behavior of the *srs2 K41A* and *srs2 K41R* mutants.** Four or five tetrads from crosses indicated above each picture are shown. Synthetic lethality with the *sgs1*Δ mutation is shown in *A*. Synthetic lethality with the *rad54*Δ mutation is suppressed by loss of *RAD51* (*B*), partially suppressed by loss of the DNA damage checkpoint gene *RAD17* (*C*), and not suppressed by loss of the DNA damage checkpoint gene *RAD9* (*D*).

the *srs2* mutants, the spontaneous mutation rate measured for forward mutations at *CAN1* remains unchanged (Table II).

Mutants of *SRS2* are sensitive to MMS and other DNA damaging agents (8), and MMS sensitivity was actually used in our study to select transplacement segregants harboring the two srs2 Walker mutant alleles (see "Materials and Methods"). The MMS sensitivity of the *srs2 K41A* and *srs2 K41R* strains is shown in Fig. 8. Both *srs2* mutants were sensitive in this assay, but the *srs2*Δ strain was significantly more sensitive than either of the two point mutants.

The *srs2*Δ mutation by itself is not lethal, but *srs2*Δ cells become inviable when *SGS1* or *RAD54* is also ablated (9, 11, 12). To determine the role of the Srs2 ATPase activity in these genetic interactions, we combined the *srs2 K41A* and *srs2 K41R* mutations with *sgs1*Δ or *rad54*Δ. The *srs2 K41A sgs1*Δ and *srs2 K41R sgs1*Δ double mutants are inviable or grow extremely

poorly (Fig. 9*A*), whereas the *srs2 K41A rad54*Δ and *srs2 K41R rad54*Δ double mutants are inviable (Fig. 9*B*). We checked the possible suppression of the *srs2 rad54*Δ lethality by *rad51*Δ, rad9Δ, or *rad17*Δ (8) by constructing the respective triple mutants. The lethality of *srs2 rad54*Δ is fully overcome by *rad51*Δ (Fig. 9*B*) and partially suppressed by *rad17*Δ (Fig. 9*C*), but *rad9*Δ was ineffective in this regard (Fig. 9*D*).

DISCUSSION

To assess the role of ATP hydrolysis in Srs2 protein functions, we have constructed variants of this protein that harbor mutations in the Walker type A motif involved in ATP binding and hydrolysis. We have overexpressed the srs2 K41A and srs2 K41R proteins in *E. coli* and purified them to near homogeneity. Our biochemical analyses show that both of these mutant proteins retain DNA binding activity and the ability to interact with Rad51, but they are defective in ATP hydrolysis and lack DNA helicase activity. Both srs2 mutant proteins are unable to dissociate the Rad51 presynaptic filament and, accordingly, do not exert any inhibitory effect on Rad51-mediated homologous DNA pairing and strand exchange. The biochemical studies reported here thus establish the requirement for ATP hydrolysis in Srs2-mediated DNA unwinding and disassembly of the Rad51 presynaptic filament.

The results from our genetic studies provide support for the premise that ATP hydrolysis by Srs2 is needed to prevent untimely recombination, as the *srs2 K41A* and *srs2 K41R* mutants both exhibit a hyperrecombinational phenotype. Interestingly, the degree of hyperrecombination (measured as intrachromosomal gene conversion between heteroalleles) is even more pronounced in the srs2 point mutants than in the *srs2*Δ strain. In this regard, the two *srs2* Walker mutants resemble the *srs2–101* mutant described previously, which harbors the amino acid change of P39L, that is also significantly more hyperrecombinogenic than the *srs2*Δ mutant (9). These observations (Ref. 9 and this study) suggest that when Srs2 is absent, other non-recombinational pathways are used to repair spontaneous DNA damage, but when Srs2 protein is present but defective, it can interfere with these DNA repair pathways. Alternatively, or in addition, the *srs2* Walker mutants and the *srs2–101* mutant could induce DNA damage that is channeled into the homologous recombination pathway for repair, convert non-recombinogenic DNA lesions into recombinogenic ones, or enhance the activities of homologous recombination proteins. Because Srs2 is also important for the maximal activation of the S phase DNA damage checkpoint (18), it remains possible that the two *srs2* Walker mutants exert a positive influence on homologous recombination efficiency through its effect on checkpoint pathways (18). Further studies are needed to distinguish among these possibilities. That the *srs2 K41A* and *srs2 K41R* mutants do not behave exactly like the *srs2*Δ mutant is further attested by the observation that they are less sensitive to MMS than the latter. Just as in the case of *srs2*Δ (8, 9), we observed synthetic lethality of both *srs2* Walker mutants with either *rad54*Δ or *sgs1*Δ. We have also shown that the lethality of *srs2 K41A rad54*Δ and *srs2 K41R rad54*Δ can be overcome by deleting *RAD51* or *RAD17*.

Recently, reports from Haber and co-workers (20) and Kupiec and co-workers (19) showed that Srs2 is also needed for the repair of a site-specific double-strand break by synthesis-dependent single-strand annealing or double-ended synthesis-dependent single-strand annealing, the major pathway of gene conversion in mitotic yeast cells. In one of these published studies, the *srs2 K41A* allele was found to be defective in synthesis-dependent single-strand annealing (20). Likewise, the function of Srs2 in promoting adaptation or recovery from DNA damage checkpoint-mediated G$_2$/M arrest is reliant on its ATPase activity, as the *srs2 K41A* mutant is defective in this regard (17). We similarly expect the *srs2 K41R* mutant to be impaired in synthesis-dependent single-strand annealing and recovery/adaptation from DNA damage checkpoint-mediated G$_2$/M arrest. However, as alluded to above, whether or not the two srs2 Walker mutants retain S phase checkpoint function (18) will have to be determined experimentally.

We have demonstrated a physical interaction between Srs2 and Rad51 by the yeast two-hybrid system and also by biochemical means with purified proteins (14). We have suggested that the physical interaction between Rad51 and Srs2 may be germane for targeting the latter to chromosomal sites, *e.g.* ssDNA gaps created at stalled DNA replication forks, where Rad51 molecules are bound. However, it remains possible that the physical interaction noted (14) enables Srs2 to specifically displace Rad51 from ssDNA. The isolation of Rad51 and Srs2 mutants defective in complex formation will be necessary to address this issue.

REFERENCES

1. Schmid, S. R., and Linder, P. (1992) *Mol. Microbiol.* **6,** 283–291
2. Howard, M. T., Neece, S. H., Matson, S. W., and Kreuzer, K. N. (1994) *Proc. Natl. Acad. Sci. U. S. A.* **91,** 12031–12035
3. Berneburg, M., and Lehmann, A. R. (2001) *Adv. Genet.* **43,** 71–102
4. Ellis, N. A., Groden, J., Ye, T. Z., Straughen, J., Lennon, D. J., Ciocci, S., Proytcheva, M., and German, J. (1995) *Cell* **83,** 655–666
5. Yu, C. E., Oshima, J., Fu, Y. H., Wijsman, E. M., Hisama, F., Alisch, R., Matthews, S., Nakura, J., Miki, T., Ouais, S., Martin, G. M., Mulligan, J., and Schellenberg, G. D. (1996) *Science* **272,** 258–262
6. Lawrence, C. W., and Christensen, R. B. (1979) *J. Bacteriol.* **139,** 866–876
7. Aguilera, A., and Klein, H. L. (1988) *Genetics* **119,** 779–790
8. Chanet, R., Heude, M., Adjiri, A., Maloisel, L., and Fabre, F. (1996) *Mol. Cell. Biol.* **16,** 4782–4789
9. Rong, L., Palladino, F., Aguilera, A., and Klein, H. L. (1991) *Genetics* **127,** 75–85
10. Lee, S. K., Johnson, R. E., Yu, S. L., Prakash, L., and Prakash, S. (1999) *Science* **286,** 2339–2342
11. Gangloff, S., Soustelle, C., and Fabre, F. (2000) *Nat. Genet.* **25,** 192–194
12. Klein, H. L. (2001) *Genetics* **157,** 557–565
13. Klein, H. L. (2000) *Nat. Genet.* **25,** 132–134
14. Krejci, L., Van Komen, S., Li, Y., Villemain, J., Reddy, M. S., Klein, H., Ellenberger, T., and Sung, P. (2003) *Nature* **423,** 305–309
15. Veaute, X., Jeusset, J., Soustelle, C., Kowalczykowski, S. C., Le Cam, E., and Fabre, F. (2003) *Nature* **423,** 309–312
16. Sung, P. (1994) *Science* **265,** 1241–1243
17. Vaze, M. B., Pellicioli, A., Lee, S. E., Ira, G., Liberi, G., Arbel-Eden, A., Foiani, M., and Haber, J. E. (2002) *Mol. Cell* **10,** 373–385
18. Liberi, G., Chiolo, I., Pellicioli, A., Lopes, M., Plevani, P., Muzi-Falconi, M., and Foiani, M. (2000) *EMBO J.* **19,** 5027–5038
19. Aylon, Y., Liefshitz, B., Bitan-Banin, G., and Kupiec, M. (2003) *Mol. Cell. Biol.* **23,** 1403–1417
20. Ira, G., Malkova, A., Liberi, G., Foiani, M., and Haber, J. E. (2003) *Cell* **115,** 401–411
21. Sherman, F. (1991) in *Guide to Yeast Genetics and Molecular Biology* (Guthrie, C., and Fink, G. R., eds) pp. 3–21, Academic Press, San Diego, CA
22. Thomas, B. J., and Rothstein, R. (1989) *Genetics* **123,** 725–738
23. Van Komen, S., Reddy, M. S., Krejci, L., Klein, H., and Sung, P. (2003) *J. Biol. Chem.* **278,** 44331–44337
24. Sugiyama, T., Zaitseva, E. M., and Kowalczykowski, S. C. (1997) *J. Biol. Chem.* **272,** 7940–7945
25. Krejci, L., Song, B., Bussen, W., Rothstein, R., Mortensen, U. H., and Sung, P. (2002) *J. Biol. Chem.* **277,** 40132–40141
26. Petukhova, G., Stratton, S., and Sung, P. (1998) *Nature* **393,** 91–94
27. Lea, D. E., and Coulson, C. A. (1949) *J. Genet.* **119,** 264–284
28. Sung, P., Higgins, D., Prakash, L., and Prakash, S. (1988) *EMBO J.* **7,** 3263–3269
29. Sung, P., and Stratton, S. A. (1996) *J. Biol. Chem.* **271,** 27983–27986
30. Sung, P., Krejci, L., Van Komen, S., and Sehorn, M. G. (2003) *J. Biol. Chem.* **278,** 42729–42732

Yeast Xrs2 Binds DNA and Helps Target Rad50 and Mre11 to DNA Ends*

Kelly M. Trujillo‡§, Dong Hyun Roh‡‖, Ling Chen, Stephen Van Komen¶, Alan Tomkinson, and Patrick Sung¶

From the University of Texas Health Science Center, Department of Molecular Medicine, Institute of Biotechnology, San Antonio, Texas 78245

Saccharomyces cerevisiae Rad50, Mre11, and Xrs2 proteins are involved in homologous recombination, non-homologous end-joining, DNA damage checkpoint signaling, and telomere maintenance. These proteins form a stable complex that has nuclease, DNA binding, and DNA end recognition activities. Of the components of the Rad50·Mre11·Xrs2 complex, Xrs2 is the least characterized. The available evidence is consistent with the idea that Xrs2 recruits other protein factors in reactions that pertain to the biological functions of the Rad50·Mre11·Xrs2 complex. Here we present biochemical evidence that Xrs2 has an associated DNA-binding activity that is specific for DNA structures. We also define the contributions of Xrs2 to the activities of the Rad50·Mre11·Xrs2 complex. Importantly, we demonstrate that Xrs2 is critical for targeting of Rad50 and Mre11 to DNA ends. Thus, Xrs2 likely plays a direct role in the engagement of DNA substrates by the Rad50·Mre11·Xrs2 complex in various biological processes.

Mutations in the *Saccharomyces cerevisiae RAD50, MRE11,* and *XRS2* genes render cells sensitive to DNA-damaging agents and defective in meiotic recombination. Cells lacking these genes also have shortened telomeres and defects in DNA damage checkpoint signaling and in DNA double strand break repair by non-homologous end joining (NHEJ).[1] In addition, these genes are needed for a pathway of long tract gene conversion called break-induced DNA replication or BIR and for the telomerase-independent lengthening of telomere, possibly by a BIR-like mechanism. Yeast two-hybrid and biochemical

studies have revealed that the products of these genes form a stable complex, referred to as the RMX complex. The formation of the RMX complex is mediated by simultaneous interactions of Mre11 with Rad50 and Xrs2 (1–3).

The equivalents of the aforementioned protein trio in humans, namely, hRad50, hMre11, and Nbs1, also combine to form a stable complex, called the RMN complex. Again, hMre11 plays a central role in complex assembly by binding hRad50 and Nbs1 (1, 3). Like the RMX complex, the RMN complex functions in DNA damage checkpoint signaling and is needed for mitotic recombination, telomere maintenance, and resistance to DNA-damaging agents (1, 4), whereas the involvement of the human complex in meiotic recombination and NHEJ has not yet been established. Importantly, mutations in hMre11 and Nbs1 lead to the cancer prone syndromes ataxia telangiectasia-like disorder and Nijmegen breakage syndrome (NBS), respectively (1, 5–7). Mouse strains deleted for Rad50 or Nbs1 suffer early embryonic lethality (8, 9) and mice harboring hypomorphic Rad50 and NBS1 alleles are hypersensitive to genotoxic stresses and cancer prone (10–12). These latter findings reveal the involvement of the RMN complex in the maintenance of genome stability and cancer avoidance in mammals, and they aptly underscore the importance of genetic and biochemical studies on this complex and its yeast equivalent.

Rad50 belongs to the <u>s</u>tructural <u>m</u>aintenance of <u>c</u>hromosomes (SMC) family and, like other members of this family, contains Walker-type nucleotide binding motifs and a long coiled-coil domain (13, 14). A zinc binding motif, referred to as a zinc hook, is located at the base of the Rad50 coiled-coil and mediates Rad50 dimerization via the chelation of a zinc ion (14). Rad50 binds DNA in an ATP-dependent manner (15). Mre11 has a 3′ to 5′ exonuclease activity and incises certain DNA structures endonucleolytically (1, 16–18). As expected, Mre11 binds both ssDNA and dsDNA (1). The Rad50 dimer combines with two Mre11 molecules to form a stable tetrameric complex (19, 20). As a result of complex formation with Rad50, the nuclease activities of Mre11 are enhanced (16–18). In studies that employed atomic force microscopy (also called scanning force microscopy), a large number of hRad50·hMre11 complexes were seen to tether linear duplex DNA molecules via their ends (13).

In congruence with genetic data implicating the RMX complex in NHEJ, previous studies have found an ability of this complex to promote end-joining reactions mediated by the Dnl4·Lif1 complex (the equivalent of mammalian DNA ligase IV·XRCC4 complex) and the Hdf1·Hdf2 complex (the equivalent of mammalian Ku heterodimer) (21). The RMX complex was seen by atomic force microscopy to engage and juxtapose DNA ends to form DNA oligomers and in biochemical experi-

[1] The abbreviations used are: NHEJ, non-homologous end joining; RMX, Rad50·Mre11·Xrs2 complex; RMN, hRad50·hMre11·Nbs1 complex; RM, Rad50·Mre11 subcomplex; MX, Mre11·Xrs2 subcomplex; NBS, Nijmegen breakage syndrome; ss, single strand; ds, double strand; AFM, atomic force microscopy; AMP-PNP, adenyl-5′-yl β,γ-imidodiphosphate; AMP-PCP, adenosine 5′-(β,γ-methylenetriphosphate); ATPγS, adenosine 5′-O-(thiotriphosphate); BIR, break-induced replication.

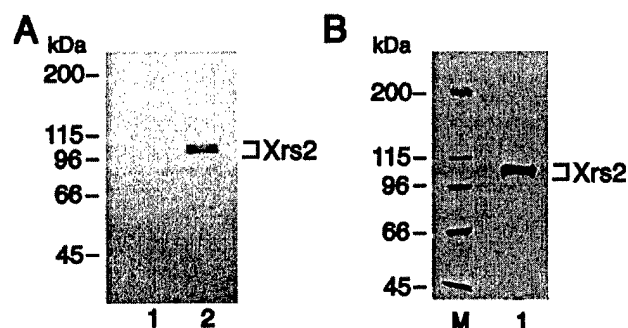*Xrs2 Binds DNA and Targets Rad50 and Mre11*

FIG. 1. **Expression and purification of Xrs2.** *A,* extracts from yeast cells harboring pX2.1 *(lane 2)* and the empty expression vector pPM231 *(lane 1)* were subjected to immunoblot analysis with anti-Xrs2 antibodies. *B,* purified Xrs2, 1.0 μg in *lane 1,* was analyzed by 7.5% SDS-PAGE and staining with Coomassie Blue. *M,* molecular size markers.

FIG. 2. **Interactions of Xrs2 with φX DNA species.** φX174 viral (+) strand *(ss;* 18 μM nucleotides; *panel I),* replicative form I DNA *(sc;* 12 μM nucleotides; *panel II),* StuI-linearized replicative form DNA *(ds;* 12 μM nucleotides; *panel III),* and a combination of all three DNA species *(panel IV)* were incubated with Xrs2 (40, 80, 150, 210, 320, 420, 520, and 1040 nM in *lanes 2–9)* at 23 °C for 15 min and then analyzed by electrophoresis. In *lanes 10,* the DNA substrates were incubated with the highest amount of Xrs2 at 23 °C for 15 min and then treated with 0.5% SDS and 0.5 mg/ml proteinase K *(SDS/PK)* for 5 min at 37 °C before gel analysis.

ments to protect DNA ends against lambda exonuclease. In this same study, Xrs2 was shown to physically interact with Lif1. The DNA end-bridging activity of RMX is believed to be important for aligning the substrate molecules to prepare them for joining, whereas the ability of Xrs2 to bind Lif1 likely endows the RMX complex with the ability to recruit the Dnl4·Lif1 complex to DNA ends to perform the joining step (21).

Toward defining the biochemical functions of Xrs2 and its contributions to the activity repertoire of the RMX complex, we have overexpressed it in yeast cells and purified it to near homogeneity. We show that Xrs2 binds DNA and is critical for DNA end binding and juxtaposition by the RMX complex. These results suggest that Xrs2 helps target the RMX complex and associated factors to DNA substrates during various chromosomal transactions.

MATERIALS AND METHODS

Overexpression and Purification of Xrs2—The *XRS2* gene was placed under the control of the galactose-inducible *GAL-PGK* promoter in the vector pPM231 to generate plasmid pX2.1 *(2μ, GAL-PGK-XRS2, LEU-2d),* which was introduced into the protease-deficient yeast strain BJ5464. Xrs2 protein was induced by growth in medium containing galactose, as described previously (18). All the purification steps were carried out at 0–4 °C. Extract was prepared from 100 g of cell pellet and clarified by centrifugation, as described (18). The clarified extract (Fraction I; 200 ml) was treated with ammonium sulfate at 0.21 g/ml. The resulting precipitate was pelleted by centrifugation (17,000 × *g,* 20 min) and dissolved in 300 ml of T buffer (40 mM Tris-HCl, pH 7.4, 10% glycerol, 0.5 mM EDTA, 0.01% Nonidet P-40, and 1 mM dithiothreitol) with protease inhibitors (18) to yield a solution with conductivity equivalent to that of 120 mM KCl (Fraction II). Fraction II was applied through a 15-ml Q-Sepharose column onto a 15-ml SP-Sepharose column with 100 mM KCl. Xrs2 bound to SP-Sepharose was eluted with a 200-ml gradient from 50 to 450 mM KCl in K buffer (20 mM KH₂PO₄, pH 7.4, 10% glycerol, 0.5 mM EDTA, 0.01% Nonidet P-40, and 1 mM dithiothreitol). The peak fractions were identified by Coomassie Blue staining of SDS-PAGE gels, pooled (Fraction III; 20 ml and ~250 mM KCl), and loaded directly onto a 6-ml Macro-Hydroxyapatite column (Bio-Rad), which was developed with a 120-ml gradient from 15 to 210 mM KH₂PO₄ in K buffer with 100 mM KCl. The peak fractions (Fraction IV; 10 ml and ~110 mM KH₂PO₄) were pooled, dialyzed for 3 h against T buffer with 60 mM KCl, and loaded onto a 1.0-ml Mono-Q column. The Mono-Q column was developed with a 33-ml gradient from 60 to 200 mM KCl in T buffer. The peak fractions (Fraction V; 3 ml and ~120 mM KCl) were loaded directly onto a 1.0-ml Mono-S column, which was developed with a 30-ml gradient from 100 to 400 mM KCl in T buffer. The pool of Xrs2 (Fraction VI; 3 ml, ~250 mM KCl and containing 3 mg of nearly homogeneous protein) was concentrated in a Centricon-30 device (Amicon) to ~5.0 mg/ml and stored in small aliquots at −80 °C. The Xrs2 protein concentration was determined by densitometric scanning of a 7.5% SDS-PAGE gel containing multiple loadings of purified Xrs2 protein previously dephosphorylated with shrimp alkaline phosphatase against known amounts of bovine serum albumin run on the same gel.

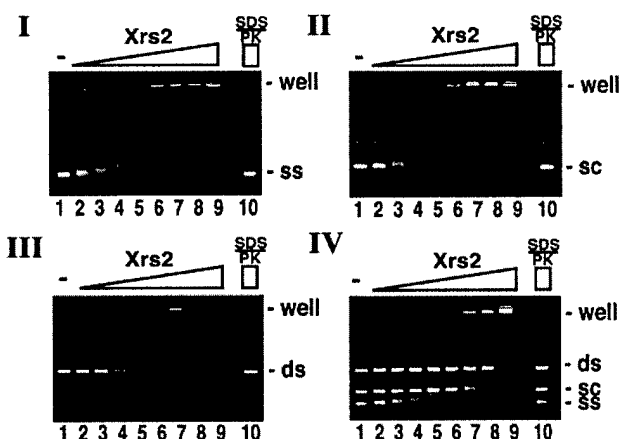*Rad50, Mre11, and Protein Complexes*—Rad50 and Mre11 were over-expressed in yeast and purified as described previously (18). The Rad50·Mre11·Xrs2 complex and the Rad50·Mre11 and Mre11·Xrs2 subcomplexes were reconstituted and purified as described (21). The concentration of Rad50 and Mre11 was determined by densitometric scanning of a 7.5% SDS-PAGE gel containing multiple loadings of the two purified proteins against known amounts of bovine serum albumin run on the same gel.

DNA Substrates—The φX174 (+) strand and replicative form I DNA (~90% supercoiled) were purchased from New England Biolabs and Invitrogen, respectively. The φX174 replicative form DNA was linearized with StuI. All the oligonucleotides were purchased from Invitrogen. OL2 is an 83-base oligonucleotide with the following sequence: 5'-TT-TATATCCTTTACTTTATTTTCTATGTTTATTCATTTACTTATTTTGT-ATTATCCTTATACTTATTTACTTTATGTTCATTT-3'. OL1 is the exact complement of OL2. HP-Y is an 80-base oligonucleotide with the following sequence: 5'-TTTTTTTTTTTTTTTTTTTTGACCTGGCACGTA-GGACAGCAGCTGCTGTCCTACGTGCCAGGTCTTTTTTTTTTTTTTT-TTTT-3'. 3'-HP is the same as HP-Y but without the 18 dT residues at the 5'-end. 5'-HP is the same as HP-Y but without the 18 dT residues at the 3'-end. HP is a 44-base oligonucleotide: 5'-GACCTGGCACGT-AGGACAGCAGCTGCTGTCCTACGTGCCAGGTC-3'. The oligonucleotides were purified and labeled at the 5'-end with ³²P, as described (18). For annealing reactions, the oligonucleotides were heated at 70 °C for 10 min and then allowed to cool slowly to room temperature. Radiolabeled nuclease substrates (HP2 and 3' Duplex) were prepared as previously described (18).

Gel Mobility Shift Assays—Xrs2 was incubated with the DNA substrates in buffer G (30 mM BisTris-HCl, pH 7.0, 100 μg/ml bovine serum albumin, 5 mM MgCl₂, 50 mM KCl, and 1 mM dithiothreitol) in 10 μl. After incubation at 25 °C for 15 min, the reaction mixtures were analyzed in 1.0% agarose gels at 4 °C in TAE buffer (40 mM Tris acetate, pH 7.4, 0.5 mM EDTA), followed by treatment with ethidium bromide to stain the DNA species. When radiolabeled oligonucleotides were used, the reaction was assembled and incubated in the same way, except that the analysis was conducted in 12% native polyacrylamide gels at 4 °C in TAE buffer. The gels were dried and subjected to phosphorimaging analysis. Deproteinization was done by incubating reaction mixtures with 0.5% SDS and 0.5 mg/ml proteinase K at 37 °C for 5 min.

Nuclease Assays—The nuclease assays were carried out in buffer that contained manganese, as described in Trujillo and Sung (18). Briefly, the DNA hairpin (HP2) and exonuclease substrate (3' Duplex) were incubated with individual proteins and protein complexes in the presence of ATP. Portions of the reactions were withdrawn at the indicated times, mixed with 1/5 volume of 3% SDS, and treated with proteinase K (0.5 mg/ml). Analyses of the endonuclease reactions in polyacrylamide gels and of the exonuclease reactions by thin layer chromatography were as described (18). Data quantitation was done by phosphorimaging analysis.

Exonuclease Protection—The exonuclease protection assay was carried out as described (21). Briefly, a 400-bp 5'-end-labeled linear DNA fragment was preincubated with individual proteins or protein complexes at 23 °C for 10 min in a total volume of 10 μl and then placed on ice. A 1.5-μl aliquot of the reaction was removed and incubated separately as control. To the remainder of the reaction, 0.1 unit of λ exonuclease (Invitrogen) was added, and the incubation continued at 0 °C. At the indicated times, 1.5-μl aliquots were removed and mixed with 0.5 μl of 3% SDS. Small portions of these samples were applied to polyethyleneimine cellulose sheets (J. T. Baker) to separate the released ^{32}P label

from the DNA substrate (18). Data quantification was done by phosphorimaging analysis.

Topological Unwinding Assay—Individual proteins and protein complexes were incubated with topologically relaxed DNA in 10 μl of buffer G containing 2 mM ATP at 23 °C. After 10 min, 3 units of calf thymus topoisomerase I (Invitrogen) was added, and the incubation was continued for another 10 min at 37 °C. The reactions were deproteinized with 0.5% SDS and 0.5 mg/ml proteinase K for 5 min at 37 °C. DNA species were resolved by electrophoresis in 1% agarose gels in TAE buffer and visualized by staining with ethidium bromide.
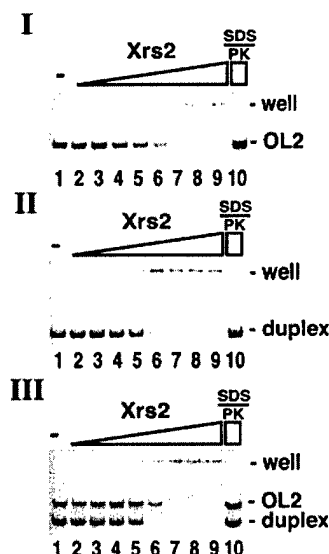
ATP Hydrolysis—Individual proteins and protein complexes were incubated at 30 °C in buffer G containing 150 μM [γ-^{32}P]ATP in a volume of 6.5 μl. At the indicated times, a 1-μl portion of the sample was removed and mixed with 0.5 μl of 1% SDS. Reaction mixtures were resolved by thin layer chromatography in polyethyleneimine cellulose sheets, followed by phosphorimaging analysis (22).

Atomic Force Microscopy—AFM was performed using a Nanoscope Scanning Probe system (Digital Instruments) in the tapping mode, following the published procedures (21). Briefly, a 400-bp DNA fragment with 5' cohesive ends (10 nM of each end) was incubated at 0 °C for 10 min with 20 nM each of the RMX, RM, and MX complexes with or without ATP in a volume of 10 μl. The reaction mixtures were diluted and applied to freshly cleaved mica disks, which were washed with water and dried with a stream of air. Images were captured at a scan rate of 1.0–1.5 Hz using Nanosensors Pointprobe silicon cantilevers (type NCL-W; length = 230 μm; resonance frequency between 177 and 191 kHz).

FIG. 3. **Interactions of Xrs2 with short DNA substrates.** Xrs2 (40, 80, 150, 210, 320, 420, 520, and 1040 nM in *lanes 2–9*) was incubated with the 83-mer oligonucleotide OL2 (300 nM nucleotides; *panel I*), its double-stranded counterpart (duplex; 300 nM bp; *panel II*), and the mixture of OL2 and duplex (*panel III*) at 23 °C for 15 min. The reaction mixtures were run in polyacrylamide gels, followed by phosphorimaging analysis of the dried gels. In *lane 10*, the DNA substrates were incubated with the highest amount of Xrs2 at 23 °C for 15 min and then treated with 0.5% SDS and 0.5 mg/ml proteinase K (*SDS/PK*) for 5 min at 37 °C before gel analysis.
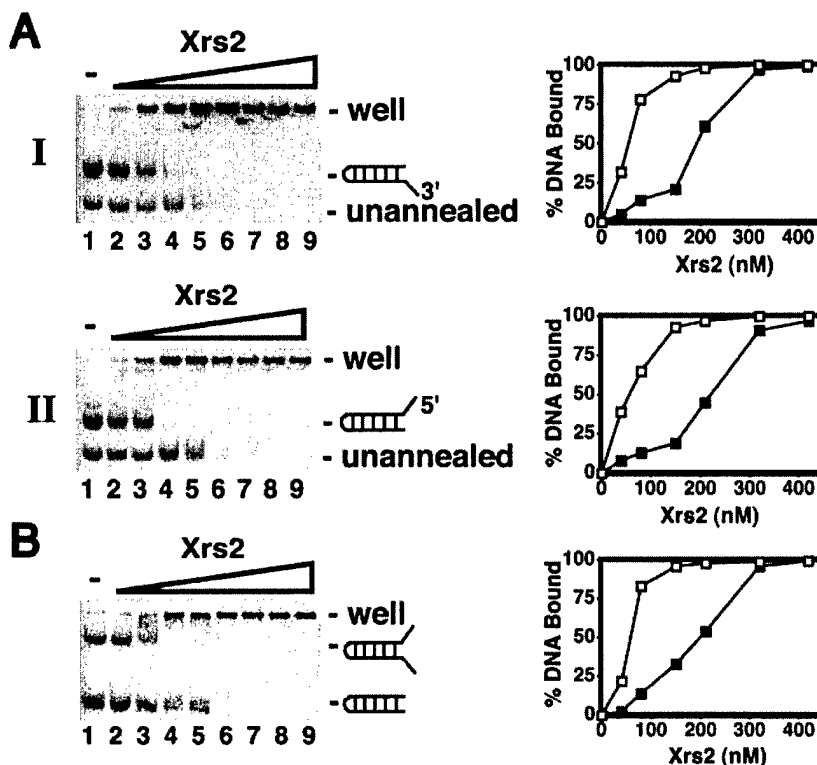
RESULTS

Expression and Purification of Xrs2—Xrs2 was expressed in yeast cells using the galactose-inducible *GAL-PGK* promoter and identified by Western blotting. A number of immunoreactive protein species ranging from ~100 to 105 kDa were detected in cell extract (Fig. 1A), which are all close to the predicted size of Xrs2 (96 kDa). A procedure was devised to purify Xrs2 to near homogeneity (Fig. 1B). The cluster of Xrs2 species detected in extract co-purified. The slower migrating forms are phosphorylated species of Xrs2, because the mobility of these forms was reduced to that of the fastest migrating form after treatment with either shrimp alkaline phosphatase or lambda phosphatase (data not shown).

Xrs2 Binds DNA—Because neither Xrs2 nor Nbs1 has been

FIG. 4. **Xrs2 binds preferentially to ssDNA secondary structures.** *A*, Xrs2 (40, 80, 150, 210, 320, 420, 520, and 1040 nM in *lanes 2–9*) was incubated with a mixture of annealed and unannealed 3'-HP (300 nM nucleotides; *panel I*) and with a mixture of annealed and unannealed 5'-HP (300 nM nucleotides; *panel II*) at 23 °C for 15 min. The reaction mixtures were run in polyacrylamide gels, which were dried and subjected to phosphorimaging analysis to obtain data points for a graphical presentation of the results. The *open squares* denote binding of the annealed oligonucleotides, and the *closed squares* denote binding of the unannealed oligonucleotides. *B*, Xrs2 (40, 80, 150, 210, 320, 420, 520, and 1040 nM in *lanes 2–9*) was incubated with a mixture of fully annealed HP-Y and HP (300 nM nucleotides each) and then analyzed as above. *Closed squares*, HP binding; *open squares*, HP-Y binding.
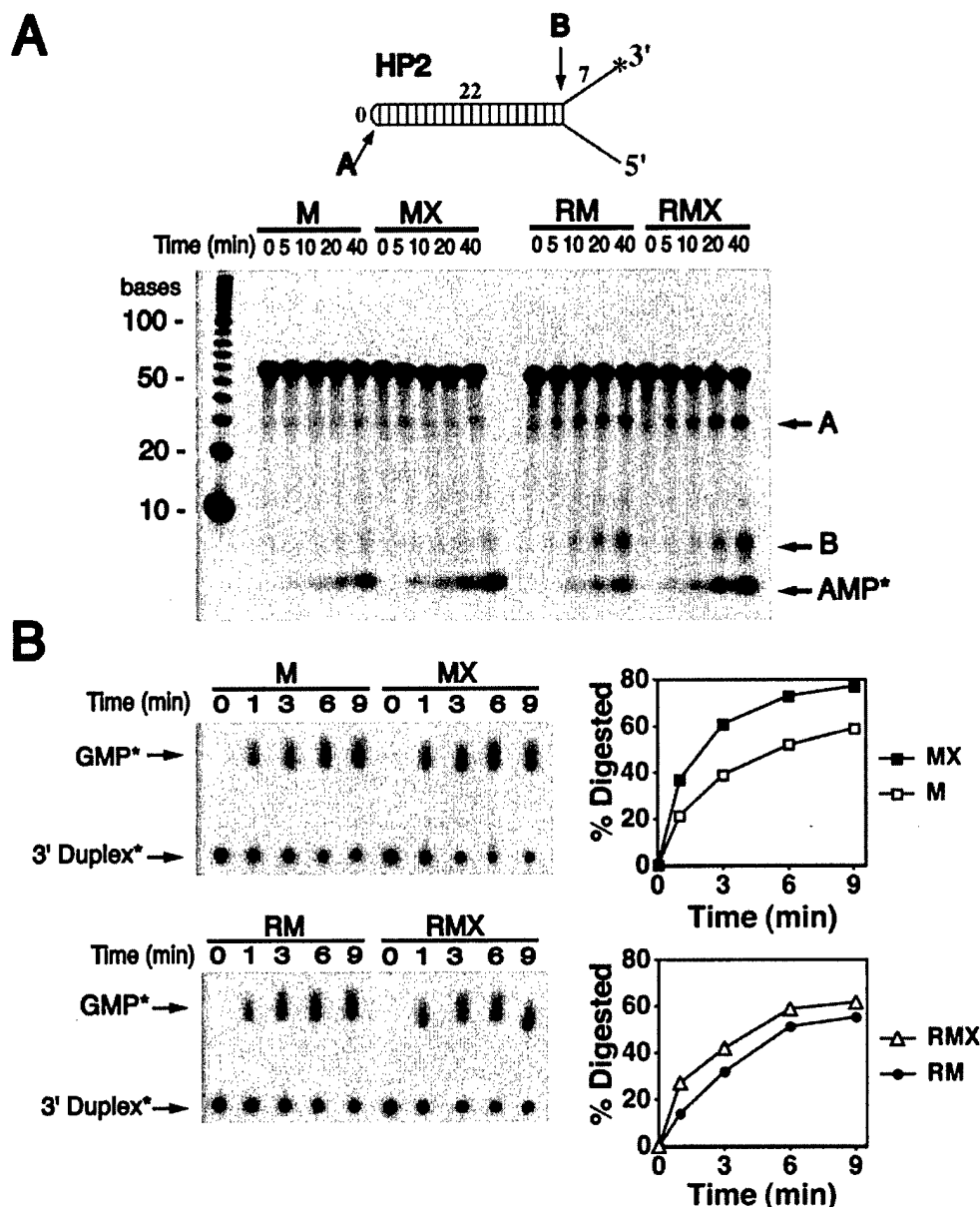
Xrs2 Binds DNA and Targets Rad50 and Mre11

FIG. 5. **Effect of Xrs2 on the nuclease activities of Mre11 and Rad50·Mre11.** *A*, the hairpin substrate (HP2; 120 nM nucleotides) was incubated with 400 nM of Mre11 (*M*), Mre11·Xrs2 (*MX*), Rad50·Mre11 (*RM*), and Rad50·Mre11·Xrs2 (*RMX*) at 37 °C. Samples were drawn at the indicated times, deproteinized, and run in a polyacrylamide gel. Two endonucleolytic products, designated *A* and *B*, and an exonuclease product, AMP, were generated (18). *B*, the 3' labeled duplex DNA substrate (7.4 μM nucleotides) was incubated with 25 nM Mre11 (*M*), Mre11·Xrs2 (*MX*), Rad50·Mre11 (*RM*), or Rad50·Mre11·Xrs2 (*RMX*) at 4 °C. Samples were drawn at the indicated times, deproteinized, and resolved by TLC. The data points from phosphorimaging analysis of the TLC plates were plotted.

examined for a DNA-binding activity, we were very interested in determining whether Xrs2 has such an activity. To do this, purified Xrs2 was incubated with φX ssDNA and φX dsDNA that was either supercoiled or linear. Nucleoprotein species were separated from the free DNA by electrophoresis in agarose gels, followed by treatment of gels with ethidium bromide to stain the DNA. In these DNA mobility shift experiments, Xrs2 bound all three species of DNA. However, Xrs2 appeared to have higher affinity for the ssDNA and supercoiled DNA. For instance, although 40 nM Xrs2 resulted in a shift of the ssDNA and supercoiled DNA, 150 nM Xrs2 was needed to see a shift of the linear duplex (Fig. 2, *I–III*). Treatment of the nucleoprotein complexes with SDS and proteinase K released the DNA substrates, indicating the absence of a nuclease activity in Xrs2.

To further examine the relative affinities of Xrs2 for the three DNA species, these substrates were mixed and then incubated with Xrs2, followed by gel electrophoresis and stain-

ing as before to detect mobility shift. As shown in Fig. 2 (*panel IV*), shifting of the ssDNA occurred with the lowest amount of Xrs2 (40 nM; *lane 2*), followed by supercoiled DNA at a significantly higher Xrs2 concentration (320 nM; *lane 6*), but the linear duplex was not shifted until the Xrs2 concentration was increased to between 520 and 1040 nM (*lane 8* and *9*). Thus, the order of preference of Xrs2 for these large DNA species is ssDNA > supercoiled DNA > linear duplex.

Xrs2 DNA-binding Activity Is Structure-specific—Due to its large size, the φX ssDNA contains substantial secondary structures. It was therefore of interest to study the DNA-binding activity of Xrs2 using short substrates that are devoid of secondary structure or that have defined structures. The first set of experiments involved the use of an 83-mer oligonucleotide (OL2) with no defined secondary structure and a duplex obtained by hybridizing OL2 to its complement. These ^{32}P-labeled DNA substrates were mixed and then incubated with Xrs2.
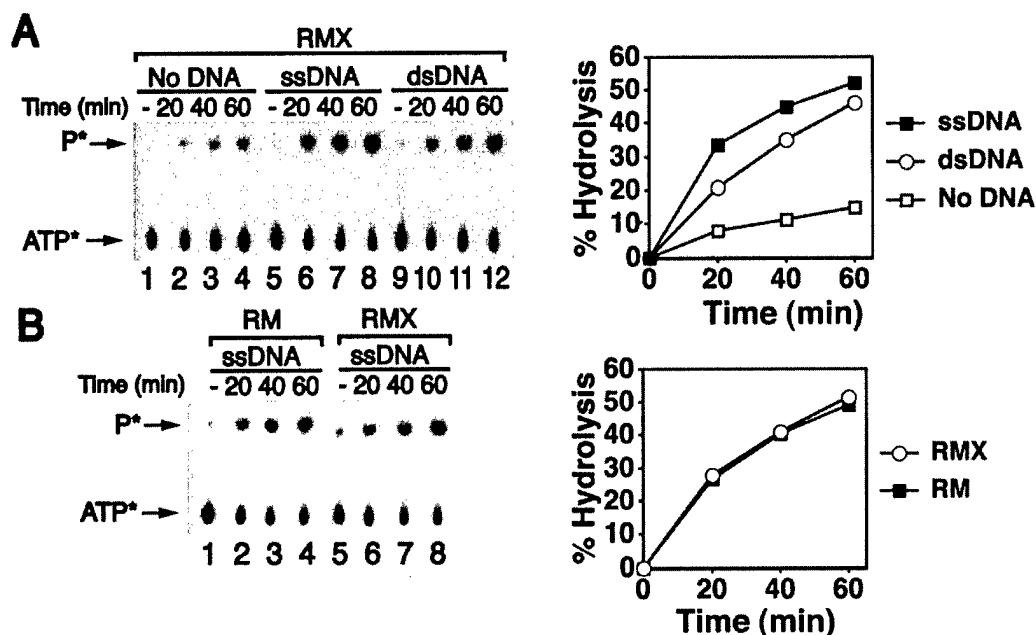
FIG. 6. **Effects of Mre11 and Xrs2 on the Rad50 ATPase activity.** *A*, the Rad50·Mre11·Xrs2 (*RMX*) complex (1.4 μM) was incubated with [γ-^{32}P]ATP (150 μM) at 30 °C without DNA and with φX174 (+) strand (ssDNA; 23 μM nucleotides) or linear duplex (dsDNA; 23 μM bp). Samples were drawn at the indicated times, deproteinized, and then analyzed by TLC. The data points from phosphorimaging analysis of the TLC plates were plotted. *B*, the Rad50·Mre11 (*RM*) and RMX complexes (1.2 μM each) were incubated at 30 °C with 150 μM [γ-^{32}P]ATP with ssDNA. Samples were drawn at the indicated times, deproteinized, and then analyzed by TLC. The data points from phosphorimaging analysis of the TLC plates were plotted.

Nucleoprotein complexes were resolved by electrophoresis in polyacrylamide gels, followed by phosphorimaging analysis of the dried gels to detect DNA mobility shift. Interestingly, unlike the experiments with the long DNA substrates (Fig. 2), wherein Xrs2 bound ssDNA preferentially, Xrs2 did not show a preference for OL2 (Fig. 3).

To test the idea that Xrs2 recognizes secondary structures in the φX ssDNA molecule, we used oligonucleotides that, when subject to heating and cooling, fold to give a hairpin structure of 22 bp with either a 3′- or 5′-single-stranded overhang of 18 dT residues. These DNA substrates were used without separation from the unannealed form in binding reactions with Xrs2. As shown in Fig. 4A, the annealed form of the substrates was bound preferentially over the unannealed form. Thus, it appeared that Xrs2 has higher affinity for a duplex/single strand junction than for either ssDNA or duplex DNA. We validated this premise by using two hairpin substrates that have either no single strand overhang or a pair of homopolymeric tails of 18 dT residues. As expected, the hairpin with tails was the preferred substrate (Fig. 4B).

Effects of Xrs2 on the Mre11 Nuclease Activities—Previous results showed that Mre11 has a 3′ to 5′ exonuclease activity and a structure-specific endonuclease activity that can cleave a hairpin, a stem-loop structure, and a 3′ ssDNA overhang that borders a duplex DNA region. Rad50 enhances the endonuclease, but not the exonuclease, activity (18). The endonuclease and exonuclease activities of the Mre11 protein are dependent on manganese, and magnesium is ineffective in this regard (16, 18).
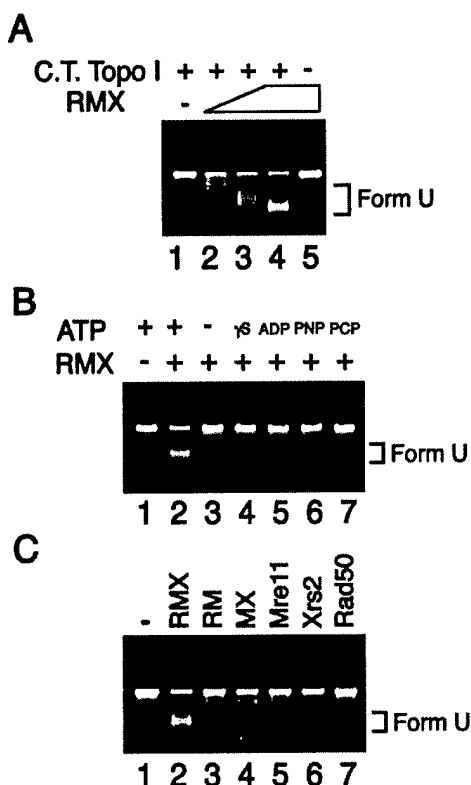
We examined whether Xrs2 regulates the Mre11 nuclease activities. For this, we used a 3′-end-labeled duplex substrate for the exonuclease assay and a hairpin that contains two 7-nucleotide dT overhangs (HP2) to assess the structure-specific endonuclease activity (18). The Mre11 exonuclease activity releases the ^{32}P label from these substrates as a mononucleotide and incises HP2 endonucleolytically at the hairpin and at the duplex/single strand junction that contains the 3′-oligonucleotide dT overhang (Fig. 5) (18).

Little, if any, stimulation of the Mre11 endonuclease activity

by Xrs2 was seen (Fig. 5A). Significantly, the RMX complex showed higher (~2-fold) endonuclease activity than the RM subcomplex (Fig. 5A), with the incisions at the hairpin (product A) and the ss/ds junction (product B) being similarly enhanced (Fig. 5A). With both the duplex and HP2, Xrs2 stimulates the exonuclease activity of Mre11 and the RM subcomplex (Fig. 5, A and B). Thus, Xrs2 potentiates the exonuclease activity of Mre11 and both the exonuclease and structure-specific endonuclease activities of the Rad50·Mre11 subcomplex.

Modulation of Rad50 ATPase Activity by Mre11 and Xrs2—Rad50 contains Walker A and B motifs believed to be involved in the binding and hydrolysis of ATP. We tested for the ability of Rad50 to hydrolyze ATP and examined possible effects of Mre11 and Xrs2 on this activity. To keep the Mre11 nuclease function dormant, the experiments were done in buffer that contained magnesium instead of manganese (16, 18). Rad50 by itself exhibited negligible ATPase activity, with k_{cat} < 0.05/min, regardless of whether DNA (ss or ds) was present or not (data not shown). As expected, Mre11 and Xrs2 were both devoid of ATPase activity (data not shown). By contrast, ATP hydrolysis was seen with the RMX complex (Fig. 6A, *panel I*). Interestingly, this activity shows a strong dependence on DNA, with ssDNA and dsDNA being equally effective. With ssDNA as cofactor, the k_{cat} for ATP hydrolysis is ~0.68 min^{-1} (Fig. 6A, *panel I*). The RM subcomplex also has a DNA-stimulated ATPase activity similar in potency to that of the RMX complex (Fig. 6A, *panel II*).
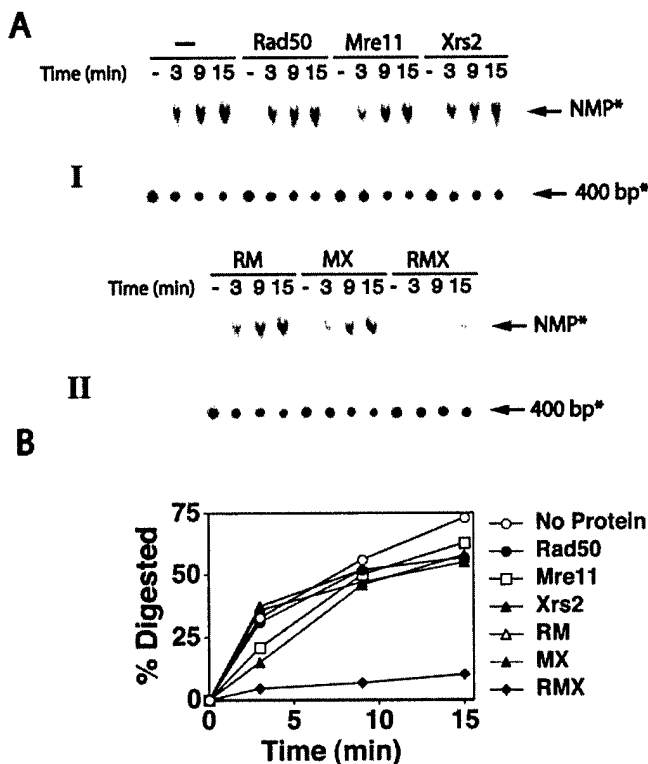
ATP-dependent Alteration of DNA Topology by the RMX Complex—We examined the ability of the RMX complex to change the topology of DNA. The experiments were done in buffer that contained magnesium to keep the Mre11 nuclease function dormant (16, 18). The reaction entailed incubating this protein complex with topologically relaxed DNA, ATP, and calf thymus topoisomerase I, followed by its deproteinization and analysis by gel electrophoresis to look for a DNA-linking number change. As shown in Fig. 7A, RMX mediated a change in the DNA-linking number, with the degree of change being proportional to the amount of protein complex (*lanes 2–4*). We

A

C.T. Topo I + + + + −
RMX −

] Form U

1 2 3 4 5

B

ATP + + − γS ADP PNP PCP
RMX − + + + + + +

] Form U

1 2 3 4 5 6 7

C

] Form U

1 2 3 4 5 6 7

FIG. 7. **RMX complex induces DNA topology change.** *A,* the Rad50·Mre11·Xrs2 (*RMX*) complex (200, 400, and 800 nM in *lanes 2–4*) was incubated with topologically relaxed ϕX174 DNA (6 μM nucleotides) and calf thymus topoisomerase I in the presence of ATP at 37 °C. In *lane 5,* the highest amount of RMX (800 nM) was incubated with the DNA substrate in the absence of topoisomerase, and in *lane 1,* the DNA substrate was incubated with topoisomerase. After deproteinization treatment, the reaction mixtures were resolved in an agarose gel, and the DNA species was stained with ethidium bromide. *Form U* denotes negatively supercoiled DNA species generated as a result of RMX binding. At 400 nM of the RMX complex, the Form U product possessed on average of five negative superhelical turns, corresponding to σ = −0.01 (*lane 3*), which is significantly less than that (σ = −0.05 to −0.06) expected for plasmid molecules isolated from cells. *B,* the RMX complex, 800 nM, was incubated with relaxed DNA (6.0 μM nucleotides) and topoisomerase in the absence of ATP (*lane 3*), with ATP (*lane 2*), ADP (*lane 5*), ATPγS (*γS; lane 4*), AMP-PNP (*PNP; lane 6*), or AMP-PCP (*PCP; lane 7*) and analyzed as above. In *lane 1,* the DNA substrate was incubated with ATP and topoisomerase. *C,* Rad50, Mre11, Xrs2, Rad50·Mre11 (*RM*), Mre11·Xrs2 (*MX*), and RMX, 800 nM each, were incubated with topologically relaxed DNA (6.0 μM nucleotides) and topoisomerase I in the presence of ATP and analyzed (*lanes 2–7*) as above. In *lane 1,* the DNA substrate was incubated with topoisomerase.

refer to the DNA species generated by RMX as Form U, because subsequent analyses indicated that it was negatively supercoiled or underwound. Omission of ATP greatly diminished the level of Form U, and substitution of ATP with ADP or the non-hydrolyzable analogues AMP-PNP, AMP-PCP, and ATPγS also reduced the Form U level by a similar degree (Fig. 7*B,* *panel II*). Neither the individual components of the RMX complex nor the RM and MX subcomplexes make Form U (Fig. 7*C*).

The calf thymus topoisomerase I used above is equally capable of removing negative supercoils and positive supercoils. Importantly, when we used *Escherichia coli* topoisomerase I, specific only for negatively supercoiled DNA, with the RMX complex, no change in the DNA linking number was detected (data not shown). Thus, it seems likely that, upon its binding to the relaxed DNA substrate, RMX generated positive supercoils that were removed by calf thymus topoisomerase I to yield Form U. That Form U harbors negative supercoils was verified by purifying it from the reaction and demonstrating its relaxation by *E. coli* topoisomerase I (data not shown).
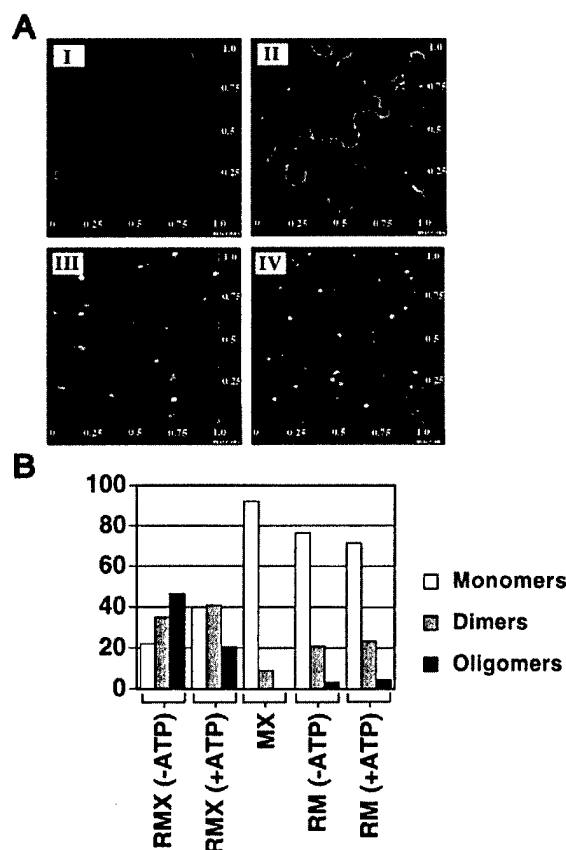
A

Time (min) − Rad50 Mre11 Xrs2
− 3 9 15 − 3 9 15 − 3 9 15 − 3 9 15

← NMP*

I

← 400 bp*

Time (min) RM MX RMX
− 3 9 15 − 3 9 15 − 3 9 15

← NMP*

II

← 400 bp*

B

FIG. 8. **Xrs2 is needed for protection of DNA ends against λ exonuclease digestion.** *A,* the 5′ ^{32}P-labeled duplex (9.5 nM DNA ends) was mixed with 60 nM each of Rad50, Mre11, Xrs2, Rad50·Mre11 (*RM*), Mre11·Xrs2 (*MX*), and Rad50·Mre11·Xrs2 (*RMX*), and then λ exonuclease was added and the incubation continued at 0 °C. Samples were drawn at the indicated times, deproteinized, and resolved by TLC. *B,* the data points from phosphorimaging analysis of the TLC plates in *A* were plotted.

Xrs2 Is Needed for Protecting DNA Ends from Exonuclease Digestion—Previously, we showed an ability of the RMX complex to engage DNA ends by two different methods: biochemically, by assessing the protection of radiolabeled DNA ends from exonuclease digestion, and physically, by examining the binding of RMX to DNA ends with atomic force microscopy. In this work, we examined a possible contribution of Xrs2 to DNA end engagement by RMX using both the biochemical means (this section) and atomic force microscopy (next section).

For the exonuclease protection experiments, a 400-bp linear DNA fragment was radiolabeled with ^{32}P at the 5′-end and subjected to digestion by λ exonuclease in the presence of RMX, the RM and MX subcomplexes, and individual components of the full complex. To avoid possible complications, the buffer used in this series of experiments contained magnesium to keep the Mre11 nuclease function dormant (16, 18). The ^{32}P-labeled mononucleotide released by λ exonuclease was separated from the undigested substrate by thin layer chromatography and quantified by phosphorimaging analysis. The results showed that only RMX protects the substrate from exonucleolytic attack (Fig. 8). Whereas nearly 75% of the ^{32}P label was removed by λ exonuclease after 15 min of incubation in the absence of another protein and with the individual components of the RMX complex, the RM subcomplex, or the MX subcomplex, less than 10% of the label was lost when RMX was used (Fig. 8). Thus, it appears that Xrs2 is indispensable for the RMX complex to shield DNA ends from λ exonuclease.

Effect of Xrs2 on DNA End Bridging by RMX Complex as Defined by AFM—AFM was employed to further characterize

A

B

FIG. 9. **Xrs2 is critical for targeting Rad50 and Mre11 to DNA ends.** *A*, the DNA substrate was incubated with the Rad50·Mre11·Xrs2 (*RMX; panel II*), Rad50·Mre11 (*RM; panel III*), and Mre11·Xrs2 (*MX; panel IV*) complexes at 0 °C for 10 min in the absence of ATP and analyzed by AFM. The DNA substrate was also analyzed alone (*panel I*). Representative scans are shown. *B*, scans of spreads from the above series of reactions and from another series of reactions carried out in the presence of ATP were analyzed to calculate the percentage of monomeric, dimeric, and oligomeric forms of the DNA substrate in each case. *RMX (−ATP)*, n = 1459 molecules examined; *RMX (+ATP)*, n = 444 molecules examined; *MX (−ATP)*, n = 1171 molecules examined; *RM (−ATP)*, n = 928 molecules examined; *RM (+ATP)*, n = 385 molecules examined.

the role of Xrs2 in targeting Rad50 and Mre11 to DNA ends. Reaction mixtures containing RMX, RM, or MX and a 400-bp DNA fragment were applied onto mica and examined in the atomic force microscope. The buffer used had magnesium in it, so as to keep the Mre11 nuclease function dormant (16, 18). Many DNA molecules were examined in each spread with representative images shown in Fig. 9A. Quantitative results are summarized in Fig. 9B. The DNA molecules alone were seen as monomers (Fig. 9A, *panel I*), but, confirming the results from the exonuclease protection experiments (Fig. 8) and our published study (21), incubation with the RMX complex resulted in the majority of the DNA fragments being converted into linear dimers and linear oligomers (Fig. 9A, *panel II*, and Fig. 9B). With the MX subcomplex, there was a low level (<10%) of DNA dimer formation but no detectable DNA oligomer (Fig. 9A, *panel IV*, and Fig. 9B). The RM subcomplex showed a somewhat higher capacity for making DNA dimers than the MX complex and a weak ability to promote DNA oligomer formation (Fig. 9A, *panel III*, and Fig. 9B). Because the above experiments were conducted in the absence of ATP, we next examined the effect of ATP on the interactions of the protein complexes with the substrate. It is clear that ATP does not enable the RM or MX complex to make more DNA dimers and oligomers, although it appears to slightly reduce the ability

of the RMX complex to generate DNA oligomers. Overall, the results (Figs. 8 and 9) indicate that only the RMX complex possesses a significant ability to engage DNA ends and bridge DNA fragments, thus revealing a specific role of Xrs2 in the interaction of the RMX complex with DNA ends.

DISCUSSION

Xrs2 Binds DNA Structures and Influences the Activities of the RMX Complex—Rad50 and Mre11 both bind DNA (1). Using gel mobility shift assays, we have presented evidence that Xrs2 has an intrinsic DNA-binding activity also. The results show that Xrs2 recognizes duplex-single strand DNA junctions. It remains to be seen whether Xrs2 also binds other DNA structures. Xrs2 exerts a slight stimulation on the nuclease activities of Mre11, with the exonuclease activity being enhanced with or without Rad50, whereas elevation of the endonucleolytic activity is realized only in the context of the RMX complex.

Genetic observations strongly suggest that the interaction of Rad50 with ATP is critical for its biological functions (1, 23). The RM and RMX complexes exhibit an ATPase activity that is stimulated by either ssDNA or dsDNA, and incubating the RMX complex with topologically relaxed DNA and calf thymus topoisomerase I results in a DNA linking number change (this work). Paull and Gellert (17) have shown an ability of the human RMN complex to melt a short duplex. The DNA unwinding activity of the RMN complex is stimulated by ATP but not by non-hydrolyzable analogues of ATP. Given this, it seems reasonable to suggest that the alteration of DNA topology induced by the yeast RMX complex also stems from an ability to separate DNA strands. The omission of ATP or its substitution with non-hydrolyzable analogues reduces the magnitude of the DNA linking number change induced by RMX, suggesting that ATP hydrolysis is needed for the expression of the DNA unwinding activity. It is important to note that even though the RM complex hydrolyzes as much ATP as the RMX complex, topological unwinding of DNA is seen only with the latter, indicating that Xrs2 plays an important role in the DNA unwinding reaction.

Previously, we reported that the RMX complex binds DNA ends and bridges linear dsDNA molecules via their ends (21). Here we have presented biochemical and physical evidence that only the RMX complex is capable of protecting DNA ends from exonuclease digestion and bridging DNA fragments. Interestingly, the DNA end binding and bridging activities of the RMX is independent of ATP. In fact, a reduced number of DNA oligomers were seen upon inclusion of ATP. At present, we do not know whether ATP attenuates the ability of the RMX complex to juxtapose DNA or it accelerates the turnover of the protein complex from DNA ends to result in disassembly of the DNA oligomers, or both. We note that the end-bridging function of the RMX complex is distinct from its endonuclease and DNA unwinding activities, in that the latter activities are stimulated, rather than attenuated, by ATP (Ref. 18 and this study).

Functional Implications—RMX enhances the end-joining efficiency of Dnl4/Lif1, and it does so by juxtaposing linear DNA fragments via their ends and recruiting Dnl4·Lif1 through an interaction between Xrs2 and Lif1 (21). Here we have demonstrated that Xrs2 is in fact also critical for targeting Rad50 and Mre11 to DNA ends and for the DNA end-bridging activity of the RMX complex. It seems reasonable to consider the possibility that the DNA-binding activity of Xrs2 contributes to the specific interactions of the RMX complex with DNA ends, perhaps by conferring end-binding specificity to this complex and stabilizing the nucleoprotein complex that contains RMX and DNA ends.

RMX is needed for BIR. During BIR, a ssDNA tail invades a homologous sequence to form a primer template junction for initiating DNA synthesis, which continues until reaching the end of the donor chromosome. BIR also requires Rad52, Rad59, and Rdh54/Tid1 (24, 25). It seems reasonable to suggest that RMX co-operates with these other factors to make the DNA joint needed for priming DNA synthesis. In this regard, the ability of RMX (and its human equivalent RMN) to melt duplex DNA may be germane for DNA joint formation and DNA synthesis in BIR.

RMX is indispensable for the formation of meiotic DNA double strand breaks catalyzed by Spo11, a topoisomerase II-like protein (26). The precise role of RMX in this reaction is not yet defined, but it is possible that it helps target the Spo11 complex to the sites of meiotic break formation and activates the topoisomerase function of Spo11. The DNA-binding activity of Xrs2 and possible interactions of Xrs2 with Spo11 or its associated factors may be critical for establishing a nucleoprotein structure conducive for the cleavage reaction. Xrs2 can likewise contribute to the DNA damage checkpoint functions of the RMX complex by interacting with the checkpoint kinases or other components of the checkpoint machineries and by targeting RMX and associated checkpoint proteins to the damage sites. In fact, a recent study has found physical interaction between Xrs2 and Tel1, the *Saccharomyces cerevisiae* equivalent of ATM kinase in mammals, and Xrs2-dependent targeting of Tel1 to a DNA double strand break (27).

Even though Nbs1 has only limited homology to Xrs2, it is clearly the functional equivalent of the latter. Nbs1 is indispensable for the functional integrity of the intra-S DNA damage checkpoint by virtue of its ability to bind ATM and serve as a substrate for the ATM kinase activity (1). In addition, Nbs1 is important for the expression of the full activity repertoire of the RMN complex (1, 17). In light of our results with Xrs2, it will be of considerable interest to test for a DNA-binding function in Nbs1.

REFERENCES

1. D'Amours, D., and Jackson, S. P. (2002) *Nat. Rev. Mol. Cell. Biol.* **3**, 317–327
2. Haber, J. E. (1998) *Cell* **95**, 583–586
3. Sung, P., Trujillo, K. M., and Van Komen, S. (2000) *Mutat. Res.* **451**, 257–275
4. Tauchi, H., Kobayashi, J., Morishima, K., van Gent, D. C., Shiraishi, T., Verkaik, N. S., vanHeems, D., Ito, E., Nakamura, A., Sonoda, E., Takata, M., Takeda, S., Matsuura, S., and Komatsu, K. (2002) *Nature* **420**, 93–98
5. Carney, J. P., Maser, R. S., Olivares, H., Davis, E. M., Le Beau, M., Yates, J. R., 3rd, Hays, L., Morgan, W. F., and Petrini, J. H. (1998) *Cell* **93**, 477–486
6. Varon, R., Vissinga, C., Platzer, M., Cerosaletti, K. M., Chrzanowska, K. H., Saar, K., Beckmann, G., Seemanova, E., Cooper, P. R., Nowak, N. J., Stumm, M., Weemaes, C. M., Gatti, R. A., Wilson, R. K., Digweed, M., Rosenthal, A., Sperling, K., Concannon, P., and Reis, A. (1998) *Cell* **93**, 467–476
7. Stewart, G. S., Maser, R. S., Stankovic, T., Bressan, D. A., Kaplan, M. I., Jaspers, N. G., Raams, A., Byrd, P. J., Petrini, J. H., and Taylor, A. M. (1999) *Cell* **99**, 577–587
8. Luo, G., Yao, M. S., Bender, C. F., Mills, M., Bladl, A. R., Bradley, A., and Petrini, J. H. (1999) *Proc. Natl. Acad. Sci. U. S. A.* **96**, 7376–7381
9. Zhu, J., Petersen, S., Tessarollo, L., and Nussenzweig, A. (2001) *Curr. Biol.* **11**, 105–109
10. Bender, C. F., Sikes, M. L., Sullivan, R., Huye, L. E., Le Beau, M. M., Roth, D. B., Mirzoeva, O. K., Oltz, E. M., and Petrini, J. H. (2002) *Genes Dev.* **16**, 2237–2251
11. Kang, J., Bronson, R. T., and Xu, Y. (2002) *EMBO J.* **21**, 1447–1455
12. Williams, B. R., Mirzoeva, O. K., Morgan, W. F., Lin, J., Dunnick, W., and Petrini, J. H. (2002) *Curr. Biol.* **12**, 648–653
13. de Jager, M., van Noort, J., van Gent, D. C., Dekker, C., Kanaar, R., and Wyman, C. (2001) *Mol. Cell* **8**, 1129–1135
14. Hopfner, K. P., Craig, L., Moncalian, G., Zinkel, R. A., Usui, T., Owen, B. A., Karcher, A., Henderson, B., Bodmer, J. L., McMurray, C. T., Carney, J. P., Petrini, J. H., and Tainer, J. A. (2002) *Nature* **418**, 562–566
15. Raymond, W. E., and Kleckner, N. (1993) *Nucleic Acids Res.* **21**, 3851–3856
16. Paull, T. T., and Gellert, M. (1998) *Mol. Cell* **1**, 969–979
17. Paull, T. T., and Gellert, M. (1999) *Genes Dev.* **13**, 1276–1288
18. Trujillo, K. M., and Sung, P. (2001) *J. Biol. Chem.* **276**, 35458–35464
19. Hopfner, K. P., Karcher, A., Shin, D. S., Craig, L., Arthur, L. M., Carney, J. P., and Tainer, J. A. (2000) *Cell* **101**, 789–800
20. Anderson, D. E., Trujillo, K. M., Sung, P., and Erickson, H. P. (2001) *J. Biol. Chem.* **276**, 37027–37033
21. Chen, L., Trujillo, K., Ramos, W., Sung, P., and Tomkinson, A. E. (2001) *Mol. Cell* **8**, 1105–1115
22. Petukhova, G., Stratton, S., and Sung, P. (1998) *Nature* **393**, 91–94
23. Alani, E., Padmore, R., and Kleckner, N. (1990) *Cell* **61**, 419–436
24. Kraus, E., Leung, W. Y., and Haber, J. E. (2001) *Proc. Natl. Acad. Sci. U. S. A.* **98**, 8255–8262
25. Signon, L., Malkova, A., Naylor, M. L., Klein, H., and Haber, J. E. (2001) *Mol. Cell. Biol.* **21**, 2048–2056
26. Keeney, S. (2001) *Curr. Top. Dev. Biol.* **52**, 1–53
27. Nakada, D., Matsumoto, K., and Sugimoto, K. (2003) *Genes Dev.* **17**, 1957–1962

Mending the break: two repair machines in eukaryotes

Department of Molecular Medicine and Institute of Biotechnology
University of Texas Health Science Center at San Antonio
15355 Lambda Drive
San Antonio, Texas 78245-3207

Lumir Krejci, Ling Chen, Stephen Van Komen, *Patrick Sung, and *Alan Tomkinson

*Corresponding authors.
  Patrick Sung
  Email: sung@uthscsa.edu
  Alan Tomkinson
  Email: tomkinson@uthscsa.edu

Abstract

DNA double-strand breaks (DSBs) pose a special challenge for cells in the maintenance of genome stability. In eukaryotes, the removal of DSBs is mediated by two major pathways: homologous recombination (HR) and non-homologous end-joining (NHEJ). Capitalizing on existing genetic frameworks, biochemical reconstitution studies have began to yield insights into the mechanistic underpinnings of these DNA repair reactions.

Introduction

Our genome is vulnerable to injury inflicted by high energy radiations, chemical agents, and also reactive intermediates that arise during cellular metabolism. In addition, stalling of DNA replication forks at certain DNA structures (e.g. DNA palindrome) or at bulky DNA lesions (e.g. ultraviolet-light induced photoproducts) and slippage of DNA polymerases will give rise to discontinuities in the DNA template that pose a potential danger to genome integrity [1, 2]. Furthermore, a pre-existing nick in DNA, which arises when cells attempt to remove oxidative or other types of DNA base damage, can lead to the formation of a double-strand break upon encountering a DNA replication fork [3]. Under these unsavory circumstances, cells promptly activate DNA damage checkpoints to momentarily halt cell cycle progression and summon DNA repair or replication restart machinery to fix the damaged DNA or rescue the stalled DNA replication forks [4-7]. As seen in genetic studies in the yeast *Saccharomyces cerevisiae*, the failure to activate the checkpoint or repair mechanisms in these times of crisis results in high mutation rates and gross chromosome rearrangements characteristic of cancer cells [8]. In fact, several well-documented cancer-prone diseases, including xeroderma pigmentosum, ataxia telangiectasia, Nijmegen breakage syndrome, and certain forms of hereditary breast and colon cancers, have been linked to defects in DNA damage checkpoint or repair mechanisms [8-10]. Taken together, the available evidence makes a compelling case that the coordinated efforts of DNA damage checkpoint responses and DNA repair/replication fork restart pathways are critical for the suppression of chromosomal rearrangements and the prevention of cell death, cell transformation, and cancer formation.

In principal, nucleotide base damages and intra-strand DNA crosslinks can be excised from the DNA strand. The resulting gap is filled in by a DNA polymerase without much danger of alteration in the genetic information. However, the DSB presents a particular challenge for cells in terms of preservation of genomic integrity, because in this particular lesion, both of the DNA strands are damaged simultaneously. Indeed, mishandling of DSBs can lead to chromosome fragmentation, deletion, and translocation, causing irreversible alterations to a cell's genomic configuration and possibly death [8].

A series of reviews on the checkpoint mechanisms and the role of DNA checkpoints and DNA repair pathways in the maintenance of genomic stability have recently appeared [1, 8, 11, 12].This article focuses on the two major DSB repair pathways employed in eukaryotic cells – homologous recombination (HR) and non-homologous DNA end joining (NHEJ). We shall first briefly review the genetic and conceptual frameworks for HR and NHEJ and then discuss the mechanistic aspects of these two repair pathways.

I. Biological Relevance of the DSB

As mentioned above, DSBs are induced by ionizing radiation, arise as intermediates of repair reactions, and occur during the course of DNA replication. The DSBs in these circumstances are perceived as lesions and dealt with promptly using one of the two repair mechanisms available. Interestingly, as briefly outlined below, DSBs also appear in a programmed fashion as an obligatory intermediate during certain biological processes.

I.A. Immunoglobulin Gene Switching

The vertebrate immune system uses V(D)J recombination to generate the diversity of immunoglobulins and T-cell receptors. During this process, DSBs are formed at specific recombination signal sequences (RSSs) by the Rag1/Rag2 protein complex [13]. The cleavage results in blunt signal ends and hairpin coding ends. Whereas the signal ends can be joined directly, the coding ends need to be opened first. A pair of NHEJ factors, Artemis/DNA-PKcs, likely carry out this hairpin opening process, which we will discuss in more detail later. The subsequent processing at the opened coding ends further increases the variety of joined products. The completion of V(D)J recombination is achieved through functions of NHEJ factors [14]. Upon the interaction with antigen, the affinity and specificity of the different immunoglobulins generated by V(D)J recombination are increased through somatic hypermutation, a process termed "affinity maturation" [15]. Furthermore, another event, class switching, alters the constant region of the immunoglobulin [16]. Recent studies have shown the creation of DSBs in somatic hypermutation [17, 18]; whether these DSBs are definite intermediates in this process remains to be determined. In contrast, class switching recombination clearly involves the concerted generation of two DSBs at the switch regions [16]. The recently identified activation-induced cytidine deaminase (AID) has been suggested to function in initiating DSB formation in class switching recombination [19, 20].

I.B. Meiotic Breaks

In *S. cerevisiae*, DSBs appear during meiosis after DNA replication. These meiotic DSBs are found at hotspots that are present in each of the sixteen chromosomes [21]. Formation of these breaks is mediated by a protein complex containing the topoisomerase II-like protein, Spo11, which is thought to introduce the DSBs at meiotic hotspots via a transesterification mechanism. Formation of the meiotic DSBs leads to recombination between chromosomal homologues to provide stable linkage between them until time for their segregation in meiosis I. Accordingly, inactivation of the machinery that makes the meiotic DSBs not only abolishes recombination, but also results in chromosomal non-disjunction during meiosis I. The mechanism for the formation of meiotic DSBs and the function of meiotic recombination are both highly conserved through evolution [22-26]. The role of DSBs in meiotic chromosome metabolism is the subject of a number of recent reviews [21, 23, 27-29].

I.C. Mating Type Switching

The switching of mating type in the yeast *S. cerevisiae* is triggered by the introduction of a site-specific DSB at the *MAT* locus on chromosome 3. Once formed, the DSB break is utilized by the recombination machinery for conducting a gene conversion event that results in the switching of one mating type to the other (a or α) via one of the gene cassettes at *HML* and *HMR*, which store the a and α mating type information, respectively. The high specificity of the HO endonuclease that makes the site-specific DSB at *MAT* has been used with great success in model systems for delineating the temporal order of events during DSB repair [30].

II. Genetic Pathways for Homologous Recombination

II.A. Initiation of Homologous Recombination

Studies in *S. cerevisiae* have revealed that in recombination events induced by a DSB, the ends of the DNA break are processed by a nuclease activity to expose single-stranded (ss) tails of considerable length, typically a few hundred bases (Step 1 in Figure 1). The ssDNA tails serve as the substrate for the recruitment of the recombination machinery, which assembles on these tails and then conducts a search for a chromosomal homologue. Subsequently, a DNA joint that links the recombining DNA molecules is formed and genetic information is transferred from the donor (the intact DNA molecule) to the recipient (the DNA molecule that has sustained the DSB). During mitotic growth, the chromosomal donor is most frequently the sister chromatid, and hence as a DNA repair tool, homologous recombination is most useful during the S and G2 phases of the cell cycle. In fact, the cell cycle stage appears to be a major determinant as to whether a DSB is repaired by a homology-directed or an end-joining mechanism [31]. In contrast, meiotic cells almost exclusively use the homologous chromosome as the donor to repair the Spo11-associated DSBs. Genetic loci that help determine meiotic recombination partner choice (i.e. exclusive usage of the homologous chromosome as recombination partner) have been described, and mutations in these genes compromise meiotic chromosome transmission, resulting in aneuploidy and death [29].

Regardless of whether the sister chromatid or homologous chromosome is used as the recombination partner, the first DNA joint molecule that forms between one of the initiating ssDNA tails (product of the nucleolytic end-processing reaction: Step 1 in Figure 1) and the undamaged DNA homologue is a structure called D-loop (Step 2 in Figure 1). Subsequent to its formation, the size of the D-loop is expanded by continual uptake of the initiating ssDNA tails into the DNA homologue, with concomitant displacement of the like strand in the DNA homologue (Step 3 in Figure 1). In widely accepted enzymological terms, the process responsible for formation of the initial DNA joint (D-loop) is commonly referred to as "homologous DNA pairing", while the extension of the D-loop is called "DNA strand exchange" or "DNA branch migration". Accordingly, the overall biochemical reaction that leads to the formation and extension of DNA joints during recombination has been termed "homologous DNA pairing and strand exchange".

II.B. Processing of the D-loop: recombination models

Concomitant with homologous DNA pairing and strand exchange, DNA synthesis initiates from the extremity of the invading single strand that is now paired with the homologous strand in the donor molecule. As a result, extension of the D-loop occurs not only by way of DNA strand exchange, but also as a consequence of *de novo* DNA synthesis (Figure 1, Step 3). Most current recombination models picture the initial step of DNA-DNA interactions as being one-ended, i.e. only one of the ssDNA tails that arise through nucleolytic end-processing is utilized for promoting DNA joint formation. As the D-loop expands in size because of DNA synthesis, the other single stranded DNA tail may also become engaged in the recombination process, resulting in a DNA intermediate that contains two crossover structures, better known as Holliday junctions. This sequence of events is envisioned in the recombination model proposed by Szostak et al in 1983 [*32*]. The presence of the Holliday structure in the DNA joint molecule allows crossover recombination products (i.e. recombinants that harbor reciprocal exchange of genetic information), as opposed to simple gene conversion products wherein the information is nonreciprocally transferred. The available evidence is consistent with the premise that crossovers are critical for proper disjunction (i.e. segregation) of the homologous chromosome pairs during the first meiotic division (i.e. meiosis I). For additional information on the subject of meiotic recombination, the reader is referred to a number of highly informative articles by [*23, 27, 29, 33-35*].

II.B.1. SDSA

Interestingly, investigations in yeast and other organisms have provided compelling evidence that the D-loop intermediate is not always processed via the reaction sequence envisioned in the 1983 Szostak et al recombination model [*32*]. For instance, it is now well established that crossover recombination products are relatively rare in mitotic cells. In fact, even during meiosis, only a fraction the DNA joint molecules mature into the double crossover structure depicted in panel I of Figure 1. The available data point to a prevalent mitotic recombination pathway that involves the dissociation of the invading single-strand from the homologue and its hybridization to the other single-strand derived from the end-processing reaction. Gap filling DNA synthesis and ligation then complete the recombination process. This type of recombination has been termed DNA synthesis dependent single-strand annealing, or SDSA (Figure 1, panel II). Variants of the SDSA model have been discussed [*36*].

II.B.2. Break Induced Replication (BIR)

Here, a D-loop is again made but is extended primarily by DNA synthesis without much heteroduplex being formed. The length of the newly synthesized DNA can cover the entire length of the donor chromosome, resulting in really long gene conversion tracts (Figure 2). It is important to emphasize that the BIR mode of recombination is not merely an extension or variation of the SDSA pathway, as it can occur in the absence of some recombination proteins, most notably Rad51, that are indispensable for the latter pathway. In fact, BIR seems to rely on a trio of proteins, Rad50, Mre11, and Xrs2, which do not appear to have any significant involvement in the Rad51-dependent pathway of D-loop formation. Even though the majority of cellular recombination events are carried out by Rad51-mediated pathways, the Rad50/Mre11/Xrs2-dependent BIR reaction appears to make important contributions to certain biological processes. For instance, Kolodner has proposed that BIR, but not Rad51-mediated recombination, is chiefly responsible for the suppression of gross chromosomal rearrangements that could arise due to delinquent DNA replication forks [*8, 37*]. In addition, the available evidence has implicated BIR as an important mechanism (as is the Rad51-dependent recombination pathway) for the elongation of shortened telomeres in cells that are defective in telomerase function [*30, 38-40*]. The biology of BIR and variants of the BIR model depicted in Figure 2 are discussed in a recent review by Haber [*30*]. The players in BIR, some of which also function in the Rad51-mediated recombination pathways, will be mentioned below.

II.B.3. Recombination by Single-Strand Annealing

Recombination by single-strand annealing (SSA) is an efficient process that occurs between directly repeated DNA sequences. In this type of recombination, regions of homology in the 3' single-stranded tails originating from the end processing reaction hybridize to form a DNA joint, followed by the trimming of the non-homologous overhangs, fill-in DNA synthesis, and ligation (Figure 3). The end result is a recombinant that has one of the DNA repeats and the intervening non-homologous DNA sequence deleted. Genetic analyses have revealed that only a subset of the factors that function in general homologous recombination events are needed for single-strand annealing. We shall return to this subject when discussing the biochemical requirements of the SSA reaction below.

III. Recombination Genes: the *RAD52* Epistasis Group

Defects in homologous recombination ablate a major pathway of DSB repair and hence render cells sensitive to break inducing agents, e.g. ionizing radiation. This phenotypic manifestation has been exploited with great success in the isolation of the majority of genes that are essential for homologous recombination and homology-directed DNA repair. Complementation assays using specific recombination substrates, yeast two-hybrid analyses, and protein homology-based computer searches have helped identify additional recombination genes. The recombination/DSB repair genes isolated using the aforementioned approaches - *RAD50, RAD51, RAD52, RAD54, RAD55, RAD57, RAD59, RDH54/TID1, MRE11,* and *XRS2* - are collectively known as the *RAD52* epistasis group.

Based on the conservation of these factors during evolution, we anticipate that the mechanistic studies with yeast recombination factors will provide a conceptual framework for the same pathways in higher eukaryotes. Below is a summary of our current knowledge on the biochemical properties of the *RAD52* group proteins and the hierarchy of physical and functional interactions among them. The biochemical attributes of functionally homologous recombination factors from *E. coli*, yeast and mammals are summarized in Table 1.

III.A. DNA End-Processing

The trio of genes – *RAD50, MRE11*, and *XRS2* - are unique among the *RAD52* group because of their multifunctional nature. Rad50 protein is a member of the SMC protein family, possessing telltale coiled coils, a weak ATPase activity, and ATP-stimulated DNA binding activity [*12, 41, 42*]. Mre11 protein has 3' to 5' exonuclease and DNA structure specific endonuclease activities [*43-45*]. The least characterized component of this trio is Xrs2. Through interactions of Mre11 with Rad50 and Xrs2, these three proteins form a stable complex with a stoichiometry of Rad50:Mre11:Xrs2 of 2:2:1 [*46, 47*]. Optimal nuclease activity of Mre11 is contingent upon complex formation with Rad50 and Xrs2/Nbs1 [*44, 45*].

Null mutants of the *RAD50, MRE11*, and *XRS2* genes are not only defective in the nucleolytic processing of meiotic DSBs made by Spo11, but also in the formation of these breaks. The nuclease activity of Mre11 is critical for meiotic DSB processing. In mitotic cells, other nucleases appear to substitute for this activity, as nucleolytic processing of DNA ends still occurs, albeit at a reduced rates in the *mre11* null mutant. Since the 3' to 5' exonuclease activity of Mre11 cannot be solely responsible for the creation of 3' single-stranded tails from DNA ends, it has been postulated that its DNA structure specific endonuclease activity is germane for this processing reaction. In this regard, the Rad50/Mre11/Xrs2 complex may target a DNA helicase to the DNA ends to initiate DNA strand separation, followed by clippage of the 5' overhanging single-strand by the DNA structure specific endonuclease activity of Mre11 [*45*]. Another, perhaps more popular, premise is that the Rad50/Mre11/Xrs2 complex recruits a nuclease (or nucleases) to help process the ends of DSBs. This latter notion stems from the observations that in cells harboring certain nuclease null alleles of *MRE11*, nucleolytic end-processing remains unaffected. However, it will be quite important to examine the products of the various presumed nuclease null alleles of *MRE11* for nucleolytic activities in conjunction with Rad50 and Xrs2, to be sure that they are indeed completely defective in nuclease function. Until more data become available, the *in vivo* role of the Mre11 nuclease function in DNA end-processing in mitotic cells will undoubtedly remain controversial.

Remarkably, in addition to its role in DNA end-processing in mitotic and meiotic cells, this trio of genes have been shown to participate in the tolerance of specific DNA structures, DNA damage checkpoint signaling, telomere maintenance, BIR, and NHEJ [*12, 48, 49*]. Mutations in two components of the equivalent complex in human, namely, Mre11 and Nbs1 (Xrs2 equivalent), give rise to the ataxia telangiectasia -like disease and Njimegen breakage syndrome, respectively. These ailments are marked by abnormal DNA damage checkpoint responses, radiation sensitivity, chromosomal fragility, and an elevated cancer incidence in afflicted individuals [*12*]. Considerable structural insights into Rad50, Mre11, and the Rad50/Mre11 complex have been garnered through crystallographic studies and analyses involving electron microscopy and scanning force microscopy [*50-54*]. The role of the yeast Rad50/Mre11/Xrs2 complex in the DNA end-joining reaction mediated by the Dnl4/Lif1 and Hdf1/Hdf2 complexes will be discussed below. A number of recent articles have exhaustively reviewed the general biology and advances in understanding the structure and function of this trio of factors and their complexes [*12, 42, 49*].

III.B. Heteroduplex DNA Formation

III.B.1. Rad51, the RecA Homologue

Mutants of *RAD51* display the classical phenotype of a gene critical for recombination, including sensitivity to ionizing radiation and alkylating agents, and also defects in mitotic and meiotic recombination. Three groups reported the cloning and characterization of *RAD51* in 1992 [*55-57*]. Importantly, sequence alignment revealed that the *RAD51* gene product is structurally related to the *E.coli* RecA protein, which plays a central role in recombination via its ability to promote the homologous DNA pairing and strand exchange reaction. Rad51 was later shown to form helical filaments on dsDNA [*58*] and ssDNA [*59, 60*]. The demonstration of Rad51 nucleoprotein filaments reinforced the presumption that Rad51 is a true functional homologue of RecA, as the latter carries out its biochemical functions in the context of a nucleoprotein filament [*61*].

That Rad51 possesses a homologous DNA pairing and strand exchange activity was first reported in 1994 [*62*]. This study utilized Rad51 purified from yeast cells, the heterotrimeric single-strand DNA binding protein replication protein A (RPA, whose role will be discussed below), and an assay system first devised for use in RecA studies [*62*]. Subsequently, recombinase activity was found in the human Rad51 protein as well [*63-65*]. Together, the biochemical studies with yeast and human Rad51 have firmly established that this protein is a *bona fide* homologue of RecA.

III.B.2. Assay Systems for Homologous DNA Pairing and Strand Exchange

During homologous recombination, a single-stranded DNA tail is used by the recombination machinery to invade a homologous duplex to form a DNA joint (Step 2 in Figure 1). This principle has guided the development of *in vitro* recombination assays, which all entail the use of a single-stranded DNA molecule as initiating substrate and a homologous

duplex molecule as the pairing partner. The three most commonly used *in vitro* systems germane for our discussions are described in Figure 4. Extensive biochemical studies with *E. coli* RecA have been instrumental for defining three kinetically distinct phases in the homologous DNA pairing and strand exchange reaction; presynapsis, synapsis, and DNA branch migration [2, 66]. The homologous DNA pairing and strand exchange characteristics of Rad51 will be discussed in the context of these three reaction phases.

The Presynaptic Phase—Rad51 nucleates onto ssDNA to form a helical protein filament, often referred to as the Rad51-ssDNA nucleoprotein filament or presynaptic filament. The presynaptic filament holds the DNA in an extended conformation. Each helical repeat in the presynaptic filament contains ~18 bases of ssDNA and ~6 Rad51 molecules [58, 59]. Since Rad51 has an ATPase activity that is greatly stimulated by ssDNA [62], the filament assembly process can be conveniently followed by measuring ATP hydrolysis [67]. Alternatively, presynaptic filament assembly has been studied by direct visualization with the electron microscope and by DNA mobility shift in agarose gels [59, 60, 68, 69]. There are two distinct DNA binding sites in the presynaptic filament: the ssDNA is situated within the primary site, and the incoming duplex molecule is bound within the secondary site. The ability to hold three DNA strands in proximity underlies the ability of the presynaptic filament to mediate homologous DNA pairing and strand exchange.

Formation of the presynaptic filament needs ATP [58-60]. However, analogues of ATP - ATP-γ-S and AMP-PNP - that are non-hydrolyzable (or only slowly-hydrolyzable) can support a substantial level of homologous DNA pairing and strand exchange [70], indicating that assembly of a functional presynaptic filament can occur with little or no ATP hydrolysis. The role of ATP binding and hydrolysis in presynaptic filament assembly has been further investigated by making mutants of yeast Rad51 that either binds but does not hydrolyze ATP (rad51 K191R) or fails to bind ATP (rad51 K191A). The rad51 K191R mutant protein can perform homologous DNA pairing and strand exchange *in vitro* and complements the DNA repair defects of a *rad51* null mutant [70, 71]. However, an increased quantity of the rad51 K191R mutant protein is needed [57, 70, 72]. Similarly, when an ATP analogue (ATP-γ-S or AMP-PNP) is used, more wild type Rad51 is required to achieve a significant level of homologous pairing and strand exchange [70]. It thus remains possible that ATP hydrolysis influences the efficiency of assembly of the presynaptic filament or its maintenance without being an absolute requirement [70]. As expected, the rad51 K191A mutant protein is incapable of DNA binding and is therefore defective in DNA pairing and strand exchange. Genetically, the *rad51 K191A* allele behaves like the null mutant, thus firmly establishing the requirement for nucleotide binding in Rad51 functions. It should be noted that studies on variants of human Rad51 (hrad51 K133A and hrad51 K133R) harboring mutations in the Walker ATP binding motif A reached the same conclusion that ATP binding alone is sufficient for the recombinase activity of this factor [73].

Synapsis—This reaction phase entails the search for DNA homology in the donor duplex and the formation of nascent DNA joints between the initiating ssDNA and the duplex. In the case of RecA, and likely with Rad51 also, the search for DNA homology in the duplex molecule appears to proceed by way of reiterative collisions between the presynaptic filament and the duplex [66]. In other words, the duplex molecule is incorporated into the presynaptic filament through multiple contact points and lingers within the secondary DNA binding site of the presynaptic filament for a finite amount of time. The duplex molecule is released if homology is not found and another segment of the duplex is sampled. This kiss-then-release process continues until homology is located in the duplex to initiate the homologous pairing process. Conceptually, for the DNA homology search process to proceed efficiently, the duplex-presynaptic filament interactions should be transient. This is clearly illustrated in the case of the presynaptic filament formed with human Rad51, where weakening of its interactions with the duplex DNA by the inclusion of relatively high levels of salts greatly stimulates the efficiency of homologous DNA pairing and strand exchange [65].

Once homology is located within the duplex molecule, DNA joint formation with the ssDNA becomes possible. The presynaptic filament is capable of making DNA joints that are either paranemic or plectonemic in nature. The paranemic joints occur within the internal regions of the recombining DNA molecules, whereas the plectonemic joints are formed at a free end located either in the ssDNA or the duplex substrate (see later). There is considerable evidence to indicate that the paranemic joints are held together by canonical Watson-Crick hydrogen bonds, but, since the two strands involved in joint formation are not topologically wound around each other, these joints are transient and will rapidly dissociate upon deproteinization. Nonetheless, the paranemic joints are thought to play an important role in bringing the recombining ssDNA and duplex substrate in homologous registry to enhance the likelihood for the formation of a plectonemic joint. Studies in the Radding group have revealed that recognition of homology, helix destabilization, and initiation of DNA joint formation are integral parts of a concerted mechanism in which A:T base pairs play a critical role [74].

With RecA, there is no evidence that the duplex slides along the presynaptic filament during the homology search process, and it seems reasonable to assume the same for Rad51. However, as discussed below, Rad54, which tracks on DNA and physically interacts with Rad51, has been suggested to actively pump the duplex DNA through the fold of the Rad51 presynaptic filament to facilitate the search for DNA homology (see later).

DNA Branch Migration (Strand Exchange) —After formation, the nascent plectonemic joint is lengthened in a unidirectional fashion. The extent of this is determined by the length of the Rad51-ssDNA nucleoprotein filament.

III.B.3. Factors that Facilitate the Rad51-Mediated Homologous DNA Pairing and Strand Exchange Reaction.

RPA—RPA, through its ability to bind and facilitate the removal of secondary structure in ssDNA, plays a central role in just about all the DNA metabolic pathways. RPA is indispensable for homologous DNA pairing and strand exchange efficiency when plasmid length DNA substrates are used [62, 67]. It was originally thought that the only significant role of RPA in homologous pairing and strand exchange was in the promotion of Rad51 presynaptic filament assembly by helping eliminate DNA secondary structure [67, 75]. However, recent studies have implicated RPA in at least two other capacities in the formation and stabilization of DNA joints in recombination reactions.

Eggler et al [76] have recently reported that when the Rad51-ssDNA nucleoprotein filament is assembled under low magnesium buffer conditions to minimize secondary structure in ssDNA, RPA is still needed for maximal DNA strand exchange efficiency with plasmid length DNA substrates (System A in Figure 4). Additional studies involving the use of exonuclease digestion of the DNA joint molecules and electron microscopy have yielded compelling evidence that RPA assures DNA strand exchange efficiency by sequestering the non-complementary DNA strand displaced from the duplex substrate as the result of DNA strand exchange. Eggler et al [76] suggested that the RPA-mediated sequestration of the displaced ssDNA ensures that the DNA strand exchange process is not reversed upon deproteinization of the reaction mixture for gel analysis.

A third role for RPA was recently revealed in the studies of Van Komen et al [77]. It has been known for quite some time that in the presence of Rad54, robust homologous DNA pairing can occur with amounts of Rad51 well below what is needed to saturate the ssDNA (i.e. 3 nucleotides of ssDNA/Rad51 monomer) [69, 78]. Interestingly, under these conditions, RPA is still indispensable for pairing efficiency [77]. It was demonstrated in this work that protein-free ssDNA inhibits the ability of Rad51 to promote homologous DNA pairing, likely by occupying the secondary DNA binding site in the presynaptic filament, and competes with duplex DNA for binding to Rad54. By sequestering free ssDNA, RPA alleviates its inhibitory effects on Rad51 and Rad54.

Thus, RPA promotes Rad51-mediated homologous DNA pairing and strand exchange by facilitating the assembly of the presynaptic filament on long ssDNA molecules [59, 67], sequestering protein-free ssDNA [77], and preventing the reversal of DNA strand exchange [76]. Paradoxically, since RPA has high avidity for ssDNA, an excess of RPA added with (or before) Rad51 to the ssDNA substrate results in exclusion of Rad51 and marked suppression of presynaptic filament assembly [65, 67, 79]. Specific recombination mediator proteins that promote the nucleation of Rad51 onto ssDNA and even onto an RPA-coated ssDNA template have been identified. The presence of these mediator proteins in the homologous DNA pairing and strand exchange reaction can effectively overcome the competitive effect imposed by RPA (Figure 5; see below).

Rad52—Rad52 is a multimeric ring-shaped molecule [80, 81], that binds ssDNA avidly [82] and physically interacts with Rad51 [57, 83]. In reactions wherein homologous pairing and strand exchange would be otherwise compromised by co-incubation of the ssDNA substrate with RPA and Rad51, an amount of Rad52 about one tenth of that of Rad51 fully restores the reaction efficiency [84, 85]. Importantly, Rad52 allows Rad51 to utilize an RPA-coated ssDNA template for recombination reactions [75, 85, 86]. This effect likely involves a specific interaction between Rad52 and RPA [87]. In addition to overcoming the suppressive effect of RPA, Rad52 exerts modest stimulation on the Rad51 recombinase activity in the absence of RPA [75, 86, 88]. However, even with Rad52, RPA is still needed for maximal homologous pairing and strand exchange [75, 86]. The physical interaction between Rad51 and Rad52 is indispensable for the recombination mediator function of the latter [89].

It should be emphasized that deletion of *RAD52* engenders defects in recombination more severe than those observed in a *rad51* null mutant. In addition, mutants of Rad52 lacking the Rad51 interaction domain [89-91] are less impaired for DSB repair and meiosis than the *rad52* null mutant [92]. These observations provide evidence that Rad52 possesses Rad51-independent functions in recombination reactions. Consistent with this premise, detailed genetic analyses have revealed a key role for Rad52 in SSA and BIR (see below).

Rad55/Rad57—*RAD55* and *RAD57* genes show a tight epistatic relationship and their encoded products interact in the yeast two hybrid system [93-95]. Consistent with these observations, Rad55 and Rad57 have been shown to form a stable heterodimer by co-immunoprecipitation and co-purification through a number of chromatographic column steps. Like Rad52, Rad55-Rad57 also has a recombination mediator function, capable of overcoming the competition posed by RPA for binding sites on the initiating ssDNA substrate (Figure 7). Through a Rad51-Rad55 association [93-95], the Rad55-Rad57 heterodimer interacts with Rad51 in the absence of ssDNA (our unpublished results). Rad55-Rad57 has a ssDNA binding function and a weak ATPase activity (our unpublished results). It seems likely that Rad55-Rad57 delivers Rad51 to the ssDNA template to facilitate the assembly of the presynaptic filament. Whether the Rad55-Rad57 heterodimer can also interact with RPA and specifically recognize an RPA-coated ssDNA template in performing its mediator function have not yet been tested.

Rad54—Despite its structural and functional similarities to RecA, Rad51 is poorly adept at making a D-loop by itself [78, 96, 97]. The addition of Rad54 protein significantly stimulates D-loop formation by Rad51 [78]. Rad54 binds Rad51 in both the yeast two-hybrid system and *in vitro* [78, 98, 99]. This interaction is likely important for DNA joint formation, as Rad54 has no effect on RecA-mediated recombination reactions *in vitro*.

Rad54 belongs to the Swi2/Snf2 protein family and, like other members of this protein family, has a DNA dependent-ATPase function. This ATPase activity prefers dsDNA as co-factor. Further insights into the role of ATP has been derived from studying Walker mutants that are either defective in nucleotide binding (rad54 K341A) or binds ATP but is inactivated for ATP hydrolysis (rad54 K341R). These *rad54* mutant alleles are defective in haploid specific mitotic

intrachromosomal gene conversion and DNA repair in both haploid and diploid cells [78, 98, 99]. Interestingly, the two rad54 Walker mutants are still capable of carrying out interchromosomal gene conversion in diploid cells [100], suggesting that Rad54 has another recombination function that is independent of its ATPase activity.

Rad54 protein has been shown to utilize the free energy from ATP hydrolysis to track along duplex DNA. This tracking motion generates a positively supercoiled domain ahead of protein movement and a compensatory, negatively supercoiled domain behind [69, 101]. The negative supercoils that accumulate lead to transient DNA strand opening. Interestingly, the ATPase, DNA supercoiling, and DNA strand opening activities of Rad54 are greatly stimulated via an interaction with Rad51 [69, 96, 97].

We envision that Rad54 exerts two major effects on the efficiency of the homologous DNA pairing reaction. First, an ability of Rad54 associated with the Rad51-ssDNA nucleoprotein complex to pull the duplex through its fold (i.e. tracking) is expected to enhance the rate at which the duplex molecule is sampled for homology. Second, the transient DNA strand opening within the negatively supercoiled domain generated by Rad54 very likely facilitates the formation of a nascent DNA joint upon DNA homology location in the duplex. This latter suggestion is supported by the demonstration that Rad54 enables Rad51 to utilize even a topologically relaxed DNA substrate for efficient DNA joint formation [69]. These ideas are summed up in Figure 5.

Notably, the DNA tracking/supercoiling function first demonstrated in Rad54 appears to be a conserved property of the Swi2/Snf2 family of proteins [102, 103]. It has been suggested that the ability to track on and supercoil DNA underlies the chromatin remodelling function of the various Swi2/Snf2-like proteins and complexes that contain them [102, 103].

Rdh54/Tid1 — A *RAD54*-related gene, *RDH54* (RAD Homologue 54), was identified through computer searches of yeast databases [104, 105]. The *RDH54* gene was also independently isolated via a yeast two-hybrid screen for genes whose products interact with the meiotic specific recombinase Dmc1 [106], and was named *TID1* (Two-hybrid Interaction with Dmc1 I). In the same study [106], the *RDH54/TID1*-encoded protein was also found to bind Rad51 in the two-hybrid assay. Consistent with this observation, purified Rdh54/Tid1 physically interacts with Rad51 [69]. Like Rad54, Rdh54 has a robust dsDNA-activated ATPase function and an ability to track on and supercoil DNA [69]. Importantly, Rdh54/Tid1 greatly stimulates Rad51-mediated D-loop formation [69].

III.C. Break-Induced DNA Replication

Genetic analyses have revealed that BIR is dependent on *RAD52, RAD59, RDH54*, and the trio of *RAD50, MRE11*, and *XRS2*. Kolodner et al have suggested that BIR is chiefly responsible for the suppression of gross chromosomal rearrangements originating from delinquent DNA replication forks [8]. Furthermore, the same set of BIR factors appear to participate in telomere elongation to yield type II survivors in cells that lack telomerase [107].

Rad59 is related in sequence to the amino-terminal portion of Rad52 and physically interacts with the latter [108, 109]. It is therefore likely that Rad52 and Rad59 work in the BIR reaction as a complex. Exactly how Rad52-Rad59 and the products of the other aforementioned genes establish a D-loop structure to initiate the DNA synthesis reaction in BIR is mysterious at the moment. However, it seems reasonable to consider the possibility that the combination of Rad52-Rad59, Rad50-Mre11-Xrs2, and Rdh54 can utilize a ssDNA template to invade a duplex template, much like what has been shown for classical recombination events mediated by Rad51, Rad52, Rad55-Rad57, and Rad54.

III.D. Single-Strand Annealing

SSA requires Rad52 and Rad59 and its efficiency is modulated by RPA in both *in vitro* and *in vivo* settings [82, 86, 110, 111]. The involvement of Rad52 and Rad59 in SSA is easily explained by the ability of these factors to promote the annealing of complementary DNA strands [82, 110]. Rad52 is capable of annealing DNA strands coated with RPA [86, 87], and it has been suggested that a specific interaction between Rad52 and RPA is necessary for the annealing reaction [87]. By contrast, the single strand annealing activity of Rad59 is inhibited by RPA [110]. Rad52 and Rad59 appear to functionally co-operate in the strand annealing reaction [109]. Rothstein and colleagues have described a RPA mutant, *rfa1-D228Y*, that allows SSA to occur in a *rad52* mutant. SSA is seen more frequently in the *rfa1-D228Y* mutant strain, suggesting that RPA normally suppresses SSA in wild type cells [111].

III.E. Recombination Machinery in Higher Organisms

In single cell eukaryotes, deleting genes of the *RAD52* epistasis group does not in general affect mitotic viability unless cells are challenged with a DNA damaging agent. In contrast, null mutations in the *RAD52* group genes often engender a defect in cell proliferation in vertebrate cells and embryonic lethality in mice. The cell proliferation defect and embryonic inviability likely reflect the fact that recombination is indispensable for the repair of spontaneous lesions that arise during DNA replication. Biochemical studies with human recombination proteins have revealed a hierarchy of physical and functional interactions among these proteins that largely follow the paradigms established with the equivalent yeast factors [65, 97, 112-114]. Importantly, the breast tumor suppressors BRCA1 and BRCA2 both affect the efficiency of recombination and recombinational DNA repair, and BRCA2 binds Rad51 [10, 115-118]. A recent study reports the finding that BRCA2 cooperates with Rad51/RPA in DNA joint formation [119]. These observations provide compelling evidence that recombination plays a major role in the maintenance of genome stability and cancer avoidance in mammals; several recent reviews on this topic are available [10, 114, 120, 121].

IV. General Introduction to NHEJ

In contrast to homologous recombination, the repair of DSBs by non-homologous end joining is conceptually much simpler. The ends of broken DNA molecules are brought together and joined in the absence of significant DNA sequence homology. An unusual feature of this repair pathway is that many of the early groundbreaking studies were carried out in the mammalian system and it is only recently that it has been examined in lower eukaryotes such as *S. cerevisiae*. One of the major reasons for this was the isolation and characterization of X-ray sensitive mutant mammalian cell lines that are defective in NHEJ (Table 2). This led to the cloning of the genes comprising NHEJ factors such as the DNA dependent protein kinase (DNA-PK), which is composed of the Ku70/Ku80 DNA binding subunit and the DNA-PKcs catalytic subunit, and XRCC4 [*122*].

The availability of the complete sequence of the *S. cerevisiae* genome [*123*] has facilitated the search for homologues of mammalian NHEJ genes and stimulated the study of NHEJ mechanisms in this model eukaryote. In contrast to mammals, inactivation of *S. cerevisiae* NHEJ genes does not usually confer a significant increase to killing by agents that cause DSBs because, in this organism, these lesions are predominantly repaired by homologous recombination. Nonetheless, these studies have shown that the fundamental mechanisms of this repair pathway are conserved among eukaryotes. The biochemical features of proteins involved in NHEJ are summarized in Table 3. In the next section, we will describe the generally accepted model for NHEJ and the role of this repair pathway in maintaining genome integrity and stability.

V. Mechanisms and Function of NHEJ in Eukaryotes.

As mentioned previously, NHEJ can simply be described as the bringing together and joining of broken DNA molecules ends. Since these events are not mediated by long tracts of DNA sequence homology, it has been proposed that the ends are held together primarily by protein-protein interactions. These so-called end-bridging factors have been central to most models of NHEJ and the focus of many investigations. However, the end-bridging model raises the question that, if a cell suffers more than one DNA double strand break, can it distinguish between ends that were once linked and ends from different DNA molecules? Studies in mammalian cells have shown that, although the joining of ends from different DNA molecules to generate chromosomal translocations does occur, these events are rare and that the cell usually rejoins the previously linked ends. One plausible explanation for these observations is that the arrangement of chromatin in loops attached to the nuclear matrix restricts the mobility of broken DNA ends and favors their rejoining to reconstitute the loop. A prediction of this idea is that chromosomal translocations will begin to occur when the cell suffers more than one DSB per chromatin loop.

The majority of DSBs caused by ionizing radiation cannot be joined directly by a DNA ligase because they have inappropriate termini. Thus, after end-bridging, the ends need to be processed to generate a ligatable structure. Analysis of *in vivo* DNA joining has revealed that many of the events occur at sites of short DNA sequence homology, ranging from 2 to 4 nucleotides in length [*124-126*]. This suggests that DNA ends are brought together in a sequence-independent manner and then the DNA sequences adjacent to the ends are sampled in some manner to identify short complementary sequences, so-called microhomologies. Presumably these sequences are used to align the DNA molecules and then ligatable structures are generated from the aligned DNA molecules by further processing. In the following sections of this review we will summarize recent advances in our understanding of the mechanisms of NHEJ in *S. cerevisiae* and mammalian cells.

V.A. S. cerevisiae NHEJ Genes

DSBs in yeast are predominantly repaired by homologous recombination. Consequently, mutation of any one of the yeast NHEJ genes generally has little effect on the sensitivity to DNA damage of proliferating cells unless the homologous recombination pathway is also inactivated. To directly examine the defect in NHEJ, several *in vivo* end-joining assays have been developed, including the most frequently used method of measuring recircularization of plasmid DNA molecules previously linearized with a restriction endonuclease.

As mentioned above, key players in NHEJ identified by biochemical and genetic studies with mammalian cells include DNA-PK, XRCC4, and by extension, DNA ligase IV because of its stable interaction with XRCC4 [*127*]. Although Hdf1 and Hdf2 have been identified as the yeast homologs of Ku70 and Ku80 [*128, 129*], respectively, yeast appears to lack a functional homologue of DNA-PKcs. Besides NHEJ, Hdf1 and Hdf2 likely participate in other cellular functions since *hdf1* and *hdf2* strains exhibit phenotypes that appear to be independent of the defect in NHEJ, such as temperature sensitive growth and pronounced telomere shortening [*128-132*]. The counterpart of the mammalian *LIG4* gene, *DNL4*, was identified in the yeast genome by sequence homology search [*133-136*]. Like DNA ligase IV, Dnl4 also forms a stable complex with a partner protein Lif1, which is likely to be the functional homologue of XRCC4 [*137*]. Consistent with their role in NHEJ, inactivation of *HDF1*, *HDF2*, *DNL4* or *LIF1* results in a similar reduction of plasmid rejoining [*130, 134-139*].

As mentioned before, the products of the *RAD50*, *MRE11* and *XRS2* genes are indispensable for NHEJ. In this regard, *rad50*, *mre11* and *xrs2* strains exhibit the same reduction in transformation efficiency of linearized plasmid DNA as the other NHEJ mutants [*125, 131, 139-141*]. These genetic studies indicate that the Hdf1/Hdf2, Rad50/Mre11/Xrs2 and Dnl4/Lif1 complexes are key components of the major NHEJ pathway. Although inactivation of any one of these NHEJ factors causes a similar reduction in transformation efficiency, there are significant differences in the type of residual end

joining. Specifically, the residual end joining activity in *dnl4*, *rad50*, *mre11*, or *xrs2* cells generates a significant number of accurately repaired products, whereas the residual repair products in *hdf* cells are mostly imprecise and suffer large deletions [*125, 130, 131, 135, 137-139*]. Epistasis studies have shown that the end joining phenotype conferred by inactivation of the Hdf1/Hdf2 complex predominates over the mutant phenotypes caused by mutating other genes, suggesting that Hdf1/Hdf2 acts earlier than the other NHEJ factors [*131, 135*]. In support of this hypothesis, the recruitment of the Dnl4/Lif1 complex to *in vivo* DSBs is dependent upon Hdf1/Hdf2 [*142*].

Although the Hdf1/Hdf2, Rad50/Mre11/Xrs2 and Dnl4/Lif1 complexes are critical for the efficient recircularization of linear plasmid DNA molecules with cohesive ends *in vivo*, the majority of DSBs induced by DNA damaging agents require additional factors to process the DNA ends. Genetic studies have implicated the nuclease encoded by the *FEN1* (*RAD27*) gene, the DNA helicase encoded by the *SRS2* gene and the DNA polymerase encoded by the *POL4* gene in NHEJ events [*143-145*].

Four laboratories have recently identified a novel NHEJ gene, *NEJ1* (*LIF2*), whose inactivation reduces transformation efficiency of linearized plasmid DNA to the same extent as the other key NHEJ genes [*146-149*]. The residual end joining products in *nej1* cells suffer large deletions similar to those seen in *hdf* cells [*148*]. The *NEJ1* gene is expressed in haploids but not diploids, providing a possible mechanism for the previously suggested regulation of NHEJ by mating type [*150, 151*]. In support of this notion, the deletion of *NEJ1* inhibited NHEJ in haploid cells, whereas its constitutive expression alleviated the repression of NHEJ in diploid cells [*147, 148*]. The identification of *NEJ1* also provides a molecular explanation for the indirect role of the *SIR* genes in NHEJ. Mutation in the *SIR* genes results in a/α mating-type heterozygosity that inhibits *NEJ1* expression and causes defective NHEJ [*147, 148, 150, 151*]. Since all naturally a/α expressing cells are diploid, it appears that NHEJ is inhibited when a homologous chromosome is present, presumably reflecting the preference for the accurate repair pathway, homologous recombination. However, haploid cells in the G1 phase of the cell cycle cannot repair DSBs by homologous recombination, providing an explanation for the activation of NHEJ in these cells.

V.B. Molecular Mechanisms of NHEJ in S. cerevisiae.
Numerous genetic studies have provided a conceptual framework for NHEJ, but the molecular mechanisms of this pathway have not been investigated to the same extent. As mentioned previously, the Mre11 subunit of the Rad50/Mre11/Xrs2 complex is a nuclease. However, mutations that inactivate nuclease activity have no effect on the efficiency of the recircularization of linear plasmid DNA molecules with cohesive ends, suggesting that Rad50/Mre11/Xrs2 has another role in NHEJ [*152*]. In a recent study, it was shown that the Rad50/Mre11/Xrs2 complex not only stimulates the catalytic activity of Dnl4/Lif1 but also alters the mechanism of ligation from intra- to intermolecular [*47*]. Consistent with this latter observation, atomic force microscopy studies have revealed that Rad50/Mre11/Xrs2 has robust end-bridging activity, forming oligomers from linear DNA molecules [*47*]. In many of the oligomers, Rad50/Mre11/Xrs2 complexes were bound at internal sites corresponding to the junctions between DNA molecules. Since these complexes were the same size as end-bound and free protein complexes, it appears that a single Rad50/Mre11/Xrs2 complex, which is composed of two Rad50 molecules, two Mre11 molecules and one Xrs2 molecule, can bind two DNA ends simultaneously. In addition to end-bridging, the Rad50/Mre11/Xrs2 complex also specifically recruits the Dnl4/Lif1 complex via an interaction between the Xrs2 and Lif1 subunits [*47*].

Similar to mammalian Ku70/Ku80, the Hdf1/Hdf2 complex binds avidly to DNA ends and can translocate inward along the DNA duplex from the end [*47, 128, 129*]. It has been shown that Ku70/Ku80 can also bridge DNA ends [*153*], but this activity appears to be much weaker than that of the Rad50/Mre11/Xrs2 complex. In accord with genetic studies, Hdf1/Hdf2 is required for efficient intermolecular ligation by Rad50/Mre11/Xrs2 and Dnl4/Lif1 at physiological salt concentrations [*47*]. The inability of mammalian Ku70/Ku80 to substitute for the yeast complex suggests that there are specific functional interactions between the Hdf1/Hdf2, Rad50/Mre11/Xrs2 and Dnl4/Lif1 complexes. In the model shown in Figure 7, we propose that, after DSB formation, Hdf1/Hdf2 binds to the ends, protecting them from degradation. The presence of Hdf1/Hdf2 at or near the DNA end enhances the recruitment of Rad50/Mre11/Xrs2, possibly in a manner similar to the recruitment of DNA-PKcs by Ku70/Ku80, and promotes end-bridging by this complex. Dnl4/Lif1 is recruited to the nucleoprotein complex containing the two DNA ends via the Xrs2 subunit of the Rad50/Mre11/Xrs2 complex. On occasions when the ends can be aligned and ligated, the reaction will be completed by the co-ordinated actions of these three complexes without additional factors. The newly identified *NEJ1* gene product is also required for the efficient recircularization of DNA molecules with cohesive ends [*146-149*]. Although Nej1 has been shown to interact with Lif1 and is necessary for the nuclear localization of Dnl4/Lif1 [*146-149*], it is not known whether Nej1 participates directly in the end joining reaction.

In most cases, the ends of DSBs will be either resected or unwound in order to expose microhomologies, with the Hdf1/Hdf2 complex functioning to limit the extent of resection. The nuclease(s) and helicase(s) involved in this step have not been definitively identified. Based on biochemical studies with hMre11, the Mre11 subunit of the Rad50/Mre11/Xrs2 complex is an attractive candidate for the nuclease whereas genetic studies have suggested a possible role for the Srs2 DNA helicase [*145*]. Once the ends of the DNA molecules have been aligned via short tracts of complementary DNA sequence, nuclease and DNA polymerase activities remove single-strand flaps and fill in the resulting gaps, respectively, to generate a ligatable structure. Genetic studies have implicated the Fen-1 (Rad27) nuclease and the Pol4 DNA polymerase in these final

end-processing reactions [143, 144]. In support of the suggested role of Pol4 in NHEJ, a recent biochemical study has shown that Pol4 efficiently catalyzes DNA synthesis on small gaps generated by the alignment of linear duplex DNA molecules with complementary ends. Furthermore, Pol4 specifically interacts with Dnl4/Lif1, resulting in the stimulation of DNA synthesis by Pol4 as well as DNA joining by Dnl4/Lif1 [154]. Since Hdf1/Hdf2, Rad50/Mre11/Xrs2 and Dnl4/Lif1 are all required for the efficient recircularization of DNA molecules with cohesive ends *in vivo*, we propose that the resection, the alignment of DNA molecules via microhomologies, and the end-processing reactions that generate a ligatable structure occur within the context of the nucleoprotein complex formed by these three core NHEJ factors.

V.C. Mammalian NHEJ Genes

NHEJ makes a much larger contribution to cell survival in response to DSBs in mammalian cells compared with yeast cells. Although mammalian somatic cells are diploid, the size and complexity of the genome, in particular the large amounts of repetitive DNA, make the identification of homologous sequences for recombinational repair a much more difficult proposition than in yeast. Interestingly, it was observed that the X-ray sensitivity of the Chinese Hamster Ovary cell line XR-1 varied as a function of cell-cycle stage [155]. The later identification of XRCC4 as the missing component in XR-1 [156] as well as a crucial NHEJ factor revealed cell-cycle regulation of NHEJ. Subsequent studies by many investigators have confirmed and extended this study and have led to the generally accepted notion that NHEJ is the major DSB repair pathway in the G1 phase of the cell cycle and in quiescent cells, whereas recombinational repair is more effective in late S and G2 phases of the cell cycle when sister chromatids are present [157].

The X-ray sensitive rodent cells have been a valuable resource for the identification of human genes (**X-R**ay **C**ross **C**omplementing, XRCC) that participate in DSB repair. Unlike yeast cells, defects in NHEJ result in X-ray sensitivity, so human genes involved in each of these pathway have been cloned by functional complementation. The mutant rodent cell lines have been used for the cloning of the *XRCC4* gene, which encodes the partner protein of DNA ligase IV, and the functional dissection of the Ku70/Ku80 and DNA-PKcs subunits of DNA-PK [122]. *ARTEMIS* is a very recent addition to the human NHEJ gene group [158]. This gene, which is mutated in an inherited form of immunodeficiency, was cloned by linkage analysis. Although the predicted amino acid sequence of this gene exhibited homology with β-lactamases, the X-ray sensitivity of artemis cell lines and the identification of additional mammalian and yeast DNA repair genes encoding β-lactamase like proteins [159, 160] indicate that *ARTEMIS* is a NHEJ gene.

Although genetic and biochemical studies in yeast have firmly established the role of the Rad50/Mre11/Xrs2 complex in NHEJ, the participation of its human equivalent, hRad50/hMre11/NBS1, in NHEJ is less clear. As mentioned above, mutations in the *hMRE11* and *NBS1* genes have been identified as the causative factors in the cancer-prone human syndromes, ataxia telangiectasia-like disorder (ATLD) and Nijmegen breakage syndrome (NBS), respectively [161-163]. However, ATLD and NBS1 cell lines do not exhibit an obvious defect in either NHEJ or V(D)J recombination [161, 164]. Unfortunately, the genes encoding subunits of the hRad50/hMre11/NBS1 complex are required for cell viability, hindering more detailed analysis of the involvement of this complex in NHEJ [165-167]. Intriguingly, individuals with *LIG4* mutations have been identified and exhibit the developmental abnormalities and mental retardation characteristic of NBS [168]. One possible explanation of these observations is that the hRad50/hMre11/NBS1 complex functions in a NHEJ subpathway that plays a critical role during embryogenesis and/or development.

Other than DSB repair, NHEJ factors also appear to participate in other cellular functions such as V(D)J recombination and retroviral integration [14, 169, 170]. Cell lines from the immunodeficient mouse strain, scid (severe combined immunodeficiency), are X-ray sensitive [171-173] and defective in DNA-PK activity [174-176], revealing the link between NHEJ and immunoglobulin gene rearrangements. Specifically, NHEJ factors are required to complete V(D)J recombination, which is initiated by the site-specific Rag1/Rag2 endonuclease [14]. Thus it was surprising that the first human individual identified with *LIG4* mutations was not immunodeficient [177, 178]. This is presumably because the residual levels of DNA ligase IV activity in this patient are sufficient for V(D)J recombination but not for NHEJ. Indeed, a recent examination of patients with uncharacterized immunodeficiency led to the identification of *LIG4* mutations that do associate with this syndrome [168].

The mouse DNA-PKcs, Ku70, Ku80, *LIG4* and *XRCC4* genes have all been inactivated by conventional gene targeting to generate mouse models of NHEJ deficiency. As expected, all of the mutant cell lines are X-ray sensitive and defective in V(D)J recombination. However, there are significant differences in the severity of the phenotype both at the cellular and organismal level. Apart from immunodeficiency, the DNA-PKcs null animal has no overt defects [179-181]. Surprisingly, there are differences in the phenotype of *Ku70* and *Ku80* null animals that include cancer predisposition and premature aging, raising the possibility that these proteins may have independent functions [182-184]. In contrast, the *XRCC4* and *LIG4* null animals have essentially identical phenotypes, exhibiting embryonic lethality at around day 16.5 [185-187]. The mutant embryos appear to die because of abnormally high levels of apoptosis in the developing central nervous system [185, 187]. Embryonic lethality can be rescued by a second mutation inactivating either Atm function or p53 function [188-191]. This suggests that unrepaired DSBs resulting from the NHEJ defect trigger apoptosis. Neuronal cells in the developing CNS appear to be particularly sensitive to apoptotic triggers, an effect that is suppressed by mutations inactivating signal transduction pathways linking DSBs to apoptosis.

The milder phenotype of cells deficient in DNA-PK compared with cells deficient in DNA ligase IV activity possibly reflects the sequestration of DNA ends into the DNA ligase IV-dependent pathway by DNA-PK assembly whereas,

in the absence of functional DNA-PK, the ends can be repaired by other DNA repair pathways. This model is supported by studies in DT40 chicken cells showing that inactivation of the Ku70/Ku80 heterodimer in *lig4* mutant cells reduces the severity of the phenotype to the same level as *ku* mutant cells [*192*]. This observation is reminiscent of the dominant nature of the end joining defect caused by *hdf* mutations compared with inactivation of other NHEJ factors in yeast.

V.D. Molecular Mechanisms of NHEJ in Mammals.

Insights into mechanisms of several different DNA transactions have been based on the development of assays with cell free extracts. For many years analysis of NHEJ by this approach was complicated by the presence of robust end joining activity in mutant cell extracts that appeared to be independent of NHEJ factors. This was a particular problem in extracts from rodent cells because they contain significantly lower levels of DNA-PK than human cells [*193*]. Baumann and West have developed an assay to detect end joining in an extract from human lymphoblastoid cells that was, in accord with genetic studies, dependent upon Ku, DNA-PKcs and DNA ligase IV/XRCC4 [*194*]. In subsequent fractionation studies, inositol 6 phosphate was unexpectedly identified as an important co-factor for efficient end joining [*195-197*]. Inositol 6 phosphate binds to Ku and could regulate DNA-PK activity [*198, 199*].

The recent determination of the structure of the Ku70/Ku80 heterodimer complexed with DNA by X-ray crystallography has provided a molecular explanation for the DNA binding properties of this complex [*200*]. Specifically, the Ku70/Ku80 complex forms an asymmetric ring around the DNA helix, suggesting a mechanism for both its ability to translocate along the DNA molecule from an end and to align and bridge DNA ends. However, the topological linking of Ku70/Ku80 to DNA creates the problem of how to remove it after repair is completed. In contrast to the contacts between the subunits of the PCNA homotrimer, the extensive and intertwined nature of the interactions between the Ku70 and Ku80 subunits argue against the dissociation of the Ku70/Ku80 heterodimer from DNA by separation of the subunits. In fact the thin section of the asymmetric ring encircling the DNA suggests that the Ku70/Ku80 heterodimer may be released by proteolysis.

Two laboratories have reported interactions between Ku70/Ku80 and DNA ligase IV/XRCC4, but the effects of Ku on DNA joining were different [*201, 202*]. In one study, Ku stimulated DNA joining whereas in the other study Ku inhibited joining by DNA ligase IV/XRCC4. The reason for the discrepancy in these studies is not clear. It is possible that the stimulatory effect is a consequence of DNA end-bridging because Ku not only stimulated DNA ligase IV/XRCC4 but also DNA ligases I and III [*202*]. However, Hdf1/Hdf2, the yeast homologue of Ku70/Ku80, inhibited DNA joining by Dnl4/Lif1 [*47*]. The effect of Ku on the DNA joining activity of DNA ligase IV/XRCC4 may not be biologically relevant because, in the yeast system, it appears that end-bridging is mediated by the Rad50/Mre11/Xrs2 complex whereas the requirement for Hdf1/Hdf1 is only apparent at ionic conditions close to physiological levels [*47*]. Similarly, the efficient interaction of DNA-PKcs with DNA ends only requires Ku70/Ku80 at ionic conditions close to physiological levels [*203*]. Interestingly, when DNA-PKcs loads onto DNA ends bound by Ku70/Ku80, the heterodimer is moved inward along the DNA helix, leaving DNA-PKcs at the end [*204*].

Recently, it was observed that DNA-PKcs was autophosphorylated in response to IR and that this autophosphorylation was necessary for DSB repair [*205*]. *In vitro* studies have shown that autophosphorylation of DNA-PKcs led to its dissociation from Ku and the loss of kinase activity [*206*], leading to the proposal that DNA-PK plays a regulatory role in NHEJ. However, there is accumulating evidence that DNA-PKcs plays an important structural role in NHEJ. The structure of DNA-PKcs determined by electron crystallography, revealed the presence of channels, suggesting that the DNA molecule is threaded through DNA-PKcs with the single strand ends protruding from the molecule [*207*]. Such an arrangement is intriguing as it suggests plausible mechanisms for DNA end-bridging, alignment and processing but, as with Ku70/Ku80, it raises questions about the removal of DNA-PKcs after repair is completed. DNA-PKcs associates with DNA ligase IV/XRCC4 at DNA ends and promotes intermolecular joining by DNA ligase IV/XRCC4 [*201*]. Indeed, under conditions compatible with DNA-PK assembly, Ku70/Ku80 still inhibited intramolecular joining by DNA ligase IV/XRCC4 so the majority of DNA joining events were intermolecular [*201*]. This change in the type of ligation resembles the effect of Rad50/Mre11/Xrs2 on Dnl4/Lif1 activity and suggests that DNA-PKcs has end-bridging activity. Interestingly, the efficient activation of kinase activity appears to require both the occupation of the open channel by double strand DNA and the simultaneous interaction with two single strand DNA ends [*208, 209*]. This provides a mechanism for DNA-PKcs to distinguish DSBs from SSBs as well as to enable the synapsis of two DNA ends. A recent study using electron microscopy has provided direct evidence for end-bridging by DNA-PKcs [*210*]. In contrast to the end-bridging by a single yeast Rad50/Mre11/Xrs2 complex, end bridging by DNA-PKcs occurs between DNA ends each bound by a DNA-PKcs molecule and involves interactions between these DNA-PKcs molecules [*210*].

Recently, physical and functional interactions between DNA-PKcs and Artemis have been described [*211*]. The assembly of a DNA-PKcs/Artemis complex on a DNA end results in the phosphorylation of Artemis and the activation of the cryptic endonuclease activity of Artemis. The DNA-PKcs/Artemis complex is able to open DNA hairpins, the unique reaction intermediate generated by the Rag1/Rag2 endonuclease during V(D)J recombination, providing a molecular explanation for the severe combined immunodeficiency of Artemis patients. The sensitivity of Artemis-deficient cell lines to ionizing radiation suggests that the Artemis nuclease is also a key player in NHEJ, presumably either contributing to exposing microhomologies for alignment or removing flaps after the alignment of microhomologies. Interestingly, the DNA-

PKcs/Artemis complex is similar to the yeast Rad50/Mre11/Xrs2 complex in that it posseses end-bridging and nuclease activities.

Although we have argued that Ku70/Ku80 is not directly involved in end-bridging and alignment, it likely remains associated with the nucleoprotein complex formed by NHEJ factors and may recruit additional NHEJ factors. In support of this idea, a functional interaction between Ku70/Ku80 and the product of the Werner's syndrome gene has been characterized [212-214]. The helicase and nuclease activities of the WS gene product may contribute to end processing. In the model shown in Figure 8, we propose that the DSBs are initially bound by Ku70/Ku80 which in turn recruits the DNA-PKcs/Artemis complex. DNA ends are then brought together by interactions between the DNA-PKcs molecules. DNA-PK phosphorylates Artemis to activate its nuclease activity. Although the identities and roles of the nucleases that expose microhomologies and remove single strand flaps after alignment remain to be determined, a recent study has provided evidence for a functional link between the Pol X family members, Pol mu and terminal deoxynucleotidyl transferase (TdT), and NHEJ factors [215]. Since Pol4, the only member of the Pol X family in *S. cerevisiae*, interacts with Dnl4/Lif1 [154], it appears that the link between Pol X DNA polymerases and NHEJ factors is conserved among eukaryotes. Presumably, TdT has evolved to play a specialized role in adding untemplated nucleotides during V(D)J recombination after the removal of Rag proteins and assembly of the NHEJ nucleoprotein complex containing Ku70/Ku80, DNA-PKcs, Artemis and DNA ligase IV/XRCC4, whereas Pol mu presumably interacts with the same NHEJ complex in non-lymphoid cells and fills in small gaps prior to ligation.

Dynan and his colleagues fractionated HeLa extracts and identified fractions that stimulated end joining by purified Ku70/Ku80 and DNA ligase IV/XRCC4. hRad50/hMre11/NBS1 but not DNA-PKcs co-purified with the stimulatory activity [216]. This result resembles the observation in the yeast system where Rad50/Mre11/Xrs2 stimulates the end joining activity of Dnl4/Lif1 [47], suggesting that hRad50/hMre11/NBS1, like the yeast counterpart, has a role in NHEJ. This idea is supported by the reported interaction between Ku and hMre11 [217]. Further evidence for the participation of the hRad50/hMre11/NBS1 complex in NHEJ comes from biochemical studies. The hMre11 nuclease is activated by non-homologous DNA ends but inhibited by complementary ends, suggesting that it has the ability to identify and align microhomologies [218]. Indeed, the processing of non-complementary DNA ends by hMre11 generated ligatable structures that were aligned at microhomologies.

In the *in vitro* system, addition of purified DNA-PKcs inhibited the stimulatory activity by hRad50/hMre11/NBS1, suggesting that hRad50/hMre11/NBS1 and DNA-PKcs compete for Ku-bound DNA ends [216]. This competition, together with the fact that both protein complexes possess end-bridging and nucleases activities, suggests that parallel NHEJ pathways may exist in mammalian system to achieve efficient DSB repair. Interestingly, the repair of DSBs appears to occur by two kinetically distinct mechanisms in mammalian cells. Inactivation of DNA-PKcs eliminates the rapid mechanism whereas the rapid and slow mechanisms are both lost in the absence of Ku function [219]. It is possible that the DNA-PKcs and Artemis have evolved in higher eukaryotes to increase the efficiency of NHEJ, giving rise to the rapid pathway. We suggest that the slow pathway may correspond to the yeast pathway involving the Rad50/Mre11/Xrs2 complex. The identification of *LIG4* mutations in patients with NBS-like symptoms also supports the existence of the hRad50/hMre11/NBS1-mediated NHEJ pathway and suggests that such pathway is critical during early development [168].

In summary, it appears that DNA end joining in mammalian cells may occur by several distinct pathways. Future studies are needed to elucidate the biological roles of the NHEJ subpathways.

References:
1. C. J. Norbury and I. D. Hickson, Cellular responses to DNA damage. *Annu Rev Pharmacol Toxicol* **41**, 367-401 (2001).
2. M. M. Cox, Recombinational DNA repair of damaged replication forks in Escherichia coli: questions. *Annu Rev Genet* **35**, 53-82 (2001).
3. B. Michel, et al., Rescue of arrested replication forks by homologous recombination. *Proc Natl Acad Sci USA* **98**, 8181-8188 (2001).
4. M. Foiani, et al., DNA damage checkpoints and DNA replication controls in *Saccharomyces cerevisiae*. *Mutat Res* **451**, 187-196 (2000).
5. J. Greenwood, V. Costanzo, K. Robertson, C. Hensey and J. Gautier, Responses to DNA damage in Xenopus: cell death or cell cycle arrest. *Novartis Found Symp* **237**, 221-230; discussion 230-224 (2001).
6. V. Kaliraman, J. R. Mullen, W. M. Fricke, S. A. Bastin-Shanower and S. J. Brill, Functional overlap between Sgs1-Top3 and the Mms4-Mus81 endonuclease. *Genes Dev* **15**, 2730-2740 (2001).
7. R. Rothstein, B. Michel and S. Gangloff, Replication fork pausing and recombination or "gimme a break". *Genes Dev* **14**, 1-10 (2000).
8. R. D. Kolodner, C. D. Putnam and K. Myung, Maintenance of genome stability in *Saccharomyces cerevisiae*. *Science* **297**, 552-557 (2002).

9.   T. Lindahl and R. D. Wood, Quality control by DNA repair. *Science* **286**, 1897-1905 (1999).
10.   A. J. Pierce, et al., Double-strand breaks and tumorigenesis. *Trends Cell Biol* **11**, S52-59 (2001).
11.   G. A. Cromie, J. C. Connelly and D. R. Leach, Recombination at double-strand breaks and DNA ends: conserved mechanisms from phage to humans. *Mol Cell* **8**, 1163-1174 (2001).
12.   D. D'Amours and S. P. Jackson, The Mre11 complex: at the crossroads of dna repair and checkpoint signalling. *Nat Rev Mol Cell Biol* **3**, 317-327 (2002).
13.   J. F. McBlane, et al., Cleavage at a V(D)J recombination signal requires only RAG1 and RAG2 proteins and occurs in two steps. *Cell* **83**, 387-395. (1995).
14.   U. Grawunder, R. B. West and M. R. Lieber, Antigen receptor gene rearrangement. *Curr Opin Immunol* **10**, 172-180 (1998).
15.   G. W. Siskind and B. Benacerraf, Cell selection by antigen in the immune response. *Adv. Immunol.* **10**, 1-50 (1969).
16.   J. Stavnezer, Immunoglobulin class switching. *Curr Opin Immunol* **8**, 199-205. (1996).
17.   L. Bross, et al., DNA double-strand breaks in immunoglobulin genes undergoing somatic hypermutation. *Immunity* **13**, 589-597. (2000).
18.   F. N. Papavasiliou and D. G. Schatz, Cell-cycle-regulated DNA double-stranded breaks in somatic hypermutation of immunoglobulin genes. *Nature* **408**, 216-221. (2000).
19.   M. Muramatsu, et al., Specific expression of activation-induced cytidine deaminase (AID), a novel member of the RNA-editing deaminase family in germinal center B cells. *J Biol Chem* **274**, 18470-18476 (1999).
20.   S. Petersen, et al., AID is required to initiate Nbs1/gamma-H2AX focus formation and mutations at sites of class switching. *Nature* **414**, 660-665 (2001).
21.   E. Martini and S. Keeney, Sex and the single (double-strand) break. *Mol Cell* **9**, 700-702 (2002).
22.   K. N. Smith, A. Penkner, K. Ohta, F. Klein and A. Nicolas, B-type cyclins CLB5 and CLB6 control the initiation of recombination and synaptonemal complex formation in yeast meiosis. *Curr Biol* **11**, 88-97 (2001).
23.   S. Keeney, Mechanism and control of meiotic recombination initiation. *Curr Top Dev Biol* **52**, 1-53 (2001).
24.   P. J. Romanienko and R. D. Camerini-Otero, Cloning, characterization, and localization of mouse and human SPO11. *Genomics* **61**, 156-169 (1999).
25.   S. Keeney, et al., A mouse homolog of the *Saccharomyces cerevisiae* meiotic recombination DNA transesterase Spo11p. *Genomics* **61**, 170-182 (1999).
26.   A. F. Dernburg, et al., Meiotic recombination in C. elegans initiates by a conserved mechanism and is dispensable for homologous chromosome synapsis. *Cell* **94**, 387-398 (1998).
27.   A. M. Villeneuve and K. J. Hillers, Whence meiosis? *Cell* **106**, 647-650 (2001).
28.   D. Zickler and N. Kleckner, Meiotic chromosomes: integrating structure and function. *Annu Rev Genet* **33**, 603-754 (1999).
29.   G. S. Roeder, Meiotic chromosomes: it takes two to tango. *Genes Dev* **11**, 2600-2621 (1997).
30.   F. Paques and J. E. Haber, Multiple pathways of recombination induced by double-strand breaks in *Saccharomyces cerevisiae*. *Microbiol Mol Biol Rev* **63**, 349-404 (1999).
31.   M. Takata, et al., Homologous recombination and non-homologous end-joining pathways of DNA double-strand break repair have overlapping roles in the maintenance of chromosomal integrity in vertebrate cells. *Embo J* **17**, 5497-5508 (1998).
32.   J. W. Szostak, T. L. Orr-Weaver, R. J. Rothstein and F. W. Stahl, The double-strand-break repair model for recombination. *Cell* **33**, 25-35 (1983).
33.   T. Allers and M. Lichten, Intermediates of yeast meiotic recombination contain heteroduplex DNA. *Mol Cell* **8**, 225-231 (2001).
34.   N. Kleckner, Meiosis: how could it work? *Proc Natl Acad Sci USA* **93**, 8167-8174 (1996).
35.   G. S. Roeder and J. M. Bailis, The pachytene checkpoint. *Trends Genet* **16**, 395-403 (2000).
36.   T. Allers and M. Lichten, Differential timing and control of noncrossover and crossover recombination during meiosis. *Cell* **106**, 47-57 (2001).
37.   K. Myung, C. Chen and R. D. Kolodner, Multiple pathways cooperate in the suppression of genome instability in *Saccharomyces cerevisiae*. *Nature* **411**, 1073-1076 (2001).
38.   V. Lundblad, DNA ends: maintenance of chromosome termini versus repair of double strand breaks. *Mutat Res* **451**, 227-240 (2000).
39.   V. Lundblad, Telomere maintenance without telomerase. *Oncogene* **21**, 522-531 (2002).
40.   V. A. Zakian, Structure, function, and replication of *Saccharomyces cerevisiae* telomeres. *Annu Rev Genet* **30**, 141-172 (1996).
41.   P. Sung, K. M. Trujillo and S. Van Komen, Recombination factors of *Saccharomyces cerevisiae*. *Mutat Res* **451**, 257-275 (2000).
42.   J. C. Connelly and D. R. Leach, Tethering on the brink: the evolutionarily conserved Mre11-Rad50 complex. *Trends Biochem Sci* **27**, 410-418 (2002).
43.   T. T. Paull and M. Gellert, The 3' to 5' exonuclease activity of Mre11 facilitates repair of DNA double-strand breaks. *Mol Cell* **1**, 969-979 (1998).

44. T. T. Paull and M. Gellert, Nbs1 potentiates ATP-driven DNA unwinding and endonuclease cleavage by the Mre11/Rad50 complex. *Genes Dev* **13**, 1276-1288 (1999).

45. K. M. Trujillo, S. S. Yuan, E. Y. Lee and P. Sung, Nuclease activities in a complex of human recombination and DNA repair factors Rad50, Mre11, and p95. *J Biol Chem* **273**, 21447-21450 (1998).

46. T. Usui, et al., Complex formation and functional versatility of Mre11 of budding yeast in recombination. *Cell* **95**, 705-716 (1998).

47. L. Chen, K. Trujillo, W. Ramos, P. Sung and A. E. Tomkinson, Promotion of Dnl4-catalyzed DNA end-joining by the Rad50/Mre11/Xrs2 and Hdf1/Hdf2 complexes. *Mol Cell* **8**, 1105-1115. (2001).

48. K. S. Lobachev, D. A. Gordenin and M. A. Resnick, The Mre11 complex is required for repair of hairpin-capped double-strand breaks and prevention of chromosome rearrangements. *Cell* **108**, 183-193 (2002).

49. K. P. Hopfner, C. D. Putnam and J. A. Tainer, DNA double-strand break repair from head to tail. *Curr Opin Struct Biol* **12**, 115-122 (2002).

50. K. P. Hopfner, et al., The Rad50 zinc-hook is a structure joining Mre11 complexes in DNA recombination and repair. *Nature* **418**, 562-566 (2002).

51. K. P. Hopfner, et al., Structural biochemistry and interaction architecture of the DNA double-strand break repair Mre11 nuclease and Rad50-ATPase. *Cell* **105**, 473-485 (2001).

52. K. P. Hopfner, et al., Mre11 and Rad50 from Pyrococcus furiosus: cloning and biochemical characterization reveal an evolutionarily conserved multiprotein machine. *J Bacteriol* **182**, 6036-6041 (2000).

53. D. E. Anderson, K. M. Trujillo, P. Sung and H. P. Erickson, Structure of the Rad50 x Mre11 DNA repair complex from *Saccharomyces cerevisiae* by electron microscopy. *J Biol Chem* **276**, 37027-37033 (2001).

54. M. de Jager, et al., Human Rad50/Mre11 is a flexible complex that can tether DNA ends. *Mol Cell* **8**, 1129-1135 (2001).

55. G. Basile, M. Aker and R. K. Mortimer, Nucleotide sequence and transcriptional regulation of the yeast recombinational repair gene RAD51. *Mol Cell Biol* **12**, 3235-3246 (1992).

56. A. Aboussekhra, R. Chanet, A. Adjiri and F. Fabre, Semidominant suppressors of Srs2 helicase mutations of *Saccharomyces cerevisiae* map in the *RAD51* gene, whose sequence predicts a protein with similarities to procaryotic RecA proteins. *Mol Cell Biol* **12**, 3224-3234 (1992).

57. A. Shinohara, H. Ogawa and T. Ogawa, Rad51 protein involved in repair and recombination in S. cerevisiae is a RecA-like protein. *Cell* **69**, 457-470 (1992).

58. T. Ogawa, X. Yu, A. Shinohara and E. H. Egelman, Similarity of the yeast RAD51 filament to the bacterial RecA filament. *Science* **259**, 1896-1899 (1993).

59. P. Sung and D. L. Robberson, DNA strand exchange mediated by a RAD51-ssDNA nucleoprotein filament with polarity opposite to that of RecA. *Cell* **82**, 453-461 (1995).

60. F. E. Benson, A. Stasiak and S. C. West, Purification and characterization of the human Rad51 protein, an analogue of E. coli RecA. *Embo J* **13**, 5764-5771 (1994).

61. X. Yu, S. A. Jacobs, S. C. West, T. Ogawa and E. H. Egelman, Domain structure and dynamics in the helical filaments formed by RecA and Rad51 on DNA. *Proc Natl Acad Sci USA* **98**, 8419-8424 (2001).

62. P. Sung, Catalysis of ATP-dependent homologous DNA pairing and strand exchange by yeast RAD51 protein. *Science* **265**, 1241-1243 (1994).

63. R. C. Gupta, L. R. Bazemore, E. I. Golub and C. M. Radding, Activities of human recombination protein Rad51. *Proc Natl Acad Sci USA* **94**, 463-468 (1997).

64. P. Baumann, F. E. Benson and S. C. West, Human Rad51 protein promotes ATP-dependent homologous pairing and strand transfer reactions in vitro. *Cell* **87**, 757-766 (1996).

65. S. Sigurdsson, K. Trujillo, B. Song, S. Stratton and P. Sung, Basis for avid homologous DNA strand exchange by human Rad51 and RPA. *J Biol Chem* **276**, 8798-8806 (2001).

66. P. R. Bianco, R. B. Tracy and S. C. Kowalczykowski, DNA strand exchange proteins: a biochemical and physical comparison. *Front Biosci* **3**, D570-603 (1998).

67. T. Sugiyama, E. M. Zaitseva and S. C. Kowalczykowski, A single-stranded DNA-binding protein is needed for efficient presynaptic complex formation by the *Saccharomyces cerevisiae* Rad51 protein. *J Biol Chem* **272**, 7940-7945 (1997).

68. E. M. Zaitseva, E. N. Zaitsev and S. C. Kowalczykowski, The DNA binding properties of *Saccharomyces cerevisiae* Rad51 protein. *J Biol Chem* **274**, 2907-2915 (1999).

69. S. Van Komen, G. Petukhova, S. Sigurdsson, S. Stratton and P. Sung, Superhelicity-driven homologous DNA pairing by yeast recombination factors Rad51 and Rad54. *Mol Cell* **6**, 563-572 (2000).

70. P. Sung and S. A. Stratton, Yeast Rad51 recombinase mediates polar DNA strand exchange in the absence of ATP hydrolysis. *J Biol Chem* **271**, 27983-27986 (1996).

71. G. S. Fortin and L. S. Symington, Mutations in yeast Rad51 that partially bypass the requirement for Rad55 and Rad57 in DNA repair by increasing the stability of Rad51-DNA complexes. *Embo J* **21**, 3160-3170 (2002).

72. E. A. Morgan, N. Shah and L. S. Symington, The requirement for ATP hydrolysis by Saccharomyces cerevisiae Rad51 is bypassed by mating-type heterozygosity or *RAD54* in high copy. *Mol Cell Biol* **22**, 6336-6343 (2002).

73. C. Morrison, et al., The essential functions of human Rad51 are independent of ATP hydrolysis. *Mol Cell Biol* **19**, 6891-6897 (1999).
74. R. C. Gupta, E. Folta-Stogniew, S. O'Malley, M. Takahashi and C. M. Radding, Rapid exchange of A:T base pairs is essential for recognition of DNA homology by human Rad51 recombination protein. *Mol Cell* **4**, 705-714 (1999).
75. B. Song and P. Sung, Functional interactions among yeast Rad51 recombinase, Rad52 mediator, and replication protein A in DNA strand exchange. *J Biol Chem* **275**, 15895-15904 (2000).
76. A. L. Eggler, R. B. Inman and M. M. Cox, The Rad51-dependent pairing of long DNA substrates is stabilized by replication protein A. *J Biol Chem* (2002).
77. S. Van Komen, G. Petukhova, S. Sigurdsson and P. Sung, Functional crosstalk among Rad51, Rad54, and RPA in Heteroduplex DNA joint formation. *J Biol Chem* (2002).
78. G. Petukhova, S. Stratton and P. Sung, Catalysis of homologous DNA pairing by yeast Rad51 and Rad54 proteins. *Nature* **393**, 91-94 (1998).
79. P. Sung, Yeast Rad55 and Rad57 proteins form a heterodimer that functions with replication protein A to promote DNA strand exchange by Rad51 recombinase. *Genes Dev* **11**, 1111-1121 (1997).
80. A. Shinohara, M. Shinohara, T. Ohta, S. Matsuda and T. Ogawa, Rad52 forms ring structures and co-operates with RPA in single-strand DNA annealing. *Genes Cells* **3**, 145-156 (1998).
81. W. Kagawa, et al., Crystal structure of the homologous-pairing domain from the human Rad52 recombinase in the undecameric form. *Mol Cell* **10**, 359-371 (2002).
82. U. H. Mortensen, C. Bendixen, I. Sunjevaric and R. Rothstein, DNA strand annealing is promoted by the yeast Rad52 protein. *Proc Natl Acad Sci USA* **93**, 10729-10734 (1996).
83. G. T. Milne and D. T. Weaver, Dominant negative alleles of RAD52 reveal a DNA repair/recombination complex including Rad51 and Rad52. *Genes Dev* **7**, 1755-1765 (1993).
84. P. Sung, Function of yeast Rad52 protein as a mediator between replication protein A and the Rad51 recombinase. *J Biol Chem* **272**, 28194-28197 (1997).
85. J. H. New, T. Sugiyama, E. Zaitseva and S. C. Kowalczykowski, Rad52 protein stimulates DNA strand exchange by Rad51 and replication protein A. *Nature* **391**, 407-410 (1998).
86. A. Shinohara and T. Ogawa, Stimulation by Rad52 of yeast Rad51-mediated recombination. *Nature* **391**, 404-407 (1998).
87. T. Sugiyama, J. H. New and S. C. Kowalczykowski, DNA annealing by RAD52 protein is stimulated by specific interaction with the complex of replication protein A and single-stranded DNA. *Proc Natl Acad Sci USA* **95**, 6049-6054 (1998).
88. J. H. New and S. C. Kowalczykowski, Rad52 protein has a second stimulatory role in DNA strand exchange that complements replication protein-A function. *J Biol Chem* **277**, 26171-26176 (2002).
89. L. Krejci, et al., Interaction with Rad51 is indispensable for recombination mediator function of Rad52. *J Biol Chem* (2002).
90. L. Krejci, J. Damborsky, B. Thomsen, M. Duno and C. Bendixen, Molecular dissection of interactions between Rad51 and members of the recombination-repair group. *Mol Cell Biol* **21**, 966-976 (2001).
91. M. D. Kaytor and D. M. Livingston, Allele-specific suppression of temperature-sensitive mutations of the *Saccharomyces cerevisiae* RAD52 gene. *Curr Genet* **29**, 203-210 (1996).
92. K. L. Boundy-Mills and D. M. Livingston, A *Saccharomyces cerevisiae RAD52* allele expressing a C-terminal truncation protein: activities and intragenic complementation of missense mutations. *Genetics* **133**, 39-49 (1993).
93. S. T. Lovett, Sequence of the *RAD55* gene of *Saccharomyces cerevisiae*: similarity of *RAD55* to prokaryotic RecA and other RecA-like proteins. *Gene* **142**, 103-106 (1994).
94. R. D. Johnson and L. S. Symington, Functional differences and interactions among the putative RecA homologs Rad51, Rad55, and Rad57. *Mol Cell Biol* **15**, 4843-4850 (1995).
95. S. L. Hays, A. A. Firmenich and P. Berg, Complex formation in yeast double-strand break repair: participation of Rad51, Rad52, Rad55, and Rad57 proteins. *Proc Natl Acad Sci USA* **92**, 6925-6929 (1995).
96. A. V. Mazin, C. J. Bornarth, J. A. Solinger, W. D. Heyer and S. C. Kowalczykowski, Rad54 protein is targeted to pairing loci by the Rad51 nucleoprotein filament. *Mol Cell* **6**, 583-592 (2000).
97. S. Sigurdsson, S. Van Komen, G. Petukhova and P. Sung, Homologous DNA pairing by human recombination factors Rad51 and Rad54. *J Biol Chem* (2002).
98. B. Clever, et al., Recombinational repair in yeast: functional interactions between Rad51 and Rad54 proteins. *Embo J* **16**, 2535-2544 (1997).
99. H. Jiang, et al., Direct association between the yeast Rad51 and Rad54 recombination proteins. *J Biol Chem* **271**, 33181-33186 (1996).
100. G. Petukhova, S. Van Komen, S. Vergano, H. Klein and P. Sung, Yeast Rad54 promotes Rad51-dependent homologous DNA pairing via ATP hydrolysis-driven change in DNA double helix conformation. *J Biol Chem* **274**, 29453-29462 (1999).
101. D. Ristic, C. Wyman, C. Paulusma and R. Kanaar, The architecture of the human Rad54-DNA complex provides evidence for protein translocation along DNA. *Proc Natl Acad Sci USA* **98**, 8454-8460 (2001).

102. K. Havas, et al., Generation of superhelical torsion by ATP-dependent chromatin remodeling activities. *Cell* **103**, 1133-1142 (2000).
103. A. Saha, J. Wittmeyer and B. R. Cairns, Chromatin remodeling by RSC involves ATP-dependent DNA translocation. *Genes Dev* **16**, 2120-2134 (2002).
104. H. L. Klein, RDH54, a RAD54 homologue in *Saccharomyces cerevisiae*, is required for mitotic diploid-specific recombination and repair and for meiosis. *Genetics* **147**, 1533-1543 (1997).
105. M. Shinohara, et al., Characterization of the roles of the Saccharomyces cerevisiae *RAD54* gene and a homologue of *RAD54, RDH54/TID1*, in mitosis and meiosis. *Genetics* **147**, 1545-1556 (1997).
106. M. E. Dresser, et al., DMC1 functions in a *Saccharomyces cerevisiae* meiotic pathway that is largely independent of the RAD51 pathway. *Genetics* **147**, 533-544 (1997).
107. E. Kraus, W. Y. Leung and J. E. Haber, Break-induced replication: a review and an example in budding yeast. *Proc Natl Acad Sci USA* **98**, 8255-8262 (2001).
108. Y. Bai and L. S. Symington, A Rad52 homolog is required for RAD51-independent mitotic recombination in *Saccharomyces cerevisiae*. *Genes Dev* **10**, 2025-2037 (1996).
109. A. P. Davis and L. S. Symington, The yeast recombinational repair protein Rad59 interacts with Rad52 and stimulates single-strand annealing. *Genetics* **159**, 515-525 (2001).
110. G. Petukhova, S. A. Stratton and P. Sung, Single strand DNA binding and annealing activities in the yeast recombination factor Rad59. *J Biol Chem* **274**, 33839-33842 (1999).
111. J. Smith and R. Rothstein, An allele of *RFA1* suppresses *RAD52*-dependent double-strand break repair in Saccharomyces cerevisiae. *Genetics* **151**, 447-458 (1999).
112. S. Sigurdsson, et al., Mediator function of the human Rad51B-Rad51C complex in Rad51/RPA-catalyzed DNA strand exchange. *Genes Dev* **15**, 3308-3318 (2001).
113. J. Y. Masson, et al., Identification and purification of two distinct complexes containing the five RAD51 paralogs. *Genes Dev* **15**, 3296-3307 (2001).
114. L. H. Thompson and D. Schild, Homologous recombinational repair of DNA ensures mammalian chromosome stability. *Mutat Res* **477**, 131-153 (2001).
115. P. L. Chen, et al., The BRC repeats in BRCA2 are critical for RAD51 binding and resistance to methyl methanesulfonate treatment. *Proc Natl Acad Sci USA* **95**, 5287-5292 (1998).
116. A. K. Wong, R. Pero, P. A. Ormonde, S. V. Tavtigian and P. L. Bartel, RAD51 interacts with the evolutionarily conserved BRC motifs in the human breast cancer susceptibility gene brca2. *J Biol Chem* **272**, 31941-31944 (1997).
117. S. K. Sharan, et al., Embryonic lethality and radiation hypersensitivity mediated by Rad51 in mice lacking Brca2. *Nature* **386**, 804-810 (1997).
118. R. Mizuta, et al., RAB22 and RAB163/mouse BRCA2: proteins that specifically interact with the RAD51 protein. *Proc Natl Acad Sci USA* **94**, 6927-6932 (1997).
119. H. Yang, et al., BRCA2 function in DNA binding and recombination from a BRCA2-DSS1-ssDNA structure. *Science* **297**, 1837-1848 (2002).
120. B. Elliott and M. Jasin, Double-strand breaks and translocations in cancer. *Cell Mol Life Sci* **59**, 373-385 (2002).
121. B. B. Zhou and S. J. Elledge, The DNA damage response: putting checkpoints in perspective. *Nature* **408**, 433-439 (2000).
122. S. E. Critchlow and S. P. Jackson, DNA end-joining: from yeast to man. *Trends Biochem Sci* **23**, 394-398. (1998).
123. A. Goffeau, et al., Life with 6000 genes. *Science* **274**, 546, 563-547. (1996).
124. D. B. Roth and J. H. Wilson, Nonhomologous recombination in mammalian cells: role for short sequence homologies in the joining reaction. *Mol Cell Biol* **6**, 4295-4304. (1986).
125. J. K. Moore and J. E. Haber, Cell cycle and genetic requirements of two pathways of nonhomologous end-joining repair of double-strand breaks in *Saccharomyces cerevisiae*. *Molecular & Cellular Biology* **16**, 2164-2173 (1996).
126. K. M. Kramer, J. A. Brock, K. Bloom, J. K. Moore and J. E. Haber, Two different types of double-strand breaks in *Saccharomyces cerevisiae* are repaired by similar RAD52-independent, nonhomologous recombination events. *Mol. Cell. Biol.* **14**, 1293-1301. (1994).
127. U. Grawunder, et al., Activity of DNA ligase IV stimulated by complex formation with XRCC4 protein in mammalian cells. *Nature* **388**, 492-495 (1997).
128. H. Feldmann and E. L. Winnacker, A putative homologue of the human autoantigen Ku from *Saccharomyces cerevisiae*. *J Biol Chem* **268**, 12895-12900. (1993).
129. H. Feldmann, et al., HDF2, the second subunit of the Ku homologue from *Saccharomyces cerevisiae*. *J Biol Chem* **271**, 27765-27769. (1996).
130. S. J. Boulton and S. P. Jackson, Identification of a *Saccharomyces cerevisiae* Ku80 homologue: roles in DNA double strand break rejoining and in telomeric maintenance. *Nucleic Acids Res* **24**, 4639-4648. (1996).
131. S. J. Boulton and S. P. Jackson, Components of the Ku-dependent non-homologous end-joining pathway are involved in telomeric length maintenance and telomeric silencing. *Embo J* **17**, 1819-1828 (1998).
132. S. E. Porter, P. W. Greenwell, K. B. Ritchie and T. D. Petes, The DNA-binding protein Hdf1p (a putative Ku homologue) is required for maintaining normal telomere length in *Saccharomyces cerevisiae*. *Nucleic Acids Res* **24**, 582-585. (1996).

133. W. Ramos, G. Liu, C. N. Giroux and A. E. Tomkinson, Biochemical and genetic characterization of the DNA ligase encoded by *Saccharomyces cerevisiae* open reading frame YOR005c, a homolog of mammalian DNA ligase IV. *Nucleic Acids Res* **26**, 5676-5683 (1998).

134. P. Schar, G. Herrmann, G. Daly and T. Lindahl, A newly identified DNA ligase of *Saccharomyces cerevisiae* involved in RAD52-independent repair of DNA double-strand breaks. *Genes Dev* **11**, 1912-1924 (1997).

135. S. H. Teo and S. P. Jackson, Identification of *Saccharomyces cerevisiae* DNA ligase IV: involvement in DNA double-strand break repair. *Embo J* **16**, 4788-4795 (1997).

136. T. E. Wilson, U. Grawunder and M. R. Lieber, Yeast DNA ligase IV mediates non-homologous DNA end joining. *Nature* **388**, 495-498. (1997).

137. G. Herrmann, T. Lindahl and P. Schar, *Saccharomyces cerevisiae* LIF1: a function involved in DNA double-strand break repair related to mammalian XRCC4. *Embo J* **17**, 4188-4198 (1998).

138. S. J. Boulton and S. P. Jackson, *Saccharomyces cerevisiae* Ku70 potentiates illegitimate DNA double- strand break repair and serves as a barrier to error-prone DNA repair pathways. *Embo J* **15**, 5093-5103. (1996).

139. G. T. Milne, S. Jin, K. B. Shannon and D. T. Weaver, Mutations in two Ku homologs define a DNA end-joining repair pathway in *Saccharomyces cerevisiae*. *Mol. Cell. Biol.* **16**, 4189-4198. (1996).

140. R. H. Schiestl, J. Zhu and T. D. Petes, Effect of mutations in genes affecting homologous recombination on restriction enzyme-mediated and illegitimate recombination in *Saccharomyces cerevisiae*. *Mol. Cell. Biol.* **14**, 4493-4500. (1994).

141. Y. Tsukamoto, J. Kato and H. Ikeda, Effects of mutations of *RAD50, RAD51, RAD52*, and related genes on illegitimate recombination in *Saccharomyces cerevisiae*. *Genetics* **142**, 383-391 (1996).

142. S. H. Teo and S. P. Jackson, Lif1p targets the DNA ligase Lig4p to sites of DNA double-strand breaks. *Curr Biol* **10**, 165-168 (2000).

143. T. E. Wilson and M. R. Lieber, Efficient processing of DNA ends during yeast nonhomologous end joining. Evidence for a DNA polymerase beta (Pol4)-dependent pathway. *J Biol Chem* **274**, 23599-23609. (1999).

144. X. Wu, T. E. Wilson and M. R. Lieber, A role for FEN-1 in nonhomologous DNA end joining: the order of strand annealing and nucleolytic processing events. *Proc Natl Acad Sci USA* **96**, 1303-1308 (1999).

145. V. Hegde and H. Klein, Requirement for the SRS2 DNA helicase gene in non-homologous end joining in yeast. *Nucleic Acids Res* **28**, 2779-2783. (2000).

146. S. L. Ooi, D. D. Shoemaker and J. D. Boeke, A DNA microarray-based genetic screen for nonhomologous end-joining mutants in *Saccharomyces cerevisiae*. *Science* **294**, 2552-2556 (2001).

147. M. Valencia, et al., *NEJ1* controls non-homologous end joining in *Saccharomyces cerevisiae*. *Nature* **414**, 666-669 (2001).

148. A. Kegel, J. O. Sjostrand and S. U. Astrom, Nej1p, a cell type-specific regulator of nonhomologous end joining in yeast. *Curr Biol* **11**, 1611-1617. (2001).

149. M. Frank_Vaillant and S. Marcand, NHEJ regulation by mating type is exercised through a novel protein, Lif2p, essential to the ligase IV pathway. *Genes & Development* **15**, 3005-3012 (2001).

150. S. U. Astrom, S. M. Okamura and J. Rine, Yeast cell-type regulation of DNA repair. *Nature* **397**, 310. (1999).

151. S. E. Lee, F. Paques, J. Sylvan and J. E. Haber, Role of yeast SIR genes and mating type in directing DNA double-strand breaks to homologous and non-homologous repair paths. *Curr Biol* **9**, 767-770. (1999).

152. S. Moreau, J. R. Ferguson and L. S. Symington, The nuclease activity of Mre11 is required for meiosis but not for mating type switching, end joining, or telomere maintenance. *Mol. Cell. Biol.* **19**, 556-566. (1999).

153. R. B. Cary, et al., DNA looping by Ku and the DNA-dependent protein kinase. *Proc Natl Acad Sci USA* **94**, 4267-4272. (1997).

154. H. M. Tseng and A. E. Tomkinson, A physical and functional interaction between yeast Pol4 and Dnl4/Lif1 links DNA synthesis and ligation in non-homologous end joining. *J Biol Chem* **in press** (2002).

155. T. D. Stamato, R. Weinstein, A. Giaccia and L. Mackenzie, Isolation of cell cycle-dependent gamma ray-sensitive Chinese hamster ovary cell. *Somatic Cell. Genet.* **9**, 165-173. (1983).

156. Z. Li, et al., The XRCC4 gene encodes a novel protein involved in DNA double-strand break repair and V(D)J recombination. *Cell* **83**, 1079-1089. (1995).

157. E. A. Hendrickson, Cell-cycle regulation of mammalian DNA double-strand-break repair. *Am J Hum Genet* **61**, 795-800. (1997).

158. D. Moshous, et al., Artemis, a novel DNA double-strand break repair/V(D)J recombination protein, is mutated in human severe combined immune deficiency. *Cell* **105**, 177-186. (2001).

159. M. L. Dronkert, et al., Disruption of mouse SNM1 causes increased sensitivity to the DNA interstrand cross-linking agent mitomycin C. *Mol Cell Biol* **20**, 4553-4561. (2000).

160. M. Brendel and J. A. Henriques, The pso mutants of *Saccharomyces cerevisiae* comprise two groups: one deficient in DNA repair and another with altered mutagen metabolism. *Mutat Res* **489**, 79-96. (2001).

161. G. S. Stewart, et al., The DNA double-strand break repair gene hMRE11 is mutated in individuals with an ataxia-telangiectasia-like disorder. *Cell* **99**, 577-587. (1999).

162. J. P. Carney, et al., The hMre11/hRad50 protein complex and Nijmegen breakage syndrome: linkage of double-strand break repair to the cellular DNA damage response. *Cell* **93**, 477-486. (1998).

163.   R. Varon, et al., Nibrin, a novel DNA double-strand break repair protein, is mutated in Nijmegen breakage syndrome. *Cell* **93**, 467-476. (1998).

164.   M. Kraakman-van der Zwet, et al., Immortalization and characterization of Nijmegen Breakage syndrome fibroblasts. *Mutat Res* **434**, 17-27. (1999).

165.   G. Luo, et al., Disruption of mRad50 causes embryonic stem cell lethality, abnormal embryonic development, and sensitivity to ionizing radiation. *Proc Natl Acad Sci USA* **96**, 7376-7381 (1999).

166.   Y. Xiao and D. T. Weaver, Conditional gene targeted deletion by Cre recombinase demonstrates the requirement for the double-strand break repair Mre11 protein in murine embryonic stem cells. *Nucleic Acids Res* **25**, 2985-2991. (1997).

167.   J. Zhu, S. Petersen, L. Tessarollo and A. Nussenzweig, Targeted disruption of the Nijmegen breakage syndrome gene NBS1 leads to early embryonic lethality in mice. *Curr Biol* **11**, 105-109. (2001).

168.   M. O'Driscoll, et al., DNA ligase IV mutations identified in patients exhibiting developmental delay and immunodeficiency. *Mol Cell* **8**, 1175-1185. (2001).

169.   L. Li, et al., Role of the non-homologous DNA end joining pathway in the early steps of retroviral infection. *Embo J* **20**, 3272-3281. (2001).

170.   R. e. Daniel, R. A. Katz and A. M. Skalka, A Role for DNA-PK in Retroviral DNA Integration. *Science* **284**, 644-647 (1999).

171.   K. A. Biedermann, J. R. Sun, A. J. Giaccia, L. M. Tosto and J. M. Brown, scid mutation in mice confers hypersensitivity to ionizing radiation and a deficiency in DNA double-strand break repair. *Proc Natl Acad Sci USA* **88**, 1394-1397 (1991).

172.   G. M. Fulop and R. A. Phillips, The scid mutation in mice causes a general defect in DNA repair. *Nature* **347**, 479-482. (1990).

173.   E. A. Hendrickson, et al., A link between double-strand break-related repair and V(D)J recombination: the scid mutation. *Proc Natl Acad Sci USA* **88**, 4061-4065. (1991).

174.   T. Blunt, et al., Defective DNA-dependent protein kinase activity is linked to V(D)J recombination and DNA repair defects associated with the murine scid mutation. *Cell* **80**, 813-823. (1995).

175.   C. U. Kirchgessner, et al., DNA-dependent kinase (p350) as a candidate gene for the murine SCID defect. *Science* **267**, 1178-1183. (1995).

176.   S. R. Peterson, et al., Loss of the catalytic subunit of the DNA-dependent protein kinase in DNA double-strand-break-repair mutant mammalian cells. *Proc Natl Acad Sci USA* **92**, 3171-3174. (1995).

177.   C. Badie, et al., A DNA double-strand break defective fibroblast cell line (180BR) derived from a radiosensitive patient represents a new mutant phenotype. *Cancer Res.* **57**, 4600-4607. (1997).

178.   E. Riballo, et al., Identification of a defect in DNA ligase IV in a radiosensitive leukaemia patient. *Curr Biol* **9**, 699-702 (1999).

179.   Y. Gao, et al., A targeted DNA-PKcs-null mutation reveals DNA-PK-independent functions for KU in V(D)J recombination. *Immunity* **9**, 367-376. (1998).

180.   Y. Gu, et al., Defective embryonic neurogenesis in Ku-deficient but not DNA-dependent protein kinase catalytic subunit-deficient mice. *Proc Natl Acad Sci USA* **97**, 2668-2673 (2000).

181.   G. E. Taccioli, et al., Targeted disruption of the catalytic subunit of the DNA-PK gene in mice confers severe combined immunodeficiency and radiosensitivity. *Immunity* **9**, 355-366. (1998).

182.   Y. Gu, et al., Growth retardation and leaky SCID phenotype of Ku70-deficient mice. *Immunity* **7**, 653-665. (1997).

183.   G. C. Li, et al., Ku70: a candidate tumor suppressor gene for murine T cell lymphoma. *Mol. Cell* **2**, 1-8. (1998).

184.   H. Vogel, D. S. Lim, G. Karsenty, M. Finegold and P. Hasty, Deletion of Ku86 causes early onset of senescence in mice. *Proc Natl Acad Sci USA* **96**, 10770-10775 (1999).

185.   D. E. Barnes, G. Stamp, I. Rosewell, A. Denzel and T. Lindahl, Targeted disruption of the gene encoding DNA ligase IV leads to lethality in embryonic mice. *Curr Biol* **8**, 1395-1398 (1998).

186.   K. M. Frank, et al., Late embryonic lethality and impaired V(D)J recombination in mice lacking DNA ligase IV. *Nature* **396**, 173-177 (1998).

187.   Y. Gao, et al., A critical role for DNA end-joining proteins in both lymphogenesis and neurogenesis. *Cell* **95**, 891-902 (1998).

188.   K. M. Frank, et al., DNA ligase IV deficiency in mice leads to defective neurogenesis and embryonic lethality via the p53 pathway. *Molecular Cell* **5**, 993-1002 (2000).

189.   Y. Lee, D. E. Barnes, T. Lindahl and P. J. McKinnon, Defective neurogenesis resulting from DNA ligase IV deficiency requires Atm. *Genes Dev* **14**, 2576-2580 (2000).

190.   Y. Gao, et al., Interplay of p53 and DNA-repair protein XRCC4 in tumorigenesis, genomic stability and development. *Nature* **404**, 897-900. (2000).

191.   J. Sekiguchi, et al., Genetic interactions between ATM and the nonhomologous end-joining factors in genomic stability and development. *Proc Natl Acad Sci USA* **98**, 3243-3248. (2001).

192.   N. Adachi, T. Ishino, Y. Ishii, S. Takeda and H. Koyama, DNA ligase IV-deficient cells are more resistant to ionizing radiation in the absence of Ku70: Implications for DNA double-strand break repair. *Proc Natl Acad Sci USA* **98**, 12109-12113. (2001).

193. N. J. Finnie, T. M. Gottlieb, T. Blunt, P. A. Jeggo and S. P. Jackson, DNA-dependent protein kinase activity is absent in xrs-6 cells: implications for site-specific recombination and DNA double-strand break repair. *Proc Natl Acad Sci USA* **92**, 320-324 (1995).

194. P. Baumann and S. C. West, DNA end-joining catalyzed by human cell-free extracts. *Proc Natl Acad Sci USA* **95**, 14066-14070 (1998).

195. L. A. Hanakahi, M. Bartlet-Jones, C. Chappell, D. Pappin and S. C. West, Binding of inositol phosphate to DNA-PK and stimulation of double-strand break repair. *Cell* **102**, 721-729 (2000).

196. L. A. Hanakahi and S. C. West, Specific interaction of IP6 with human Ku70/80, the DNA-binding subunit of DNA-PK. *Embo J* **21**, 2038-2044. (2002).

197. Y. Ma and M. R. Lieber, Binding of inositol hexakisphosphate (IP6) to Ku but not to DNA-PKcs. *J Biol Chem* **277**, 10756-10759. (2002).

198. L. A. Hanakahi and S. C. West, Specific interaction of IP6 with human Ku70/80, the DNA-binding subunit of DNA-PK. *Embo J* **21**, 2038-2044 (2002).

199. Y. Ma and M. R. Lieber, Binding of inositol hexakisphosphate (IP6) to Ku but not to DNA-PKcs. *J Biol Chem* **277**, 10756-10759 (2002).

200. J. R. Walker, R. A. Corpina and J. Goldberg, Structure of the Ku heterodimer bound to DNA and its implications for double-strand break repair. *Nature* **412**, 607-614. (2001).

201. L. Chen, K. Trujillo, P. Sung and A. E. Tomkinson, Interactions of the DNA ligase IV-XRCC4 complex with DNA ends and the DNA-dependent protein kinase. *J Biol Chem* **275**, 26196-26205 (2000).

202. D. A. Ramsden and M. Gellert, Ku protein stimulates DNA end joining by mammalian DNA ligases: a direct role for Ku in repair of DNA double-strand breaks. *Embo J* **17**, 609-614. (1998).

203. O. Hammarsten and G. Chu, DNA-dependent protein kinase: DNA binding and activation in the absence of Ku. *Proc Natl Acad Sci USA* **95**, 525-530. (1998).

204. S. Yoo and W. S. Dynan, Geometry of a complex formed by double strand break repair proteins at a single DNA end: recruitment of DNA-PKcs induces inward translocation of Ku protein. *Nucleic Acids Res* **27**, 4679-4686. (1999).

205. D. W. Chan, et al., Autophosphorylation of the DNA-dependent protein kinase catalytic subunit is required for rejoining of DNA double-strand breaks. *Genes Dev* **16**, 2333-2338 (2002).

206. D. W. Chan and S. P. Lees-Miller, The DNA-dependent protein kinase is inactivated by autophosphorylation of the catalytic subunit. *J Biol Chem* **271**, 8936-8941 (1996).

207. K. K. Leuther, O. Hammarsten, R. D. Kornberg and G. Chu, Structure of DNA-dependent protein kinase: implications for its regulation by DNA. *Embo J* **18**, 1114-1123. (1999).

208. O. Hammarsten, L. G. DeFazio and G. Chu, Activation of DNA-dependent protein kinase by single-stranded DNA ends. *J Biol Chem* **275**, 1541-1550. (2000).

209. S. Martensson and O. Hammarsten, DNA-dependent protein kinase catalytic subunit. Structural requirements for kinase activation by DNA ends. *J Biol Chem* **277**, 3020-3029. (2002).

210. L. G. DeFazio, R. M. Stansel, J. D. Griffith and G. Chu, Synapsis of DNA ends by DNA-dependent protein kinase. *Embo J* **21**, 3192-3200. (2002).

211. Y. Ma, U. Pannicke, K. Schwarz and M. R. Lieber, Hairpin opening and overhang processing by an Artemis/DNA-dependent protein kinase complex in nonhomologous end joining and V(D)J recombination. *Cell* **108**, 781-794. (2002).

212. M. P. Cooper, et al., Ku complex interacts with and stimulates the Werner protein. *Genes Dev* **14**, 907-912. (2000).

213. B. Li and L. Comai, Functional interaction between Ku and the werner syndrome protein in DNA end processing. *J Biol Chem* **275**, 28349-28352. (2000).

214. D. K. Orren, et al., A functional interaction of Ku with Werner exonuclease facilitates digestion of damaged DNA. *Nucleic Acids Res* **29**, 1926-1934. (2001).

215. K. N. Mahajan, S. A. Nick McElhinny, B. S. Mitchell and D. A. Ramsden, Association of DNA polymerase mu (pol mu) with Ku and ligase IV: role for pol mu in end-joining double-strand break repair. *Mol Cell Biol* **22**, 5194-5202. (2002).

216. J. Huang and W. S. Dynan, Reconstitution of the mammalian DNA double-strand break end-joining reaction reveals a requirement for an Mre11/Rad50/NBS1-containing fraction. *Nucleic Acids Res* **30**, 667-674. (2002).

217. W. Goedecke, M. Eijpe, H. H. Offenberg, M. van Aalderen and C. Heyting, Mre11 and Ku70 interact in somatic cells, but are differentially expressed in early meiosis. *Nat Genet* **23**, 194-198. (1999).

218. T. T. Paull and M. Gellert, A mechanistic basis for Mre11-directed DNA joining at microhomologies. *Proc Natl Acad Sci USA* **97**, 6409-6414. (2000).

219. S. J. DiBiase, et al., DNA-dependent protein kinase stimulates an independently active, nonhomologous, end-joining apparatus. *Cancer Res* **60**, 1245-1253. (2000).

Figure Legends

Figure 1
Recombination Models. The DSB is resected to yield 3' single stranded (ss) tails (Step 1). One of the ssDNA tails invades the DNA homologue to form a D-loop (Step 2). The D-loop is extended by continual strand exchange and by *de novo* DNA synthesis. The D-loop can be processed through two separate pathways. In one case (Classical DSB Repair Mechanism in Panel I), the second ssDNA tail anneals with the DNA strand displaced by the expanding D-loop structure, leading to the formation of a second Holliday junction. Alternatively (SDSA Mechanism in Panel II), the invading DNA strand dissociates from the donor DNA molecule and then anneals with the second ssDNA tail. Gap filling DNA synthesis and ligation then complete the process.

Figure 2
Recombination by BIR. A 3' ssDNA tail invades the donor chromosome to form a short DNA joint, which is then stabilized by DNA synthesis. The invading DNA strand continually dissociates from the donor chromosome as DNA synthesis continues. Second strand DNA synthesis then initiates on the non-dissociated invading strand. This recombination process can result in the copying of a substantial portion of the donor chromosome, resulting in gene conversion tracts that are many kilo bases in length. Alternative models of BIR have been discussed (Kraus et al, 2001).

Figure 3
Recombination between direct repeats by single-strand annealing. Resection of the ends of a DSB located between two direct DNA repeats (light boxes) results in 3' ssDNA tails that can hybridize within the homologous region. Following trimming of the flap structure, gap-filling DNA synthesis and ligation lead to a recombinant that has one of the DNA repeats and the intervening DNA sequence deleted.

Figure 4
In vitro systems for examining homologous DNA pairing and strand exchange. **A.** In this system, circular single-stranded DNA (ss) from a bacteriophage, typically φX174, is paired with the homologous linear duplex (ds) to yield a joint molecule (jm). DNA strand exchange, if successful over the entire length of the DNA molecules (5.4 kilo base pairs for fX DNA), generates a nicked circular duplex (nc) and a linear ssDNA (lss) as products.
B. The second system for characterizing the recombinase activity of Rad51 utilizes an oligonucleotide as the initiating substrate. The joint molecule that results from pairing between the oligonucleotide and the homologous duplex is rapidly resolved by DNA strand exchange, leading to the release of the ^{32}P-labeled strand from the duplex. Since the substrates are short, this system has its utility limited to studying homologous pairing.
C. This system has been specifically designed to study D-loop formation. Herein, a linear single strand (lss), either an oligonucleotide or a plasmid length DNA molecule, invades a covalently closed, typically negatively supercoiled, duplex molecule (sc) to form a D-loop. Biochemical studies have revealed that Rad51 needs the co-operation of Rad54 or Rdh54 to make D-loop efficiently.

Figure 5
Function of recombination mediators. RPA has high affinity for ssDNA and can therefore effectively compete with Rad51 for binding to the DNA, resulting in the suppression of presynaptic filament assembly. The recombination mediators help overcome the suppressive effect of RPA.

Figure 6
Cooperation between Rad51 and Rad54 in DNA joint formation. In this model, the incoming duplex is actively pumped through the presynaptic complex (consisting of Rad51, Rad54, RPA, and ssDNA) by Rad54, creating positively and negatively supercoiled domains as depicted. The Rad51-ssDNA nucleoprotein filament samples the negatively supercoiled domain for DNA homology. Once homology is located, formation of a DNA joint molecule ensues. The nascent joint molecule formed will be paranemic in nature if it occurs away from the end of the initiating ssDNA molecule. However, if DNA joint formation occurs near the end of the ssDNA molecule, it has the potential of being converted into a plectonemic linkage.

Figure 7
A model for NHEJ in S. cerevisiae. After DSB formation, Hdf1/Hdf2 binds to the DNA ends. The presence of Hdf1/Hdf2 at or near DNA ends enhances the recruitment of Rad50/Mre11/Xrs2 and promotes its end-bridging activity. Dnl4/Lif1 is in turn recruited to the nucleoprotein complex via the Xrs2 subunit. If necessary, end processing by factors such as Pol4 may take place within the nucleoprotein complex. H, Hdf1/Hdf2; R, Rad50; M, Mre11; X, Xrs2; D, Dnl4; L, Lif1; and P, Pol4.

Figure 8

A model for NHEJ in mammals. After DSB formation, Ku binds to DNA ends and recruits DNA-PKcs/Artemis. The binding of DNA-PKcs to DNA ends causes the inward translocation of Ku, leaving DNA-PKcs at the ends. Protein-protein interactions between end-bound DNA-PKcs molecules mediates the synapsis of the ends. Assembly of the DNA-PK complex on DNA ends activates the kinase activity that results in the phosphorylation of Artemis and XRCC4. DNA ends may be processed by Artemis and/or Pol μ. Finally, DNA ends are joined by DNA ligase IV/XRCC4. PKcs, DNA-PKcs; IV/4, DNA ligase IV/XRCC4.

Figure 1.

DSB

Step 1 — Nucleolytic end-processing

Step 2 — Strand invasion

Step 3 — D-loop extension

DNA synthesis ⇐   ⇒ Strand exchnage

(I) Strand stabilization

(II) Strand displacement

Strand annealing

Strand annealing

DNA synthesis

Classical DSBR (crossover)

SDSA (noncrossover)

Figure 2.

DSB

5' resection

Strand invasion

Strand displacement
synthesis

Synthesis of
complementary strand

Figure 3.

DSB

5' resection

Complementary
strand annealing

Flap processing
& Ligation

Figure 6.

Figure 7.

DSB Formation

Recognition

Recruitment and Synapsis
(Nej1?)

Processing and Ligation
(Fen-1? Srs2?)

Figure 8.

DSB Formation

Recognition

Artemis

PKcs

Artemis

Recruitment

PKcs **Ku**

**Synapsis, Processing
and Ligation**

Artemis

Ku **PKcs** **PKcs** **Ku**

Pol μ

Table 1. Biochemical Properties of Recombination Factors

Protein	Biochemical function	E.coli homologue	Human homologue	Features
Rad50	DNA-binding ATPase	SbcC	hRad50	Member of SMC family; interacts with Mre11 and Xrs2
Mre11	ssDNA endonuclease 3' to 5' exonuclease	SbcD	hMre11	Homology to phosphoesterases; interacts with Rad50 and Xrs2
Xrs2	not known	none	NBS1	Interacts with Mre11, Rad50 and Lif1
Rad51	ATP-dependent homologous DNA pairing and strand exchange	RecA	hRad51	Forms nucleoprotein filaments; interacts with Rad52, Rad54 and Rad55/Rad57
Rad52	ssDNA binding and annealing	none	hRad52	Mediator of strand exchange; single strand annealing activity
Rad55 and Rad57	ssDNA binding	none	XRCC2 XRCC3 Rad51B Rad51C Rad51D	Forms heterodimer; mediator of strand exchange
Rad54	DNA-dependent ATPase	none	hRad54 hRad54B	Member of Swi2/Snf2 family; promotes homologous DNA pairing by Rad51; DNA tracking/supercoiling function
Rdh54/Tid1	DNA-dependent ATPase	none	hRad54 hRad54B	Member of Swi2/Snf2 family; Promotes homologous DNA pairing by Rad51; interacts with Dmc1 and Rad51
Rad59	ssDNA binding and annealing	none	not known	Homology to Rad52; required for single strand annealing and BIR
RPA	ssDNA binding	SSB	hRPA	Removes secondary structure in ssDNA; sequester ssDNA during homologous pairing and strand exchange

Table 2. IR Sensitive Rodent Mutants Defective in NHEJ

IR group	Gene defective	Protein	Identifed mutants
4	*XRCC4*	XRCC4	XR-1
5	*XRCC5*	Ku80	xrs1-7
6	*XRCC6*	Ku70	
7	*XRCC7*	DNA-PKcs	Mouse scid cell line, V-3

Table 3. Biochemical Properties of NHEJ Factors

Protein	Biochemical function	S. cerevisiae homologue	Features
Ku70/Ku80	DNA end binding	Hdf1/Hdf2	Interacts with DNA-PKcs
DNA-PKcs	DNA activated serine-threonine protein kinase	none	Interacts with Ku70/Ku80 and Artemis
Artemis	5' to 3' exonuclease	not known	Interacts with DNA-PKcs
	Acquires structure specific endonuclease activity when complexed with DNA-PKcs		
DNA ligase IV	ATP-dependent DNA ligase	Dnl4	Interacts with XRCC4; Dnl4 also interacts with Pol4
XRCC4	DNA binding	Lif1	Interacts with DNA ligase IV; Lif1 also interacts with Xrs2
Pol μ	DNA polymerase	Pol4	
Fen-1	flap endonuclease	Rad27	

hRad50/hMre11/NBS1: please refer to Table 1

letters to nature

$b = 75.8$ Å and $c = 121.8$ Å, with one holotoxin complex in the asymmetric unit. For cryoprotection, crystals were transferred directly into a buffer with PME (M_r 5K), concentration 5–10% higher than the conditions in which the crystals grew, with 20% glycerol, supplemented with 1 M sodium bromide, and flash-cooled immediately afterward to −160 °C (total transfer/soak time between 20–30 s). Phases were determined by single-wavelength anomalous diffraction from the scattering of 26 partially ordered bromine ions introduced into the crystal from the cryo-buffer. Crystallographic methods and statistics can be found in Supplementary Information. The final model was refined to 2.0 Å and has R/R_{free} values of 18.2% and 21.4%, respectively. 90% of the residues fall into the most favourable region of the Ramachandran plot without outliers. The N-terminal 38 residues (18–56) of the crystallized construct of CdtA are not visible in the electron density, nor are residues 183–185 of CdtB (internal loop). Four residues at the N terminus and eight at the C terminus of CdtC are also not modelled, owing to disorder.

Mutagenesis

The amino-acid substitutions were introduced into *cdt* genes by *in vitro* site-directed mutagenesis using oligonucleotide primer pairs containing the appropriate base changes. The amplification of the mutant plasmid was carried out by Pfu Turbo DNA polymerase (Stratagene) in the thermal temperature cycler, and wild-type template plasmid was removed by digestion with *DpnI* before transformation. The double mutant is CdtB with His160Gln and Asp199Ser. The DNA binding mutant has the mutations Arg117Ala, Arg144Ala and Asn201Ala. The aromatic patch mutant contains Trp91Gly, Trp98Gly, Trp100Gly and Try102Ala substitutions in CdtA. The deletion mutant (CdtC Δ21–35) was generated by PCR and cloned as N-terminal hexahistidine fusion protein into the same vector as wild-type gene. All mutants created were verified by DNA sequencing. Purification of the mutant proteins and assembly into the mutant CDT holotoxin was performed as previously described for the wild-type complex.

Cell cycle analysis

Cell cycle progression of HeLa cells treated with CDT holotoxin was analysed by flow cytometry. HeLa cells (2×10^6 cells) were treated with indicated concentrations of wild-type or mutant CDT holotoxin for 3 h at 37 °C, 5% CO_2, and were subsequently washed of toxin and maintained in culture media. 48 hours after treatment with CDT, cells were collected and fixed by addition of cold 70% ethanol during continuous vortexing, and left at 4 °C for 16 h. The cells were then stained for 2 h at 23 °C with propidium iodide solution (25 μg ml^{-1} propidium iodide, 100 U ml^{-1} DNase-free RNase A, 0.04% TritonX-100 in PBS). Relative DNA content was measured by flow cytometry with FACSCalibur flow cytometer (Beckton Dickinson).

Plasmid-digestion assay

The DNase activity of CdtB was tested by a plasmid-digestion reaction as previously described[9,30] Wild-type and mutant CdtB proteins used in this assay were purified using the same protocol described above for the CDT holotoxin. The reaction contained 20 mM HEPES pH 7.5, 150 mM NaCl, 5 mM $MgCl_2$, 5 mM $CaCl_2$, supercoiled pUC19 plasmid (2.5 μg) as substrate, and indicated concentrations of wild-type or mutant CdtB (1, 3, or 9 μg), or CDT holotoxin (3, 9, and 27 μg). The reaction was incubated for 5 h at 37 °C, and quenched by addition of 10 mM EDTA. Supercoiled, linear and relaxed plasmid forms were separated by agarose gel electrophoresis (0.8%), stained with ethidium bromide, and photographed using Gel Doc 2000 Documentation system (Bio-Rad).

1. Johnson, W. M. & Lior, H. A new heat-labile cytolethal distending toxin (CLDT) produced by *Campylobacter* spp. *Microb. Pathog.* **4**, 115–126 (1988).
2. Pickett, C. L. & Whitehouse, C. A. The cytolethal distending toxin family. *Trends Microbiol.* **7**, 292–297 (1999).
3. De Rycke, J. & Oswald, E. Cytolethal distending toxin (CDT): a bacterial weapon to control host cell proliferation? *FEMS Microbiol. Lett.* **203**, 141–148 (2001).
4. Lara-Tejero, M. & Galan, J. E. Cytolethal distending toxin: limited damage as a strategy to modulate cellular functions. *Trends Microbiol.* **10**, 147–152 (2002).
5. Lara-Tejero, M. & Galan, J. E. CdtA, CdtB, and CdtC form a tripartite complex that is required for cytolethal distending toxin activity. *Infect. Immun.* **69**, 4358–4365 (2001).
6. Cortes-Bratti, X., Chaves-Olarte, E., Lagergard, T. & Thelestam, M. Cellular internalization of cytolethal distending toxin from *Haemophilus ducreyi. Infect. Immun.* **68**, 6903–6911 (2000).
7. Frisan, T., Cortes-Bratti, X., Chaves-Olarte, E., Stenerlow, B. & Thelestam, M. The *Haemophilus ducreyi* cytolethal distending toxin induces DNA double-strand breaks and promotes ATM-dependent activation of RhoA. *Cell. Microbiol.* **5**, 695–707 (2003).
8. Frisan, T., Cortes-Bratti, X. & Thelestam, M. Cytolethal distending toxins and activation of DNA damage-dependent checkpoint responses. *Int. J. Med. Microbiol.* **291**, 495–499 (2002).
9. Elwell, C. A. & Dreyfus, L. A. DNase I homologous residues in CdtB are critical for cytolethal distending toxin-mediated cell cycle arrest. *Mol. Microbiol.* **37**, 952–963 (2000).
10. Lara-Tejero, M. & Galan, J. E. A bacterial toxin that controls cell cycle progression as a deoxyribonuclease I-like protein. *Science* **290**, 354–357 (2000).
11. Elwell, C., Chao, K., Patel, K. & Dreyfus, L. *Escherichia coli* CdtB mediates cytolethal distending toxin cell cycle arrest. *Infect. Immun.* **69**, 3418–3422 (2001).
12. Mao, X. & DiRienzo, J. M. Functional studies of the recombinant subunits of a cytolethal distending holotoxin. *Cell. Microbiol.* **4**, 245–255 (2002).
13. Cortes-Bratti, X., Frisan, T. & Thelestam, M. The cytolethal distending toxins induce DNA damage and cell cycle arrest. *Toxicon* **39**, 1729–1736 (2001).
14. Hassane, D. C., Lee, R. B., Mendenhall, M. D. & Pickett, C. L. Cytolethal distending toxin demonstrates genotoxic activity in a yeast model. *Infect. Immun.* **69**, 5752–5759 (2001).
15. Cortes-Bratti, X., Karlsson, C., Lagergard, T., Thelestam, M. & Frisan, T. The *Haemophilus ducreyi* cytolethal distending toxin induces cell cycle arrest and apoptosis via the DNA damage checkpoint pathways. *J. Biol. Chem.* **276**, 5296–5302 (2001).
16. Alby, F. *et al.* Study of the cytolethal distending toxin (CDT)-activated cell cycle checkpoint. Involvement of the CHK2 kinase. *FEBS Lett.* **491**, 261–265 (2001).
17. Deng, K., Latimer, J. L., Lewis, D. A. & Hansen, E. J. Investigation of the interaction among the components of the cytolethal distending toxin of *Haemophilus ducreyi. Biochem. Biophys. Res. Commun.* **285**, 609–615 (2001).
18. Lewis, D. A. *et al.* Characterization of *Haemophilus ducreyi* cdtA, cdtB, and cdtC mutants in *in vitro* and *in vivo* systems. *Infect. Immun.* **69**, 5626–5634 (2001).
19. Comayras, C. *et al.* *Escherichia coli* cytolethal distending toxin blocks the HeLa cell cycle at the G2/M transition by preventing cdc2 protein kinase dephosphorylation and activation. *Infect. Immun.* **65**, 5088–5095 (1997).
20. Escalas, N. *et al.* Study of the cytolethal distending toxin-induced cell cycle arrest in HeLa cells: involvement of the CDC25 phosphatase. *Exp. Cell Res.* **257**, 206–212 (2000).
21. Nishikubo, S. *et al.* An N-terminal segment of the active component of the bacterial genotoxin cytolethal distending toxin B (CDTB) directs CDTB into the nucleus. *J. Biol. Chem.* **278**, 50671–50681 (2003).
22. Montfort, W. *et al.* The three-dimensional structure of ricin at 2.8 A. *J. Biol. Chem.* **262**, 5398–5403 (1987).
23. Holm, L. & Sander, C. Protein structure comparison by alignment of distance matrices. *J. Mol. Biol.* **233**, 123–138 (1993).
24. Lee, R. B., Hassane, D. C., Cottle, D. L. & Pickett, C. L. Interactions of *Campylobacter jejuni* cytolethal distending toxin subunits CdtA and CdtC with HeLa cells. *Infect. Immun.* **71**, 4883–4890 (2003).
25. Deng, K. & Hansen, E. J. A CdtA-CdtC complex can block killing of HeLa cells by *Haemophilus ducreyi* cytolethal distending toxin. *Infect. Immun.* **71**, 6633–6640 (2003).
26. Shenker, B. J. *et al. Actinobacillus actinomycetemcomitans* cytolethal distending toxin (Cdt): evidence that the holotoxin is composed of three subunits: CdtA, CdtB, and CdtC. *J. Immunol.* **172**, 410–417 (2004).
27. Suck, D., Lahm, A. & Oefner, C. Structure refined to 2A of a nicked DNA octanucleotide complex with DNase I. *Nature* **332**, 464–468 (1988).
28. Weston, S. A., Lahm, A. & Suck, D. X-ray structure of the DNase I-d(GGTATACC)2 complex at 2.3 A resolution. *J. Mol. Biol.* **226**, 1237–1256 (1992).
29. Jones, S. J., Worrall, A. F. & Connolly, B. A. Site-directed mutagenesis of the catalytic residues of bovine pancreatic deoxyribonuclease I. *J. Mol. Biol.* **264**, 1154–1163 (1996).
30. Pan, C. Q., Ulmer, J. S., Herzka, A. & Lazarus, R. A. Mutational analysis of human DNase I at the DNA binding interface: implications for DNA recognition, catalysis, and metal ion dependence. *Protein Sci.* **7**, 628–636 (1998).

● ●

Human meiotic recombinase Dmc1 promotes ATP-dependent homologous DNA strand exchange

Michael G. Sehorn[1]*, **Stefan Sigurdsson**[2]*, **Wendy Bussen**[2], **Vinzenz M. Unger**[1] & **Patrick Sung**[1]

[1]*Department of Molecular Biophysics and Biochemistry, Yale University School of Medicine, 333 Cedar Street, New Haven, Connecticut 06520, USA*
[2]*Department of Molecular Medicine, Institute of Biotechnology, University of Texas Health Science Center at San Antonio, 15355 Lambda Drive, San Antonio, Texas 78245, USA*

* These authors contributed equally to this work

Homologous recombination is crucial for the repair of DNA breaks and maintenance of genome stability[1-3]. In *Escherichia coli*, homologous recombination is dependent on the RecA protein. In the presence of ATP, RecA mediates the homologous DNA pairing and strand exchange reaction that links recombin-
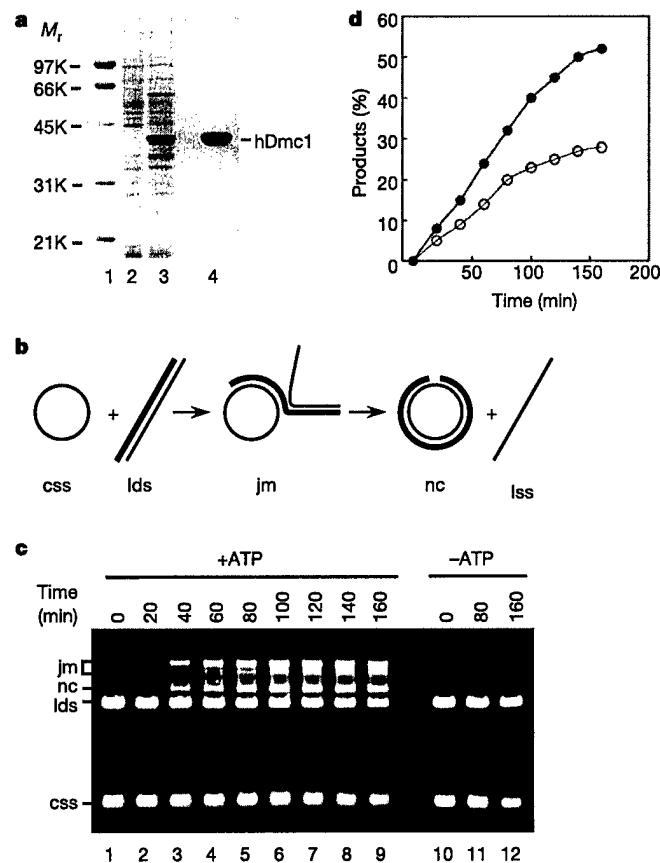
ing DNA molecules. DNA joint formation is initiated through the nucleation of RecA onto single-stranded DNA (ssDNA) to form helical nucleoprotein filaments[4-6]. Two RecA-like recombinases, Rad51 and Dmc1, exist in eukaryotes[1]. Whereas Rad51 is needed for both mitotic and meiotic recombination events, the function of Dmc1 is restricted to meiosis[3,7]. Here we examine human Dmc1 protein (hDmc1) for the ability to promote DNA strand exchange, and show that hDmc1 mediates strand exchange between paired DNA substrates over at least several thousand base pairs. DNA strand exchange requires ATP and is strongly dependent on the heterotrimeric ssDNA-binding molecule replication factor A (RPA). We present evidence that hDmc1-mediated DNA recombination initiates through the nucleation of hDmc1 onto ssDNA to form a helical nucleoprotein filament. The DNA strand exchange activity of hDmc1 is probably indispensable for repair of DNA double-strand breaks during meiosis and for maintaining the ploidy of meiotic chromosomes.

The *RAD51* gene is required for mitotic and meiotic recombination[3,8]. Like RecA, Rad51 forms helical nucleoprotein filaments and mediates homologous DNA pairing and strand exchange in an ATP-dependent manner[2,4]. Mutations in *DMC1* (disrupted meiosis cDNA 1) cause no discernible mitotic phenotype but lead to a constellation of meiotic abnormalities, primarily due to a failure to pair homologous chromosomes properly[7,9-11]. Surprisingly, even

though Dmc1 protein has a weak homologous DNA pairing activity, it does not seem to catalyse DNA strand exchange[1,12-14]. The apparent lack of DNA strand exchange activity in Dmc1 is counter-intuitive, because genetic studies in yeast have shown that *DMC1* deletion suppresses meiotic recombination, and Dmc1 protein seems to form recombinants in the absence of Rad51 (refs 7, 15). Additionally, Dmc1 is thought to bind DNA as stacked protein rings and to mediate homologous DNA pairing by means of this nucleo-protein intermediate[13,16].

We cloned hDmc1 cDNA and introduced it into a baculovirus vector that adds a 5' six-histidine tag. A recombinant His$_6$-hDmc1 baculovirus was made and used to infect High-Five insect cells. We purified hDmc1 by three chromatographic fractionation steps and affinity chromatography on Ni^{2+}-nitrilotriacetate agarose (Fig. 1a); the identity of the purified protein was verified by matrix-assisted laser desorption ionization–time-of-flight MS analysis. Three different hDmc1 preparations gave the same results in all the analyses.

Figure 1 hDmc1 catalyses ATP-dependent DNA strand exchange. **a**, Extracts from cells without (lane 2) or with (lane 3) hDmc1, and purified hDmc1 (4 μg in lane 4), were analysed by SDS–polyacrylamide-gel electrophoresis on 10% polyacrylamide gels. M_r, relative molecular mass. **b**, Reaction diagram: pairing of (+) strand (css) with linear duplex (lds) yields a joint molecule (jm), and DNA strand exchange generates a nicked circular duplex (nc) and linear ssDNA (lss). **c**, DNA strand exchange as a function of reaction time (lanes 1–9). ATP is needed for product formation (lanes 10–12). **d**, Time course of DNA strand exchange. Open circles, nicked circular duplex; filled circles, joint molecules and nicked circular duplex combined

Figure 2 Dependence of hDmc1-mediated DNA strand exchange on hRPA and salt. **a**, Dependence of hDmc1-mediated DNA strand exchange on hRPA. The agarose gel containing samples from the 3-h time point is shown in the upper panel; labels are as described in Fig. 1b. Lower left, nicked circular duplex; lower right, nicked circular duplex and joint molecules combined. **b**, Dependence of hDmc1/hRPA-mediated DNA strand exchange on KCl. Left, nicked circular duplex; right, nicked circular duplex and joint molecules combined. Symbols: filled circles, 60 min of incubation; open circles, 120 min of incubation; squares, 180 min of incubation.
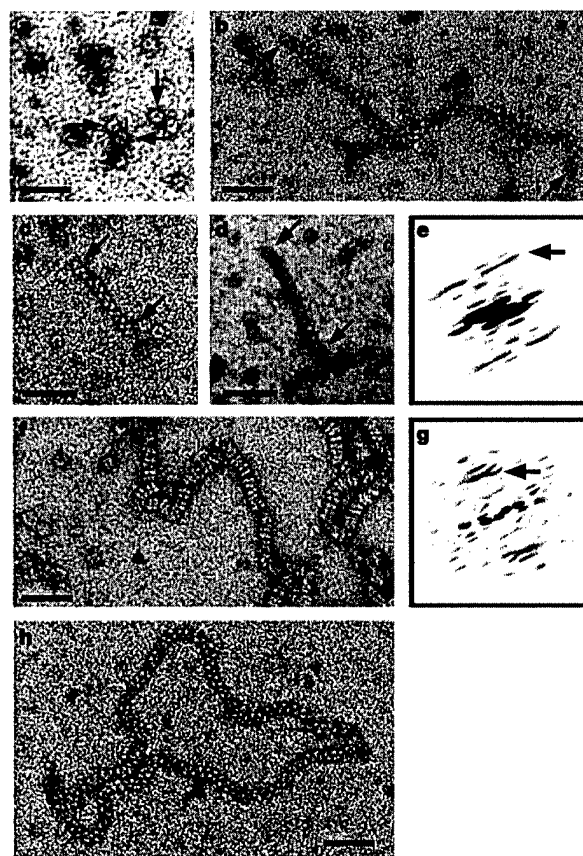
We examined whether hDmc1 can mediate DNA strand exchange with plasmid-length φX174 ssDNA and double-stranded DNA (dsDNA)[2–4]. Pairing yields a DNA joint molecule, and DNA strand exchange over the length (5.4 kilobases) of the synapsed substrates produces nicked circular duplex and linear ssDNA[2–4] (Fig. 1b). We included hRPA in the reaction, because this ssDNA-binding factor enhances the Rad51 recombinase activity[2–4]. We first verified that the hDmc1 and hRPA used were devoid of nuclease contamination by incubating them with the appropriate test substrates (data not shown). For DNA strand exchange, we preincubated hDmc1 with

ssDNA in the presence of ATP, and then incorporated hRPA and dsDNA. A substantial level of nicked circular duplex was seen. Specifically, at 80 min, about 20% of the input duplex was converted into nicked circular duplex (Fig. 1c). The use of duplex substrates labelled with ^{32}P at either the 3′ or 5′ end confirmed the displacement of linear ssDNA and provided assurance that hDmc1 catalyses genuine DNA strand exchange (Supplementary Fig. 1). Maximal DNA strand exchange occurs within the range of two nucleotides to one nucleotide per hDmc1 monomer (data not shown).

No product was seen when ATP was omitted (Fig. 1c) or when it was replaced with ADP or one of the slowly hydrolysable ATP analogues ATP-γS, AMP-PNP or AMP-PCP (data not shown). Thus, ATP hydrolysis seems to be indispensable for the hDmc1-mediated recombination reaction. As shown in Fig. 2a, the omission of hRPA completely abolished the formation of nicked circular duplex and greatly decreased the amount of DNA joint molecules. The optimal level of hRPA for the hDmc1-mediated reaction was between 10 and 15 nucleotides per RPA monomer (Fig. 2a). As expected, no product was seen with heterologous DNA species (for example, φX (+) strand and linear pBluescript duplex), confirming the requirement for DNA homology (data not shown). Interestingly, physiological ionic strength (100–200 mM KCl) is essential for revealing the recombinase activity of hDmc1 (Fig. 2b). The recombination reaction is also highly sensitive to pH, with optimal activity being observed between pH 7.3 and 7.8 (data not shown).

Figure 3 hDmc1 mediates robust D-loop formation. **a**, Reaction diagram: pairing of OL2 (lss) with pBluescript replicative form I DNA (sc) yields D-loop. **b**, D-loop formation as a function of time. Bl, reaction blank without hDmc1. **c**, The dependence of D-loop formation on ATP and DNA homology. The heterologous DNA (φX174 replicative form I DNA, designated as Het in lane 10) was used with hDmc1 and ATP. Bl, reaction blank with the homologous DNA substrates but no hDmc1. **d**, The level of D-loop was examined as a function of the order of addition of reaction components.

Figure 4 Analysis of hDmc1-ssDNA complexes by electron microscopy. **a**, hDmc1 protein rings (several marked by arrows). **b–d**, hDmc1-ssDNA filaments formed with ATP; the filament ends are marked by arrows. **e**, Fourier transform of the filament in **d**. A pair of layer lines (marked by the arrow) was observed 1/82 Å from the equator, indicating helical symmetry. **f**, Without ATP, only stacked rings of hDmc1 are formed on ssDNA. **g**, Fourier transform of the stacked rings shows one strong layer line (marked by the arrow) crossing the meridian. **h**, A helical hRad51–ssDNA filament formed with ATP. Scale bar, 50 nm.

We also examined the ability of hDmc1 to catalyse DNA pairing and strand invasion in the D-loop assay, which monitors the assimilation of a radiolabelled oligonucleotide into a homologous duplex[2–4] (Fig. 3a). The hDmc1-mediated D-loop reaction is robust (Fig. 3b) and requires ATP, which cannot be replaced by ATP-γS or AMP-PNP (Fig. 3c). Importantly, preincubation of hDmc1 with ssDNA resulted in a robust reaction, whereas less product was seen when the duplex substrate was preincubated with hDmc1, or when the recombinase was mixed with both DNA substrates simultaneously (Fig. 3d). These results implicate a hDmc1–ssDNA complex as the active nucleoprotein species in recombination, a conclusion that was independently verified by experiments on the order of addition with the use of the φX174 DNA substrates (data not shown). As shown in Supplementary Fig. 2, the ability of hDmc1 to form D-loop is enhanced by the Rad54B protein, which is probably the orthologue of the yeast Rdh54/Tid1 protein known to be involved in meiotic recombination with Dmc1 (ref. 3).

The functional form of hDmc1 is thought to comprise stacked protein rings on DNA[13,16]. We used electron microscopy to examine the nature of the hDmc1–ssDNA nucleoprotein complex, adhering to the buffer conditions for DNA strand exchange. Consistent with previous studies[13,16] was our observation that only hDmc1 protein rings were seen in the absence of DNA (Fig. 4a). hDmc1 protein filaments were formed upon the addition of ssDNA; three examples of these filaments are shown in Fig. 4b–d. The hDmc1–ssDNA nucleoprotein filaments had the striated appearance characteristic of helical nucleoprotein filaments made by Rad51 (Fig. 4h) and RecA[1,4,6]. A Fourier transform further confirmed that the hDmc1–ssDNA nucleoprotein filaments were helical (Fig. 4e). Although abundant, the hDmc1–ssDNA helical nucleoprotein filaments were shorter than those assembled with hRad51, with a mean length of 98 ± 43 nm ($n = 152$), although longer filaments were seen occasionally (see Fig. 4b, for example). Importantly, from several independent spreads, we found no evidence of stacked hDmc1 rings when ATP was present. However, when ATP was omitted there was no sign of hDmc1 helical filaments; instead, linear arrays of stacked hDmc1 rings on ssDNA were seen (Fig. 4f); a Fourier transform helped to establish the non-helical nature of these nucleoprotein complexes (Fig. 4g).

In recombination reactions, ssDNA is used to initiate genetic exchange with a homologous duplex[2–5]. RecA and Rad51 function in recombination by assembling into a helical protein filament on ssDNA often referred to as the presynaptic filament[2,4]. The presynaptic filament contains a binding site for duplex DNA, and this ability of the presynaptic filament to hold three DNA strands in close proximity underlies the basis for seeking out DNA homology and forming DNA joints[2,4]. Here we show that hDmc1 also forms a helical nucleoprotein filament on ssDNA and mediates extensive DNA strand exchange. In experiments that used fluorescence resonance energy transfer, hDmc1 was seen to form a three-stranded synaptic intermediate[17]. It is likely that the hDmc1–ssDNA nucleoprotein filament represents the critical catalytic intermediate for this recombinase. That the hDmc1 filaments in our electron microscopic analysis did not extend over the entire length of the DNA might reflect an inherent instability of these filaments. We find that a relatively high concentration of salt and a narrow pH range are required to reveal the DNA strand exchange potential of hDmc1. It remains to be seen whether these reaction parameters help to modulate the affinity of the hDmc1 presynaptic filament for duplex DNA or affect another step in the reaction path[2,18].

Our results show that hRPA is critical for DNA strand exchange efficiency. hRPA could promote hDmc1-mediated DNA strand exchange by minimizing secondary structure in the ssDNA[2–4] and sequestering the displaced strand that results from DNA strand exchange[19,20]. In addition, we have found that hRad54B protein enhances the ability of hDmc1 to form D-loop. It is very likely that the hDmc1 recombinase activity is modulated by other protein

factors that function with Dmc1 in meiosis[21]; in this regard, the biochemical systems devised here will be valuable for defining the role of these factors in hDmc1-mediated recombination reactions. □

Methods

Purification of hDmc1 and hRPA

High-Five insect cells were infected with His_6-hDmc1 baculovirus at a multiplicity of infection of 10 and were harvested after 48 h. Extract from 200 ml of insect cell culture was subjected to chromatographic fractionation in Q Sepharose, Mono Q and Mono S, and also to affinity purification with Ni2+-nitrilotriacetate agarose (Qiagen) to purify hDmc1 to near homogeneity. A total of 5 mg protein was obtained, which was concentrated in a Centricon-30 microconcentrator to 15 mg ml^{-1} and stored in small aliquots at $-70\,^{\circ}$C. Human RPA was purified to near homogeneity from *E. coli*[22] as described[18].

DNA substrates

The φX174 circular ssDNA and replicative form I DNA (about 95% supercoiled) were purchased from New England Biolabs and Life Technologies, respectively. The replicative form I DNA was linearized with *ApaL*1. OL2 is a 90-mer oligonucleotide complementary to pBluescript SK DNA and was ^{32}P-labelled at the 5' end as described[23]. DNA substrates were stored in TE buffer (10 mM Tris-HCl pH 7.2, 0.5 mM EDTA).

DNA strand exchange reaction

The cited reactant concentrations corresponded to the final values and the incubation steps were performed at 37 °C. The time course experiment shown in Fig. 1 had a final volume of 50 μl and was performed in 35 mM Tris-HCl pH 7.6, 1 mM dithiothreitol, 2 mM ATP, 2.5 mM $MgCl_2$, with an ATP-regenerating system consisting of 8 mM creatine phosphate and 30 μg ml^{-1} creatine kinase. To assemble the reaction, hDmc1 (30 μM) was incubated with φX174 (+) strand (30 μM nucleotides) for 5 min. At this time, hRPA (2 μM) and KCl (200 mM) were added, and after a 5-min incubation, linear φX dsDNA (22 μM nucleotides) was incorporated to complete the reaction. At the indicated times, a 5 μl aliquot of the reaction mixture was withdrawn, deproteinized and subjected to analysis in agarose gels, as described[24]. In other experiments the volume of the reaction was scaled down appropriately. The experiments in Fig. 2 used the same hDmc1 and DNA concentrations as above.

D-loop reaction

The reaction buffer was 20 mM Tris-HCl pH 7.3, 100 μg ml^{-1} BSA, 5 mM $MgCl_2$, 2 mM ATP, containing the ATP-generating system described above. For the experiment in Fig. 3 (37.5 μl final volume), hDmc1 (6.5 μM) was incubated with 5'-labelled OL2 (2.5 μM nucleotides) for 3 min at 37 °C. The reaction was completed with the addition of pBluescript SK replicative form I DNA (190 μM nucleotides). The reaction mixture was incubated at 30 °C and 3.3 μl aliquots were withdrawn at the indicated times, deproteinized, and run in 1% agarose gels in Tris/acetate/EDTA buffer as described[23]. The gels were dried and D-loop levels were quantified by phosphorimaging analysis. The reactions in which ATP was omitted or replaced by a non-hydrolysable analogue were scaled down to 12.5 μl final volume.

Electron microscopy and image analysis

Reaction mixtures were assembled in the buffer used for DNA strand exchange. The reactions contained hDmc1 (30 μM) or Rad51 (30 μM) and ssDNA (120 μM nucleotides) in the absence or presence of 2 mM ATP and were incubated for 1 h at 37 °C. After dilution 1:40 with the reaction buffer, 3 μl of the diluted mixture was applied to 400-mesh grids coated with fresh carbon film that had been glow-discharged in air. After staining for 15 s with 2% uranyl acetate, samples were examined in a Tecnai 12 transmission electron microscope equipped with a LaB6 filament and operated at 120 keV. Digital images were captured with a GATAN 794, 1,024 × 1,024-pixel charge-coupled device camera at a nominal magnification of ×26,000. For further analysis, images were converted to Medical Research Council (MRC) format, and ordered segments of the nucleoprotein complexes were identified with the fast Fourier transform option in the image display program XIMDISP[25]. Diffraction patterns were calculated after boxing short, straight segments of the nucleoprotein complexes with the program BOXIMAGE[25].

1. Masson, J. Y. & West, S. C. The Rad51 and Dmc1 recombinases: a non-identical twin relationship. *Trends Biochem. Sci.* **26**, 131–136 (2001).
2. Sung, P., Krejci, L., Van Komen, S. & Sehorn, M. G. Rad51 recombinase and recombination mediators. *J. Biol. Chem.* **278**, 42729–42732 (2003).
3. Symington, L. S. Role of RAD52 epistasis group genes in homologous recombination and double-strand break repair. *Microbiol. Mol. Biol. Rev.* **66**, 630–670 (2002).
4. Bianco, P. R., Tracy, R. B. & Kowalczykowski, S. C. DNA strand exchange proteins: a biochemical and physical comparison. *Front. Biosci.* **3**, D570–D603 (1998).
5. Roca, A. I. & Cox, M. M. RecA protein: structure, function, and role in recombinational DNA repair. *Prog. Nucleic Acid Res. Mol. Biol.* **56**, 129–223 (1997).
6. Yu, X., Jacobs, S. A., West, S. C., Ogawa, T. & Egelman, E. H. Domain structure and dynamics in the helical filaments formed by RecA and Rad51 on DNA. *Proc. Natl Acad. Sci. USA* **98**, 8419–8424 (2001).
7. Bishop, D. K., Park, D., Xu, L. & Kleckner, N. DMC1: a meiosis-specific yeast homolog of *E. coli recA* required for recombination, synaptonemal complex formation, and cell cycle progression. *Cell* **69**, 439–456 (1992).
8. Shinohara, A. *et al.* Cloning of human, mouse and fission yeast recombination genes homologous to

9. Lydall, D., Nikolsky, Y., Bishop, D. K. & Weinert, T. A meiotic recombination checkpoint controlled by mitotic checkpoint genes. *Nature* 383, 840–843 (1996).

10. Yoshida, K. *et al.* The mouse RecA-like gene Dmc1 is required for homologous chromosome synapsis during meiosis. *Mol. Cell* 1, 707–718 (1998).

11. Pittman, D. L. *et al.* Meiotic prophase arrest with failure of chromosome synapsis in mice deficient for Dmc1, a germline-specific RecA homolog. *Mol. Cell* 1, 697–705 (1998).

12. Li, Z., Golub, E. I., Gupta, R. & Radding, C. M. Recombination activities of HsDmc1 protein, the meiotic human homolog of RecA protein. *Proc. Natl Acad. Sci. USA* 94, 11221–11226 (1997).

13. Masson, J. Y. *et al.* The meiosis-specific recombinase hDmc1 forms ring structures and interacts with hRad51. *EMBO J.* 18, 6552–6560 (1999).

14. Hong, E. L., Shinohara, A. & Bishop, D. K. *Saccharomyces cerevisiae* Dmc1 protein promotes renaturation of single-strand DNA (ssDNA) and assimilation of ssDNA into homologous super-coiled duplex DNA. *J. Biol. Chem.* 276, 41906–41912 (2001).

15. Shinohara, A., Ogawa, H. & Ogawa, T. Rad51 protein involved in repair and recombination in *S. cerevisiae* is a RecA-like protein. *Cell* 69, 457–470 (1992).

16. Passy, S. I. *et al.* Human Dmc1 protein binds DNA as an octameric ring. *Proc. Natl Acad. Sci. USA* 96, 10684–10688 (1999).

17. Gupta, R. C., Golub, E., Bi, B. & Radding, C. M. The synaptic activity of HsDmc1, a human recombination protein specific to meiosis. *Proc. Natl Acad. Sci. USA* 98, 8433–8439 (2001).

18. Sigurdsson, S., Trujillo, K., Song, B., Stratton, S. & Sung, P. Basis for avid homologous DNA strand exchange by human Rad51 and RPA. *J. Biol. Chem.* 276, 8798–8806 (2001).

19. Van Komen, S., Petukhova, G., Sigurdsson, S. & Sung, P. Functional crosstalk among Rad51, Rad54, and RPA in heteroduplex DNA joint formation. *J. Biol. Chem.* 277, 43578–43587 (2002).

20. Eggler, A. L., Inman, R. B. & Cox, M. M. The Rad51-dependent pairing of long DNA substrates is stabilized by replication protein A. *J. Biol. Chem.* 277, 39280–39288 (2002).

21. Zickler, D. & Kleckner, N. Meiotic chromosomes: integrating structure and function. *Annu. Rev. Genet.* 33, 603–754 (1999).

22. Henricksen, L. A., Umbricht, C. B. & Wold, M. S. Recombinant replication protein A: expression, complex formation, and functional characterization. *J. Biol. Chem.* 269, 11121–11132 (1994).

23. Sigurdsson, S., Van Komen, S., Petukhova, G. & Sung, P. Homologous DNA pairing by human recombination factors Rad51 and Rad54. *J. Biol. Chem.* 277, 42790–42794 (2002).

24. Sung, P. & Robberson, D. L. DNA strand exchange mediated by a RAD51-ssDNA nucleoprotein filament with polarity opposite to that of RecA. *Cell* 82, 453–461 (1995).

25. Crowther, R. A., Henderson, R. & Smith, J. M. MRC image processing programs. *J. Struct. Biol.* 116, 9–16 (1996).

Functional Dissection of Transcription Factor ZBRK1 Reveals Zinc Fingers with Dual Roles in DNA-binding and BRCA1-dependent Transcriptional Repression*

Wei Tan‡, Lei Zheng‡, Wen-Hwa Lee§, and Thomas G. Boyer‡¶

From the ‡Department of Molecular Medicine and Institute of Biotechnology, University of Texas Health Science Center, San Antonio, Texas 78245-3207 and the §Department of Biological Chemistry, University of California, Irvine, California 92697-1700

The breast- and ovarian-specific tumor suppressor BRCA1 has been implicated in both activation and repression of gene transcription by virtue of its direct interaction with sequence-specific DNA-binding transcription factors. However, the mechanistic basis by which BRCA1 mediates the transcriptional activity of these regulatory proteins remains largely unknown. To clarify this issue, we have examined the functional interaction between BRCA1 and ZBRK1, a BRCA1-dependent KRAB eight zinc finger transcriptional repressor. We report here the identification and molecular characterization of a portable BRCA1-dependent transcriptional repression domain within ZBRK1 composed of zinc fingers 5–8 along with sequences in the unique ZBRK1 C terminus. This C-terminal repression domain functions in a BRCA1-, histone deacetylase-, and promoter-specific manner and is thus functionally distinguishable from the N-terminal KRAB repression domain in ZBRK1, which exhibits no BRCA1 dependence and broad promoter specificity. Significantly, we also find that the BRCA1-dependent transcriptional repression domain on ZBRK1 includes elements that modulate its sequence-specific DNA binding activity. These findings thus reveal the presence within ZBRK1 of functionally bipartite zinc fingers with dual roles in sequence-specific DNA-binding and BRCA1-dependent transcriptional repression. We discuss the implications of these findings for the role of BRCA1 as ZBRK1 co-repressor.

Germ line inactivation of the gene encoding BRCA1 confers a cumulative lifetime risk of female breast and ovarian cancer (1–3). Although the mechanistic basis for its tissue- and gender-specific tumor suppressor activity remains poorly defined, BRCA1 nonetheless fulfills a broad function in the maintenance of global genome stability (4–10). The underlying basis for this caretaker activity likely derives from the role of BRCA1 as a conduit in the cellular DNA damage response, wherein it serves to couple DNA damage-induced signals to downstream

responses including DNA damage repair and cell cycle checkpoint activation (6, 7, 11–21). Several potentially overlapping cellular activities have been ascribed to BRCA1, each of which could underlie its ability to control signal output. For example, BRCA1 has been implicated in chromatin remodeling, ubiquitinylation, recombination, and transcriptional regulation (6, 22–28). The extent to which these pleiotropic activities contribute to the caretaker function of BRCA1 is presently unknown; however, the fact that each of these BRCA1-associated activities are similarly abrogated by cancer-predisposing BRCA1 missense mutations suggests a strong correlative link between their discharge and BRCA1-mediated tumor suppression.

With respect to its role in transcription control, BRCA1 has been implicated in both activation and repression of genes linked to a variety of biological processes, including cell growth control and DNA replication and repair (21, 29–31). Thus, by virtue of its transcriptional regulatory activity, BRCA1 could influence cellular responses downstream of DNA damage signals, and this activity could contribute to its caretaker function.

The precise role of BRCA1 in gene-specific transcription control has yet to be definitively established. Because it exhibits no sequence-specific DNA binding activity, it seems likely that BRCA1 is targeted to specific genes through its functional interaction with sequence-specific DNA-binding transcription factors. Direct evidence to support this hypothesis has come from the identification of multiple DNA-binding transcription factors with which BRCA1 has been shown to physically interact and functionally synergize, including p53, c-Myc, estrogen receptor α, androgen receptor, OCT-1, NF-YA, and ZBRK1 (32–40). However, the underlying mechanism by which BRCA1 mediates the transcriptional stimulatory or repressive effects of these regulatory proteins has not been established.

We have been studying the functional interaction between BRCA1 and the transcriptional repressor ZBRK1 as a model system to understand the mechanistic basis by which BRCA1 mediates sequence-specific transcription control. Initially identified by virtue of its physical interaction with BRCA1, ZBRK1 (Zinc finger and BRCA1-interacting protein with a KRAB domain 1) is a member of the Kruppel-associated box-zinc finger protein (KRAB-ZFP) family of transcriptional repressors (39, 41). Typically, KRAB-ZFPs bind to their corresponding target genes through tandem C-terminal C_2H_2 zinc fingers and repress transcription through an N-terminal KRAB domain, which silences gene expression through the indirect recruitment of histone deacetylases, histone methyltransferases, and heterochromatin proteins (41–47). Like other KRAB-ZFPs, ZBRK1 harbors an N-terminal KRAB domain. However, ZBRK1 is atypical among KRAB-ZFPs due to the fact that it harbors 8 central C_2H_2 zinc fingers and a unique C terminus

that is absent among the larger family of KRAB-ZFPs.

Through its 8 central zinc fingers, ZBRK1 binds to a compositionally flexible 15-bp DNA sequence, GGG*xxx*CAG*xxx*TTT (where *x* is any nucleotide) (39). A search for potential ZBRK1 DNA-binding sites in existing genes led to intron 3 of GADD45a, a functionally important DNA damage-response effector known to be regulated transcriptionally by BRCA1 (21, 32, 39). Functional analysis revealed that ZBRK1 represses *GADD45a* gene transcription through its intron 3 DNA-binding site in a BRCA1-dependent manner, thus revealing BRCA1 to be a ZBRK1 co-repressor (39). Significantly, familial breast cancer-derived mutants of BRCA1 that disrupt its interaction with ZBRK1 abrogate its co-repressor activity, suggesting that its co-repressor function may be important for the tumor suppressor properties of BRCA1 (39). The regulation of *GADD45a* gene transcription is likely to be complex and controlled coordinately by ZBRK1 and BRCA1 in concert with other trans-acting factors, including p53, OCT1, and NF-YA, that function through cis-acting sequences present in the *GADD45a* promoter and intron 3 regions (21, 32, 39, 48, 49).

In addition to *GADD45a*, potential ZBRK1-binding sites have been identified in other DNA damage-response genes that are also regulated by BRCA1, including p21, Bax, and GADD153 (39). This observation suggests a potentially broader role for BRCA1 and ZBRK1 in the coordinate transcriptional regulation of diverse DNA damage-response genes. To begin to explore the mechanism by which BRCA1 mediates sequence-specific transcriptional repression through ZBRK1, we have pursued in greater depth the physical and functional interaction between these two proteins. We report here the identification and molecular characterization of a portable BRCA1-dependent transcriptional repression domain within ZBRK1 composed of zinc fingers 5–8 along with sequences in the unique ZBRK1 C terminus. This C-terminal repression domain functions in a BRCA1-, histone deacetylase (HDAC)-,[1] and promoter-specific manner and is thus functionally distinguishable from the N-terminal KRAB repression domain in ZBRK1, which exhibits no BRCA1 dependence and broad promoter specificity. Significantly, we also find that the BRCA1-dependent C-terminal transcriptional repression domain within ZBRK1 is composed of elements that modulate sequence-specific DNA-binding by zinc fingers 1–4. These findings thus reveal an unanticipated dual function for the ZBRK1 zinc fingers in DNA binding and transcriptional repression, and further shed new light on the mechanistic role of BRCA1 in sequence-specific transcriptional control.

EXPERIMENTAL PROCEDURES
Plasmid Construction and Mutagenesis

Expression Plasmids—pMAL-C2-TEV-ZBRK1 ΔK for expressing MBP-ZBRK1 ΔK in *Escherichia coli* was derived from pGEPK3-ZBRK1 ΔK, which is a derivative of pCNF-ZBRK1 ΔK (39). Briefly, a BamHI-XhoI fragment carrying ZBRK1 cDNA sequences encoding ZBRK1 amino acids 144–532 (lacking the N-terminal KRAB domain) was subcloned into the BamHI and XhoI sites of pMAL-C2-TEV (provided by Dr. P. Renee Yew), thereby generating a translational fusion of MBP and ZBRK1 ΔK. C-terminal truncation mutants of MBP-ZBRK1 ΔK bearing stepwise deletions of individual ZBRK1 zinc fingers were expressed from pMAL-C2-TEV-ZBRK1 ΔK deletion derivatives, each of which was constructed by PCR-based subcloning. Briefly, sequences encoding ZBRK1 ΔK within pMAL-C2-TEV-ZBRK1 ΔK were liberated as a BamHI-HindIII fragment and replaced with corresponding PCR-

generated ZBRK1 deletion fragments using a common upstream primer corresponding to MBP sequences and unique downstream primers within the C terminus of each zinc finger (defined here as the seventh amino acid residue C-terminal to the last histidine residue of each C_2H_2 zinc finger). Individual MBP-ZBRK1 ΔK deletion derivatives encode the following ZBRK1 amino acids (aa): MBP-ZBRK1 ΔK 8ZF (aa 144–431); 7ZF (aa 144–403); 6ZF (aa 144–377); 5ZF (aa 144–347); 4ZF (aa 144–319); 3ZF (aa 144–291); 2ZF (aa 144–263); and 1ZF (aa 144–235). Individual MBP-ZBRK1 ΔK broken finger (BF) mutants were generated by PCR-based site-directed mutagenesis of pMAL-C2-TEV-ZBRK1 ΔK using the QuickChange II site-directed mutagenesis kit following the manufacturer's recommendations (Stratagene, La Jolla, CA). Each broken finger mutant bears a histidine (CAT codon) to asparagine (aaT codon) substitution mutation at the first of the two conserved histidine residues within the targeted C_2H_2 zinc finger.

ZBRK1 5ZFC was expressed as a GAL4 DNA-binding domain fusion in mammalian cells from the plasmid GAL4-ZBRK1 5ZFC, constructed by subcloning a PCR-amplified ZBRK1 cDNA fragment encoding amino acids 319–532 (encompassing zinc finger 5 through the C terminus) into the SalI and HindIII sites of pM (Clontech, Palo Alto, CA). N- and C-terminal truncation derivatives of GAL4-ZBRK1 5ZFC bearing stepwise deletions of individual zinc fingers and C-terminal sequences, respectively, were generated by PCR-based subcloning. Briefly, the SalI-HindIII fragment within GAL4-ZBRK1 5ZFC encoding ZBRK1 5ZFC was replaced with corresponding PCR-generated ZBRK1 deletion fragments. Individual GAL4-ZBRK1 5ZFC deletion derivatives encode the following ZBRK1 amino acids (aa): GAL4-ZBRK1 6ZFC (aa 347–532); 7ZFC (aa 375–532); 8ZFC (aa 403–532); C (aa 431–532); GAL4-ZBRK1 5ZFC Δ1 (aa 319–523); 5ZFC Δ2 (aa 319–503); and 5ZFC Δ3 (aa 319–483). Broken finger derivatives of GAL4-ZBRK1 5ZFC were generated by PCR amplification of ZBRK1 sequences encoding amino acids 319–532 from individual pMAL-C2-TEV ZBRK1 ΔK BF mutants and subsequent replacement of the SalI-HindIII wild-type ZBRK1 fragment in GAL4-ZBRK1 5ZFC.

ZBRK1 5ZFC and its truncation and broken finger derivatives were expressed in yeast as GAL4 activation domain fusions using pGADT7 (Clontech, Palo Alto, CA). Briefly, ZBRK1 5ZFC and its truncation (6ZFC, 7ZFC, 8ZFC, 0ZFC, 5ZFC Δ1, 5ZFC Δ2, and 5ZFC Δ3) and broken finger (BF5, BF6, BF7, and BF8) derivatives were excised as BamHI-blunted SalI fragments from GAL4-ZBRK1 5ZFC and its corresponding derivative plasmids, and subcloned into the BamHI and blunted XhoI sites in pGADT7. A BRCA1 cDNA fragment (encoding amino acids 341–748) encompassing the ZBRK1-binding domain (39) was PCR-amplified and subcloned into the EcoRI and SalI sites of pGBKT7, thereby generating a translational fusion of the GAL4 DNA-binding domain with BRCA1 amino acids 341–748 in the plasmid pGBKT7-BRCA1.
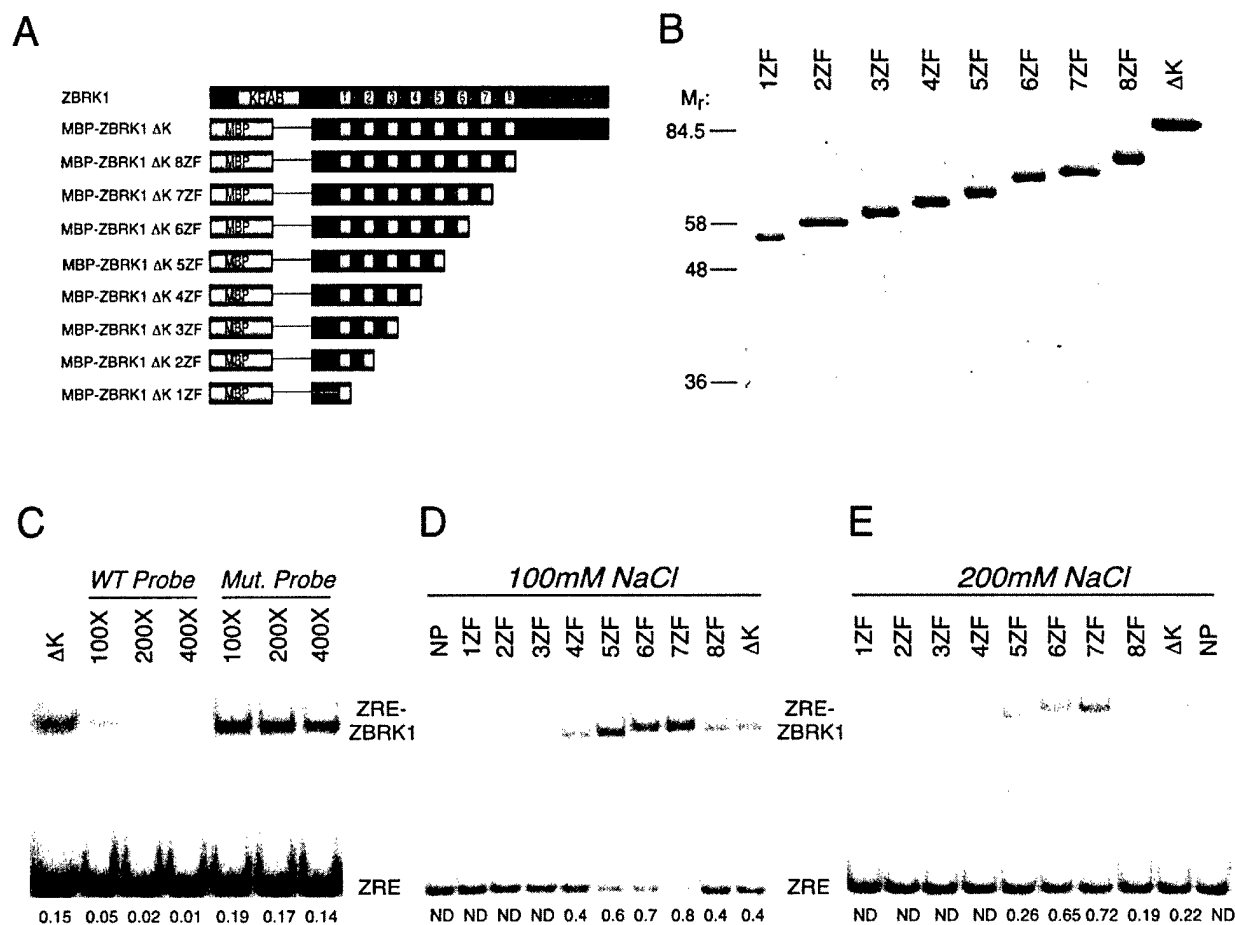
The ZBRK1 KRAB domain was expressed as a GAL4 DNA-binding domain fusion in mammalian cells from GAL4-ZBRK1 KRAB, constructed by subcloning a PCR-amplified ZBRK1 cDNA fragment encoding amino acids 1–85 into the BamHI and blunted XbaI sites of pM2 (50). All PCR-based subcloning was performed using *Pfu* DNA polymerase (Stratagene, La Jolla, CA), and the integrity of individual deletion and substitution mutations was confirmed by DNA sequence analysis.

Reporter Plasmids—pG₅TK-Luc carrying five copies of the GAL4 DNA-binding site upstream of the herpes simplex virus thymidine kinase (TK) promoter (sequences corresponding to −105 to +51, where +1 is the transcription start site) driving expression of the gene encoding firefly luciferase was constructed by replacing a HindIII-BglII fragment from pSBS-GAL-TK-Luc (provided by Dr. Tony Ip) with a HindIII-BglII fragment from pG₅TK-CAT (provided by Dr. P. Renee Yew), thus positioning five copies of the GAL4 DNA-binding site and the TK promoter upstream of the firefly luciferase gene. pG₅SV40-Luc carrying five GAL4 DNA-binding sites upstream of the SV40 promoter driving expression of the firefly luciferase gene has been described previously (39). pG₅SNRPN-Luc (provided by Dr. Paul A. Wade) carries five GAL4 DNA-binding sites upstream of the human small nuclear ribonucleoprotein N promoter driving expression of the firefly luciferase gene (51).

Recombinant Protein Expression and Purification

MBP-ZBRK1 fusion proteins were expressed in and purified from *E. coli* strain BL21 Star (DE3) pLysS (Invitrogen). Briefly, cells were grown at 37 °C to an A_{600} of 0.6. Isopropyl-1-thio-β-D-galactopyranoside was added to a final concentration 0.3 mM, and the cells were transferred to 25 °C for another 3.5 h. Cells were pelleted, washed once with phosphate-buffered saline, and then resuspended in MBP binding buffer (25 mM Tris-HCl, pH 7.5; 1 mM EDTA; 200 mM NaCl; 20 μM

---

[1] The abbreviations used are: HDAC, histone deacetylase; EMSA, electrophoretic mobility shift assay; MEFs, mouse embryo fibroblasts; aa, amino acids; MBP, maltose-binding protein; PMSF, phenylmethylsulfonyl fluoride; TSA, trichostatin A; ZRE, ZBRK1-response element; BF, broken finger; TK, thymidine kinase; WT, wild type; Mut., mutant; HSV, herpes simplex virus.

FIG. 1. **Identification of DNA binding determinants on ZBRK1.** *A*, schematic representation of ZBRK1 (the KRAB domain and numbered zinc fingers are indicated), MBP-ZBRK1 ΔK, and MBP-ZBRK1 ΔK truncation derivatives. *B*, purified MBP-ZBRK1 ΔK and its corresponding truncation derivatives as indicated were resolved by SDS-10% PAGE and visualized by Coomassie Blue staining. Molecular weight marker positions (M_r) are indicated. *C*, competition EMSA. EMSA was performed using a ^{32}P-labeled double-stranded oligonucleotide probe corresponding to a wild-type consensus ZRE and purified MBP-ZBRK1 ΔK (*1st lane*). A 100-, 200-, or 400-fold molar excess of an unlabeled wild-type (*WT*) ZRE probe (*2nd to 4th lanes*) or mutated (*Mut.*) ZRE probe corresponding to a double-stranded oligonucleotide identical in length but different in sequence (*5th to 7th lanes*) was added to the binding reaction as indicated. The positions of the unbound ZRE oligonucleotide probe (*ZRE*) and the ZRE·MBP-ZBRK1 ΔK nucleoprotein complex (*ZRE-ZBRK1*) are indicated. For each EMSA reaction, the proportional fraction of ZRE probe bound by MBP-ZBRK1 ΔK is indicated *below* each lane and was determined by dividing the number of radioactive counts in the bound probe by the number of radioactive counts in the bound plus the unbound probe. *D* and *E*, sequence-specific DNA binding activity of MBP-ZBRK1 ΔK and its corresponding truncation derivatives. EMSA was performed using the consensus ZRE probe and 50 ng of either MBP-ZBRK1 ΔK or each of its corresponding deletion derivatives as indicated. *NP* indicates no protein added to the EMSA reaction. The positions of the unbound ZRE oligonucleotide probe (*ZRE*) and the ZRE·MBP-ZBRK1 ΔK nucleoprotein complex (*ZRE-ZBRK1*) are indicated. DNA-binding reactions were performed in 100 mM NaCl (*D*) or 200 mM NaCl (*E*). For each EMSA reaction, the proportional fraction of ZRE probe bound by MBP-ZBRK1 ΔK or its truncation derivatives is indicated *below* each lane and was determined by dividing the number of radioactive counts in the bound probe by the number of radioactive counts in the bound plus the unbound probe. *ND*, not detectable.

ZnCl$_2$; and 10 mM β-mercaptoethanol) supplemented with protease inhibitors (aprotinin 0.4 μg/ml; chymostatin 0.5 μg/ml; leupeptin 0.5 μg/ml; pepstatin 0.5 μg/ml; PMSF 0.5 mM; and benzamidine-HCl 0.5 mM). Resuspended cells were frozen and thawed one time, followed by sonication (3 times for 1 min) and clarification by centrifugation at 30,000 × *g* for 30 min. MBP-ZBRK1 fusion proteins were purified from clarified lysates by affinity chromatography on amylose resin (New England Biolabs, Beverly, MA). Briefly, clarified lysates were incubated with amylose resin in batch for 1 h at 4 °C, washed 3 times with MBP binding buffer, and then eluted with MBP binding buffer containing 0.5% maltose for 30 min at 4 °C. Purified proteins (estimated to be >95% homogeneous by SDS-PAGE and subsequent visualization by Coomassie Blue staining) were dialyzed for 1 h at 4 °C against EMSA storage buffer (25 mM Tris-HCl, pH 7.5; 100 mM NaCl; 20 μM ZnCl$_2$; 10% glycerol; 10 mM β-mercaptoethanol; and 0.5 mM PMSF) before long term storage at −80 °C.
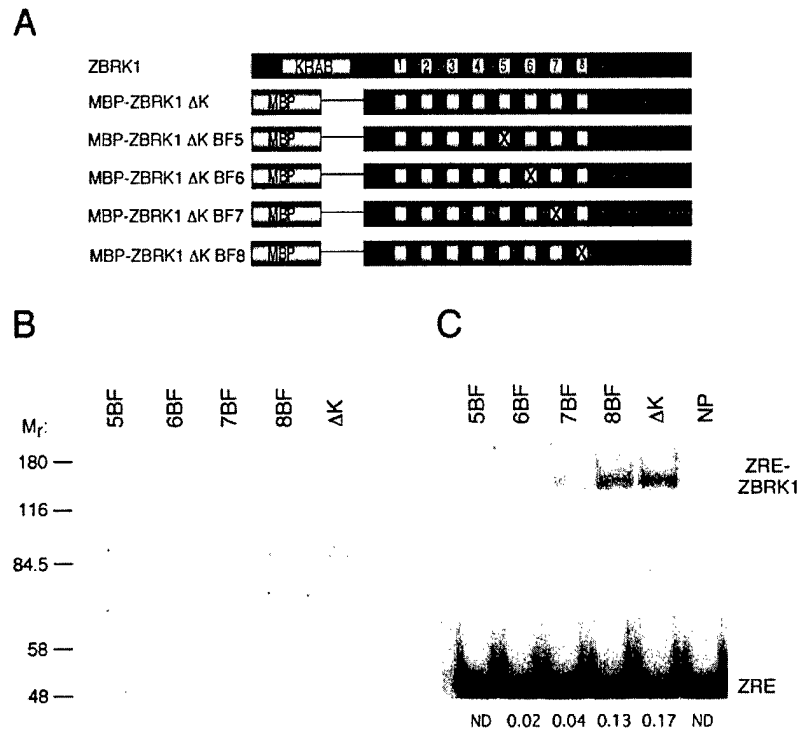
Electrophretic Mobility Shift Assay (EMSA)

For EMSA, the ZRE probe was obtained by annealing two complementary oligonucleotides corresponding in sequence to the consensus ZBRK1 DNA-binding site: 5'-GATCCACGGGACGCAGGTGTTTTGT-GCCG-3' and 5'-GATCCGGCACAAAACACCTGCGTCCCGTG-3' (39). Mutant (Mut) probe was obtained by annealing two oligonucleotides,

5'-GATCCACCTCACGTTCGTGCACTGTGCCG-3' and 5'-GATCCG-GCACAGTGCACGAACGTGAGGTG-3' (39). Each of these double-stranded probes carried overhanging ends, which were filled in with [α-^{32}P]dCTP by Klenow enzyme. In each reaction, purified MBP-ZBRK1 fusion proteins (50 ng) were incubated with 6000 cpm of a ^{32}P-labeled double-stranded oligonucleotide probe in 30 μl of EMSA binding buffer (25 mM Tris-HCl pH 7.5; 20 μM ZnCl$_2$; 12.5% glycerol; 0.5 mM PMSF; and a variable concentration of NaCl as indicated). Following 30 min of incubation at room temperature, reaction mixtures were loaded onto a 5% non-denaturing polyacrylamide gel and electrophoresed at 200 V for 2 h at 4 °C in 0.5× TBE. Dried gels were subjected to PhosphorImager analysis (Amersham Biosciences).

Cell Culture, Transfections, and Reporter Assays

Brca1−/−, p53−/− (*Brca1−/−*), and p53−/− (*Brca1+/+*) mouse embryo fibroblasts (MEFs) (39) and U2OS human osteosarcoma cells were cultured in Dulbecco's modified Eagle's medium (Invitrogen) supplemented with 10% fetal bovine serum (Hyclone, Logan, UT). *Brca1+/+*, *Brca1−/−*, and U2OS cells were transfected at 60% confluency using Effectene reagent (Qiagen, Valencia, CA), and the expression and reporter plasmids are indicated in each figure. Each transfection also included an internal control plasmid, pCH110 (40), expressing β-galactosidase under control of the SV40 promoter. Forty-eight hours

FIG. 2. **Identification of DNA-binding determinants on ZBRK1.** *A*, schematic representation of ZBRK1, MBP-ZBRK1 ΔK, and MBP-ZBRK1 ΔK broken finger derivatives. *B*, purified MBP-ZBRK1 ΔK and its corresponding broken finger derivatives as indicated were resolved by SDS-10% PAGE and visualized by Coomassie Blue staining. Molecular weight marker positions (M_r) are indicated. *C*, sequence-specific DNA binding activity of MBP-ZBRK1 ΔK and its corresponding broken finger derivatives. EMSA was performed using the consensus ZRE probe and 50 ng of either MBP-ZBRK1 ΔK or each of its corresponding broken finger derivatives as indicated. *NP* indicates no protein added to the EMSA reaction. The positions of the unbound ZRE oligonucleotide probe (*ZRE*) and the ZRE·MBP-ZBRK1 ΔK nucleoprotein complex (*ZRE-ZBRK1*) are indicated. DNA-binding reactions were performed in 200 mM NaCl. For each EMSA reaction, the proportional fraction of ZRE probe bound by MBP-ZBRK1 ΔK or its broken finger derivatives is indicated *below* each lane and was determined by dividing the number of radioactive counts in the bound probe by the number of radioactive counts in the bound plus the unbound probe. *ND*, not detectable.

post-transfection, cells were harvested and lysed in Reporter Lysis buffer (Promega, Madison, WI). Transfected cell lysates (20 μl) were analyzed for luciferase activity using the luciferase assay system (Promega, Madison, WI) and for β-galactosidase activity using the Galacto-light Plus Chemiluminescent Reporter Assay (BD Biosciences). Each transfection was repeated a minimum of 3 times in duplicate.

Yeast Two-hybrid Interaction Assay

pGADT7-ZBRK1 5ZFC and its truncation (6ZFC, 7ZFC, 8ZFC, 0ZFC, 5ZFC Δ1, 5ZFC Δ2, and 5ZFC Δ3) and broken finger (BF5, BF6, BF7, and BF8) derivatives were individually co-transformed along with pG-BKT7-BRCA1 (expressing BRCA1 amino acids 341–748) into the yeast strain Y187 (BD Biosciences/Clontech). After selection, colonies were expanded in liquid culture for assay of β-galactosidase activity following previously established procedures (39).

Transient Expression Analysis

Steady-state levels of GAL4-ZBRK1 5ZFC protein and its truncation and substitution derivatives were comparatively analyzed by immunoblot analysis of transfected whole cell extracts in order to verify equivalent levels of ectopic protein expression. Briefly, U2OS cells transfected with GAL4-ZBRK1 5ZFC, truncation mutants GAL4-ZBRK1 6ZF, 7ZFC, 8ZFC, 0ZFC, 5ZFC Δ1, 5ZFC Δ2, and 5ZFC Δ3, and broken finger mutants GAL4-ZBRK1 5ZFC BF5, BF6, BF7, and BF8 were lysed in Laemmli sample buffer, resolved by SDS-10% PAGE, and subjected to immunoblot analysis using an antibody directed against the GAL4 DNA-binding domain (sc-510, Santa Cruz Biotechnology, Santa Cruz, CA) and, as an internal control protein, the p89 subunit of TFIIH (sc-293, Santa Cruz Biotechnology, Santa Cruz, CA). Immunodetection was performed using ECL Western blotting detection reagents (Amersham Biosciences).

RESULTS

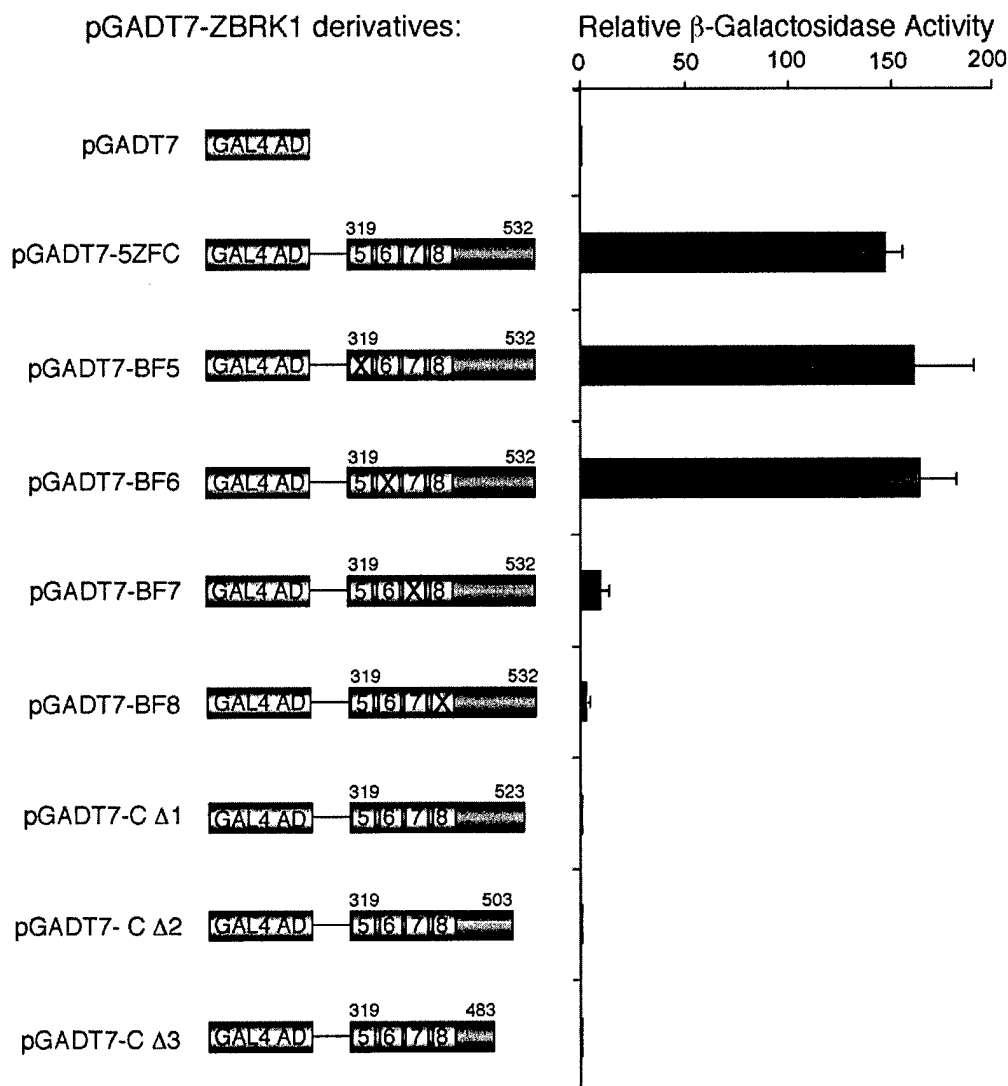*Identification of DNA-binding Determinants on ZBRK1*—Previously, we demonstrated a strict requirement for BRCA1 in ZBRK1 repression. Specifically, we showed that ZBRK1 repression function was similarly abrogated by genetic ablation of *Brca1* or by deletion of the BRCA1-binding domain on ZBRK1 (39). The BRCA1-binding domain on ZBRK1 includes the last four of eight ZBRK1 zinc fingers (zinc fingers 5–8) along with the ZBRK1 C terminus (39). Whether and how this zinc finger domain contributes to the sequence-specific DNA binding activity of ZBRK1, however, is presently unknown.

Because the specification of individual zinc fingers required to bind to DNA and/or BRCA1 could illuminate the underlying mechanism(s) by which BRCA1 mediates ZBRK1 repression, we initially sought to establish both the number and identity of the ZBRK1 zinc fingers required to bind DNA and BRCA1.

With respect to DNA binding, we showed previously (39) that the eight central ZBRK1 zinc fingers collectively recognize a 15-bp consensus sequence, GGGxxxCAGxxxTTT. Based on the observation that one C_2H_2 zinc finger can bind to ~3 bp of DNA (52–54), only five of the eight ZBRK1 zinc fingers would be predicted to bind to its 15-bp consensus sequence. To test this prediction, we analyzed a panel of ZBRK1 zinc finger deletion derivatives for their respective abilities to bind to the consensus ZBRK1 DNA-binding site in an EMSA.

To this end, we expressed ZBRK1 as a maltose-binding protein (MBP) chimera in *E. coli*, which permitted the purification of otherwise insoluble ZBRK1 protein. Full-length MBP-ZBRK1 is expressed poorly, whereas MBP-ZBRK1 ΔK (a deletion derivative lacking the N-terminal 143 amino acids of the 532-amino acid full-length ZBRK1 protein) is abundantly expressed. ZBRK1 ΔK lacks the N-terminal KRAB domain but retains the ZBRK1 zinc fingers and the C terminus, elements that are required for binding to both DNA and/or BRCA1 (Fig. 1, *A* and *B*). We have therefore utilized this recombinant ZBRK1 derivative as the background into which truncation and substitution mutations have been introduced for purposes of DNA binding assays.

In an EMSA, MBP-ZBRK1 ΔK produced a discrete nucleoprotein complex on a double-stranded oligonucleotide probe corresponding to the consensus ZBRK1-response element (ZRE); a molar excess of unlabeled WT ZRE probe (WT probe), but not a mutant probe (Mut probe), efficiently competed for the formation of this complex, thus establishing sequence-specific DNA binding by MBP-ZBRK1 ΔK in this assay (Fig. 1C). To determine the number and identity of the ZBRK1 zinc fingers required to bind to its consensus sequence, we analyzed a series of C-terminal truncation derivatives bearing stepwise deletions of individual ZBRK1 zinc fingers (Fig. 1, *A* and *B*). In
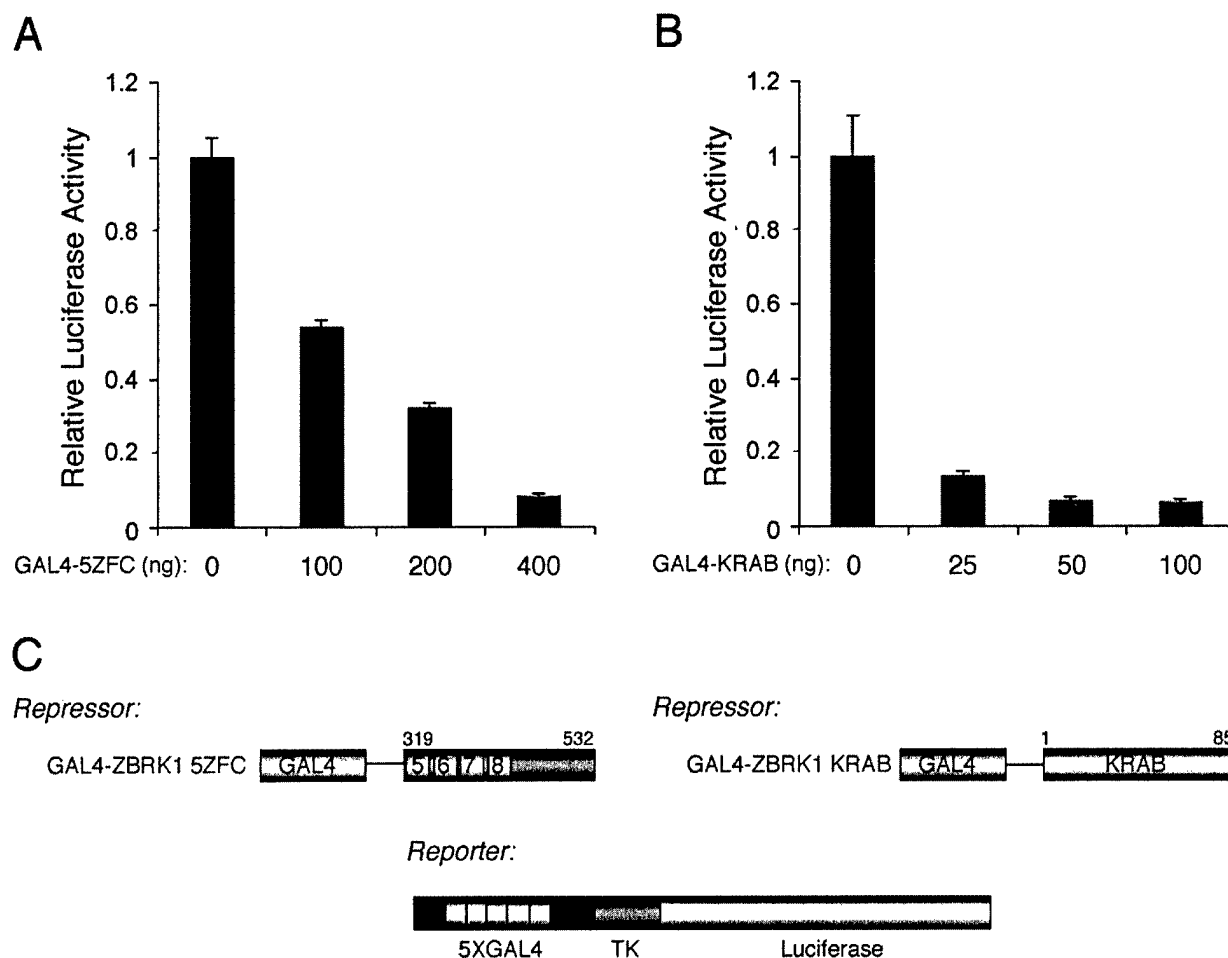
FIG. 3. **Identification of BRCA1-binding determinants on ZBRK1.** The ZBRK1-binding region on BRCA1 (amino acids 341–748) (39), expressed as a GAL4 DNA-binding domain fusion protein (in the plasmid pGBKT7), was tested for interaction with the indicated fragments of ZBRK1 fused to the GAL4 transactivation domain (plasmid pGADT7) in yeast two-hybrid assays. β-Galactosidase activities were quantified as described previously (39). Corresponding β-galactosidase activities obtained with each pGADT7-ZBRK1 5ZFC derivative are expressed relative to that observed with the backbone pGADT7 expression vector alone, which was arbitrarily assigned a value of 1. Values represents the average of three independent assays, each performed in triplicate, and *error bars* represent the mean ± S.D. As a comparative measure of interaction strength, the average β-galactosidase activity obtained with pGBKT7-p53 and pGADT7-Large T antigen was 512 ± 13.5. The validity of two-hybrid interactions observed in these experiments was further substantiated by the following controls. First, we confirmed that the observed β-galacto-sidase activities were dependent upon BRCA1 sequences expressed from the plasmid pGBKT7-BRCA1 by performing a parallel series of interaction assays with individual pGADT7-ZBRK1 5ZFC derivatives and the backbone vector pGBKT7 as a negative control. Second, immunoblot analyses of yeast whole cell extracts confirmed that each of the pGADT7-ZBRK1 5ZFC fusion proteins was expressed at roughly equivalent levels, thus excluding the possibility that differences in β-galactosidase activities derive from difference in fusion protein expression.

100 mM NaCl, truncation of the ZBRK1 C terminus (MBP-ZBRK1 ΔK 8ZF) did not appreciably affect DNA binding relative to intact MBP-ZBRK1 ΔK (Fig. 1D). Interestingly, deletion of the eighth and last ZBRK1 zinc finger along with the C terminus (MBP-ZBRK1 ΔK 7ZF) led to an increase in DNA binding activity, suggesting that ZBRK1 ZF8, and possibly the C terminus, constrains sequence-specific DNA binding mediated by the first seven zinc fingers (Fig. 1D). This effect was exacerbated under more stringent DNA binding conditions (200 mM NaCl) (Fig. 1E). At 100 mM NaCl, stepwise truncation of zinc fingers 7 to 5 led to a slight incremental reduction in sequence-specific DNA binding activity (Fig. 1D). ZBRK1 derivatives bearing less than four zinc fingers failed to bind to DNA, thereby establishing zinc fingers 1–4 as the minimal ZBRK1 DNA-binding domain under these conditions (Fig. 1D). Identical results were observed at 50 mM NaCl (data not

shown). At 200 mM NaCl, zinc fingers 1–5 were required for stable DNA binding, and the inclusion of zinc fingers 6 and 7 incrementally stabilized binding (Fig. 1E).

To examine more rigorously the role of zinc fingers 5–8 in sequence-specific DNA binding by ZBRK1, we examined a set of "broken finger" mutants bearing substitution mutations within each of these zinc fingers. This approach permitted us to assess the individual contribution of each finger within the BRCA1-binding domain to overall DNA binding activity in the context of the eight-fingered ZBRK1 ΔK protein and thereby circumvent potential artifacts arising from analyses of truncation mutants. Each broken finger mutant bears a His-to-Asn substitution mutation at the first of the two conserved His residues within the targeted C_2H_2 zinc finger (Fig. 2, A and B). The relative conservative nature of this substitution eliminates zinc coordination within the targeted finger, thereby disrupting
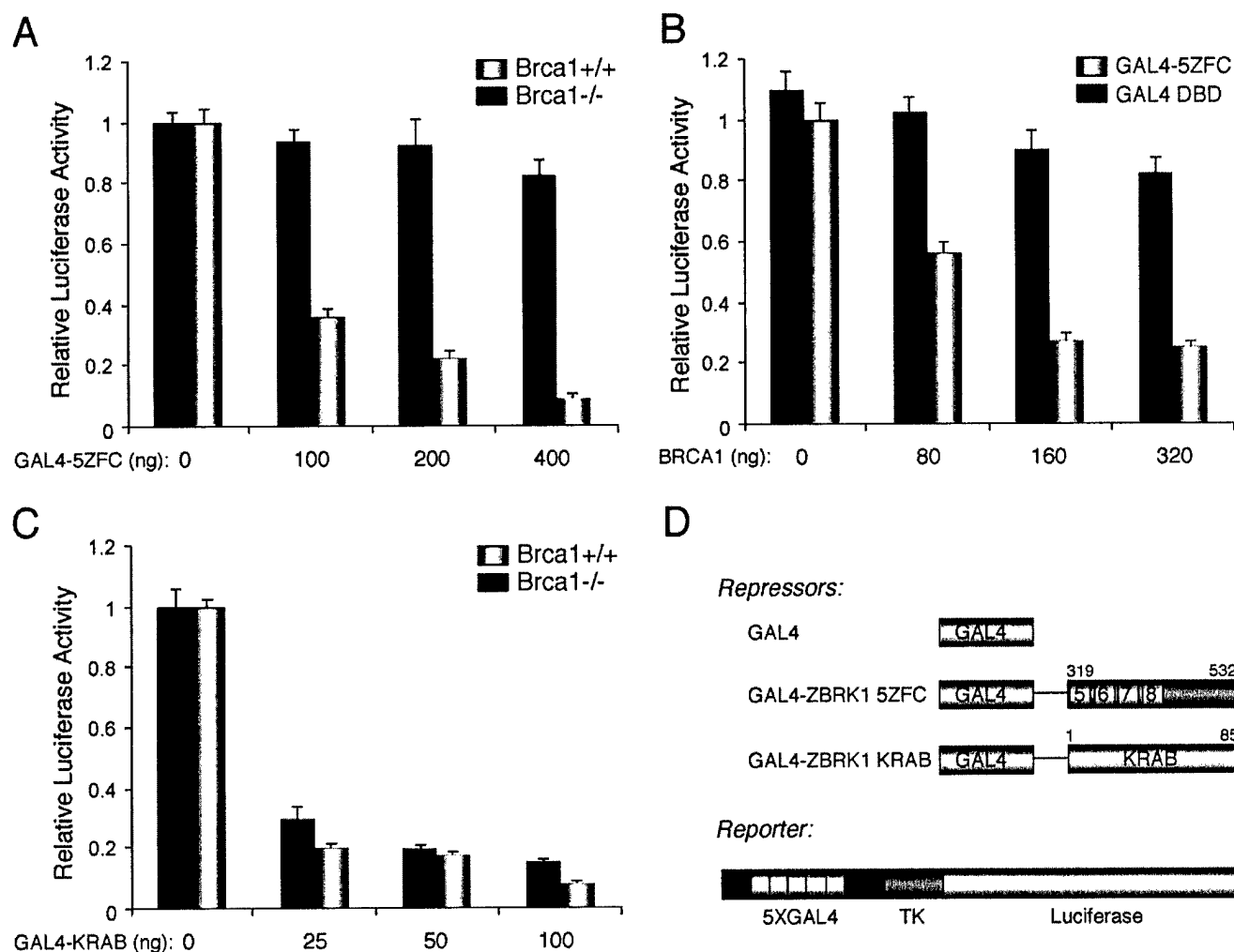
A

GAL4-5ZFC (ng): 0   100   200   400

B

GAL4-KRAB (ng): 0   25   50   100

C

Repressor:

GAL4-ZBRK1 5ZFC

Repressor:

GAL4-ZBRK1 KRAB

Reporter:

5XGAL4   TK   Luciferase

FIG. 4. **ZBRK1 harbors two independent transcriptional repression domains.** *A* and *B*, human U2OS cells were transfected with 30 ng of pG$_5$TK-Luc bearing five copies of the GAL4 DNA-binding site sequence upstream of the TK promoter without or with the indicated nanogram amounts of GAL4-ZBRK1 5ZFC (*A*) or GAL4-KRAB (*B*). In this and all subsequent transfection experiments involving effector plasmid titrations, the total amount of DNA in each transfection was fixed by reciprocal titration of the corresponding backbone expression plasmid. Also, in this and all subsequent transfection experiments, the relative luciferase activity represents the ratio of the luciferase activity obtained in a particular transfection to that obtained in cells transfected with only the reporter and pM (GAL4 DNA-binding domain) expression vectors alone. Luciferase activities were first normalized to β-galactosidase activity obtained by co-transfection of the SV40-β-gal vector (15 ng) as described previously (39). *Error bars* represent the S.D. from the average of at least three independent transfections performed in duplicate. *C*, schematic representation of GAL4-ZBRK1 5ZFC and GAL4-ZBRK1 KRAB chimeras (amino acid sequences fused to the GAL4 DNA-binding domain are indicated *numerically above* each chimera) and the pG$_5$TK-Luc reporter template used in transfection assays.

its local structure with little effect on the integrity of the remainder of the protein (55, 56). Consistent with the results obtained using C-terminal truncation mutants, analysis of individual BF mutants 5–8 revealed zinc finger 5 to be an important ZBRK1 determinant for stable DNA binding, whereas zinc fingers 6 and 7 promote but are not essential for binding (Fig. 2C). Disruption of zinc finger 8 did not appreciably affect the DNA binding activity of MBP-ZBRK1 ΔK, suggesting that zinc finger 8 is largely dispensable for stable association with DNA (Fig. 2C). Furthermore, local disruption of zinc finger 8 did not relieve constraints on the DNA binding activity of MBP-ZBRK1 ΔK, suggesting that the C terminus of ZBRK1 can also mask the inherent DNA binding activity of ZBRK1 zinc fingers 1–7 (Fig. 2C). In summary, the results of DNA-binding analyses delimit the core ZBRK1 DNA-binding domain to zinc fingers 1–4; these zinc fingers are minimally required for stable DNA binding under relatively non-stringent conditions of ionic strength. Zinc finger 5 is a critical and context-dependent determinant of stable binding and represents the extent of the minimal DNA-binding domain under more stringent binding conditions. Zinc fingers 6 and 7, although nonessential, nonetheless further stabilize DNA binding mediated by zinc fingers 1–5. Finally, zinc finger 8 and the C terminus apparently

destabilize the maximum potential DNA binding activity inherent in zinc fingers 1–7.

Identification of BRCA1-binding Determinants on ZBRK1— Next, we sought to establish more precisely the molecular determinants on ZBRK1 required for BRCA1 binding. Previously, we mapped the BRCA1-binding domain on ZBRK1 to encompass a broad region extending from zinc finger 5 through the C terminus (5ZFC) (39). To more narrowly define the BRCA1-binding determinants on ZBRK1, we examined the contribution of individual zinc fingers 5–8 as well as sequences within the ZBRK1 C terminus to BRCA1 binding using a yeast two-hybrid interaction assay. To this end, individual substitution and truncation mutations within ZBRK1 5ZFC were translationally fused to the GAL4 transactivation domain and tested for their respective abilities to bind to the ZBRK1-interaction domain on BRCA1 (amino acids 341–748), translationally fused to the GAL4 DNA-binding domain in yeast (Fig. 3). Corresponding β-galactosidase activities identified critical determinants of BRCA1 interaction on ZBRK1 to include the C terminus as well as zinc fingers 7 and 8 (Fig. 3). Deletion of only 9 amino acids from the C terminus significantly compromised BRCA1 binding, indicating that the unique C terminus on ZBRK1 is required in its entirety for efficient interaction with BRCA1 (Fig. 3). This observation sug-
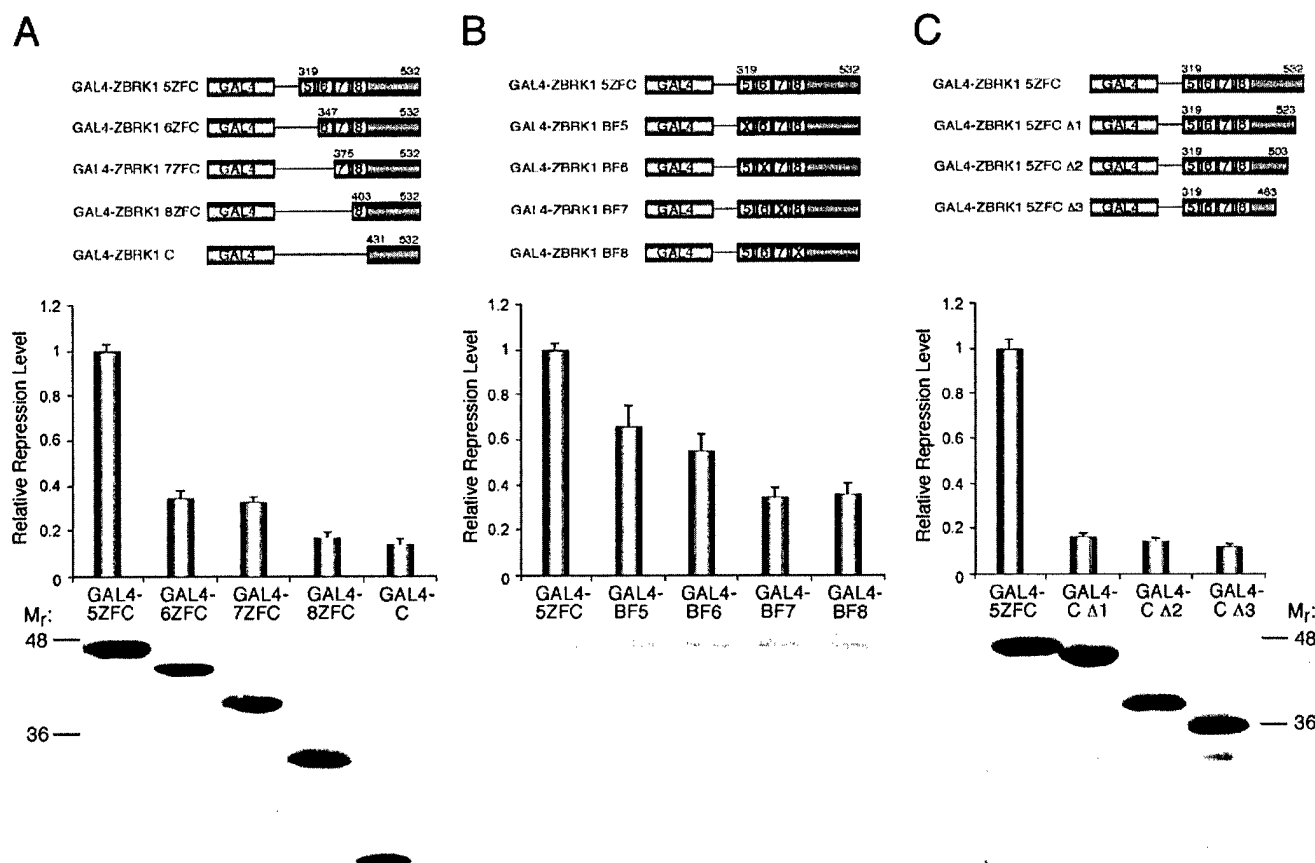
BRCA1-dependent Repression through ZBRK1 Zinc Fingers

A

B

C

D

Fig. 5. **The ZBRK1 5ZFC and KRAB repression domains function in a BRCA1-dependent and BRCA1-independent manner, respectively.** *A, Brca1+/+* and *Brca1−/−* MEF cells (39) as indicated were transfected with 100 ng of pG$_5$TK-LUC without or with the indicated nanogram amounts of GAL4-ZBRK1 5ZFC. *B, Brca1−/−* MEF cells were transfected with 100 ng of pG$_5$TK-Luc and 20 ng of either pM (expressing the GAL4 DNA-binding domain (*DBD*) alone) or GAL4-ZBRK1 5ZFC, respectively, without or with the indicated nanogram amounts of pCS2+-BRCA1 expressing wild-type human BRCA1. *C, Brca1+/+* and *Brca1−/−* MEF cells as indicated were transfected with 100 ng of pG$_5$TK-Luc without or with the indicated nanogram amounts of GAL4-ZBRK1 KRAB. *A–C*, relative luciferase activities were calculated as described in the legend to Fig. 4. *D*, schematic representation of the GAL4 DNA-binding domain, the GAL4-ZBRK1 5ZFC and GAL4-ZBRK1 KRAB chimeras, and the pG$_5$TK-Luc reporter template used in transfection assays.

gests that the overall conformation of the C terminus is likely to be important for BRCA1 interaction. Whereas ZBRK1 zinc fingers 7 and 8 are critical for BRCA1 interaction, zinc fingers 5 and 6 do not appear to contribute to BRCA1 binding (Fig. 3). Taken together, these results indicate that important BRCA1-binding determinants on ZBRK1 include those that also modulate its sequence-specific DNA binding activity in both a positive (zinc finger 7) and negative (zinc finger 8 and the C terminus) manner.

The BRCA1-binding Domain on ZBRK1 Functions as an Autonomous BRCA1-dependent Transcriptional Repression Domain—The fact that BRCA1 contacts ZBRK1 through surfaces that are not essential but nonetheless modulatory with respect to DNA binding suggests several potential mechanisms by which BRCA1 might mediate transcriptional repression by ZBRK1. First, BRCA1 could mediate ZBRK1 repression, at least in part, by modulating its sequence-specific association with DNA. This possibility is currently under investigation. Alternatively, or additionally, BRCA1 could mediate repression by DNA-bound ZBRK1. This possibility is supported by our previous observation that clinically validated missense mutations within the BRCA1 C terminus that do not disrupt its interaction with ZBRK1 nonetheless abrogate its ZBRK1 co-

repressor activity (39). To test this possibility directly, we examined whether the BRCA1-binding domain on ZBRK1 could function as a BRCA1-dependent transcriptional repression domain when tethered to a heterologous DNA-binding domain. This approach permitted us to assess the influence of BRCA1 on the repression function of ZBRK1 independently of any effects that it might have on the DNA binding activity of ZBRK1. Accordingly, we initially tested the ability of ZBRK1 5ZFC (extending from zinc finger 5 to the C terminus) to function as an independent repression domain when linked to the GAL4 DNA-binding domain. GAL4-ZBRK1 5ZFC was transiently expressed in U2OS human osteosarcoma cells, and its influence on transcription from a pG$_5$TK-Luc reporter template bearing five copies of the consensus GAL4 DNA-binding site upstream of the herpes simplex virus (HSV) TK gene promoter was examined. GAL4-ZBRK1 5ZFC conferred greater than 10-fold repression upon reporter gene expression in a dose-dependent manner (Fig. 4A). We also confirmed the presence of a potent KRAB repression domain within the ZBRK1 N terminus by examining its ability repress pG$_5$TK-Luc reporter gene expression when tethered to the GAL4 DNA-binding domain (Fig. 4B). Based on quantitative immunoblot analysis of transfected
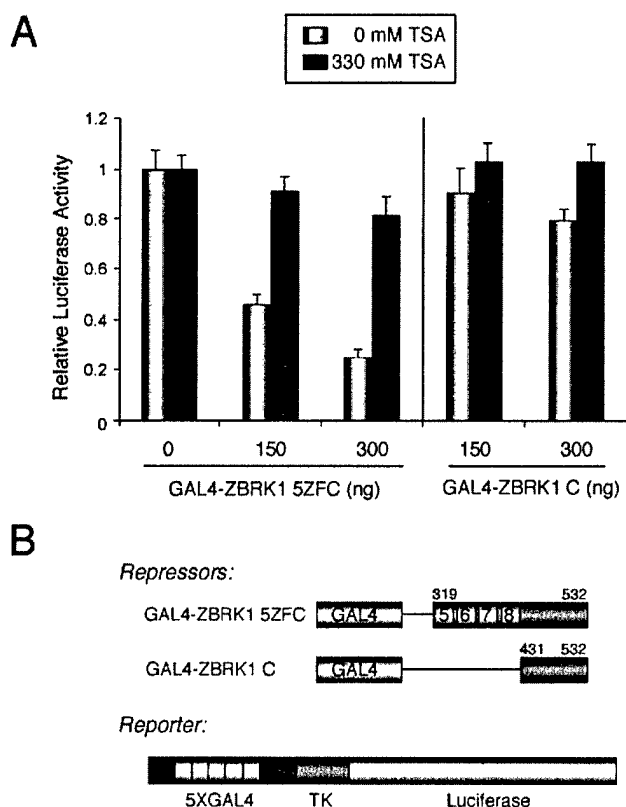
FIG. 6. **Functional analysis of ZBRK1 5ZFC truncation and substitution derivatives.** *A–C*, U2OS cells were transfected with 30 ng of pG$_5$TK-Luc and the following amounts of GAL4-ZBRK1 5ZFC or its indicated derivatives: *A*, 5ZFC, 400 ng; 6ZFC, 7ZFC, 8ZFC, and C, 200 ng; *B*, 5ZFC or its indicated broken finger derivatives, 200 ng; *C*, 5ZFC, 400 ng; Δ1, 200 ng; Δ2, 400 ng; Δ3, 200 ng. In each panel, the relative repression level represents the relative luciferase activity obtained with a particular GAL4-ZBRK1 5ZFC derivative divided by that obtained with GAL4-ZBRK1 5ZFC. Relative luciferase activities were calculated as described in the legend to Fig. 4. In these experiments, the relative luciferase activity observed with GAL4-ZBRK1 5ZFC (three independent transfections performed in duplicate) was as follows: *A*, 0.10 corresponding to 10-fold repression of reporter template activity; *B*, 0.21 corresponding to an approximate 5-fold repression of reporter template activity; *C*, 0.08 corresponding to 12.5-fold repression of reporter template activity. To confirm that GAL4-ZBRK1 5ZFC and its truncation and substitution derivatives are expressed at roughly equivalent levels, lysates from U2OS cells transfected with GAL4-ZBRK1 5ZFC or its derivatives (the same amounts used in functional analysis and indicated above) were resolved by SDS-10% PAGE and subjected to immunoblot analysis using antibodies specific for the GAL4 DNA-binding domain. Molecular weight marker positions (*M*$_r$) are indicated. GAL4-ZBRK1 5ZFC and its derivatives are represented schematically at the *top* of each panel.

cell extracts, the ZBRK1 KRAB domain, on a molar basis, appears to be a stronger transcriptional repression domain than the ZBRK1 BRCA1-binding domain (data not shown). Nonetheless, this result indicates the presence within ZBRK1 of two portable transcriptional repression domains, an N-terminal KRAB domain and a novel C-terminal transcriptional repression domain (5ZFC) that encompasses the BRCA1-binding domain.

To confirm the requirement for BRCA1 in transcriptional repression by ZBRK1 5ZFC, we tested the repression function of GAL4-ZBRK1 5ZFC in *Brca1+/+* and *Brca1−/−* MEF cells. GAL4-ZBRK1 5ZFC conferred up to 10-fold repression in *Brca1+/+* MEFs, whereas little or no repression activity was observed in *Brca1−/−* MEFs (Fig. 5A). Ectopic expression of BRCA1 in *Brca1−/−* MEFs restored ZBRK1 5ZFC-directed transcriptional repression (Fig. 5B), establishing conclusively that BRCA1 mediates repression by DNA-bound ZBRK1 5ZFC. In contrast to ZBRK1 5ZFC, the ZBRK1 KRAB domain repressed transcription equivalently in both *Brca1+/+* and *Brca1−/−* MEFs (Fig. 5C). Thus, the N-terminal KRAB and C-terminal 5ZFC repression domains within ZBRK1 can be distinguished functionally on the basis of their respective requirements for BRCA1.

BRCA1-binding Is Necessary but Not Sufficient for ZBRK1

5ZFC Repression Function—To more narrowly define the boundaries of the BRCA1-dependent 5ZFC repression domain within ZBRK1, we examined a panel of ZBRK1 5ZFC truncation and substitution mutants for their respective repression activities *in vivo*. Relative to the intact 5ZFC domain, deletion or disruption of zinc fingers 5 or 6 individually reduced repression activity by 2–3-fold (Fig. 6, *A* and *B*), whereas individual deletion or disruption of zinc fingers 7 or 8 reduced repression activity by 3–6-fold (Fig. 6, *A* and *B*). These results indicate that zinc fingers 5–8 are all required for the integrity of the 5ZFC repression domain, although zinc fingers 7 and 8 appear to be quantitatively more important. Deletion of only 9 amino acids from the C terminus of ZBRK1 severely compromised the repression function of the 5ZFC domain, indicating that the entire C terminus is likely to be important for 5ZFC repression activity (Fig. 6C). Thus, the 5ZFC repression domain extending from ZBRK1 zinc finger 5 through the C terminus appears to constitute an intact repression domain that cannot be further delimited. This analysis also reveals an imperfect correlation between BRCA1 binding and transcriptional repression by the 5ZFC repression domain. Thus, disruption of ZBRK1 zinc fingers 7 or 8 or truncation of the C terminus severely compromised BRCA1 binding (Fig. 3) and transcriptional repression (Fig. 6). By contrast, disruption of zinc fingers 5 or 6, which are

A

B

Repressors:

GAL4-ZBRK1 5ZFC

GAL4-ZBRK1 C

Reporter:

FIG. 7. **ZBRK1 5ZFC-directed repression is reversed by tricho-statin A.** *A,* U2OS cells were transfected with 30 ng of pG$_5$TK-Luc without or with the indicated nanogram amounts of GAL4-ZBRK1 5ZFC or GAL4-ZBRK1 C. Where indicated, TSA (330 nM) was also included. Relative luciferase activities were calculated as described in the legend to Fig. 4. *B,* schematic representation of the GAL4-ZBRK1 5ZFC and GAL4-ZBRK1 C chimeras and the pG$_5$TK-Luc reporter template used in transfection assays.

not required for BRCA1 binding (Fig. 3), nonetheless signifi-cantly compromised transcriptional repression (Fig. 6, *A* and *B*). On this basis we conclude that BRCA1 binding is necessary but not sufficient for 5ZFC repression function. This suggests that ZBRK1 zinc fingers 5 and 6 may possibly contact an additional co-repressor(s).

The BRCA1-dependent 5ZFC Repression Domain Is Histone Deacetylase-dependent and Promoter-specific—Previously, BRCA1 has been shown to interact through its C-terminal BRCT repeats with histone deacetylases (HDACs) 1 and 2 (57). HDACs remove acetyl groups from lysine residues on histone tails and thus promote the formation of transcriptionally re-pressive chromatin. To determine the contribution of HDAC activity to repression mediated by ZBRK1 5ZFC, we tested the effect of the selective HDAC inhibitor trichostatin A (TSA) on repression mediated by GAL4-ZBRK1 5ZFC. TSA largely re-versed GAL4-ZBRK1 5ZFC repression in U2OS cells, implicat-ing HDAC activity in this process (Fig. 7).

Like the ZBRK1 5ZFC repression domain, KRAB repression domains function through HDACs as well as through histone methyltransferases and heterochromatin proteins (41–47). This prompted us to comparatively examine the promoter spec-ificities of the ZBRK1 5ZFC and KRAB repression domains. The ZBRK1 N-terminal KRAB domain repressed transcription potently from each of three different RNA polymerase II pro-moters tested: the SV40 major late, the HSV TK, and the human small nuclear ribonucleoprotein N (SNRPN) promoters (Fig. 8*B*). By contrast, ZBRK1 5ZF5C repressed transcription potently from the HSV TK promoter, moderately from the SV40
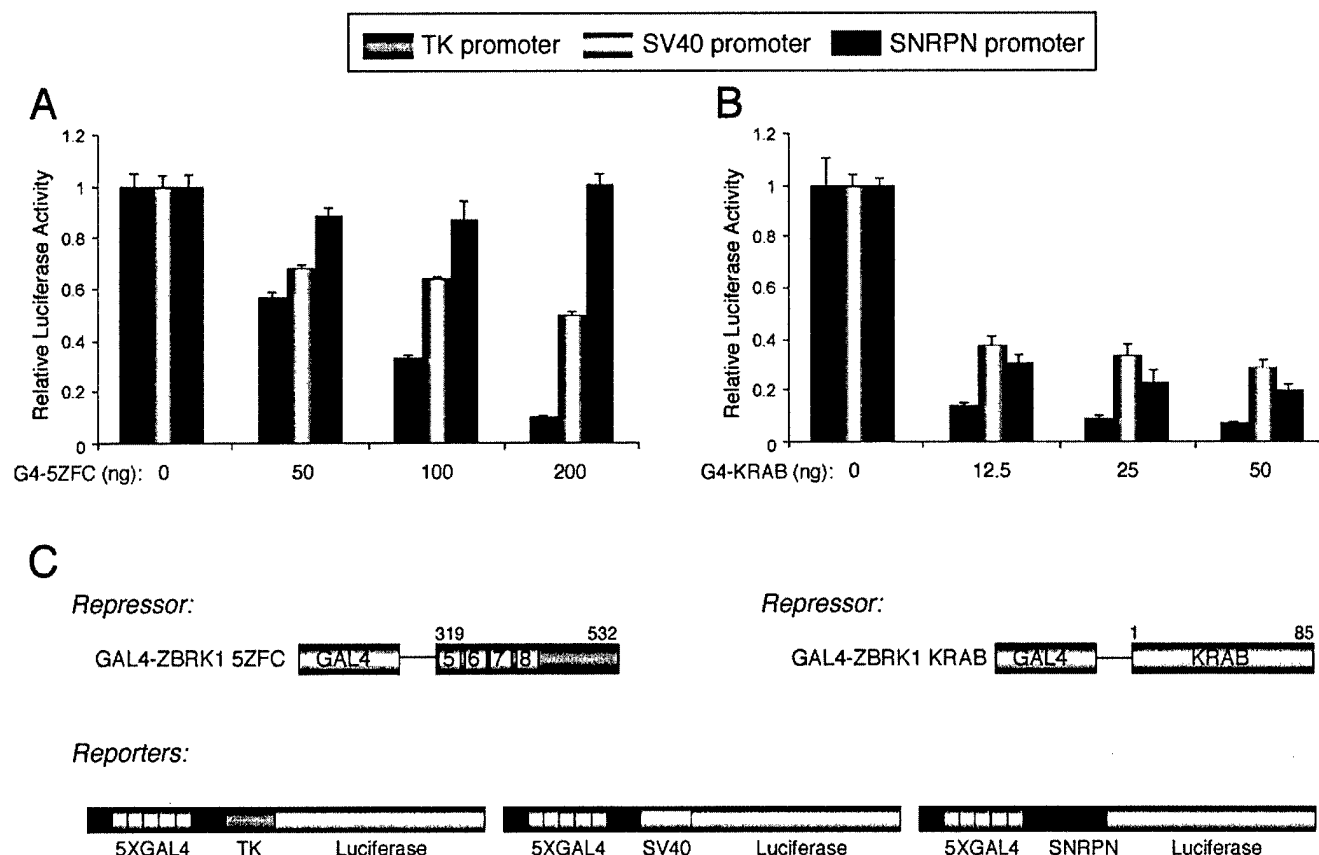
promoter, and not at all from the SNRPN promoter (Fig. 8*A*). These results indicate that the ZBRK1 KRAB and 5ZFC re-pression domains can be distinguished functionally not only by their requirement for BRCA1 but also on the basis of their promoter specificities; whereas the ZBRK1 KRAB repression domain exhibits broad promoter selectivity, the BRCA1-de-pendent 5ZFC repression domain exhibits a more restricted promoter bias.

DISCUSSION

A central question regarding the role of BRCA1 in transcrip-tion control concerns the means by which it mediates gene-specific regulation in the absence of sequence-specific DNA binding activity. In part, this question has been answered by the identification of a growing number of sequence-specific DNA-binding transcription factors with which BRCA1 physi-cally and functionally interacts. In this regard, our previous identification of ZBRK1 as a BRCA1-dependent transcriptional repressor provided a molecular basis to link BRCA1 directly to the regulation of *GADD45a* gene expression (39). Other work has rendered it clear that the BRCA1 regulation of *GADD45a* gene transcription is likely to be complex and mediated not only through ZBRK1 but other trans-acting factors, including OCT1 and NF-YA (21, 32, 39). Presently, however, little is known regarding the mechanism(s) by which BRCA1 mediates sequence-specific transcriptional control through the various transcription factors with which it interacts. Here we have investigated the functional interaction between ZBRK1 and BRCA1 in an effort to understand the role of BRCA1 in se-quence-specific transcriptional repression.

Our studies suggest that BRCA1 mediates ZBRK1 repres-sion, at least in part, through its targeted recruitment to a novel C-terminal repression domain (5ZFC) within ZBRK1. Structurally, this repression domain comprises the last four zinc fingers and the unique C-terminal extension of ZBRK1. The identification of 5ZFC as a discrete functional domain was revealed by its ability to repress transcription when tethered to a heterologous DNA-binding domain (Fig. 4) and its functional resistance to truncation or substitution mutagenesis (Fig. 6). Importantly, we demonstrated that 5ZFC repression function is dependent upon BRCA1; genetic ablation of *Brca1* or disrup-tion of BRCA1-binding determinants on 5ZFC similarly abro-gates the repression function of this domain (Figs. 5 and 6). The functional contribution of this domain to BRCA1-dependent ZBRK1 repression is reflected by our previous observation that deletion of the ZBRK1 C terminus abrogates ZBRK1 repression through natural ZBRK1-response elements (39). However, whereas BRCA1 binding is necessary, our studies here suggest that it is not sufficient for 5ZFC-directed repression. First, BRCA1 binding and repression determinants within this do-main can be separated, suggesting a possible functional re-quirement for a co-repressor(s) in addition to BRCA1 (Figs. 3 and 6). Second, 5ZFC-directed repression is HDAC-dependent (Fig. 7). Thus, we propose that the ZBRK1 5ZFC repression domain recruits BRCA1 as part of a higher order repression complex that minimally includes an associated HDAC activity. Targeted attempts to identify the functionally relevant BRCA1-associated co-repressor activities are currently underway.

Our work further reveals unique insight into the structural and functional organization of ZBRK1, a member of the KRAB-ZFP family. The ~220 members of this family make up a significant proportion of the transcription factor complement of the human proteome and are believed to occupy important regulatory roles in development, differentiation, and transfor-mation (41, 58–63). Despite their potential biological signifi-cance, our current understanding of the mechanisms through

FIG. 8. **The ZBRK1 KRAB and 5ZFC repression domains exhibit unique promoter specificities.** *A* and *B*, U2OS cells were transfected with 30 ng of pG$_5$TK-Luc, 15 ng pG$_5$SV40-Luc, or 90 ng pG$_5$SNRPN-Luc as indicated without or with the indicated nanogram amounts of GAL4-ZBRK1 5ZFC (*A*) or GAL4-ZBRK1 KRAB (*B*). Relative luciferase activities were calculated as described in the legend to Fig. 4. *C*, schematic representation of the GAL4-ZBRK1 KRAB and GAL4-ZBRK1 5ZFC chimeras, and the pG$_5$TK-Luc, pG$_5$SV40-Luc, and pG$_5$SNRPN-Luc reporter templates used in transfections.

which individual members of this protein family function is still rather limited. Thus, although considerable mechanistic insight into the repression function of the KRAB domain has been revealed in recent years (41–47), comparatively little is known regarding the role of KRAB domain-associated zinc fingers in transcriptional repression apart from their presumed role in sequence-specific DNA binding. In part, this gap in knowledge derives from the limited availability of KRAB-ZFP target sequences with which structure-function analyses may be carried out. In the case of several KRAB-ZFPs whose corresponding binding site sequences have been identified, an additional function(s) for individual zinc fingers beyond DNA binding seems implicit. For example, based on the observation that one C$_2$H$_2$ zinc finger can bind to ~3 bp of DNA (52–54), the established target sequence lengths of 5 and 27 bp, respectively, for the 8- and 10-fingered ZNF202 and KS1 proteins are incompatible with DNA contact mediated by every zinc finger (61, 63). Our previous derivation of a consensus binding sequence for ZBRK1 has permitted us here to dissect a long array KRAB-ZFP and examine the contribution of individual zinc fingers to both sequence-specific DNA-binding and transcriptional repression. Our studies reveal the ZBRK1 zinc fingers to be multifunctional in nature, with dedicated roles in binding DNA, BRCA1, or both.

First, zinc fingers 1–4 are essential for DNA binding activity and compose the minimal DNA-binding domain under moderate conditions of ionic strength (Fig. 1). Zinc finger 5 appears to be a critical and context-dependent DNA-binding zinc finger; this finger represents the extent of the minimal DNA-binding domain under more stringent conditions (Fig. 1). Zinc fingers 6

and 7 are not essential for DNA binding but nonetheless enhance the stability of DNA binding (Figs. 1 and 2). Finally, zinc finger 8 (along with the C terminus) is dispensable for, and may possibly destabilize, DNA binding mediated by zinc fingers 1–7 (Fig. 1). Taken together, these findings reveal the ZBRK1 zinc fingers to compose at least two functional classes: those that make minimal essential contacts with DNA (fingers 1–4) and those that modulate the stability of these contacts (fingers 5–8). Importantly, zinc fingers 5–8 that modulate ZBRK1 DNA binding activity also represent critical determinants of repression by DNA-bound ZBRK1 through association with co-repressors, including BRCA1. These findings thus extend the established role of KRAB-zinc fingers to include protein-protein interactions critical for transcriptional repression, and also identify within ZBRK1 dual specificity zinc fingers with twin roles in DNA-binding and transcriptional repression.

Our work advances the understanding of DNA recognition by KRAB-ZFPs in several respects. First, we provide further empirical evidence to support predictive models for C$_2$H$_2$ zinc finger-DNA recognition. Structural studies of 3- and 5-fingered proteins in complex with DNA have indicated that individual zinc fingers bind to ~3 bp of DNA (52–54). Based on this model, five of the eight ZBRK1 zinc fingers would be predicted to bind to its 15-bp recognition sequence. In fact, DNA-binding analyses revealed that under mild conditions of ionic strength, the first four ZBRK1 zinc fingers are sufficient to confer stable binding to its consensus sequence. However, more stringent conditions unmasked a requirement for the fifth finger, consistent with the aforementioned structural models. Second, our identification of ZBRK1 zinc finger 5 as a critical and context-

dependent DNA-binding determinant could clarify recent issues concerning selectivity among KRAB-ZFPs that recognize overlapping DNA-binding site sequences. In this regard, a four-fingered KRAB-ZFP called SZF1 was recently shown to recognize a DNA-binding site in common with ZBRK1 (64). The observation that SZF1 and ZBRK1 exhibit overlapping DNA-binding specificities *in vitro* raises the possibility that these proteins might compete for a common binding site(s) *in vivo* (64). This, in turn, could have significant implications for the biological regulation of target gene transcription by each of these proteins. However, as we show here, ZBRK1 zinc finger 5 is a critical DNA-binding determinant under more stringent conditions of increased ionic strength and also increased non-specific competitor concentrations *in vitro* (Fig. 1 and data not shown). Because these conditions are more likely to approximate those of the cellular milieu, in which target site location must be achieved in the presence of a vast excess of like and unlike DNA sequences, ZBRK1 zinc finger 5 could represent a critical determinant of target site selection *in vivo*. Beyond zinc finger 5, zinc fingers 6 and 7 through enhanced affinity and/or protein-protein interactions could further influence ZBRK1 target site selectivity.

Our identification within ZBRK1 of a C-terminal BRCA1-dependent repression domain in addition to the N-terminal KRAB domain represents the first demonstration of a KRAB-ZFP harboring two independent repression domains. More importantly, the presence of two inherent repression domains could have important implications for gene-specific transcription control by ZBRK1. As we show here, the KRAB and C-terminal repression domains within ZBRK1 can be distinguished functionally on the basis of their respective requirements for BRCA1; the C-terminal repression domain is BRCA1-dependent, whereas the KRAB domain is not. This functional distinction may in part underlie the unique promoter specificities of the two repression domains. Whereas the KRAB repression domain exhibits broad promoter specificity, the BRCA1-dependent repression domain exhibits a more restricted promoter bias. Thus, the relative contribution of the BRCA1-dependent repression domain to overall ZBRK1 repression may vary among different ZBRK1 target promoters, effectively expanding the regulatory potential available at ZBRK1 target genes. It will be of interest in future studies to determine whether and how these discrete repression domains function synergistically to confer ZBRK1 repression.

Finally, although our work suggests that BRCA1 mediates repression by DNA-bound ZBRK1, we cannot exclude the additional possibility that BRCA1 also mediates ZBRK1 repression, at least in part, by modulating it sequence-specific DNA binding activity. Our observation that the BRCA1-binding surface on ZBRK1 includes zinc fingers that modulate its DNA binding activity in both a positive (zinc finger 7) and negative (zinc finger 8) manner is consistent with this possibility, and studies are currently underway to address this important issue. Nonetheless the studies presented here shed new light on the functional organization of ZBRK1 as a model KRAB-ZFP and further define the role of BRCA1 in sequence-specific transcription control.

REFERENCES

1. Miki, Y., Swensen, J., Shattuck-Eidens, D., Futreal, P. A., Harshman, K., Tavtigian, S., Liu, Q., Cochran, C., Bennett, L. M., Ding, W., Bell, R., Rosenthal, J., Hussey, C., Tran, T., McClure, M., Frye, C., Hattier, T., Phelps, R., Haugen-Strano, A., Katcher, H., Yakumo, K., Gholami, Z., Shaffer, D., Stone, S., Bayer, S., Wray, C., Bogden, R., Dayananth, P., Ward, J., Tonin, P., Narod, S., Bristow, P. K., Norris, F. H., Helvering, L., Morrison, P., Rosteck, P., Lai, M., Barrett, J. C., Lewis, C., Neuhausen, S., Cannon-Albright, L., Goldgar, D., Wiseman, R., Kamb, A., and Skolnick, M. H. (1994) *Science* 266, 66–71
2. Hall, J. M., Lee, M. K., Newman, B., Morrow, J. E., Anderson, L. A., Huey, B., and King, M. C. (1990) *Science* 250, 1684–1689
3. Wooster, R., and Weber, B. L. (2003) *N. Engl. J. Med.* 348, 2339–2347
4. Tirkkonen, M., Johannsson, O., Agnarsson, B. A., Olsson, H., Ingvarsson, S., Karhu, R., Tanner, M., Isola, J., Barkardottir, R. B., Borg, A., and Kallioniemi, O. P. (1997) *Cancer Res.* 57, 1222–1227
5. Venkitaraman, A. R. (2002) *Cell* 108, 171–182
6. Zheng, L., Li, S., Boyer, T. G., and Lee, W. H. (2000) *Oncogene* 19, 6159–6175
7. Xu, X., Weaver, Z., Linke, S. P., Li, C., Gotay, J., Wang, X. W., Harris, C. C., Ried, T., and Deng, C. X. (1999) *Mol. Cell* 3, 389–395
8. Scully, R., and Livingston, D. M. (2000) *Nature* 408, 429–432
9. Welcsh, P. L., and King, M. C. (2001) *Hum. Mol. Genet.* 10, 705–713
10. Deng, C. X. (2001) *Mutat. Res.* 477, 183–189
11. Rosen, E. M., Fan, S., Pestell, R. G., and Goldberg, I. D. (2003) *J. Cell Physiol.* 196, 19–41
12. Xu, B., Kim, S., and Kastan, M. B. (2001) *Mol. Cell. Biol.* 21, 3445–3450
13. Cortez, D., Wang, Y., Qin, J., and Elledge, S. J. (1999) *Science* 286, 1162–1166
14. Lee, J. S., Collins, K. M., Brown, A. L., Lee, C. H., and Chung, J. H. (2000) *Nature* 404, 201–204
15. Scully, R., Chen, J., Ochs, R. L., Keegan, K., Hoekstra, M., Feunteun, J., and Livingston, D. M. (1997) *Cell* 90, 425–435
16. Li, S., Ting, N. S., Zheng, L., Chen, P. L., Ziv, Y., Shiloh, Y., Lee, E. Y., and Lee, W. H. (2000) *Nature* 406, 210–215
17. Moynahan, M. E., Chiu, J. W., Koller, B. H., and Jasin, M. (1999) *Mol. Cell* 4, 511–518
18. Zhong, Q., Chen, C. F., Li, S., Chen, Y., Wang, C. C., Xiao, J., Chen, P. L., Sharp, Z. D., and Lee, W. H. (1999) *Science* 285, 747–750
19. Scully, R., Chen, J., Plug, A., Xiao, Y., Weaver, D., Feunteun, J., Ashley, T., and Livingston, D. M. (1997) *Cell* 88, 265–275
20. Somasundaram, K., Zhang, H., Zeng, Y. X., Houvras, Y., Peng, Y., Wu, G. S., Licht, J. D., Weber, B. L., and El-Deiry, W. S. (1997) *Nature* 389, 187–190
21. Harkin, D. P., Bean, J. M., Miklos, D., Song, Y. H., Truong, V. B., Englert, C., Christians, F. C., Ellisen, L. W., Maheswaran, S., Oliner, J. D., and Haber, D. A. (1999) *Cell* 97, 575–586
22. Deng, C. X., and Brodie, S. G. (2000) *BioEssays* 22, 728–737
23. Monteiro, A. N. (2000) *Trends Biochem. Sci.* 25, 469–474
24. Starita, L. M., and Parvin, J. D. (2003) *Curr. Opin. Cell Biol.* 15, 345–350
25. Jasin, M. (2002) *Oncogene* 21, 8981–8993
26. Baer, R., and Ludwig, T. (2002) *Curr. Opin. Genet. Dev.* 12, 86–91
27. Bochar, D. A., Wang, L., Beniya, H., Kinev, A., Xue, Y., Lane, W. S., Wang, W., Kashanchi, F., and Shiekhattar, R. (2000) *Cell* 102, 257–265
28. Miyake, T., Hu, Y. F., Yu, D. S., and Li, R. (2000) *J. Biol. Chem.* 275, 40169–40173
29. MacLachlan, T. K., Somasundaram, K., Sgagias, M., Shifman, Y., Muschel, R. J., Cowan, K. H., and El-Deiry, W. S. (2000) *J. Biol. Chem.* 275, 2777–2785
30. Aprelikova, O., Pace, A. J., Fang, B., Koller, B. H., and Liu, E. T. (2001) *J. Biol. Chem.* 276, 25647–25650
31. Welcsh, P. L., Lee, M. K., Gonzalez-Hernandez, R. M., Black, D. J., Mahadevappa, M., Swisher, E. M., Warrington, J. A., and King, M. C. (2002) *Proc. Natl. Acad. Sci. U. S. A.* 99, 7560–7565
32. Fan, W., Jin, S., Tong, T., Zhao, H., Fan, F., Antinore, M. J., Rajasekaran, B., Wu, M., and Zhan, Q. (2002) *J. Biol. Chem.* 277, 8061–8067
33. Ouchi, T., Monteiro, A. N., August, A., Aaronson, S. A., and Hanafusa, H. (1998) *Proc. Natl. Acad. Sci. U. S. A.* 95, 2302–2306
34. Chai, Y. L., Cui, J., Shao, N., Shyam, E., Reddy, P., and Rao, V. N. (1999) *Oncogene* 18, 263–268
35. Fan, S., Ma, Y. X., Wang, C., Yuan, R. Q., Meng, Q., Wang, J. A., Erdos, M., Goldberg, I. D., Webb, P., Kushner, P. J., Pestell, R. G., and Rosen, E. M. (2001) *Oncogene* 20, 77–87
36. Park, J. J., Irvine, R. A., Buchanan, G., Koh, S. S., Park, J. M., Tilley, W. D., Stallcup, M. R., Press, M. F., and Coetzee, G. A. (2000) *Cancer Res.* 60, 5946–5949
37. Wang, Q., Zhang, H., Kajino, K., and Greene, M. I. (1998) *Oncogene* 17, 1939–1948
38. Zhang, H., Somasundaram, K., Peng, Y., Tian, H., Bi, D., Weber, B. L., and El-Deiry, W. S. (1998) *Oncogene* 16, 1713–1721
39. Zheng, L., Pan, H., Li, S., Flesken-Nikitin, A., Chen, P. L., Boyer, T. G., and Lee, W. H. (2000) *Mol. Cell* 6, 757–768
40. Zheng, L., Annab, L. A., Afshari, C. A., Lee, W. H., and Boyer, T. G. (2001) *Proc. Natl. Acad. Sci. U. S. A.* 98, 9587–9592
41. Collins, T., Stone, J. R., and Williams, A. J. (2001) *Mol. Cell. Biol.* 21, 3609–3615
42. Friedman, J. R., Fredericks, W. J., Jensen, D. E., Speicher, D. W., Huang, X. P., Neilson, E. G., and Rauscher, F. J., III (1996) *Genes Dev.* 10, 2067–2078
43. Kim, S. S., Chen, Y. M., O'Leary, E., Witzgall, R., Vidal, M., and Bonventre, J. V. (1996) *Proc. Natl. Acad. Sci. U. S. A.* 93, 15299–15304
44. Moosmann, P., Georgiev, O., Le Douarin, B., Bourquin, J. P., and Schaffner, W. (1996) *Nucleic Acids Res.* 24, 4859–4867
45. Lechner, M. S., Begg, G. E., Speicher, D. W., and Rauscher, F. J., III (2000) *Mol. Cell. Biol.* 20, 6449–6465
46. Schultz, D. C., Ayyanathan, K., Negorev, D., Maul, G. G., and Rauscher, F. J., III (2002) *Genes Dev.* 16, 919–932
47. Schultz, D. C., Friedman, J. R., and Rauscher, F. J., III (2001) *Genes Dev.* 15, 428–443
48. Kastan, M. B., Zhan, Q., el-Deiry, W. S., Carrier, F., Jacks, T., Walsh, W. V., Plunkett, B. S., Vogelstein, B., and Fornace, A. J., Jr. (1992) *Cell* 71,

587–597

49. Hollander, M. C., Alamo, I., Jackman, J., Wang, M. G., McBride, O. W., and Fornace, A. J., Jr. (1993) *J. Biol. Chem.* **268,** 24385–24393
50. Sadowski, I., Bell, B., Broad, P., and Hollis, M. (1992) *Gene (Amst.)* **118,** 137–141
51. Fujita, N., Jaye, D. L., Kajita, M., Geigerman, C., Moreno, C. S., and Wade, P. A. (2003) *Cell* **113,** 207–219
52. Pavletich, N. P., and Pabo, C. O. (1991) *Science* **252,** 809–817
53. Pavletich, N. P., and Pabo, C. O. (1993) *Science* **261,** 1701–1707
54. Wolfe, S. A., Nekludova, L., and Pabo, C. O. (2000) *Annu. Rev. Biophys. Biomol. Struct.* **29,** 183–212
55. Del Rio, S., Menezes, S. R., and Setzer, D. R. (1993) *J. Mol. Biol.* **233,** 567–579
56. Del Rio, S., and Setzer, D. R. (1993) *Proc. Natl. Acad. Sci. U. S. A.* **90,** 168–172
57. Yarden, R. I., and Brody, L. C. (1999) *Proc. Natl. Acad. Sci. U. S. A.* **96,** 4983–4988
58. Jheon, A. H., Ganss, B., Cheifetz, S., and Sodek, J. (2001) *J. Biol. Chem.* **276,** 18282–18289
59. Bellefroid, E. J., Poncelet, D. A., Lecocq, P. J., Revelant, O., and Martial, J. A. (1991) *Proc. Natl. Acad. Sci. U. S. A.* **88,** 3608–3612
60. Bellefroid, E. J., Marine, J. C., Ried, T., Lecocq, P. J., Riviere, M., Amemiya, C., Poncelet, D. A., Coulie, P. G., de Jong, P., Szpirer, C., Ward, D. C., and Martial, J. A. (1993) *EMBO J.* **12,** 1363–1374
61. Gebelein, B., and Urrutia, R. (2001) *Mol. Cell. Biol.* **21,** 928–939
62. Gebelein, B., Fernandez-Zapico, M., Imoto, M., and Urrutia, R. (1998) *J. Clin. Investig.* **102,** 1911–1919
63. Wagner, S., Hess, M. A., Ormonde-Hanson, P., Malandro, J., Hu, H., Chen, M., Kehrer, R., Frodsham, M., Schumacher, C., Beluch, M., Honer, C., Skolnick, M., Ballinger, D., and Bowen, B. R. (2000) *J. Biol. Chem.* **275,** 15685–15690
64. Peng, H., Zheng, L., Lee, W. H., Rux, J. J., and Rauscher, F. J., III (2002) *Cancer Res.* **62,** 3773–3781

Purified Human SUV3p Exhibits Multiple-Substrate Unwinding Activity upon Conformational Change[†]

Zhanyong Shu,[‡,§] Sangeetha Vijayakumar,[§,‖] Chi-Fen Chen,[‖] Phang-Lang Chen,[‖] and Wen-Hwa Lee*,[‡]

Department of Biological Chemistry, College of Medicine, University of California, Irvine, California 92697, and Department of Molecular Medicine, Institute of Biotechnology, University of Texas Health Science Center at San Antonio, San Antonio, Texas 78245

ABSTRACT: Suv3 of *Saccharomyces cerevisiae* has been classified as a mitochondrial RNA helicase. However, the helicase domain in both yeast and human SUV3 varies considerably from the typical RNA helicase motifs. To investigate its enzymatic activities, a homogeneously purified preparation of SUV3 is required. Expression of a processed form of human SUV3 carrying an N-terminal deletion of 46 amino acids (SUV3ΔN46) in a yeast suv3 null mutant, which otherwise fails to grow in a nonfermentable carbon source and forms petite colonies in glucose medium, rescues the null phenotype. Through a five-step chromatographic procedure, an 83 kDa SUV3ΔN46 protein (SUV3−83) and a partially degraded 70 kDa product (SUV3−70) containing amino acids 68−685 were purified to homogeneity. Single- or double-stranded DNA and RNA stimulated ATPase activity of both proteins. SUV3−70, which retains core catalytic domains, can bind and unwind multiple duplex substrates of RNA and DNA with a 5′−3′ directionality over a wide range of pH, while SUV3−83 has helicase activity at only acidic pH. ATP, but not nonhydrolyzable ATP, is essential for the unwinding activity, suggesting the requirement of the energy derived from ATP hydrolysis. Consistent with this notion, suv3 mutants containing alanine (A) or arginine (R) substitutions at the conserved lysine residue in the ATP binding site (K213) lost ATPase activity and also failed to unwind the substrates. Importantly, circular dichroism (CD) spectral analysis showed that SUV3−83, at pH 5.0, adopts a conformation similar to that of SUV3−70, suggesting a conformational change in SUV3−83 is required for its helicase activity. The physiological relevance of the multiple-substrate helicase activity of human SUV3 is discussed.

DNA helicases play a significant role in DNA replication, repair, and recombination (*1*). Likewise, RNA−RNA and RNA−DNA helicases play major roles in transcription, translation, and RNA splicing (*2, 3*). Consistent with their roles in nucleic acid metabolism, mutations in helicases have been linked to several human genetic diseases, including Werner syndrome (WRN), Bloom syndrome (BLM), and Xeroderma pigmentosum (*2*). The basic biochemical reactions catalyzed by all helicases, namely, nucleic acid binding, NTP[1] binding, and NTP hydrolysis-dependent unwinding of nucleic acids, may be similar. However, their affinity for different nucleic acid substrates, a preference for a particular NTP, and active assembly state (monomer, dimer, or hexamer) can be

different (*4, 5*). WRN, BLM, and RecG are examples of helicases exhibiting specificity toward specialized structures, such as replication forks or Holliday junctions (*6, 7*). Identification of substrate specificity is an important step toward unraveling the molecular function of helicases.

Suv3 of *Saccharomyces cerevisiae* is a putative ATP-dependent RNA helicase in the DEAD/DExH family that functions in turnover and processing of RNA in mitochondria (*8−10*). Human SUV3 was identified on the basis of the homology of its sequence to that of yeast Suv3 (*11*). Sequence homology analysis of databases also identified other putative Suv3 homologue in *Caenorhabditis elegans, Arabidopsis thaliana*, and mouse (*11*). Suv3-like proteins have been proposed to form a distinct and conserved family, as they share more homology within the group than with any other family of helicases (*11, 12*). One biochemical defect detected in yeast suv3 null mutants is a failure to process mitochondrial RNA precursors (*9, 10*), which results in overaccumulation of excised group I introns. These observations led to the concept that Suv3 plays a major role in RNA metabolism in yeast mitochondria; the absence of a fully functional Suv3 results in mitochondrial genomic loss and respiratory incompetence. A partially purified RNA "degradosome" from yeast mitochondria, consisting of Suv3 and an exoribonuclease, Dss1, possesses RNA helicase activity (*10*). However, whether purified Suv3 alone has any helicase activity is unclear.

* To whom correspondence should be addressed. Phone: (949) 824-4492. Fax: (949) 824-9767. E-mail: whlee@uci.edu.
[‡] University of California, Irvine.
[§] These authors contributed equally to this work.
[‖] University of Texas Health Science Center at San Antonio.

[1] Abbreviations: NTP, nucleoside triphosphate; ds, double-stranded; ss, single-stranded; ssc, single-stranded circular; DTT, dithiothreitol; SDS, sodium dodecyl sulfate; BSA, bovine serum albumin; PAGE, polyacrylamide gel electrophoresis; KOAc, potassium acetate; KO(Cit)$_2$, potassium citrate; CD, circular dichroism; UV, ultraviolet; HD, heat-denatured; Sub, substrate; TE, Tris-EDTA buffer; TBE, Tris-boric acid-EDTA buffer; PMSF, phenylmethanesulfonyl fluoride; QFF, Q-Sepharose fast flow.

In this study, we expressed a processed form of human SUV3, which has an N-terminal deletion of 46 amino acids (SUV3ΔN46), in a yeast suv3 null mutant. Expression of SUV3ΔN46 rescues the SUV3 null phenotype. To investigate their enzymatic activities, a SUV3ΔN46 protein, SUV3−83, and a partially degraded SUV3−70 were purified to homogeneity from the rescued yeast. Both proteins have the ATPase activity that is stimulated by polynucleotide acids. SUV3−70 can bind and unwind multiple duplex substrates of RNA and DNA with a 5′−3′ directionality in a pH-independent manner, while SUV3−83 has the helicase activity at only acidic pH. Significantly, circular dichroism spectral analysis showed that SUV3−83, at pH 5.0, adopts a conformation similar to that of SUV3−70, suggesting that a conformational change in SUV3−83 is required for its helicase activity. Although several other helicases exhibit multisubstrate specificity (6, 13, 14), this is, to our knowledge, the first helicase in which a conformational change can govern its enzymatic activity.

EXPERIMENTAL PROCEDURES

Yeast Strain and Plasmids. S. cerevisiae strain BWG1 [MATa his134−519 ura3 ade1 leu2 $\omega^+\rho^+$ (8)] was from R. A. Butow (University of Texas Southwestern Medical Center, Dallas, TX). A SUV3 cDNA encoding SUV3ΔN46 was constructed by deleting the first 46 amino acids and replacing threonine 47 with methionine by site-directed mutagenesis (Quick Change site-directed mutagenesis kit, Stratagene, La Jolla, CA) using the full-length cDNA as the template. Expression of SUV3ΔN46 in multicopy plasmid pJJ1 was driven by a phosphoglycerate kinase (PGK) promoter to form pJJ1-SUV3ΔN46. To investigate the potential function of the Walker A motif (GXXXXGKT, amino acids 207−214) (15), two plasmids, pJJ1-SUV3ΔN46K213A and pJJ1-SUV3ΔN46K213R, carrying the indicated point mutations at lysine 213, were constructed by site-directed mutagenesis using pJJ1-SUV3ΔN46 as the template.

Disruption and Rescue Experiments. Yeast strain BWG1 [MATa his134−519 ura3 ade1 leu2 $\omega^+\rho^+$ (8)] was first transformed with pJJ1, pJJ1-SUV3ΔN46, pJJ1-SUV3ΔN-46K213A, or pJJ1-SUV3ΔN46K213R and was plated on synthetic medium lacking leucine (SC-Leu). Individual colonies were picked from the SC-Leu plate, and the corresponding competent cells were then transformed with the yeast Suv3 knockout construct in which URA3 replaced a part of yeast Suv3 (C.-F. Chen, W.-H. Lee, et al., manuscript submitted for publication). Transformants were selected on synthetic media lacking leucine and uracil. Disruptions were confirmed by PCR genotyping using primers outside the target region and inside the URA3 gene. Yeast cells lacking yeast Suv3 and carrying pJJ1, pJJ1-SUV3ΔN46, pJJ1-SUV3ΔN46K213A, or pJJ1-SUV3ΔN46K213R were grown in YP glucose (1% yeast extract, 2% bactopeptone, and 2% glucose) or in YP glycerol (1% yeast extract, 2% bactopeptone, and 2% glycerol).

Immunoblot Analysis. Immunoblotting analysis was performed as described previously (16) using a mouse anti-SUV3 monoclonal antibody generated against the GST−SUV3 fusion protein (amino acids 144−786) as the probe.

Overexpression and Purification of SUV3−83. A suv3 null BWG1 yeast strain harboring pJJ1-SUV3ΔN46 was cultured in medium lacking leucine and uracil. Detection of the human SUV3 protein was performed by immunoblotting using an anti-SUV3 monoclonal antibody. All the following steps were conducted at 4 °C. Yeast (25 g wet weight) were resuspended in cell breakage buffer [50 mM Tris-HCl (pH 8.0), 5% sucrose, 2.5 mM EDTA, 600 mM KCl, 2 mM DTT, 0.01% Nonidet P-40 with protease inhibitors, including aprotinin, antipain, leupeptin, and pepstatin at 1 µg/mL each, and 1 mM PMSF] at the ratio of 1:5 (w/v) and lysed using a French press at a high pressure. Cellular lysates were clarified by centrifugation (100000g for 45 min), and the supernatants were then subjected to ammonium sulfate precipitation at 0.21 g/mL (0−35%). The precipitates were collected by centrifugation (20000g for 20 min) and resuspended in ∼50 mL of T buffer [25 mM Tris-HCl (pH 8.0), 5% glycerol, 1 mM EDTA, 2 mM DTT, and protease inhibitors]. After the conductivity was adjusted to the value of buffer A (T buffer with 100 mM KCl), the supernatant was applied to a Q-Sepharose Fast Flow (QFF) column (8 mL) pre-equilibrated with buffer A and developed in a gradient of 10 to 50% buffer B (T buffer with 1 M KCl) over 5 column volumes. The peak of SUV3−83, which eluted at approximately 32% buffer B, was then directly applied to a HiTrap heparin column (5 mL), which was developed in a gradient of 20 to 50% buffer B over 4 column volumes. The peak fractions containing SUV3−83 which eluted around 32% buffer B were pooled and applied to a G-25 Sephadex column (50 mL) to remove the salt, and the protein fractions were then applied to a Mono Q (HR 5/5, 1 mL) column, which was developed in a gradient of 0 to 30% buffer B over 20 column volumes. SUV3−83, which eluted between 16 and 19% buffer B from the Mono Q column, was then applied to a Superdex 200 column (HR 10/30, 24 mL) in buffer A. Peak fractions were pooled and concentrated using Centricon concentrators (models YM-30 and YM-50) and stored at −70 °C.

Purification of SUV3−70. SUV3−70, a stable proteolytic product of SUV3−83, was first detected in QFF fractions in which SUV3−83 and SUV3−70 were eluted together. QFF fractions were loaded onto a HiTrap Blue affinity column (5 mL) and developed in a gradient of 20 to 100% buffer C (T buffer with 2 M KCl) over 4 column volumes. SUV3−70 was eluted at around 46% buffer C whereas SUV3−83 around 75%. The fractions containing SUV3−70 were dialyzed against buffer A and applied to the Mono Q (HR 5/5, 1 mL) column which was developed in a gradient of 0 to 30% buffer B over 20 column volumes. The SUV3−70 was eluted at around 9% buffer B, and the pooled fractions were then applied to a Superdex-200 column. Identification of SUV3−70 was based on its characteristic peptide pattern analyzed by mass spectrometry. The peak fractions from the Superdex-200 column were concentrated and stored at −70 °C.

All the columns and media used in the purification were from Amersham Pharmacia Biotech. The protein concentration was determined by UV absorption using a DU650 spectrophotometer (Beckman Instruments) with molar extinction coefficients for SUV3−83 and SUV3−70 being 67 110 and 61 420 M^{-1} cm^{-1}, respectively. Both SUV3−83 and SUV3−70 were more than 95% pure after Coomassie blue staining of an 8% SDS−PAGE gel (Figure 2C).

Mass Spectrometry and Edman Degradation. SUV3 proteins were digested in-gel using trypsin (Promega), and the resulting peptides were analyzed with Voyager DE-Pro (Applied Biosystems) based on matrix-assisted laser desorption ionization time-of-flight (MALDI-TOF) mass spectrometry as described previously (*17*). The N-terminal sequence of the purified SUV3−70 was determined by Edman degradation using a PROCISE-cLC instrument (Applied Biosystems) as described previously (*17*)

ATPase Assays. The ATPase assay was carried out in a reaction volume of 20 μL containing ATPase buffer [25 mM Tris-HCl (pH 7.5), 1 mM DTT, 5 mM MgCl$_2$, 50 mM KCl, and 100 ng of BSA], 0.05 mCi/mL [γ-^{32}P]ATP (Amersham Biosciences), 100 μM ATP, and varying amounts of SUV3 proteins at 37 °C for 60 min as described previously (*12*). The reaction was terminated by adding 2 μL of 0.5 M EDTA. One microliter of each reaction mixture was then spotted onto polyethyleneimine cellulose thin-layer chromatography plates (Selecto Scientific, Suwanee, GA) and developed in 1 M formic acid with 0.5 M LiCl. The amounts of ^{32}P$_i$ and [γ-^{32}P]ATP in the reaction mixture were determined using a Storm 320 Phosphor Imager (Molecular Dynamics, Piscataway, NJ) and quantified as picomoles of ATP hydrolyzed.

Factors that could potentially affect the ATPase activity, including cations and polynucleotide acids, were also tested under various conditions. To determine the effect of cations, 0.1 mM EDTA was used to remove contaminating divalent cations, and then CaCl$_2$, MgCl$_2$, MnCl$_2$, or ZnCl$_2$ was added to a final concentration of 5 mM. To assay the effect of polynucleotide acids, ssRNA (R40), ssDNA (D40), dsRNA (R40−R14), or dsDNA (D40−D14) was added to the reaction mixture at a concentration of 20−200 μM (nucleotide base). Different pH conditions were also tested for the ATP hydrolysis activity of SUV3−83.

Helicase Substrates. Linear substrates (RNA−RNA, DNA−DNA, RNA−DNA, and DNA−RNA) were prepared by annealing 40-base oligonucleotides with complementary 5′-end-labeled 14-base oligonucleotides as previously described (*16*). The sequences of R14 and D14 were as described previously (*18*); R40 and D40 were identical to R44 and D44 (*18*), respectively, except for omission of four bases at the 3′-end. The shorter oligonucleotide was 5′-end-labeled with [γ-^{32}P]ATP using T$_4$ polynucleotide kinase (Roche Applied Science, Indianapolis, IN). In separate reactions, 5′-end-labeled DNA or RNA was mixed and annealed with a 2-fold excess of unlabeled complementary oligonucleotides in annealing buffer (1× TE with 200 mM NaCl). The annealed substrates were gel purified as described previously (*6*) and named R40−R14, R40−D14, D40−R14, and D40−D14.

The circular DNA helicase substrate was prepared by annealing a complementary 26-base oligonucleotide labeled at the 5′-end to ϕ×174 sscDNA (New England Biolabs, Beverly, MA), thus generating a partial duplex DNA as described previously (*19*).

The substrate for the directionality assay was constructed by hybridizing a 52-mer oligonucleotide (5′-CGA ACA ATT CAG CGG CTT TAA CCG GAC GCT CGA CGC CAT TAA TAA TGT TTT C-3′) to residues 702−753 of ϕ×174 sscDNA (*20*). After *Hpa*II digestion at the partial duplex region, the circular ϕ×174 sscDNA became a linear fragment containing a 22-nucleotide duplex region at its 5′-end and a 30-nucleotide duplex at its 3′-end. To blunt both ends, the linear substrate was filled in with one [α-^{32}P]dCTP and one cold dGTP using the Klenow fragment of DNA polymerase I. The resulting partial duplex substrate contained 24 and 32 bp at the 5′- and 3′-ends, respectively.

Helicase Assay. Unwinding reactions (20 μL) were carried out in helicase buffer [25 mM Tris-HCl (pH 7.5), 5 mM DTT, 0.1 mg/mL BSA, 2.5 mM MgCl$_2$, and 3 mM ATP] containing 1 nM substrate and an increasing amount of SUV3−83 or SUV3−70 at 37 °C for 60 min. Reactions were terminated by adding 5 μL of "stop mix" loading buffer containing 0.1 M Tris-HCl (pH 7.5), 20 mM EDTA, 0.5% SDS, 0.1% Nonidet P-40, 0.1% bromophenol blue, 0.1% xylene cyanol, and 25% glycerol. Aliquots of the reaction were electrophoresed through 15% native polyacrylamide gels in 1× TBE to separate the displaced labeled short strand. Gels were dried, and the radioactivity of the labeled DNA was quantified using a Storm 320 Phosphor Imager (Molecular Dynamics).

The helicase directionality assay was performed under the same conditions except that 0.8 nM of labeled substrate was used. The mixtures were then loaded on an 8% PAGE gel containing 1× TBE, 0.1% SDS, and 3 M urea, and run in 1× TBE buffer. Urea was used to interfere with the potential folding of released fragments.

The effect of pH on the helicase activity of SUV3−83 was analyzed as described above, except that the helicase buffer contained the following different buffer reagents (all at 25 mM): sodium citrate (pH 3.5), sodium acetate (pH 4.5, 5.0, and 5.5), phosphate buffer (pH 6.5 and 7.5), Tris buffer (pH 8.5), and ethanolamine buffer (pH 9.5).

The effect of different salts on the helicase activity was analyzed by preincubating 4 μg of SUV3−83 in 100 μL of 1 M salts [KCl, KOAc, KO(Cit)$_2$, MgSO$_4$, or (NH$_4$)$_2$SO$_4$] for 15 min. One microliter of this mixture was then added to the unwinding reaction mixture as described above. The effect of different salt concentrations on helicase activity was measured by varying the concentration of 0−500 mM KCl directly in the helicase reaction mixtures as described above.

Substrate Binding Assays. Gel mobility shift assays on dsRNA and dsDNA were performed exactly as described for the helicase assay except that the nonhydrolyzable ATP analogue ATPγS, instead of ATP, was used. The reaction mixture was incubated with increasing amounts of SUV3−83 for 30 min at 37 °C and the reaction terminated by adding a stop mix (lacking SDS) as described for the helicase assay. SDS (1%) was added separately to an aliquot of reaction mixture with the largest amount of protein to disrupt the binding of protein and nucleic acid to indicate the migration position of the labeled nucleic acids. The reaction mixtures were loaded on 10% native polyacrylamide gels for linear RNA−RNA substrates and 1% agarose gel for circular DNA−DNA substrates and electrophoresed at 4 °C as described above.

Circular Dichroism. Circular dichroism experiments were conducted using an Olis RSM-1000 CD spectrophotometer at 20 °C with continuous nitrogen flow protection in a 1 mm path length cylindrical quartz cuvette. CD spectra were scanned in the far-UV region (195−250 nm) by setting a stepwise increment of 0.5 nm and integrated time of 5 s with a protein concentration of 0.3 mg/mL for SUV3−70 and 0.2

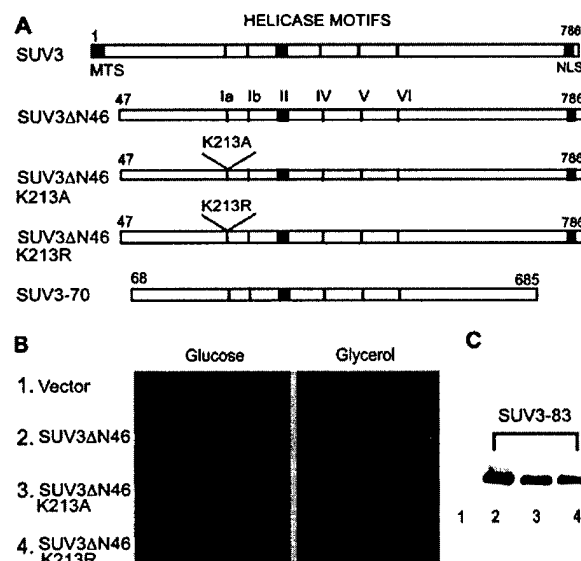mg/mL for SUV3−83 in 25 mM sodium acetate (pH 5.0) and 25 mM Tris-HCl (pH 7.0). Each datum was collected four times and averaged.

RESULTS

Expression of SUV3ΔN46 Rescues the Growth Defects of suv3 Null S. cerevisiae. Deletion of Suv3 in *S. cerevisiae* is associated with respiratory incompetence (*8*). Cells fail to grow in a nonfermentable carbon source like glycerol and form petite colonies in glucose media (*8*). To test whether human SUV3 can rescue a null phenotype, full-length human SUV3 and an endogenously processed form lacking the 46 N-terminal amino acids, SUV3ΔN46, were expressed in suv3 null yeast from a single-copy plasmid (C.-F. Chen, W.-H. Lee, *et al.*, manuscript submitted for publication). Both forms rescue the lethal phenotype in glycerol growth medium, indicating that human SUV3 is a functional homologue in yeast. To investigate if SUV3 has intrinsic helicase activity, we attempted to overexpress a full-length human SUV3 protein using a pJJ1 vector that contains a 2μ replication origin to facilitate purification. However, this was problem-atic due to the insolubility and instability of the protein (data not shown). To circumvent this difficulty, SUV3ΔN46, the processed form of SUV3, and its point mutants (SUV3ΔN46-K213A and SUV3ΔN46K213R) carrying A and R substitu-tion at an invariant K213 of the Walker A motif (*15*) were expressed in suv3 null yeast using a 2μ replication origin to test whether they can rescue the null phenotype (Figure 1A). SUV3ΔN46 complemented suv3 null cells as they no longer formed petite colonies on glucose and were also growth-competent in glycerol medium, while the vector alone and the two point mutants failed to rescue the growth defects of the suv3 null yeast (Figure 1B). Because the amounts of expressed protein from SUV3−83, SUV3−83K213A, and SUV3−83K213R were comparable (Figure 1C, lanes 2−4), these results suggest that SUV3−83, expressed from SUV3ΔN46, is a functional homologue of yeast SUV3 and the Walker A motif of SUV3−83 is critical to its function. Hence, we decided to purify SUV3−83 to elucidate the biochemical properties of SUV3.

Identification of SUV3−83 and SUV3−70. While puri-fying SUV3−83 from yeast (Figure 2A), we observed that SUV3−83 was processed into several truncated forms (Fig-ure 2B, lane 2). The most stable proteolytic form was purified and named SUV3−70 (Figure 2C). Both SUV3−83 and SUV3−70 were identified by mass spectroscopy after trypsin digestion with peptides covering more than 50% of the amino acids being identified in each of these proteins (Figure 3). Identities of both SUV3−83 and SUV3−70 were further confirmed by immunoblotting using an anti-SUV3 antibody.

Since our initial experiments showed that SUV3−70, instead of SUV3−83, contains detectable helicase activity, we decided to characterize SUV3−70 that may serve as a comparison if the deleted region(s) has its influence in its enzymatic activity. N-Terminal sequencing revealed that SUV3−70 initiated at the residue 68 (Figure 3A). The molecular mass of SUV3−70 was determined to be 70 004 Da by mass spectrometry analysis without proteolysis (Fig-ure 3C). On the basis of the molecular mass and the N-terminal sequence, the C-terminal residue was deduced to be amino acid 685 (calculated mass of 70 014 Da). Thus,

FIGURE 1: Human SUV3−83 is a functional homologue of yeast Suv3. (A) Schematic diagram of amino acid sequences of SUV3 proteins. The black boxes at the N- and C-termini represent the putative mitochondrial targeting signal (MTS) and the putative nuclear localization signal (NLS), respectively. Roman numerals (I−VI) denote the conserved helicase motifs. SUV3ΔN46 lacks the putative mitochondrial targeting signal (the first 21 residues) and an additional 25 amino acids at the N-terminus. SUV3−83K213A and SUV3−83K213R carry a mutation in the conserved lysine residue in motif I. SUV3−70 is a processed form of SUV3−83, which lacks 67 amino acids at the N-terminus and 101 amino acids at the C-terminus. (B) Growth of 5-fold dilutions of suv3 null yeast complemented with vector alone, SUV3ΔN46, SUV3−83K213A, or SUV3−83K213R on glucose- and glycerol-containing media. (C) Detection of SUV3 protein expression in suv3 null yeast transformed with vector alone (lane 1), SUV3ΔN46 (lane 2), SUV3−83K213A (lane 3), and SUV3−83K213R (lane 4) by immunoblotting using an anti-SUV3 monoclonal antibody.

SUV3−70 contains 618 residues from amino acids 68−685 of SUV3 and includes all the essential core helicase motifs (Figure 1A).

We next purified SUV3−83, SUV3−70, SUV3−83K213A, and SUV3−83K213R proteins on a large scale to near homogeneity as described in Experimental Procedures. Purified proteins were loaded on an 8% SDS−PAGE gel and found to be more than 95% pure by Coomassie blue staining (Figure 2C).

SUV3−83 and SUV3−70 Have ATPase Activity. SUV3 contains a Walker A motif at residues 207−214 that is involved in ATP hydrolysis in many other helicases (*21, 22*). Thus, purified SUV3 proteins were tested for ATPase activity. SUV3−83 and SUV3−70 each exhibited ATPase activity that showed a linear relationship with the amount of enzyme at the given concentration and condition (Figure 4A). However, SUV3−70 exhibited higher activity than SUV3−83 (Figure 4A). In contrast, the Walker A motif mu-tants, SUV3−83K213A and SUV3−83K213R, were defec-tive in ATP hydrolysis. Thus, SUV3 has intrinsic ATPase activity, which requires K213 within the Walker A motif.

We next investigated the effect of divalent cations on ATPase activity. A strict requirement for certain divalent cations, including Mg^{2+}, Mn^{2+}, and Co^{2+}, was observed, as ATPase activity was abolished in their absence, while replacement with Ca^{2+} and Zn^{2+} reduced the activity by ~60−80% (Figure 4B).
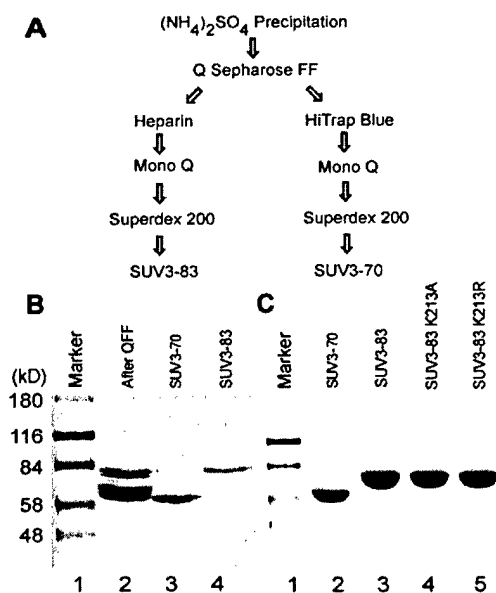
FIGURE 2: Purification of SUV3—83 and SUV3—70 expressed in yeast. (A) Purification schemes for SUV3—83 and SUV3—70 from yeast lysates. (B) Coomassie blue-stained 8% SDS—PAGE gel showing both SUV3—83 and SUV3—70 appear in the same fraction before purification (lane 2) and their subsequent separation: SUV3—70 (lane 3) and SUV3—83 (lane 4). Lane 1 contained molecular mass markers (kilodaltons). (C) SUV3—70 (3 μg, lane 2), SUV3—83 (4 μg, lane 3), SUV3—83K213A (4 μg, lane 4), and SUV3—83K213R (4 μg, lane 5) were analyzed via 8% SDS—PAGE and stained with Commassie blue for their purity. Lane 1 contained molecular mass markers (kilodaltons).

To test whether polynucleotide acids have any affect on the ATPase activity, we added a different amount of ssRNA, ssDNA, dsRNA, and dsDNA to the reaction mixture. At 20 μM (nucleotide base) polynucleotide acids, the ATPase activity of SUV3—70 was enhanced by 4.8-fold with ssRNA and by 1.2-fold with ssDNA (Figure 4C). Similarly, dsRNA and dsDNA were able to increase the ATP hydrolysis activity of SUV3—70, but not that of SUV3—83, at pH 7.5 (Figure 4C). To resolve this distinctive property, the ATPase activity assay was performed at different pHs for SUV3—83 because the enzymatic activity of SUV3—83 is apparently sensitive to pH change (see below). As shown in Figure 4D, dsDNA was able to enhance the ATP hydrolysis significantly at pH 5.0, but not at other pHs. The enhancement by dsDNA (5.4-fold) was even stronger than that of ssDNA (2.0-fold) at 40 μM (nucleotide base, data not shown). These results demonstrate that polynucleotide acids can stimulate the ATPase activity of SUV3.

SUV3—70 Has Multiple-Substrate Helicase Activity. Yeast Suv3 has been suggested to have RNA helicase activity (9). However, when compared to the consensus sequence motif for RNA and DNA helicases, the motif in SUV3 appears to be diverged from those found in RNA helicases. Therefore, we tested whether SUV3—83 and SUV3—70 have unwinding activity with a classical DNA substrate, circular single-stranded φ×174 DNA annealed with 26-mer complementary oligonucleotide labeled at the 5′-end, at pH 7.5. SUV3—70 unwound this substrate efficiently, while SUV3—83 exhibited little to no activity (Figure 5A,B). This suggests that SUV3 can use DNA as a substrate and unwind duplex DNA. To test whether the unwinding activity is ATP-dependent, we repeated the analysis in the absence of ATP or in the presence
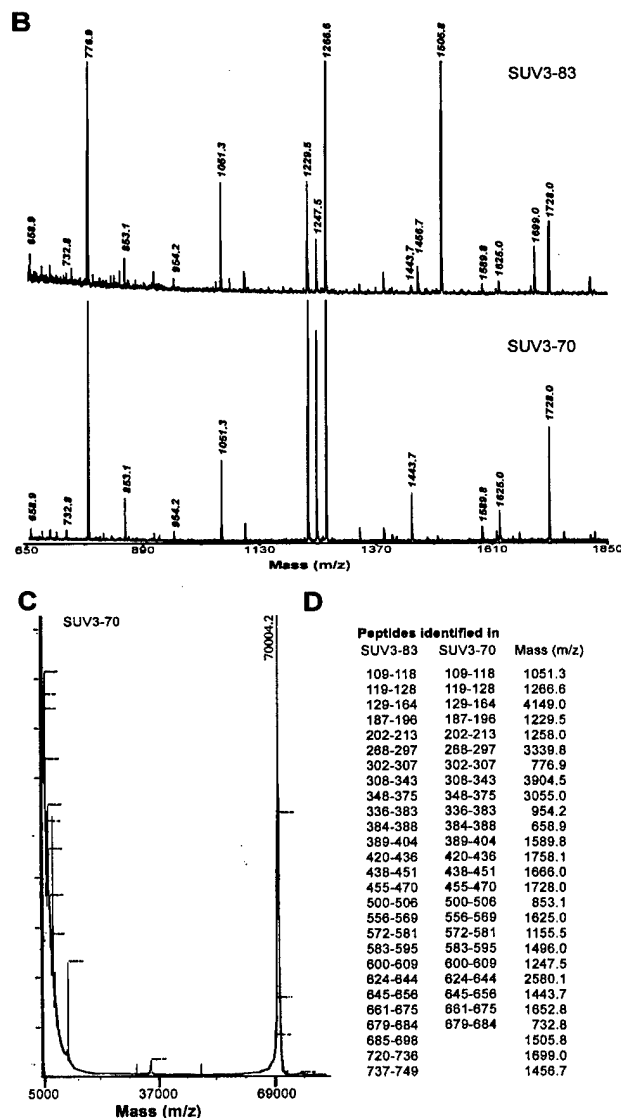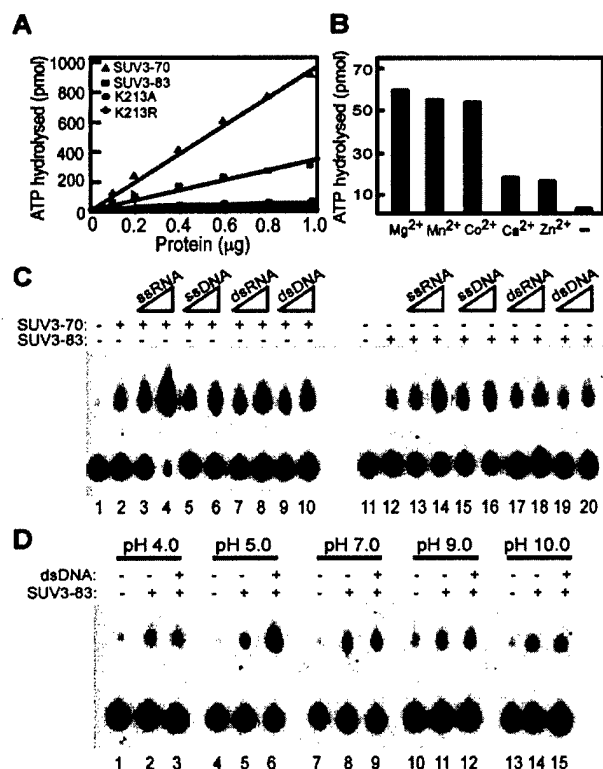

FIGURE 3: Sequence comparison between SUV3—83 and SUV3—70. (A) The N-terminal sequence of SUV3—70 was determined by Edman degradation. The 10 residues listed were obtained. (B) Comparison of the MALDI-TOF mass spectra between trypsin-digested SUV3—83 and SUV3—70. Only a limited m/z range is shown. (C) The mass of SUV3—70 was determined by mass spectrometry. SUV3—70 exhibited an m/z value of 70 004.2 in the experiment. (D) Tryptic peptides identified in SUV3—83 and SUV3—70 with their corresponding m/z values. SUV3—83 has all peptides from SUV3—70 in addition to three peptides at the C-terminal region.

of nonhydrolyzable analogue ATPγS. The results demonstrate that SUV3—70 requires a hydrolyzable form of the ATP for its unwinding activity (Figure 5C).
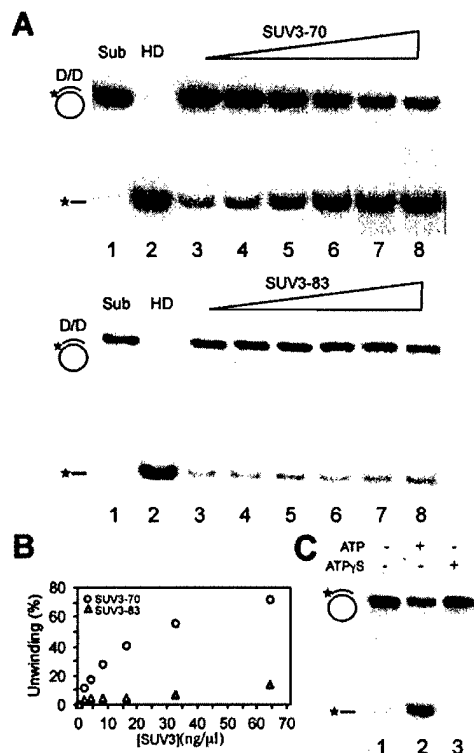
Next, we tested whether SUV3—70 could unwind linear polynucleotide substrates, including R40—R14, R40—D14, D40—R14, and D40—D14, each of which consisted of a 14 bp duplex region and a 26-nucleotide 5′-overhang. SUV3—70 could efficiently unwind R40—R14, R40—D14, and D40—R14 (Figure 6). In contrast, SUV3—83 could not unwind these substrates under identical conditions (data not shown). Under the same condition, neither SUV3—70 nor SUV3—83 could unwind the D40—D14 substrate (Figure 6D).
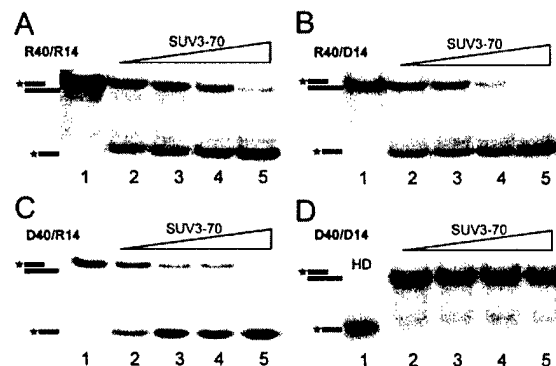
A

B

C

D

FIGURE 4: Characterization of the ATPase activity of SUV3. (A) Comparison of the ATPase activities of SUV3−83, SUV3−70, and two mutants. The ATPase reaction mixtures consisted of 25 mM Tris-HCl (pH 7.5 and 37 °C), 1 mM DTT, 5 mM $MgCl_2$, 50 mM KCl, and 100 ng/μL BSA. The reactions were carried out at 37 °C for 60 min, including 0.05 μCi/μL [γ-^{32}P]ATP, 100 μM ATP, and varying amounts of SUV3 proteins, including SUV3−83, SUV3−70, SUV3−83K213A, and SUV3−83K213R. SUV3−70 has a higher ATPase activity than SUV3−83. Both Walker A motif mutants lack ATPase activity. (B) Requirement of divalent cations for the ATPase activity of SUV3−83. The ATPase required divalent cations of Mg^{2+}, Mn^{2+}, Co^{2+}, Ca^{2+}, or Zn^{2+} for its activity and was inactive without it (−). (C) Polynucleotide acids stimulate SUV3 ATPase activity. The reaction was carried out at pH 7.5 as described for panel A, and the mixture contained SUV3−70 (lanes 2−10) or SUV3−83 (lanes 12−20) at 50 ng/μL each, and 20 or 200 μM (nucleotide base) ssRNA, ssDNA, dsRNA, or dsDNA as indicated. Lanes 1 and 11 were control reactions without protein. Polynucleotide acids stimulated both SUV3 ATPase activities, but the SUV3−83 ATPase activity was not enhanced by double-stranded RNA or DNA under the conditions that were used. (D) dsDNA stimulates the ATPase activity of SUV3−83 at pH 5.0. The conditions of the reaction were the same as those for panel A, except the buffer was changed to acetate buffer (pH 4.0 and 5.0), Tris-HCl buffer (pH 7.0), or ethanolamine buffer (pH 9.0 and 10.0). dsDNA [40 μM (nucleotide base)] was added to the mixtures as indicated. Panels C and D show the separation of free phosphate (top spots) from ATP (bottom spots) on the thin layer plates.

Similar results were seen when the experiments were performed using R26−R14, R26−D14, D26−R14, and D26−D14 linear substrates which had an eight-nucleotide 5′-overhang and a four-nucleotide 3′-overhang (data not shown). Collectively, these results indicate that SUV3 is a multiple-substrate helicase.

SUV3−70 Displays 5′−3′ Unwinding Activity. To unwind duplex DNA or RNA efficiently, helicases usually initiate the reaction at single-strand regions adjacent to the duplex (23). To determine the directionality of SUV3, we used a long linear DNA substrate containing partial duplex regions at either end blunted (Figure 7A). The release of a 24-mer fragment indicates movement in the 3′−5′ direction, while
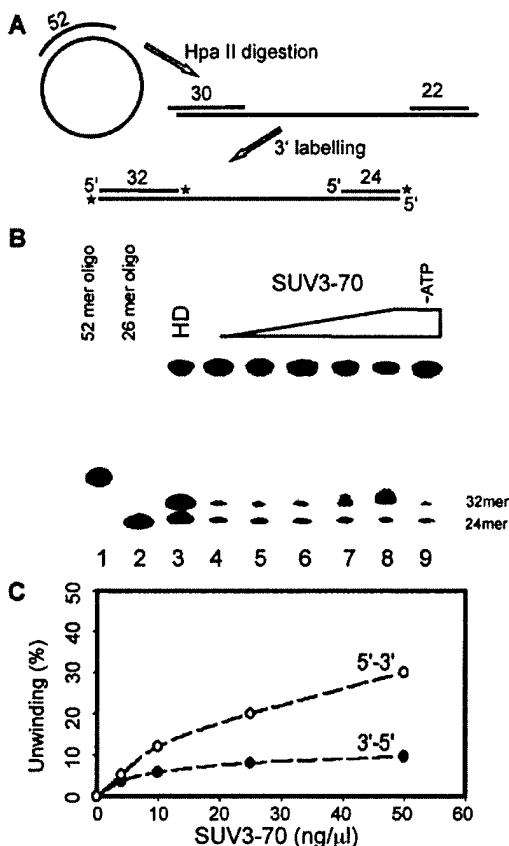
A

B

C

FIGURE 5: Unwinding activity of SUV3−70 and SUV3−83 on a circular DNA substrate. (A) Unwinding of the circular DNA−DNA substrate with increasing amounts of SUV3−70 and SUV3−83. Reactions were carried out in helicase buffer at pH 7.5 (25 mM Tris-HCl, 5 mM DTT, 0.1 mg/mL BSA, 2.5 mM $MgCl_2$, and 3 mM ATP) containing 1 nM circular DNA−DNA substrate. Lane 1 contained the substrate without enzyme and lane 2 the heat-denatured substrate; from lane 3 to 8, the enzyme concentrations were 2, 4, 8, 16, 32, and 64 ng/μL, respectively. (B) Quantitative plot of the unwinding efficiency of SUV3−70 and SUV3−83 at various enzyme concentrations. (C) The unwinding activity is ATP-dependent. The reaction conditions were the same as those described for panel A, except no ATP was present in lane 1 and ATPγS was added in lane 3 instead of ATP.

A **B** **C** **D**

FIGURE 6: Unwinding activity of SUV3−70 on linear substrates. Reactions were carried out in helicase buffer at pH 7.5 with increasing concentrations of SUV3−70, at 2, 4, 8, and 16 ng/μL in lanes 2−5, respectively. Different substrates, including (A) R40−R14, (B) R40−D14, (C) D40−R14, and (D) D40−D14, were used in each reaction.
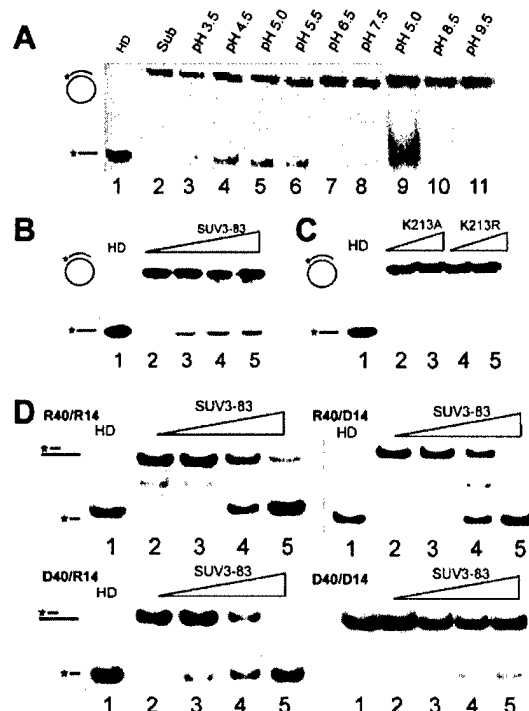
release of a 32-mer fragment indicates movement in the 5′−3′ direction. When this substrate was incubated with increasing amounts of SUV3−70, the 32-mer was preferentially displaced in an ATP-dependent manner (Figure 7B, lanes 5−9), indicating that SUV3−70 prefers the 5′−3′ direction (Figure 7B,C), although a slight displacement of 24-mer was also observed.

FIGURE 7: Determining the directionality of SUV3 helicase. (A) Methods of construction of the partial duplex substrate with blunted ends used to determine directionality. Details are given in Experimental Procedures. (B) Directionality assay of SUV3−70 helicase activity. Lanes 1 and 2 contained the labeled 52- and 26-mer as markers, respectively. Lanes 3 and 4 contained the heat-denatured substrate (HD) and native substrate, respectively. Lanes 5−8 show reactions with increasing amounts of SUV3−70 (4, 10, 25, and 50 ng/µL, respectively). Lane 9 had the same conditions as lane 8 but without ATP. (C) Quantitative plots of the unwinding percentage in panel B. An increasing amount of 32-mer from the reaction indicated that SUV3 helicase has a 5′−3′ directionality.

FIGURE 8: SUV3−83 exhibits helicase activity under acidic conditions. (A) Reaction mixtures containing 4 ng/µL SUV3−83 and 1 nM circular DNA substrate were incubated in 25 mM helicase buffers at different pHs: sodium citrate at pH 3.5 (lane 3), sodium acetate at pH 4.5 (lane 4) and pH 5.0 (lanes 5 and 9), phosphate buffer at pH 5.5 (lane 6), pH 6.5 (lane 7), and pH 7.5 (lanes 8), Tris-HCl buffer at pH 8.5 (lane 10), and ethanolamine buffer at pH 9.5 (lane 11). (B) Helicase reactions at pH 5.0 (25 mM sodium acetate, 5 mM DTT, 0.1 mg/mL BSA, 2.5 mM MgCl$_2$, and 3 mM ATP) with increasing amounts of SUV3−83 (2, 4, 8, and 16 ng/µL for lanes 2−5, respectively) and 1 nM partial duplex circular DNA substrate. (C) SUV3−83K213A and SUV3−83K213R have no detectable helicase activity. Reactions were carried out at pH 5.0 as described for panel B. Lane 1 contained the heat-denatured substrate. Lanes 2 and 3 contained 8 and 16 ng/µL SUV3−83K213A, respectively. Lanes 4 and 5 contained 8 and 16 ng/µL SUV3−83K213R, respectively. (D) Reaction mixtures contained increasing amounts of SUV3−83 (2, 4, 8, and 16 ng/µL in lanes 2−5, respectively) were incubated with R40−R14, R40−D14, D40−R14, or D40−D14 substrates in the pH 5.0 helicase buffer.

Optimizing SUV3−83 Helicase Activity. Although it contains the same helicase motif as SUV3−70, SUV3−83 did not display helicase activity under standard reaction conditions (pH 7.5). It is possible that SUV3−83 may require conditions different from those needed by SUV3−70 for the activity. Addition of salts can stimulate the strand exchange activity of human Rad51 (24) and ATPase activity of yeast Mot1 (24). Consequently, we tested the effect of various salt concentrations on the helicase activity of SUV3−83. The activity of SUV3−83 on the circular DNA−DNA substrate remained undetectable despite the presence of 0−500 mM KCl in the helicase reaction mixture (data not shown). Changing the order of treatment by preincubation of SUV3−83 in different salts before addition to the reaction mixtures also had no effect on stimulating helicase activity.

Next, we tested whether the SUV3−83 helicase activity on a circular DNA−DNA substrate was pH-dependent. Interestingly, SUV3−83 exhibited DNA−DNA helicase activity at only acidic pHs ranging from 4.5 to 5.5 but not at neutral or basic pHs (Figure 8). For example, SUV3−83 unwinds circular DNA−DNA substrates at pH 5.0 in a dose-dependent manner (Figure 8B). To further test whether ATPase activity is essential for the helicase activity, two

Walker A motif mutants, SUV3−83K213A and SUV3−83K213R, which were deficient in ATPase activity (Figure 4A), were used for an unwinding assay with a circular DNA−DNA substrate at pH 5.0. Both mutants were inactive (Figure 8C), consistent with the notion that hydrolysis of ATP is required for the SUV3 helicase activity.

Other linear substrates used in the helicase assay for SUV3−70 were also tested for SUV3−83 at pH 5.0. As shown in Figure 8D, SUV3−83 unwound linear RNA−RNA, RNA−DNA, and DNA−RNA substrates efficiently, although only minimal activity was detected using a linear DNA−DNA substrate. These results indicate that SUV3−83 has multiple-substrate helicase activity under acidic conditions.

Effect of pH on Substrate Binding of SUV3−83. Many helicases first bind substrate then translocate along the substrate template to unwind the duplex (23). The inability of SUV3−83 to unwind duplex substrates could be due to its low affinity with these substrates at pH 7.5. Therefore, we compared the binding of SUV3−83 to an RNA−RNA substrate at pH 7.5 and 5.0 by incubating various concentra-
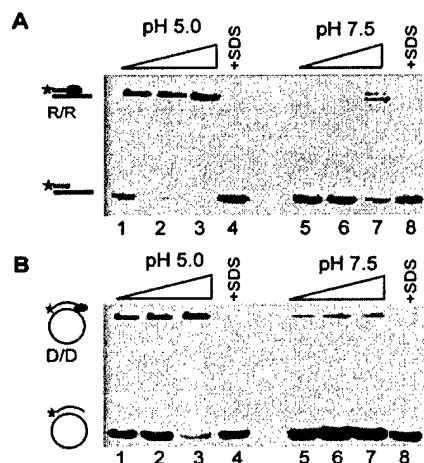
FIGURE 9: SUV3−83 preferentially binds its substrates at acidic pH. (A) Binding assay of SUV3−83 with the R40−R14 substrate at pH 5.0 (lanes 1−3) and pH 7.5 (lanes 5−7) with increasing amounts of protein (4, 8, and 16 ng/μL). Lane 4 was the same as lane 3 but was treated with 1% SDS; lane 8 was the same as lane 7 but was treated with 1% SDS. (B) Binding assay of SUV3−83 with a circular DNA−DNA substrate (1 nM) at pH 5.0 (lanes 1−3) and pH 7.5 (lanes 5−7) with increasing amounts of SUV3−83 (4, 8, and 16 ng/μL). Lane 4 was the same as lane 3 but was treated with 1% SDS; lane 8 was the same as lane 7 but was treated with 1% SDS.

tions of SUV3−83 with the substrate in the presence of nonhydrolyzable ATP analogue ATPγS. SUV3−83 bound the RNA−RNA substrate strongly at pH 5.0, while it bound weakly to the same substrate at pH 7.5 (Figure 9A). Similarly, SUV3−83 bound the circular DNA−DNA substrate with greater affinity at pH 5.0 than at pH 7.5 (Figure 9B). Thus, substrate binding of SUV3−83 is pH-dependent, which is consistent with the observation that SUV3−83 has unwinding activity at acidic pHs.

Conformational Change Regulates the Helicase Activity of SUV3. The difference in the helicase activity of SUV3−83 and SUV3−70 can be ascribed to the sequences missing from both the N- and C-termini of SUV3−83 (Figure 1A). These sequences may affect the conformation of SUV3−83 by altering the affinity for substrates. In the case of SUV3−70, these putative regulatory domains are missing, and hence, the catalytic site is readily accessible under all conditions. On the basis of this rationale, an acidic pH would be expected to induce a conformational change in SUV3−83 to expose its active sites. To test this possibility, we used far-UV CD spectroscopy to detect the conformational changes in the secondary structure of these proteins. As shown in Figure 10A, the CD spectra of SUV3−70 suggest that it is an α-helix rich protein (*26−28*) which did not change in shape significantly when the pH was decreased to 5.0 (data not shown). The CD spectrum of SUV3−83 at pH 7.0 is much different from that of SUV3−70 (Figure 10B). However, when the pH was decreased to 5.0, the spectrum closely resembled that of SUV3−70 (Figure 10B). This result indicated that SUV3−83 underwent a significant conformational change at pH 5.0 and adopted a conformation similar to that of SUV3−70.

DISCUSSION

S. cerevisiae Suv3 has been classified as a mitochondrial RNA helicase. In work yet to be published, we showed that
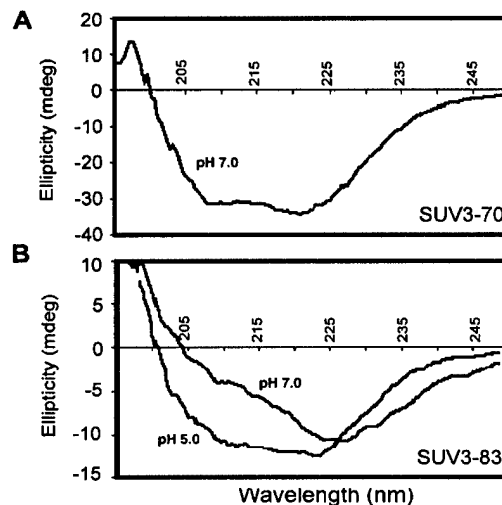

FIGURE 10: Circular dichroism spectra of SUV3−70 and SUV3−83 at different pHs. The far-UV CD spectrum was recorded for (A) SUV3−70 (0.3 mg/mL) in 25 mM Tris-HCl buffer (pH 7.0) and (B) SUV3−83 (0.2 mg/mL) in 25 mM sodium acetate buffer (pH 5.0) or in 25 mM Tris-HCl buffer (pH 7.0).

SUV3 is processed by protease at the mitochondria to remove 46 amino acids from the N-terminus, and it is the major functional component of SUV3 ubiquitously expressed in different types of mammalian cells (C.-F. Chen, W.-H. Lee. *et al.*, manuscript submitted for publication). Consistent with this finding, expression of SUV3ΔN46 in the yeast suv3 null mutant restores their ability to grow in a nonfermentable carbon source and form healthy colonies in glucose medium, suggesting that SUV3−83 is a functional homologue of yeast Suv3 *in vivo*. Through a five-step chromatographic procedure, both SUV3−83 and SUV3−70 were purified to more than 95% homogeneity. Both SUV3−83 and SUV3−70 have moderate ATPase activities that can be stimulated by polynucleotide acids. At neutral pH (7.5), SUV3−70 can bind and unwind multiple substrates, including homo- and heteroduplexes of RNA and DNA, while SUV3−83 has little helicase activity. At acidic pHs (4.5−5.5), SUV3−83 unwinds multiple substrates, like SUV3−70. Consistent with this observation, SUV3−83, at pH 5.0, adopts a conformation similar to that of SUV3−70. These results indicate that SUV3−83 is a multiple-substrate helicase that can be modulated by conformational change.

ATPase Activity of SUV3−83 and SUV3−70. Purified SUV3−83 and SUV3−70 each displayed ATPase activity, but SUV3−70 exhibited activity higher than that of SUV3−83 when assayed at neutral pH. The reason for the lower activity of SUV3−83 is currently unclear. The ATPase activity exhibited strict cation dependence and was supported almost equally by Mg^{2+}, Mn^{2+}, and Co^{2+}, with Ca^{2+} and Zn^{2+} being less effective. Two mutants with amino acid substitution in the conserved Walker A motif completely lost ATPase activity, indicating that the Walker A motif is required for ATP hydrolysis.

At neutral pH, single-stranded RNA or DNA at >20 μM (nucleotide base) stimulated the ATPase activities of both SUV3−83 and SUV3−70, while double-stranded RNA and DNA significantly enhanced the ATPase activity of SUV3−70 but not of SUV3−83. After the assay condition had been changed to pH 5.0, both double-stranded RNA and DNA significantly stimulated SUV3−83 ATPase activity. These

results are consistent with the known observation that polynucleotide acids stimulate the ATPase activity of helicase (*15*). Although it remains to be verified how these polynucleotide acids stimulate the ATPase activity of SUV3, it is likely that binding to these polynucleotide acids may facilitate the ATP hydrolysis by these two proteins, which is consistent with the result that SUV3−83 bound strongly to dsRNA or dsDNA at only acidic pHs (Figure 9).

Substrate Specificity of SUV3 Helicase. Suv3 of *S. cerevisiae* has been categorized as a putative ATP-dependent mitochondria RNA helicase member of the DEAD/DExH family (*8−10*). On the basis of our results, we conclude that human SUV3 is an ATP-dependent multiple-substrate helicase. In addition to dsRNA and dsDNA unwinding activity, SUV3−70 and SUV3−83 can unwind heteroduplexes of RNA and DNA. The latter substrate specificity of SUV3 provides an ample opportunity for executing its biological function. It was recently reported that SUV3 preferentially unwinds duplex DNA over duplex RNA (*12*). However, we did not find any such preferential unwinding of DNA by either SUV3−83 or SUV3−70. The SUV3 protein used in this previous report had 22 amino acids deleted at the N-terminus, as opposed to 46 amino acids deleted in the SUV3−83 described here. Because the proteolytic processing at the mitochondria is critical for the biological function of SUV3 (C.-F. Chen, W.-H. Lee, *et al.*, manuscript submitted for publication), SUV3 with 22 amino acids deleted from the N-terminus is not able to complement suv3 null yeast (*12*), perhaps because of its inability to be processed correctly at mitochondria. Thus, the biochemical properties exhibited by SUV3−83 are more likely to reflect *in vivo* function. Alternatively, the preferential unwinding of DNA could be attributed to the nature of the DNA substrate used in their assay. In our study, unwinding activity was seen on only substrates with partial duplex circular DNA or long partially duplex linear DNA, but not on substrates with short linear duplex DNA. The shorter linear duplex DNAs, including D40−D14 and D26−D14 used in this study, were poor substrates despite the fact that they had a short nucleotides overhang, while the substrate used by Minczuk et al. (*12*) had a forked structure at the 5′-end. It is possible that SUV3, like BLM and WRN (*6*), may have a higher affinity for specialized DNA structures such as forked DNA or X-junctions.

Conformation Change Induced by pH. It is known that pH is a critical factor influencing helicase activity (*29, 30*). RepA, a DNA helicase from *Escherichia coli*, exhibits optimal helicase activity and DNA binding activity at pH 5.5, while at pH 7.5, these activities are greatly diminished (*29*). Similarly, SUV3−83 was unable to engage in productive dsDNA and dsRNA binding and unwinding activity at pH 7.5; however, it exhibited optimal binding and unwinding activities at pH 5.0. How the conformational change induced by pH affects the enzyme activity is very intriguing. SUV3−83 adopts different secondary structures as observed by its CD spectra at two distinctive pH conditions. On the basis of this information, it is reasonable to assume that the protein conformation changes at acidic pH may modulate the active site and the nucleotide binding domain, thus facilitating its polynucleotide binding, ATP hydrolysis, and duplex unwinding function. It is noted that SUV3−70, which lacks 21 amino acids at the N-terminus and 101 amino acids at the

C-terminus, in contrast to SUV3−83, has a helicase activity at neutral and acidic pH, suggesting that these residues that are absent in SUV3−70 may have a regulatory role in SUV3 protein folding.

Physiological Relevance of the SUV3−83 Helicase Activity. The pH-induced conformational change of SUV3−83 observed *in vitro* could be mimicked *in vivo* by a post-translational modification or by interaction with an accessory protein. For example, phosphorylation and acetylation of p53, a tumor suppressor and transcription factor, has been shown to stimulate its specific DNA binding activity (*31, 32*). In the case of ATM, a DNA damage checkpoint protein, autophosphorylation was shown to result in a conformational change, which, in turn, activated its kinase activity (*33*). Whether SUV3 is subjected to secondary modification by phosphorylation is not yet known. Alternatively, binding to other proteins may activate the helicase activity of SUV3−83. It was reported that Mre11 and the Mre11−Rad50 complex exhibit differential nuclease activity (*34*), indicating that the binding of Rad50 affects Mre11 activity. Our preliminary result showing that binding to Mre11 activated SUV3 helicase activity supports this possibility.

Although SUV3 has been classified as a mitochondrial helicase, our preliminary results suggest that SUV3 exists in two compartments of the cell, mitochondria and nucleus (C.-F. Chen, W.-H. Lee, *et al*, manuscript submitted for publication). SUV3−83 is rapidly processed from full-length SUV3 at mitochondria and then translocates to nucleus and mitochondria matrix. Yeast Suv3 has been shown to play a very important role in mitochondrial RNA stability and has been postulated to be responsible for the degradation of aberrant RNAs (*10*). It is currently unclear whether the RNA−RNA helicase activity displayed by SUV3 has any role in the nucleus. It is also possible that in these two different organelles SUV3 recognizes different substrates as dictated by the environment and its binding partners. The RNA−DNA helicase activity of SUV3 could point toward its role in transcription, lagging strand synthesis, mitochondrial DNA replication, and/or telomere maintenance where such RNA−DNA hybrid structures are commonly encountered. The DNA−DNA helicase activity exhibited by human SUV3 could be employed in DNA recombination as suggested by our preliminary results (C.-F. Chen, W.-H. Lee, *et al*, manuscript submitted for publication). Thus, SUV3 may serve as a critical helicase for many physiological functions because of its substrate diversity and highly regulated unwinding activity.

REFERENCES

1. Matson, S. W., and Kaiser-Rogers, K. A. (1990) DNA helicases, *Annu. Rev. Biochem. 59*, 289−329.
2. Tanner, N. K., and Linder, P. (2001) DExD/H box RNA helicases: from generic motors to specific dissociation functions, *Mol. Cell 8*, 251−262.

3. Sancar, A., and Sancar, G. B. (1988) DNA repair enzymes, *Annu. Rev. Biochem. 57*, 29−67.

4. Van Brabant, A. J., Stan, R., and Ellis, N. A. (2000) DNA helicases, genomic instability, and human genetic disease, *Annu. Rev. Genomics Hum. Genet. 1*, 409−459.

5. Hall, M. C., and Matson, S. W. (1999) Helicase motifs: the engine that powers DNA unwinding, *Mol. Microbiol. 34*, 867−877.

6. Mohaghegh, P., Karow, J. K., Brosh, R. M., Jr., Bohr, V. A., and Hickson, I. D. (2001) The Bloom's and Werner's syndrome proteins are DNA structure-specific helicases, *Nucleic Acids Res. 29*, 2843−2849.

7. McGlynn, P., and Lloyd, R. G. (2001) Rescue of stalled replication forks by RecG: simultaneous translocation on the leading and lagging strand templates supports an active DNA unwinding model of fork reversal and Holliday junction formation, *Proc. Natl. Acad. Sci. U.S.A. 98*, 8227−8234.

8. Stepien, P. P., Margossian, S. P., Landsman, D., and Butow, R. A. (1992) The yeast nuclear gene suv3 affecting mitochondrial post-transcriptional processes encodes a putative ATP-dependent RNA helicase, *Proc. Natl. Acad. Sci. U.S.A. 89*, 6813−6817.

9. Margossian, S. P., Li, H., Zassenhaus, H. P., and Butow, R. A. (1996) The DExH box protein Suv3p is a component of a yeast mitochondrial 3′-to-5′ exoribonuclease that suppresses group I intron toxicity, *Cell 84*, 199−209.

10. Dziembowski, A., Piwowarski, J., Hoser, R., Minczuk, M., Dmochowska, A., Siep, M., van der Spek, H., Grivell, L., and Stepien, P. P. (2003) The yeast mitochondrial degradosome. Its composition, interplay between RNA helicase and RNase activities and the role in mitochondrial RNA metabolism, *J. Biol. Chem. 278*, 1603−1611.

11. Dmochowska, A., Kalita, K., Krawczyk, M., Golik, P., Mroczek, K., Lazowska, J., Stepien, P. P., and Bartnik, E. (1999) A human putative Suv3-like RNA helicase is conserved between *Rhodobacter* and all eukaryotes, *Acta Biochim. Pol. 46*, 155−162.

12. Minczuk, M., Piwowarski, J., Papworth, M. A., Awiszus, K., Schalinski, S., Dziembowski, A., Dmochowska, A., Bartnik, E., Tokatlidis, K., Stepien, P. P., and Borowski, P. (2002) Localisation of the human hSuv3p helicase in the mitochondrial matrix and its preferential unwinding of dsDNA, *Nucleic Acids Res. 30*, 5074−5086.

13. Matson, S. W. (1989) *Escherichia coli* DNA helicase II (uvrD gene product) catalyzes the unwinding of DNA·RNA hybrids in vitro, *Proc. Natl. Acad. Sci. U.S.A. 86*, 4430−4434.

14. Stahl, H., Droge, P., and Knippers, R. (1986) DNA helicase activity of SV40 large tumor antigen, *EMBO J. 5*, 1939−1944.

15. Caruthers, J. M., and McKey, D. B. (2002) Helicase structure and mechanism, *Curr. Opin. Struct. Biol. 12*, 123−133.

16. Zheng, L., Chen, Y., and Lee, W. H. (1999) Hec1p, an evolutionarily conserved coiled-coil protein, modulates chromosome segregation through interaction with SMC proteins, *Mol. Cell. Biol. 19*, 5417−5428.

17. Kinter, M., and Sherman, N. E. (2000) *Protein Sequencing and Identification using Tandem Mass Spectroscopy*, John Wiley, New York.

18. Rogers, G. W., Jr., Lima, W. F., and Merrick, W. C. (2001) Further characterization of the helicase activity of eIF4A. Substrate specificity, *J. Biol. Chem. 276*, 12598−12608.

19. Whitby, M. C., Vincent, S. D., and Lloyd, R. G. (1994) Branch migration of Holliday junctions: identification of RecG protein as a junction specific DNA helicase, *EMBO J. 13*, 5220−5228.

20. Seo, Y. S., Lee, S. H., and Hurwitz, J. (1991) Isolation of a DNA helicase from HeLa cells requiring the multisubunit human single-stranded DNA-binding protein for activity, *J. Biol. Chem. 266*, 13161−13170.

21. Brocchieri, L., and Karlin, S. (1998) A symmetric-iterated multiple alignment of protein sequences, *J. Mol. Biol. 276*, 249−264.

22. Walker, J. E., Saraste, M., Runswick, M. J., and Gay, N. J. (1982) Distantly related sequences in the α- and β-subunits of ATP synthase, myosin, kinases and other ATP-requiring enzymes and a common nucleotide binding fold, *EMBO J. 1*, 945−951.

23. Soultanas, P., and Wigley, D. B. (2001) Unwinding the 'Gordian knot' of helicase action, *Trends Biochem. Sci. 26*, 47−54.

24. Sigurdsson, S., Trujillo, K., Song, B., Stratton, S., and Sung, P. (2001) Basis for avid homologous DNA strand exchange by human Rad51 and RPA, *J. Biol. Chem. 276*, 8798−8806.

25. Adamkewicz, J. I., Mueller, C. G., Hansen, K. E., Prud'homme, W. A., and Thorner, J. (2000) Purification and enzymic properties of Mot1 ATPase, a regulator of basal transcription in the yeast *Saccharomyces cerevisiae*, *J. Biol. Chem. 275*, 21158−21168.

26. Pellaud, J., Schote, U., Arvinte, T., and Seelig, J. (1999) Conformation and self-association of human recombinant transforming growth factor-β3 in aqueous solutions, *J. Biol. Chem. 274*, 7699−7704.

27. Nam, G. H., and Choi, K. Y. (2002) Association of human tumor necrosis factor-related apoptosis inducing ligand with membrane upon acidification, *Eur. J. Biochem. 269*, 5280−5287.

28. Johnson, W. C., Jr. (1988) Secondary structure of proteins through circular dichroism spectroscopy, *Annu. Rev. Biophys. Chem. 17*, 145−166.

29. Scherzinger, E., Ziegelin, G., Barcena, M., Carazo, J. M., Lurz, R., and Lanka, E. (1997) The RepA protein of plasmid RSF1010 is a replicative DNA helicase, *J. Biol. Chem. 272*, 30228−30236.

30. Sung, P., Higgins, D., Prakash, L., and Prakash, S. (1988) Mutation of lysine-48 to arginine in the yeast RAD3 protein abolishes its ATPase and DNA helicase activities but not the ability to bind ATP, *EMBO J. 7*, 3263−3269.

31. Gu, W., and Roeder, R. G. (1997) Activation of p53 sequence-specific DNA binding by acetylation of its C-terminal domain, *Cell 90*, 595−606.

32. Saito, S., Goodarzi, A. A., Higashimoto, Y., Noda, Y., Lees-Miller, S. P., Appella, E., and Anderson, C. W. (2002) ATM mediates phosphorylation at multiple p53 sites, including Ser (46), in response to ionizing radiation, *J. Biol. Chem. 277*, 12491−12494.

33. Bakkenist, C. J., and Kastan, M. B. (2003) DNA damage activates ATM through intermolecular autophosphorylation and dimer dissociation, *Nature 421*, 499−506.

34. Paull, T. T., and Gellert, M. (1998) The 3′ to 5′ exonuclease activity of Mre 11 facilitates repair of DNA double-strand breaks, *Mol. Cell 1*, 969−979.

BI0356449

Physical and Functional Interaction between the XPF/ERCC1 Endonuclease and hRad52*

Teresa A. Motycka‡§, Tadayoshi Bessho§¶, Sean M. Post‡∥, Patrick Sung**,
and Alan E. Tomkinson‡‡§§

From the ‡Molecular Medicine Graduate Program, Institute of Biotechnology, The University of Texas Health Science
Center, San Antonio, Texas 78245, ¶Eppley Institute, University of Nebraska Medical Center, Omaha, Nebraska 68198-
6805, the **Department of Molecular Biophysics and Biochemistry, Yale University, New Haven, Connecticut 06520-8024,
and ‡‡Radiation Oncology Research Laboratory, Department of Radiation Oncology, University of Maryland,
Baltimore, Maryland 21201-1509

The XPF/ERCC1 heterodimer is a DNA structure-specific endonuclease that participates in nucleotide excision repair and homology-dependent recombination reactions, including DNA single strand annealing and gene targeting. Here we show that XPF/ERCC1 is stably associated with hRad52, a recombinational repair protein, in human cell-free extracts and that these factors interact directly via the N-terminal domain of hRad52 and the XPF protein. Complex formation between hRad52 and XPF/ERCC1 concomitantly stimulates the DNA structure-specific endonuclease activity of XPF/ERCC1 and attenuates the DNA strand annealing activity of hRad52. Our results reveal a novel role for hRad52 as a subunit of a DNA structure-specific endonuclease and are congruent with evidence implicating both hRad52 and XPF/ERCC1 in a number of homologous recombination reactions. We propose that the ternary complex of hRad52 and XPF/ERCC1 is the active species that processes recombination intermediates generated during the repair of DNA double strand breaks and in homology-dependent gene targeting events.

In the yeast *Saccharomyces cerevisiae*, Rad1 and Rad10 proteins form a stable complex with DNA structure-specific endonuclease activity (1, 2). During the removal of DNA lesions by nucleotide excision repair (NER),[1] Rad1-Rad10 complex makes the 5′ incision in a bubble structure generated as a result of localized unwinding of the damaged DNA (2, 3). A stable interaction with the DNA damage recognition protein Rad14 appears to mediate the specific recruitment of Rad1/Rad10 to the damaged strand (4). Interestingly, unlike the other members of the *RAD3* epistasis group that constitute the yeast NER path-

way, the *RAD1* and *RAD10* genes also participate in specialized forms of mitotic recombination including the single strand annealing (SSA) pathway of recombination between direct sequence repeats and the integration of plasmid DNA into homologous chromosomal sequences (reviewed in Ref. 5).

In mammalian NER, XPF/ERCC1, the equivalent of Rad1/Rad10, interacts with XPA, the equivalent of Rad14, and makes the 5′ incision in the damaged strand (6–12). Similar to its yeast counterpart, XPF/ERCC1 is multifunctional, participating in intrachromosomal recombination between direct sequence repeats, the repair of DNA interstrand cross-links, and gene targeting (13–17). Although the XPF/ERCC1 endonuclease removes non-homologous single strand tails during targeted homologous recombination and SSA (17), a recent study (13) has revealed that XPF/ERCC1 is still required for gene targeting even when the targeting construct is homologous with the genomic locus. At the present time it is not known how XPF/ERCC1 is recruited to the specific recombination intermediates generated during SSA and targeted homologous recombination.

In yeast, the majority of DNA double strand breaks are repaired by recombinational repair pathways mediated by the products of genes in the *RAD52* epistasis group (18, 19). Within this epistasis group, inactivation of the *RAD52* gene results in the most severe phenotype (18, 19). Interestingly, genetic studies have implicated Rad52 in the same types of specialized mitotic recombination, SSA and homology-dependent integration of plasmid DNA, as the Rad1/Rad10 endonuclease (20, 21). Although inactivation of vertebrate *RAD52* homologs does not significantly affect cellular sensitivity to agents that cause DNA double-strand breaks, these mutant cell lines are defective in the targeting of DNA molecules to homologous chromosomal loci, although to a lesser extent than that observed in yeast *rad52* mutants (22, 23).

Eukaryotic Rad52 protein contains a conserved N-terminal domain that binds to DNA and self-associates to form a heptameric ring structure (24–27). Consistent with their role in SSA, both human (h) and yeast (y) Rad52 proteins promote the renaturation of complementary DNA single strands (28, 29). In this study, we provide evidence that the function of the XPF/ERCC1 DNA structure-specific endonuclease is modulated by a direct interaction with hRad52. These results reveal a novel role for hRad52 in recombination and suggest a mechanism for the targeting and activation of the XPF/ERCC1 endonuclease in recombination reactions.

EXPERIMENTAL PROCEDURES

Fractionation of HeLa Extract by Immunoaffinity Chromatography with XPF Antibody—XPF antibodies (NeoMarkers, 50 μg) and anti-

[1] The abbreviations used are: NER, nucleotide excision repair; GST, glutathione S-transferase; SSA, single strand annealing; hRad52, human Rad52; yRad52, yeast Rad52.

His$_6$ antibodies (Clontech, 50 μg) were coupled to protein A beads (Invitrogen, 50 μl) as described (30). The beads were incubated with cell-free extract (500 μg, total protein) from HeLa cells (31) for 1 h at 4 °C in 500 μl of Buffer A (25 mM HEPES-KOH, pH 7.8, 100 mM KCl, 1 mM MgCl$_2$, 0.1 mM EDTA, 12.5% glycerol, 1 mM dithiothreitol). After washing the beads with 137 mM NaCl, 2.7 mM KCl, 10 mM Na$_2$HPO$_4$, 2 mM KH$_2$PO$_4$, pH 7.2, bound proteins were eluted in a stepwise fashion with 50 μl of Buffer A containing 0.2, 0.5, 1 M KCl and then 0.2 M glycine, pH 2.0. Aliquots (10 μl) of the eluates were separated by SDS-PAGE, and XPF, ERCC1, and hRad52 were detected by immunoblotting. ERCC1 antibodies were from Neomarkers, and hRad52 antibodies (32) were a gift from Dr. Eva Lee.

Immunoprecipitation—HeLa cells were lysed in Buffer B (50 mM Tris-HCl, pH 7.5, 300 mM NaCl, 2 mM EDTA, and 1% Nonidet P-40) containing a mixture of protease and phosphatase inhibitors (1 mM benzamidine-HCl, 1 mM phenylmethylsulfonyl fluoride, 10 μg/ml aprotinin, 100 mM sodium fluoride, 1 mM sodium orthovanadate, and 1 mM β-glycerophosphate) and a final concentration of 20 μg/ml ethidium bromide. Clarified lysates (2 mg) were incubated with protein G beads (Amersham Biosciences, 20 μl) and either anti-hRad52 rabbit antiserum (2 μl), pre-immune antiserum (2 μl), anti-XPF antiserum (2 μl), or anti-ERCC1 antiserum (2 μl, Santa Cruz Biotechnology) for 2 h at 4 °C. After extensive washing with Buffer B, immunoprecipitated proteins were separated by SDS-PAGE, and XPF was detected by immunoblotting.

Purification of Recombinant hRad52—*Escherichia coli* BL21(DE3) cells harboring pET28b-hRad52 that encodes hRad52 with a C-terminal His$_6$ tag were grown in Terrific Broth (33) and induced with 1 mM isopropylthiogalactoside for 5 h at 30 °C. Cells were lysed in 50 mM Tris-HCl, pH 7.5, 10% sucrose, 10 mM EDTA, 600 mM KCl, containing a mixture of protease inhibitors (1 mM benzamidine-HCl, 1 mM phenylmethanesulfonyl fluoride, 0.4 μg/ml aprotinin, 0.5 μg/ml leupeptin, 0.7 μg/ml pepstatin) using a French press. After centrifugation (100,000 × g, 60 min), ammonium sulfate (0.32 g/ml) was added to the cleared lysate. The resulting precipitate was collected by centrifugation (18,000 × g, 30 min) and then resuspended in Buffer C (50 mM potassium phosphate, pH 7.4, 10% glycerol, 0.5 mM EDTA, 1 mM β-mercaptoethanol) containing the mixture of protease inhibitors. The conductivity of the protein solution was adjusted to that of 100 mM KCl with Buffer C and then mixed with nickel nitrilotriacetic acid-agarose beads (Qiagen) pre-equilibrated with Buffer C containing 100 mM KCl and 50 mM imidazole. After being poured into a column, the beads were washed extensively with the same buffer, followed by the sequential elution of bound hRad52 with 200 and 500 mM imidazole in Buffer C containing 100 mM KCl. Fractions containing hRad52 were loaded onto an 8-ml Source S column (Amersham Biosciences) and eluted with a linear gradient from 100 to 600 mM KCl in Buffer C. Nearly homogenous hRad52 (~11 mg from a 1-liter culture) was stored in small aliquots at −80 °C.

The hRad52 open reading frame was subcloned from pET28b-hRad52 into pTAG (34) to generate the plasmid pTAG-hRad52 that expresses full-length hRad52 as a glutathione S-transferase (GST) fusion protein. Fragments of the hRad52 open reading frame that encode the N-terminal domain (residues 1–176) and the remainder (residues 177–418) of hRad52 were introduced into pTAG to generate the plasmids, pTAG-hRad52N and pTAG-hRad52C, that express these hRad52 fragments as GST fusion proteins. Plasmids encoding GST and GST-hRad52 fusion proteins were introduced into BL21(DE3) cells. When cultures grown at 25 °C reached A_{600} ~0.8, 1 mM isopropylthiogalactoside was added, and growth continued for 4 h. Cells were harvested by centrifugation, resuspended in Buffer D (50 mM Tris-HCl, pH 7.5, 250 mM KCl, 10% glycerol, 1 mM EDTA) containing the mixture of protease inhibitors, and lysed by sonication. After centrifugation (100,000 × g, 60 min), the lysate was rocked for 1 h with glutathione-Sepharose beads (Amersham Biosciences) at 4 °C. The beads were collected by centrifugation and then washed extensively with Buffer D. Bound proteins were eluted with Buffer C containing 10 mM reduced glutathione. Fractions containing either GST or GST fusion proteins were stored at −80 °C.

Purification of Recombinant yRad52—His-tagged yRad52 was purified from *E. coli* as described previously (35).

Purification of Recombinant XPF/ERCC1—The XPF-ERCC1 complex was overexpressed in and purified from *E. coli* as described (36), except the cobalt column was omitted and Superdex 200 (Amersham Biosciences) was used for the gel filtration step. Approximately 3 μg of nearly homogenous XPF-ERCC1 complex was obtained from a 1-liter culture.

In Vitro Transcription and Translation—The plasmids pTB-E1 and pTB-F that encode ERCC1 and XPF, respectively (11), were used as

templates to synthesize ^{35}S-labeled ERCC1 and XPF by coupled *in vitro* transcription and translation using the T7 Quick-coupled TNT kit from Promega.

Pull-down Assays—Glutathione-Sepharose beads (10 μl) and purified recombinant XPF/ERCC1 (13 pmol) were incubated with either GST-hRad52 (25 pmol) or GST (25 pmol) in 250 μl of Buffer D (50 mM HEPES-KOH, pH 7.5, 100 mM KCl, 1 mM EDTA, 0.05% Nonidet P-40) with or without 20 μg/ml ethidium bromide for 30 min at 4 °C. Beads were collected by centrifugation and then washed extensively with Buffer D. Proteins were released from the beads by the addition of SDS sample buffer followed by incubation at 95 °C for 5 min. After separation by SDS-PAGE, ERCC1 and XPF were detected by immunoblotting.

Glutathione-Sepharose beads, GST fusion proteins and *in vitro* translated ERCC1 and XPF were incubated in 50 mM Tris-HCl, pH 7.5, 150 mM KCl, 1 mM EDTA, 0.5% Nonidet P-40 as described above. Labeled proteins that bound to the beads were separated by SDS-PAGE and then detected by PhosphorImaging analysis (Amersham Biosciences).

DNA Substrates—The following oligonucleotides were purchased from Operon: Ya, 5'-<u>ACGTTGTAAAACGACGGCCAGTGAATTCGAG</u>-CTCGGTACCCGGAGATCCTCTAGAGTCGACCTGCAGTGGCTT-3', and Yb, 5'-CCTAACAGTACTTGATCAGAGCTCTTCGAGAATTT<u>TAC</u>-<u>CGAGCTCGAATTCACTGGCCGTCGTTTTACAACGT</u>-3'. The underlines in Ya and Yb are complementary. Ya (200 pmol) was labeled with [γ-^{32}P]ATP (PerkinElmer Life Sciences, 6000 Ci/mmol) by T4 polynucleotide kinase (New England Biolabs). Labeled Ya was annealed with Yb (400 pmol) in 10 mM Tris-HCl, pH 7.5, 50 mM NaCl, 0.1 mM EDTA by heating at 70 °C for 5 min followed by slow cooling to room temperature. The splayed arm substrate was purified after electrophoresis through a 5% non-denaturing polyacrylamide gel as described previously (11).
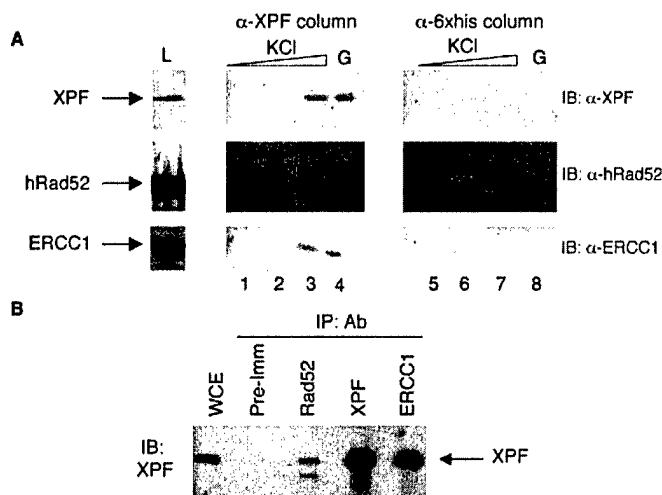
Endonuclease Assay—XPF-ERCC1 complex (0.4 pmol) was pre-incubated on ice for 5 min with the indicated amount of hRad52 (0–4.4 pmol) in 10 mM HEPES-KOH, pH 7.8, 15 mM KCl, 1 mM MgCl$_2$, 0.1 mg/ml bovine serum albumin, 4.5% glycerol, 0.3 mM dithiothreitol in a final volume of 10 μl. After the addition of labeled DNA substrate (3 fmol), reaction mixtures were incubated at 37 °C for the indicated times. Reactions were stopped by the addition of EDTA to a final concentration of 2 mM. After phenol/chloroform extraction and ethanol precipitation, reaction products were separated by denaturing PAGE. Labeled oligonucleotides in the dried gel were detected and quantitated by PhosphorImaging analysis (Amersham Biosciences).

Single Strand Annealing—The assay (reaction volume 50 μl) was performed essentially as described (37). For reactions containing both XPF/ERCC1 (0.5 pmol) and hRad52 or yRad52 (3.6 pmol), the proteins were preincubated on ice for 5 min. For zero time point samples, the reaction components were mixed directly in stop buffer.

RESULTS

Specific Association between XPF/ERCC1 and hRad52 in Human Cell Extracts—To identify proteins that associate with XPF/ERCC1, we fractionated a HeLa cell extract by immunoaffinity chromatography with either anti-XPF antibodies or anti-His$_6$ antibodies as the ligand. As expected, both XPF and ERCC1 were specifically retained by the anti-XPF beads and detected in the 1 M KCl and 0.2 M glycine eluates by immunoblotting (Fig. 1A, compare *lanes 3* and *4* with *lanes 7* and *8*). Interestingly, hRad52 was detected in the 1 M KCl eluate from the anti-XPF beads (Fig. 1A, *lane 3*) but not in an equivalent fraction from either the anti-His$_6$ beads (Fig. 1A, *lane 7*) or protein A-agarose beads alone (data not shown). To provide further evidence for a specific association between XPF/ERCC1 and hRad52, we fractionated a HeLa nuclear extract by hRad52 affinity chromatography. ERCC1 specifically bound to the hRad52 beads and was eluted by the same ionic conditions that disrupted the association between hRad52 and the anti-XPF beads (data not shown).

Because both the XPF-ERCC1 complex and hRad52 bind to DNA, their association in the affinity chromatography experiments may have been mediated by DNA in the extract. To examine this issue, proteins were immunoprecipitated from a HeLa cell extract in the presence of ethidium bromide to disrupt DNA-protein interactions (Fig. 1B). As expected, XPF was immunoprecipitated by XPF antibodies and by antibodies spe-
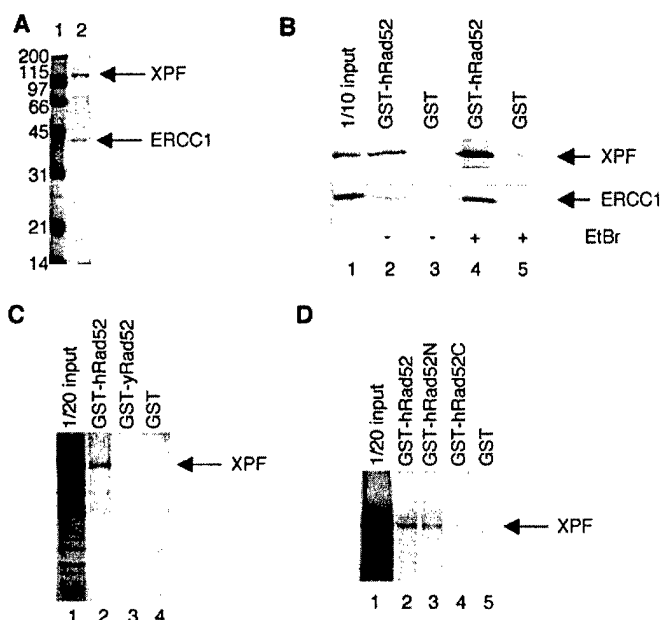
FIG. 1. **Association of ERCC1 and XPF with hRad52 in human cell extracts.** *A*, HeLa cell-free extract (500 µg) was incubated with either α-XPF beads or α-His$_6$ beads as described under "Experimental Procedures." Bound polypeptides were eluted stepwise with 0.2 (*lanes 1* and *5*), 0.5 (*lanes 2* and *6*), and 1.0 M KCl (*lanes 3* and *7*) and then finally with 0.2 M glycine, pH 2.0 (*lanes 4* and *8*, *G*). An aliquot of the cell-free extract (50 µg, *L*) and peak fractions from the eluates of the immuno-affinity beads were separated by SDS-PAGE, transferred to a nitrocellulose membrane, and then probed with the indicated antibody. *B*, HeLa cell-free extract (2 mg) was immunoprecipitated (*IP*) with the indicated antibody (*Ab*) as described under "Experimental Procedures." After separation of immunoprecipitated proteins by SDS-PAGE, XPF was detected by immunoblotting (*IB*).

FIG. 2. **Mapping of the interaction between hRad52 and XPF/ERCC1.** *A*, recombinant XPF-ERCC1 complex purified from *E. coli*. *Lane 1*, molecular mass standards (kDa); *lane 2*, XPF/ERCC1 (0.9 µg, 6.7 pmol). *B*, binding of hRad52 to the ERCC1-XPF complex. Glutathione beads and purified XPF-ERCC1 complex were incubated with either GST-hRad52 (*lanes 2* and *4*) or GST alone (*lanes 3* and *5*) in the presence or absence of ethidium bromide as described under "Experimental Procedures." The binding of XPF/ERCC1 to the beads was detected by immunoblotting. *Lane 1/10 input* contained one-tenth of the XPF/ERCC1 used in the binding reactions. *C*, binding of hRad52 to XPF. Glutathione beads and labeled *in vitro* translated XPF were incubated with GST-hRad52 (*lane 2*), GST-yRad52 (*lane 3*), or GST alone (*lane 4*) as described under "Experimental Procedures." *D*, binding of XPF to the N-terminal domain of hRad52. Glutathione beads and labeled *in vitro* translated XPF were incubated with either GST (*lane 5*) or the GST fused to full-length Rad52 (GST-hRad52, *lane 2*), the N-terminal domain of hRad52 (GST-hRad52N, *lane 3*), and the C-terminal domain of hRad52 (GST-hRad52C, *lane 4*). The binding of labeled XPF to the beads was detected by PhosphorImaging analysis.

cific for its partner protein, ERCC1 (Fig. 1*B*). In accord with the affinity chromatography experiments, XPF was specifically co-immunoprecipitated by hRad52 antibody (Fig. 1*B*). Together these results strongly suggest that XPF/ERCC1 and hRad52 stably associate under physiological conditions.

Direct Physical Interaction between the DNA Binding Domain of hRad52 and the XPF Subunit of the XPF-ERCC1 Complex—To determine whether there is a direct interaction between hRad52 and XPF/ERCC1, we performed pull-down assays with purified recombinant XPF/ERCC1 (Fig. 2*A, lane 2*) and GST-hRad52. XPF/ERCC1 bound to glutathione-Sepharose beads liganded by GST-hRad52 but not to beads liganded by GST (Fig. 2*B*, compare *lanes 2* and *3*). A similar result was obtained when the pull-down assays were carried out in the presence of ethidium bromide (Fig. 2*B, lanes 4* and *5*) confirming that the association between XPF/ERCC1 and hRad52 is not mediated by DNA.

The interaction of hRad52 with the subunits of the XPF-ERCC1 complex was examined in pull-down assays using *in vitro* translated polypeptides. Labeled XPF bound to GST-hRad52 beads but not to either GST-yRad52 or GST beads alone (Fig. 2*C, lanes 2–4*). In contrast, no specific binding of *in vitro* translated ERCC1 to GST-hRad52 beads was observed (data not shown). To map the region of hRad52 that interacts with XPF, we expressed and purified the N- and C-terminal domains of hRad52 as GST fusion proteins. XPF bound to full-length hRad52 and its N-terminal domain but not to the C-terminal domain (Fig. 2*D*). Together, these results demonstrate that XPF/ERCC1 and hRad52 physically interact in a species-specific reaction that is mediated by the XPF subunit of the XPF-ERCC1 complex and the N-terminal DNA binding domain of hRad52.
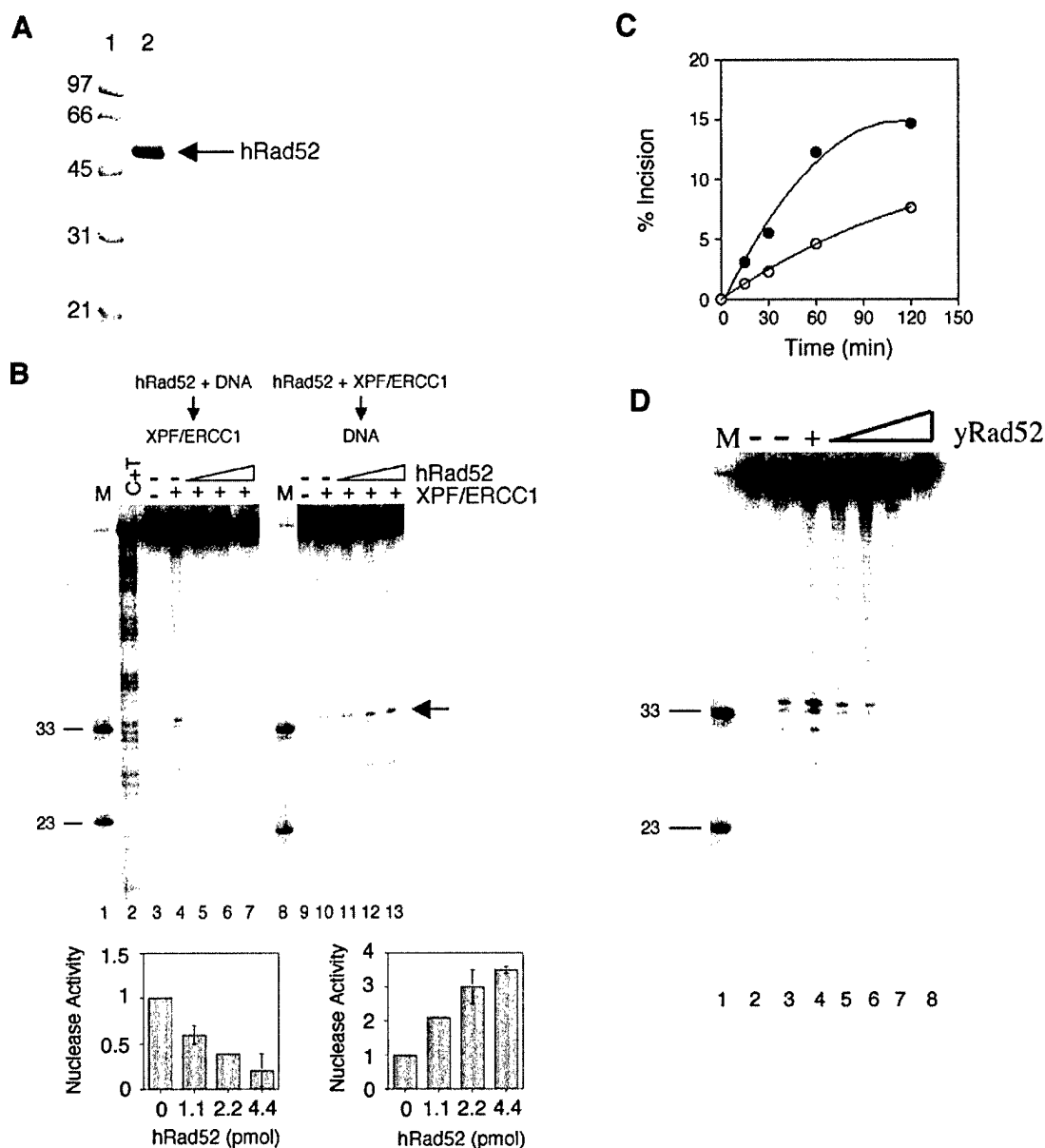
hRad52 Stimulates the DNA Structure-specific Endonuclease Activity of XPF/ERCC1—To elucidate the functional consequences of the interaction between hRad52 and XPF/ERCC1, the effect of purified hRad52 (Fig. 3*A, lane 2*) on the nuclease activity of XPF/ERCC1 was examined. In these assays we used

the preferred DNA substrate of XPF/ERCC1, a splayed arm structure formed that is cleaved by XPF/ERCC1 at the duplex/single strand junction releasing the 3' single-stranded tail (3, 8, 10–12, 38). Pre-incubation of the DNA substrate with increasing amounts of hRad52 progressively inhibited XPF/ERCC1 nuclease activity (Fig. 3*B, lanes 4–7*). In contrast, pre-incubation of XPF/ERCC1 with the same amounts of hRad52 before mixing with the DNA substrate stimulated nuclease activity (Fig. 3*B, lanes 10–13*). Maximal stimulation occurred at a ratio of about 6 hRad52 molecules to 1 XPF-ERCC1 complex (Fig. 3*B*). Further increases in the amount of hRad52 progressively reduced nuclease activity (data not shown). At the optimum ratio, hRad52 enhanced the initial rate of endonucleolytic cleavage catalyzed by XPF/ERCC1 about 3-fold (Fig. 3*C*). Because hRad52 forms a heptameric ring (24, 25), these results suggest that a single XPF/ERCC1 heterodimer interacts with the hRad52 heptamer to yield a ternary complex that has increased nuclease activity. To provide further support for this model, we examined the effect of yRad52, which has similar biochemical properties to hRad52 but does not appear to bind XPF (Fig. 2*C*). In contrast to hRad52 (Fig. 3*B, lanes 10–13*), pre-incubation of XPF/ERCC1 with increasing amounts of yRad52 inhibited nuclease activity (Fig. 3*D, lanes 5–8*). Thus, the increased endonuclease activity of XPF/ERCC1 is dependent upon a specific physical interaction with hRad52.

Because Rad52 is a DNA-binding protein, we considered the possibility that the interaction of hRad52 with XPF/ERCC1 may change the DNA substrate specificity of this endonuclease.
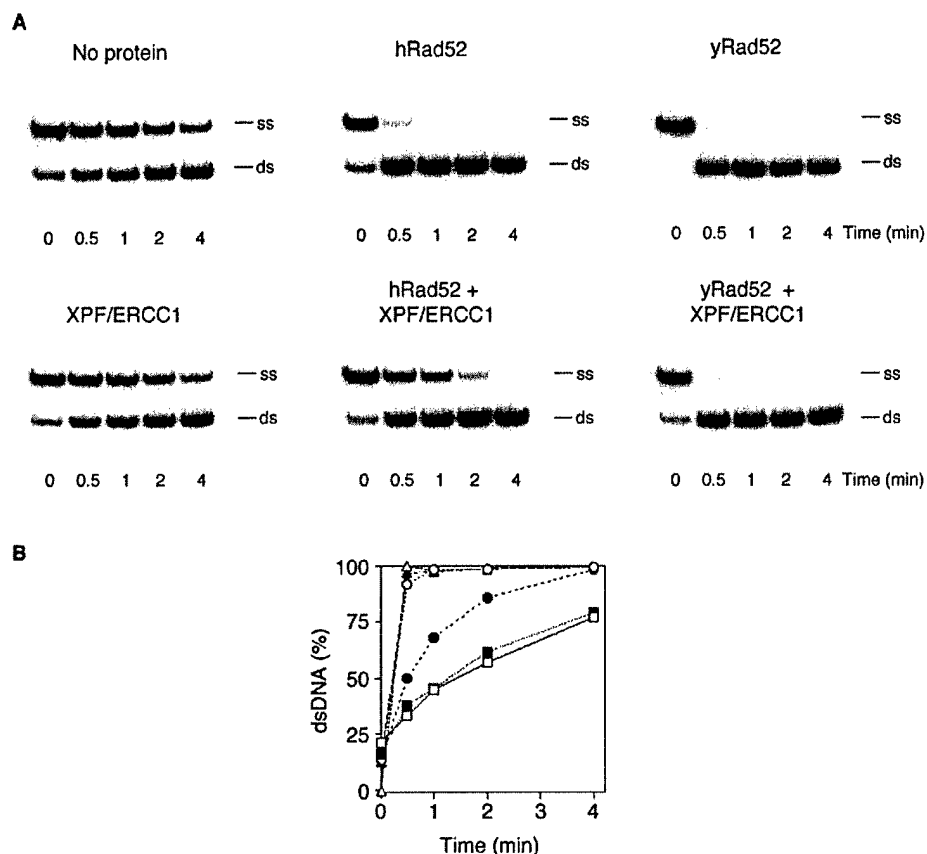
FIG. 3. **Effect of order of addition of hRad52 on the endonuclease activity of XPF/ERCC1.** *A*, recombinant hRad52 purified from *E. coli*. *Lane 1*, molecular mass standards (kDa); *lane 2*, hRad52, (4 μg, 87 pmol). *B, left panel*, hRad52 was pre-incubated with the labeled splayed arm DNA substrate (3 fmol) on ice for 5 min, prior to the addition of XPF/ERCC1 (0.4 pmol). *Right panel*, hRad52 was pre-incubated with XPF/ERCC1 (0.4 pmol) prior to the addition of the labeled splayed arm DNA substrate (3 fmol). Reactions were incubated as described under "Experimental Procedures." After separation by denaturing gel electrophoresis, labeled oligonucleotides were detected by PhosphorImaging analysis. *Lanes 1* and *8*, splayed arm DNA substrate digested with SacI and EcoRI to generate the labeled 33 and 23 nucleotide oligomers; *lane 2*; C + T Maxam-Gilbert sequencing ladder of labeled oligonucleotide Ya; *lanes 3* and *9*, splayed arm DNA substrate alone. Splayed arm DNA substrate and XPF/ERCC1 with no hRad52 (*lanes 4* and *10*), 1.1 pmol of hRad52 (*lanes 5* and *11*), 2.2 pmol of hRad52 (*lanes 6* and *12*), and 4.4 pmol of hRad52 (*lanes 7* and *13*). The *arrow* on the *right* indicates the major incision site of XPF/ERCC1. The *bar graphs* below the gels indicate the relative nuclease activity from two independent experiments quantitated by PhosphorImaging analysis and expressed relative to the activity of XPF/ERCC1 alone. *C*, kinetic analysis of the effect of hRad52 on the XPF/ERCC1 endonuclease. XPF/ERCC1 (0.4 pmol) was pre-incubated either in the presence (*filled circles*) or absence (*open circles*) of hRad52 (2.2 pmol) prior to the addition of the splayed arm DNA substrate. Aliquots were taken at the indicated time points. After separation by denaturing gel electrophoresis, cleavage of the DNA substrate was quantitated by PhosphorImaging analysis and is shown graphically. *D*, XPF/ERCC1 (0.4 pmol) was pre-incubated either in the presence or absence of hRad52 or yRad52 prior to the addition of the labeled splayed arm DNA substrate and further incubation as described under "Experimental Procedures." After separation by denaturing gel electrophoresis, labeled oligonucleotides were detected by PhosphorImaging analysis. *Lane 1*, splayed arm DNA substrate digested with SacI and EcoRI to generate the labeled 33- and 23-nucleotide oligomers indicated on the *left* (*M*); *lane 2*, DNA substrate alone. XPF/ERCC1 and DNA substrate with no Rad52 (*lane 3*), 2.2 pmol of hRad52 (*lane 4*), 0.9 pmol of yRad52 (*lane 5*), 1.8 pmol of yRad52 (*lane 6*), 3.6 pmol of yRad52 (*lane 7*), and 9 pmol of yRad52 (*lane 8*).

A duplex Y structure was not cleaved by XPF/ERCC1 either with or without hRad52 (data not shown). In contrast, hRad52 did stimulate the weak cleavage activity of XPF/ERCC1 on a duplex substrate with a 3′ single strand flap, but the degree of stimulation was similar to that observed with the preferred splayed arm substrate (data not shown). Thus, under the reac-

tion conditions used, hRad52 does not seem to alter DNA substrate specificity of XPF/ERCC1.

XPF/ERCC1 Attenuates the DNA Strand Annealing Activity of hRad52—The ability of eukaryotic Rad52 to bind to single strand DNA and to promote the annealing of complementary DNA single strands (25, 28) is consistent with the involvement

FIG. 4. **Attenuation of hRad52-mediated single strand annealing by XPF/ERCC1.** *A*, hRad52 or yRad52 (3.6 pmol) was pre-incubated either in the presence or absence of XPF/ERCC1 (0.5 pmol) prior to the addition of complementary single strand 83-mer oligonucleotides (18 pmol of each), one of which was end-labeled, as described under "Experimental Procedures." For the zero time point (*lane 0*), reaction constituents were mixed directly in stop buffer. Aliquots were removed at the indicated time points. After native gel electrophoresis, labeled oligonucleotides were detected and quantitated by PhosphorImaging analysis. The positions of single strand (*ss*) and duplex oligonucleotides (*ds*) are indicated on the right. *B*, the results of the annealing reactions described above are shown graphically. No protein, *open square*; XPF/ERCC1, *filled square*; hRad52, *open circle*; hRad52 and XPF/ERCC1, *filled circle*; yRad52, *open triangle*; yRad52 and XPF/ERCC1, *filled triangle*.

of this factor in SSA (21, 28, 29, 39–43). Because XPF/ERCC1 interacts with the DNA binding domain of hRad52, we examined whether this interaction modulates the ability of hRad52 to anneal complementary DNA single strands. As expected (28, 29), both hRad52 and yRad52 promoted the annealing of complementary DNA single strands, whereas XPF/ERCC1 had no significant annealing activity (Fig. 4). Interestingly, pre-incubation with XPF/ERCC1 markedly attenuated the strand annealing activity of hRad52 (Fig. 4) but had no effect on strand annealing by yRad52 (Fig. 4). Thus, inhibition of hRad52-mediated strand annealing is dependent upon a specific physical interaction with XPF/ERCC1, suggesting that the binding of hRad52 to DNA and to XPF/ERCC1 are mutually exclusive. Taken together our results provide evidence that hRad52 and XPF/ERCC1 form a stable ternary complex that cleaves specific recombination intermediates.

DISCUSSION

During NER, protein-protein interactions with XPA and RPA position XPF/ERCC1 to make the 5′ incision in the damaged DNA strand (6–12). In contrast, the molecular mechanisms that underlie the recruitment and activation of XPF/ERCC1 in homology-dependent recombination reactions have not been identified. Here we have shown an association between XPF/ERCC1 and hRad52 in human cell extracts and demonstrated a direct interaction between XPF and the N-terminal DNA binding domain of hRad52. The physical link between XPF/ERCC1 and hRad52 is congruent with results from genetic studies in mammalian cells (21–23, 39, 44–48) and *S. cerevisiae* (21–23, 39, 44–48), implicating these proteins in mitotic recombination pathways that include SSA and the integration of DNA molecules into homologous chromosomal sequences.

The yeast Rad1/Rad10 endonuclease removes non-homologous 3′ single strand tails from recombination intermediates

that would otherwise prevent completion of the recombination event (39, 48). Similar studies with Chinese hamster ovary *ercc1* mutant cell lines have provided evidence that the XPF-ERCC1 complex also participates in intrachromosomal recombination between direct sequence repeats and removes non-homologous single strand tails in homology-mediated gene targeting events (15, 17). However, more recently, it was found that ERCC1 is also essential for targeted gene replacement in mouse ES cells even when the ends of the targeting construct are homologous with the genomic locus (13). Thus, it appears that XPF/ERCC1 plays a critical role in the processing of a different type of recombination intermediate that does not have a non-homologous single strand tail, namely the heteroduplex intermediate that is generated as a result of stalled branch migration during gene targeting (13).

Based on the biochemical properties of eukaryotic Rad52 (28, 29), it has been assumed that it would be involved in the annealing of complementary DNA single strands to generate the DNA structures that are subsequently recognized and cleaved by Rad1/Rad10 in yeast and XPF/ERCC1 in mammalian cells. Although our studies do not exclude the involvement hRad52 in the strand annealing reaction, they have revealed a novel and unexpected role for Rad52 at a different and later stage in these pathways, the cleavage of recombination intermediates. Specifically we have shown that hRad52 and XPF/ERCC1 form a stable complex in human cell extracts. Because formation of this ternary complex not only enhances the structure-specific endonuclease activity of XPF/ERCC1 but also inhibits DNA binding by hRad52, we suggest that the role of hRad52 in the ternary complex is to recruit, via protein-protein interactions, the DNA structure-specific endonuclease to specific recombination intermediates generated during SSA and in gene targeting.

REFERENCES

1. Tomkinson, A. E., Bardwell, A. J., Bardwell, L., Tappe, N. J., and Friedberg, E. C. (1993) *Nature* **362,** 860–862
2. Bardwell, A. J., Bardwell, L., Tomkinson, A. E., and Friedberg, E. C. (1994) *Science* **265,** 2082–2085
3. Davies, A. A., Friedberg, E. C., Tomkinson, A. E., Wood, R. D., and West, S. C. (1995) *J. Biol. Chem.* **270,** 24638–24641
4. Guzder, S., Sung, P., Prakash, L., and Prakash, S. (1996) *J. Biol. Chem.* **271,** 8903–8910
5. Praksash, S., and Prakash, L. (2000) *Mutat. Res.* **451,** 13–24
6. Park, C. H., Bessho, T., Matsunaga, T., and Sancar, A. (1995) *J. Biol. Chem.* **270,** 22657–22660
7. van Duin, M., de Wit, J., Odijk, H., Westerveld, A., Yasui, A., Koken, M. H. M., Hoeijmakers, J. H. J., and Bootsma, D. (1986) *Cell* **44,** 913–923
8. Sijbers, A. M., de Laat, W. L., Ariza, R. R., Biggerstaff, M., Wei, Y.-F., Moggs, J. G., Carter, K. C., Shell, B. K., Evans, E., de Jong, M. C., Rodemakers, S., de Rooij, J., Jaspers, N. G. J., Hoeijmakers, J. H. J., and Wood, R. D. (1996) *Cell* **86,** 811–822
9. Brookman, K. W., Lamerdin, J. E., Thelen, M. P., Hwang, M., Reardon, J. T., Sancar, A., Zhou, Z. Q., Walter, C. A., Parris, C. N., and Thompson, L. H. (1996) *Mol. Cell. Biol.* **16,** 6553–6562
10. de Laat, W. L., Appeldoorn, E., Jaspers, N. G., and Hoeijmakers, J. H. J. (1998) *J. Biol. Chem.* **273,** 7835–7842
11. Bessho, T., Sancar, A., Thompson, L. H., and Thelen, M. P. (1997) *J. Biol. Chem.* **272,** 3833–3837
12. Matsunaga, T., Park, C.-H., Bessho, T., Mu, D., and Sancar, A. (1996) *J. Biol. Chem.* **271,** 11047–11050
13. Niedernhofer, L. J., Essers, J., Weeda, G., Beverloo, B., de Wit, J., Muijtens, M., Odijk, H., Hoeijmakers, J. H. J., and Kanaar, R. (2001) *EMBO J.* **20,** 6540–6549
14. Westerveld, A., Hoeijmakers, J. H. J., van Duin, M., de Wit, J., Odijk, H., Pastink, A., Wood, R. D., and Bootsma, D. (1984) *Nature* **310,** 425–429
15. Sargent, R. G., Rolig, R. L., Kilburn, A. E., Adair, G. M., Wilson, J. H., and Nairn, R. S. (1997) *Proc. Natl. Acad. Sci. U. S. A.* **94,** 13122–13127
16. Hoy, C. A., Thompson, L. H., Mooney, C. L., and Salazar, E. P. (1985) *Cancer Res.* **45,** 1737–1743
17. Adair, G. M., Rolig, R., Moore-Faver, D., Zabelshansky, M., Wilson, J. H., and Nairn, R. S. (2000) *EMBO J.* **19,** 5552–5561
18. Symington, L. (2002) *Microbiol. Mol. Biol. Rev.* **630,** 630–670
19. Krejci, L., Chen, L., Van Komen, S., Sung, P., and Tomkinson, A. (2003) *Prog. Nucleic Acid Res. Mol. Biol.* **75,** 159–201
20. Sugawara, N., and Haber, J. E. (1992) *Mol. Cell. Biol.* **12,** 563–575
21. Fishman-Lobell, J., Rudin, N., and Haber, J. E. (1992) *Mol. Cell. Biol.* **12,** 1291–1303
22. Yamaguchi-Iwai, Y., Sonoda, E., Buerstedde, J. M., Bezzubova, O., Morrison, C., Takata, M., Shinohara, A., and Takeda, S. (1998) *Mol. Cell. Biol.* **11,** 6430–6435
23. Rijkers, T., ven den Ouweland, J., Morolli, B., Rolink, A. G., Baarends, W. M., van Sloun, P. H. P., Lohman, P., and Patsink, A. (1998) *Mol. Cell. Biol.* **18,** 6423–6429
24. Stasiak, A. Z., Larquet, E., Stasiak, A., Muller, S., Engel, A., van Dyck, E., West, S. C., and Egelman, E. H. (2000) *Curr. Biol.* **10,** 337–340
25. Shinohara, A., Shinohara, M., Ohta, T., Matsuda, S., and Ogawa, T. (1998) *Genes Cells* **3,** 145–156
26. Singleton, M. R., Wentzell, L. M., Liu, Y., West, S. C., and Wigley, D. B. (2002) *Proc. Natl. Acad. Sci. U. S. A.* **99,** 13492–13497
27. Kagawa, W., Kurumizaka, H., Ishitani, R., Fukai, S., Nureki, O., Shibata, T., and Yokoyama, S. (2002) *Mol. Cell* **10,** 359–371
28. Mortensen, U. H., Bendixen, C., Sunjevaric, I., and Rothstein, R. (1996) *Proc. Natl. Acad. Sci. U. S. A.* **93,** 10729–10734
29. Reddy, G., Golub, E. I., and Radding, C. M. (1997) *Mutat. Res.* **377,** 53–59
30. Harlow, E., and Lane, D. (1988) *Antibodies: A Laboratory Manual,* pp. 522–523, Cold Spring Harbor Laboratory Press, Cold Spring Harbor, NY
31. Manley, J. L., Fire, A., Cano, A., Sharp, P. A., and Gefter, M. L. (1980) *Proc. Natl. Acad. Sci. U. S. A.* **77,** 3855–3859
32. Chen, G., Yuan, S.-S. F., Liu, W., Xu, Y., Arlinghaus, R., Baltimore, D., Gasser, P. J., Park, M. S., Sung, P., and Lee, E. Y.-H. P. (1999) *J. Biol. Chem.* **274,** 12748–12752
33. Ausubel, F. M., Brent, R., Kingston, R., Morre, D., Seidman, J., Smith, A., and Struhl, K. (1994) *Current Protocols in Molecular Biology,* p. 3, John Wiley & Sons, Inc., New York
34. Ron, D., and Dressler, H. (1992) *BioTechniques* **13,** 866–868
35. Song, B., and Sung, P. (2000) *J. Biol. Chem.* **275,** 15895–15904
36. Kuraoka, I., Kobertz, W. R., Ariza, R. R., Biggerstaff, M., Essigmann, J. M., and Wood, R. D. (2000) *J. Biol. Chem.* **275,** 26632–26636
37. Krejci, L., Song, B., Bussen, W., Rothstein, R., Mortensen, U. H., and Sung, P. (2002) *J. Biol. Chem.* **277,** 40132–40141
38. Rodriguez, K., Wang, Z., Friedberg, E. C., and Tomkinson, A. E. (1996) *J. Biol. Chem.* **271,** 20551–20558
39. Fishman-Lobell, J., and Haber, J. E. (1992) *Science* **258,** 480–484
40. Benson, F. E., Baumann, P., and West, S. C. (1998) *Nature* **335,** 337–338
41. New, J. H., Sugiyama, T., Zaitseva, E., and Kowalczykowski, S. C. (1998) *Nature* **391,** 407–410
42. Shinohara, A., and Ogawa, T. (1998) *Nature* **391,** 404–407
43. Sung, P. (1997) *J. Biol. Chem.* **272,** 28194–28197
44. Schiestl, R. H., and Prakash, S. (1988) *Mol. Cell. Biol.* **8,** 3619–3626
45. Schiestl, R. H., and Prakash, S. (1990) *Mol. Cell. Biol.* **10,** 2485–2491
46. Aguilera, A., and Klein, H. L. (1989) *Genetics* **122,** 503–517
47. Thomas, B. J., and Rothstein, R. (1989) *Genetics* **123,** 725–738
48. Ivanov, E. L., and Haber, J. E. (1995) *Mol. Cell. Biol.* **15,** 2245–2251